Movements around a tunnel in two-layer ground

by

Richard John Grant

A dissertation submitted for the
Degree of Doctor of Philosophy

The City University, London
Department of Civil Engineering
Geotechnical Engineering Research Centre

July 1998

CONTENTS

LIST OF TABLES

LIST OF FIGURES

ACKNOWLEDGEMENTS

The Geotechnical Engineering Research Centre (GERC) at City University has been a fantastic place to learn and conduct research in Geotechnical Engineering. The supportive atmosphere has been nurtured over many years by everybody associated with the Group, but especially by the current academic and technical members mentioned below.

I first wish to acknowledge the commitment of my supervisors, Professor Neil Taylor and Dr. Sarah Stallebrass, and their unstinting help and support in all respects. My grateful thanks go to them both for their unerring dedication, good humour and time. The analytical and technical skills of both are well known, but their patience and friendship have been equally important.

Special thanks to Professor John Atkinson and Dr. Matthew Coop for their support throughout, especially for their perseverance in helping me understand the fundamental principles of soil behaviour. John Atkinson always had time to advise, and particular thanks to Matthew Coop for imparting some of his immense experience of laboratory testing and knowledge of (and data on) the mechanical behaviour of sands.

The physical experiments, in particular the centrifuge model testing, required considerable input from the technical staff within the Group. My sincere thanks go to Keith Osbourne, to Lloyd Martyka and to Reg Allen, and also to Harvey Skinner, now of the University of Southampton, for guiding me through the early centrifuge tests and solving many of the initial difficulties.

The quantity and quality of information gained from the centrifuge model testing was greatly enhanced by the use of digital image processing. I wish to acknowledge the contribution of those members of the Engineering Surveying Research Centre at City University who developed the new system for the centrifuge during the course of this work. Many thanks are due to Dr. Stuart Robson, Dr. Jin Chen, Professor Mike Cooper and Dr. Dong Ning Qu.

My research was funded for three years by the Engineering and Physical Sciences Research Council. I have been able to continue working at City University thanks to funding from the GERC and an agreement with the Geotechnical Consulting Group (GCG), and I gratefully acknowledge the support of all.

I am indebted to Dr. Toshiyuki Hagiwara (formerly of Gunma University, Japan) and Michele Calvello for their collaborative input, and also to Caesar Kerali for data from one of his tests.

Thanks are also due to the many people that have conducted research within the Group during the period of this work. These include: Paul Morrison, for guidance in the early stages; Vojkan Jovicic, for instruction in the use of bender elements; Ruth Fearon, for making me laugh throughout; and Jiro Kuwano (Tokyo Institute of Technology), for a fresh outlook. Thanks also to both old and current members of the Group who have made the period of this work so enjoyable for me.

I would like to give special thanks to Deborah for her continuous encouragement and for contributing in many ways to the contents of this dissertation. I should also include our families and our friends, especially my parents. Finally, thanks to Sam, our first child, who postponed entry into this world for long enough for me to finish.

DECLARATIONS

I grant powers of discretion to the University Librarian to allow this dissertation to be copied in whole or in part without further reference to me. This permission covers only single copies made for study purposes, subject to normal conditions of acknowledgement.

ABSTRACT

An increasing need for accurate predictions of tunnelling-induced ground movements and potential damage to structures has produced a number of publications over the past 30 years. Few, however, have addressed the problem of tunnelling in ground consisting of more than one soil layer or the associated subsurface movements. The aim of the research was to investigate ground movements in two-layer ground conditions, specifically movements above tunnels driven in clay overlain by coarse grained materials. The principal methods of investigation were geotechnical centrifuge model testing and finite element analysis using the 3-Surface Kinematic Hardening (3-SKH) model, an elasto-plastic soil model implemented in the finite element program CRISP at City University, London. Both methods use effective stress path modelling to produce soil behaviour representative of prototype situations.

Twenty-eight plane strain centrifuge model tests are reported in which the tunnel was represented by a 50mm diameter cylindrical cavity supported by compressed air pressure. The tunnel cavity was located within a layer of overconsolidated kaolin clay and in most cases the clay had an overlying layer of coarse grained material. The main variables in the tests were: the type of overlying strata; the thicknesses of the two strata; and the position of the water table. Tests were conducted at an acceleration of 100*g* when the cavity then represented a 5m diameter tunnel with a maximum depth to tunnel axis of 22.5m at prototype scale. After effective stress equilibrium was achieved, ground movements were generated by reducing the tunnel support pressure at a rate which produced essentially undrained behaviour in the clay. Transducers were used to measure pore pressures in the clay near the tunnel and displacements at the ground surface and at the clay/sand interface. Subsurface movements in the clay were obtained from images from a CCD camera, mounted on the centrifuge swing to view the front of the model in-flight, using a new digital image processing system developed at City University to track targets in the vertical face of the clay.

Stress path triaxial tests were performed on some of the sands used in the centrifuge experiments, to determine stiffness properties for analysis of centrifuge test results and input for numerical analyses. Values of shear stiffness at very small strains, G'_{max}, were determined using the bender element technique.

Finite element analyses were conducted at centrifuge model scale with carefully simulated model stress histories. Some were direct simulations of physical model tests and were fully evaluated by comparison with centrifuge test data. Numerical predictions could be used with confidence, therefore, within the known limitations of the analyses. As well as evaluating the numerical model, the main points of investigation were the effects of: modelling conditions such as boundary proximity and stress history; the constitutive model used for the sand; the stiffness and depth of the upper strata on the movements in the clay.

The results are applicable to predicting ground movements in the plane perpendicular to single, long tunnels, and the most important findings of the research are as follows.

i) Both surface and subsurface settlement troughs are well represented by Gaussian distributions, except within a vertical distance of approximately 0.5*D* of the tunnel crown when considerably steeper settlement profiles should be anticipated.
ii) The form of the settlement profiles is constant until the tunnel begins to collapse (V~20%).
iii) The equations of Mair et al (1993) adequately describe the distribution of vertical movements with depth for tunnels in clay-only soil profiles, although, near a "free" ground surface the distribution of movements may be considerably wider (also see (i) above).
iv) For tunnels in clay with an overlying layer of different material the ratio of the shear stiffnesses at the interface between the materials should be taken into account.
v) For undrained (constant volume) conditions, horizontal displacements may be inferred from the vertical displacements as the vectors of movement focus on the point where the tangent to the distribution of i with depth intersects the vertical tunnel axis.

LIST OF SYMBOLS

A	coefficient of p' in relationship for $G'_{max\ (nc)}$, or
	A^* for describing G'_{max} measured for compacted sands
D	tunnel diameter
E	Young's modulus
G	tangent shear modulus
G'_{max}	G' at very small strains, when the soil response is considered to be elastic (sometimes referred to by others as G'_0)
H	drainage path length
I	second moment of area
K	dimensionless width parameter for Gaussian settlement troughs [$K = i/(z_0 - z)$]
$K_{s\ (grad)}$	gradient of distribution of i through the sand
K_0	coefficient of earth pressure at rest
N	gravity scaling factor, or
	stability ratio in plasticity solutions ($N = \Delta\sigma_T/s_u$)
R_0	overconsolidation ratio in terms of p' ($R_0 = 2p'_0/p'$)
R_{pnl}	radius of the plastic zone in plasticity solutions (assuming non-linear elasticity)
S	settlement, or
	ratio of size of yield surface to bounding surface (for the 3-SKH model)
T	ratio of size of history surface to bounding surface (for the 3-SKH model)
T_v	time factor (for consolidation)
V	volume loss (usually as percentage of tunnel volume)
a	radial acceleration
	or radius of tunnel ($D = 2a$)
a_c	Coriolis acceleration
s_u	undrained shear strength
c_v	coefficient of consolidation
d	depth of layer
e	voids ratio
g	acceleration due to gravity (9.81m/s^2)
h	depth
i	distance from the centreline to the point of inflexion of a Gaussian distribution
k	coefficient of permeability
m	exponent of R_0 in relationship for $G'_{max\ (oc)}$

n exponent of p' in relationship for $G'_{max\,(nc)}$, or
n^* for describing G'_{max} measured for compacted sands

p' mean normal effective stress

p'_0 half the value of p' at the intersection of an unload-reload line with the isotropic normal compression line

p'_e value of p' on the INCL at a given v

p'_r reference pressure in relationship for G'_{max} (p'_r = 1kPa)

q' deviator stress

r radius from centre of rotation (for centrifuge acceleration), or
radius from centre of tunnel (for plasticity solutions)

$\dot{r}$ velocity of a particle in a radial direction

t time

u pore pressure

u_e excess pore pressure

v specific volume of the soil

v_s velocity of the shear wave (bender element measurements)

v_κ specific volume on a given unload-reload line p' = 1kPa

x distance from tunnel centreline in transverse direction

z distance from ground surface in vertical direction (positive downwards)

z_* distance from the tunnel axis in vertical direction (positive upwards) - Appendix A

z_e effective depth

z_1 depth to clay/sand interface

z_0 depth to tunnel axis

Γ specific volume on the critical state line when p' = 1kPa

M stress ratio at critical state (q'/p')

N specific volume on the isotropic normal compression line when p' = 1kPa

γ unit weight of soil

γ_d unit weight of dry soil

γ_s unit weight of saturated soil

γ_w unit weight of water

ε strain

η stress ratio (q'/p')

θ subtended angle

κ average gradient of an unload-reload line in v: lnp' space

κ^* gradient of an unload-reload line in $\ln v$: $\ln p'$ space

λ gradient of normal compression line in v: $\ln p'$ space

λ^* gradient of normal compression line in $\ln v$: $\ln p'$ space

ν Poisson's ratio

ρ mass density

σ stress

σ_T tunnel support pressure

ϕ' angle of friction

ϕ'_c critical state angle of friction

ψ exponent in the hardening modulus (for the 3-SKH model)

ω angular velocity

Superscripts

' in terms of effective stress (as in σ' is effective stress)

Subscripts

a axial

c clay

fin final

h horizontal

i interface

m model

max maximum

nc normally consolidated

oc overconsolidated

p prototype

r radial

s sand, or

shear (in ε_s), or

soil (in N_s)

v vertical

w water

Abbreviations

3-SKH 3-Surface Kinematic Hardening (model)

AC alternating current

BSP	British Standard Pipe (size scale for pipe fittings)
CCD	charged couple device (television cameras on centrifuge)
CCTV	closed-circuit television (television system on centrifuge)
cl	centreline
CSL	critical state line
CRISP	CRItical State Program (finite element program)
CSSM	Critical State Soil Mechanics
DPI	digital pressure indicator
FEA	finite element analysis
INCL	isotropic normal compression line
IP	image processing
LBS	Leighton Buzzard Sand (washed silica sand)
LE	linear elastic
med	medium
SBS	state boundary surface
LVDT	linearly variable differential transformer (displacement transducer)
PC	personal computer (IBM compatible)
PPT	pore pressure transducer
RAM	random access memory (relating to computers)
rpm	revolutions per minute
URL	unload-reload line
VCR	video cassette recorder
VHS	magnetic recording video tapes
S-VHS	high quality magnetic recording video tapes

Note

In general, standard SI (Système International) units are used.

CHAPTER 1 INTRODUCTION

The research described in this dissertation concerns the soil movements due to tunnelling in two-layer ground conditions. In this introductory chapter the objectives and background of the work are presented, followed by an overview of the methodology used to investigate the problem and an outline of the following chapters.

1.1 Objectives

The principal aim of the research was to develop properly validated rules for estimating the distribution of short-term ground movements induced by tunnelling in ground consisting of more than one soil layer. The scope of the work was limited to movements in the plane perpendicular to tunnels driven in clay overlain by sands and gravels. By definition, the work includes an investigation of both vertical and horizontal ground movements, as well as the development of numerical analyses and empirical formulae for predicting the shape of tunnelling-induced transverse settlement troughs.

1.2 Background

Underground excavation is not a new practice. Minerals have been extracted from the ground by mining techniques for hundreds of years. However, with regard to tunnelling, perhaps the first modern approach may be attributed to the famed Victorian Engineers, Marc Isambard Brunel and his son Isambard Kingdom Brunel. In the first half of the 19th Century they battled and finally succeeded in excavating a tunnel underneath the River Thames (Skempton and Chrimes, 1994). The Thames Tunnel was the first major subaqueous tunnel constructed anywhere in the world and inspired the first use of a tunnelling shield. Originally opened for pedestrian traffic, it later became a rail tunnel and still forms part of the London Underground railway network today.

Tunnelling inevitably induces ground movements, which in built-up areas can cause damage to existing services and structures. In fact, there were reports of damage to adjacent buildings during construction of the historic Thames Tunnel. Over recent years, damage to existing structures due to tunnelling has been experienced world-wide. Often, individual cases are not published for contractual and insurance reasons, but movement of existing buildings adjacent

to tunnel construction is expected. One well-reported case is the movement, and protection, of the Mansion House in London during the extension of the Docklands Light Railway (Frischmann et al, 1994).

Pressure on land use within urban areas has led to an increase in the number of tunnelling projects for services and mass transit purposes, both in the UK and abroad. An obvious example is the ongoing Jubilee Line Extension in London, which involves tunnelling close to many prestigious structures including the Houses of Parliament and the Clock Tower of Big Ben. With the increase in tunnelling in the urban environment accurate prediction of the associated deformations has become a major issue.

1.2.1 *Prediction of tunnelling-induced ground movements*

Current practice for the prediction of tunnelling-induced near surface settlement profiles is usually based on an empirical approach, formulated largely from field observations of tunnels in uniform ground conditions. Little is known about ground response due to tunnelling in ground consisting of more than one soil layer. The geology of London, in common with many other major cities, generally consists of a layer of coarse grained material overlying overconsolidated clay. Structures are founded at various depths within the soil mass and it is therefore desirable to develop a method of predicting both surface and subsurface movements in multi-layered ground.

Field measurements of subsurface ground movements are expensive and difficult to obtain. The prediction of subsurface displacements and their effect on underground services and structures is commonly based on extrapolations from surface measurements, with relatively little subsurface data either available or used. It is clear that significant improvements in predictions may be achieved by a better understanding of the development of ground movements around tunnels.

1.2.2 *Assessment of damage to existing structures due to tunnelling*

Settlement predictions are generally carried out because of concern over damage to existing structures. Although the role of this research is to investigate ground movements caused by tunnelling and not the effect of these movements on structures, it is important to be aware of the ultimate use of the findings. Below is a brief description of the commonly used methods of assessing the effect of tunnel-induced movements on structures.

Burland and Wroth (1975) used simple beam theory to determine "critical tensile strains" within a plane wall subjected to distortions. The ratio of height to length and the mode of distortion imposed, hogging or sagging, determines whether bending or shear strains are critical. The magnitude of the strains is also a function of the angular distortion imposed on the wall. Burland et al (1977) produced a classification of visible damage to walls by defining severity of damage by the width and number of cracks. Boscardin and Cording (1989) proposed "limiting tensile strains" for the boundaries of these categories and suggested that horizontal tensile ground strains should be added directly to the building strains in order to determine the critical tensile strain of the structure. This allows prediction of likely structural damage to a plane masonry wall if the imposed angular distortion and directly applied horizontal tensile strain can be determined, which are both functions of the ground movement. This procedure has been modified by Mair et al (1996), who suggested using a deflection ratio in place of the angular distortion and imposing the average horizontal ground strain beneath the structural element. Further comments on assessment of building damage may be found in Chapter 2.

1.3 Methodology

The key elements of the investigation were:

i) to use centrifuge model testing techniques to investigate both vertical and horizontal ground movements caused by tunnelling in two-layer ground conditions, particularly sands and gravels overlying clay; and

ii) to develop numerical analyses and empirical formulae for predicting the shape of settlement troughs induced by tunnelling in two-layer ground.

The primary methods of investigation are introduced in the following sections.

1.3.1 *Centrifuge model testing*

Centrifuge model testing was the principal method of investigation for this research and formed the largest section of work by far. A total of twenty model tests were carried out by the author, directly for this study. A further eight tests are reported which were conducted in collaboration with visitors and students at City University to extend the work.

Centrifuge testing allows the simulation of full scale prototype stress distributions with depth, simply as a consequence of the increase in inertial radial acceleration imposed by the rotation of the centrifuge. With careful experimental procedures the stress history of the soil can be controlled so that the soil strength and stiffness throughout the model are known.

The model tests were conducted under plane strain conditions with a circular tunnel cavity in overconsolidated kaolin clay, usually overlain by a layer of silica sand. The tunnel cavity was lined with a latex rubber membrane and initially supported by compressed air pressure equal to the total overburden stress at tunnel axis level. Movements were generated by reducing the pressure in the tunnel so that the cavity contracted. Measurements were made during the tests by conventional displacement transducers and pore pressure transducers. Digital image analysis of marker beads pressed into the front surface of the soil model was also used, so allowing subsurface movements to be monitored.

The main variables were the geometry (total cover and ratio of sand to clay depth), the type or stiffness of the overlying strata and the position of the water table.

1.3.2 *Triaxial testing*

A small number of stress path triaxial tests were conducted on some of the sands used in the centrifuge tests to help determine parameters for analysis of the centrifuge test data and for finite element analyses. The properties of kaolin are well reported in the literature, including the shear stiffness at very small strains, G'_{max}. Properties for some silica sands have been published, though not for the specific sands used in the centrifuge tests. Attention was focused on determining values of G'_{max} for the sands and this was achieved using the bender element technique.

1.3.3 *Numerical modelling*

Finite element analyses were carried out using a modified version of the finite element program CRISP (CRItical State Program). All were conducted at centrifuge model scale in which the clay was represented by the 3-Surface Kinematic Hardening (3-SKH) model, a non-linear elasto-plastic model incorporating kinematic hardening, and the sand by a linear elastic (LE) model or the 3-SKH model.

A total of twenty-three finite element analyses were conducted. The numerical modelling was evaluated by direct comparison with centrifuge model test results and used to investigate concerns about the physical model tests, such as boundary conditions, the effect of modelling the upper strata, and to aid the investigation of patterns of ground movements.

1.4 Outline of the dissertation

This dissertation describes the process and outcome of an investigation into ground movements caused by tunnelling in two-layer ground conditions. In Chapter 2, the literature relating to the research is reviewed, with particular emphasis on the behaviour of stiff soils and the prediction of tunnelling-induced ground movements. Details of the experimental work undertaken follows. Firstly, in Chapter 3, centrifuge model testing is introduced including the principles, relevant scaling laws and inherent errors. The facilities used for the centrifuge modelling are fully described as are the test equipment, experimental procedure and the tests undertaken. Secondly, in Chapter 4, details of the triaxial testing are presented including the objectives, the equipment used, the sample preparation procedure, and the data obtained. Material properties derived from the triaxial tests, or from the literature, and used for analysis of the centrifuge test data and numerical modelling are also presented in Chapter 4.

In Chapter 5, basic centrifuge model test results are presented to illustrate the main features of the tests and the quality of data obtained from them. The fundamental results are examined including: interpretation of image processing data; settlement trough width; horizontal ground movements; changes in pore pressure around the tunnel and collapse loads. The experimental results are drawn together in Chapter 6 and the trends observed are analysed and discussed. The general patterns of ground movement that can develop are identified and suggestions to improve predictions of movements due to tunnelling in two-layer ground conditions are made. The numerical analysis is presented in Chapter 7 including a brief illustration of the basic concepts of an elasto-plastic soil model developed at City University and the determination of material parameters for the model. The stress history followed in the analyses, which accurately represents that of the centrifuge models, is described, together with the finite element analyses conducted and the pertinent results. Finally, the conclusions are presented in Chapter 8. The limitations of the work are discussed, leading to suggestions for further work, and the implications of the results are highlighted.

CHAPTER 2 BACKGROUND AND PREVIOUS WORK

Within this chapter, the key literature important to the understanding of deformations around tunnels, before collapse, is presented and reviewed. Firstly, the present understanding of the behaviour of stiff soils is outlined within the context of the research. This is followed by a review of the work related to field measurements, physical modelling, analytical solutions and numerical modelling which has been combined to produce the methods commonly used to predict ground movements due to tunnelling.

2.1 Behaviour of stiff soils

The review will focus on the behaviour of relatively stiff soils as related to tunnelling, which include overconsolidated clays and most coarse grained materials. With some notable exceptions, such as the Singapore Mass Rapid Transit System (Hulme et al, 1989), tunnels in normally consolidated clays are relatively uncommon.

2.1.1 *Critical State Soil Mechanics*

In this dissertation the investigation of soil response to loading is presented within the framework of Critical State Soil Mechanics, CSSM, (Schofield and Wroth, 1968), which has been used successfully for the analysis and prediction of soil behaviour for some time. A variety of texts (Atkinson and Bransby, 1978; Wood, 1990; Atkinson, 1993) have made CSSM increasingly more accessible to students, researchers and practising engineers alike, providing a logical and consistent framework in which the mechanics of soil behaviour can be analysed. Although originally developed for saturated remoulded clay soils many researchers have extended the framework for coarse grained, unsaturated and natural soils (Coop and Lee, 1993; Wheeler and Sivakumar, 1993; Cotecchia and Chandler, 1997).

CSSM is generally presented using the stress invariants p', the mean normal effective stress, and q', the deviatoric stress, plus v, the specific volume of the soil. These stress invariants were developed for analysing triaxial tests for which:

$$p' = (\sigma'_a + 2\sigma'_r)/3 \; ; \tag{2.1}$$

$$q' = \sigma'_a - \sigma'_r \; ; \tag{2.2}$$

where σ'_a and σ'_r are the axial and radial effective stresses respectively.

The expression for p' under plane strain or general stress conditions stays relatively straightforward and simply accounts for the intermediate principal stress. Expressions for q' are more complex as the shear stresses, τ, must also be accounted for. General expressions for p' and q' are given by Wood (1990).

The fundamental principle of CSSM is that soils subjected to shearing will ultimately reach a constant state. At this critical state shear distortions will continue at constant shear stress, with no volumetric straining. It is reached only after significant shear strains (usually in excess of 10-20%) at which stage the soil has been effectively reconstituted and reached a new, unique state, associated with turbulent flow, which is independent of its initial state. Therefore, for a given soil there exists a unique critical state line, CSL, which is illustrated in Figure 2.1(a & b) and defined by equations 2.3 and 2.4 as;

$$v = \Gamma - \lambda \ln p' \; ; \tag{2.3}$$

$$q' = Mp' \; ; \tag{2.4}$$

where v is the specific volume of the soil,

Γ is the value of v on the CSL when $p' = 1$kPa,

λ is the gradient of the CSL in v:lnp' space, and

M is the stress ratio at critical state (q'/p').

The isotropic normal compression line, INCL, is parallel to the CSL in v:lnp' space and represents the boundary of all possible isotropic states. It is given by;

$$v = N - \lambda \ln p' \; ; \tag{2.5}$$

where N is the value of v on the INCL when $p' = 1$kPa, and

λ is the gradient of the INCL in v:lnp' space.

Normal compression of the soil at different stress ratios, $\eta = q'/p'$, produces a family of lines parallel to the INCL in v:lnp' space and a state boundary surface, SBS, in stress space. Figure 2.1(a) shows one of these lines of particular importance, the 1-dimensional normal compression line. 1-dimensional compression of any soil occurs at a particular stress ratio, required to give zero lateral strain.

If the soil is overconsolidated, its current mean normal effective stress is, in general, less than it has been previously, and the soil state lies inside the SBS on an unload-reload line, URL.

There are an infinite number of URLs each associated with a mean normal effective stress on the INCL, labelled $2p'_0$ in Figure 2.1(a), and each with the equation

$$v = v_\kappa - \kappa \ln p' \ ; \tag{2.6}$$

where v_κ is the value of v on a given URL when $p' = 1$kPa, and

κ is the gradient of an URL in v:lnp' space.

The section through the SBS shown in Figure 2.1(b) is the elliptical Modified Cam-clay yield locus (Roscoe and Burland, 1968), projected onto an URL, which has been used for the numerical analyses presented in Chapter 7.

For clays there is only one way to reach a state inside the SBS and that is by swelling back along an URL from a normal compression line. However, coarse grained materials are rarely truly overconsolidated and are more commonly compacted to the current volumetric state. This means that the material has not been subjected previously to a higher effective stress, but nonetheless, in CSSM, a large SBS consistent with a high preconsolidation stress is implied by the volumetric state. Loose samples of sand are notoriously difficult to make and the position of the normal compression lines are such that extremely high pressures are required to reach the INCL. The size of the SBS is usually very large for coarse grained materials found in situ and for most of the centrifuge tests and numerical analyses conducted for this research.

CSSM can be used as a framework into which models of material behaviour, constitutive relations, can be implemented. Most early critical state models, including the original Modified Cam-clay, assume that the soil behaves elastically within the SBS. A soil state will remain on a given URL until the SBS is reached and only then can plastic strains develop. Another assumption of the early models is that the behaviour within the SBS is linear, a simplification which has been shown to be grossly inaccurate by many researchers including Jardine et al (1984) and Atkinson et al (1990). Modified Cam-clay with linear elasticity within the SBS requires a total of only five soil parameters; M, Γ, λ, κ and the shear stiffness G'; all of which can be easily obtained by standard triaxial tests, making the model relatively friendly to use. However, real soil behaviour inside the SBS is highly non-linear and not elastic. Consideration of problems where the initial stress state is well inside the SBS, such as heavily overconsolidated soils, or where small changes in stress or strain are important, such as pre-failure deformations, requires a more sophisticated approach if realistic predictions are to be achieved.

2.1.2 *Non-linear soil behaviour and high stiffness at very small strains*

Jardine et al (1984) demonstrated that the behaviour of soil is highly non-linear. Atkinson et al (1990) showed that the response of soil to a change in stress is dependent not only on the current stress state but also on the recent stress history, defined as the length and direction of the previous stress path. Figures 2.2 (a & b), given by Stallebrass and Taylor (1997), illustrate the effect of changes in stress path direction on the stiffness of a typical soil. The reduction in stiffness of a single curve is dependent on the change in stress or strain, but the particular curve being followed depends on the recent stress history. For example, a full stress path reversal, $\theta = 180°$, will result in a considerably higher stiffness than a 90° reversal.

From back analysis of soil displacements around geotechnical structures in London clay, Simpson et al (1979) suggested that the soil stiffnesses being used to make predictions were perhaps significantly under-estimated. Burland (1989) highlighted the fact that the stiffness of soils at very small strains was orders of magnitude higher than at levels of strain more commonly measured in the laboratory or in the field at the time.

Given the highly non-linear nature of soil stiffness, it is difficult to compare intrinsic stiffnesses except at very small strains (say <0.001%) where the behaviour may be considered to be linear and elastic. The shear stiffness at these very small strains will be referred to here as G'_{max}, although it is also known in some texts as G'_0. Recently, considerable efforts have been made to develop methods of determining G'_{max}, both in the field and the laboratory. Work conducted by Viggiani (1992) on fine grained soils and Jovicic (1997) on coarse grained soils compared measurements of G'_{max} made using high resolution local displacement transducers with measurements made using the dynamic bender element technique on reconstituted triaxial samples. Further details of the bender element technique are given in Chapter 4. Both concluded that the bender element technique could be used successfully to determine G'_{max} in the laboratory for their particular soils.

Viggiani and Atkinson (1995) presented an equation similar to that suggested by Wroth and Houlsby (1985) for the value of G'_{max} on the INCL, $G'_{max(nc)}$, as:

$$\frac{G'_{max(nc)}}{p'_r} = A\left(\frac{p'}{p'_r}\right)^n ; \qquad (2.7)$$

where p'_r is a reference pressure of 1kPa, and

A and n are dimensionless material properties which can be determined from triaxial tests.

They went on to relate the stiffness of an overconsolidated soil, $G'_{max(oc)}$, to that of the normally consolidated soil through a newly defined overconsolidation ratio, as:

$$G'_{max(oc)} = G'_{max(nc)} \, R_0^{\,m} \; ; \quad R_0 = \frac{2p'_0}{p'} \; ; \qquad (2.8a \,\&\, b)$$

where $2p'_0$ is the intersection of the current URL with the INCL, and the exponent m is a dimensionless material property which can be determined from triaxial tests.

Jovicic and Coop (1997) showed that equation (2.7) was valid for coarse grained soils as well as for fine grained soils and that the parameters A and n could be determined in the same way. However, the factor by which $G'_{max(nc)}$ should be multiplied to obtain a value of G'_{max} for a coarse grained material which is not on the INCL depends on the method by which it reached its current state. That is, for a coarse grained material at a given state the value of G'_{max} will be higher if the soil is truly overconsolidated than if it is compacted. Figure 2.3 shows how the ratio of $G'_{max}/G'_{max(nc)}$ varies for a carbonate sand, a decomposed granite and a silica sand, depending on whether the soil is in a compacted or truly overconsolidated state. The figures were given by Jovicic and Coop (1997) and show the variation of G'_{max} (denoted by G_0) with normalised volumetric state p'/p'_e. p'_e is the value of p' on the INCL for a given value of v, and therefore all measurements taken on the INCL collapse onto a single point at $p'/p'_e = 1$. All three materials indicate differences between compacted and truly overconsolidated states, the largest being exhibited by the Dogs Bay sand (a carbonate sand). Jovicic and Coop (1997) suggested that this may be due to the fact that the carbonate sand is more susceptible to particle breakage than the other two. It follows that the silica sand has the strongest particles as the difference between the truly overconsolidated and compacted values is by far the smallest. Values of the parameters A and n for a silica sand, a carbonate sand and a decomposed granite are given by Jovicic (1997).

2.1.3 *A non-linear elasto-plastic model for soil*

The importance of modelling the non-linear behaviour of soil to predicting ground movements has been demonstrated by many authors, including Jardine et al (1986), Jardine et al (1991) and Gunn (1993), amongst many others.

To include the important features of high stiffness at small strains and the effect of recent stress history in a critical state model, Stallebrass (1990) incorporated two additional kinematic yield surfaces within the standard Modified Cam-clay SBS. The model is shown schematically in Figure 2.4 and is known as the 3-Surface Kinematic Hardening (3-SKH) model. If the stress state stays within the inner surface the soil behaviour is elastic. Contact with this surface marks the onset of plastic deformations and the stress path is able to move across the URLs within the SBS. The inner yield surface translates and moves with the stress state producing the non-linear behaviour. When the stress state reaches the second kinematic surface it will also translate and follow the stress path, marking the end of the effect of recent stress history. These types of models are often referred to as "bubble" models; Al-Tabbaa (1987) and Al-Tabbaa and Wood (1989) described a two surface bubble model for clay.

By allowing plasticity within the SBS, the 3-SKH model gives a realistic representation of the behaviour of soil which is far better than the more simple linear elastic (LE) models. Further details of the model are given by Atkinson and Stallebrass (1991), Stallebrass and Taylor (1997) and also in Chapter 7, as it has been used for the numerical analysis presented in this dissertation.

2.1.4 *The importance of small strain behaviour of soil to tunnelling-induced movements*

Having established that the behaviour of soil within the small strain region is highly non-linear, the importance to predicting tunnel-induced settlements should be assessed. In the Unwin Memorial Lecture of 1992, Mair (1993) added a range of strains typical of certain geotechnical structures to a figure provided by Atkinson and Sallfors (1991). The figure is reproduced in Figure 2.5 and shows that the strains applicable to deformations around tunnels, under normal working conditions, are in the range of 0.03% to 1%, well within the non-linear region of most soils. Clearly, there is a need to consider the small strain behaviour of soils when predicting tunnelling-induced ground movements.

2.2 Prediction of ground movements due to tunnelling

The movements around a tunnel heading are 3-dimensional and arise from many sources. They are illustrated in Figure 2.6 which was adapted from a figure given by Mair and Taylor (1997), after Cording (1991), who listed them as follows:

1) face loss - deformation of the ground towards the face resulting from stress relief;
2) passage of the shield - the presence of an over-cutting edge (bead) combined with any tendency of the machine to plough or yaw will lead to radial ground movements;
3) closure of the tail void - the lining will be smaller than the tailskin of the shield resulting in further radial ground movements;
4) lining deflection - as the loading from the ground increases; and
5) consolidation - dissipation of excess pore pressures and therefore changes in effective stress will lead to additional movements (long-term in clay).

The summation of these movements at any discrete time is commonly termed the volume loss. Sources (2) and (3) are often considered together. With the exception of the face loss (1) all occur in the plane perpendicular to the tunnel lining.

Many authors, including Peck (1969) and O'Reilly and New (1982), have concluded that transverse surface settlement distributions above single long tunnels are well represented by a Gaussian distribution thus;

$$S = S_{max} \exp\left(\frac{-x^2}{2i^2}\right) ; \qquad (2.9)$$

where S is settlement,
x is distance from the tunnel centreline in the transverse direction,
S_{max} is settlement at $x = 0$, and
i is distance from the centreline to the point of inflexion.

The first published observation of this is generally attributed to Martos (1958) with regard to settlements above mine openings.

It has been applied extensively in practice to make predictions of settlement troughs perpendicular to long tunnels. Figure 2.7 illustrates the Gaussian distribution in relation to this study of ground movements around a tunnel in two-layer ground conditions, extending its application to the subsurface regions. The subscripts c and s relate to the clay and sand respectively.

Integrating equation (2.9) with respect to x yields the area of the settlement trough, or volume per unit length, V, as,

$$V = \frac{S_{max}}{\sqrt{2\pi}.i} \quad . \tag{2.10}$$

If values of V and i can be determined then the settlement at any point of the trough can be calculated from equation (2.9).

As noted by Cording and Hansmire (1975) and others, for short-term settlements caused by tunnelling in clay it is reasonable to assume undrained conditions and therefore no change of volume of the soil. Consequently, the volume of the short-term settlement troughs in clay can be estimated from the movements at the tunnel boundary. The response of sands and gravels to tunnelling-induced movements may be assumed to be drained. As such, volume changes may occur in the soil, and settlement trough volumes may not equate to the movements at the tunnel.

It is not the aim of this research to investigate the determination of values of V in detail, but it should be noted that this is not a trivial matter. It is clear that the volume loss at the tunnel must be dependent on some soil properties, overburden and the degree of support to the tunnel cavity, amongst others. Variables such as methods of tunnelling, ease of supporting different materials and the skill of the tunnellers, will affect the degree of support achieved and these cannot be predicted easily. Experience and back-analysis of similar projects is probably the most reliable way of predicting volume losses. However, the potential variability of ground conditions usually requires the use of the Observational Method and predictions should be updated as tunnelling proceeds.

There is sufficient evidence in support of the assumption that the surface settlement troughs above tunnels are well represented by Gaussian distributions. The question of the distribution of i with depth and the associated horizontal movements in non-homogeneous ground conditions still need to be addressed.

A variety of expressions exist for predicting the value of i. In a well known and much used paper, O'Reilly and New (1982) performed regression analyses on data collected from a variety of surface measurements of settlement in the field, which resulted in;

$$i = 0.43z_0 + 1.1 \quad \text{(for clays)} \tag{2.11}$$

and

$$i = 0.28z_0 - 0.1 \quad \text{(for sands).} \tag{2.12}$$

O'Reilly and New (1982) also considered the distribution of movements with depth in clay. They assumed that displacements were radial to the tunnel, so that they could be modelled as originating from a point sink at the tunnel axis, and that plane strain undrained conditions applied, that is deformation at constant volume. This suggests a linear variation of trough width with tunnel depth resulting in an expression for i as ;

$$i = K(z_0 - z)\,; \tag{2.13}$$

such that K is the gradient of the distribution of i with height above the tunnel $(z_0 - z)$.

On further review of the field data, O'Reilly and New suggested that equation (2.13) was valid and that $K = 0.5$ was reasonable for most clays, though it varied between 0.4 for stiff clays and 0.7 for soft clays, and that $K = 0.25$ for coarse grained soils. They conceded that subsurface data were negligible, but suggested that vectors obtained from plane strain centrifuge tests by Mair (1979) indicated that the assumption of radial movement was reasonable when considering movements near the ground surface in clay.

The other commonly used expression for i in clay was suggested by Clough and Schmidt (1981) as;

$$i = \frac{D}{2}\left(\frac{z_0}{D}\right)^{0.8}\,; \tag{2.14}$$

where D is the tunnel diameter.

This expression was also based on surface measurements and shows a dependence on tunnel diameter as well as depth.

Figure 2.8 shows the range of surface i values suggested by Peck (1969) for a variety of tunnels in different ground conditions. From Figure 2.8 it is interesting to note that the widths of surface settlement troughs in sands above the water level are considerably less than those in sands below the water table, which in fact are shown to be wider than those in clay. Superimposed on the limits given by Peck (1969) are lines representing equation (2.14) and different values of the trough width parameter K in equation (2.13).

It can be seen that the line suggested by Peck (1969) as the limit for soft clays corresponds approximately to a value of $K = 0.5$, as proposed for London clay by O'Reilly and New (1982) and confirmed by Rankin (1988), for tunnels less than approximately three diameters deep.

For tunnels deeper than three diameters, the lines diverge, with Peck's indicating narrower troughs for deeper tunnels.

The majority of work published regarding tunnelling-induced settlements concerns surface troughs. However, subsurface displacements are of great concern when assessing the impact of tunnelling on all underground structures and most surface structures, particularly those with relatively deep foundations. Predictions made for movements beneath foundations are commonly based on assuming free-surface displacements at depth. Mair et al (1993) suggested a relationship for the width of subsurface troughs in clay, based on the limited field data available and centrifuge test data published by Mair (1979). They concluded that subsurface troughs are reasonably well represented by Gaussian distributions but that they are significantly wider, and therefore less steep, than the free-surface troughs at equivalent distances above the tunnel. The distribution of i with depth given by Mair et al (1993) is shown in Figure 2.9. The depth below the ground surface and the value of i have been non-dimensionalised by the depth to the tunnel axis, z_0. Mair et al (1993) suggested the following distribution of i with depth;

$$i / z_0 = 0.175 + 0.325(1 - z / z_0) \; ; \tag{2.15}$$

which fits reasonably well with the data. The width of the settlement troughs at depth would be under-predicted if a constant value of $K = 0.5$ was assumed in equation (2.13), which would be a gross extrapolation from surface measurements, and is also plotted in Figure 2.9. To express the distribution of i in the form of equation (2.13), a value of K which varies with depth is required. As stated by Mair et al (1993), equation (2.15) implies a distribution of K given by;

$$K = \frac{0.175 + 0.325(1 - z / z_0)}{1 - z / z_0} \; ; \tag{2.16}$$

which is plotted in Figure 2.10. A constant value of $K = 0.5$ would be a vertical line on this plot and the data clearly indicate otherwise. At the ground surface $z/z_0 = 0$ and equation (2.15) yields the same value of i as equation (2.13) with $K = 0.5$.

Recently, two papers have been published regarding subsurface movements in materials other than clay. Moh et al (1996) looked at data from the Taipei Rapid Transit System with tunnels in silty clays, and silty sands overlain by silty clays. With the commonly used equations of O'Reilly and New (1982) and Clough and Schmidt (1981), equations (2.13) and (2.14) above, they extrapolated downwards towards the tunnel, concluding that the width of the subsurface

settlement profiles was significantly under-estimated if subsurface horizons were considered as free-surfaces. Similarly, Dyer et al (1996) produced surface and subsurface data for a 1.43m diameter sewer in sand with overlying clay and made ground, drawing similar conclusions to Moh et al (1996). Dyer et al (1996) plotted the variation of K with depth, and Mair and Taylor (1997) added to this the variation of K with depth interpreted from the data of Moh et al (1996). Figure 2.11 shows these distributions with that of Mair et al (1993) added. The three lines represent three different ground conditions but the increase of K with depth has a similar form for each case.

Good measurements of horizontal movements due to tunnelling are rare and therefore their prediction has relied largely on assumptions and lack of conflicting evidence. If constant volume conditions apply and a Gaussian distribution is assumed for the vertical settlement profile, it can be shown that the maximum horizontal movement occurs at a horizontal distance i from the tunnel centreline (O'Reilly and New, 1982; Attewell et al, 1986; Rankin, 1988). If constant volume conditions are not applicable then the horizontal movements are not restricted by the assumption of a Gaussian distribution for the vertical settlement trough. O'Reilly and New (1982) suggested that the vectors of movement may be directed at the tunnel axis, so that;

$$S_h = S_v \frac{x}{(z_0 - z)} \; ; \qquad (2.17)$$

and this can also be shown to imply undrained (constant volume) conditions if a constant value of K is assumed in equation (2.13). O'Reilly and New (1982) used movement vectors from centrifuge tests by Mair (1979) to support this, but conceded that the assumption of movements directed towards the tunnel axis was not valid, apart from near the ground surface. Of course, K has been shown to vary with depth which will affect the direction of the movement vectors. Taylor (1995b) stated that equation (2.16), for the variation of K with depth in clay, implied that the vectors of movement were directed at a single point, $0.175z_0/0.325$ below the tunnel axis. Horizontal movements could therefore be predicted by adding $0.175z_0/0.325$ to the denominator, $z_0 - z$, in equation (2.17).

2.2.1 *Field measurements*

With regard to ground movements caused by tunnelling in soft ground, the work conducted on case history data by Schmidt (1969), and more widely reported by Peck (1969), confirmed the validity of the Gaussian distribution for the shape of surface settlement troughs. The form of

the trough appears to be independent of the type of tunnelling method employed. The majority of the data collated by O'Reilly and New (1982) were for hand excavated tunnels, some using a shield and some not. However, Clough et al (1983) reported Gaussian surface settlement troughs above a tunnel in San Francisco Bay Mud constructed using an Earth Pressure Balance machine, even though the majority of the overburden was man made fill. Fujita (1981) examined data from tunnels in Japan constructed using a wide variety of techniques and concluded that the trough width was independent of construction technique. Rankin (1988) cites centrifuge test results reported by Kimura and Mair (1981) which indicate that the settlement trough width is independent of the degree of support and therefore of the tunnel construction technique. This final statement is perhaps not defensible. The tunnel support in the centrifuge tests reported by Kimura and Mair (1981) was provided by compressed air pressure. The stress paths around the tunnel would be of similar form regardless of the tunnel support pressure, only the magnitude of the stress changes would be different. This does not necessarily apply to the degree of support offered by real tunnelling techniques where the stress paths around the tunnel could vary and may result in different distributions of movements.

Attewell and Farmer (1974) presented details of ground movements measured during hand excavation of a 4.146m diameter shield driven tunnel at a depth of 29.3m in London clay. Surface movements were monitored using precise levelling techniques as well as theodolites and extensometers. Subsurface movements were measured using inclinometers and magnetic extensometers. The surface troughs measured were well defined by a Gaussian distribution but the value of i was 50% higher than suggested by Peck (1969), which the authors attributed to post-shield contraction. Referring back to Figure 2.8 this tunnel would have a z_0 / D value of around 7, which places it in a zone well after the divergence of Peck's line from the line for $K = 0.5$. In fact, the value of i measured was well predicted by $K = 0.5$. Attewell and Farmer (1974) also present a good example of the difficulties and cost associated with obtaining sufficient good quality subsurface data. The authors comment that within the reasonable limits of the project it was not possible to obtain sufficient subsurface data to allow the full determination of the subsurface settlement troughs, but that there was a "*characteristic steepening with depth*".

Barratt and Tyler (1976) presented a study of ground movements and lining behaviour during construction of London Underground tunnels beneath Regents Park using expanded concrete linings. Their primary objective was to compare the behaviour with a similar tunnel constructed beneath Green Park, London, using cast iron linings. They concluded that the

settlements during construction of the expanded concrete lined tunnels were marginally less than those experienced during construction of the cast iron lined tunnels. The reduction was attributed to the more rapid rate of progress and support of the concrete lined tunnels. However, this is perhaps another example of the difficulties involved in field measurement. The data presented for the transverse troughs are far from smooth and the accuracy of some of the measurements or the stability of some of the measurement stations must be questioned. Although the authors state that the temporary bench mark used for the measurements was located well outside the zone of influence of the tunnels, this was clearly not the case. In fact, even their main datum was probably subjected to some degree of tunnelling-induced movement. In addition, the authors note that the temporary bench mark was found to be subjected to seasonal movements of the same order of magnitude as the measured settlements due to tunnelling, which illustrates the need for long pre-construction measurement periods to establish datum values.

In 1992 a tunnelling trial to assess methods of construction using a modified version of the New Austrian Tunnelling Method (NATM) in London clay was conducted for the Heathrow Express Link, London. Key papers describing the work were published by New and Bowers (1994) and Deane and Bassett (1995). New and Bowers (1994) presented some results in the context of evaluating a ground movement model for the trial. The model was a refinement of the methods described in 2-dimensions by O'Reilly and New (1982) who assumed that the ground movements originated from a point sink at tunnel axis level. In other words, ground movements were assumed to be radial to the tunnel. Subsurface vectors of ground movement from the trial, obtained from inclinometers and magnetic ring extensometers, indicated that the movements were not truly radial and that the vectors were directed generally at points well below the tunnel axis. The authors tried several different methods of generating ground movements in their model to try and improve the predictions. These included describing the ground losses over the full cross-section of the tunnel, around the periphery of the tunnel or across a horizontal "ribbon" at the tunnel invert of the same width as the tunnel diameter. Figure 2.12(a & b) was given by New and Bowers (1994). It demonstrates a significant improvement in the predicted displacement vectors when using the "ribbon" model over a point sink at tunnel axis level, even though the model is clearly not describing a real physical event. Deane and Bassett (1995) provide more details of the construction process and produced contours of vertical and horizontal ground movements around the tunnels, which are reproduced in Figure 2.13. It is worth noting that the tunnel was constructed beneath an area of existing pavement. Near-surface measurements were made beneath the paved area as it was considered that the surface measurements may not be representative of the real ground

movements. This is probably true, but it is also the case that the surface pavement may have modified the ground movements, to a degree depending on the type and stiffness of the pavement. It may not be applicable to describe this as a green-field site.

Even though the Heathrow Express trial tunnel yielded some of the most comprehensive measurements from a full scale tunnel to date, the quantity of data was still limited. The bold vectors in Figure 2.12 represent the field measurements from which, presumably, the contours of vertical and horizontal movement in Figure 2.13 were derived. Considerable interpretation of the results must have been required to produce the contour plots given the density of the field measurements.

In 1996 the International Symposium on Geotechnical Aspects of Underground Construction in Soft Ground (ed. Mair and Taylor, 1996) was held at City University, London. With several large tunnelling projects being conducted world-wide at the time, particularly the Jubilee Line Extension (JLE) in London, it brought in a great many papers concerned with tunnelling. Many of the papers included measurements of ground movements but it is inevitable that these measurements are rarely comprehensive, owing to the difficulties and expense of obtaining field data. Standing et al (1996) gave details of two control sites being monitored for the JLE. The instrumentation and measurement techniques were fully described but very few data were presented. The preliminary results showed that the surface settlement troughs were not exactly described by Gaussian distributions, particularly at the extremes of the troughs. It is anticipated that these sites will provide considerable data and insight into the ground movements due to tunnelling over the coming years, though at the time of writing this dissertation the results have still to be published. Two of the most applicable contributions to the symposium, those of Moh et al (1996) and Dyer et al (1996), produced surface and subsurface displacements in mixed ground conditions and were reviewed in the preceding section.

It has been noted previously that few data have been published regarding horizontal movements. One exception to this is reproduced in Figure 2.14 from the work of Hong and Bae (1995). It shows the horizontal movements at the ground surface above a tunnel driven in predominantly sandy strata. The horizontal distance, x, has been normalised by i and the horizontal movement, S_h, has been normalised by $S_{h\,max}$. Hong and Bae (1995) plotted the predicted distribution of horizontal movements assuming that the vectors were directed at the tunnel axis as;

$$\frac{S_h}{S_{h\,max}} = 1.65\frac{x}{i}\exp\left(\frac{-x^2}{2i^2}\right) \quad ; \qquad (2.18)$$

which is derived from equation (2.9) and also requires a single point of displacement vector focus for a given horizon. The data are in good agreement with the prediction except at the horizontal limits of movement.

Measurements of long-term settlement due to tunnelling in clay are not common, probably due to the cost of maintaining long-term monitoring. Movements can continue after the passage of the tunnel heading due to dissipation of excess pore pressures in the surrounding ground, generated either from loading/unloading of the soil or from changes to the equilibrium pore pressure regime if the tunnel acts as a drain. Glossop and O'Reilly (1982) presented settlement data from the construction of a 3.0m diameter tunnel through very soft marine silty-clay at Grimsby. In some sections the tunnel was constructed under compressed air and this clearly retarded ground movements. Settlements increased after the compressed air pressure was switched off and the transverse settlement troughs widened. The movements at this site were monitored for a further eleven years and O'Reilly et al (1991) showed that the magnitude and width of the settlement trough continued to increase until equilibrium was achieved. They noted however that the increases in settlement and trough width led to only very slight increases in the curvatures of the settlement profiles. It was suggested that this is probably the reason that few problems have been reported regarding the damaging effects of long-term settlements due to tunnelling. The CIRIA Report CP/5 (1992) agrees with these comments with reference to tunnels in London. It suggests that although vertical settlements and trough widths may increase with time there is little increase in horizontal ground strains. Bowers et al (1996) presented data from the Heathrow Express trial tunnel (discussed above) some three years after completion. Their results agreed with the above, showing increases in the magnitude of settlement and trough width but very little increase in horizontal strains. Bowers et al (1996) concluded that although the zone of influence due to tunnelling had widened, any structure within the vicinity of the tunnel was unlikely to have been damaged further by the consolidation settlements.

Shirlaw (1995) presented an extensive review of long-term settlements above tunnels which showed that the consolidation component could be considerable, between 30% and 90% of the total settlement, and often wider settlement troughs developed in the long-term. In their general review of tunnelling, Mair and Taylor (1997) cited the cases presented by Shirlaw (1995) and others to conclude that wider long-term settlement profiles may be anticipated if

the tunnel acts as a drain. In soft clays positive excess pore pressures may be generated locally due to pressure from the earth support system or the grouting of the tail void. Dissipation of these excess pressures may result in further movements of similar width to those in the short-term. In stiff clays the excess pore pressures generated are generally negative and therefore swelling may be anticipated, resulting in no additional long-term settlement. However, if the tunnel lining is of high permeability compared with the surrounding ground, the long-term change in the equilibrium pore pressures could have a wide zone of influence, producing wider long-term settlement troughs. In general, long-term settlements are unlikely to produce more arduous conditions in terms of structural damage than short-term construction settlements.

The papers reviewed above are just a few of many which have presented measurements of ground movements around tunnels. It is clear that measurements are often difficult to obtain, particularly below the ground surface, and are rarely complete. Most of the rules suggested for predicting settlements due to tunnelling have been developed from back-analysis of published measurements, including data from the USA and Asia. The trends from the most relevant of these have been presented to highlight the present view.

2.2.2 *Physical modelling*

Soil is a frictional material, which means that the increase in stress with depth must be modelled correctly if realistic soil behaviour is to be reproduced in small scale models being used to investigate geotechnical problems. This is difficult to achieve without a centrifuge, although studies at 1*g*, using surcharge loading to produce appropriate stress levels in the model, have been conducted successfully. For example, Kim et al (1998) investigated the interaction between closely spaced tunnels using 1*g* model tests. Nakai et al (1997) conducted small scale model tests at 1*g* without attempting to achieve appropriate stress levels in the soil. The results were used largely to evaluate numerical analyses and the data are not explored further here owing to the extremely low stress levels in the models.

A more appropriate modelling technique is that of centrifuge model testing which has been used successfully in the past for modelling the behaviour of ground due to tunnelling. It is a very powerful tool for research and forms the major part of this investigation. Some aspects of centrifuge testing are discussed within this report but further details on the technique generally may be found in Schofield (1980) and in two texts on the subject, Centrifuges in Soil Mechanics edited by Craig, James and Schofield (1988) and Geotechnical Centrifuge

Technology edited by Taylor (1995a). Papers concerning specific geotechnical problems investigated using centrifuge techniques may be found in the Proceedings of the International Conferences held approximately every three years, the most recent being "Centrifuge 94" (ed. Leung, Lee and Tan, 1994).

During the 1970's and early 1980's the then Transport and Road Research Laboratory (TRRL) devoted considerable research effort to investigating the behaviour of tunnels in soft ground. In addition to studying tunnels under construction several research projects were commissioned at Cambridge University based on physical model tests (Potts, 1976; Seneviratne, 1979; Mair, 1979; Taylor, 1984).

Full 3-dimensional modelling of a modern tunnelling event is highly complex. Work conducted by many researchers, particularly at Cambridge University, showed that 2-dimensional idealisation of a tunnelling event can give considerable insight into the deformations in the transverse plane around a long tunnel. In the 2-dimensional idealisation only the movements in the plane perpendicular to the tunnel lining are simulated. It would be reasonable to assume that these movements, due to (2) and (3) in Figure 2.6, will dominate the deformations in the plane transverse to the tunnel in the short-term. However, it should be noted that in a real event the soil has been subjected to straining towards the tunnel face, in the longitudinal direction, before the transverse movements occur. This may affect the distribution of movements.

Much of the work at Cambridge focused on stability, and solutions for tunnelling in sand were published by Atkinson and Potts (1977a) and for tunnelling in clay by Davis et al (1980). However, the work also produced data on ground deformations before tunnel collapse.

Atkinson and Potts (1977b) reported data from 1*g* model tests, and a limited number of centrifuge tests, on shallow tunnels in sand and overconsolidated kaolin clay. They concluded that the surface settlement troughs were well represented by Gaussian distributions but that they departed from them at distances greater than $2i$ horizontally from the tunnel. They also reported that the width of the troughs did not vary significantly until failure. For sands above the water table and for overconsolidated clay their results agreed well with the classifications of Peck (1969) presented in Figure 2.8. Some of the model tests had a surface surcharge loading and the authors note that this served to increase the value of i in dense sands but not in stiff clays. Unfortunately few data are presented regarding subsurface movements.

Mair et al (1981) reported measurements made during centrifuge model tests on plane strain tunnels in soft clay. They too observed that the troughs were reasonably represented by Gaussian distributions and that the *i* values fell within the range suggested by Peck (1969).

Following the work conducted at Cambridge University there appears to be little fundamental research published regarding investigations of ground movements due to tunnelling using a geotechnical centrifuge. Chambon et al (1991) and Chambon and Corté (1994) addressed the problem of the face stability of shallow tunnels in granular soils, concluding that the tunnel support pressure required to prevent collapse was independent of the ratio of tunnel depth to diameter (*C/D*), which is in agreement with Atkinson and Potts (1977a). König et al (1991) investigated stress redistributions during tunnel construction in dry sand. They found that considerable arching/stress redistribution occurred around a tunnel heading with temporary support of less than the total overburden stress. This led to significant increases in the lining stresses in the section immediately adjacent to the unlined heading, which should be accounted for in design.

The increase in tunnelling projects around the world has lead to more specific studies of particular tunnel related problems. These include compensation grouting (Bolton et al 1994), lining behaviour (König et al, 1994; Yoshimura et al, 1994), face stability (see above plus Skiker et al, 1994), soil nailing (Kuwano et al 1997 and 1998) and the interaction of structures and tunnel-induced movements (Bezuijen and van der Schrier, 1994; Taylor and Grant, 1998).

Bezuijen and van der Schrier (1994) presented an interesting study on the influence of a bored tunnel on pile foundations. A series of plane strain centrifuge tests was reported in which a contracting mechanical device was used to generate the ground movements, simulating a tunnel through sand with overlying clay layers or through sand with the tunnel crown partially in the overlying clay (total soil cover to tunnel diameter ratio ranged from approximately 1.5 to 3). The response of model piles adjacent to the tunnel was monitored. Ground surface measurements were limited to three locations but fitted well with the predicted trough forms: the test with the tunnel partially in the upper clay layer yielding an *i* value 30% bigger than the test with the tunnel completely within the lower sand layer. Two methods of prediction were used and these are plotted in Figure 2.15 for comparison with the test data. The first method assumed a Gaussian distribution and the second was developed from the analytical solution given by Sagaseta (1987), which is discussed in the following section. Neither prediction is favoured in particular as both fit the data well. However, there is one concern with the experimental set-up, as it is not clear how the mechanical tunnel was operated and it

may have been fixed to the model container. If it was not free to move there would be a redistribution of stresses around the tunnel due to the centrifuge acceleration and possibly a significant effect on the movements around the tunnel during the test. Also, the piles would certainly restrict the movements of the soil such that differences in the surface troughs in the tests can be used only qualitatively with regard to green-field site conditions.

Nomoto et al (1994), Imamura et al (1996) and Nomoto et al (1996) described the development and testing of a miniature shield tunnelling machine for the centrifuge. Few results have been presented as yet but this machine may well lead to improved understanding of tunnel-induced movements in 3-dimensions.

Much of the physical modelling data, particularly from the centrifuge tests at Cambridge University, has been used along with field measurements to produce the design rules for predicting tunnelling-induced settlements (O'Reilly and New, 1982; O'Reilly, 1988; New and O'Reilly, 1991; Mair et al, 1993). With advances in image processing techniques (see Chapter 3) plane strain centrifuge model testing is a powerful tool for investigating the movements around tunnels in non-uniform ground conditions. To date, generally, predictions have been made by extrapolating from previous studies with single soil geological profiles.

2.2.3 *Analytical solutions*

The few published closed form analytical solutions for stress changes and ground movements around tunnels have not been used extensively as predictive tools owing to their difficulty, limiting assumptions and poor comparison with measured data. One of the more successful approaches was given by Mair and Taylor (1993) who used plasticity solutions to predict the behaviour of clay around tunnels. Conditions of axisymmetry and an isotropic stress state were imposed, but solutions for the unloading of both a spherical and cylindrical cavity in a linear elastic perfectly plastic continuum compared favourably with physical data for movements ahead of an advancing tunnel and adjacent to a long tunnel respectively. Similar solutions for predicting pore pressure changes adjacent to the cylindrical cavity were improved by assuming non-linearity in the elastic region and also compared well with results from centrifuge model tests by Mair (1979) and field measurements from around a deep tunnel in Boom clay. Predictions of the pore pressure changes in some of the centrifuge tests conducted for this research are compared to measurements from the physical tests in Chapter 5. The solutions are useful in zones close to a tunnel where the limitation of axisymmetry may not be so important, but clearly become less useful in the proximity of

boundaries such as free-surfaces. As a result, the solutions cannot be used directly to predict surface settlement troughs. The assumption of an isotropic stress state must also be a concern, particularly in heavily overconsolidated clays where horizontal stresses may be considerably greater than the vertical stresses.

Sagaseta (1987) presented a 2-dimensional solution for deformation due to ground loss in an incompressible elastic material. The solution accounts for a free-surface by considering a virtual source/sink, symmetric around the boundary with the source of movements. It is applicable to many geotechnical problems and details of the application to a plane strain tunnel was given. Predictions were compared to measurements from construction of the Caracas Metro and the trough widths were found to be considerably over-predicted. A further problem with the approach is that it requires an assumption of the magnitude of the volume loss. Referring back to the previous section (2.2.2), Figure 2.15 shows settlement troughs from centrifuge tests on tunnels in sand with overlying clay layers and included an analytical prediction based on that of Sagaseta (1987) above, but for a compressible material. The prediction compared favourably with the limited measured data presented, but the overlying clay layers could not be described as compressible, in the short-term. Sagaseta (1988), in response to Schmidt (1988), suggested that narrower troughs were predicted by assuming a compressible material but this cannot really be justified for short-term predictions in clay. However, notwithstanding the problems highlighted, the solution does appear to predict some aspects of the general patterns of movement around a tunnel. In Figure 2.16 (after Uriel and Sagaseta, 1989) the predicted "stream-lines" of ground movement, assuming incompressible material, and observed "stream-lines" of ground movement (Cording and Hansmire, 1975) for the Washington Metro are presented. The over-prediction of the width of movement is still apparent but the patterns are similar. Also in Uriel and Sagaseta (1989), the solution was extended to include stiffness and stress anisotropy, but predictions were not compared to physical measurements. To summarise, the work of Sagaseta in deriving analytical solutions may lead to improved methods of prediction, but currently these are not sufficiently close to measured data to replace empirical methods. The need to estimate a magnitude of volume loss detracts from the possible usefulness of the solution.

2.2.4 *Numerical modelling*

Predicting settlements due to tunnelling using numerical modelling techniques has always proved to be a difficult problem. It is, of course, a boundary value problem which requires the behaviour of the entire soil mass to be modelled accurately if realistic predictions are to be

expected. Soil strains are generally small, which means that the non-linear behaviour must be modelled, and the measurement boundary, usually the ground surface, is far from the source of movement, the tunnel. This is in contrast to predicting displacements of a retaining wall, for example, which can usually be done satisfactorily as it relies primarily on modelling correctly the active pressures applied to the wall and the stiffness of the wall itself. Predicting ground settlements behind a retaining wall requires much more careful simulation of the soil behaviour.

Clough and Leca (1989) produced a review of the use of finite element methods applied to tunnelling. Even though developments in the field of numerical modelling are very rapid, many of their points are still relevant today, mainly;

- full 3-dimensional simulation of the tunnelling event is complex and (still) prohibitively expensive,
- many of the parameters which influence the outcome are difficult to define including degree of support and hence stress relaxation around the tunnel (crudely volume loss),
- the important soil properties are rarely known with confidence, and
- no constitutive model has shown itself to be successful at simulating all the aspects of soil behaviour important to tunnelling.

Some of these difficulties with relevance to this work will be addressed below.

Whether in 2- or 3-dimensions the actual process of excavating the tunnel is practically impossible to simulate exactly. Focusing on plane strain conditions, several methods of generating the ground movements for 2-dimensional analyses are used. The first and most commonly used involves reducing the stresses in the ground radial to the tunnel boundary by some factor, before installing, or effectively installing, a lining. The factor can be estimated but it is more common to fix it by prescribing a pre-determined volume loss, that is reducing the stresses proportionally until a certain volume loss is achieved. It is therefore the distribution of ground movements due to the stress relaxation which is being predicted rather than their magnitude. In finite element analysis it is possible to impose displacements at the tunnel boundary to generate ground movements. The volume loss is dictated by these displacements which may be uniform around the boundary or, at the other extreme, varied by trial and error to try and alter the shape of the predicted surface settlement trough. A more practically based approach was suggested by Rowe et al (1983) termed the "gap" method. The gap is defined as the distance across an effective void between the tunnel lining at the crown and the soil. The invert of the tunnels stays in contact with the soil at the bottom and

the annulus of the surrounding ground is described by a circle between these points. The ground is then allowed to relax onto the lining in order to generate the movements. Physically, the gap represents the clearance between the lining and the outer skin of the tunnelling shield, but allowance can be made in 2-dimensional analyses to account for stress relaxation at the tunnel face. Rowe and Kack (1983) presented back-analyses of four case histories and demonstrated that the "gap" method could be used successfully to predict surface settlement profiles above tunnels. However, determining the "gap" is akin to determining the volume loss, which remains difficult and critical to the results. A further concern with regard to applying the "gap" method is whether the tunnel is allowed to move freely. Although the tunnel lining stays in contact with the soil at the invert it should not be fixed to prevent invert movement.

Another method is simply to replace the soil in the tunnel with a constant radial support stress and then reduce the stress to generate the ground movements. The support stress would usually be the vertical total stress acting at tunnel axis level but may be the vertical total stress acting at the tunnel crown. If the axis level stress is chosen, the soil at the tunnel crown will be slightly overstressed creating a stress path reversal on reduction of the tunnel pressure.

As detailed in Chapter 7, all of the numerical modelling conducted for this research was designed to replicate plane strain centrifuge tests in which the tunnel cavity was supported by an all round compressed air pressure. The pressure was reduced to generate the soil movements. The final method outlined above is the exact simulation of this process and was therefore implemented for the numerical analyses.

Selby (1988) approached the problem of predicting settlement troughs in two-strata situations, either clay overlain by coarse grained material or vice-versa, in a different way. Free-surface predictions for the top of the lower stratum, given as displacements in the form of a Gaussian distribution, were imposed on the base of the upper stratum. The movements then propagated through the upper stratum on the basis of the properties of that soil. A linear elastic constitutive model was used to predict the movements in the upper stratum after the settlement trough from the lower stratum was imposed at its base. The concept is simple but flawed. It treats the interface between the two soils as a free-surface, which it clearly is not. The movements at this interface will almost certainly be affected by the pressure imposed from and the presence of the soil above. It is quite likely that the settlement trough at the interface will be wider than the equivalent free-surface trough. While it may be valid to consider the movements in the upper stratum from imposed movements at its base, it is

essential to impose the correct displacements. Not surprisingly, the results showed a large dependence on the properties of the upper stratum. Superposition of the empirical equations suggested by O'Reilly and New (1982) was suggested as a more practical approach and this was reiterated by New and O'Reilly (1991), based on the above work.

The need for careful modelling of the soil behaviour when predicting ground deformations due to tunnelling using the finite element method was well illustrated by Gunn (1993). A non-linear elastic perfectly plastic soil model, developed to replicate the non-linear elastic stiffness of overconsolidated clays at small strains, was used to make settlement predictions. The results were compared with those using a linear elastic model and a linear elastic perfectly plastic model and are reproduced in Figure 2.17. It is clear that the settlement troughs from the linear elastic and linear elastic perfectly plastic models were extremely flat and wide, and that the results from the non-linear elastic perfectly plastic model were far more realistic. However, when compared to the expected Gaussian distribution, all of the models under-predicted the anticipated maximum settlements, and so, for equal volume losses, produced troughs which were too wide. The linear elastic model and the linear elastic perfectly plastic model both predicted maximum settlements of less than 10% of the expected value whereas the non-linear elastic perfectly plastic model predicted approximately 40% of the anticipated maximum settlement. None of the soil models adequately simulated the surface settlement troughs but modelling the non-linearity of soil stiffness at small strains made a clear improvement.

Incorporating the non-linear behaviour of soil in numerical models has been approached in several ways. The approach by researchers at Imperial College, London, has been to use non-linear elastic models which have been described by many authors including, most recently, Addenbrooke et al (1997) regarding analyses of tunnels. Simpson (1992 and 1993) described a non-linear elasto-plastic model termed the "brick model" which was analogous to a man dragging bricks on strings of different lengths through strain-space, the lengths of the strings and the changes in strain path directions producing the non-linear behaviour. The approach adopted at City University was developed by Stallebrass (1990) and uses kinematic yield surfaces inside the state boundary surface to produce the non-linear behaviour due to changes in stress path direction.

Stallebrass et al (1994 a & b) used the 3-SKH model to investigate the settlements around tunnels in stiff clay. In the first paper, predicted surface settlement troughs were presented for both short and long-term conditions. The short-term settlement troughs compared favourably

with field data from Barratt and Tyler (1976), except that movements were exaggerated in the far-field. The long-term settlement trough showed an increase in movement which reduced with horizontal distance from the tunnel, so that a steeper ground profile was predicted than in the short-term. The additional movements were explained in terms of the dissipation of excess pore pressures. As described previously, increases in settlement due to consolidation have been observed in the field but it is generally more widespread and, in contrast to these numerical predictions, does not usually cause a steepening of the ground profile. In the second paper, a carefully considered parametric study exploring the effect of recent stress history on the movements around tunnels was presented. The main finding was that surface settlement troughs in clay where the soil had been unloaded and reloaded before tunnel construction, as in London clay, were much steeper and narrower than settlement troughs in clay where the soil had been unloaded only. The study also examined the effect of the previous overburden stress on the settlement troughs, which not only dictates the length of the unloading stress path but also the value of the coefficient of earth pressure at rest, K_0. It was stated that increasing the previous overburden stress produces wider and shallower settlement troughs, though this is not obvious from the results presented. The volume of the settlement troughs is certainly lower when the previous overburden stress is high, due to the increase in soil strength, but it is not clear that the point of inflexion of the settlement distributions is displaced.

It has been suggested that modelling the anisotropic behaviour of soil may play an important role in improving predictions due to tunnelling. A number of researchers have investigated this by incorporating anisotropic elastic shear moduli in their soil models. Lee and Rowe (1989) used an anisotropic linear elastic perfectly plastic model and showed that predictions were considerably affected by anisotropy. Simpson et al (1996) used an anisotropic linear elastic model and the highly non-linear Brick model in both isotropic and anisotropic forms, concluding that anisotropy had considerably more effect on the settlement predictions above tunnels in London clay than non-linearity. The results of the anisotropic models compared favourably with measurements from the Heathrow Express trial tunnel (Deane and Bassett, 1995). Addenbrooke et al (1997) made a similar study of tunnels in London clay using a variety of Imperial College soil models, including linear elastic and non-linear elastic models. They concluded that both non-linearity and anisotropy had significant effects on the predictions of the surface settlement troughs. However, by comparison with field data from Standing et al (1996), they illustrated that unrealistic values for the ratio of the anisotropic shear moduli (G'_{vh} / G'_{hh}) were required to significantly improve the predictions over isotropic models. In contrast, Jovicic (1997) used anisotropic shear moduli in the non-linear elasto-

plastic 3-SKH model at City University to predict settlements over tunnels, concluding that the effect of anisotropy was small. It is clear that the effect of anisotropic elastic shear moduli is highly dependent on the soil model used, and it is logical that this should depend on the degree of elastic behaviour implicit in the particular constitutive model.

Evaluation of numerical models is essential if they are to be used with confidence to make predictions. It is not sufficient to compare the model with results from single element laboratory tests from which the model was developed or the material parameters derived. Comparison with closed form solutions or measurements from physical boundary value problems is required. Field data are often used for this but the uncertainties concerning material properties and boundary conditions make this less than ideal. Limited measurements, usually only at the boundaries, also add to the difficulties. All of these problems can be overcome by comparisons with well controlled effective stress centrifuge tests (Grant et al, 1997), to either aid further development of the model or increase understanding and therefore confidence in the predictions. The analyses carried out for this work were conducted using a modified version of the incremental finite element program CRISP, as given in Britto and Gunn (1987), in which the 3-SKH model has been incorporated. Evaluation of the model has been ongoing for many years (Stallebrass and Taylor, 1997) and was continued within this research to identify the limitations of the predictions.

2.2.5 *Combined observations and current practice*

Many papers have been produced which attempt to set out rules for predicting ground movements due to tunnelling. The key points of many of them were introduced at the beginning of this section. O'Reilly and New (1982) produced rules for estimating surface settlement troughs in the plane transverse to a long tunnel in what they termed cohesive and granular soils, but which are better described as clay and coarse grained soils. As suggested by Attewell and Woodman (1982), if the transverse troughs are of Gaussian form it follows that the longitudinal trough should be described by a cumulative distribution. They produced a full set of equations to describe the surface trough above a tunnel in 3-dimensions. Various additions to these rules have been made by other authors but current practice for predicting surface settlements above tunnels, particularly in the UK, was largely set out in these two papers. The details are well described in a text by Attewell et al (1986). New and O'Reilly (1991), after Selby (1988), suggested that the movements due to tunnelling in ground made up of more than one soil layer could be estimated by summing the distributions through each layer using the equations of O'Reilly and New (1982). They also suggested that predictions

above twin tunnels could be made by superposition of the equations for single tunnels. Most of the rules used in UK practice stem from O'Reilly and New (1982) and so this is reviewed in more detail here to illustrate current practice.

O'Reilly and New (1982), in agreement with many other authors, stated that the surface settlements perpendicular to long tunnels could be described by a Gaussian distribution (equation 2.9). From this the values of ground slope and curvature can be obtained by differentiation, and the area of the trough obtained by integration with respect to the horizontal distance x. The area of the settlement trough may be considered a volume per unit length advance of the tunnel and is commonly termed the settlement volume. For consideration of short-term displacements due to tunnelling in clays undrained conditions are assumed and the volume of the settlement trough is equal to the extra volume of soil excavated over and above that occupied by the tunnel, including the lining. This is termed tunnel volume loss, V, and is often expressed as a percentage of the tunnel volume. O'Reilly and New (1982) correctly state that the constant volume condition is not a reasonable assumption for the coarse grained material but do not pursue this problem any further; there is simply the supposition that the settlement volume can be related to the tunnel volume by an empirically determined value of percentage volume loss. Another assumption made is that ground movement is radial to the tunnel. It is noted that evidence from small scale tests suggest that the movements in clays tend to be towards some point below the tunnel axis but it is suggested that the error in the assumption is small at the ground surface. This is true for deeper tunnels but not so for the shallower cases. Horizontal movements and ground strains can be derived from this assumption and equation (2.9). It should be noted that these will be overpredicted if the actual displacements are indeed directed to a point below the tunnel axis.

Movements in the coarse grained materials are discussed by O'Reilly and New (1982) but they do not put forward a model or parameters for their prediction. The vector plot illustrated for tests conducted in sand by Potts (1976) suggests significantly higher horizontal movements, and hence ground strains, at the surface than would be predicted assuming radial flow.

Empirical relationships for the important trough width parameter i are suggested for both the clay and the coarse grained soil, based on case study data. It should be noted that the range of tunnel depths for which data are presented is limited, particularly for the coarse grained soils. It is also important to note, and perhaps not stressed sufficiently by O'Reilly and New (1982), that the data all relate to surface settlement profiles. No data for subsurface profiles are

presented, probably due to the difficulties in obtaining subsurface measurements of movement. It is not reasonable to extrapolate the relationships given to subsurface movements. The authors note that the trough width parameter i may be defined in terms of some fraction K of the depth to the tunnel axis. They state that a value of $K = 0.5$ for clay soils and 0.25 for granular soils can be used for most practical purposes.

The paper presented by O'Reilly and New (1982) may be summarised as follows.

i) Adequate predictions of surface troughs in uniform clay soils can be achieved using the methods described.

ii) General movements in coarse grained material cannot confidently be predicted with the information given, especially horizontal displacements and ground strains.

iii) Subsurface movements cannot be predicted owing to lack of data.

The need to predict subsurface movements is probably more critical in urban areas than the need for accurate green-field site surface predictions. With little published guidance the equations described above were often extrapolated downwards assuming a free-surface at the level for which displacements were required. Mair et al (1993) investigated the distribution of trough width with depth in clays using limited field data and centrifuge tests data from Mair (1979). They concluded that they were considerably underestimated by assuming the above and suggested an expression for K which varied with depth (equation 2.16).

The end use of predictions of ground movement due to tunnelling is generally to estimate potential damage to existing structures. It is common to use green-field site settlement predictions to impose angular distortions or deflection ratios and strains directly onto a structure. This was covered briefly in Section 1.2.2. Mair et al (1996) summarised a procedure for assessing potential damage due to tunnelling advising, through much experience, that the average horizontal tensile ground strains should be imposed on the building rather than the maximum. The results of these predictions are generally conservative as the presence of a building significantly modifies the shape of the trough, usually to flatten it. The effect of a building on the settlement trough due to tunnelling is perfectly illustrated in Figure 2.18 (after Frischmann et al, 1994). It shows the observed settlement profile and green-field site predictions for settlements during construction of part of the Docklands Light Railway beneath the Mansion House in London. The building is a substantial structure and clearly had the effect of considerably spreading the ground movements due to tunnelling. Potts and Addenbrooke (1996 and 1997) presented the results of a numerical study to examine the effect of having an overlying surface structure on the transverse settlement trough due to

tunnelling. As expected the presence of the building modified the trough such that the damage was less than would be predicted by assuming green-field site displacements. They produced plots of modification factors for deflection ratios, used to calculate building strains, based on the relative stiffnesses of the building and the soil. Useful though this was, evidence from field data or physical tests is required to confirm the modification factors.

It is likely that the presence of a layer of coarse grained material overlying clay through which a tunnel is bored will affect the ground movements in the clay. If the correct trough at the interface between the clay and the sand can be predicted, the distribution of movement through the upper sand layer may be well predicted by superposition of the assumed distribution of movements through the sand. However, the influence of the upper stratum on the movements in the lower layer must be known.

2.3 Summary

In this chapter the background and previous work relevant to the prediction of ground movements due to tunnelling in soft ground has been presented.

The first section introduced the theoretical models within which the current research is considered. This included a brief illustration of the mechanical framework of critical state soil mechanics and the current knowledge of soil behaviour, with particular emphasis on the stiffness and behaviour of soils before failure. A non-linear elasto-plastic soil model, the 3-Surface Kinematic Hardening model, which was used for the numerical analyses presented in this dissertation, has been introduced and the importance of correctly modelling the pre-failure behaviour of soil in predicting tunnelling-induced ground movements has been addressed.

In the second half of the chapter the previous work regarding the prediction of ground movement due to tunnelling was presented. The important work in the areas of field measurements, physical modelling, analytical solutions and numerical modelling were all reviewed, and the combination of these which dictate current practice was presented.

CHAPTER 3 CENTRIFUGE MODEL TESTING

After a brief introduction to the form of model used for this investigation the background and fundamental principles of centrifuge model testing are highlighted within this chapter. Following this an overview of the centrifuge testing facility at City University, including the new image processing capability which has played an important role in this research, is given. Finally, the equipment and adopted test procedure is described fully and an outline of the complete model test series is presented.

3.1 Introduction

The focus of the centrifuge test series was to examine the short term surface and subsurface deformations, before tunnel collapse, in the plane perpendicular to a single long tunnel in two-layer ground, concentrating on overconsolidated clay with an overlying layer of coarse grained material.

Figure 3.1 is a schematic diagram of a typical centrifuge model used for this investigation. The tests were conducted under plane strain conditions such that only radial movements towards the tunnel were simulated. Generally the models consisted of a layer of pre-consolidated kaolin clay overlain by a layer of coarse grained material. A cylindrical cavity lined with a latex rubber membrane was supported by compressed air as the overburden pressure was increased during acceleration of the centrifuge. All tests were conducted at a centrifuge acceleration of 100*g*, at which the models represented a prototype tunnel of 5m diameter in a block of soil some 55m wide. To generate the movements the compressed air pressure within the tunnel was reduced over a period of around 3 minutes. Data were recorded from displacement transducers (at the sand surface and the clay/sand interface), miniature pore pressure transducers and by using image processing techniques to track the movement of marker beads pushed into the soil face. As the research was focused on short term movements, no structural tunnel lining was necessary. This enabled investigation of displacements over the full range of volume losses up to failure.

A total of twenty centrifuge tests (RJG1 to 20) were conducted by the author within the main part of this study, the key variables being the geometry (soil cover above the tunnel crown, ratio of clay to sand cover), the type of overlying strata (stiffness) and the position of the water table. A further eight tests (TH1 to 6, MC01 and CK1) were carried out in collaboration

with visitors and students at City University to investigate various associated issues: TH1 to 6 with Dr. Toshiyuki Hagiwara of Gunma University, Japan; MC01 with Michele Calvello, a visitor from Italy; CK1 with Caesar Kerali, an undergraduate at City University.

3.2 Background to centrifuge model testing

The first use of centrifuge testing for geotechnical purposes is attributed to Davidenkov and Pokrovskii of the USSR in the 1930's (Craig et al, 1988). Possibly owing to the onset of the Second World War and the following isolation of the Soviet block, the method was largely ignored internationally until the 1960's. Papers on centrifuge testing appeared in the Proceedings of the seventh conference of the International Society for Soil Mechanics and Foundation Engineering, Mexico 1969, for the first time since 1936. They were submitted by researchers from the USA, Japan and England. Since then rapid technical advances have led to an increase in centrifuge facilities world-wide and flexibility in accurately modelling many geotechnical problems.

Further reading on the history and development of geotechnical centrifuges may be found in Geotechnical Centrifuge Technology (ed. Taylor, 1995a).

3.2.1 *Principles of centrifuge modelling*

In contrast to most testing methods for soils and soil models, with a centrifuge it is possible to create a stress distribution, in a small-scale model, which increases with depth from zero at the model surface, corresponding to a large-scale prototype. Soil strength and stiffness is governed by the current state of stress within the soil and the stress history to which it has been subjected. Careful consideration must be given to the second of these matters but the first is simply achieved in the centrifuge by the increase in inertial radial acceleration on a small-scale soil model.

According to Newton's laws of motion the action of pulling a mass out of a straight flight path into a radial path will impose an inward acceleration on the mass towards the axis of rotation (see Figure 3.2). If the frame of reference is switched to the centrifuge package, it can be seen that the block of soil is trying to accelerate through the bottom of its container with an equal and opposite acceleration to the radial acceleration. The radial acceleration is a function of the angular velocity and radius from the centre of rotation thus;

$$a = \omega^2 r \ ; \tag{3.1}$$

where a is the radial acceleration (m/s^2),

ω is the angular velocity (rad/s),

r is the radius from centre of rotation (m).

It is convenient to define a gravity scaling factor as;

$$N = \frac{a}{g} \ ; \tag{3.2}$$

where N is the gravity scaling factor, and

g is the acceleration due to gravity ($9.81 m/s^2$).

With careful choice of model dimensions and radial acceleration, prototype stress profiles which vary with depth, from zero at the model surface, can be simulated closely.

3.2.2 *Scaling laws*

The fundamental principle behind centrifuge testing is the reproduction of the stress distribution in the prototype. This can be written as;

$$\sigma_{vp} = \sigma_{vm} \ ; \tag{3.3}$$

or

$$\rho g h_p = \rho N g h_m \ ; \tag{3.4}$$

where suffix p denotes prototype,

suffix m denotes model,

ρ is the density of the material, and

h is the depth.

If the density of the material in the model is the same as that in the prototype and g is a constant, the scale factor for length in the model is;

$$\frac{h_m}{h_p} = \frac{1}{N} \quad ; \tag{3.5}$$

that is, the 1 : N scale model must be accelerated to N times gravity to simulate the prototype stress distribution.

The other scaling law which is important to this research concerns consolidation, which is a diffusion (of excess pore pressures) event. It is often convenient when examining scale factors for modelling to form dimensionless groups of the variables involved. In the case of consolidation, the time factor T_v is used to describe the degree of consolidation and is itself dimensionless.

$$T_v = c_v \frac{t}{H^2} \tag{3.6}$$

where c_v is the coefficient of consolidation,
t is time, and
H is the drainage path length.

For a given degree of consolidation, T_v in the prototype and the model will be the same and;

$$c_{vp} \frac{t_p}{{H_p}^2} = c_{vm} \frac{t_m}{{H_m}^2} \quad ; \tag{3.7}$$

which gives;

$$t_m = t_p \frac{{H_m}^2}{{H_p}^2} \frac{c_{vp}}{c_{vm}} \quad ; \tag{3.8}$$

and using the scaling relationship of equation 3.5 this leads to;

$$t_m = t_p \frac{1}{N^2} \frac{c_{vp}}{c_{vm}} \quad . \tag{3.9}$$

If the prototype soil is used in the centrifuge model the values of c_v are equal and time has a scale factor of N^{-2} for consolidation in the centrifuge. For example, a one year consolidation event being modelled at 100g will take place in less than an hour.

3.2.3 *Inherent Errors*

It is almost inevitable that errors exist in simulation exercises. Problems with boundary conditions are common in physical testing situations and are discussed later in this dissertation. This section identifies the errors caused by the radial acceleration field in centrifuge testing.

The vertical stress profile within a homogeneous soil in a prototype situation increases linearly with depth, from zero at the surface, if gravity can be considered to be constant for the depth involved. In the case of the centrifuge model, the acceleration is not constant with depth but varies linearly with radius from the axis of rotation (equation 3.1). Typical vertical stress profiles for the centrifuge model and corresponding prototype are illustrated in Figure 3.3, where the difference between the profiles has been exaggerated for clarity. The vertical stress at any point within the centrifuge model is calculated by taking the average acceleration acting upon the soil above. As acceleration varies linearly with radius this corresponds to the acceleration midway between the point under consideration and the model surface. The variation in radial acceleration within the centrifuge model inevitably results in regions where the stresses do not correspond to the prototype situation.

It is advantageous to minimise the amount of under stress and over stress. By finding expressions for the ratios of under stress or over stress to the prototype stresses at the same depth and equating the two, it can be shown that the least variation is obtained when the required scaling acceleration is set at one third of the model depth (Taylor, 1995a). This gives a correct stress at two thirds model depth (see Figure 3.3). This rule has been applied to the centrifuge tests in this series and the maximum vertical stress error was approximately 3% for the geometrical conditions of the tests and the City University centrifuge.

An error in principal stress magnitude and direction occurs within the reference frame of the soil model due to the fact that the acceleration field is radial. Consider that the model is set up on the centrifuge such that the centreline of the soil, perpendicular to the model base, passes through the axis of rotation (Figure 3.4). In moving away from this centreline in a direction normal to it, horizontally within the frame of reference of the model, the direction and magnitude of acceleration, and hence the principal stresses, change with the radius to the axis of rotation. In other words, there is an increasing component of lateral acceleration within the model as the distance from the centreline increases. This lateral acceleration will be greatest at the largest offset from the centreline and the smallest model radius, that is at the

boundaries of the soil surface. It is therefore desirable to put the shortest plan dimension of the model in the horizontal radial plane. For the tests conducted in this research program, the largest lateral accelerations were approximately 7% of the vertical and occurred at the extremes of the model top surface.

A third potential source of error associated with the radial acceleration field is known as the Coriolis acceleration. It occurs in a direction tangential to the radial acceleration and acts on a particle as it moves to a different radius. This is due to the fact that tangential velocity is proportional to radius, i.e. there is a tangential velocity gradient, or an acceleration, as the particle moves to a different radius. In the frame of reference of the model this amounts to a horizontal acceleration.

Consideration of the motion of a particle across a radial acceleration field results in;

$$a_c = 2\frac{\mathrm{d}r}{\mathrm{d}t}\frac{\mathrm{d}\theta}{\mathrm{d}t} \quad ; \quad a_c = 2\dot{r}\omega \; ; \tag{3.10a \& b}$$

where a_c is the Coriolis acceleration,

θ is the subtended angle (radians),

t is time (sec), and

$\dot{r}$ is the velocity of the particle in the radial direction (m/s).

Taylor (1995a) suggests that for relatively slow events the Coriolis effect is not significant if $\dot{r}$ is less than $0.05\omega r$. Within the bounds of the models tested for this research this amounts to a velocity of around 1.9m/s which is orders of magnitude faster than any event occurring in the tests reported. Thus any errors due to Coriolis accelerations can be considered insignificant.

In general, the soil used in centrifuge models is the same as the prototype soil. This can lead to problems of compatibility between grain size and scaling. The question of whether the centrifuge scaling laws should be applied to particle size is not easily answered. In some situations it is important that the soil behaves as a continuum displaying the same characteristics as the prototype soil. In other situations it may be important to model correctly localised effects and the ratio of the grain size to some dimension or zone of shearing may be critical. The tests conducted for this research are primarily concerned with deformations before tunnel collapse and it is important to replicate the stress-strain response of the prototype soil continuum. Taylor (1995a) suggests that the grain size should be compared

with some important dimension in the model to assess potential problems of grain size effects. In this case, it would seem reasonable to consider the least value of the trough width parameter, i, and the tunnel diameter as critical dimensions for the clay and the value of i alone for the sand. The minimum ratio of critical dimension to grain size for the tests conducted is in excess of 100 and so effects of grain size are assumed to be negligible.

3.3 The London Geotechnical Centrifuge Testing Facility

City University became only the third centre in the UK to have a geotechnical centrifuge testing facility when it came into operation in 1989. It is continually undergoing upgrades and modifications to improve the capability and facilitate new experiments.

3.3.1 *The Acutronic 661 geotechnical centrifuge*

The London Geotechnical Centrifuge Centre at City University has a purpose built Acutronic 661 geotechnical centrifuge. The important geometrical details are shown in Figure 3.4. The radius to the swing platform during centrifuge flight is 1.8m which generally results in a working radius for a soil model of around 1.5m to 1.6m. It has an operating capacity of 40 gravity tonnes and a maximum operating speed of 345rpm, which gives 200g acting at 1.5m radius. This allows testing of a 400kg package at 100g or a 200kg package at 200g for maximum capacity. The available volume on the swinging platform is 500mm x 700mm x 500mm high.

Significant enhancement of the centrifuge was carried out whilst the testing programme described herein was being conducted. Figures 3.5 and 3.6 show schematically the general set up of the centrifuge testing facility before and after August 1995. The main difference concerns the data acquisition system which was completely renewed. Details of both systems are given in the following section.

To minimise the required energy input a fairing is positioned on the leading edge of the swing and the entire rotating assembly is enclosed within an aerodynamic shell. For safety purposes, a containment system is provided which consists of a sacrificial block wall surrounding the testing area which is itself contained by a reinforced concrete housing.

The centrifuge is balanced before operation by means of a moveable counterweight. Load cells are built into the centrifuge mounting to detect out-of-balance forces during operation. The system is set up such that an out of balance force of 20kN will prompt an automatic shut down. This allows continuous unmanned overnight operation. In the tests reported, the monitored out-of-balance forces rarely exceeded 4kN.

Communications with the model in-flight are made through a rotating slip ring stack above the rotor arm on the machine axis consisting of both electrical and fluid slip rings. The fluid slip rings allow oil, water and compressed air to be supplied to the model. The electrical slip rings are used to transmit transducer signals and for supplying power, relaying closed circuit television signals and operation of solenoid valves, as required.

3.3.2 *Data acquisition*

Before August 1995

The data acquisition system used before August 1995 is illustrated in Figure 3.5. Tests RJG1 to 16 were conducted using this system.

Onboard junction boxes with filters and amplification were used to convey transducer signals to the slip rings. It was possible to amplify the signals in the boxes by factors of 1, 10 or 100 before being passed through the rotating stack. Further filtering and amplification were located after the slip rings, in the control room, where the signals could be increased by 2, 4 or 8 times before being logged on a personal computer or passed to a direct output rack.

A 12 bit analogue to digital converter data logging card was installed in the computer which interfaced with the commercial data logging program Labtech Notebook (version 4.1). It allowed signals to be logged at various frequencies within given voltage ranges. For all tests conducted with this system the output voltage range was fixed at ±10.0V throughout. This allowed relatively high level signals to be passed through the slip rings which were then adjusted at the control room amplifier to optimise the data logging range. During the key phases of the centrifuge tests data were logged at a rate of 1 reading/second per transducer.

After August 1995

Figure 3.6 illustrates the data acquisition system used after August 1995, for tests RJG17 to 20. The new system was designed, manufactured and installed specifically for the City University facility by Chiker Technologies Limited, Cambridge.

Junction boxes mounted permanently on the centrifuge swing receive signals from the transducers and pass them to an onboard signal conditioning unit for filtering and amplification. The output from individual transducers can be amplified by 1, 2, 10, 100, 500 or 1000 times. The unit is located within a new housing installed near the centrifuge axis. Also located within the housing is a 16 bit analogue to digital converter and purpose built computer which employs a multiplexing technique to transfer the data through the slip rings as a single signal. The signal is received by a PC in the control room which runs data logging software written specifically for this system. The transducer output voltage after amplification has to be in the range of ±5.0V, so the signals for individual transducers were amplified to maximise this range. Data were recorded at a rate close to 1 reading/second for each transducer during the key stages of the centrifuge tests, depending on the number of instruments being logged. This frequency could have been increased by reducing the integration time of the readings.

3.3.3 *Instrumentation and calibration*

The main function of the centrifuge testing was to measure ground movements caused by contraction of a circular cavity at various depths. Linearly variable differential transformers (LVDTs), manufactured by Schlumberger and supplied by RS Components Limited, Northants, were used to measure accurately vertical movements on the surface of the model and the clay/sand interface.

For most tests, 13 transducers with a range of ±5mm and 5 transducers with a range of ±15mm were used, based solely on availability. The transducers of both ranges have an output of ±3.5V at the limits of their displacement range. The output from both types of instrument was amplified to maximise their output in the ±5mm range, within the range of the data logging system. They were calibrated individually over that range in steps of 1mm using a screw micrometer within an instrument clamping block.

To measure pore pressure changes around the tunnel during contraction of the cavity, PDCR81 miniature pressure transducers (PPTs), manufactured by Druck Limited, Leicester, were positioned in the clay through access ports in the rear wall of the strong-box. The diaphragm of the transducers was protected from the soil pressure by a porous stone, glued to the instrument body. For correct measurement of pore pressures it is important to ensure that the porous stone is saturated with water and the cavity between it and the diaphragm of the transducer is also full of water. To achieve this the transducers were de-aired in a calibration

chamber by immersing them in distilled water and imposing a vacuum of around 100kPa, until they were clearly de-aired (usually at least 1 hour). In all but the first two (preliminary) tests an additional pressure transducer of the same type but with the porous stone removed was used to confirm the level of water in the stand-pipe supplying the model. By applying pressure to a chamber using a Bishop ram, the transducers were calibrated against a Druck DPI101 Digital Pressure Indicator (DPI), which was itself calibrated against a dead-weight system (Budenburg Gauge Company Ltd., Broadheath, Manchester).

The pore pressure transducers can operate at pressures up to 300kPa, at which the output is around ±0.1V. Amplification was applied to optimise the output signal within the logging range of the data acquisition system.

A miniature pressure transducer, model XTM-103-190 6bar gauge, supplied by Kulite Sensors Limited, Basingstoke, was used to measure the air pressure in the tunnel. The transducer was also calibrated against the Druck DPI.

Calibration of all transducers was carried out through the equipment used during the tests, that is, on board junction boxes followed by one of the systems described above. Generally, all transducers were re-calibrated for every test, though pressure transducers were occasionally only checked against their previous calibration. LVDTs were calibrated in 1mm steps over a ±5mm range and pressure transducers were generally calibrated in steps of 20kPa over the anticipated range of measurement.

3.3.4 *Image processing*

Image processing has been used to record displacements in centrifuge model tests for some time. At Cambridge University images are captured on photographic film, with a camera located off the centrifuge, and a flash light synchronised with the rotation of the arm. The data recovery is not continuous and determination of the displacements is largely a manual process. Allersma (1991), Garnier et al (1991) and Ethrog (1994) all reported using video images to measure displacements during centrifuge experiments, which allows continuous recovery of data. Allersma (1996) reported the use of digital image processing for measurement of a slope failure in the field.

A joint research project with the Engineering Surveying Research Centre at City University was undertaken to develop a system to measure automatically the movements of targets

during centrifuge tests. The aim was to produce displacement and strain data in close to real time. The system was being developed in parallel with the test series which forms the basis of this dissertation and as such, the techniques and quality of data produced were continually being improved.

To enable subsurface movements to be monitored during a test a small charged couple device (CCD) camera was mounted on the swing of the centrifuge to observe the model, in-flight, through a perspex window forming one side of the model container. During model preparation a grid of black marker beads (3mm dia. cylinders) was pressed into the clay surface to give observable targets. For early tests, black dyed sand was used to create horizontal lines in the sand layer to enable observation of movement mechanisms in the overlying coarse grained material. To try and improve data recovery from image processing a system of placing individual targets in the sand was devised and implemented from test RJG10 onwards. The CCD camera relayed the signal through the slip rings to a monitor for immediate viewing. Images were also stored either on video tape (VHS or S-VHS) or directly on computer via a frame grabber. The system can be seen in both the centrifuge layout diagrams, Figures 3.5 and 3.6.

The mathematics behind the close range photogrammetry used within the image processing system are beyond the scope of this dissertation. Much of the background to the photogrammetry is given by Cooper and Robson (1996) and the image analysis system by Taylor et al (1998). However, the general methodology is described briefly below. It can be split into two almost separate procedures. The first involves recording and tracking the targets in the image plane (on the pixel board of the CCD camera) and the second is the calibration from image space to object space (a co-ordinate system in the soil plane). A digitised image of one of the centrifuge tests, before movements due to tunnelling have been generated, is shown in Figure 3.7. The image is in effect a print of the camera pixel board (the image plane). Figure 3.8 below shows the calibrated positions of the targets in the clay layer (the white layer in Figure 3.7) in the soil plane (the object plane). The distortion due to the camera and the camera position have been calibrated out, as has the refractive effect of the 80mm thick perspex window through which the model is viewed. The larger black targets on white squares (Figure 3.7) are fixed control targets on the outside of the perspex window which were required for the calibration procedure. The effect of calibration can be seen clearly, bearing in mind that the targets were installed on a regular square grid. In Figure 3.7 the columns of targets, particularly at the edges of the image, are far from vertical and the

image gives the appearance of being squashed in the vertical direction. The calibrated positions in Figure 3.8 show the true locations of the targets in the object plane.

Figure 3.9 shows a flow chart for the image processing system. The analogue signal from the CCD camera was either recorded on video tape (S-VHS quality from RJG7 onwards) and converted to a digital image after the test, or converted directly by a frame grabber (from RJG17 onwards). The frame grabber digitises discrete images and the current system requires about one second to transfer and store the information, so limiting logging rates to around 1 frame/second. The target location, calibration to co-ordinates in object space and calculation of strains have all been conducted post-test, although work on the system is continuing so that movements in object space may be observed in real time for future experiments.

The quality of the measurements depends on the calibration. but firstly on the precision with which the targets can be located in the image plane. For the tests described here a single target covered 6 to 7 pixels of the camera's view in each direction, giving a total of 36 or 49 pixels. Each pixel has a single grey level or intensity. If the grey level across a target is plotted a three dimensional intensity distribution is formed. The key to the quality of tracking a target is to determine the movement of this intensity distribution, or grey level map. To achieve usable measurements this must be done to sub-pixel level. Following the centre of mass of the intensity distribution is a common method of doing this but the quality is limited. To improve this technique it is possible to use an adaptive threshold limit to separate noise but minimise loss of useful information. Both of these techniques were used in the development of the measurement system, but area-based image matching proved to be best by far. This involves using least squares techniques to follow the entire grey level map of a patch in which a target is included and, with the current set-up, allows the tracking of a target to within around one tenth of a pixel. With better lighting, targets or reduced coverage this could be improved. Apart from test RJG15, all results from image processing reported in this dissertation are from the back-analysis of test images, digitised directly by the frame grabber, using the area based image matching technique.

Transforming the target locations from the image plane to the object plane requires knowledge of the camera and camera lens (focal point, focal length etc.), camera position and orientation (derived from the permanent control targets) and the refractive properties of the perspex window. The procedures are relatively common in digital photogrammetry and result in co-ordinates of the targets, in millimetres, in the soil plane for discrete times during the centrifuge tests (usually at 1 second intervals). Knowledge of the camera position and

orientation has proved crucial to the quality of the results. It is dependent on the number and position of the permanent control targets which have varied considerably during this test series, the later tests having the better control.

Generally, the quality of the results from image processing has improved through the test series due to improvements in:

i) the image quality (from test RJG15 a monochrome camera and frame grabber were used to improve image quality);
ii) the recording medium (VHS tape before test RJG7, S-VHS tape from RJG7 to RJG16, directly digitised images from RJG17 onwards), and
iii) the quality of control for the camera position and orientation (the number and position of the permanent control targets).

Accuracy is a measure of systematic errors, which were accounted for in the calibration procedure. Precision is a measure of the random errors, which were assessed independently and found to be between 50μm and 80μm when viewing an area of approximately 250mm x 250mm (covering up to 625 targets on a 10mm grid). It should be noted that this is an overall measurement precision and not the error in measurement of movement of an individual target. This is best assessed by comparison of co-ordinates from consecutive images and was generally of the order of 30-40μm in the horizontal direction and 10-20 μm in the vertical direction. The horizontal line jitter of the camera electronics causing the increased error in the lateral measurements.

As far as the author is aware, the image processing described here is by far the most sophisticated that has been used for monitoring centrifuge experiments. The quality of measurements from other systems has not often been assessed so thoroughly, and the displacements are often used simply to determine general patterns of movement. The system uses software developed at City University which is still being improved to increase the measurement quality and further automate the processing. For example, since completion of this test series control of the camera location has been improved by locating the fixed control targets behind the perspex window, in the object plane, which allows the effects of refraction through the window to be accounted for directly.

Strains within the ground for a typical tunnelling event may be in the range of 0.1 to 1.0% (Mair, 1993). LVDTs can measure displacements at the model boundaries in this range but this cannot give real insight into the patterns of deformations within the soil mass.

Considerable effort has therefore been concentrated on the image processing for this research and on achieving quality of measurement within this range (10-100μm over 10mm). In later tests this has been achieved.

3.4 Model test equipment

A schematic diagram of a typical centrifuge model used for this work was presented in Figure 3.1. In this section the materials and equipment used in the model are described in detail. A summary of the experimental equipment and test procedure was given by Grant and Taylor (1996).

3.4.1 *Soils used for testing*

Pre-consolidated Speswhite kaolin clay was used for the clay layer in all tests. It is a widely used laboratory material owing to its relatively high permeability and inert nature. A large body of data is available on the properties and behaviour of kaolin, which has been studied in great depth over the years, and it is readily available in bagged powder form.

A variety of washed silica sands were used for the sand layers in the tests. Gradings for the sands are given in Figure 3.10. One of the sand types, called Flint Gravel, was a medium sand with sub-angular to sub-rounded particles and was supplied by Civil Engineering Developments Limited, Grays. Three of the sand types were supplied directly by the David Ball Company Limited, Cambridge, and are commonly known as Leighton Buzzard Sand (LBS). The particles of the LBS could be described as sub-rounded and the three gradings supplied were coarse, medium and medium fine. The medium sand had practically the same grading as the Flint Gravel sand. For one of the centrifuge tests a fourth grading was made up from the above LBS to form a well graded material.

3.4.2 *The model container*

The box which contained the model (the strong-box) was made of Duraluminium and had a front perspex window to allow the model to be viewed during the tests. To resist the high stresses acting on the container during testing the perspex was nominally 80mm thick, and aluminium channel sections were used to strengthen the rear wall. The container can be seen

in Figure 3.11. It had an inner plan area of 550mm x 200mm. Working at 100*g* it was possible to represent over 30m depth of soil at prototype scale (300mm at model scale).

3.4.3 *The ground water supply*

A stand-pipe arrangement was used to maintain the level of water in the model during the tests. The stand-pipe was positioned on the centrifuge swing adjacent to the strong-box. The arrangement can be seen in Figure 3.11. Water was supplied to the stand-pipe via the fluid slip rings, the level being kept constant by the pre-determined height of the overflow pipe. From there the water was fed into the model through the base drainage system. The base of the strong-box had a herring-bone pattern of channels cut into it, on top of which was a 3mm thick porous plastic sheet to prevent the clay from blocking the drainage system.

In this way the height of the water table required in the model could be established and the corresponding height of the stand-pipe overflow determined, accounting for the radial acceleration field. Typically, the stand-pipe was offset from the model centreline by 240mm which required that the overflow pipe was around 19mm higher than the height of the water table, when measured from the centrifuge platform.

To shorten the drainage path in tests where the water table was in the upper sand layer, water was also supplied from the stand-pipe to the sand through a port in the rear wall of the strong-box.

3.4.4 *Location and fixing of instrumentation*

Sketched details of the position and fixings of all instrumentation can be seen in Figure 3.11.

For most tests, nine LVDTs were used to measure the movements at each of the sand and the clay surfaces. They were fixed to an aluminium box section bridge above the model using ring clamps. The bridge structure was designed to allow flexibility in positioning of the instruments in all directions. Additions to the instrument cores, made of brass or steel studding, extended to the measurement surface. The extensions positioned on the model surface were fitted with plastic feet to prevent penetration under increased loading. The cores of the instruments measuring the clay/sand interface extended through the sand through perspex tubing, finished with circular feet. Figure 3.12 shows the positions of the LVDTs

which were maintained for all the tests. The formation was designed to give maximum details of the full settlement troughs at each interface.

Miniature pore pressure transducers (PPTs) were installed through the rear wall of the strong-box to check the equilibrium pore water pressures and monitor pore water pressure changes around the tunnel during the contraction of the cavity. Standard brass fittings were modified to seal around the PPT cable using rubber washers, in a manner similar to that described by Mair (1979). Figure 3.13 shows the location of ports that were made in the rear wall of the strong-box to accommodate PPT or drainage fittings. For this test series an average of five PPTs were used for each test, their locations limited to those in close proximity of the tunnel, that is columns b and c.

An additional pressure transducer was positioned in the stand-pipe to double check the water level. It was the same type as those used in the clay but with an exposed diaphragm. The radial acceleration ensured that the transducer remained at the base of the stand-pipe provided that sufficient slack was left in the cable.

The tunnel pressure was monitored by a transducer connected to the tunnel fitting immediately outside the strong-box, as described in the following section.

3.4.5 *The tunnel, tunnel support and fitting details*

The tunnel cavity was supported by compressed air pressure within a latex rubber membrane. It was necessary to increase the air pressure supplied to the tunnel during centrifuge acceleration to balance the increasing overburden pressure and, likewise, to reduce it to generate the ground movements. This required a means of accurately monitoring and varying the pressure within the tunnel.

The details of the tunnel fitting arrangement are given in Figure 3.14. Unlike previous arrangements such as those used at Cambridge University by Mair (1979) and Taylor (1984), the tunnel membrane did not have a top hat flange sealed on the outside of the box, so requiring a hole the same diameter as the tunnel through the model container. Instead, the membrane was almost a complete cylinder with a small diameter hole in one end through which a flanged stainless steel tunnel fitting was inserted. The geometry of the tunnel fitting is given in Figure 3.15. The tunnel and fitting were installed from the inside of the strong-box, requiring only a 14mm diameter hole to be cut in the rear wall. The arrangement was

clamped into place externally using a brass nut, the rubber membrane forming a good seal between the flange arrangement of the tunnel fitting and the rear wall. The tunnel membranes were 0.75mm thick and produced by Precision Dippings Limited, Bristol. based on a former supplied by City University.

A brass manifold was manufactured to accommodate the tunnel pressure transducer and the connector for the compressed air, which was supplied to the centrifuge platform through the fluid slip rings. Details are given in Figure 3.14. The compressed air supply was controlled manually from the centrifuge control room using a constant relief pneumatic pressure regulator. Initially a model manufactured by Hale Hamilton (Valves) Limited, Uxbridge, was used, but problems occurred during test RJG7 in the form of a considerable drift in air supply pressure. A Fairchild Model 10 regulator, Winston-Salem (USA), was found to be much more stable and was used, without fault, for the remainder of the test series.

3.5 Experimental procedure

The preparation of the centrifuge experiments was a long and complex process. In this section the procedure is broken down into the basic steps involved and presented in detail, with reference to the equipment described in the previous section. The stress history of the model is also discussed.

3.5.1 *Preparation of the clay in the model*

Speswhite kaolin clay was mixed with distilled de-aired water using a large paddle mixer to give a slurry with a moisture content of around 120%. The kaolin used was either in dry powdered form or as reused material from other tests with a moisture content of approximately 35-40%. Care was taken to ensure uniform mixing over a period of around 4 hours.

The base of the strong-box had a herring-bone pattern of drainage channels which fed to external ports in the ends of the box. A 3mm porous plastic sheet and filter paper barrier was placed in the bottom of the box to allow the passage of water between the model and the drainage system but prevent the loss of clay. Water-pump grease (Mair, 1979) was applied to the side walls of the box to limit the friction between the clay and the metal. The slurry was then carefully placed into the box ensuring that no air voids were formed. If the volume of

slurry required exceeded the volume of the strong box a 300mm extension section was bolted to the top of the box.

A porous plastic sheet and filter paper barrier were placed on the top of the sample which was then positioned in the computer controlled consolidation press, a photograph of which is given in Figure 3.16. The consolidation was controlled by applying pressure to a ram which loaded the sample through a rigid piston plate. The pressure was maintained and adjusted by communication through a PC. An in-house control program monitored ram pressures and vertical movement of the sample detected by transducers. It communicated through a multi-function PC super card, supplied by Computer Instrumentation Limited, West Sussex, and updated as necessary the voltage supply to an air pressure converter. The converter controlled a hydraulic pump which amplified the air pressure, through a diaphragm, to an oil pressure which supplied the loading ram.

The pre-consolidation history was practically the same for all tests. The piston was lowered to the sample and a sample height measured for a consolidation pressure of 5-15kPa. This was considered to be the initial height of the slurry. The consolidation pressure was then increased to an initial pressure over a period of around 30 minutes. It was found that the seal around the sample was capable of holding a pressure of 125kPa at this time without loss of clay. The consolidation pressure was subsequently doubled twice over the following two days, to 250kPa and 500kPa respectively. The pressure was held constant at 500kPa (the maximum pre-consolidation pressure) for around one week, after which vertical movements were observed to be negligible. The sample was then allowed to swell, with free water available at the drainage boundaries, under a pressure of 250kPa for approximately 3 days before miniature pressure transducers were installed through the ports in the rear wall of the box. This was carried out by boring holes with a guide tube and auger whilst maintaining the 250kPa consolidation pressure. A small quantity of de-aired kaolin slurry was then injected into the end of the hole into which the transducer was bedded. The gap behind the transducer was then back-filled with slurry and the port sealed around the cable. Finally, the sample was maintained under a pressure of 250kPa for a further 3-4 days before testing. The exceptions to the above procedure were preliminary tests RJG1 and 2, in which the samples were subjected to a maximum vertical pre-consolidation pressure of 250kPa, with no swelling phase.

The effects on the clay samples of removal from the consolidation press, preparation of the model and re-consolidation on the centrifuge are discussed in the following sections.

3.5.2 *Preparation of the model*

The clay sample was removed from the consolidation press on the day of the test. The drainage at the base of the sample was closed before removal of the pressure to prevent the passage of free water into the sample and so minimise further swelling.

The surface of the clay was trimmed to the correct height before removing the front wall of the box. Both free surfaces were coated in liquid paraffin to prevent loss of moisture from the sample. Marker beads required for the image processing were then pressed into the front clay surface through a carefully positioned template before the tunnel cavity was cut. The details of the tunnel cutting process are shown in Figure 3.18. A jig was bolted onto the front of the box in order to guide accurately a thin walled cylinder, previously lubricated with viscous liquid paraffin, through the clay from front to back of the sample. The clay was excavated from within and the tube removed to leave a circular hole through the width of the model. The axis of the tunnel was fixed such that there was a minimum of 1 tunnel diameter of soil (>50mm) below the tunnel invert and up to 4 tunnel diameters of cover above the tunnel crown. The interface between the clay and the sand was fixed at various positions above the crown of the tunnel, depending on the test.

The latex tunnel membrane was then stretched and pulled through the cavity, from front to back, on the stainless steel tunnel fitting, which was passed through the hole in the rear wall of the box and fixed in place to form an airtight seal against the box wall.

Following the placement of the tunnel, the perspex window of the strong box was firmly bolted in place, the area in contact with the clay having been coated in viscous paraffin liquid as a lubricant. The viscosity of the lubricating fluid is discussed in Section 5.2. The horizontal surface of the clay, which was to become the clay/sand interface, was then lightly scraped to remove the sealing oil. Perspex tubes with circular feet were positioned on this surface and held in place by a light-weight jig fastened to the top of the box. These sleeves were required to give access to the clay surface for measurement by LVDTs. It was necessary to place the sleeves before the sand to avoid sample disturbance.

3.5.3 *Preparation of the sand in the model*

In many of the tests conducted there was a layer of sand overlying the clay. For tests RJG2 and RJG3 this was simply poured slowly from a height of 1.5m. All sand placement for tests

RJG4 onwards was made using a raining system which is illustrated in Figure 3.19. Sand was dropped from a hopper through 3 offset sieves set at a minimum of 800mm above the top model surface. The height of this drop ensured that the particles reached their terminal velocity and hence, repeatable, consistent samples were produced (Eid, 1987).

After fixing sharp edges around all four sides of the box, to deflect away sand falling outside the model, the sand was rained into place. For all tests involving sand before RJG10, the raining was interrupted periodically to place a thin strip of dyed black sand next to the perspex window. This allowed visualisation of movements from the video images.

Due to small effects of uneven sand raining, believed to be caused by air currents, it was always necessary to place slightly more sand than required and to level the surface by removing the surplus with a vacuum. The required depth of sand was achieved by connecting an adjustable height fitting through which the vacuum was applied.

From test RJG10 onwards a system of placing marker beads in the sand after raining was implemented. This is illustrated in Figure 3.20. Basically, by clamping securely a plate in contact with the sand surface, the LVDT sleeves protruding through holes in the plate, it was possible to swivel the strong-box through 90° so that the window could be removed with the sand remaining in place, giving access to the front sand surface. Marker beads could then be placed in the sand in a similar manner to those in the clay before carefully reversing the process. The disturbance to the sample was minimal but problems were encountered as the targets in the sand tended to become partly obscured by the grains.

3.5.4 *Centrifuge test procedure*

At several stages during the model preparation the package was weighed to enable calculation of the weight of individual components, particularly the clay and the sand, for centrifuge balance calculations and determination of the soil state.

Once the soil model was complete and the necessary pre-test measurements taken the LVDTs were installed on top of the strong-box before it was placed on the centrifuge swing. A photograph of the package at this stage is given in Figure 3.17. The time required to complete the procedure described above, from removal from the consolidation press to positioning on the centrifuge swing, was approximately 5 to 6 hours. Once on the swing, a further 2 to 3

hours were usually required to prepare the model before the centrifuge was accelerated to test speed (spin-up).

Tasks carried out during this phase include: positioning of the stand-pipe for water feed to the model; installation of the pressure transducer in the stand-pipe; positioning of the CCD camera and lighting; checks on amplification gains, data acquisition and vertical positioning the LVDTs close to their electrical zero; connection of all transducers to junction boxes (and junction boxes to slip rings); safely strapping down the various cables, tubes and boxes around the model. When balance calculations, counter-weight positioning and final safety checks were complete the water feeds from the stand-pipe to the model were connected and the model was ready for spin-up.

As the centrifuge was accelerated to full speed the pressure within the tunnel was manually increased from the control room to balance the overburden pressure at tunnel axis level. The water feed to the stand-pipe and hence to the model was turned on. Data were logged and images recorded during spin-up and until the pre-set water level was reached in the model.

The model was left overnight to reach equilibrium. During this time data were logged periodically. Figures 3.21 and 3.22 show data recorded during a typical test, RJG16, from spin-up of the centrifuge to spin-down, for the pressure transducers and LVDTs respectively. The data are plotted against the square root of time so that the response during the early stages of the test is clearly visible. Figure 3.21 shows that the tunnel support pressure was increased from approximately zero to a maximum of around 315kPa, where it was kept constant until being reduced quite rapidly to zero after a period of around 17 hours. The initial increase of tunnel support pressure represents the increase in centrifuge acceleration and the period of constant support pressure represents the consolidation phase. Soon after the centrifuge spin-up the stand-pipe was allowed to fill with water and the increase in pressure measured by the stand-pipe transducer can be seen in Figure 3.21. The pore pressure transducers responded rapidly to the new stress regime during centrifuge spin-up and then slowly came into equilibrium with the stand-pipe pressure. As shown in Figure 3.22, the LVDTs measured a positive displacement during spin-up due to the deflection of the instrument support structure. Soon afterwards there was a marked negative displacement, probably associated with shrinkage of the clay or embedment of the LVDT feet into the soil surface, until the stand-pipe was filled with water and the clay began to swell. The LVDTs continued to register positive displacements due to swelling of the clay until consolidation was complete.

The following morning the test was conducted by reducing the tunnel pressure to zero, or until the tunnel collapsed, at a rate of approximately 100kPa/minute (equivalent to a period of around 3 weeks for a tunnel at prototype scale with a cover of $3D$). During this event, data were logged as close to every second as possible and images recorded digitally or on video tape.

3.5.5 *Summary of the model stress history*

The probable stress history of the clay in the model is illustrated in Figures 3.23 and 3.24.

The label A represents the stress state after 1-dimensional compression to the maximum pre-consolidation pressure, and B is the stress state after swelling back in the consolidation press. With the sample in equilibrium, the pore water pressures will be close to zero and so the lines A and B in Figure 3.23 also represent the total stress distributions in the model at these stages. On removal from the consolidation press the total stress will be close to zero and the pore pressures will immediately become negative maintaining an effective stress of 250kPa in the sample. If this state were maintained throughout model preparation then the response of the soil to the new stress conditions imposed by the centrifuge acceleration would be further swelling to C, the degree being dependent on the depth, z, in the model [1].

Of course, the degree to which the 250kPa suction was maintained in the soil during model preparation affects the stress paths of the soil. The PPTs used for the experiments are unable to measure suctions of greater than around 60kPa reliably and so pore pressures were not measured during model preparation. However, the immediate response of the PPTs to the new stress conditions imposed by the centrifuge acceleration can indicate the effective stress in the model. This relies on a good immediate response from a number of PPTs over a significant depth. For many tests the PPTs were located over a relatively small range of depths, immediately around the tunnel. This causes difficulties in obtaining a clear indication of the pore water pressure profile. However, for some tests, such as RJG4, the PPTs were positioned over a reasonable depth, in excess of 100mm, and the pore water pressure profile immediately after spin-up could be determined with some confidence. In the case of RJG4 it was parallel to the total stress profile and offset by -125kPa, suggesting that the effective stress profile at the end of model preparation was vertical but at a value of 125kPa, half of the

[1] When the front wall of the strong-box is removed there will be a change in horizontal total stress leading to changes in pore pressure and therefore mean normal effective stress unless the ratio of σ_h'/σ_v' is unity. For the tests conducted it is likely that the ratio of σ_h'/σ_v' was close to unity and the consequence of not allowing for the change in σ_h would then be negligible.

assumed 250kPa. Clearly this will change the stress paths within the soil mass, particularly around the tunnel in experiments with greater soil cover, where a significant proportion of the model may be subject to re-compression.

Knowledge of the stress history and stress paths followed in the clay is particularly important in interpretation of the data and especially when undertaking realistic finite element analyses. This will be examined in more detail in later chapters.

3.6 Tests undertaken

The key aim of the research was to define the surface and subsurface movements caused by tunnelling in two-layer ground. Having limited the investigation to tunnels in overconsolidated clay with a different overlying strata, the main variables were: geometry (total soil cover, ratio of the strata depths), the type of upper strata (stiffness and state) and the position of the water-table.

Table 3.1 presents a summary of the twenty centrifuge tests carried out by the author as the main test series for this research. Table 3.2 details a further series of eight tests conducted in collaboration with visitors to City University to continue the investigation of this problem.

The first two tests were of a preliminary nature designed primarily to test equipment and methodology, although useful results were obtained. They were conducted without a re-consolidation phase on the centrifuge, and so, at all points in the model the soil had experienced approximately the same stress history.

All of the other tests were conducted with similar stress histories to each other. They were pre-consolidated to 500kPa and allowed to swell back to a vertical effective stress of 250kPa. Pore pressure equilibrium conditions were achieved at full acceleration on the centrifuge before the pressure reduction in the tunnel was carried out.

The first nine tests were all variations on a geometry in which the total soil cover above the tunnel crown was four times the diameter of the tunnel ($4D$ cover). This is approaching the maximum achievable cover with the test set up. They were designed to investigate the effect of the position of the clay/sand interface, that is varying the ratio of sand to clay depth, and

the influence of sand type. To compare results of different total cover test RJG10 was conducted with 2*D* cover, equally divided between the sand and clay layers.

There then followed a series of tests designed to investigate the effect of the stiffness of the upper strata by using different materials (RJG11 to 16), such as water, uniformly graded sand, no material, clay and well graded sand. Within this series the effect of having a water table below or near the top of the sand layer above the clay was also investigated.

A series of four tests (RJG17 to 20) again looked at the effect of the upper sand layer being predominantly above or below the water table but also at the effect of the layer being in a dense or loose state.

The concept of TH1 to 6 and MC01 was to maintain the same vertical effective stress profile within a pre-defined clay layer of 1.5*D* depth above the tunnel crown, whilst varying the type of the upper strata; clay, dry sand in various states, saturated dense sand and water. This isolated the effect of the upper strata on the movements in the clay.

Not including the first (preliminary) test RJG1, a total of six tests were conducted with different clay covers and no sand layer present. As well as investigating the effect of total cover above the tunnel crown these tests also act as reference tests for the other variables being investigated.

Problems which may have affected results were encountered in a number of tests and are highlighted in Tables 3.1 and 3.2. Some of the comments are simply included to help identify the differences between tests. Others include observations of the physical model which may have affected the response of the soil during the tests and may help to explain some of the unaccountable results. Also recorded are problems with electrical equipment, of which failure (or part-failure) of the junctions boxes carrying the transducer signals was the most common. Data from these tests may be limited, or less reliable than the others. Although the quality of the tests tended to improve chronologically, all tests produced at least some useful data. The quality of the image processing measurements improved significantly for the later tests and this is addressed in Chapter 5.

3.7 Summary

The purpose of Chapter 3 was to give full details of the centrifuge modelling conducted for this research so that the reader can fully understand the experiments. The background and principles of centrifuge model testing have been introduced, including the scaling laws and inherent errors relevant to the work. The centrifuge testing facility, data acquisition and instrumentation have been described, and details of the new image processing system highlighted. Full descriptions of the centrifuge model experiments have been given including the test equipment, experimental procedure and the stress history of the soil in the models. Finally, details of all the model tests conducted and the problems associated with each have also been presented.

CHAPTER 4 TRIAXIAL TESTING AND MATERIAL PROPERTIES

The triaxial testing and determination of material properties for analysis are described within this chapter. Following a brief introduction details are given of; the objectives of the triaxial testing; the equipment used; the sample preparation; the testing procedure; the tests conducted and the results obtained. Finally, material properties derived from the triaxial tests or from the literature, and used for analysis of the centrifuge test data and numerical modelling, are presented.

4.1 Introduction

Triaxial testing was not originally envisaged as a key element of this research work. The properties of kaolin are well reported, including the tangent shear modulus at very small strains, G'_{max}, (Viggiani, 1992) and critical state parameters for silica sands likewise (Coop and Lee, 1993). However, it became clear that there were insufficient published data to estimate reliably values for the shear modulus of the sands used in the centrifuge tests. Soil parameters were required for finite element analyses and it was considered that the relative shear stiffness of the clay and overlying sand layers could be important for analysis of the centrifuge test results.

4.2 Objectives

The objectives of the triaxial testing were to determine properties for some of the sands used in the centrifuge tests, specifically, the tangent shear stiffness at typical values of mean normal effective stress experienced in the model tests. Values for the shear stiffness of the sands at very small strains, G'_{max}, and the reduction in shear stiffness due to straining were the main requirements.

4.3 Equipment

All tests were conducted using a computer controlled hydraulic stress path cell in a temperature-controlled laboratory. Initially, the response of the soil at small strains was measured with local miniature LVDTs, both axially and radially, using fixings of the type

described by Cuccovillo and Coop (1997) and a radial strain belt (Coop, 1996). However, after experiencing some difficulties with the cell, an apparatus fitted with vertical bender elements became available and it was decided that the objectives could be better met using this equipment.

4.3.1 *The stress path cell*

A diagram of the stress path cell used for the triaxial testing conducted is given in Figure 4.1 (Jovicic, 1997). It is based on a standard hydraulic triaxial cell (Bishop and Wesley, 1975). In-house software on a BBC micro-computer monitored the instrumentation and controlled electronic pressure converter units through a Spectra ms interface unit. The converter units were supplied by a constant air pressure from a screw compressor (800-900kPa) and in turn delivered pressure to air/fluid interfaces with the triaxial cell, the axial ram and the sample pore water (back-pressure via the volume gauge). Data were recorded on floppy-disks. Axial strain control could be achieved by applying load through a Bishop ram powered by a stepper motor and controlled by a timed relay device. The system was developed by various researchers at City University over the last fifteen years and is well described by Viggiani (1992).

4.3.2 *Instrumentation*

The instrumentation illustrated in Figure 4.1 includes two external LVDTs for measuring axial and volumetric strains, two pressure transducers for measuring cell pressure and pore pressure, and a load cell for measuring deviatoric force. All calibrations were conducted through the full test set-up.

The external LVDTs had a range of ±15mm and were supplied by RDP Electronics, Leicester. The axial strain transducer was fixed to the top of the cell and measured the displacement of the ram beneath the sample. The volumetric strain was determined externally by measuring the displacement of the diaphragm in an Imperial College type volume gauge. Both transducers were calibrated using a screw micrometer within an instrument clamp. Accuracies of the order of ±5μm are expected from such instruments within this system (less than ±0.01% in terms of volumetric and axial strain for a 38mm dia. sample).

The pressure transducers were supplied both by Druck Limited, Leicester, and Wykeham Farrance Limited, Slough. The capacities varied but were generally 1000kPa or above.

Calibration was carried out with a DPI 101 Digital Pressure Indicator also supplied by Druck, by applying pressure with a Bishop ram. Accuracies of the order of ±0.2kPa were expected within this set-up. The DPI was calibrated with a dead-weight system supplied by Budenberg Gauge Company Limited, Cheshire.

The deviatoric force was measured by a 5kN capacity pressure compensating Surrey University type load cell, also supplied by Wykeham Farrance, positioned within the triaxial cell and in direct line with the top platen. Calibration was carried out by applying dead-weights. An accuracy of the order of ±1.0kPa was expected.

The initial tests conducted using local instrumentation also had three miniature LVDTs with through bobbin cores and ±5mm range. To improve their performance AC amplifiers (type S7) were used to amplify the signal. Both the LVDTs and the amplifiers were supplied by RDP. Cuccovillo and Coop (1997) suggested that measurements in the fourth decimal place of percentage strain (0.0001%) are achievable but the third decimal place (0.001%) is closer to the magnitude achieved with the set-up used.

4.3.3 *Bender elements*

The bender element method for determining G'_{max} of soils in laboratory tests was developed by Schulteiss (1982) and Dyvik and Madshus (1985). The technique and apparatus used for these tests is described by Jovicic (1997), who gives extensive details. Figure 4.1 illustrates the main features of the bender element set-up within the testing apparatus.

The technique involves propagating a shear wave through the soil by the excitation of a piezo-electric ceramic bender element, embedded in the top of the sample. The wave is received by a second element embedded at the base of the sample and the time taken for the shear waves to pass through a known length of sample is measured using a digital oscilloscope. The velocity of the shear wave is directly related to the shear modulus, for an isotropic elastic material, as;

$$G = \rho v_s^2 \; ; \tag{4.1}$$

where ρ is the mass density of the material, and

v_s is velocity of the shear wave.

4.4 · Sample preparation

Triaxial testing was carried out on compacted saturated sand samples only, which were prepared using conventional split moulds. The sample membrane was attached to the bottom pedestal in the cell by rubber O-rings, a porous stone and filter paper preventing blockage of the base drainage system. The membrane was held against the sides of the mould by a vacuum, achieved by attaching a medical pump to a port in the split mould. The sand was placed into distilled, de-aired water in three layers, each layer being tamped carefully with an aluminium rod to achieve the most dense sample possible by this method. The mass of sand in the sample was recorded.

On reaching the required sample height the water was drained to the level of the top of the sand and the top platen, with protruding bender element, was carefully pushed into place, taking care to align the transmitting element with the receiving element in the bottom platen. The membrane and O-rings were then positioned in the usual manner. It should be noted that the O-rings must be below the level of the top platen, either around a split stretching ring or on the mould itself, before the top platen is placed. The O-rings cannot be positioned over the top platen once it is located due to the cable carrying the bender element signal. At this stage a rubber suction cap was positioned on the top platen to aid the alignment of the sample and reduce errors due to loading of non-parallel surfaces (Atkinson and Evans, 1985).

A manometer, located on the laboratory floor, was attached to the drainage system of the sample which produced a pressure of around -10kPa in the pore water, and an effective stress of 10kPa in the soil. The effective stress was sufficient to allow the split mould to be removed whilst maintaining the integrity of the sample for the short period until a cell pressure could be applied. It was at this stage that the local strain gauges were attached to the sample during the early tests. The fixings for the instruments were simply glued to the membrane, the radial belt fixed in two places around mid-height of the sample and two axial gauges, fixed one either side of the sample, over a gauge length of approximately 50mm.

The next phase was to apply a small cell pressure of around 10kPa, after which the tap to the manometer was closed and the integrity of the sample was maintained by a small effective stress. The drainage tap to the volume gauge, with zero back-pressure, was then carefully opened and both the cell pressure and back-pressure increased in parallel, maintaining a small effective stress of the order of 10kPa throughout. A back-pressure of 300kPa was chosen to aid saturation of the sample. The relatively high back-pressure was possible, even though the

apparatus was limited to a cell pressure of around 800kPa, because the tests were to be conducted at quite low effective stresses, similar to those experienced by the sands in the centrifuge tests. The sample was generally left overnight with a pore water back-pressure of 300kPa, $\sigma_v' = 10$kPa, to allow saturation to occur. B value tests were conducted the following morning and rarely produced values less than 0.98.

In the centrifuge tests the sands were initially subjected to K_0 compression due to the increase in centrifuge acceleration. The suction cap was therefore connected to the load cell at this stage, by carefully raising the axial ram, to allow different radial and axial stresses to be applied. In this state the sample was ready for the test stages to begin.

4.5 Tests conducted

Table 4.1 lists the successful triaxial tests conducted on four different types of washed silica sand, giving the initial and final specific volumes, the type of measurement used and the strain level reached at the end of shearing. It should be noted that the tests using local LVDTs were carried out on 60mm diameter samples (120mm nominal height) and the bender element tests were carried out on 38mm diameter samples (76mm nominal height).

Having achieved a saturated sample with a pore water back-pressure of 300kPa, $\sigma_v' = 10$kPa, all tests began by attempting K_0 compression of the sample to simulate the stress path of the sand in a centrifuge test. K_0 compression of samples in the triaxial apparatus, that is increasing axial stress and radial stress independently depending on the change in radial strain, can be difficult to control and so it was decided to make an estimate of K_0 for the sands and effect a pre-determined stress path whilst observing radial strain. It was thought unlikely that the slight errors in the simulation of the stress path direction would have any significant effect on the measurements required.

Although only really applicable to normally consolidated fine grained soils, an initial estimate of horizontal effective stress was made assuming that $K_0 = 1\text{-}\sin\phi'$ (Jaky, 1944). In fact, the compacted sand was on the dry side of the critical state line and could be described as having an apparent overconsolidation ratio, OCR (the ratio of the maximum previous vertical effective stress to the current vertical effective stress for an element of soil). An expression relating K_0 to OCR, such as presented by Mayne and Kulhawy (1982), may have been slightly more appropriate, although this was also developed for fine grained soils. However, this

would have involved making some assumptions about the apparent OCR. Taking $K_0 = 1\text{-}\sin\phi'$ and using ϕ'_c of 36° (from preliminary shear box tests by the author), $K_0 = 0.41$, which conveniently approximates to increasing both the mean normal effective stress, p', and the deviatoric stress, q', at the same rate.

Based on measurements on Ham river sand, Coop and Lee (1993) suggested that $K_{0\,(nc)}$ of around 0.57 is likely to be reasonable for most silica sands which indicates that the above estimate for $K_{0\,(oc)}$ may be too low. Radial strains from tests TT1 and TT2 (Table 4.1) were measured directly using a local strain belt and were also inferred from external measurements of axial and volumetric strain. The two methods produced similar values. Radial strains for the other tests were derived from external measurements only. During compression at the stress ratio corresponding to $K_0 = 0.41$, the observed radial strains varied between +0.1% and -0.1%. A negative radial strain, implying an increasing horizontal dimension due to a low radial stress, indicates that the assumed value of K_0 was too low. It is likely that $K_0 = 0.41$ is a low value and therefore the spread of radial strains during K_0 compression is attributed to strain measurement inaccuracies associated with the very low effective stresses. However, as stated previously, the small deviations from the true K_0 stress path should not have any significant effect on the results presented here.

Figure 4.2 shows the stress path followed in test 7, and is typical of all tests conducted. The stress state (in q': p' space) before K_0 compression began lay on the isotropic axis with a value approximately equal to 10kPa. The first event in the compression of the sample was therefore to return the stress state to the desired position, in this case $q' = p' = 15$kPa. The stress path then followed the estimated K_0 compression line until $q' = p' = 60$kPa. This corresponds to a $\sigma_v' = 100$kPa, approximately 100mm depth of saturated sand in centrifuge tests at 100g or 60 to 70mm depth of dry sand. This is slightly higher than the average stress state for the sands in the centrifuge tests but it is a reasonable value. Conducting triaxial tests at low effective stresses can be difficult, particularly for bender element measurements.

During triaxial tests TT3 to TT7, bender element measurements were taken during the compression stage when $q' = p' = 20$, 40 & 60kPa. This phase was conducted relatively quickly over a period of around 2 to 3 hours.

The final testing stage was to shear the sample at constant p'. As can be seen from Figure 4.2 the change in q' required to reach the peak state was relatively small and so after the first few preliminary tests this stage was conducted by controlling axial strain. An axial strain rate of

0.5 - 1.0% per hour was used initially to ensure that sufficient data were recorded in the small strain region. The strain rate was usually increased after this to a rate of around 2% per hour.

4.6 Results

The key observations made directly from the triaxial test results are presented in this section.

Table 4.2 lists the centrifuge tests in which the different sands were used and the specific volumes assumed for the sand samples in those tests, for comparison with the triaxial tests. The samples in the centrifuge tests were prepared by raining the sand from a considerable height into the model container. The accuracy of the measurements made during the centrifuge model preparation was not sufficient to determine specific volumes with confidence and so thorough independent checks were made by raining sand into smaller containers using the same set-up. This resulted in the consistent and repeatable specific volumes and dry unit weights given in Table 4.2. It was not possible to prepare the triaxial samples by the same method but compaction of the samples under water yielded similar values.

As mentioned previously, Figure 4.2 shows the stress path from triaxial test 7 tending towards the CSL suggested by Coop and Lee (1993) for Ham river sand. However, reference to Figure 4.3, which shows the volumetric state of the sample and the CSLs and INCLs for various silica sands (after Coop and Lee, 1993 & Coop and Cuccovillo, 1998), reveals that it is in fact a very long way from achieving a critical state. This is to be expected as extremely loose samples and/or high pressures are generally required to reach critical states for sands. The CSLs and INCLs for the silica sands referred to above show a relatively consistent grouping which suggests that critical state parameters for silica sands are reasonably similar. Clearly, all of the sands in the centrifuge and triaxial tests were compacted to states well dry of critical and had extremely high apparent OCRs.

The results of the bender element measurements are presented in Figure 4.4. The relationship between G'_{max} and p' is approximately linear over this narrow and low stress range. The 52/100 Leighton Buzzard sand and the Flint Gravel sand which have very similar and uniform gradings also have very similar stiffnesses. As expected the well graded mixed Leighton Buzzard sand has a higher stiffness by around 20%. It is interesting that the coarsest material, the 14/25 LBS, which had a similar uniformity of grading to those first mentioned above,

displayed the highest G'_{max}. There is no reason to doubt the result as the bender element signal was good; nevertheless it is perhaps a little surprising that sands of the same mineralogy and uniformity of grading can show such significantly different values of G'_{max}. One possible cause is that the coarse grains may have inhibited the movement of the bender elements, especially if they became trapped between the piezo-ceramic and the porous drainage plates. Another possibility is that the ratio of the size of the soil grains to the bender elements is important for coarse grained material, particularly at low confining pressures.

The same data are plotted on logarithmic axes in Figure 4.5, along with data from Coop (1998) for $G'_{max\ (nc)}$ measured for a variety of other soils; Coop (1998) noted that the data for the non-plastic materials lie close to each other with G'_{max} reducing with increasing plasticity. The data from the triaxial tests presented here were obtained at lower confining pressures than the other data plotted, but it can be seen that they lie slightly above those for the non-plastic materials on the INCL, although within the same region. Overconsolidated soils are expected to display higher stiffnesses than those on the INCL, with particular reference to Figure 2.3 and the work of Jovicic and Coop (1997) on the stiffness of coarse grained materials. This gives a degree of confidence in the measurements for use in analysing the tunnel problem.

The final results presented from the triaxial tests show the decay of stiffness with shear strain (Figure 4.6) and change in deviatoric stress (Figure 4.7). The strains were measured using LVDTs, locally for tests 1 and 2 and externally for the remainder. Good small strain measurements were not achieved but the data are sufficient to give an idea of the rate of decay of shear stiffness of the particular materials in various states. The differences are best observed with the change in deviatoric stress. The well graded mixed LBS shows the slowest decay of stiffness followed by the 52/100 LBS. As the Flint Gravel sand has a very similar grading, particle mineralogy and shape to the 52/100 LBS, and produced very similar values for G'_{max} from bender element measurements, it is rather surprising that the decay of stiffness is not comparable. In fact, the Flint Gravel sand data shows no tendency for higher stiffnesses at small strains and, although there are no known physical reasons to mistrust the measurements, it is thought that the extremely rapid decay of stiffness observed may not be reliable. Tests TT1 and TT2 produced data at smaller strain levels as local transducers were used and produced faster decays of stiffness associated with the looser volumetric states of the 14/25 LBS and the mixed LBS respectively.

The data, in the form presented in Figure 4.7, are used in Chapter 7 to determine material parameters for use in the finite element analyses.

4.7 · Material properties

Basic material properties for both kaolin and silica sands are given in Table 4.3. Most of these were derived from the literature as detailed below.

Speswhite kaolin is a well tested laboratory clay and a significant body of test data exist for this material. The values presented in Table 4.3 are considered to be the most likely average values for kaolin derived mainly from tests conducted at City University by various researchers. G'_{max} is determined using equations 2.7 and 2.8 (Viggiani and Atkinson, 1995) for which the coefficient A and exponents n and m are given by Viggiani (1992). These parameters have been used successfully for analysing many geotechnical problems at City University.

Values of K_0 were required to determine horizontal effective stresses. For use in analysis of centrifuge test results, K_0 for the overconsolidated clay was taken as;

$$K_0 = 1 - \sin\phi' . \mathrm{OCR}^{\sin\phi'} \tag{4.2}$$

(Mayne and Kulhawy, 1982); and for the silica sands $K_0 = 0.57$ (Coop and Lee, 1993).

The critical state parameters for silica sand were also reported by Coop and Lee (1993) who conducted triaxial tests at elevated stresses in order to determine them. The grouping of the CSLs and INCLs for a variety of silica sands in Figure 4.3 suggests that these parameters are unlikely to vary greatly for silica sands of different origins.

The shear stiffness at very small strains, G'_{max}, varies depending on the sand tested, or, probably more accurately for silica sands, on the volumetric state of the sand tested. As mentioned before, the values determined from the bender element measurements are given directly in Figure 4.4. At these low stresses and over a short stress range the value of G'_{max} for a particular sand varies approximately linearly with p' and could be reasonably described by a straight line. As presented in Chapter 2, Jovicic (1997) and Jovicic & Coop (1997) suggested that G'_{max} for coarse grained materials could be described by an expression similar to that used for clays, but that the method by which the material reached an overconsolidated state had an effect on the magnitude. Referring back to Figure 2.3 for the Ham river sand (silica sand), most of the sands tested here fall between the lines denoting the different methods of attaining their current state. The degree of scatter of the results for Ham river sand in Figure 2.3 is considerable and the fact that measurements from the tests presented here

appear slightly high is not of great concern. It is not possible to be sure whether the values of A and n or the ratio of $G'_{max\ (oc)}$ / $G'_{max\ (nc)}$ quoted by Jovicic (1997) for Ham river sand are different from the sands tested here. However, it would be sensible to describe the variation of G'_{max} measured in these tests using a similar expression. The simplest way to do this is to fit values of A and n to the measurements on the overconsolidated (compacted) samples tested such that;

$$\frac{G'_{max(oc)}}{p'_r} = A^* \left(\frac{p'}{p'_r} \right)^{n^*} \quad ; \tag{4.3}$$

where * denotes that they are in terms of an overconsolidated state.

In this way the stiffnesses measured over the limited stress range can be well described but there is no dependence on R_0. This is unlikely to be a problem for the analysis presented in this dissertation but extrapolation to higher stresses would lead to inaccuracies. Fundamentally, this is not ideal as the parameters A and n become state dependent and will be different for the same material in different states of compaction. However, the assumptions should adequately serve the requirements of this research. Fitting to the measured data in Figure 4.4 yields the following:

	A^*	n^*
med/dense 52/100 LBS and Flint Gravel sand - tests 3, 4 & 6	6000	0.63
med/dense 14/25 LBS - test 5	9000	0.61
med/dense mixed LBS - test 7	13000	0.56

4.8 Summary

The determination of the parameters of the materials used in the centrifuge tests has been described, with particular emphasis on the measurement of G'_{max} of the sands, and the decay of shear stiffness, using the bender element technique and a stress path triaxial apparatus. Other material properties have been presented from the relevant literature. These values have been summarised for general analysis of centrifuge test data. Parameters specific to the numerical modelling are given in Chapter 7.

CHAPTER 5 CENTRIFUGE MODEL TEST RESULTS

The important data obtained from the centrifuge tests described in Chapter 3 are presented in this chapter. Individual experiments are used to illustrate the main features of the tests, and the type and quality of the data obtained from them. Results from image processing are reviewed and the difficulties in interpretation are assessed. The key observations from the results are presented including: distributions of the settlement trough width, which are described by determining values of i from the test data; assessment of horizontal movements; examination of measured changes in pore pressures around the tunnel; and the effect of surface layers on collapse. The main findings are summarised in Section 5.4.

5.1 Illustrative results

The results presented in this section are intended to illustrate the basic data obtained from the centrifuge model tests. The data shown correspond to the tunnel pressure reduction phase by which time all models had reached equilibrium conditions at the required speed on the centrifuge.

5.1.1 *Ground movements at the surface and clay/sand interface*

Movements at the upper soil surface of the model and the interface between the clay and the sand, if present, were monitored by conventional LVDT type displacement transducers. Typically, nine transducers were used at each level.

Figure 5.1 shows the displacement measured by the transducer directly above the tunnel centreline, at the ground surface, during centrifuge test RJG15 ($3D$ clay cover only). As expected the settlement increased with the reduction in tunnel support pressure, the test progressing from the right of the graph to the left. For a single tunnel with homogeneous soil layers and a uniform stress distribution in the horizontal plane, that is no overlying surcharge eccentric to the tunnel, the settlement directly above the tunnel centreline should be the maximum settlement, S_{max}, at any given level. Typically, the tunnel support pressure was reduced at a rate of around 100kPa/minute, whereby it took a little over three minutes to reduce the pressure to zero for this particular test. The plot in Figure 5.1 is comparable to a load-deflection curve for a foundation test and it is practically impossible to identify a single yield point. Data were logged at a constant rate throughout each test at between one and two

readings per second, depending on the number of transducers involved in the experiment. The spacing of the data points indicates that the settlement increased rapidly as the tunnel support pressure approached zero. Approximate volume losses calculated from the displacements at the clay/ground surface are included above the graph. As this work is concerned largely with deformations prior to tunnel collapse, the majority of the results presented are from stages in the tests before 20% volume loss was reached. Although a little low to be described as failure, a volume loss of 20% would be a serious concern and it will be shown that pre-collapse predictive methods may not be appropriate for volume losses in excess of this.

Figure 5.2 shows a similar plot for RJG16 (1.5*D* sand over 1.5*D* clay). The two traces show data from the clay/sand interface and the sand/ground surface. As expected, settlement above the tunnel centreline was consistently found to be less at the sand/ground surface than at the clay/sand interface.

Figures 5.3 and 5.4 show the development of the transverse settlement troughs for the same tests. Data are plotted for a range of volume losses from 2% to 20%. Figure 5.3 for the clay-only test shows clearly how the troughs developed smoothly, with the settlement decreasing with horizontal distance from the tunnel centreline. It is clear that the transducers farthest from the tunnel were still registering movements. The LVDT at x = -240mm was only 35mm from the boundary of the model container and it is likely that movements were still occurring at the lateral boundaries. Movements associated with the volume loss at the tunnel are constrained by the model container. If the interface between the sides of the container and the soil is frictionless then the movements measured at the lateral boundaries may be greater than at analogous points in a model of infinite width. If there is friction at the interface between the soil and the model container then this will tend to hold up the soil against the sides of the box. Either way there may be some effect on the displacements measured by the far-field transducers and this will increase with the vertical distance from the tunnel as the movements spread away from their source. It is likely that there will be a small amount of friction between the sides of the box and the soil. The effect on the displacements at the limits of measurement are unlikely to be large but it is important to be aware of them, particularly for the tests with the greatest depth of soil cover.

The point is reiterated in Figure 5.4 which shows the development of the transverse troughs at both the clay/sand interface and the sand/ground surface for test RJG16. The far-field transducers registered practically no movement at the clay/sand interface which was only

1.5D above the crown of the tunnel. The sand/ground surface was 3D above the tunnel crown and the movements measured by the outlying transducers were significantly larger.

Figure 5.4 also demonstrates the differences between the sand/surface troughs and the subsurface clay/sand interface troughs. The subsurface troughs measured on the top of the clay (1.5D above the tunnel crown) were deeper and steeper than those measured at the sand/ground surface (3D above the tunnel crown). It will be seen later that this is a function of the relative positions of the horizons at which settlement is measured, both from the tunnel and the ground surface. There is not sufficient information here to investigate the distribution of movements through the sand layer, except to say that the trough width increased. In all tests, volume losses determined from measurements at the clay/sand interface and the sand/ground surface were broadly similar, and trends in the differences were not consistent, probably due to there being insufficient measurement points.

It is commonly assumed that the transverse surface settlement profiles due to single tunnels are of Gaussian form. The simplest way to check vertical settlement profiles against this assumption is to plot the data such that they produce a straight line if they are well described by the Gaussian function, which can be expressed in linear form as;

$$\frac{x}{i} = \pm\sqrt{-2\ln S / S_{max}} \quad . \tag{5.1}$$

Data from centrifuge tests RJG15 and RJG16 respectively have been plotted in this manner in Figures 5.5 and 5.6. Best fit straight lines have been calculated by least squares estimation and drawn through the data. For the LVDT measurements S_{max} was taken to be directly above the tunnel centreline as the number of data points available, a maximum of nine for each trough at each discrete time interval, was not considered sufficient to examine offsets in the centrelines of the settlement troughs and the tunnel. The same data are re-plotted in more familiar form in Figures 5.7 and 5.8. Settlements have been normalised by S_{max} and the horizontal distance, x, non-dimensionalised by the tunnel diameter, D. In fact, the latter operation is unnecessary for reviewing the data, as the tunnel diameter was 50mm in all of the experiments undertaken. Figures 5.5 to 5.8 are typical of the data obtained from the centrifuge tests, and show that the data fit well with the form of the Gaussian distribution and that the assumption that S_{max} occurs directly above the tunnel centreline is valid. The clay/sand interface (Figures 5.6a and 5.8a), which is a subsurface trough, shows an especially good fit. However, Figures 5.5 and 5.7 illustrate a point which is common to most of the tests. Larger movements occurred in the far-field than predicted by the best fit Gaussian distribution. This immediately suggests the possibility that the movements at the edges of the

trough may be greater than normally expected due to the proximity of the lateral boundary of the model, as described above. However, similar features were observed in field data obtained during construction of the Jubilee Line Extension (Nyren, 1998), which, to some extent, negates the concerns regarding the side wall boundary effects.

Given the concerns over the movements at the edges of the troughs in the centrifuge tests, the fact that settlement troughs in the field stray from the Gaussian distribution at their edges, and that these movements are outside the zone of interest for most predictive purposes anyway, the least squares estimations have been applied to data within $x = \pm 2i$ of the tunnel centreline only (for a Gaussian distribution the settlement is 13.5% of S_{max} at $x = \pm 2i$). The horizontal distance from the vertical centreline of the tunnel to the point of inflexion of the Gaussian distribution, i, is the inverse of the gradient on the plots given in Figures 5.5 and 5.6. Some iteration is required when finding the best fit to determine which points are within $x = \pm 2i$ of the tunnel centreline. Generally, the measurements of the sand surfaces show more scatter about the trend line but do not consistently tend away from it. The relatively large movements at the edges of the trough are associated with surface settlement troughs and so it is possible that the unrestrained free-surface is the cause of the wider movements.

Figures 5.9 and 5.10 show the variation of i with volume loss for two tests, again RJG15 and RJG16. In each case consistent values of i have been derived after volume losses of between 1% and 2%: at volume losses lower than this there is considerable scatter in the values of i. Although there is a slight rise and fall in the magnitude of i, it stays remarkably constant for volume losses between 2% and 20%, after which it tends to reduce. In practical terms a volume loss of 20% is effectively collapse and the settlement troughs become increasingly steep thereafter. The range of volume loss shown in Figure 5.9 has been deliberately extended well beyond 20% to illustrate the trend, which is also apparent in Figure 5.10 for both the subsurface clay/sand interface and the sand/ground surface. It should be noted that the volume losses have been calculated from the best fit Gaussian distributions at the clay surface. As such, errors will increase as the troughs steepen or stray from the Gaussian form. The importance of the small variation in i at pre-collapse volume losses is that distributions of movement up to collapse are seen to be reasonably constant. Data from stages in the tests well beyond the usual range of volume losses experienced by tunnelling (say 1% to 5%) can be used in investigating the pattern of deformations around tunnels.

In summary, Gaussian distributions do seem to describe the transverse settlement troughs well including the subsurface troughs at the clay/sand interface. Relatively large movements at the

edges of troughs occur at free-surfaces, which may be associated with the lack of restraint from above. The form of the settlement troughs stays approximately constant until the tunnel begins to collapse. This is important as it indicates that all pre-collapse data from the centrifuge tests may be used to aid the investigation, even though most settlement predictions due to tunnelling are made for low volume losses.

5.1.2 *Subsurface ground movements measured by image processing*

As well as monitoring the vertical movements at the clay/sand interface using LVDTs, subsurface ground movements were monitored using image processing techniques. Digital images at several stages during centrifuge test RJG20 are given in Figure 5.11. The majority of the marker beads seen in the images were on a regular 10mm grid. As described in Chapter 3, the system involved measuring the displacement of marker beads pushed into the front vertical face of the soil which could be viewed, in-flight, through a thick perspex window using a CCTV camera mounted on the centrifuge swing. Post-test processing of the images produced co-ordinates of all the marker beads in real (object) space. Saving images at a rate of approximately one per second produced complete details of the subsurface movements during the reduction in tunnel support pressure. From the four images in Figure 5.11, the change in the size of the tunnel is obvious but the movement of most of the marker beads was relatively small until high volume losses were reached.

Figure 5.12a shows the level of measurement noise in the system by plotting vectors of movement between consecutive images immediately prior to the reduction in tunnel support pressure. The location of the measurement targets in the first frame is marked by a "+" and a line is drawn from this to the position of the target in the second frame. Movements have been magnified 200 times and a bar indicating 1mm in length at vector scale is given at the top of the plot. In general, the noise is spacially random and can also be seen in the control targets used to determine the camera position, demarked by circles, and in this case positioned on the outside of the window. The occasional rows of regular horizontal movement are due to "horizontal line jitter" caused by the camera electronics. Generally, the level of noise is around 20μm.

Figure 5.12b is included to show the level at which meaningful patterns of displacement can reasonably be observed. Movement near the tunnel crown was approximately 0.15mm and that near the clay/sand interface was considerably less. The vectors are magnified 100 times and again a 1mm bar is given to illustrate the magnitude of movements. Even at these small

displacements it is possible to observe patterns of movement above the level of the noise. At this stage in the test the volume loss measured by the LVDTs at the clay/sand interface was around 1%.

Figures 5.13(a & b) show the vectors of movement (magnified 15 times) during RJG20 at volume losses of 5% and 10% respectively (as measured by LVDTs at the clay/sand interface). The pattern of movement is extremely regular apart from the occasional, clearly mis-directed vector, which is likely to be a function of the target tracking method and can be caused by slight lighting fluctuations or partial obscuring of the marker. It can be seen that the measurements in the sand layer were considerably less regular than those in the clay. Generally, measuring movements in sand using image processing has proved more difficult than in clay. Apart from the problem of installing the marker beads (targets), there is a greater tendency for the soil grains to obscure the targets during a test. If the shape of the target changes, the tracking algorithms perceive a change in target position. In addition, the quality of the target tracking relies on the difference in the intensity of light reflected by the targets and the background (the difference in grey-scale level). The difference in intensity of black targets on a white background (kaolin clay) is relatively large and sufficient to produce good results, whereas the intensity difference is not as great for black targets on a background of yellow silica sand. In order to achieve more reliable measurements by image processing in sand, either a new target design would be required or a different technique employed such as tracking patches denoted by surface texture. Some work has been conducted to develop retro-reflective targets to maximise the difference in intensity of light reflected. This would improve measurements not only in sand but also in clay. However, the lighting requirements for this type of target would be different and may prove difficult to resolve. Owing to the above difficulties, little attention has been focused on the results from image processing in the sand. Nevertheless, it is clear that considerable insight into subsurface movements in the clay can be gained from the results obtained by image processing.

Figure 5.14 shows one way in which these data can be used. Best fit Gaussian distributions have been superimposed on the vectors of movement for several subsurface levels. In this case, the centrelines of the troughs are not coincident with the centreline of the tunnel, but are offset to the left by up to 10mm. It is also apparent that the settlement profiles near to the tunnel do not fit the form of a Gaussian distribution as well as those at shallower depths. Close to the tunnel crown the vectors indicate steeper troughs than those implied by the best fit Gaussian profiles.

The issue is explored further in Figure 5.15, which is also indicative of the quality of the measurements made. From the co-ordinates of the targets throughout test RJG20, normalised settlement profiles for a wide range of volume losses and a range of subsurface levels have been produced. Figure 5.15(a) shows movements of the top row of targets in the clay, nearest to the clay/sand interface, 105mm above the tunnel crown ($z_0 - z = 130$mm). Imposed on top of the measured data is the best fit Gaussian distribution. There is a slight offset to the left of the tunnel centreline, at $x = 0$, but the data form a remarkably tight group around the best fit line. The profile is very well described by a Gaussian distribution. With the exception of two points, the same is true of the profile given in Figure 5.15(b), some 40mm closer to the tunnel, where $z_0 - z = 90$mm. However, the movements $0.5D$ above the tunnel crown (Figure 5.15c) show a little more scatter and a steeper profile than the best fit Gaussian curve. The difference is even greater in Figure 5.15(d) which shows the normalised settlement profile immediately above the tunnel crown.

Clearly, there is potential for considerable insight to be gained through image processing measurements in centrifuge model tests, especially for detailed investigations of pre-collapse deformations.

5.1.3 *Pore pressure response*

Pore pressure transducers in the clay during the centrifuge tests were used largely to measure equilibrium pore water pressure profiles in the model. However, as they were located in the vicinity of the tunnel they also produced measurements of the changes in pore water pressures during the reduction in tunnel support pressure.

The pore pressure response around the tunnel during unloading depends on the rate of stress change, the type and the state of the soil, in particular the permeability, compressibility and overconsolidation ratio. In all of the tests conducted the tunnel lay within an overconsolidated clay layer. Significant negative excess pore pressures were produced around the tunnel, associated with the largely undrained conditions (in the short term) and the general reduction in mean normal total stress. This is illustrated in Figures 5.16 and 5.17, which show the actual pore pressures in the vicinity of the tunnel during the reduction in support pressure for centrifuge tests RJG15 and RJG16. The data for Figure 5.16 were shown previously in Figure 3.23 to illustrate the centrifuge spin-up phase of the experiment, the difference in Figure 5.16 being that the x-axis has been changed to show the reduction in tunnel support pressure.

The results presented are typical of all the centrifuge tests conducted. Changes in pore pressure decreased with distance from the tunnel boundary and significant negative pore pressures developed as the tunnel support pressure approached zero.

5.2 Assessment of image processing measurements

Use of image processing for determining movements in plane strain centrifuge models is not a new technique. However, the work presented here is the first to be conducted at City University using the advanced digital system described. Although thorough checks can be made to ensure that the system is measuring real displacements, it is also important to assess the effect on the movements of the boundary condition at the front of the model. For the centrifuge tests described, this has been done by comparing data from LVDTs on the clay surface with vertical displacements of the marker beads near the clay surface, obtained by the image processing system. The LVDTs were located near to the central vertical plane of the model, and as such should have measured displacements unaffected by the front and rear boundaries.

Results presented here are for test RJG20, though similar comparisons have been made for all centrifuge tests where the image processing results were expected to be of good quality (RJG17 onwards). Table 5.1 lists all of the centrifuge tests conducted with details of the image processing conducted for each and the anticipated quality of the data.

Figure 5.18 shows a direct comparison of the measured displacement above the tunnel centreline from a LVDT at the clay/sand interface with that measured by image processing of the corresponding target nearest to the LVDT. The upper plot suggests that the two displacements compare favourably throughout the reduction in tunnel support pressure, but that the image processing measured slightly less displacement until large settlements were reached. As the image processing target was marginally closer to the tunnel crown the movements from image analysis should be marginally larger than those from the LVDT. The lower plot shows the same data for only the early stages of the test with the displacement scale magnified by ten. As with the vector plot in Figure 5.12a, the level of noise for the image processing can be seen to be in the region of 20μm. At this exaggerated scale the discrepancy between the two methods of measurement can be seen more clearly. The image processing displacement appears to lag behind the LVDT displacement by approximately 15kPa in terms of tunnel support pressure. Once the image processing target began to move it

seemed to do so at the same rate as the LVDT, in that the gradients of the traces are similar. The similarity of the shape of the curves with a constant offset between them could simply suggest an error in the recording of data. The recording systems for the electronic transducers and the image processing were independent and the timing between them was recorded manually. However, similar exercises have been conducted on all of the tests from RJG15 onwards and a similar pattern emerged for each. An error of ±5kPa is considered the maximum possible due to the independent recording systems.

Differences between the displacements measured by each of the LVDTs for test RJG20 on the clay/sand interface and those of the corresponding targets measured by image processing are presented in Figure 5.19. Displacements measured by one method have simply been plotted against those made by the other. If the measurements corresponded exactly they would fall on the bold 45° line indicated. In fact, all show a similar trend with gradients close to 45° but only after a certain displacement has been reached. With the exception of one data series, there is a reasonably small spread of data around a mean offset of 0.1mm.

Clearly, friction exists between the perspex window and the clay. This interface was generally lubricated using viscous paraffin liquid or, in some later tests, by silicone fluid. From analysis of the other test data it is apparent that the type, or at least the viscosity, of the lubricant is important. It appears that reasonably high viscosity lubricant is necessary to minimise the frictional component of sliding between the clay and the perspex; lower viscosity lubricants perhaps do not ensure sufficient cover between the soil and the perspex. It is estimated that the viscosity of the paraffin liquid used in the majority of the tests was in the order of 100cS (water has a viscosity of 1cS). All of the tests showed similar trends and the offset of 100μm was an average value for most tests, where the lubrication was reasonably viscous (around 100cS). A number of tests in the TH series were conducted using no or low viscosity lubrication (30cS) and although they show a similar trend to the others, the magnitude of the offset is considerably greater. The implication is that a stick-slip mechanism acting at the interface between the clay and the perspex is responsible for the initial offset between the LVDT measurements and the image processing measurements. Once the soil at the interface has moved a certain distance, it continues to do so at the same rate as the rest of the soil mass. Current practice is to use a silicone fluid of very high viscosity (12500cS) to ensure that the clay is not in contact with the perspex throughout the test, although further experiments are required to confirm the optimum method of minimising the effect of friction.

The effect of friction on the displacement of the soil will only remain constant whilst the ratio of driving stress to normal stress remains constant. In the centrifuge tests presented the driving stress is the total vertical stress and will increase linearly with depth in the model. The normal stress is the total horizontal stress in the soil and so the ratio of driving stress to normal stress will vary with K_0 through the soil profile, being a maximum near the soil surface. This might suggest that the component of friction is not constant throughout the model depth. Figure 5.20 shows the volume losses calculated during centrifuge test RJG20 from LVDT data and from the image processing displacement vectors at subsurface horizons. Volume loss calculated from the LVDTs is based on the best fit Gaussian distribution, but volume losses calculated from the displacement vectors are based on the summation of the vector cross products. No attempt was made to include the volume loss due to movements outside the lateral limits of the image processing measurements. However, it can be seen by reference to Figure 5.15 that this component is likely to have been very small. The offset between the LVDT data and the image processing data is still apparent. Data from the image processing shows a little random scatter but, in general, there is no tendency for the volume loss to increase, or decrease, with depth. This exercise has been carried out on data from a number of centrifuge tests with the same result. The implication is that the component of friction must be reasonably consistent with depth. However, to develop more confidence in the use of the image processing results for the future, an independent experiment, in which a mass of soil is moved down a known distance whilst using image processing to observe the movements throughout the depth of the soil at the soil/perspex boundary, should be conducted. More detailed investigation of the quality of different lubricating materials would also be beneficial for future experiments.

The primary use of the image processing measurements in this research is to establish distributions of settlement trough width with depth, and thus it is important to be aware of any effect of the friction on the trough width, indicated by the value of i. Gaussian distribution curves are datum dependent; they tend towards zero at the limits, and therefore offsets in the measured displacements will change the value of i interpreted from settlement data. This is illustrated in Figure 5.21. A real set of image analysis data from centrifuge test RJG20 has been plotted and from the best fit Gaussian distribution curve, a value of i = 75mm has been determined. If it is assumed that the measured settlement data are 0.1mm less than the actual movements, as suggested by Figure 5.19, and this offset is taken into account, it would imply that the real value of i is 81mm. Therefore, the i value would have been under-estimated by 7%. Clearly the effect of friction must be considered when using the image processing data.

The effect on distributions of i typical of results from the centrifuge tests has been investigated further in Figures 5.22 and 5.23. A constant error in settlements, S, will affect the values of S_{max}, V and i to different degrees depending on their changing magnitudes. The effect is most easily investigated numerically and the results of such an investigation are presented in Figure 5.22. Values of S were determined for Gaussian distributions with i values ranging from 40mm (typically near the tunnel crown) to 120mm (typically near the ground surface) and over a range of volume losses up to 20%. An offset of -0.1mm was applied to the settlement values to represent the under-measurement due to friction of the image processing results. New "best fit" Gaussian distributions were then determined for the new settlements, using the values within $x = \pm 2i$ only. As the Gaussian distribution must tend towards zero settlement at the limits, the new distributions were "best fit" distributions. However, the process is analogous to the calculations performed on the real image processing data and so the results obtained should produce realistic errors in the value of i. Figure 5.22 shows the calculated percentage error in i with increasing S_{max}. Errors in i are the differences between the i values for the real Gaussian distributions, representing the real settlement troughs, and the offset data, representing the under-measured settlements, relative to the i values for the real Gaussian distributions. Values of S_{max} in Figure 5.22 are those representing the under-measured values so that errors could be estimated directly from measured data. At small values of S_{max} the error in i is considerable but as S_{max} increases the error in i reduces rapidly to a relatively low value.

The possible effect on the distribution of i values with depth is illustrated in Figure 5.23, where the $3D$ cover above the tunnel crown is made up of clay only. The distribution of i with depth has been plotted in accordance with Mair et al (1993) for a volume loss of 10% (taken as a mid-range volume loss when considering trends from image processing data). This line is then taken to be the true distribution of i. Assuming that the settlements have been under-measured by 0.1mm, the errors calculated in the above investigation have been applied to the distribution according to the magnitude of S_{max}. The results have been plotted adjacent to the "true" distribution in Figure 5.23. Errors in i increase with distance from the tunnel as S_{max} decreases but, generally, the difference between the two distributions is relatively small.

Friction effects are present in all model tests. The improvement in measurement techniques described above has allowed some of the effects to be quantified approximately, however, the exact effect on displacements is not yet known. If it could be specified absolutely, it would be simple to formulate a model which takes the friction into account and corrects the vectors or i values. Factoring the results from this research to account for friction is not considered

appropriate owing to the incomplete knowledge of the friction component of movements determined from digital image measurement. However, having explored the potential magnitude and effects of friction it seems that at least the distribution of derived i values is not affected greatly, provided that the friction component is not excessive (the example in Figure 5.23 was for an offset due to friction of 0.1mm) and that the values of S_{max} are not too low (say in excess of 1mm).

5.3 Overall patterns of results

Displacement vectors can be a useful tool to identify trends of movements in tests. Vectors in the clay for tests conducted from RJG17 onwards (except CK1) are presented in Figures 5.24 to 5.26. Image processing results from tests conducted before RJG17 are not considered to be of quantitative value. Good results in the sand layer were not achieved and so are not considered here.

Figure 5.24 shows the vectors from tests RJG17 to RJG20 in each of which the clay cover above the tunnel crown was 2.5D, but the surface layer varied. In each case the clay was overlain by the following: nothing in test RJG17; 1.5D of dense, largely saturated sand in test RJG18; 1.5D of medium/dense dry sand in test RJG19; 1.5D of loose dry sand in test RJG20. By visual inspection of the vectors in the clay, it can be seen that the widest spread of movements occurred in test RJG19, in which the effective stress in the clay was the highest, but also the stiffness of the sand layer would have been the greatest. The second widest spread of movements in this series appears to be in test RJG18, even though in test RJG20 the clay would have had higher values of effective stress and the stiffness of the sand layer may also have been greater. The narrowest zone of movements occurred in test RJG17 which had the lowest values of effective stress in the clay and no overburden. It is interesting to note that at the clay surface in test RJG17, which was a free-surface, significantly higher horizontal movements can be seen than at analogous points in the other tests. This is presumably due to the lack of horizontal restraint provided by an overlying layer. However, it is not clear from these tests whether the effective stress in the clay or the stiffness of the overlying layer, or both, influence the distribution of movements in the lower clay layer.

For this reason, the test series labelled TH1 to 5 and MC01 was conducted. Vectors of movement from these tests are given in Figure 5.25. The vertical effective stress profile in the clay, which extends to 100mm above the tunnel axis, was kept the same for each test but the

surface layer was varied. In this way the effect of stiffness of the upper strata could be isolated. Types and conditions of the upper layers are labelled in Figure 5.25, and were: saturated clay; medium/dense dry sand; medium/loose dry sand; loose dry sand; fluid surcharge contained within a latex membrane; medium/dense saturated sand. Visually, the narrowest spread of movements is from test TH5 in which a fluid surcharge, of no shear stiffness, was used. This is followed by the loose and medium/loose dry sand tests (TH4 and TH3), then the clay-only and medium/dense dry sand tests (TH1 and TH2) and the widest movements appear to have occurred in the test with an overlying layer of medium/dense saturated sand (MC01). The properties of the upper layer must be the cause of the differences observed in this test series and this is explored further in Chapter 6.

Though not directly comparable with the other tests presented, the vectors of movement from TH6, in which a layer of clay was overlain by a significant layer of medium/dense saturated sand, are given in Figure 5.26 for completeness. Movements in the clay are slightly wider than those in the test with medium/dense saturated sand described above (MC01), although both the depth of saturated sand and the vertical effective stress in the clay were higher in this particular test.

5.3.1 *Vertical movements*

Gaussian distributions are a very useful way of representing vertical ground movements due to tunnelling. The distribution or extent of movement for a settlement trough is fully defined by the value of i, the distance from the centreline to the point of inflexion of the curve. Except in the vicinity of the tunnel, measured data have already been shown to be well represented by Gaussian distributions. For each test, the vertical movements in the clay above the tunnel are therefore fully defined by the distribution of i with depth. For those tests where the quality of image processing measurements is good, tests RJG17 onwards, the value of i has been plotted against the height above the tunnel axis in Figures 5.27 to 5.30. Data points at the surfaces of the soil layers, including the subsurface clay/sand interface, were determined from LVDT measurements and the remaining data points were determined from image processing results.

Figure 5.27 shows the distributions of i from tests in which clay was the only soil present. Three different clay covers above the tunnel crown are represented by the tests and these are $2D$ (CK1), $2.5D$ (RJG17) and $3D$ (RJG15 and TH1). The quality of image processing measurement for RJG15 cannot be confirmed and so should strictly be considered only

qualitatively. However, there is excellent agreement with the results from the other $3D$ test. TH1, which suggests that data from test RJG15 may be included for consideration. The distributions of i with depth appear to have three zones: the region close to the tunnel, the region close to the free-surface and the zone between the two. In the vicinity of the tunnel the values of i reduce rapidly. However, care must be taken in this region as it has been shown that the settlement troughs close to the tunnel can be steeper than the best fit Gaussian distributions. Although the data lying within $0.5D$ of the tunnel have been included on the plots for completeness, strictly they should not be included when defining distributions of i with depth. It is also clear, especially in the $3D$ cover tests (RJG15 and TH1), that there is a trend for markedly higher values of i in the vicinity of the ground surface. Part of this apparent widening of the settlement troughs may be attributed to the under-measurement from the image processing; the values of i derived from the LVDT measurements may be wider than those from the image analysis. However, the highest data point determined from the image processing in each case tends to agree with the trend for rapidly increasing values of i near the free-surface. Further data are required to investigate the causes of this observation but it may be due to the lack of horizontal restraint, as with the increased horizontal movements in this region, or the rapid reduction in soil stiffness in the near surface zone. In the middle zone, the remaining (majority) of the data suggest a series of reasonably straight lines of similar gradient, offset from each other in the horizontal direction by perhaps a function of depth of cover above the tunnel.

Figure 5.28 shows a similar plot for centrifuge tests RJG17 to RJG20, in which the clay cover above the tunnel was $2.5D$ in all cases but the layer above was varied as follows: RJG17 had no overlying layer; RJG18 had $1.5D$ of medium/dense saturated sand above; RJG19 had $1.5D$ of medium/dense dry sand above; RJG20 had $1.5D$ of loose dry sand above. There is some scatter in the data, but general trends show that test RJG17 had the narrowest distribution of i with depth and RJG19 had the widest. In between, and on this plot almost coincident, lie the data for RJG18 and RJG20. In this figure the trend for wider movements with increasing vertical effective stress and/or stiffness of the upper strata is apparent. There appears to be a slight tendency for the gradient of the distributions to reduce with increasing stiffness of the upper layer, as well as the horizontal offset of the distributions from the vertical centreline of the tunnel increasing with increasing vertical effective stress.

As explained previously, the test series TH1 to 5 and MC01 was designed to isolate the effect of stiffness of the upper strata by maintaining the same vertical effective stress profile in the lower clay layer for each test. These tests formed an important series and the conditions for

each will be reiterated. Each had 100mm of clay above the tunnel axis, in which the vertical effective stress profiles were the same, and the following layers above: 75mm of saturated clay (TH1); 36mm of medium/dense dry sand (TH2); 40mm of medium/loose dry sand (TH3); 42mm of loose dry sand (TH4); 57mm of fluid surcharge (TH5); 58mm of medium/dense saturated sand (MC01). Figure 5.29 shows that the narrowest distribution of *i* with depth in the clay layer is for TH5 where the overlying material had no shear stiffness. This is followed by the test with loose dry sand (TH4), then the test with the medium/loose sand (TH3). Somewhat wider are the distributions for the test with medium/dense dry sand (TH2) and clay only (TH1), which are very similar to one another; marginally wider than these is the distribution for the test with medium/dense saturated sand (MC01). As the vertical effective stress profile in the clay was the same for each test, the differences in the results can only be attributed to the differences in the properties of the upper layers. Generally, the stiffer upper layers produce wider troughs in the lower strata, but it is not obvious from the plot whether both the offset and the gradient of the distribution of *i* is affected.

It is unfortunate that there is some doubt about the effects of friction on the image processing data for tests TH3, TH4 and TH5. As discussed in Section 5.2, it is possible that friction between the clay and the perspex window may have caused the narrow distributions of *i* observed in these tests. However, there are differences in the values of *i* determined from LVDT measurements at the clay/sand interface. For the tests with an overlying layer of dry sand, the values of *i* at the clay/sand interface are all very similar, but the LVDT measurements from test TH5 (overlying fluid surcharge) produce a lower value of *i* and those for test MC01 (overlying saturated sand) produce a higher value of *i*. This suggests that even though the absolute distributions of *i* with depth for tests TH3, TH4 and TH5 are in doubt, the general pattern of increasing trough width in the clay with increasing stiffness of the overlying strata is real.

Again for completeness, the final figure in this series (Figure 5.30) shows the distribution of *i* with depth for test TH6. This test had the same clay cover above the tunnel axis as the tests just described but had a surface layer consisting of 93mm of medium/dense saturated sand. As the vertical effective stress around the tunnel was higher than in the tests above the results are not directly comparable, but it is clear that this geometry produced a wider distribution of *i* through the clay layer.

A full listing of the *i* values derived from the LVDT measurements for all tests is given in Table 5.2, including the *i* values for the upper sand surface. The values of *i* at both the sand

and the clay surfaces, plus the subsurface distributions in the clay layers are investigated in more detail in Chapter 6.

5.3.2 *Horizontal movements*

Predictions of ground movements due to tunnelling are generally made to assess potential damage to existing services and structures. Distortions imposed by the vertical ground movements are obviously a potential problem, but in addition, horizontal ground strains caused by differential horizontal movements are of concern. It is useful to extend the framework developed for predicting vertical movements above tunnels to include horizontal movements. This can be done by assuming that the vectors focus on a point source of ground loss somewhere on the vertical centreline of the tunnel, $x = 0$, although the point of focus may change as a function of distance above the tunnel axis.

Centrifuge tests RJG17 ($2.5D$ clay only above tunnel crown) and RJG20 ($1.5D$ loose dry sand over $2.5D$ clay above tunnel crown) have been used to assess whether a vector focus can be established for individual centrifuge tests. For each test, movements at a range of measurement horizons within the clay have been explored. However, in the first case, test RJG17, the movements near the free-surface of the clay have been considered in detail and in the second case, test RJG20, the movements near to the tunnel crown have been investigated in detail.

Figure 5.31 shows the focus of individual vectors at different heights above the tunnel axis level, at a range of volume losses, for test RJG17. In all cases the data used to establish the average vector focus was limited to points between $x = 0.5i$ and $1.5i$ ($\pm$) where the horizontal movements were expected to be largest. Data outside this range tended to be too noisy to draw meaningful conclusions. In the figures, points are shown for a limited number of discrete stages in the test, but the average focus was determined from all available data between volume losses of 5 and 20%. Results presented in Figure 5.31(a) are for a horizon 140mm above the tunnel axis, which is only 10mm from the free ground surface. The average vector focus is slightly above the tunnel crown, but it is clear that there is a trend for the vectors to project higher on the tunnel centreline as the horizontal distance from the tunnel increases. This indicates a higher proportion of horizontal to vertical movement with width and is consistent with the observations from the vectors in Figure 5.24(a). Figure 5.31(b) shows data for a horizon some 20mm closer to the tunnel and the average vector focus was found to have shifted to a point 132mm below the tunnel axis. The trend for an increasing

component of horizontal movement with width is less pronounced, though there is considerable scatter in the data. Figure 5.31(c) shows similar results for the horizon 80mm above the tunnel centreline, which is slightly greater than 1*D* above the tunnel crown. The average vector focus is fractionally lower than the preceding level at 143mm below the tunnel axis. No trend for an increase in the horizontal component of movement with width is apparent at this level, but the scatter in the data is still large.

Figure 5.32(a, b & c) shows the vertical and horizontal movements at the same horizons, for the same test, relative to the maximum vertical settlement. The suffix 'v' refers to vertical movement and 'h' to horizontal movement. Also plotted on the figure are the best fit Gaussian curves, determined from all available data between volume losses of 5 and 20%, and the distributions of horizontal movement assuming the previously determined average vector foci. High components of horizontal movement with increasing distance from the vertical centreline of the tunnel are obvious in Figure 5.32(a), which shows the data for the level only 10mm from the ground surface. Near to the surface the vectors do not seem to focus on a single point and the horizontal movements are therefore not well described by assuming a single vector focus. However, the horizontal movements 30mm below the ground surface are well described by assuming the average vector focus, with the possible exception of the region to the far right of the tunnel centreline where the data show slightly higher components of horizontal movement. At the horizon 80mm above the tunnel axis the movements are extremely well described by the average vector focus even though there is considerable scatter around the average value (Figure 5.31c).

A similar exercise was conducted for test RJG20. Figure 5.33(a, b & c) shows the average vector foci for levels 130mm, 90mm and 50mm above the tunnel axis. In this case the clay was overlain by a layer of loose dry sand. The data presented in Figure 5.33(a) are for a level 20mm below the clay/sand interface. The data are grouped together more tightly than for RJG17 but show that the movements were not completely symmetrical about the tunnel axis. An average vector focus of 145mm below the tunnel axis level was obtained. Some 40mm below, 90mm above the tunnel axis (Figure 5.33b), the average vector focus is slightly lower at 152mm below tunnel axis. In Figure 5.33(c), just 0.5*D* above the tunnel crown, the average vector focus has moved up to 102mm below the tunnel axis and a trend for higher components of horizontal movement near the tunnel centreline is apparent.

The relative vertical and horizontal movements for test RJG20 are plotted in Figure 5.34(a, b & c). Vertical movements presented previously in Figure 5.15. showed a settlement trough

offset by -10mm from the tunnel centreline. This explains the apparent asymmetry of the data plotted in Figure 5.33(a) used for determining the average vector focus. The data would have been symmetrical if the focus on x = -10mm had been plotted; however, the same average focus should have been determined. The best fit lines have been shifted to the left by 10mm to account for this. The average vector focus represents the data plotted at 130mm above tunnel axis level extremely well, and the comparison at the 90mm level is certainly satisfactory. At the horizon $0.5D$ above the tunnel crown the horizontal component of movement is greater near to the tunnel centreline than represented by the average vector focus. This is consistent with the vertical movement data which suggests a steeper settlement trough than described by the best fit Gaussian distribution.

The data presented above suggests that although attempting to determine a vector focus may produce some scatter in the results, the average focus tends to represent the horizontal movements reasonably successfully for a given distance above tunnel axis level. At or near a free ground surface the horizontal components of movement are considerably greater than those at depth. In this region, an average focus may not represent the movements well, as the horizontal component tends to increase with horizontal distance from the tunnel centreline. Also, vectors at this level tend to be directed above the tunnel axis. At horizons near to the tunnel, say within $0.5D$ of the crown, vertical settlements are not well represented by a Gaussian distribution and similarly horizontal movements cannot be considered to focus on a single point. However, the difference in vector focus at levels between these limits, that is between the regions near to the tunnel and the free ground surface, tends to be small. The vector focus for the middle zone can be approximated to a single point, and this point is significantly lower than the tunnel axis level.

5.3.3 *Pore pressures*

Pore pressure measurements were made around the tunnel during the centrifuge model tests, largely to determine equilibrium pore pressure profiles and hence vertical effective stresses. However, it is also interesting to examine the response around the tunnel during the reduction of support pressure.

Figure 5.35 shows the excess pore pressures generated around the tunnel during the support pressure reduction phase of test RJG15 ($3D$ clay only above the tunnel crown). It can be seen that significant negative excess pore pressures were developed, the magnitude reducing with distance from the tunnel. The pore pressure transducer b1, just below the tunnel axis, showed

a rapid increase in the rate of excess pore pressure production beyond $\Delta\sigma_T$ = -250kPa, presumably as the tunnel began to collapse.

As discussed in Chapter 2, Mair and Taylor (1993) produced plasticity solutions for changes in pore pressure around an unloaded cylindrical cavity under axisymmetric conditions. They found that an isotropic linear elastic-perfectly plastic soil model predicted zero pore pressure change in the elastic region, in contrast to measurements from centrifuge tests (Mair, 1979) and a deep tunnel in Boom clay (Neerdael and De Bruyn, 1989, Mair et al, 1992). They suggested that the difference between the predictions and observations may be due to one or all of the assumptions of isotropic soil behaviour, axisymmetric conditions and linear elastic soil behaviour. The condition of axisymmetry was probably reasonable for the deep tunnel in the Boom clay and may be applicable around the tunnel in the centrifuge tests here, where the ratio of σ_h' / σ_v' is equal to unity. Mair and Taylor (1993) went on to develop an expression for a non-linear elastic-perfectly plastic soil which was in better agreement with the observations, the solutions of which are produced below. R_{pnl} is the radius of the plastic zone (ie. limit of zone in which plastic strains develop) from the tunnel centreline and is given by;

$$\frac{R_{pnl}}{a} = \exp\left(\frac{N}{2} - 1\right) \tag{5.2}$$

where a is the radius of the tunnel ($D = 2a$), and for these tests,

$$N = \frac{\Delta\sigma_T}{s_u} \tag{5.3}$$

and s_u is the undrained shear strength of the soil around the tunnel. The change in pore pressure within the plastic zone is given by;

$$\frac{\Delta u}{s_u} = 1 - N + 2\ln\left(\frac{r}{a}\right) \tag{5.4}$$

and in the elastic zone;

$$\frac{\Delta u}{s_u} = -\frac{R_{pnl}}{r} \quad . \tag{5.5}$$

Predictions of the pore pressure changes around the tunnel in test RJG15 have been made using these solutions and compared with the centrifuge test data in Figure 5.36. One difficulty in applying the solutions is in determining a value for the undrained shear strength of the clay,

which was not measured directly in the centrifuge tests. Applying Critical State Soil Mechanics:

$$s_u = \frac{M}{2}.\exp\left(\frac{\Gamma - v}{\lambda}\right) \quad ; \tag{5.6}$$

which presents another problem as this expression is highly dependent on the specific volume, v. Using a value of $v = 2.07$, consistent with a saturated unit weight for kaolin of 17.5kN/m^3, gives an undrained shear strength of 75kPa. Mair (1979) produced a plot of undrained shear strength for one-dimensionally consolidated kaolin, which was dependent on overconsolidation ratio, current vertical effective stress and test conditions (plane strain or triaxial, extension or compression). Using this approach for RJG15 gives a range of s_u around the tunnel of between 50 and 75kPa, the lower value being for shearing in extension.

The value of s_u was varied within this range and compared with the measured response from test RJG15 for a range of changes in tunnel support pressure. It was found that the lower limit, s_u = 50kPa, gave the best comparison with the observations, and this has been plotted in Figure 5.36. Though not perfect the comparison is encouraging. Both extension and compression stress paths exist around a tunnel, but soil elements near the crown and invert are generally in extension. The lower value of s_u associated with these regions means that they are likely to be the first to experience the onset of gross plastic deformation and so the extension stress path may be considered to be dominant. The lower value of s_u = 50kPa may therefore be justified.

Figure 5.37 shows the excess pore pressures generated during centrifuge test RJG16 (1.5D medium/dense saturated sand overlying 1.5D clay above the tunnel crown). The negative excess pore pressures generated are similar in pattern and magnitude to those in test RJG15, the magnitude reducing with distance from the tunnel. A sudden increase in the rate of generation of excess pore pressures as $\Delta\sigma_T$ reduced, as in RJG15, is not apparent. Referring back to Figures 5.1 and 5.2 it is clear that much larger ground movements were generated around the tunnel in RJG15 at an earlier stage of the test, causing the greater excess pore pressures.

The plasticity solutions presented above were also compared to the measured response in test RJG16 and the results are presented in Figure 5.38. Again, a value of s_u = 50kPa was used and the comparison between predicted and measured response was similar to that for RJG15.

It is clear that significant negative excess pore pressures can be developed around a tunnel in overconsolidated clay. Localised increase in the excess pore pressures may occur as the soil around the tunnel approaches collapse. The plasticity solutions presented by Mair and Taylor (1993) can give reasonable predictions of the changes in pore pressure around an unloaded tunnel, but here they have been compared only with measured data from situations were the ratio of σ_h' / σ_v' around the tunnel was approximately equal to unity.

5.3.4 *Tunnel collapse*

Insight into the deformations around tunnels can be gained by plane strain idealisations, but the collapse of a tunnel is really a 3-dimensional event. It almost always occurs during construction at the tunnel heading or, less often and still 3-dimensional in nature, a failure of the lining at a discrete point along the tunnel. The collapse of a tunnel in two-layer ground conditions is therefore not a major part of this work. However, it is interesting to see what effect the different upper strata have on the collapse of the tunnel in plane strain conditions. The collapse load is a function of driving stress, supporting stress and shear strength of the soil around the tunnel. The effect of the upper strata on collapse loads can therefore be investigated by comparing the values of S_{max} or volume loss, V%, with change in tunnel support pressure for tests in which the vertical effective stress around the tunnel, and therefore undrained shear strength, were similar. The latter has been done for the centrifuge tests and the results are shown in Figure 5.39(a, b, c, d & e) with the tests divided into groups of similar vertical effective stress around the tunnel.

Many tests have been grouped together in Figure 5.39(a). All had 4D total cover above the tunnel crown and a water table slightly below the ground surface. Although the tests with an overlying sand layer are not tightly grouped together, they all reached higher volume losses for a given change in tunnel support pressure than the clay-only test presented (RJG9). In qualitative terms test RJG3 collapsed first, though in this test the sand was placed by hand and may not have been as dense as the overlying material in the other tests. RJG18 collapsed later than the other tests with overlying sand layers and the reason for this is not clear. The only identifying feature is that it was the only test in this group in which 52/100 LBS was used. A general trend for higher collapse loads with lower ratios of sand to clay cover is apparent.

Two tests are presented in Figure 5.39(b). One had an overlying layer of fluid surcharge (RJG11) and the other had an overlying layer of medium/dense sand (RJG12). Not

surprisingly the fluid surcharge caused the tunnel to reach higher volume losses for a given change in support pressure.

Figure 5.39(c) shows a different trend to that in Figure 5.39(a) above. The test with an overlying sand layer (RJG16) reached lower volume losses than the clay-only test (RJG15) for a given change in support pressure. In test RJG16 the sand layer consisted of medium/dense mixed LBS, which, in contrast to any other test conducted, was a well graded material. This suggests that a well graded coarse grained material may be more prone to arching than a uniformly graded material and hence may increase the collapse load of the tunnel to one greater than that for the equivalent clay-only soil profile.

Figure 5.39(d) presents data from tests RJG19 and RJG20 in which a clay layer was overlain by a medium/dense and a loose sample of 52/100 LBS respectively. It is not surprising that the test with the loose sand sample reached higher volume losses for a given change in support pressure. Clearly the dense material was more prone to arching than the loose material.

Finally, Figure 5.39(e) gives the results from the test series TH1 to 5 and MC01 in which the vertical effective stress in the clay was kept the same for each test. Four of the tests (TH1, TH3, TH4 and TH5) fall into the expected pattern. The volume loss for the test with an overlying fluid surcharge (TH5) was greatest for a given change in support pressure, followed by the test with the loose sand (TH4), the test with the medium/loose sand (TH3) and finally the test with clay only (TH1). However, the test with the overlying medium/dense dry sand (TH2) reached higher volume losses with change in support pressure than expected and the test with saturated medium/dense sand (MC01) reached extremely high volume losses for comparatively small changes in support pressure. The surprising relation of test TH2 to the other tests may be attributed to small differences in the model and experimental variability, but this is not adequate to explain the large differences seen in MC01. Either the clay had a considerably lower undrained shear strength than the other tests, possibly due to errors during preconsolidation of the clay or model preparation, or something fundamental is missing from the analysis, such as a reduction in the tendency for arching caused by the sand lying below the water table.

Tentatively, it may said that the presence of an overlying coarse grained material may increase or reduce the collapse load relative to a tunnel at the same depth in an all-clay soil profile, depending on the tendency for arching of the upper material. Compared to the

equivalent clay-only test, the collapse load was lower in all tests that had an upper stratum of poorly graded material and lower still if the material was loose. In the single test in which the upper stratum was well graded the collapse load was higher than the equivalent clay-only test. It appears that the tendency for arching increases with density and is considerably greater in well graded material than in poorly graded material. The collapse load will also vary with the ratio of sand to clay cover above the tunnel, depending on the tendency for arching in the sand.

5.4 Summary

Results from the centrifuge tests have been used in this chapter to illustrate the tests and the type and quality of data obtained. Basic trends in vertical movements, horizontal movements, pore pressure response and tunnel collapse have been presented and potential difficulties in using the image processing data have been addressed. The fundamental data important to the work have been given.

The main points highlighted by the data presented in this chapter are summarised below and refer mainly to a tunnel in clay overlain by a coarse grained layer.

i) Advances in digital image processing allow pre-collapse deformations to be studied in detail using centrifuge modelling techniques, and a thorough check on the quality of the measurement method can be achieved if used in combination with conventional LVDTs.

ii) Both surface and subsurface transverse settlement troughs are well described by Gaussian distributions, except in the immediate vicinity of the tunnel (within $0.5D$ of the crown) and at the "tails" of the troughs (beyond $\pm 2i$) where movements may be under-estimated.

iii) The form of the distributions, given by the value of i, is constant for a wide range of volume losses, at least 1% to 20%, at which point the tunnel may be considered to have started to collapse.

iv) The spread of movements in the clay, and therefore the distribution of i with depth, varies with the depth of cover for soil profiles made up of clay only, and the differences for cases when some of the cover is made up of coarse grained material have been measured.

v) Allowing for a degree of scatter, vectors of movement in the clay generally focus close to a point on the vertical centreline of the tunnel well below the tunnel axis, except near a free-surface where significantly larger components of horizontal movement occur and in the immediate vicinity of the tunnel (say within $0.5D$ of the crown).

vi) Significant negative excess pore water pressures are generated around a tunnel in overconsolidated clay if the soil is being unloaded, and these have been predicted adequately using plasticity solutions when the ratio of σ_h' / σ_v' near the tunnel is close to unity.

vii) A tunnel in clay with an overlying layer of coarse grained material may have a lower collapse load than a tunnel at the same depth in a clay-only soil profile, unless the upper material is prone to arching. Results from a single test suggest that a tunnel in clay with an overlying layer of dense well graded coarse grained material may have a higher collapse load than a tunnel at the same depth in a clay-only soil profile.

CHAPTER 6 SYNTHESIS AND DISCUSSION OF EXPERIMENTAL RESULTS

Within this chapter, the key experimental observations concerning ground movements around single tunnels in two-layer ground conditions are examined. The existing framework, referred to in Chapter 2, is used to explore trends in results. Results for the clay-only centrifuge tests are shown to be consistent and predictable within the current framework, but the distribution of movements through the upper sand layers are seen to be less consistent. Wider settlement troughs were observed in the lower clay stratum when an overlying layer of coarse grained material was present, than at the same depth in a clay-only soil profile. Reasons for the differences in settlement trough widths from those of an all-clay soil profile are examined including the magnitude of vertical effective stress and the ratio of stiffness of the two materials. Accounting for the ratio of the shear stiffness of the two materials at the interface between them provided the best correlation with the test data. Further analysis and discussion suggests that this is the most appropriate approach when predicting tunnelling-induced movements in two-layer ground conditions. Statements are made regarding the focus of vectors of ground movement in clays which, combined with the observations mentioned above, leads to suggested improvements to prediction procedures for both vertical and horizontal movements. The recommended procedures are assessed by direct comparison with centrifuge test data.

6.1 Vertical movements in the clay

Vertical movements are usually the primary concern when predicting ground movements due to tunnelling and potential damage to existing structures. Horizontal movements tend to be inferred as a function of the vertical movements, and the distance above the tunnel axis, and this is investigated later in the chapter.

6.1.1 *Existing framework*

The terms used for defining the geometry associated with ground movements around tunnels in two-layer ground conditions were presented in Chapter 2. These terms are fundamental to describing the existing framework and observations from the experimental results, and are illustrated in Figure 6.1. An important point to note is that the term $(z_0 - z)$ is simply the vertical distance above the tunnel axis.

Rules for predicting vertical ground movements due to tunnelling have been discussed generally in Chapter 2. O'Reilly and New (1982) reported that the transverse surface settlement trough width is characterised by i, the horizontal distance from the tunnel centreline to the point of inflexion of the settlement trough. They stated that for the excavation of a single long tunnel in London clay, i can be defined simply as a function of the tunnel depth as;

$$i = 0.5z_0 \ . \tag{6.1}$$

Many field measurements have shown this expression to be reasonable for surface settlement troughs and some have extended the use to subsurface regions such that

$$i = 0.5(z_0 - z) \ . \tag{6.2}$$

Using field measurements and centrifuge test data given by Mair (1979), Mair et al (1993) suggested that although the above expression was reasonable at the surface for an all-clay soil profile, the subsurface trough width was considerably under-estimated. They presented the following:

$$i/z_0 = 0.175 + 0.325(1 - z/z_0) \ . \tag{6.3 (2.15 bis)}$$

It should be noted that at the ground surface $z/z_0 = 0$ and equation (6.3) reverts to equation (6.1). Equation (6.3) was presented in Figure 2.9 along with the data from which it was derived. As an apparently reasonable representation of the spread of vertical subsurface movements in clay, equation (6.3) is the datum to which trends in the centrifuge test data obtained are referred and it represents the framework against which the results are considered.

6.1.2 *Results from centrifuge tests with all-clay soil profiles*

Figure 6.2 shows the distribution of i with depth, non-dimensionalised by the depth to the tunnel axis, for the centrifuge tests with all-clay soil profiles and in which the quality of measurements from image processing was assessed as adequate for quantitative use. In the plot the tunnel axis is at $z/z_0 = 1$, and at the ground surface $z/z_0 = 0$. As with all the results presented in this chapter, the values of i are considered to be the "best fit" for each test and were determined from data over a range of volume losses from 2% to 20% (or up to $\sigma_T = 0$) for LVDT measurements, and usually from 5% to 20% (or up to $\sigma_T = 0$) for image processing measurements. The lower limits represent the smallest volume losses, approximately, at which values of i could be determined, with confidence, above the level of noise for that measurement method. In between the limits, the values of i determined were practically

constant. After volume losses of approximately 20% had been reached the values of i tended to reduce quite rapidly and this is thought to be caused by the onset of collapse at the tunnel. Also shown on Figure 6.2 are the lines representing equations (6.2) and (6.3). It is clear that the centrifuge test data are in very close agreement with equation (6.3) (Mair et al, 1993). Although the majority are marginally to the right of the line it is interesting to note that the scatter is considerably less than the data from which the line was originally determined (Figure 2.9). Having established that the distribution of i with depth determined from the centrifuge tests with all-clay soil profiles is well described by this equation it will be used as a reference to assess the other data and referred to as the all-clay or clay-only line.

The points on the line $z/z_0 = 0$ are from LVDT measurements and the values of i/z_0 at this horizon for tests RJG15 and TH1 plot significantly further from equation (6.3) than those determined from image processing data. Initially it was thought that the values of i determined from image processing measurements may be artificially small due to the under-measurement caused by friction, which, as it was shown in Chapter 5, may lead to low values of i. Although there may be some effect on the data shown in Figure 6.2, the tendency to deviate from the clay-only line is also apparent in the data points just below the surface which were determined from image processing measurements. This suggests that the rate of widening of the trough may increase in close proximity to the (unrestrained) surface of the clay.

As the depth approaches $z/z_0 = 1$, in close proximity to the tunnel axis, there is a tendency for values of i to decrease more rapidly than implied by equation (6.3). The data points representing the horizon $0.5D$ above the tunnel crown have been identified for each test shown and the rapid narrowing of the trough which occurs between the crown and these points is evident. Although the data in this region do represent best fit values of i, it was shown in Chapter 5 that the settlement troughs are unlikely to be well represented by Gaussian distributions within $0.5D$ of the tunnel crown. In fact, the troughs are likely to be even narrower than the representative values of i from the best fit Gaussian distributions.

Thus, in general, the tests with all-clay soil profiles produced data which are in very close agreement with the clay-only line of Mair et al (1993), although the distribution of i with depth appears to be slightly 'S' shaped at the extremes.

Figure 6.3 shows similar plots for values of i determined from LVDT measurements at the top horizon of the clay, that is at the clay/sand interface if present, or at the clay surface for clay-

only soil profiles. Figure 6.3(a) shows the data points labelled by test (one per test in which the prefix R refers to the RJG test series, T the TH series and M1 is test MC01) and Figure 6.3(b) shows the data points identified by the type of overlying layer. The data at the clay surface for clay-only soil profiles lie on the $z/z_0 = 0$ axis. The fluid surcharge used in tests RJG11 and TH5 has been treated as a layer of material with zero shear stiffness and so the depth of the tunnel for these tests, z_0, has been measured from the surface of the fluid. There is quite a spread along this axis which emphasises the observation made above concerning the rapid widening of the troughs in the proximity of the clay surface. There is no obvious correlation between the geometry of the tests, or the depth to the water table, and the offset in the value of i/z_0 from the clay-only line at the ground surface, $z/z_0 = 0$.

6.1.3 *Results from centrifuge tests with clay and different overlying materials*

Figure 6.3 also illustrates the effect on the distribution of i in the clay when there is an overlying layer of different material. z_0 is taken as the depth from the surface of the upper layer to the tunnel axis and a direct comparison can be made with the distribution of i from all-clay soil profiles, represented by equation (6.3). Clearly, the majority of the data show that significantly wider values of i were observed at the clay/sand interface than would have been expected at the same depth had the soil profile consisted only of clay. The two tests in which water (contained in a rubber bag) was used as a flexible surcharge (RJG11 and TH5) plot inside the clay-only line (z_0 was measured from the surface of the surcharge). The remaining tests plot outside the all-clay line with the two closest to it representing tests RJG20 and TH4, which were the only two tests in which the sand layer was in a loose state. In the remainder of the tests the soil profiles were either all-clay or had a surface layer of medium/dense sand (of various types), with the exception of TH3 which had a surface layer of medium/loose sand. It is difficult to determine a pattern without further reference to material properties, except to say that generally the offset from the all-clay line increased with the depth of sand.

Stiffnesses measured in the triaxial tests and presented in Chapter 4 showed that the 14/25 Leighton Buzzard Sand (LBS) was the stiffest material used, followed by the mixed LBS. These sands were used in two of the tests only but both showed significant proportional differences in the observed values of i from that observed for an all-clay soil profile. Again, there is no obvious effect of the position of the water table.

It is clear that rules for predicting the distribution of i in single soil ground profiles may not be adequate for situations where there is an overlying strata of a different material. The simple rules of superposition suggested by Selby (1988) and New and O'Reilly (1991), and discussed in Section 2.2.4, treat each layer independently and do not account for interaction between the layers. Assessing when the presence of an overlying layer has a significant influence on the distribution of i requires detailed examination.

6.2 Vertical movements in the overlying sand

Owing to the difficulties of measuring movements using image processing in the sand layers, the only reliable data available for the movement of the sand are the vertical displacements obtained using LVDTs. Therefore, it is possible only to investigate the average spread of vertical movements through the sand by examination of LVDT data at the boundaries of the layers: the clay/sand interface below and the sand/ground surface above.

6.2.1 *Existing framework*

Recent work by Dyer et al (1996) suggested that the spread of movements with depth due to tunnelling in coarse grained material may be represented by an expression similar to equation (6.3) for clay. A linearly varying distribution of i with depth requires both an offset and a gradient. The values of i are generally smaller than for clay, so in the expression describing the distribution of i with depth the magnitudes of both the offset and gradient are smaller than for clay. However, for the centrifuge tests conducted the tunnel was not constructed in the sand, but in clay with an overlying layer of coarse grained material. As such the offset of the distribution of i was dictated by the spread of movements through the clay, and so defined by the value of i at the clay/sand interface. Consequently, only the gradient of the distribution of i through the sand layer can be examined.

O'Reilly and New (1982) suggested that the width of the surface settlement trough in sands could be determined in a similar way to that for clays, and concluded that

$$i = 0.25 z_0 \tag{6.4}$$

was appropriate.

The factor 0.25, and 0.5 for clays in equations (6.1) and (6.2), is often referred to as the settlement trough width parameter, K. When considering distributions of movement with depth,

$$i = K(z_0 - z) \ , \tag{6.5}$$

and a constant value of K implies that the distribution of i has a constant gradient and starts from zero at the tunnel axis; thus the offset is zero. As stated by Mair et al (1993), equation (6.3) for the distribution of i with depth in clay implies a value of K which changes with depth, and after Dyer et al (1996) this also appears to be true for tunnels in sand. However, the distribution of i through the sand layers for the centrifuge tests can be examined by the average gradient only, and this gradient will be referred to as;

$$K_{s\,(grad)} = \frac{(i_s - i_c)}{(z_0 - z)} = \frac{(i_s - i_c)}{z_1} \ . \tag{6.6}$$

It should be noted that $K_{s\,(grad)}$ here is not being used in the conventional manner as it does not account for the offset in the distribution of i. The expression should be written as;

$$\Delta i_s = K_{s\,(grad)} \Delta z_1 \tag{6.7a}$$

and the absolute value is

$$i_s = i_c + K_{s(grad)} z_1 \ . \tag{6.7b}$$

In this case, $K_{s\,(grad)}$ is the gradient of the distribution of i through the layer, the offset is not a function of tunnel depth (z_0), as it would be if the tunnel was in the sand, but is provided by the value of i imposed at the base of the layer from the movements at the clay/sand interface.

The average gradient of the distribution of i through the sand layers, $K_{s\,(grad)}$, is used to investigate the vertical movements in the sand.

6.2.2 *Results from centrifuge model tests*

Figure 6.4(a & b) shows the increase in the value of i through the sand layer, (i_s - i_c), plotted against the depth of the sand layer, z_1. Figure 6.4(a) shows the data points labelled by test (one per test in which the prefix R refers to the RJG test series, T the TH series and M1 is test MC01) and Figure 6.4(b) shows the data points identified by the type and condition of the sand. Lines depicting a range of values of $K_{s\,(grad)}$ from 0.15 to 0.35 have been plotted as an approximate envelope to the data, and the line for $K_{s\,(grad)} = 0.25$ has also been included.

Before examining the data, it should be noted that the values of i determined for the sand surfaces are not as reliable as those determined for the clay surfaces. Firstly, the movement data tended to be slightly more erratic. Secondly, the sand surface lay further from the tunnel than the clay/sand interface. As such, the settlement troughs were wider than for the clay/sand interface, thus increasing the risk of including far-field data in the determination of values of i (data used within $x = \pm 2i$), which may have been influenced by lateral boundary effects.

There is an additional concern regarding the use of average distributions of i through the sand layers, determined from measurements at the boundaries only. The upper surface of the sand was in all cases a free-surface and, following the patterns observed in the clay-only tests, it is likely that the distributions of i increased more rapidly in the proximity of the free-surface. In these circumstances the average distributions of i through the sand layers would be of less relevance. However, the data in Figure 6.4 are quite widely and evenly spread between $K_{s\ (grad)} = 0.15$ and $K_{s\ (grad)} = 0.35$. If rapid widening of the distribution of i was occurring towards the free-surface, there should be a tendency for larger average values of $K_{s\ (grad)}$ in the tests with the thinnest sand layers. There is no clear evidence of this.

One pattern that may be extracted from Figure 6.4 is a slight tendency for the sands below the water table to have lower values of $K_{s\ (grad)}$ (in the region of 0.15 to 0.2) and those above the water table to have higher values (approaching 0.35). The lower values, for which the sands were below the water table, are also associated with the medium/dense Flint gravel sand and 52/100LBS, which have very similar particle size distributions and very similar stiffnesses (low relative to the other sands used). In the cases where sands below the water table have relatively high values of $K_{s\ (grad)}$, the material is associated with relatively high stiffnesses, as shown in Chapter 4. The above observations are by no means conclusive and in all cases some contradictory data exist.

Using the parameter in the more conventional manner, Peck (1969) suggested that values of K for surface settlement troughs due to tunnels in sands below the water table were higher than those in clays, and that values in sands above the water table were lower than in clays. In contrast, Mair and Taylor (1997) in reviewing a number of case histories, suggested there was no significant difference in the values of K for surface settlement troughs in sands above or below the water table. The data presented here suggests that the difference, if any, is relatively small, but that higher values of K may be assumed for sands above the water table than for those below.

6.3 Analysis of settlement trough widths in clay from centrifuge test data

It is clear from Figures 6.2 and 6.3 that the centrifuge tests for clay-only soil profiles produced results that were consistent with current practice but that ground profiles of more than one soil layer require further consideration. Figure 6.3 showed that the movements due to tunnelling in clay can be modified significantly from that of the clay-only soil profile if the upper part of the profile is a different material. Differences in the distribution of movements in sands overlying clay were observed in Figure 6.4, although the trends were not conclusive.

The validity of equation (6.3), after Mair et al (1993), for clay-only soil profiles has been confirmed and is therefore a good reference from which to explore the differences in the other test data.

6.3.1 *Characterising differences between tests*

When considering the movements due to tunnelling in a layer of clay with different overlying materials, the main differences between cases are the stresses in the clay imposed by the overlying material and the stiffness characteristics of the two materials.

Equation (6.3), proposed by Mair et al (1993) for clay-only soil profiles is illustrated in Figure 6.5. Distributions of i are plotted against distance from the tunnel axis (z_0 - z) for three different tunnel depths z_0. Increasing the depth of the tunnel increases the offset of the distribution of i from the vertical centreline of the tunnel but the gradient remains the same. These distributions were shown to be valid for clay-only soil profiles, especially overconsolidated clays, in which the unit weight of the soil is reasonably constant with depth. In these cases the depth, z_0, may be considered to represent the effective stress at the tunnel axis. However, if a layer of soil of different unit weight is overlying the clay the effective stress at the tunnel axis level is not represented by z_0 alone. It is relatively simple to determine an effective depth z_e to represent the effective stress at the tunnel axis if all of the soil above is saturated clay as;

$$z_e = \frac{\sigma_{v'T}}{\gamma_c - \gamma_w} \tag{6.8}$$

where $\sigma_{v'T}$ is the vertical effective stress at tunnel axis level,

γ_c is the unit weight of the saturated clay,

γ_w is the unit weight of water, and

z_e is the equivalent depth to the tunnel axis.

Differences in stiffness between the clay and overlying material are not so straightforward to characterise. However, it is more important to have a consistent method of characterising the ratio of stiffnesses of the two materials, rather than to have an absolute measure of stiffness. The stiffness of soil is known to be highly non-linear and so the shear stiffness at very small strains, G'_{max}, has been chosen, as the only intrinsic stiffness. The determination of the stiffnesses was described in Chapter 4. For the kaolin they have been calculated using the work of Viggiani and Atkinson (1995) and for the sands they have been calculated from bender element measurements in triaxial tests and using the framework of Jovicic and Coop (1997), with a slight modification. The assumed variation of stiffness with depth in both the sand and the clay layers is given in Figure 6.6 for centrifuge test RJG18 (1.5D sand over 2.5D clay above the tunnel crown). It is a good illustration of the calculated distribution of G'_{max} for the centrifuge tests. Of course, the actual distributions of stiffness at low values of mean normal effective stress, p', are not well defined and the profile of stiffness at the interface, where the soil type changes, may not be the sudden step change shown. However, it is thought to be a representative profile for the purposes of analysis.

If only vertical stress is considered to influence the movements in the clay and the value of z_0 was converted to a value of z_e as defined by equation (6.8), the stiffness profile from the clay layer may be considered to extend above the clay/sand interface to a height z_e above the tunnel axis. This will have accounted for the stress and stiffness in the lower clay layer but not the stiffness of the sand, which in this instance is higher at the interface than that of the clay.

Table 6.1 lists all of the centrifuge tests conducted and the shear stiffnesses, G'_{max}, which may characterise the soils in the tests. These include: the average value of G'_{max} for each layer, calculated by integrating the distributions with depth for each test and dividing by the depth of each layer; the value of G'_{max} at the interface for both the clay and the sand; and the value of G'_{max} at the tunnel axis. For the clay-only tests a value of G'_{max} has been quoted assuming that full pore suction is maintained at the ground surface corresponding to the depth of the water table.

If stiffness can be used to characterise the modification of ground movements then the solution should be based on a sensible, physical mechanism which should be supported by the data. One particular mechanism is investigated in detail below and others are considered in the discussion that follows.

6.3.2 *Accounting for vertical effective stress in the clay*

Equation (6.8) describes a way of accounting for different vertical effective stresses in the lower clay layer caused by overlying layers of different unit weights or by variations in the position of the water table. Although it amounts to the same thing, rather than consider the vertical effective stress at the tunnel axis, it is perhaps more appropriate to think of the thickness of the sand layer being increased to correspond to a depth consistent with the vertical effective stress at the interface with the clay, as if it had the same value of $(\gamma - \gamma_w)$ as the saturated clay. The expression for z_e, accounting for vertical effective stress, would then be written;

$$z_e = (z_0 - z_1) + \frac{\sigma_{v'(i)}}{(\gamma_c - \gamma_w)} \tag{6.9}$$

where z_1 is the thickness of the upper layer, so that
$(z_0 - z_1)$ is simply the depth of clay above the tunnel axis, and
$\sigma_{v'(i)}$ is the vertical effective stress at the interface (or at the clay surface in the case of a clay-only soil profile - see below).

This has been applied to the test data and the results are shown in Figure 6.7. The plots show data for the clay layers only which have been non-dimensionalised by the effective depth to the tunnel axis, z_e, determined from equation (6.9). They are analogous to the plots shown in Figures (6.2) and (6.3), and presented by Mair et al (1993) as given in Figure 2.9, except that the depth below ground surface (z) has been replaced by the depth above the tunnel axis $(z_0 - z)$. Using the level of the tunnel axis as a datum seems sensible when considering movements in the lower clay layer. The ordinate has been inverted such that a value of zero represents the tunnel axis. As the reference material is saturated clay, it should be noted that for a clay-only test a value of $(z_0 - z) / z_e = 1$ represents the ground surface only if the water table is coincident with the ground surface. If the water table is below ground surface, z_e will be greater than z_0 according to equation (6.9). The vertical effective stress will not be zero at the ground surface if pore suctions are assumed due to a water table some distance below. This effective stress is accounted for by adding an additional depth of saturated clay to z_0.

Figure 6.7(a) shows the data determined from LVDT measurements of the clay surface and clay/sand interface. As described above, the data points at the clay surface for the clay-only tests do not correspond to $(z_0 - z) / z_e = 1$ because the water table was below the ground surface and pore suctions were assumed. Having factored the data for effective stress there is a

reasonable fit to the all-clay line, although most of the data still fall to the right of it. The tests with proportionally greater depths of sand are amongst the furthest away.

Figure 6.7(b) shows the subsurface data from image processing and LVDT measurements for tests TH1 to 5 and MC01. In this test series the vertical effective stress profile in the clay layer was deliberately kept the same for each test and z_e had a value of 175mm, corresponding to the value of z_0 for the saturated all-clay test, TH1. The spread of the distributions of i is therefore identical to that of the raw test data which was shown in Figure 5.29. There is a clear tendency for the values of i in the clay to be greater when the upper layer is stiff and narrower when it is less stiff.

In Figure 6.7(c) the results of tests RJG17 to 20, including subsurface movements in the clay layer, have been factored for vertical effective stress. They plot relatively close to the clay-only line, especially the points representing measurement by LVDTs (the highest point in each series). Unlike the data in Figures 6.7(a & b) almost all of the points are to the left of the all-clay line, those farthest from it are very close to the tunnel (within $0.5D$ of the crown) in the region where the troughs have been shown to be very steep and not well represented by Gaussian distributions.

All of the above results, factored for vertical effective stress using equation (6.9), have been plotted together in Figures 6.8(a and b). Figure 6.8(a) shows the factored data compared to the clay-only line defined by equation (6.3). There is a spread of data but the scatter is quite balanced around the clay-only line. Figure 6.8(b) shows the same data but this time they are compared to the results from the clay-only tests, which, being measured in the same way, are the most appropriate reference data from which the differences should be assessed. It is interesting that factoring for vertical effective stress has produced a greater spread in the clay-only test data than the unfactored data (see Figure 6.2).

From the evidence in the figures above, it appears that accounting for vertical effective stress may not be sufficient to explain the differences in the test results. This is particularly evident in Figure 6.7(a) for the tests with proportionally large amounts of sand, that is those with low $(z_0 - z) / z_e$ values, and in Figure 6.7(b) where there is quite a spread of results despite having isolated the vertical effective stress throughout the test series.

6.3.3 *Accounting for shear stiffness at the clay/sand interface*

For a subsurface horizon in a mass of clay subjected to tunnelling-induced movements, the value of i can be predicted using equation (6.3). However, if the clay above that horizon was replaced by a material of different stiffness and the tunnelling event repeated, a different value of i would be produced. This has been illustrated clearly by the centrifuge test data and it has also been shown that the difference is not completely accounted for by considering the vertical effective stress.

In the first case, the all-clay soil profile, the elements of clay just above and below the horizon had practically the same properties. In moving incrementally up through a layer of clay the ratio of stiffnesses of the elements of soil above and below each other is very close to unity. These soil elements vertically adjacent to each other have the same resistance to distortion. However, at an interface with a layer of different material there is generally a distinct change in the ratio of stiffnesses. The elements above and below the interface have different resistance to distortion, and it is logical that this could cause a change in the pattern of ground movements.

A measure of the resistance of elements to distort, in a manner which may be associated with ground movements due to tunnelling, is simply the shear stiffness, G, for which the value at very small strains, G'_{max}, can be used. It seems appropriate to consider the ratio of the shear stiffnesses of the soil elements at the interface to assess the impact of an overlying soil layer on the distribution of tunnelling-induced ground movements.

The effect of the ratio of stiffness could be applied by factoring the depth of the upper layer by the ratio of stiffnesses at the interface, so that;

$$z_e = (z_0 - z_1) + \frac{G'_{max\,(si)}}{G'_{max\,(ci)}} . z_1 \qquad (6.10)$$

where $G'_{max\,(si)}$ and $G'_{max\,(ci)}$ are the shear stiffnesses at very small strains of the sand and clay respectively, at the interface between the two materials.

Figure 6.9 shows the test data with equation (6.10) applied. Again, the first plot, Figure 6.9(a), is for the LVDTs at the clay/sand interface or the clay surface. In this case, the results for the ground surface in the clay-only tests are at a value of $(z_0 - z) / z_e = 1$, as there is no material with stiffness overlying the surface elements. The same is true of the tests in which

water was used as a flexible surcharge. The value of z_e is the depth of clay only, as water has no shear stiffness. The clay-only data therefore show the same scatter at the free-surface as previously seen in the unfactored data, and included in this scatter are two points from the tests with the fluid overburden. With the exception of one test, the results for the clay/sand interface generally fall closer to the clay-only line than when they were factored for vertical effective stress.

The same is true for the data from TH1 to 5 and MC01 shown in Figure 6.9(b). Although not falling on a single line, the grouping of the results is considerably closer to the clay-only line than seen previously in Figure 6.7(b).

Figure 6.9(c) shows the data from tests RJG17 to RJG20. Applying a factor for stiffness to these data has moved them slightly to the left of the clay-only line, but the grouping is still relatively close.

Figure 6.10 shows all of the data together, factored for the ratio of shear stiffnesses at the interface. The data are compared to the clay-only line, equation (6.3), in Figure 6.10(a). There is still a degree of scatter but it is less than when the data are factored for vertical effective stress and it is well balanced around the clay-only line. The same data appear in Figure 6.10(b), factored in the same way but now compared to the clay-only test results. The spread of results for the clay-only tests does not alter when the factor for stiffness is applied in accordance with equation (6.10) and, therefore, the grouping is much closer than in Figure 6.8(b).

Factoring for stiffness seems to offer more promise than factoring for vertical effective stress. In factoring for stiffness in these frictional materials, the vertical effective stress (or more correctly the mean normal effective stress) is also being considered, since stiffness is stress dependent.

6.3.4 *Discussion*

As mentioned above, the stiffness of soils depends partly on effective stress. It is likely, therefore, that applying equation (6.10) also accounts to some extent for the stress in the soils. With regard to the centrifuge tests results, applying factors for both vertical effective stress and stiffness to the data would clearly move them well to the left of the clay-only line.

It has been shown that equation (6.3) may be used to predict the spread of movements through a layer of clay with an overlying layer of different material, if the tunnel depth is modified to account for the differences between the layers. Accounting for the different unit weights of the soil would improve predictions, but good correlation between the spread of data and the ratio of stiffness at the interface between the two materials has been demonstrated. This correlation has been investigated simply by using G'_{max} of the soils at the interface between the layers but it is important to investigate alternative methods of quantifying the relative stiffness of the two layers.

Many researchers over the years have simplified the behaviour of buildings overlying soil by considering it to be analogous to that of deep beams. Recently Potts and Addenbrooke (1996, 1997) adopted a similar method in attempting to characterise the effect of building stiffness on reducing the impact on structures of ground movements due to tunnelling.

It seems reasonable to explore the possibility of adopting a similar approach in characterising the effect of stiffness when one layer of soil is overlying another. For a long tunnel, as for the plane strain centrifuge model tests, the out of plane dimension is effectively unity. The resistance to shearing of a rectangular section beam of unit breadth may be considered as;

$$\text{resistance to shear} = Gd \quad , \tag{6.11}$$

and to bending;

$$\text{resistance to bending} = EI = \frac{Ed^3}{12} \tag{6.12}$$

For the soil layers, d is simply the depth of the layer, E is Young's modulus and I is the second moment of area. Average stiffness moduli for the layers should be used and average values of G'_{max} for the layers of soil in the centrifuge tests are given in Table 6.1. For the purposes of this analysis values of E may be estimated by assuming isotropic elasticity, so that

$$E = 2G(1+\nu) \quad , \tag{6.13}$$

and Poisson's ratio, ν, should assume values for undrained behaviour (ν=0.5) and drained behaviour ($\nu \approx 0.3$) as necessary.

Clearly, the relative stiffnesses of the layers in terms of equations (6.11) and (6.12) above are significantly influenced by the depth of the layers, d. Ratios of stiffness, or resistance, for the upper soil layer to the lower clay layer in the centrifuge tests range from 0.2, for test RJG4, to

8.6, for test RJG8, using equation (6.11). Applying equation (6.12) results in a range of relative bending stiffness ratios from 0.02, for test RJG4, to 186, for test RJG8. In terms of both shear and bending resistance the clay layer is proportionally stiffer than the sand stratum unless the depth of sand exceeds that of the clay. The data suggest that these relative stiffness ratios are not appropriate to this problem.

The response of an element of soil to perturbations is governed by the in situ stress conditions, or the depth of soil above it. The relative stiffness of the two soils must be characterised by their stiffnesses at analogous points in the soil profile, that is, the interface between the two soils. The depth of soil is already accounted for in the existing framework, equation (6.3), and any difference in unit weights of the soil forms part of the calculation of stiffnesses. The equivalent depth to the tunnel, z_e, should not include independent factors for both effective stress and stiffness.

Another consideration is the change in stress at the interface between two materials. Although the vertical effective stress profile with depth may be relatively smooth, there will be a change in the horizontal stresses at an interface between two soils, represented by the change in K_0, and it is possible that this may affect the distribution of movements. For the clay-only centrifuge tests, as the free-surface is approached from beneath, the value of K_0 increased rapidly due to the rapidly increasing overconsolidation ratio. The increasing proportion of horizontal to vertical stresses may be responsible for the marked widening of the settlement troughs and associated high horizontal movements observed in this vicinity. However, in the centrifuge tests with an overlying sand layer the value of K_0 in the clay near the clay/sand interface did not increase in the same way due to the overburden of the sand. No rapid widening of the settlement troughs in the clay was observed in the vicinity of an interface with a sand layer, unlike in the region below a free-surface. The values of K_0 in the materials at the interface will be different but it is unlikely that the change in K_0 alone could cause the significant influence on the movements throughout the clay layer. For calculating stiffnesses in the sands a value of $K_0 = 0.57$ has been used throughout, which is a reasonable value for a 1-dimensionally compressed silica sand (Coop and Lee, 1993). Values of K_0 at the interface for the clay ranged from 0.84 to 1.42 (equation 4.2 after Mayne and Kulhawy, 1982), depending on the depth of sand and position of the water table. Compared to the changes in K_0 as a free-surface is approached in overconsolidated clay, the differences between the values in the sand and the clay at the interface are relatively small. With regard to the overall patterns of movement throughout the underlying clay layer, the horizontal stress change at an

interface with a different overlying layer is included in equation (6.10), if values of G'_{max} are dependent on p', as in the analysis presented.

Considering the mechanism for the distortion of soil elements above a tunnel and having observed the differences in the data presented here, factoring the depth of the overlying layer by the ratio of the shear stiffnesses at the soil interface (equation 6.10), would seem the most appropriate method of taking into account the differences in soil stiffnesses when predicting ground movements above tunnels in two-layer ground conditions. In field situations it may prove more practical to use alternative, but consistent, directly measured stiffness moduli to account for the effect of relative stiffness.

6.4 Predicting tunnelling-induced ground movements

6.4.1 *Discussion*

Assuming that settlement troughs are Gaussian distributions and that i varies with depth in accordance with equation (6.5), $i = K(z_0 - z)$, O'Reilly and New (1982) stated that if a constant value of the trough width parameter K is assumed and the constant volume condition applies (valid for the short-term in clay), vectors of movement are directed towards the axis of the tunnel. Equation (6.3), suggested by Mair et al (1993), implies that K increases with depth as;

$$K = \frac{0.175 + 0.325(1 - z / z_0)}{1 - z / z_0} \quad . \qquad (6.14)\ (2.16\ \text{bis})$$

Taylor (1995b) stated that with this distribution of K and assuming constant volume conditions, the vectors of movement would then be directed at a point $0.175z_0/0.325$ below the tunnel axis, which is the intersection of the distribution of i with depth, described by equation (6.3), with the vertical centreline of the tunnel.

In both of the above cases the distribution of i with depth is a straight line, and in both cases it has been stated that the vectors of movement are directed at the point where the straight line distribution of i intersects the vertical centreline of the tunnel. Similarly, it may be assumed that if the distribution of i with depth is not a straight line, the vectors of movement at any horizon will be directed towards the point where the tangent to the distribution intersects with the tunnel centreline. The validity of this is demonstrated in Appendix A, assuming that: vertical settlement profiles are of Gaussian form; constant volume conditions apply; and that

the focus of ground movements at any particular horizon does not vary with distance, x, from the vertical centreline of the tunnel.

The distributions of i with depth seen earlier in this chapter suggest a rapid narrowing of the troughs in close proximity to the tunnel, although the Gaussian distribution is less valid in this region. They also suggest a rapid widening of the troughs as a free-surface is approached. An exaggerated curve of this form has been sketched in Figure 6.11(a) with tangents to the distribution and the associated intersections with the tunnel centreline. Figure 6.11(b) illustrates how the vectors focus on the intersections of the tangents to the distribution of i with the tunnel centreline. If a straight line is assumed for most of the depth, the vectors focus at a single point, shown well below the tunnel axis, for the majority of the depth of soil. Near the tunnel the focus may be closer to the tunnel axis, and towards the free-surface the vector focus may be above the tunnel axis. All of these characteristics were observed in the movement vectors from the centrifuge tests examined in detail in Chapter 5, and in the distributions of i with depth for the clay-only tests (Figures 6.2 and 6.10(b)).

Coarse grained materials respond in a drained manner to tunnelling-induced ground movements. As such they are not constrained by conditions of constant volume and the horizontal movements do not depend on the vertical movements. The vectors of movement can be directed anywhere.

6.4.2 *Procedure*

Both surface and subsurface settlement troughs are generally well described by Gaussian distributions (equation 2.9). Equation (6.3), given by Mair et al (1993), has been shown to predict adequately the width of settlement troughs above a tunnel in a clay-only soil profile. The width of the settlement trough at any particular horizon above the tunnel is basically a function of the distance above the source of movement and the vertical effective stress at that horizon. Mair et al (1993) used the ground surface as a reference horizon, but when considering movements in a layer of clay which is overlain by a layer of coarse grained material it seems more appropriate to use the tunnel axis level as the reference horizon. Equation (6.3) can be re-written as;

$$i/z_0 = 0.175 + 0.325\left(\frac{z_0 - z}{z_0}\right) \quad . \tag{6.15}$$

The effect of the overlying layer on the movements in the clay can be taken into account by determining an equivalent depth, z_e, which accounts for the difference in stiffness between the two materials such that;

$$i/z_e = 0.175 + 0.325\left(\frac{z_0 - z}{z_e}\right) \tag{6.16}$$

where

$$z_e = (z_0 - z_1) + \frac{G'_{\max(si)}}{G'_{\max(ci)}}.z_1 \quad . \tag{6.17) (6.10 bis}$$

Assuming a Gaussian distribution for the vertical settlement profiles, the horizontal ground movements can be described as a function of the vertical movements via the distribution of i with depth, provided that the constant volume condition applies and the vector focus at any particular horizon is not a function of horizontal distance from the vertical centreline of the tunnel, x. The vectors of movement can be assumed to be directed towards the point at which the tangent to the distribution of i with depth intersects the vertical axis of the tunnel. For the majority of the clay profile the distribution of i with depth can be assumed to be linear and it intersects the vertical centreline of the tunnel at a distance $0.175z_e/0.325$ below the centre of the tunnel. Generally, horizontal movements can be expressed as a function of the vertical movements as;

$$S_h = \frac{S_v.x}{z_0 + \frac{0.175}{0.325}z_e} \quad . \tag{6.18}$$

In the vicinity of a free-surface, or for horizons within $0.5D$ of the tunnel crown, the vector focus will be somewhat higher than $0.175z_e/0.325$ below the tunnel axis and therefore the horizontal movements will be greater.

Vertical movements in the overlying coarse grained material can be predicted by superposition of the settlement trough at the top of the clay layer onto the base of the upper layer. The spread of movements through the coarse grained layer can be assumed to be the same as the gradient of the distribution of i with depth, $K_{(grad)}$, if the tunnel were driven through that material; an indication of $K_{(grad)}$ values for sands was given in Figure 6.4. The offset of the distribution of i with depth from the vertical centreline of the tunnel is that given by the imposed trough at the base of the layer. It should be noted that this is not simply superposition of single soil profile predictions. The movements imposed at the base of the sand layer, the settlement trough at the clay/sand interface, is not the equivalent clay-only

trough, as it has been modified by the presence of the overlying layer. Horizontal movements cannot be predicted in the same way as for clays as constant volume conditions to not apply. Rules for predicting horizontal movements in sands due to tunnelling cannot be determined from this research, although assuming constant volume conditions for a material which will dilate should lead to conservative predictions of the component of horizontal to vertical movement.

6.4.3 *Comparison of predicted and measured vertical and horizontal movements*

Assuming a linear variation of i with depth, and applying the points made above regarding vector focus, predictions of vertical and horizontal movement have been made for direct comparison with some of the centrifuge test data. In Figure 6.12 image processing data, used previously in Chapter 5 to demonstrate the tests, are plotted and predictions are shown as solid lines. Both the vertical and horizontal movements have been normalised by the maximum vertical movement (the suffix 'h' is for horizontal and the suffix 'v' is for vertical).

Figure 6.12(a, b & c) shows data from the clay-only test RJG17 (2.5D clay cover above the crown). As the clay-only test data have validated equation (6.3), after Mair et al (1993), this has been applied to test predictions of both vertical and horizontal movement at several subsurface levels. The vertical troughs at all levels, including that only 10mm from the ground surface, are well predicted, even though the data are slightly asymmetric. The horizontal movements 80mm above the tunnel axis and 30mm below the ground surface are adequately predicted, although the magnitude of the maximum movement tends to be over-estimated whilst the movements at the edges of the troughs are under-estimated, particularly near the ground surface. At the level 10mm below the ground surface, the horizontal movements are significantly under-predicted, which represents the shift of vector focus in the free-surface region which is not accounted for in the predictive equations.

Figure 6.13(a, b & c) shows data and predictions for centrifuge test TH6 which consisted of 93mm of saturated sand overlying 75mm of clay above the tunnel crown. Data from this test have not been used significantly to establish the method of accounting for stiffness described by equation (6.17) above and therefore present an ideal examination of the procedure. Figures 6.13(a & b) show predicted movements and test data for a horizon in the clay 90mm above the centre of the tunnel. The prediction shown in the first figure assumes that the soil is all clay and the width of the predicted settlement trough is clearly narrower than the measured movements. However, the predicted horizontal movements using equation (6.18) were very

close to the measured data. In Figure 6.13(b) the relative stiffness of the two soils was taken into account using equations (6.16) and (6.17). The predicted vertical settlement troughs are approximately 14% wider than assuming a clay-only soil profile and the comparison with the measured data is considerably better. Conversely, in this instance the predicted horizontal movements, although still adequate, are not as close to the measured data as those predicted assuming an all-clay soil profile. Figure 6.13(c) shows the measured distribution of i with depth and the predicted lines assuming an all-clay soil profile and accounting for stiffness. Discounting the data within $0.5D$ of the tunnel crown it is clear that the predicted distribution of i which accounts for the ratio of stiffnesses of the soils is closer to the distribution measured in the centrifuge test.

Generally, except in the vicinity of the tunnel or near a free-surface, the predictions appear to agree well with the test data, including the horizontal movements, assuming a fixed vector focus based on a straight line distribution of i with depth.

6.5 Summary

Differences in the results from the centrifuge tests have been observed and attempts to characterise the possible causes of them have been explained and discussed. The key findings are highlighted below.

Generally, short term ground movements due to tunnelling in clay-only soil profiles are well described by equation (6.3), after Mair et al (1993). If account is taken of the change in shear stiffness at the interface of the two materials, using equation (6.10), reasonable predictions can be made of ground movements due to tunnelling in clay with an overlying coarse grained layer. Horizontal movements in the clay can be predicted by assuming that the vectors focus on the point where the tangent to the distribution of i intersects the vertical centreline of the tunnel. Difficulties arise in the vicinity of the tunnel where vertical settlement troughs may be steeper than the best fit Gaussian distributions, and at a free-ground surface where vertical settlement troughs may be wider than predicted but, more importantly, horizontal movements may be considerably larger than predicted.

Vertical movements through an overlying layer of coarse grained material may be predicted by superposition of the settlement trough from the clay surface and the spread of movements through the upper layer. The settlement trough imposed from the clay must account for the

influence of the upper stratum, as described above, and the spread of movements through the sand is the gradient of the distribution of i with depth only: the offset of the distribution from the vertical centreline of the tunnel at the base of the layer is the value of i at the clay surface. Horizontal movements in sands have not been investigated due to difficulties with image processing measurements. The focus of vectors of movement cannot be predicted in the same way as for clays because constant volume conditions do not apply.

CHAPTER 7 NUMERICAL ANALYSIS

The numerical analyses presented in this chapter were conducted using a non-linear elasto-plastic soil model (the 3-Surface Kinematic Hardening model) and the finite element method. The purpose of the analyses was to investigate how closely the physical behaviour observed in the centrifuge model tests could be predicted by the numerical approach and to undertake parametric studies within the known limitations of the analyses. The chapter includes: details of the 3-Surface Kinematic Hardening (3-SKH) model and the material parameters required; a description of the stress history followed in the analyses and the procedure adopted to do this; and finally, pertinent results from the analyses and a summary of the key findings.

7.1 Introduction

The finite element method used in conjunction with a suitable material model is a useful tool for research and design purposes. The model must be capable of simulating accurately the stress-strain behaviour of the material being analysed, in this case soil.

The analyses presented were conducted using a modified version of the finite element program CRISP, CRItical State Program, (Britto and Gunn 1987). CRISP is an incremental finite element program which was developed at Cambridge University during the 1970's specifically to carry out geotechnical analyses using the Critical State framework to describe soil behaviour. It has been used extensively both in industry and for research purposes for many years. The main model used to represent the soil was the 3-Surface Kinematic Hardening model (Stallebrass, 1990; Stallebrass and Taylor, 1997). It is a non-linear elasto-plastic soil model which was developed and implemented into CRISP at City University and has been used successfully for a number of years to model the behaviour of overconsolidated soils.

7.2 Objectives

The finite element analyses (FEA) were intended to supplement the centrifuge tests and provide further detail of the ground movements around tunnels under plane strain conditions. As such they were designed to simulate centrifuge model tests, the main objectives being:

i) to evaluate the numerical model using data from the centrifuge tests;

ii) to examine the effects of the limitations in the physical modelling, such as boundary proximity; and

iii) to extend the investigation beyond the scope of the centrifuge test series.

7.3 Overview of the analyses

A total of twenty three FEA are reported and details of these are given in Tables 7.1 and 7.2. It is useful to present a general overview of the analyses at this point. They can be divided into a number of series, each designed to investigate specific points, some of which overlap.

The main focus of the research is concerned with ground movements around tunnels in two-layer ground conditions. However, twelve analyses were conducted in which clay was the only material. A single clay stratum is a limiting case, of course, and not only produces a useful datum against which to measure the effect of overlying sand layers, but also provides the simplest situation with which to investigate a variety of modelling concerns.

Four main groups of clay-only, or all-clay, analyses were conducted. The first group provided data for evaluating the numerical model by replicating specific centrifuge tests that had been carried out. The investigation then continued to look more broadly at the effect of the depth of clay cover above the tunnel crown. Other clay-only analyses were designed to investigate various modelling concerns, either physical or numerical, including the effect of:

i) the proximity of the rigid model boundaries;

ii) changing the stress history of the model by starting from different values of $\sigma_{T\ max}$ or allowing additional swelling to occur during model preparation;

iii) allowing additional reconsolidation time under centrifuge acceleration;

iv) assuming drained conditions before and undrained conditions during σ_T reduction; and

v) assuming no movement at the lateral boundaries of the model.

Following the clay-only analyses an upper sand layer was introduced, initially as a linear elastic (LE) material. The purpose was to determine whether the basic characteristics of the effect of an overlying layer of sand on the deformations around a tunnel in clay could be predicted when using a LE model to represent the sand. It should be noted that this was anticipated as a preliminary study and was instigated largely because a realistic constitutive model, designed to predict the behaviour of sand, was not available. Again, a centrifuge test

was replicated to evaluate the numerical model and further analyses were conducted to investigate the effect of the sand depth.

Modifications to the computer code allowed the use of the 3-SKH model to simulate the upper sand layers and the above series of numerical analyses was repeated to compare the results.

The final series of analyses again included simulation of one of the centrifuge tests conducted, to help evaluate the numerical model and increase confidence in its performance. The main purpose of the series was to vary the stress-strain response of the upper strata in order to assess the effect on the movements in the lower clay layer. This was done by varying the stiffness parameters of the sand, within realistic limits.

7.4 The 3-Surface Kinematic Hardening (3-SKH) model

Stallebrass et al (1994a) stated that soil strains mobilised during tunnel construction are likely to be small, provided a failure condition is not reached, and so the behaviour will be governed by the soil stiffness. In predicting deformations, therefore, it is important to use a model which is capable of simulating the highly non-linear stiffness of soil.

The 3-Surface Kinematic Hardening (3-SKH) model, described by Stallebrass (1990) and Stallebrass and Taylor (1997), is a non-linear elasto-plastic soil model developed to simulate both the decrease in soil stiffness during loading and the effects of recent stress history (Atkinson et al, 1990). The basic features of the model were highlighted in Chapter 2. Defined in triaxial stress space it comprises two kinematic surfaces inside the standard Modified Cam-clay state boundary surface (SBS), as shown in Figure 7.1. Whilst the stress state of an element of soil stays within the inner (yield) surface, strains are elastic. If the stress state reaches the boundary of this region, plastic straining begins and the surface will translate and move along with it. The same is true of the second kinematic surface, known as the history surface, which denotes the limit of the effect of recent stress history. If the stress path changes direction strains may become elastic again until contact with the innermost kinematic (yield) surface is restored. In this way the non-linear behaviour of soil can be simulated by the position of the stress state relative to, and the translation of, the kinematic surfaces.

Figure 7.2 illustrates the translation rule which ensures that the three surfaces cannot intersect. The surfaces move along vectors joining their conjugate points, whose position is dictated by the position of the stress state on the inner surface.

It should be noted that although the 3-SKH model is a relatively sophisticated soil model and is capable of simulating many of the important aspects of soil behaviour, it does have its limitations. The model was developed initially to improve predictions for overconsolidated clays. The ways in which the behaviour of sand differs from that of clay, in particular the effect of particle crushing, is not considered in the current formulation. However, in the absence of a more appropriate model, the 3-SKH model was used to simulate the sand behaviour in some of the analyses presented herein. Work is currently in progress to develop constitutive models which reproduce the effects of structure in natural soils and particle crushing, particularly in coarse grained material (Baharom, 1998).

7.4.1 *Determination of material parameters*

Modified Cam-clay requires five material parameters: G', κ, λ, Γ and M.

The 3-SKH model requires three additional parameters: T, S and ψ. T is the ratio of the size of the history surface to the bounding surface and likewise, S is the ratio of the size of the yield surface to the history surface. The product TS therefore is the ratio of the size of the yield surface to the bounding surface. These relationships are illustrated in Figure 7.1. ψ is an exponent in the hardening rule.

The values of the product TS and parameter T represent the change required in p' to extend the soil behaviour beyond the region of assumed elastic response and the effect of recent stress history respectively. Values can be obtained from triaxial tests by conducting 180° isotropic stress path reversals. Values of ψ cannot be observed directly and must be determined by parametric studies and evaluated by experimental data.

Butterfield (1979) suggested that swelling and compression indices were linear over larger ranges when plotted in ln: ln space, and the 3-SKH model utilizes this, so requiring the gradient of the unload-reload lines, κ, and normal compression lines, λ, in ln$v$: lnp' space where they are denoted as κ^* and λ^*.

Also, in the 3-SKH model the elastic shear modulus is defined as a compliance. For the purpose of these analyses it has been taken to be G'_{max}, and for the kaolin it was calculated in accordance with equations (2.7) and (2.8a & b), developed by Viggiani and Atkinson (1995) for fine grained soils. For each increment and each soil element, G'_{max} varied depending on the current values of p' and R_0, the input coefficient A, and exponents n and m.

Values of the parameters used for the FEA are given in Table 7.3.

All of the parameters for kaolin are well reported and are summarised by Stallebrass and Taylor (1997) following work by Stallebrass (1990) and Viggiani (1992). For consolidation analyses, values of vertical and horizontal permeability, k_v and k_h, were calculated from formulae suggested by Al Tabbaa (1987), using average voids ratios measured in centrifuge model tests, as:

$$k_v = 0.5e^{3.25} \times 10^{-6} \text{ (mm/s);} \tag{7.1}$$

$$k_h = 1.43e^{2.09} \times 10^{-6} \text{ (mm/s).} \tag{7.2}$$

Parameters for the sands were determined from the triaxial tests described in Chapter 4 and other published data. Coop and Lee (1993) reported critical state parameters for Ham River sand, which is a medium silica sand of very similar grading to the Flint gravel sand and the 25/52 Leighton Buzzard Sand used in some of the centrifuge tests. They also stated that the critical state parameters for all silica sands were unlikely to vary much from their reported values, and this is particularly true if the uniformity of the gradings are similar. For use in the 3-SKH model, values of κ and λ given by Coop and Lee (1993) were converted to $\ln v$:$\ln p'$ space, denoted by κ^* and λ^*, over an appropriate stress range, and values of Γ and M were used directly. Chapter 4 describes triaxial tests conducted on some of the sands used in the centrifuge test series, which were designed specifically to determine values of G'_{max}. Parameters determined in Chapter 4 for the stiffness of 52/100 LBS and Flint Gravel sand were used in most of the FEA.

The parameters governing the decay of stiffness in the 3-SKH model, T, S and ψ, were estimated for the sands from the triaxial test data, by numerical simulation of single element tests. Illustrative results from some of the simulations are presented in Figure 7.3. The size of the SBS was estimated from the critical state parameters given in Table 4.3 (after Coop and Lee, 1993) and the specific volume of the sands used in the triaxial tests. As expected this resulted in a very large SBS and so very low values of the parameter T were required to produce an appropriate region in which the effect of recent stress history applied. The

exponent in the hardening modulus, ψ, interacts with the parameters T and S. It was found that although a reasonable approximation of the general decay of stiffness for the sands could be simulated, reproducing the exact decay of specific sands was not possible with the current model. The values of the parameters used for TTR1 were considered to be appropriate values for the sands and they are included in Table 7.3.

For the isotropic LE sand model E' is a function of G', by definition, and G' was taken as a value measured in preliminary triaxial tests at a shear strain of 0.01%. A Poisson's ratio of 0.3 was assumed.

7.5 Stress history

The stress history in a typical centrifuge model was discussed and illustrated in section 3.5.5. The stiffness of the soil will vary depending on the degree of loading and the stress history. In order to obtain the appropriate stiffnesses for all points within the soil mass when using the 3-SKH model it is necessary to simulate the stress history and so produce the correct orientation of the kinematic surfaces, before the important loading phases begin.

For all of the analyses reported here the simulated stress history was designed to replicate the centrifuge model tests. The general principle of simulating the stress history is to ensure that the effective stresses are always correct. The simulation began at the end of 1-dimensional compression of the kaolin to a vertical effective stress of 500kPa in the consolidation press. At this point $\sigma_v' = 500$kPa throughout the clay and σ_h' was calculated by assuming $K_0 = 0.63$ for normally consolidated kaolin (Pantelidou, 1994). This provided an in situ stress state from which to begin. At the start of the first loading stage the kinematic surfaces would usually be centred around the in situ stress state. The soil stiffness and therefore the response of the soil to loading cannot be reproduced correctly until sufficient stress history has been followed to position the surfaces appropriately. However, the kinematic surfaces are not allowed to intersect with each other or the SBS. If the in situ stress state is on the SBS, as in this case for a normally consolidated material, all three surfaces are in contact at the in situ stress state and orientated tangential to the SBS. The positions of the surfaces at the in situ stage are therefore appropriate and the response to the first load perturbation should be correct.

The first stage for all analyses was to allow swelling throughout the clay to $\sigma_v' = 250$kPa, as experienced by the kaolin in the consolidation press. After this first unloading the orientation

of the kinematic surfaces should be correct and, from this point onwards, should produce the correct soil stiffness and hence response to loading. Due to the difficulties in determining pore water pressure profiles and therefore effective stresses in the clay during the centrifuge model preparation, the standard stress history simulated for the FEA assumed that $\sigma_v' = 250$kPa was maintained throughout the clay until the centrifuge acceleration was increased. One analysis (RC3AM) was conducted to investigate the effect of assuming additional swelling to $\sigma_v' = 125$kPa before increasing the centrifugal acceleration, as it was thought that this may occur during centrifuge model preparation.

The final history stage required the change of the effective stress profile from being constant with depth to one increasing with depth, as appropriate for a model in equilibrium on the centrifuge in flight. For the majority of analyses, in which the change was from a constant $\sigma_v' = 250$kPa, swelling occurred over the full soil depth, from being small in magnitude at the bottom of the model, to reaching a maximum at the top. For the analysis which was brought to the centrifuge equilibrium effective stress profile from constant $\sigma_v' = 125$kPa, recompression was experienced by the soil in the lower regions. The effect of this is illustrated by the sketched stress paths in Figure 7.4. Both finish at the same σ_v' but have very different stress paths. The relative positions and orientations of the kinematic surfaces will produce a different response of the soil to the next loading stage.

The stress history of the sand in the centrifuge tests would be 1-dimensional compression only, due to the acceleration of the centrifuge. This was automatically achieved in the FEA by building up the sand in layers at the maximum centrifuge acceleration of 100*g*, each layer being compressed by the correct amount by the soil above.

7.6 Procedure

As detailed in Tables 7.1 and 7.2, a total of twenty-three analyses were carried out. All were conducted under plane strain conditions using linear strain triangular elements and the coupled consolidation facility in CRISP, with the exception of RC4U which was a drained/undrained analysis. The mesh used for those with 4*D* total soil cover above the tunnel crown is shown in Figure 7.5. For all analyses the mesh represented a centrifuge model test at model scale. As the problem has an axis of symmetry about the vertical axis of the tunnel it was necessary to model half of the continuum only, which in this case contained approximately 340 elements and 620 vertex nodes. The mesh was arranged in layers so that:

rows of elements could be removed easily to conduct analyses with less total cover (3*D* or 2*D*); the surface layers could be specified with different material properties to the lower regions; and subsurface displacement data could be abstracted easily from the output files. Strict convergence tests were not applied to the mesh, but it was optimised by careful observation of the stresses throughout the analyses.

It is necessary to maintain an effective stress increment considerably smaller than the inner yield surface to ensure that the 3-SKH model is able to function properly. This can lead to a large number of increments required to conduct an analysis including the stress history phases. However, modern PCs with sufficient RAM are more than capable of running these problems. Most of the analyses required between 3000 and 5000 stress increments and were carried out on a Pentium Pro200 with 32Mb of RAM, which ran at an average rate of around 1000 increments/hour of processing time.

The size of time increments is also important for the stability of the pore pressure distribution in consolidation analyses. Guide-lines are given by Britto and Gunn (1987) and these were followed for the analyses described herein. In addition, periodic checks on equilibrium pore pressure distributions were carried out.

Generally, the boundary conditions were as follows:

- top boundary impermeable with free movement in all directions;
- bottom boundary permeable with no excess pore pressures allowed, and fixed against movement in all directions; and
- left and right boundaries impermeable with excess pore pressures allowed, free movement in the vertical direction and fixed against movement in the horizontal direction.

The vertical centreline of the tunnel represents an axis of symmetry and the boundary conditions imply a mirrored mesh on the left hand side. However, the boundary conditions on the right hand side also imply an axis of symmetry. The analyses will effectively consider the presence of another implied tunnel at twice the mesh width to the right of the first. In fact, this continues on both sides of the initial tunnel ad infinitum. In consequence, if the settlement trough is wider than the mesh it will be influenced by the settlements of the implied adjacent tunnels. This point is illustrated later in the presentation of results.

To begin an analysis using CRISP it is necessary to specify a complete mesh which includes all elements to be considered throughout the analysis. In this case, that includes those depicting both the clay and sand layers, plus the soil in the tunnel. As the clay layer must be subjected to a specific stress history before the sand layer is added, the first stage in the analyses involved removal of the elements forming the sand layer to produce what is known as the primary mesh.

In the numerical analyses, as in real events, the soil responds to changes in effective stress. The underlying principle behind the procedure followed for the numerical simulations was, therefore, to model correctly the effective stress at all times, which in certain circumstances requires the manipulation of surcharge loads.

In situ stresses were specified to match those in a centrifuge model under maximum preconsolidation pressure in the consolidation press. For all the analyses reported here, $\sigma_v' = 500$kPa and $\sigma_h' = 315$kPa throughout the full depth of the clay, assuming $K_0 = 0.63$ for normally consolidated kaolin (Pantelidou, 1994). In most cases, the boundary conditions were fixed as above and external loading was applied to be in equilibrium with the in situ stress state. Figure 7.6 illustrates a typical stress history for the FEA.

The formulation of CRISP is such that it does not apply gravitational accelerations to pore water. To avoid the need for changing boundary conditions at a later stage it was convenient to begin from a pore pressure profile which was hydrostatic under the maximum gravitational accelerations to be imposed. To achieve an equilibrium in situ effective stress state that was constant with depth, it was necessary to specify an in situ gravity level such that the gravitational stresses induced by the unit weight of the soil were exactly the same as the pore water pressures. In terms of effective stresses, these two then balanced out and the effective stress profile was dictated purely by a surcharge loading applied to the mesh surface. This observation was made by Labouise (1995) and the requirement is:

$$N_w \gamma_w = N_s \gamma_s \ , \tag{7.3}$$

noting that N_w is the effective gravity scaling factor applied to the water, in this case $N_w = 100$, and N_s is the gravity scaling factor required for the soil. γ_w and γ_s are the unit weights of water and saturated soil respectively. For a model made of kaolin to be subjected to a final gravity scaling factor of 100, the value of N_s which produces an effective stress profile due to self-weight of zero throughout the model is

$$N_s = \frac{100 \times 9.81\,\text{kN/m}^3}{17.44\,\text{kN/m}^3} = 56.25g\,. \qquad (7.4)$$

So, at the beginning of an analysis, σ_v' = 500kPa and σ_h' = 315kPa throughout the clay, which is in equilibrium with a pore pressure profile specified as hydrostatic at 100*g*, a gravity acceleration of 56.25*g* imposed on the soil and a surcharge loading of around 500kPa. The stress state throughout the clay then lies on the K_0 compression line. The exact value of the surcharge loading depends on the position of the water table. For these analyses the pore pressure profile was assumed to have a constant gradient. If the water table was below the surface then a negative pore pressure was present at the surface, the hydrostatic gradient dictating the value. For the majority of analyses the water table was positioned 25mm below the model surface producing a pore pressure of -0.025m x 9.81kN/m^3 x 100*g* = -24.525kPa at the ground surface. Effectively, this implies an offset which then has to be removed from the surcharge. In the analyses where a sand layer was present, a further addition to the initial surcharge was required, equivalent to the effective stress imposed on the clay due to the introduction of the sand, as detailed later.

The first loading phase of the analyses was to remove 250kPa of the surcharge, so simulating the reduction of vertical effective stress in the consolidation press. This allowed all elements in the model to swell back from σ_v' = 500kPa to σ_v' = 250kPa. It was conducted over a long time period, sufficient to allow full equilibrium conditions to be achieved.

The second loading phase was to increase the in situ gravity level to the required value, N = 100, and at the same time remove additional surcharge. This simulated the change in effective stress due to centrifuge acceleration. It was conducted over a short time period followed by a consolidation phase to allow equilibrium conditions to be reached, though it would be equally valid to conduct the loading phase over a long time period. For analysis RC3AM, 375kPa of surcharge was removed in the first loading phase and 125kPa in the second, to simulate additional swelling occurring during centrifuge model preparation.

Unlike the centrifuge model tests, at this stage the tunnel cavity was not present in the clay. This was due largely to the problems of numerical instability if too many different load perturbations were conducted, in parallel or in series, without achieving equilibrium between each stage. The tunnel was installed after full acceleration had been reached by removing the soil elements and replacing them with a pressure equal to the total stress at tunnel axis level. Again, this was conducted over a short time period and was followed by a consolidation

period corresponding to around 20 hours at model time to allow equilibrium to be achieved. Analysis RC4X explored the effect of allowing additional consolidation time before reducing the tunnel pressure.

Having carefully simulated the preparation stages of the centrifuge model tests, all elements within the clay were at the appropriate stress state and had been subjected to sufficient stress history for the kinematic surfaces to be orientated correctly. The response to the next load perturbation should be close to that in the corresponding centrifuge model.

For the clay-only analyses the next and final stage was to reduce the supporting pressure within the tunnel and so generate movements within the soil. This was conducted at a similar rate to the centrifuge tests, which would produce an effectively undrained response in the clay.

For analyses with an upper sand layer it was necessary to build the sand on top of the clay without changing the effective stress, and therefore the stress history, within the clay. This was done by building the sand in layers whilst removing the equivalent surcharge from the top of the clay. Generally, the sand was specified to behave in a drained manner. For the analyses using the LE sand, this process could be conducted over very few stress increments as the clay (3-SKH model) did not experience any stress change and the simple LE sand was not troubled by large stress increments.

Later analyses were conducted using a further modified version of CRISP. The modifications were necessary to allow in situ conditions to be specified in a material which was being used to build layers during the analysis. This allowed the overlying sand layer to be represented by the 3-SKH model. The value of K_0 and an initial percentage of the overburden stress were specified as starting stresses, and the initial size of the SBS was also defined by the user. This was important for the sand which was in a compacted state such that the size of the SBS was not dictated by the relatively low starting stresses. A value of 10% of the overburden stress was generally used as a starting condition for a built element, the remaining stress being induced in the element over a specified number of increments. As when using the LE sand, an overburden stress was removed from the surface of the clay during the building phase so that no stress changes were experienced by the lower clay layer during this operation.

It was not possible to specify pore pressures within the built elements for either the LE model or the 3-SKH model. To produce the correct vertical effective stress profile in saturated sand

it was necessary to use a unit weight equal to the difference between that of the saturated soil and water (γ - γ_w). In these analyses, a surcharge was kept on the clay surface throughout to maintain the correct vertical effective stress profile through the clay layer.

As with the clay-only analyses, the final stage was to reduce the supporting pressure within the tunnel to generate the ground movements in the model.

7.7 Results and comparison with centrifuge test data

To illustrate the progression of a typical analysis, the effective stress paths for soil elements near the crown, shoulder (springing) and invert of the tunnel during a clay-only analysis are given in Figure 7.7. Following the stress history described above, all the stress paths follow a line of 1-dimensional swelling from the end of K_0 compression. As the tunnel support pressure was calculated to correspond to the vertical total stress at tunnel axis level, the elements near the tunnel crown and invert have slightly different stress histories. Near the crown the tunnel support pressure was too high, resulting in some recompression of the elements in this vicinity. The opposite was the case at the invert resulting in further swelling. Both of the elements were subjected to extension upon the rapid decrease in tunnel support pressure, as the major principal effective stress (σ_v') decreased. On the other hand, the element at the shoulder of the tunnel was subjected to compression as the tunnel pressure was reduced, with the minor principal effective stress (σ_h') reducing. Extension at the crown and invert with compression at the shoulder (springing) was anticipated. For the elements at the crown and invert, the difference in the stress histories, and therefore the change in stress path direction upon unloading at the tunnel boundary, are a function of the modelling exercise, in which a constant pressure is used to support the tunnel.

Figure 7.8 allows a more detailed examination of the total and effective stress paths in the soil elements at the crown and the shoulder of the tunnel. Atkinson and Mair (1981), and later Mair and Taylor (1993), considered stress paths around a tunnel during unloading. They noted that for axisymmetric unloading of an isotropic elastic material the changes in both the mean normal total and effective stresses are zero, because changes in radial and tangential stresses are equal and opposite. However, for an anisotropic or non-elastic material the mean normal total stress decreases. This can be seen in the total stress paths in Figure 7.8. Initially the changes are small, but as the length of the stress path increases so does the change in mean normal total stress. This is associated with the degree of plastic straining, controlled by the

effective stress path and the position and orientation of the kinematic surfaces. The pore pressure at any discrete stage is the difference between the mean normal total and effective stresses. Initially the pore pressure reduced slightly, but the rate of change increased dramatically with the increase in plastic straining. Small changes in pore pressure when the soil behaviour is dominated by elasticity and increasing changes in pore pressure with increasing plasticity is consistent with the relatively simple plasticity solutions of Mair and Taylor (1993). The sharp change in direction, which is particularly evident in the stress path for the soil element at the tunnel shoulder, marks the end of the influence of the kinematic history surface, and therefore the end of the effect of recent stress history and the onset of large plastic deformations.

Before the ground movement results are presented and discussed it is important to define the method used for calculating volume loss (V) from the FEA predictions. Volume loss is often used when predicting tunnelling-induced settlement. It refers strictly to the movement generated at the tunnel but is often measured at the ground surface and inferred by assuming undrained/constant volume conditions. This is the case for the centrifuge tests where LVDT measurements at the clay surface produced the most reliable data. In coarse grained material V is often calculated from surface measurements also, but the volume loss at the tunnel is usually unknown. For the FEA the volume loss can be determined directly from the displacements of the element nodes immediately around the tunnel. The simple method used here involved calculating an average radial displacement for the tunnel from the nodal displacements, from which a volume loss could be determined.

7.7.1 *Clay-only analyses*

Figures 7.9 and 7.10 show a comparison between FEA predictions and centrifuge test data. The data are from centrifuge test RJG15 and the corresponding FEA, RC3A, in which the tunnel had a total cover of $3D$ clay only. Figure 7.9 is the equivalent of a load displacement curve and shows vertical displacement above the tunnel centreline at the ground surface against the tunnel support pressure. It is clear that the FEA initially under-predicted the soil stiffness at high tunnel support pressures, compared to measurements from an LVDT in the centrifuge test, but as the support pressure was reduced further, the decay of stiffness predicted was not as rapid as that in the centrifuge model. Although there are discrepancies, the prediction is encouraging over a large range of support pressure. Figure 7.10 shows the transverse settlement troughs from the analysis and experiment. The vertical displacement has been normalised by S_{max} to allow comparisons of trough shape to be made at several

stages during the reduction of tunnel support pressure. In addition, the horizontal distance from the tunnel centreline, x, has been non-dimensionalised by the tunnel diameter, D. As shown in Chapter 5, the centrifuge test data indicates a consistent normalised trough shape over a considerable range of volume loss (at least from 2% to 20%) whereas the FEA predictions show a narrowing of the settlement trough with increasing volume loss. Such a trend has been observed only at conditions close to failure in the centrifuge tests. The FEA predictions all indicate a wider spread of movements than the centrifuge test data, particularly as the value of x/D increases. This is consistent with the findings of other authors who have applied the finite element method to predict transverse settlement profiles due to tunnelling, for example, Addenbrooke et al (1997). In fact, these predictions are considerably closer to the measured results than would have been expected if a less sophisticated soil model had been used (Gunn, 1993). The FEA predictions are reasonable but significantly over-estimate the movements at the edge of the trough, particularly at low volume losses. Flattening of the settlement trough at the very extremes may be explained by the limited width of the mesh and the "adjacent tunnel" implied by the axis of symmetry. This will be considered in more detail later in this section.

The shape of the settlement troughs from most of the centrifuge tests, including RJG15, have been shown to be reasonably represented by Gaussian distributions. It is clear from Figure 7.10 that the considerable far-field movement predicted by the FEA would not be well described by a Gaussian distribution. For this reason, no attempt has been made to suggest Gaussian parameters to describe the settlement troughs predicted by the FEA. The quality of predictions have been assessed against centrifuge test data and the trends from predictions described by other means.

The presentation of results for the groups of clay-only analyses has been kept consistent to allow comparisons between them. Four plots (a to d) are given for each of Figures 7.11 to 7.14, showing respectively:

a) volume loss (V%) against tunnel support pressure;
b) movement at springing and invert level of the tunnel normalised by movement at the tunnel crown for V ranging from 0 to 25%;
c) normalised movements $1D$ above the tunnel crown (horizontal and vertical movement normalised by the vertical settlement above the tunnel centreline (S_{max}) against normalised horizontal distance, x/D); and
d) normalised movements at the ground surface (horizontal and vertical movement normalised by S_{max} against x/D).

(a) indicates the progress of the analyses but really it is useful only when considering analyses with the same total stress at the tunnel axis; (b), (c) and (d) give far more insight into the patterns of displacement around the tunnel and the propagation of movements towards the ground surface.

To avoid repetition, an overview of Figures 7.11 to 7.14 is presented first, in which the key consistent features are highlighted. Individual points are discussed afterwards.

The figures focus on the effect of different conditions on the ground movement around the tunnel, that is, at the crown, springing level and invert, and the propagation of these movements through the clay to the ground surface. Movements at the springing level always exceeded those at the invert and a variety of conditions resulted in movements at the springing level in excess of those at the crown. The movements at the springing level and invert of the tunnel will be referred to as deep-seated movements.

Deep-seated movements around the tunnel increased with depth of clay, both above and below the tunnel, varied with the recent stress history around the tunnel, and were low when undrained conditions were imposed during tunnel support pressure reduction. Relative differences in the movements around the tunnel were evident in the vertical movements $1D$ above the crown. Larger deep-seated movements around the tunnel produced wider settlement profiles $1D$ above the crown, however, this was not always evident at the ground surface.

The ratios of horizontal to vertical movement were variable and seemed to be sensitive to the proximity of the right hand boundary. However, the approximate position of the maximum horizontal movement tended to correspond with the point of inflexion of the vertical profile.

The first series of clay-only analyses was conducted to investigate the effect of depth of clay cover above the tunnel crown. Results are presented in Figure 7.11 comparing FEA predictions for $2D$ (RC2), $3D$ (RC3A) and $4D$ (RC4) clay cover only. The plot of volume loss against tunnel support pressure (Figure 7.11(a)) shows, as expected, that for a given support pressure, the analysis with the greatest total stress at the tunnel produced the greatest volume loss. Deep-seated ground movements around the tunnel increased with depth of clay cover and tended to produce wider settlement troughs $1D$ above the tunnel crown. This became exaggerated at the ground surface due to the depth of soil through which the movements propagated. The horizontal movements $1D$ above the tunnel crown were similar for each

case, the maximum ranged from approximately $0.25S_{max}$ for the $2D$ clay cover to $0.3S_{max}$ for the $4D$ clay cover. At the ground surface the maximum horizontal movements ranged from approximately $0.25S_{max}$ to $0.4S_{max}$ but here the larger movements were associated with the narrow trough from the $2D$ cover analysis. The relative magnitude of the horizontal movement may be greater for the $2D$ analysis simply because of the proximity of the ground surface to the tunnel. However, it may also be the case that the restraint of the lateral right hand boundary was more significant as the movements propagated further from the tunnel, as in the analyses with greater clay cover.

Figure 7.12 shows the results from analyses exploring the effect of boundary proximity. All had $4D$ clay cover above the tunnel crown. The series included: a standard mesh (RC4 described above); a wide mesh extended to twice the width of the standard mesh (RC4W); a deep mesh extended to $4D$ below the tunnel invert (RC4D); and a wide/deep mesh which incorporated both extensions to the mesh (RC4WD). All of the analyses had the same total overburden stress at the tunnel and the volume losses generated during the reduction in tunnel support pressure were almost identical. The volume loss predicted using the standard mesh was marginally less than the others. The deep meshes (RC4D and RC4WD) produced greater deep-seated movements around the tunnel whereas the effect of the mesh width on these movements appeared to be small. Predictions using the wide/deep mesh showed slightly larger movements at the springing level than those using the deep mesh. Of course, for the standard mesh the bottom boundary was significantly closer to the tunnel than the right hand boundary, $1.1D$ compared to $5D$, and so changes in the proximity of this boundary had considerably more influence on the movements near the tunnel. Again, the movements around the tunnel were evident at the horizon $1D$ above the tunnel crown. All the analyses predicted very similar trough shapes within the inner portion of the trough, say within $x/D = 2.5$, where it is clear that the movements were dominated by the displacements in the vicinity of the tunnel crown. Analyses using the deep mesh of standard width showed considerably more vertical movement in the outer regions of the trough than those using the standard mesh, consistent with the deeper movements around the tunnel. The same pattern is clear in the predictions with the wide meshes. Again the maximum horizontal movements tended to occur around the point of inflexion of the settlement troughs, their magnitudes being over a limited range from approximately $0.25S_{max}$ to $0.35S_{max}$, with analyses using the wider meshes producing the highest values.

It is interesting to consider the potential problems associated with the conditions at the right hand boundary. The fixity at this boundary, which prevents movement in the lateral direction

but allows movement in the vertical direction, implies an axis of symmetry and consequently implies the presence of another tunnel. If the movements from one tunnel extended to this lateral boundary they would be superimposed on the movements from the implied tunnel, and at the boundary itself the vertical displacement would be exactly twice the value of that from a single tunnel. This is illustrated by the results in Figures 7.12 (c) and (d) where it is clear that the settlement troughs from the standard width meshes display significantly greater vertical movements at the limits of the mesh than the corresponding results from the wide meshes.

There is little difference between the patterns of vertical movement $1D$ above the tunnel and the ground surface, except for the proportionally greater movements between $x/D = 2$ and $x/D = 4$ for predictions with the wide/deep mesh. The horizontal movements at the ground surface were significantly different. The analyses using the wide meshes produced maximum horizontal movements approaching $0.5S_{max}$ in contrast to $0.2S_{max}$ when using standard width meshes. Clearly the proximity of the laterally fixed right hand boundary had considerable influence on the horizontal movements and it was most significant at the ground surface (free-boundary).

The results presented in Figure 7.13 show the effect of changing the recent stress history around the tunnel. All of the analyses had $3D$ clay cover only above the tunnel crown and were designed to simulate histories that may occur during centrifuge testing, but with exaggerated conditions. The first was a reference analysis in which the maximum tunnel support pressure ($\sigma_{T\,max}$) was equal to the total overburden stress at tunnel axis level (RC3A); the second and third analyses began from a $\sigma_{T\,max}$ that was 50kPa low (RC3B) and 50kPa high (RC3C). In the fourth and final analysis in this series (RC3AM), the clay was allowed to swell back to 125kPa, rather than the usual 250kPa, before being subjected to $100g$ acceleration. This simulated the effect of swelling occurring in the clay during model preparation, before being accelerated on the centrifuge. For a given tunnel support pressure, the least volume loss was predicted by the analysis beginning from the low $\sigma_{T\,max}$ and the highest volume loss from the analysis beginning from the high $\sigma_{T\,max}$; the analysis in which additional swelling was allowed also predicted a relatively high volume loss. The reference data from which the volume losses were calculated were all from the stage immediately before the reduction in support pressure. Some movement towards the tunnel had already occurred for the low $\sigma_{T\,max}$ analysis during the consolidation phase, which is not accounted for in the volume loss calculation and, similarly, some movement away from the tunnel had occurred for the high $\sigma_{T\,max}$ analysis.

The FEA starting from a low $\sigma_{T\ max}$ and the analysis in which additional swelling was allowed produced the largest deep-seated movements, the invert movement being particularly high for the analysis with additional swelling. These movements can be related to the changes in stress paths. For analyses with $3D$ total cover the clay all around the tunnel usually swelled back from $\sigma_v' = 250$kPa during the increase in centrifuge acceleration. When the correct $\sigma_{T\ max}$ was used in the tunnel the crown was reloaded slightly (compression), the invert unloaded slightly (extension) and the soil at the springing level experienced no change. The crown, and to a lesser extent the springing, underwent a minor stress path reversal when the tunnel support pressure was reduced. Starting from a low $\sigma_{T\ max}$ the springing had previously been unloaded in compression immediately before the tunnel support pressure was reduced, generating a softer response when the unloading continued and therefore a greater proportion of movement. A similar argument applies to the analysis in which additional swelling was allowed before the centrifuge acceleration and the tunnel support pressure was applied. In this case, all the soil swelled back to $\sigma_v' = 125$kPa and was then reloaded under the centrifuge acceleration. The correct $\sigma_{T\ max}$ was applied at the tunnel so that the crown was reloaded (compression), the invert unloaded slightly (extension) and elements of soil at springing level experienced no change. The crown had undergone more reloading than normal, producing a stiffer response on unloading of the tunnel when the stress path reversed. This resulted in proportionally greater movements at both springing and invert levels.

As with the previous analyses, the larger deep-seated movements were associated with wider settlement profiles $1D$ above the tunnel crown. The horizontal movements were all very similar with the maximum being approximately $0.25S_{max}$. The same trend manifests itself at the ground surface though the analysis with the low $\sigma_{T\ max}$ produced a wider trough than the analysis with the additional swelling, which is the reverse of the troughs $1D$ above the crown.

Results from the final series of clay-only analyses are presented in Figure 7.14. All of the analyses had $4D$ clay cover only and they included: a reference analysis (RC4); an analysis with additional time for re-consolidation under $100g$ conditions (RC4X); an analysis in which the soil behaviour was undrained during the tunnel pressure reduction phase (RC4U); an analysis in which the right hand boundary was fixed against movement in the vertical direction (RC4P). In RC4U the history stages of the analysis were conducted under drained conditions and only the reduction in tunnel support pressure was carried out under undrained conditions. RC4P was designed to examine an extreme case, where it was assumed that the friction between the clay and the strong-box in a centrifuge test prevented vertical movement of the soil at the boundary. The difference in predicted movements between the standard

analysis and the one in which additional re-consolidation time was allowed are imperceptible, indicating that the re-consolidation was complete under standard conditions. Slightly higher volume losses were predicted under undrained conditions. Fixing the right hand boundary against vertical displacement produced slightly smaller movements at the tunnel invert than the standard analysis, but the major significant difference in movements around the tunnel was the low invert movement predicted by the undrained analysis. Interestingly, this is observed in the width of vertical movement trough $1D$ above the crown but not at the ground surface, though the settlement profile was not very smooth. Fixing the right hand boundary against vertical displacement obviously reduced the settlement at the edge of the mesh but produced an uncharacteristic U-shaped trough at the ground surface. The patterns of horizontal movement showed little change from those already observed.

7.7.2 *Analyses with an overlying sand layer*

The first set of analyses in which the clay had an overlying sand layer compared the effect of the amount of sand to clay cover. All of the analyses had $3D$ total soil cover but four different geometries were used: no sand with $3D$ clay only; $1D$ sand over $2D$ clay; $1.5D$ sand over $1.5D$ clay; $2D$ sand over $1D$ clay. Each of the four cases were analysed using a LE model and the 3-SKH model for the sand. The results are compared using normalised settlement troughs. This series of analyses was originally presented by Stallebrass et al (1996).

Figures 7.15 (a & b) show the normalised vertical movements predicted by the FEA using the LE model and the 3-SKH model for the sand respectively. The data are for the horizon $1D$ above the tunnel crown and, therefore, the movements were in the clay layer for all cases. When using either the LE or 3-SKH model for the sand, the vertical settlement profile in the lower clay layer became flattened with increasing depth of sand above. There are small differences in the movements of the clay depending on the constitutive model used for the sand, particularly around $x/D = 0.8$, and these become greater with the depth of sand being modelled. Although the exact movements predicted $1D$ above the tunnel crown depend on the constitutive model used for the sand, the trend of movements with increasing depth of the overlying sand layer is very similar.

Figure 7.15 (c) shows the vertical movements at the model surface when the 3-SKH model was used for the sand (note:- the movements in the sand produced using the LE model were unrealistic and are shown later in the Figure 7.17). The surface troughs were narrower if a

layer of sand was present although, in this instance, there is little difference between the results of the analyses for different sand depths.

Figure 7.16 compares directly the differences between the settlement profiles predicted at the clay/sand interface for the different sand covers. Figure 7.16 (a) also shows the best fit Gaussian distribution for data from centrifuge test RJG16. It is clear from Figures 7.16 (a to c) that the predicted settlement profiles at the clay surface were smoother when the 3-SKH model was used for the sand than when the LE model was used, although the results are very similar. Both over-estimated the width of settlement trough when compared to the corresponding centrifuge test for the 1.5*D* sand over 1.5*D* clay case.

Figure 7.17 shows the corresponding results at the upper sand surface. It is immediately clear that using the LE sand model produces unrealistic settlement profiles. Again, the best fit Gaussian distribution curve from centrifuge test RJG16 has been plotted in Figure 7.17 (a). The prediction from the analysis with the 3-SKH model for the sand compares more favourably than the corresponding results for the clay/sand interface.

Analysis RSG1 was a simulation of centrifuge test RJG20. This was selected because comparisons could be made not only with the boundary measurements from the centrifuge test but also with detailed, high quality image processing measurements. The soil cover above the tunnel crown was 1.5*D* of dry silica sand over 2.5*D* of saturated kaolin. For the analysis both materials were modelled using the 3-SKH model.

Figure 7.18 compares the displacements above the tunnel crown at both the clay/sand interface and the sand/ground surface, as predicted by the FEA and observed in the centrifuge test. As with the previous clay-only comparison, the initial stiffness was under-predicted by the FEA and the decay of stiffness with change in stress/strain was not sufficiently rapid. However, the magnitude of the displacements were of the same order and, as such, were encouraging. Difficulties in the analysis arose as the tunnel neared collapse due to the small stress increments required by the 3-SKH model, and so the comparison does not continue beyond around 25% volume loss.

Figures 7.19 (a & b) compare the normalised settlement troughs at the clay/sand interface and the sand/ground surface. The normalisation allows data from more than one stage in the experiments to be included on the same plot. In this case, data have been plotted when the tunnel support pressure was 130kPa and 100kPa. Corresponding volume losses from the

centrifuge test are indicated in Figure 7.18. Predicted settlement profiles were sufficiently close to the measured profiles to suggest that further analyses would produce useful qualitative trends. It is interesting to note that the prediction for the upper sand surface was better than that for the clay/sand interface. These predictions are considered to be good when compared to other numerical simulations of this notoriously difficult boundary value problem. Nevertheless, the distribution of predicted movements is still much wider than that observed in the centrifuge test.

The vectors plotted in Figure 7.20 provide more detail of the spread of movements in the centrifuge test and the FEA. It can be seen that the FEA considerably over-predicted the movements at the invert of the tunnel and possibly also at the springing, which led to much wider propagation of movements through the clay layer. Comparison of the contour plots of engineering shear strain around the tunnel, given in Figure 7.21, gives more insight into the cause of the discrepancies. Zones of high shear strain around the upper half of the tunnel are familiar to tunnel analysts and can be seen in both plots, although the FEA produced higher values. However, in the centrifuge test there was less shear strain generated around the lower half of the tunnel than the upper half, in contrast to the FEA which predicted slightly more. Clearly the FEA under-predicted the stiffness in the vicinity of the tunnel, especially around the tunnel invert. This contributed to the wider spread of movements observed in the FEA when compared to the centrifuge test results.

The numerical analyses have been fully evaluated here by detailed comparison with high quality data from well controlled centrifuge model tests. Only after thorough evaluation can the analyses be used with confidence, within the observed limitations, to aid prediction of ground movements. Comparisons such as those presented above can also aid the development and improvement of the numerical model.

In the final series of analyses the effect of varying the shear stiffness characteristics of the upper sand layer was examined. All of the analyses had a total cover above the tunnel crown of 4*D*. The clay-only analysis (RC4) and the sand over clay analysis (RSG1), described immediately above, were used as references for comparison. Both clay and sand were represented by the 3-SKH model. RSG2 had a higher shear stiffness in the sand than RSG1, and RSG3 had lower shear stiffness in the sand than RSG1. The sand parameters were calculated such that the shear stiffness of the sand in RSG2 was twice that in RSG1, and in RSG3 the shear stiffness of the sand was half that in RSG1. This produced values which were still within a realistic range for sands (Jovicic, 1997). The rate of shear stiffness decay with

change in stress/strain was the same for each of these analyses. For RSG4, the shear stiffness parameters for the sand were the same as for RSG1 except that the shear stiffness decayed at the same rate as for kaolin, that being a reduced rate of change of stiffness with change in stress/strain.

Predicted normalised vertical displacement profiles at various depths are given in Figure 7.22. Varying the shear stiffness characteristics of the sand had minimal effect on the movements within the clay layer, as seen in Figures 7.22 (a & b). There was also very little difference between the movements predicted at the sand/ground surface for the sands with different stiffness characteristics (Figure 7.22c). However, in line with established design rules, there was clearly less lateral spreading of movement in the sand layers compared to that in the clay. In other words, the distribution of width of movement with depth was steeper than that in the corresponding clay layer, by comparison with the ground surface trough of RC4. Figure 7.23 shows the relative movements around the tunnel and generally confirms that the differences between the analyses were small.

The numerical results do not show the same significant effect of the shear stiffness of the upper sand layer on the spread of movements in the lower clay layer as the experimental results shown in Chapter 6. However, it should be noted that in contrast to the physical model tests, in the numerical simulations the shear stiffness only was varied; the bulk modulus remained constant. To accurately simulate the physical tests it would be necessary to change the value of κ^* in the numerical analyses to give a bulk modulus consistent with the change in shear stiffness. This was not done and unfortunately the result of this series of analyses is therefore inconclusive.

A final analysis (RSG1U) was conducted to investigate the effect of the drainage conditions in the upper layer on the distribution of ground movements. As described above, varying the stiffness characteristics resulted in only small changes. RSG1U was the same analysis as RSG1 but with the behaviour of the upper sand layer specified as undrained during the tunnel pressure reduction phase. The results are presented in Figure 7.24. Only small differences between the drained and undrained analysis were observed in the lower clay layer. However, the sand/ground surface trough for the undrained upper sand layer was shallower than that for the drained upper sand layer. The lateral spread of movements was less for the drained case than for the undrained case. This implies that the steeper distribution of movements with depth in coarse grained material is not solely a function of the stiffness but also of the

drainage conditions, although these are related by effective stress. When constant volume conditions were imposed the distribution of movements was not so steep.

7.8 Summary

FEA has been used as a tool to aid the investigation of ground movements around tunnels. A sophisticated soil model was applied with care using intrinsic soil properties, without fixing input parameters. Well controlled centrifuge model tests have been simulated numerically and the results compared with high quality data retrieved from the physical centrifuge events. This allowed evaluation of the numerical simulations, highlighting the strengths and weaknesses of the analyses, and so allowing FEA to be used with confidence in the investigation.

Twenty-three analyses were conducted, twelve of which were clay-only and focused largely on the modelling concerns which could not be assessed easily or economically by centrifuge testing. The remaining analyses included an upper sand layer and examined the effect of using different models to represent the sand, the influence of the sand depth, stiffness and the drainage conditions within the upper layer.

For the clay-only analyses, comparison with the centrifuge test data showed that although movements were not being predicted exactly, they were of similar magnitude and distribution, and this gave confidence that further analyses could produce meaningful results. The key findings from the clay-only analyses are given below.

i) The relative width of settlement troughs can be related to the distribution of movements around the tunnel, with the wider troughs being associated with proportionally larger movements at the springing and invert of the tunnel. Similar findings from numerical simulations were reported by Addenbrooke et al (1997).
ii) The proportion of movement at the springing and invert increased with depth of soil cover (increasing effective stress).
iii) Increasing the depth of soil beneath the tunnel invert caused an increase in the proportion of movements at the invert and the springing levels.
iv) Horizontal movements were sensitive to mesh fixities, but the position of the maximum horizontal movement was generally coincident with the point of inflexion of the settlement trough.

v) Increasing the distance from the tunnel to the laterally fixed boundary did not necessarily increase the trough width, but it did allow significantly greater proportions of horizontal movement.

vi) The distribution of movements at the tunnel boundary varied in accordance with the stress history of the soil in the vicinity.

vii) Preventing vertical movements at the lateral boundary produced unrealistic U-shaped settlement troughs.

viii) Analyses assuming undrained soil behaviour predicted less movement at the invert than the corresponding coupled consolidation analyses, which led to narrower settlement troughs. Also, the settlement profiles were not smooth.

The analyses conducted with a layer of sand overlying the clay were also compared directly with results from centrifuge model tests. Again, trough widths were over-predicted but the results were encouraging and allowed qualitative trends to be observed. Detailed comparisons with centrifuge test data gave a good indication of the reasons for the over-predicted trough widths. The key findings from these analyses are given below.

i) When considering movements in the lower clay layer, using a LE model for the upper sand layer produced similar, but not identical, trends of movements in the clay compared to those observed when the 3-SKH model was used for the sand.

ii) Using a LE model for the sand resulted in unrealistic movements in the sand layer, whereas use of the 3-SKH model produced more appropriate results.

iii) Detailed evaluation of the FEA by comparison with centrifuge test data showed that the analyses under-predicted the stiffness around the tunnel, particularly at the invert, which contributed to the wide settlement profiles predicted.

iv) Varying the stiffness characteristics of the upper sand layer, within realistic limits, resulted in minimal variation in the settlement profiles, although this may result from specifying changes in shear stiffness only and not in bulk modulus.

v) Characteristic steepening of the distribution of ground movements in the sand layer was achieved by using the 3-SKH model with appropriate sand parameters.

vi) The steepening of the distribution of movements in the sand layer may be a function of the drainage conditions imposed as well as the material parameters, although stiffness is a function of effective stress and therefore drainage conditions.

CHAPTER 8 SUMMARY, CONCLUSIONS AND FURTHER WORK

The work that has been presented was conducted to investigate movements around a tunnel in two-layer ground conditions, specifically ground movements above a tunnel in clay overlain by coarse grained materials. The purpose of this final chapter is to summarise the methods used, draw conclusions, highlight the limitations of the work, including suggestions for how the research could be taken further, and consider the implications.

8.1 Methodology

The principal methods of investigation were physical model studies using a geotechnical centrifuge and finite element analysis using a suitable constitutive model for soil. Both of these methods use effective stress path modelling to produce soil behaviour representative of prototype situations.

A total of twenty-eight plane strain centrifuge model tests were reported in which the tunnel was represented by a 50mm diameter cylindrical cavity, lined only by a latex membrane. The tunnel cavity was located within a layer of overconsolidated Speswhite kaolin clay, which had been preconsolidated at 1*g*, and in most cases the clay had an overlying layer of coarse grained material. The main variables in the tests were: the type of overlying strata; the thicknesses of the two strata; and the position of the water table. As the centrifuge acceleration was increased, compressed air pressure was supplied to the tunnel membrane to balance the increasing overburden stress. Tests were conducted at an acceleration of 100*g* when the cavity then represented a 5m diameter tunnel with a maximum depth to tunnel axis of 22.5m at prototype scale. Effective stress equilibrium was achieved at this acceleration before the ground movements were generated by reducing the tunnel support pressure reasonably rapidly to ensure a largely undrained response in the clay. Pore pressures were monitored using miniature pore pressure transducers and vertical displacements were measured at the ground surface and the clay/sand interface using conventional LVDTs. In addition, subsurface movements in the clay were obtained from analysis of images from a CCD camera mounted on the centrifuge swing. The camera viewed the front face of the model in-flight through a thick perspex window and images were recorded digitally throughout the test. A new image processing system developed at City University was used to track the displacement of targets pressed into the front vertical face of the soil producing a continuous record of calibrated co-ordinates in real-space. In this way both vertical and horizontal subsurface ground movements were obtained.

A limited series of stress path triaxial tests were conducted, largely to determine stiffness properties of the sands used in the centrifuge tests for analysis of the physical modelling test results and input for numerical analyses. The bender element technique was used to measure values of the small strain shear stiffness, G'_{max}, during K_0 compression, at stress levels similar to those experienced by the sands in the centrifuge model tests.

Twenty-three plane strain finite element analyses (FEA) were conducted using the 3-Surface Kinematic Hardening (3-SKH) model, an elasto-plastic soil model developed and implemented in the finite element program CRISP, at City University. The constitutive model allows plasticity within the state boundary surface and is capable of reproducing important aspects of soil behaviour including high stiffness at small strains, the decay of stiffness with increasing strain and the effect of recent stress history. The analyses were used mainly to enhance understanding of the events in the centrifuge tests and were therefore conducted at model scale. The procedure used for the centrifuge tests was followed carefully to simulate the stress history of the soil in the models as closely as possible. Direct and detailed comparison with results from the centrifuge model tests allowed full evaluation of the simulations so that the results could be used with confidence within the known limitations of the analyses. As well as evaluating the numerical model, the main points of investigation were: the effect of modelling conditions such as boundary proximity and stress history; the effect of using a linear elastic model for the sand; and the effect of the stiffness and depth of the upper strata on the movements in the clay.

8.2 Conclusions

A considerable amount of literature regarding tunnelling-induced ground movements has been published, including empirical, analytical and numerical solutions sometimes supported by field measurements and physical model testing. The problem of predicting movements due to tunnelling in ground made up of more than one soil layer had not been properly addressed until now. Generally, the literature shows that predictions rely on simple rules of superposition which have been grossly extrapolated from rules for single-layer soil profiles. To date, the interaction between the different layers of soil has been largely ignored. In addition, subsurface vertical and horizontal ground movements are expensive and difficult to obtain in the field and their prediction relies on limited reported data.

The work presented has shown that the integrated approach of combining physical modelling techniques, using a geotechnical centrifuge, and numerical analyses, using the finite element

method with a sophisticated constitutive model, is a very powerful method of investigating geotechnical problems. Recent advances in digital image processing have allowed detailed measurements of pre-collapse deformations to be made in scale models, not only at the boundaries of the model but throughout the full soil depth. This wealth of information has given considerable insight into ground movements around tunnels, and the knowledge gained has been applied to predicting ground movements in the plane perpendicular to single, long tunnels.

From the centrifuge test results the following observations were made.

i) Both surface and subsurface settlement troughs are well represented by Gaussian distributions, except within a vertical distance of approximately $0.5D$ above the tunnel crown, when settlement profiles can be expected to have significantly steeper gradients than the best-fit Gaussian curves.

ii) The form or shape of the distributions remains constant for a wide range of volume losses, until the tunnel begins to collapse (V~20%).

iii) Gaussian settlement profiles are characterised by i, the horizontal distance from the tunnel centreline to the point of inflexion of the curve. The variation of i with vertical distance above the tunnel axis suggested by Mair et al (1993), and given by Equation (2.15), adequately describes the distribution of vertical movements with depth for tunnels in overconsolidated, clay-only soil profiles. However, near a "free" ground surface the distribution of movements may be considerably wider and in close proximity of the tunnel crown it is likely to be considerably narrower (as indicated in (i) above) than that given by Mair et al (1993).

iv) For tunnels in clay with an overlying layer of different material, the upper layer affects the distribution of settlement trough width with depth in the lower layer and the ratio of shear stiffness at the interface between the materials should be taken into account; a procedure for this has been proposed using equations (6.16) and (6.17). If the upper layer is stiffer than the lower layer the settlement trough widths in the lower layer will be wider than at a similar depth in a single-soil ground profile.

v) For undrained (constant volume) conditions, horizontal displacements may be determined from the vertical displacements, since it has been shown that movement vectors focus on the point where the tangent to the distribution of i with depth intersects the vertical axis of the tunnel. The vector focus is generally below the tunnel invert except in the near vicinity of the tunnel or the upper unrestrained free ground surface. Generally, the maximum horizontal movement is approximately 20% of the maximum vertical movement and occurs at the point of inflexion of the vertical profile. At an

unrestrained free ground surface the maximum horizontal movement may be as high as 40% of the maximum vertical movement.

vi) Changes in pore pressure due to tunnelling may be approximated by the plasticity solutions of Mair and Taylor (1993), although this has been investigated only when the ratio of σ_h' / σ_v' is close to unity in the vicinity of the tunnel.

vii) Collapse loads of tunnels in clay with overlying coarse grained material may be lower or higher than for the corresponding clay-only situation if the coarse grained layer has respectively a low or high tendency for arching.

Finite element analysis, using a sophisticated constitutive model capable of representing well the soil behaviour over a wide range of strains, proved to be an extremely useful tool during the investigation. Comparison with the centrifuge test data showed that although movements were not being predicted exactly, they were of similar magnitude and distribution. Trough widths tended to be slightly over-predicted in comparison with the centrifuge test data but the results were encouraging and this allowed qualitative trends to be observed with confidence.

The key findings from the finite element analyses are listed below.

i) In part, settlement trough widths can be related to the distribution of movements at the tunnel boundary. The wider troughs were associated with proportionally larger movements at the springing and invert of the tunnel. The degree of movement at the springing and invert increased with depth of soil cover and also with the depth of soil beneath the tunnel invert. The relative distribution of movements at the tunnel boundary also varied in accordance with the stress history of the soil in the vicinity of the tunnel. Detailed comparison with centrifuge test data showed that the analyses under-predicted soil stiffness around the tunnel, particularly at the invert, which contributed to the wider settlement profiles predicted.

ii) Close lateral boundaries limit horizontal movements but may not significantly affect the distance to the point of inflexion of the vertical settlement profile.

iii) Analyses assuming undrained soil behaviour may predict less smooth settlement profiles than the corresponding coupled consolidation analyses, and also less movement at the invert which consequently leads to narrower settlement troughs.

iv) Realistic movements can be predicted in the lower clay layer by assuming that the upper sand layer is a linear elastic material. However, it is necessary to use a more sophisticated model for the sand, such as the 3-SKH model, if realistic movements through the sand layer are to be predicted. By using the 3-SKH model for the sand, with appropriate parameters for sand, it is possible to produce the characteristic steepening of the distribution of ground movements through the sand layer. However, it was shown

that this could be a function of the drainage conditions of the sand layer as well as the material parameters.

v) In contrast to the centrifuge model test results, varying the stiffness characteristics of the upper sand layer, represented by the 3-SKH model, within realistic limits, resulted in only small variations in the settlement profiles. There was no obvious explanation for the difference between the observations from the physical and numerical experiments but it may result from only specifying changes in shear stiffness and not bulk modulus of the sand in the FEA.

Following a detailed analysis of the experimental observations, a method was presented of predicting tunnelling-induced movements in the plane transverse to a tunnel in two-layer ground conditions. It is likely that the procedure could also be applied to situations with more soil layers. Superposition of movements predicted by assuming single-soil ground profiles is not sufficient as differences in stiffnesses between adjacent soil layers can have a significant effect on the movements in the lower layer. In addition, although the existing predictive equations for ground movements due to tunnelling in clay-only soil profiles have been shown to be generally adequate, there can be significant variations in close proximity to a tunnel or an unrestrained free ground surface.

The research has shown that centrifuge model testing combined with sophisticated numerical analysis is a very powerful method of investigating geotechnical problems. Valuable insight into the ground movements around a plane strain tunnel in two-layer ground conditions has been gained which should be of benefit to future tunnelling projects. The quantity and quality of data retrieved by the new image processing techniques described, combined with the more conventional methods, is worthy of particular note. Generally, the analysis and synthesis of data were specific to exploring the particular problem of the development of ground movements above a tunnel, but the techniques and methodology should be equally applicable to other investigations.

8.3 Limitations and further work

The applicability of the findings are intrinsically linked to the limitations of the work. An obvious limitation is that the model experiments were limited to green-field site conditions, although this is a necessary starting point for understanding the fundamental nature of ground movement around tunnels. Furthermore, the findings have not been assessed rigorously

against field observations, apart from the agreement of the all-clay test results with the field data presented by Mair et al (1993).

There are a number of limitations specifically concerning the centrifuge model testing which could be investigated further.

i) The initial stress state around the tunnel was limited to conditions of the ratio of σ_h' / σ_v' being close to unity because of the method of tunnel support (compressed air pressure). Different stress states could be achieved by using a retractable, rigid support system to impose the tunnelling-induced movements.

ii) The results from numerical modelling indicated that the proximity of the lateral and bottom boundaries may have some effect on the development of ground movements. However, movements both in the far-field and near to the tunnel invert were over-predicted by the FEA, suggesting that the numerical simulations were not appropriate near to the boundaries of the model. These effects could be investigated in the centrifuge by using the same model containers but with a reduced tunnel diameter and higher test accelerations, or by modelling a half-tunnel (semi-circular) against one of the lateral boundaries.

iii) Some model tests could be designed specifically to investigate the effects of friction on the measurements from image processing. For example, a block of preconsolidated clay could be moved by a ram, whilst displacements were measured both by LVDTs and image processing. In the same way, different methods of minimising the friction could be evaluated.

Although the stress history of the clay in the centrifuge models was practically the same for all the tests and the range of intrinsic stiffnesses for the sands was limited (Figure 4.4), the relative stiffnesses between the soil layers were realistic. It would be interesting to investigate a wider range of relative stiffnesses, for example, sand overlain by normally consolidated clay, although considerable thought would be required to achieve this on the centrifuge.

Limitations specific to the numerical analysis include (i) above regarding the initial stress conditions around the tunnel. In situ stress states with the ratio of σ_h' / σ_v' not equal to unity are more easily modelled using finite element analysis than physical testing because complex mechanical equipment is not required. In addition, although the 3-SKH model was used with some success to model the sands, it had been developed to simulate the behaviour of overconsolidated clays. Improvements in numerical predictions may be made with the development of a more appropriate model for sands.

Clearly, determination of the relative stiffness of the materials used in the centrifuge model tests was important in the synthesis of results and suggestions for improving predictions. There is potential for errors in estimating the stiffness moduli of the materials in the centrifuge tests but a consistent procedure was used and the relative values should be adequate. As stated above, if field data were examined it may be found that different ratios of other, directly measured, stiffness moduli are appropriate to use.

8.4 Implications of results

The research was conducted to improve predictions of ground movements due to tunnelling. Assessment of potential damage to existing services and structures is generally the end use of such predictions. Protective measures such as compensation grouting have proved to be very successful in limiting building damage on recent large scale tunnelling projects such as the Jubilee Line Extension in London. However, protecting buildings against tunnelling-induced movements in this way is extremely expensive and improvements to predictive methods have the obvious benefits of allowing more selective ground treatment and improving tunnel alignment optimisation.

The results have shown that the equations given by Mair et al (1993) are adequate for predicting green-field settlements induced by tunnelling for surface and subsurface movements in clay-only soil profiles (and possibly where there is only modest and smooth variation of stiffness with depth). The equations predict wider subsurface movements than would be obtained using surface based equations such as those given by O'Reilly and New (1982). Of course, this implies that more subsurface foundations, services and underground structures may be affected than would previously have been considered, but the damaging aspects of the movements, such as differential settlements and ground curvature, are less severe.

The presence of a layer of different material overlying the clay will modify the movements in the clay layer from those for a tunnel of equivalent depth in an all-clay soil profile. The research concentrated on ground movements due to tunnelling in clay with overlying stiff coarse grained materials. It was found that the presence of an overlying material which is stiff relative to the underlying clay causes wider movements in the clay than for a tunnel of equivalent depth in an all-clay soil profile. The zone of movement due to tunnelling is therefore wider but, as stated above, this implies that the damaging aspects are reduced. It

was shown in Chapter 6 that the relative stiffness of the two layers could be accounted for by considering the ratio of G'_{max} of the two materials at the interface. It would be useful to confirm this by field measurements, and it may be found that other, directly measured, in situ stiffness moduli are just as appropriate.

It has been shown that for undrained (constant volume) conditions horizontal ground displacements can be inferred from the vertical displacements as the ground movement vectors focus on the point where the tangent to the distribution of i with depth intersects the vertical tunnel axis. For the majority of the soil depth this focal point will be below the tunnel invert level, which implies lower magnitudes of horizontal movement than inferred by the commonly applied assumption of movements directed at the tunnel axis. The settlement trough widths decrease rapidly within a vertical distance of $0.5D$ of the tunnel crown and increase rapidly in the vicinity of a free-surface. The implication is that relatively high horizontal movements occur in these regions, if the soil behaviour is undrained. However, the presence of a building on top of the soil, or possibly even a pavement, will almost certainly reduce these horizontal movements as the soil surface is not then an unrestrained free-surface. In fact, very low horizontal movements at building foundation level have been reported by Standing (1998). If a pavement is sufficient to modify these near-surface movements, the free-surface effect is only of real concern for near-surface services across green-field sites.

It is clear that settlement trough widths are a function of the movements at the tunnel boundary, to some degree, and that relative movements can be assessed by considering the stress paths of soil elements in the vicinity of the tunnel. Analysing tunnelling-induced movements by investigating stress paths around the tunnel may prove particularly useful in specific situations where controlling ground movements is the critical issue.

The main findings of the research strictly apply to green-field site conditions and the presence of an existing structure will modify the ground movements due to tunnelling, probably in much the same way as a stiff overlying soil layer. However, it is necessary to be able to predict, and preferably to understand, the green-field movements before considering the effect of existing structures in modifying the ground movements. It is hoped that the findings of this research will make a useful contribution towards predicting ground movements due to tunnelling, especially for ground profiles consisting of more than one soil layer.

REFERENCES

Addenbrooke, T.I., Potts, D.M. and Puzrin, A.M. (1997). The influence of pre-failure soil stiffness on the numerical analysis of tunnel construction. *Géotechnique* 47, No.3, 693-712.

Allersma, H.G.B. (1991). Using image processing in centrifuge research. *Proc. Int. Conf. Centrifuge 91, Colorado* (ed. Hon-Yim Ko and F.G. McLean), 551-558. Balkema, Rotterdam.

Allersma, H.G.B. (1996). Using digital image processing field measurement. *Géotechnique* 46, No.3, 561-563.

Al-Tabbaa, A. (1987). *Permeability and stress-strain response of Speswhite kaolin.* Ph.D. thesis, University of Cambridge.

Al-Tabbaa, A. and Wood, D.M. (1989). An experimentally based 'bubble' model for clay. *Proc. 3rd Int. Conf. Numerical Models in Geomechanics* (ed. S. Pietruszczak and G.N. Pande), 91-99. Elsevier, London.

Atkinson, J.H. (1993). *An Introduction to the Mechanics of Soils and Foundations through Critical State Soil Mechanics.* McGraw-Hill, Maidenhead.

Atkinson, J.H. and Bransby, P.L. (1978). *The Mechanics of Soil. An Introduction to Critical State Soil Mechanics.* McGraw-Hill, Maidenhead.

Atkinson, J.H. and Evans, J.S. (1985). Discussion on: The measurement of soil stiffness in the triaxial apparatus by Jardine, R.J., Symes, M.J. and Burland, J.B.. *Géotechnique* 35, No.3, 378-382.

Atkinson, J.H. and Mair, R.J. (1981). Soil mechanics aspects of soft ground tunnelling. *Ground Engineering*, 20-24, 26 and 38.

Atkinson, J.H. and Potts, D.M. (1977a). Stability of shallow circular tunnels in cohesionless soil. *Géotechnique* 27, No.2, 203-215.

Atkinson, J.H. and Potts, D.M. (1977b). Subsidence above shallow tunnels in soft ground. *Proc. ASCE, J. Geotech. Eng.,* Vol.103, No.GT4, 307-325.

Atkinson, J.H., Richardson, D. and Stallebrass, S.E. (1990). Effect of recent stress history on the stiffness of overconsolidated soil. *Géotechnique* 40, No.4, 531-540.

Atkinson, J.H. and Sallfors, G. (1991). Experimental determination of stress-strain-time characteristics in laboratory and in situ tests. *Proc. 10th Eur. Conf. Soil Mechanics and Foundation Engineering, Florence,* 915-956.

Atkinson, J.H. and Stallebrass, S.E. (1991). A model for recent history and non-linearity in the stress-strain behaviour of overconsolidated soil. *Computer Methods and Advances in Geomechanics* (ed. Beer, Booker and Carter), 555-560. Balkema, Rotterdam.

Attewell, P.B. and Farmer, I.W. (1974). Ground deformations resulting from shield tunnelling in London clay. *Can. Geotech. J.*, 11, 380-395.

Attewell, P.B. and Woodman, J.P. (1982). Predicting the dynamics of ground settlement and its derivatives caused by tunnelling in soil. *Ground Engineering,* Vol.15, No.8, 13-22 and 36.

Attewell, P.B., Yeates, J. and Selby, A.R. (1986). *Soil Movements Induced by Tunnelling and their Effects on Pipelines and Structures.* Blackie and Son Ltd., Glasgow and London.

Baharom, B. (1996). *Development of a constitutive model for coarse-grained soils.* 1st year report during Ph.D. research, Geotechnical Engineering Research Centre Report GE/96/12, City University, London.

Barratt, D.A. and Tyler, R.G. (1976). Measurements of ground movement and lining behaviour on the London Underground at Regent's Park. *Transport and Road Research Laboratory Report* LR684.

Bezuijen, A. and van der Schrier, J. (1994). The influence of a bored tunnel on pile foundations. *Proc. Int. Conf. Centrifuge 94, Singapore* (ed. C.F. Leung, F.H. Lee and T.S. Tan), 681-686. Balkema, Rotterdam.

Bishop, A.W. and Wesley, L.D. (1975). A hydraulic triaxial apparatus for controlled stress path testing. *Géotechnique* 25, No.4, 657-670.

Bolton, M.D., Chin, C.Y. and Lu, Y.C. (1994). Compensation grouting. *Proc. Int. Conf. Centrifuge 94, Singapore* (ed. C.F. Leung, F.H. Lee and T.S. Tan), 719-724. Balkema, Rotterdam.

Boscardin, M.D. and Cording, E.J. (1989). Building response to excavation-induced settlement. *Proc. ASCE, J. of Geotech. Eng.*, Vol.115, No.1, 1-21.

Bowers, K.H., Hiller, D.M. and New, B.M. (1996). Ground movement over three years at the Heathrow Express Trial Tunnel. *Proc. Int. Symp. Geotechnical Aspects of Underground Construction in Soft Ground, London* (ed. R.J. Mair and R.N. Taylor), 647-652. Balkema, Rotterdam.

Britto, A.M. and Gunn, M.J. (1987). *Critical State Soil Mechanics via Finite Elements.* Ellis Horwood, Chichester.

Burland, J.B. (1989). The 9th Laurits Bjerrum Memorial Lecture: Small is beautiful - the stiffness of soils at small strains. *Can. Geotech. J.*, 26, 499-516.

Burland, J.B., Broms, B.B. and de Mello, V.F.B. (1977). State of the art report: Behaviour of foundations and structures. *Proc. 9th Int. Conf. Soil Mechanics and Foundation Engineering, Tokyo,* 495-546.

Burland, J.B. and Wroth, C.P. (1975). Settlements of buildings and associated damage. *Proc. Conf. Settlement of Structures*, 611-654. Pentech Press, London.

Butterfield, R. (1979). A natural compression law for soils. *Géotechnique* 29, No.4, 469-480.

Chambon, P. and Corté, J.-F. (1994). Shallow tunnels in cohesionless soil: stability of tunnel face. *Proc. ASCE, J. of Geotech. Eng.*, Vol.120, No.7, 1150-1163.

Chambon, P., Corté, J.-F., Garnier, J. and König, D. (1991). Face stability of shallow tunnels in granular soils. *Proc. Int. Conf. Centrifuge 91, Colorado* (ed. Hon-Yim Ko and F.G. McLean), 99-106. Balkema, Rotterdam.

CIRIA Report CP/5 (1992). *Prediction and effects of ground movements caused by tunnelling in soft ground beneath urban areas.*

Clough, G.W. and Leca, E. (1989). With focus on use of finite element methods for soft ground tunnelling. Review paper, *Tunnels et Micro-Tunnels en Terrain Meuble-du Chantier à la Théorie,* 531-573. Presse de l'Ecole National des Ponts et Chaussées, Paris.

Clough, G.W. and Schmidt, B. (1981). Design and performance of excavations and tunnels in soft clay. *Soft Clay Engineering*, 569-634. Elsevier.

Clough, G.W., Sweeney, B.P. and Finno, R.J. (1983). Measured soil response to EPB shield tunnelling. *Proc. ASCE, J. of Geotech. Eng.*, Vol.109, No.2, 131-149.

Coop, M.R. (1996). Personal communication.

Coop, M.R. (1998). Personal communication.

Coop, M.R. and Cuccovillo, T. (1998). The influence of geological origin on the behaviour of carbonate sands. *Proc. Int. Symp. Problematic Soils, IS-Tohoku 98, Japan,* to be published.

Coop, M.R. and Lee, I.K. (1993). The behaviour of granular soils at elevated stresses. *Predictive Soil Mechanics. Proc. Wroth Memorial Symp., Oxford, July 1992* (ed. G.T. Houlsby and A.N. Schofield), 186-198. Thomas Telford, London.

Cooper, M.A.R. and Robson, S. (1996). Chapter 2: Theory of close range photogrammetry. *Close Range Photogrammetry and Machine Vision* (ed. K.B. Atkinson), Whittles, Caithness, Scotland.

Cording, E.J. (1991). Control of ground movements around tunnels in soil. General report, *Proc. 9th Pan-American Conf. Soil Mechanics and Foundation Engineering, Chile.*

Cording. E.J. and Hansmire, W.H. (1975). Displacements around soft ground tunnels. General report, *Proc. 5th Pan-American Conf. Soil Mechanics and Foundation Engineering, Buenos Aires,* 571-632.

Cottechia, F. and Chandler, R.J. (1997). The influence of structure on the pre-failure behaviour of a natural clay. *Géotechnique* 47, No.3, 523-544.

Craig, W.H., James, R.G. and Schofield, R.N. (ed.) (1988). *Centrifuges in Soil Mechanics.* Balkema, Rotterdam.

Cuccovillo, T. and Coop, M.R. (1997). The measurement of local axial strains in triaxial tests using LVDTs. *Géotechnique* 47, No.1, 167-171.

Davis, E.H., Gunn, M.J., Mair, R.J. and Seneviratne, H.N. (1980). The stability of shallow tunnels and underground openings in cohesive material. *Géotechnique* 30, No.4, 397-416.

Deane, A.P. and Bassett, R.H. (1995). The Heathrow Express trial tunnel. *Proc. ICE. London, Geotechnical Engineering,* 113, 144-156.

Dyer, M.R., Hutchinson, M.T. and Evans, N. (1996). Sudden Valley Sewer: a case history. *Proc. Int. Symp. Geotechnical Aspects of Underground Construction in Soft Ground, London* (ed. R.J. Mair and R.N. Taylor), 671-676. Balkema, Rotterdam.

Dyvik, R. and Madshus, C. (1985). Laboratory measurements of G_{max} using bender elements. *Proc. ASCE Annual Convention: Advances in the Art of Testing Soils under Cyclic Conditions, Detroit, Michigan,* 186-197.

Eid, W.K. (1987). *Scaling effects in cone penetration testing in sand.* Ph.D. dissertation, Virginia Polytechnic and State University, Blacksburg, Virginia, USA.

Ethrog, U. (1994). Strain measurement by video image processing. *Recent advances in experimental mechanics, Lisbon* (ed. Silva Gomes et al), 411-415. Balkema, Rotterdam.

Frischmann, W.W., Hellings, J.E., Gittoes, G. and Snowden, C. (1994). Protection of the Mansion House against damage caused by ground movements due to the Docklands Light Railway Extension. *Proc. ICE, London, Geotechnical Engineering,* 107, 65-76.

Fujita, K. (1981). On the surface settlements caused by various methods of shield tunnelling. *Proc. 11th Int. Conf. Soil Mechanics and Foundation Engineering,* Vol.4, 609-610.

Garnier, J., Chambon, P., Ranaivoson, D., Charrier, J. and Mathurin, R. (1991). Computer image processing for displacements measurement. *Proc. Int. Conf. Centrifuge 91, Colorado* (ed. Hon-Yim Ko and McLean, F.G.), 543-550. Balkema, Rotterdam.

Glossop, N.H. and O'Reilly, M.P. (1982). Settlement caused by tunnelling through soft marine silty clay. *Tunnels and Tunnelling, October 1982,* 13-16.

Grant, R.J., Stallebrass, S.E. and Taylor, R.N. (1997). Prediction of pre-failure ground movements: Physical and numerical techniques. *Proc. 14th Int. Conf. Soil Mechanics and Foundation Engineering, Hamburg,* September 1997, 663-668. Balkema, Rotterdam.

Grant, R.J. and Taylor, R.N. (1996). Centrifuge modelling of ground movements due to tunnelling in layered ground. *Proc. Int. Symp. Geotechnical Aspects of Underground Construction in Soft Ground, London* (ed. R.J. Mair and R.N. Taylor), 507-512. Balkema, Rotterdam.

Gunn, M.J. (1993). The prediction of surface settlement profiles due to tunnelling. *Predictive Soil Mechanics. Proc. Wroth Memorial Symp., Oxford, July 1992* (ed. G.T. Houlsby and A.N. Schofield), 304-316. Thomas Telford, London.

Hong, S.W. and Bae, G.J. (1995). Ground movements associated with subway tunnelling in Korea. *Proc. Int. Symp. Underground Construction in Soft Ground, New Delhi* (ed. K. Fujita and O. Kusakabe), 229-232. Balkema, Rotterdam.

Hulme, T.W., Potter, L.A.C. and Shirlaw, J.N. (1989). Singapore Mass Rapid Transit System: construction. *Proc. ICE, London, Part 1, Transportation Engineering Group,* 86, 709-770.

Imamura, S., Nomoto, T., Mito, K., Ueno, K. and Kusakabe, O. (1996). Design and development of underground construction equipment in a centrifuge. *Proc. Int. Symp. Geotechnical Aspects of Underground Construction in Soft Ground, London* (ed. R.J. Mair and R.N. Taylor), 531-536. Balkema, Rotterdam.

Jaky, J. (1944). The coefficient of earth pressure at rest. *J. Soc. Hungarian Archit. Engrs.*, Vol.22, 355-358.

Jardine, R.J., Potts, D.M., Fourie, A.B. and Burland, J.B. (1986). Studies of the influence of non-linear stress-strain characteristics in soil-structure interaction. *Géotechnique* 36, No.2, 377-396.

Jardine, R.J., St John, H.D., Hight, D.W. and Potts, D.M. (1991). Some practical applications of a non-linear ground model. *Proc. 10th Eur. Conf. on Soil Mechanics and Foundation Engineering, Florence,* Vol.1, 223-228.

Jardine, R.J., Symes, M.J.R.P. and Burland, J.B. (1984). The measurement of soil stiffness in the triaxial apparatus. *Géotechnique* 34, No.3, 323-340.

Jovicic, V. (1997). *The measurement and interpretation of small strain stiffness of soils.* Ph.D. thesis, City University, London.

Jovicic, V. and Coop, M.R. (1997). Stiffness of coarse-grained soils at small strains. *Géotechnique* 47, No.3, 545-562.

Kim, S.H., Burd, H.J. and Milligan, G.W.E. (1998). Model testing of closely spaced tunnels in clay. *Géotechnique* 48, No.3, 375-388.

Kimura, T. and Mair, R.J. (1981). Centrifugal testing of model tunnels in soft clay. *Proc. 10th Int. Conf. Soil Mechanics and Foundation Engineering, Stockholm,* Vol.1, 319-322.

König, D., Güttler, U. and Jessberger, H.L. (1991). Stress redistributions during tunnel and shaft constructions. *Proc. Int. Conf. Centrifuge 91, Colorado* (ed. Hon-Yim Ko and F.G. McLean), 129-138. Balkema, Rotterdam.

König, D., Jessberger, H.L., Chambon, P. and Dangla, P. (1994). Behaviour of a tunnel lining embedded in a Bentonite quartz flour water mixture in granular soil. *Proc. Int. Conf. Centrifuge 94, Singapore* (ed. C.F. Leung, F.H. Lee and T.S. Tan), 705-712. Balkema, Rotterdam.

Kuwano, J., Taylor, R.N. and Grant, R.J. (1997). Centrifuge study on stability around tunnels in clay reinforced by soil nails. *Proc. 30th Year Anniversary Symp. Southeast Asian Geotechnical Society, Deep Foundations, Excavations, Ground Improvements and Tunnelling, Bangkok,* 4.35-4.48.

Kuwano, J., Taylor, R.N. and Grant, R.J. (1998). Modelling of deformations around tunnels in clay reinforced by soil nails. *Proc. Int. Conf. Centrifuge 98, Tokyo,* to be published. Balkema, Rotterdam.

Labiouse, V. (1995). Personal communication.

Lee, K.M. and Rowe, R.K. (1989). Deformations caused by surface loading and tunnelling: the role of elastic anisotropy. *Géotechnique* 39, No.1, 125-140.

Leung, C.F., Lee, F.H. and Tan, T.S. (ed.) (1994). Centrifuge 94. *Proc. Int. Conf. Centrifuge 94, Singapore.* Balkema, Rotterdam.

Mair, R.J. (1979). *Centrifugal modelling of tunnel construction in soft clay.* Ph.D. thesis, University of Cambridge.

Mair, R.J. (1993). Developments in geotechnical engineering research: applications to tunnels and deep excavations. *Unwin Memorial Lecture (1992), Proc. ICE, London,* Vol.97, No.1 (February 1993), 27-41.

Mair, R.J., Gunn, M.J. and O'Reilly, M.P. (1981). Ground movements around shallow tunnels in soft clay. *Proc. 10th Int. Conf. Soil Mechanics and Foundation Engineering, Stockholm,* 323-328. Balkema, Rotterdam.

Mair, R.J. and Taylor, R.N. (1993). Prediction of clay behaviour around tunnels using plasticity solutions. *Predictive Soil Mechanics. Proc. Wroth Memorial Symp., Oxford, July 1992* (ed. G.T. Houlsby and A.N. Schofield), 449-463. Thomas Telford, London.

Mair, R.J. and Taylor, R.N. (ed.) (1996). Geotechnical aspects of underground construction in soft ground. *Proc. Int. Symp. Geotechnical Aspects of Underground Construction in Soft Ground, London.* Balkema, Rotterdam.

Mair, R.J. and Taylor, R.N. (1997). Theme lecture: Bored tunnelling in the urban environment. *Proc. 14th Int. Conf. Soil Mechanics and Foundation Engineering, Hamburg.* Balkema, Rotterdam.

Mair, R.J., Taylor, R.N. and Bracegirdle, A. (1993). Subsurface settlement profiles above tunnels in clays. *Géotechnique* 43, No.2, 315-320.

Mair, R.J., Taylor, R.N. and Burland, J.B. (1996). Prediction of ground movements and assessment of risk of building damage due to bored tunnelling. *Proc. Int. Symp. Geotechnical Aspects of Underground Construction in Soft Ground, London* (ed. R.J. Mair and R.N. Taylor), 713-718. Balkema, Rotterdam.

Mair, R.J., Taylor, R.N. and Clarke, B.G. (1992). Repository tunnel construction in deep clay formations. *Commission of the European Communities* Report EUR 13964 EN.

Martos, F. (1958). Concerning an approximate equation of subsidence trough and its time factors. *Int. strata control congress, Leipzig (Berlin: Deutsche Akademie der Wissenschaften zu Berlin, Sektion fur Bergbau,* 1958*)*, 191-205.

Mayne, P.W. and Kulhawy, F.H. (1982). K_0 - OCR relationships in soil. *Proc. ASCE, J. Geotech. Eng.,* Vol.108.6, 851-872.

Moh, Z.-C., Ju, D.H. and Hwang, R.N. (1996). Ground movements around tunnels in soft ground. *Proc. Int. Symp. Geotechnical Aspects of Underground Construction in Soft Ground, London* (ed. R.J. Mair and R.N. Taylor), 725-730. Balkema, Rotterdam.

Nakai, T., Xu, L. and Yamazaki, H. (1997). 3D and 2D model tests and numerical analysis of settlements and earth pressures due to tunnel excavation. *Soils and Foundations,* Vol.37, No.3, 31-42.

Neerdael, B. and de Bruyn, D. (1989). Geotechnical research in the test drift of the HADES underground research facility at Mol. *Proc. CEC Technical Session, Geomechanics of clays for radioactive waste disposal, Commission of the European Communities* Report EUR 12027 EN/FR, 83-94.

New, B.M. and O'Reilly, M.P. (1991). Tunnelling induced ground movements; predicting their magnitude and effects. Invited review paper *4th Int. Con. Ground Movements and Structures, Cardiff*, 671-697. Pentech Press (1992).

New, B.M. and Bowers, K.H. (1994). Ground movement model validation at the Heathrow Express trial tunnel. *Proc. Tunnelling '94 Symp., Institution of Mining and Metallurgy, London,* 301-329. Chapman and Hall.

Nomoto, T., Mito, K., Imamura, S., Ueno, K. and Kusakabe, O. (1994). A miniature shield tunnelling machine for a centrifuge. *Proc. Int. Conf. Centrifuge '94, Singapore* (ed. C.F. Leung, F.H. Lee and T.S. Tan), 699-704. Balkema, Rotterdam.

Nomoto, T., Mito, K., Imamura, S., Ueno, K. and Kusakabe, O. (1996). Centrifuge modelling of construction processes of shield tunnel. *Proc. Int. Symp. Geotechnical Aspects of Underground Construction in Soft Ground, London* (ed. R.J. Mair and R.N. Taylor), 567-572. Balkema, Rotterdam.

Nyren, R. (1998). Personal communication.

O'Reilly, M.P. (1988). Evaluating and predicting ground settlements caused by tunnelling in London clay. *Proc. Tunnelling '88 Symp., Institution of Mining and Metallurgy, London*, 231-240.

O'Reilly, M.P., Mair, R.J. and Alderman, G.H. (1991). Long-term settlements over tunnels: an eleven-year study at Grimsby. *Proc. Tunnelling '91 Symp., Institution of Mining and Metallurgy, London,* 55-64.

O'Reilly, M.P. and New, B.M. (1982). Settlements above tunnels in the United Kingdom - their magnitude and prediction. *Proc. Tunnelling '82 Symp., Institution of Mining and Metallurgy, London* (ed. M.J. Jones), 173-181.

Pantelidou, H. (1994). *Changes in soil stiffness associated with diaphragm walling.* Ph.D. thesis, University of London, Queen Mary and Westfield College.

Peck, R.B. (1969). Deep excavations and tunnelling in soft ground. *Proc. 7th Int. Conf. Soil Mechanics and Foundation Engineering, Mexico,* State of the Art Volume, 225-290.

Potts, D.M. (1976). *Behaviour of lined and unlined tunnels in sand.* Ph.D. thesis, University of Cambridge.

Potts, D.M. and Addenbrooke, T.I. (1996). The influence of an existing surface structure on the ground movements due to tunnelling. *Proc. Int. Symp. Geotechnical Aspects of Underground Construction in Soft Ground, London* (ed. R.J. Mair and R.N. Taylor), 573-578. Balkema, Rotterdam.

Potts, D.M. and Addenbrooke, T.I. (1997). A structure's influence on tunnelling-induced ground movements. *Proc. ICE, London, Geotechnical Engineering,* 125, 109-125.

Rankin, W.J. (1988). Ground movements resulting from urban tunnelling: prediction and effects. *Engineering Geology of Underground Movements,* (ed. F.G. Bell, M.G. Culshaw, J.C. Cripps and M.A. Lovell), Geol. Soc. Engineering Geology Special Publication No.5, 79-92.

Roscoe, K.H. and Burland, J.B. (1968). On the generalised stress-strain behaviour of "wet" clay. *Engineering plasticity* (ed. J. Heyman and F.A. Leckie), 535-609. Cambridge University Press.

Rowe, R.K. and Kack, G.J. (1983). A theoretical examination of the settlements induced by tunnelling: four case histories. *Can. Geotech. J.*, 20, 299-314.

Rowe, R.K., Lo, K.Y. and Kack, G.J. (1983). A method of estimating surface settlement above tunnels constructed in soft ground. *Can. Geotech. J.*, 20, 11-22.

Sagaseta, C. (1987). Analysis of undrained soil deformation due to ground loss. *Géotechnique* 37, No.3, 301-320.

Sagaseta, C. (1988). Discussion on "Analysis of undrained soil deformation due to ground loss" by C. Sagaseta. *Géotechnique* 38, No.4, 647-649.

Schmidt, B. (1969). *Settlements and ground movements associated with tunnelling in soil.* Ph.D. thesis, University of Illinois.

Schmidt (1988). Discussion on "Analysis of undrained soil deformation due to ground loss" by C. Sagaseta. *Géotechnique* 38, No.4, 647-649.

Schofield, A.N. (1980). (The 20th Rankine lecture) Cambridge Geotechnical Centrifuge operations. *Géotechnique* 30, No.3, 227-268.

Schofield, A.N. and Wroth, C.P. (1968). *Critical State Soil Mechanics.* McGraw-Hill, London.

Schulteiss, P.J. (1982). *Influence of packing structure on seismic wave velocities in sediments.* Ph.D. thesis, University College of North Wales.

Selby, A.R. (1988). Surface movements caused by tunnelling in two-layer soil. *Engineering Geology of Underground Movements*, (ed. F.G. Bell, M.G. Culshaw, J.C. Cripps and M.A. Lovell), Geol. Soc. Engineering Geology Special Publication No.5, 71-77.

Seneviratne, H.N. (1979). *Deformations and pore pressure variations around shallow tunnels in soft clay.* Ph.D. thesis, Cambridge University.

Shirlaw, J.N. (1995). Observed and calculated pore pressures and deformations induced by an earth pressure balance shield: Discussion. *Can. Geotech. J.*, 32, 181-189.

Simpson, B. (1992). (The 32nd Rankine lecture) Retaining structures - displacement and design. *Géotechnique* 42, No.4, 539-576.

Simpson, B. (1993). Development and application of a new soil model for prediction of ground movements. *Predictive Soil Mechanics. Proc. Wroth Memorial Symp., Oxford, July 1992* (ed. G.T. Houlsby and A.N. Schofield), 628-643. Thomas Telford, London.

Simpson, B., Atkinson, J.H. and Jovicic, V. (1996). The influence of anisotropy on calculations of ground settlements above tunnels. *Proc. Int. Symp. Geotechnical Aspects of Underground Construction in Soft Ground, London* (ed. R.J. Mair and R.N. Taylor), 591-595. Balkema, Rotterdam.

Simpson, B., O'Riordan, N.J. and Croft, D.D. (1979). A computer model for the behaviour of London clay. *Géotechnique* 29, No.2, 149-177.

Skempton, A.W. and Chrimes, M.M. (1994). Thames Tunnel: geology, site investigation and geotechnical problems. *Géotechnique* 44, No.2, 191-216.

Skiker, A., Chambon, P., Leca, E. and Garnier, J. (1994). Face stability of tunnels constructed using the mechanical precutting tunnelling method. *Proc. Int. Conf. Centrifuge '94, Singapore* (ed. C.F. Leung, F.H. Lee and T.S. Tan), 713-718. Balkema, Rotterdam.

Stallebrass, S.E. (1990). *Modelling the effect of recent stress history on the deformation of overconsolidated soils.* Ph.D. thesis, City University, London.

Stallebrass, S.E., Grant, R.J. and Taylor, R.N. (1996). A finite element study of ground movements measured in centrifuge model tests of tunnels. *Proc. Int. Symp. Geotechnical Aspects of Underground Construction in Soft Ground, London* (ed. R.J. Mair and R.N. Taylor), 595-600. Balkema, Rotterdam.

Stallebrass, S.E., Jovicic, V. and Taylor, R.N. (1994a). Short term and long term settlements around a tunnel in stiff clay. *Proc. Eur. Conf. Numerical Methods in Geotechnical Engineering, Manchester,* 235-240. Balkema, Rotterdam.

Stallebrass, S.E., Jovicic, V. and Taylor, R.N. (1994b). The influence of recent stress history on ground movements around tunnels. *Proc. Conf. Pre-failure Deformation Characteristics of Geomaterials, IS-Hokkaido, Japan,* 615-620. Balkema, Rotterdam.

Stallebrass, S.E. and Taylor, R.N. (1997). The development and evaluation of a constitutive model for the prediction of ground movements in overconsolidated clay. *Géotechnique* 47, No.2, 235-255.

Standing, J.R. (1998). Personal communication.

Standing, J.R., Nyren, R.J., Burland, J.B. and Longworth, T.I. (1996). The measurement of ground movements due to tunnelling at two control sites along the Jubilee Line Extension. *Proc. Int. Symp. Geotechnical Aspects of Underground Construction in Soft Ground, London* (ed. R.J. Mair and R.N. Taylor), 751-756. Balkema, Rotterdam.

Taylor, R.N. (1984). *Ground movements associated with tunnels and trenches.* Ph.D. thesis, University of Cambridge.

Taylor, R.N. (ed.) (1995a). *Geotechnical Centrifuge Technology.* Blackie Academic and Professional, Glasgow.

Taylor, R.N. (1995b). Tunnelling in soft ground in the UK. *Proc. Int. Symp. Underground Construction in Soft Ground, New Delhi* (ed. K. Fujita and O. Kusakabe), 123-126. Balkema, Rotterdam.

Taylor, R.N. and Grant, R.J. (1998). Centrifuge modelling of the influence of surface structures on tunnelling induced ground movements. *Proc. World Tunnelling Congress 98 on Tunnels and Metropolises, Sao Paulo, Brazil, April 1998* (ed. A. Negro Jr. and A.A. Ferreira), 261-266. Balkema, Rotterdam.

Taylor, R.N., Robson, S., Grant, R.J. and Kuwano, J. (1998). An image analysis system for determining plane and 3-D displacements in centrifuge models. *Proc. Int. Conf. Centrifuge 98, Tokyo,* to be published. Balkema, Rotterdam.

Uriel, A.O. and Sagaseta, C. (1989). General Report: Discussion Session 9; Selection of design parameters for underground construction. *Proc. 12th Int. Conf. Soil Mechanics and Foundation Engineering, Rio de Janeiro,* Vol.4, 2521-2551. Balkema, Rotterdam.

Viggiani, G. (1992). *Small strain stiffness of fine grained soils.* Ph.D. thesis, City University, London.

Viggiani, G. and Atkinson, J.H. (1995). Stiffness of fine-grained soils at very small strains. *Géotechnique* 45, No.2, 249-267.

Wheeler, S.J. and Sivakumar, V. (1993). Development and application of a critical state model for unsaturated soil. *Predictive Soil Mechanics. Proc. Wroth Memorial Symp., Oxford, July 1992* (ed. G.T. Houlsby and A.N. Schofield), 709-728. Thomas Telford, London.

Wood, D.M. (1990). *Soil Behaviour and Critical State Soil Mechanics.* Cambridge University Press.

Wroth, C.P. and Houlsby, G.T. (1985). Soil mechanics - property characterisation, and analysis procedures. *Proc. 11th Int. Conf. Soil Mechanics and Foundation Engineering, San Francisco,* Vol.1, 1-55. Balkema, Rotterdam.

Yoshimura, H. Miyabe, K. and Tohda, J. (1994). Response of a tunnel lining due to an adjacent twin shield tunnelling. *Proc. Int. Conf. Centrifuge 94, Singapore* (ed. C.F. Leung, F.H. Lee and T.S. Tan), 693-698. Balkema, Rotterdam.

test	date	clay cover (above crown)		upper layer (above clay)		total cover (above crown)		water table (below surface)		type of upper layer	comments
		mm	no. of D	mm	no. of D	mm	no. of D	mm	no. of D		
RJG1	08/03/94	200	4	0	0	200	4	N/A	N/A	none	preliminary not in equilibrium, oil on surface
RJG2	22/03/94	100	2	100	2	200	4	N/A	N/A	52/100 LBS	ditto, sand placed by hand
RJG3	04/05/94	100	2	100	2	200	4	25	0.5	Flint Gravel	in equilibrium
RJG4	07/06/94	150	3	50	1	200	4	25	0.5	Flint Gravel	preconsolidation interrupted, σ_T jumpy
RJG5	21/06/94	50	1	150	3	200	4	25	0.5	Flint Gravel	clay visibly softer than RJG4
RJG6	27/07/94	12.5	0.25	187.5	3.75	200	4	25	0.5	Flint Gravel	preconsolidation interrupted
RJG7	23/08/94	12.5	0.25	187.5	3.75	200	4	25	0.5	52/100 LBS	15% loss in σ_T overnight
RJG8	04/10/94	12.5	0.25	187.5	3.75	200	4	25	0.5	14/25 LBS	junction box problems
RJG9	26/10/94	200	4	0	0	200	4	25	0.5	none	junction box part-failure, oil on surface
RJG10	17/11/94	50	1	50	1	100	2	25	0.5	Flint Gravel	first markers in sand
RJG11	08/03/95	75	1.5	67(e)	1.34(e)	142	2.84	17	0.34	water	flexible overburden
RJG12	05/04/95	75	1.5	67	1.34	142	2.84	17	0.34	25/52 LBS	slight leak at window seal during test
RJG13	10/05/95	75	1.5	67	1.34	142	2.84	67	1.34	25/52 LBS	dry sand
RJG14	05/06/95	75	1.5	0	0	75	1.5	25	0.5	none	oil on clay surface to prevent evaporation
RJG15	29/06/95	150	3	0	0	150	3	25	0.5	none	oil on clay surface to prevent evaporation
RJG16	25/07/95	75	1.5	72	1.44	147	2.94	22	0.44	mixed	sand is mixed LBS
RJG17	28/03/96	125	2.5	0	0	125	2.5	25	0.5	none	partially blocked base drainage
RJG18	23/04/96	125	2.5	75	1.5	200	4	25	0.5	52/100 LBS	
RJG19	09/05/96	125	2.5	75	1.5	200	4	75	1.5	52/100 LBS	dense dry sand, junction box problem
RJG20	30/05/96	125	2.5	75	1.5	200	4	75	1.5	52/100 LBS	loose dry sand, junction box problems

Note:

1. The clay in each test had a similar pre-consolidation history. 1-dimensional compression to 500kPa ($\sigma_v'_{max}$) followed by swelling to 250kPa ($\sigma_v'_{fin}$) throughout. Care was taken to minimise swelling during model preparation. RJG1 and 2 were preliminary tests and $\sigma_v'_{max}$ was 250kPa with no swelling phase.
2. Each test was conducted on the centrifuge at 100g, and, with the exception of preliminary tests RJG1 and 2, the model was allowed to come into equilibrium with the new stress conditions overnight (approx. 16 hours) before the tunnel support pressure was reduced.
3. Flint Gravel is a sub-angular medium silica sand. Leighton Buzzard Sand (LBS) is a sub-rounded washed silica sand with gradings as follows; 14/25 - coarse sand, 25/52 - medium sand, 52/100 - medium fine sand.

(e) Water in latex membrane representing this equivalent depth of sand.

Table 3.1 Centrifuge tests conducted in main series

test	date	clay cover (above crown)		upper layer (above clay)		total cover (above crown)		water table (below surface)		type of upper layer	comments
		mm	no. of D	mm	no. of D	mm	no. of D	mm	no. of D		
TH1	19/06/96	150	3	0	0	150	3	5	0.1	clay	datum test
TH2	10/07/96	75	1.50	36	0.72	111	2.22	36	0.72	med/dense dry sand	
TH3	24/07/96	75	1.50	40	0.80	115	2.30	40	0.80	med/loose dry sand	poor lubrication on window
TH4	22/08/96	75	1.50	42	0.84	117	2.34	42	0.84	loose dry sand	ditto above
TH5	06/09/96	75	1.50	57(w)	1.14(w)	132	2.64	57	1.14	water	ditto above
TH6	20/09/96	75	1.50	93	1.86	168	3.36	5	0.1	med/dense saturated sand	incorrect σ_v' in clay
MC01	07/11/97	75	1.50	58	1.16	133	2.66	5	0.1	med/dense saturated sand	as TH6 with correct σ_v' in clay
CK1	12/02/97	100	2	0	0	100	2	20	0.4	none	image processing only

Note:

1. The clay in each test had a similar pre-consolidation history. 1-dimensional compression to 500kPa ($\sigma_v'_{max}$) followed by swelling to 250kPa ($\sigma_v'_{fin}$) throughout. Care was taken to mimimise swelling during model preparation.
2. Each test was conducted on the centrifuge at 100g, and the model was allowed to come into equilibrium with the new stress conditions overnight (approx. 16 hours) before the tunnel support pressure was reduced.
3. The object of the above test series was to isolate the effect of the upper layer on the movements in the lower layer by having the same σ_v' profile throughout the lower clay layer in each test.
4. The sand used in the above tests was 52/100 Leighton Buzzard Sand (LBS) which is a sub-rounded washed medium fine silica sand.

(w) Water in latex membrane.

Table 3.2 Additional centrifuge tests (conducted in collaboration)

test	sand type	initial v	final v	measurements attempted/achieved		
				bender elements	local LVDTs	strain level *
TT1	14/25 LBS	1.76	1.78	no	yes	ε_s = 0.001 - 17%
TT2	mixed LBS	1.54	1.64	no	yes	ε_s = 0.001 - 12%
TT3	52/100 LBS	1.61	N/A	yes	no	none
TT4	52/100 LBS	1.61	1.70	yes	no	ε_s = 0.01 - 8%
TT5	14/25 LBS	1.53	1.72	yes	no	ε_s = 0.01 - 33%
TT6	Flint Gravel	1.47	1.63	yes	no	ε_s = 0.01 - 34%
TT7	mixed LBS	1.46	1.62	yes	no	ε_s = 0.01 - 24%

Note:

* using displacement transducers

1. Details of the sands are given in Section 3.4.1. Gradings are given in Figure 3.10.
2. All samples were compacted during preparation and subjected to K_0 compression to $p' = q' = 60$kPa followed by constant p' shearing (pore water back pressure = 300kPa).

Table 4.1 Triaxial tests conducted

sand type	used in centrifuge tests	specific volume v	dry unit weight γ_d (kN/m^3)
Flint Gravel (med/dense)	(RJG3, 4, 5, 6 & 10)	1.50	17.3
52/100 LBS (med/dense)	(RJG2, 7, 18 & 19), (TH2 & 6) & (MC1)	1.62	16.0
52/100 LBS (med/loose)	(TH3)	1.80	14.4
52/100 LBS (loose)	(RJG20) & (TH4)	1.90	13.7
25/52 LBS (med/dense)	(RJG12 & 13)	1.49	17.4
14/25 LBS (med/dense)	(RJG8)	1.50	17.3
mixed LBS (med/dense)	(RJG16)	1.49	17.4

Note:

1. Details of the sands are given in Section 3.4.1. Gradings are given in Figure 3.10.
2. v and therefore γ_d were determined from independent tests.

Table 4.2 Specific volumes and dry unit weights for the sands used in the centrifuge tests

symbol	parameter	value	
		kaolin	silica sand
A	coefficient in relationship for $G'_{max\,(nc)}$	1964 (1)	see 4.7
n	exponent in relationship for $G'_{max\,(nc)}$	0.65 (1)	see 4.7
m	exponent in relationship for $G'_{max\,(oc)}$	0.2 (1)	see 4.7
κ	average gradient of swelling line in v:lnp' space	0.035 (1)	0.014 (3)
λ	gradient of compression line in v:lnp' space	0.18 (1)	0.16 (3)
M	stress ratio at critical state (q': p')	0.89 (1)	1.28 (3)
Γ	specific volume at critical state when p'=1kPa	2.994 (1)	2.99 (3)
N	specific volume on INCL when p'=1kPa	3.05 (2)	3.17 (3)
ϕ'_c	critical state angle of shearing resistance	23°	32°
γ	unit weight of soil (saturated for clay)	17.5 (kN/m^3) (4)	γ_d given above
γ_w	unit weight of water	9.81 (kN/m^3)	9.81 (kN/m^3)

Note:

1. Material properties from:
   - (1) Stallebrass and Taylor (1997)
   - (2) Pantelidou (1994)
   - (3) Coop and Lee (1993)
   - (4) many laboratory tests at City University by other researchers (for average volumetric state in the centrifuge tests)
2. Additional material parameters used specifically for numerical modelling are given in Chapter 7.

Table 4.3 General material parameters

test	date	recording medium	camera/lens	camera located by	comments	quality of measurement/use
RJG1	08/03/94	VHS tape	colour/wide	soil targets or window edge	preliminary test	visual only
RJG2	22/03/94	VHS tape	colour/wide	soil targets or window edge	preliminary test	visual only
RJG3	04/05/94	VHS tape	colour/wide	soil targets or window edge	poor lighting	very low/visual
RJG4	07/06/94	VHS tape	colour/wide	soil targets or window edge	poor lighting	very low/visual
RJG5	21/06/94	VHS tape	colour/wide	soil targets or window edge	poor lighting	very low/visual
RJG6	27/07/94	VHS tape	colour/wide	soil targets or window edge	small clay cover	very low/visual
RJG7	23/08/94	S-VHS tape	colour/wide	soil targets or window edge	small clay cover	very low/visual
RJG8	04/10/94	S-VHS tape	colour/wide	soil targets or window edge	small clay cover	very low/visual
RJG9	26/10/94	S-VHS tape	colour /wide	few control targets on front	poor control	very low/visual
RJG10	17/11/94	S-VHS tape	colour/wide	control targets on front		low/visual
RJG11	08/03/95	S-VHS tape	colour/standard	control targets on front		low/visual
RJG12	05/04/95	S-VHS tape	colour/standard	control targets on front		low/qualitative
RJG13	10/05/95	S-VHS tape	colour/standard	control targets on front	poor control	very low/qualitative
RJG14	05/06/95	S-VHS tape	colour/standard	control targets on front		low/qualitative
RJG15	29/06/95	S-VHS tape	mono./standard	good control targets on front		medium/qualitative
RJG16	25/07/95	S-VHS tape	mono./standard	good control targets on front		medium/qualitative
RJG17	28/03/96	DIGITAL	mono./standard	good control targets on front		medium/quantitative
RJG18	23/04/96	DIGITAL	mono./standard	good control targets on front		medium/quantitative
RJG19	09/05/96	DIGITAL	mono./standard	good control targets on front		medium/quantitative
RJG20	30/05/96	DIGITAL	mono./standard	good control targets on front		medium/quantitative
TH1	19/06/96	DIGITAL	mono./standard	good control targets on front		medium/quantitative
TH2	10/07/96	DIGITAL	mono./standard	good control targets on front		medium/quantitative
TH3	24/07/96	DIGITAL	mono./standard	good control targets on front	bad friction	medium/quantitative
TH4	22/08/96	DIGITAL	mono./standard	good control targets on front	bad friction	medium/quantitative
TH5	06/09/96	DIGITAL	mono./standard	good control targets on front	bad friction	medium/quantitative
TH6	20/09/96	DIGITAL	mono./standard	good control targets on front		high/quantitative
MC01	07/11/97	DIGITAL	mono./standard	control targets in soil plane		high/quantitative
CK1	12/02/97	DIGITAL	mono./standard	control targets in soil plane		high/quantitative

Table 5.1 Details of image processing for the centrifuge tests

test	depth of clay above tunnel axis (mm)	i_c at clay surface (mm)	depth of sand, z_l (mm)	i_s at sand surface, if present, (mm)
RJG1	225	118	0	N/A
RJG2	125	106	100	124
RJG3	125	99	100	113
RJG4	175	112	50	117
RJG5	75	99	150	130
RJG6	37.5	79	187.5	115
RJG7	37.5	95	187.5	137
RJG8	37.5	94	187.5	154
RJG9	225	122	0	N/A
RJG10	75	68	50	82
RJG11	100	61	124 of water	N/A
RJG12	100	82	67	103
RJG13	100	80	67	99
RJG14	100	61	0	N/A
RJG15	175	104	0	N/A
RJG16	100	82	72	103
RJG17	150	76	0	N/A
RJG18	150	96	75	108
RJG19	150	108	75	133
RJG20	150	92	75	108
TH1	175	111	0	N/A
TH2	100	65	36	77
TH3	100	66	40	81
TH4	100	59	42	74
TH5	100	58	57 of water	N/A
TH6	100	84	93	98
MC01	100	74	58	82
CK1	125	no LVDTs	0	N/A

Figure 5.2 *i* values at clay and sand surfaces (determined from measurements by LVDTs)

		UPPER LAYER			CLAY			
test	**depth to water table (mm)**	**depth (mm)**	G'_{max} **(MPa) interface**	G'_{max} **(MPa) average**	**depth (mm)**	G'_{max} **(MPa) interface (surface +)**	G'_{max} **(MPa) tunnel axis**	G'_{max} **(MPa) average**
RJG1	N/A	0	N/A		225	σ_v' not known in clay		
RJG2	N/A	100	118.9	72.8	125	σ_v' not known in clay		
RJG3	25	100	101.2	66.5	125	60.4	73.1	67.1
RJG4	25	50	70.7	46.6	175	50.1	71.4	61.9
RJG5	25	150	127.0	82.5	75	68.1	74.9	71.6
RJG6	25	187.5	145.6	93.8	37.5	73.3	76.2	74.7
RJG7	25	187.5	138.7	89.4	37.5	71.4	74.4	72.9
RJG8	25	187.5	197.4	128.6	37.5	73.3	76.2	74.7
RJG9	25	0	N/A		225	35.9	70.5	56.7
RJG10	25	50	70.7	46.6	75	50.1	60.9	55.9
RJG11	17	124	0	0	100	52.4	65.3	59.3
RJG12	17	67	77.0	50.4	100	52.4	65.3	59.3
RJG13	67	67	95.5	58.4	100	58.6	69.6	64.4
RJG14	25	0	N/A		100	35.9	56.5	47.7
RJG15	25	0	N/A		175	35.9	65.5	53.5
RJG16	22	72	140.2	96.1	100	55.8	67.6	62.1
RJG17	25	0	N/A		150	35.9	64.9	53.7
RJG18	25	75	82.6	54.6	150	54.3	71.4	63.6
RJG19	75	75	99.2	60.7	150	59.7	74.8	67.8
RJG20	75	75	80.7	49.4	150	56.7	72.9	65.4
TH1	5	0	N/A		175	22.1	62.0	48.5*
TH2	36	36	62.5	39.2	100	47.0	62.0	55.3
TH3	40	40	55.5	34.7	100	47.0	62.0	55.3
TH4	42	42	52.9	33.0	100	47.0	62.0	55.3
TH5	57	57	0	0	100	47.0	62.0	55.3
TH6	5	93	87.1	54.7	100	55.8	67.6	62.1
MC01	5	58	62.6	38.9	100	47.0	62.0	55.3
CK1	20	0	N/A		125	33.5	59.0	47.2

* average G'_{max} for lower 100mm of clay only is 55.3MPa (47.0MPa at $z_0 - z = 100$mm)

\+ ground surface for clay only tests, assuming negative pore pressure corresponding to the depth of the water table

Table 6.1 Stiffnesses of layers in centrifuge model tests

analysis	cover above tunnel crown		comments
	(mm)	(no. of D)	
RC2	100	2	centrifuge model test not conducted
RC3A	150	3	typical centrifuge test simulation with correct $\sigma_{T\ max}$ (300kPa)
RC3B	150	3	as RC3A with low $\sigma_{T\ max}$ (250kPa)
RC3C	150	3	as RC3A with high $\sigma_{T\ max}$ (350kPa)
RC3AM	150	3	as RC3A with additional swelling to σ_v' = 125kPa before imposing full gravity level (100g)
RC4	200	4	typical centrifuge test simulation
RC4W	200	4	as RC4 with mesh extended to twice normal width
RC4D	200	4	as RC4 with mesh extended to 4D below the tunnel invert
RC4WD	200	4	as RC4 with mesh extended in width and depth as above
RC4X	200	4	as RC4 with consolidation time extended by 10 hours before σ_T reduction phase
RC4U	200	4	as RC4 with history phase conducted under drained conditions and σ_T reduction phase conducted under undrained conditions
RC4P	200	4	as RC4 with mesh fixed vertically at right hand boundary

Note:

1. With the exception of RC4U, all analyses listed above were conducted using the coupled consolidation facility in CRISP, with the water table 25mm (0.5D) below the soil surface.
2. The parameters used are those given in Table 7.3.
3. Unless stated otherwise the analyses were conducted using the following procedure.
   a. Surcharge on soil surface with insitu gravity level = 56.25g, producing σ_v' = 500kPa throughout soil depth (assumed K_0 = 0.63).
   b. 250kPa surcharge removed from soil surface with time increment set to allow full consolidation, producing σ_v' = 250kPa throughout soil depth.
   c. Rapid increase in gravity to 100g whilst removing remaining surcharge, followed by consolidation phase.
   d. Elements in tunnel removed and $\sigma_{T\ max}$ applied over short time period followed by consolidation phase, producing equilibrium σ_v' profile.
   e. Reduction of σ_T at a rate of 1kPa/second.

Table 7.1 Finite element analyses (all-clay)

analysis	clay cover (above crown)		upper stratum depth (cover above clay)		total cover (above tunnel crown)		comments
	(mm)	(no. of D)	(mm)	(no. of D)	(mm)	(no. of D)	
RS1	75	1.5	75	1.5	150	3	simulation of centrifuge tests RG16, LE model for sand, water table effectively 25mm (0.5D) below the sand surface
RS2	100	2	50	1	150	3	as RS1
RS3	50	1	100	2	150	3	as RS1
RSN1	75	1.5	75	1.5	150	3	as RS1 with 3-SKH model for sand (silica sand 1)
RSN2	100	2	50	1	150	3	as RS2 with 3-SKH model for sand (silica sand 1)
RSN3	50	1	100	2	150	3	as RS3 with 3-SKH model for sand (silica sand 1)
RSG1 & RSG1U	125	2.5	75	1.5	200	4	simulation of centrifuge test RJG20, 3-SKH model for sand, water table at clay/sand interface - 2 analyses, upper layer drained and undrained (silica sand 2)
RSG2	125	2.5	75	1.5	200	4	as RSG1 with higher G'_{max} (silica sand 3)
RSG3	125	2.5	75	1.5	200	4	as RSG1 with lower G'_{max} (silica sand 4)
RSG4	125	2.5	75	1.5	200	4	as RSG1 with slower decay of stiffness - same as kaolin (silica sand 5)

Note:

1. All analyses listed above were conducted using the 3-SKH model and coupled consolidation facility in CRISP for the lower clay layer. The modelling of the upper strata is highlighted in the table.
2. The parameters used are those given in Table 7.3.
3. The procedure for the above analyses varied depending on the position of the water table and the need to simulate the effective stresses in the clay. The following is a general procedure only.
   a. No upper layer. Surcharge on clay surface with insitu gravity level = 56.25g, producing constant σ_v'=500kPa throughout clay depth (assumed $K_0 = 0.63$).
   b. 250kPa surcharge removed from clay surface with time increment set to allow full consolidation, producing constant σ_v'=250kPa throughout clay depth.
   c. Rapid increase in gravity to 100g whilst removing more surcharge, followed by consolidation phase.
   d. Elements in tunnel removed and $\sigma_{T\,max}$ applied over very short time period followed by consolidation phase.
   e. Upper layer built whilst removing surcharge equivalent to sand weight from clay surface (some surcharge may remain to maintain correct σ_v' profile in clay).
   f. Reduction of σ_T at a rate of 1kPa/second.

Table 7.2 Finite element analyses (including an upper stratum)

symbol	parameter	value					
3-Surface Kinematic Hardening model							
		kaolin	**silica sand (1)**	**silica sand (2)**	**silica sand (3)**	**silica sand (4)**	**silica sand (5)**
A or A^*	coefficient in relationship for G'_{max}	1964	4000	6000	23500	1200	6000
n or n^*	exponent in relationship for G'_{max}	0.65	0.59	0.63	0.40	0.95	0.63
m	exponent in relationship for G'_{max}	0.2	0.103	0	0	0	0
κ^*	gradient of swelling line in $\ln v : \ln p'$ space	0.005	0.000375	0.000375	0.000375	0.000375	0.000375
λ^*	gradient of compression line in $\ln v : \ln p'$ space	0.073	0.06	0.06	0.06	0.06	0.06
M	stress ratio at critical state (q' / p')	0.89	1.28	1.28	1.28	1.28	1.28
Γ	specific volume at critical state when p' =1kPa	2.994	2.99	2.99	2.99	2.99	2.99
k_v (m/sec)	vertical permeability	0.7E-9	drained	drained/undrained	drained	drained	drained
k_h (m/sec)	horizontal permeability	1.8E-9	drained	drained/undrained	drained	drained	drained
T	size ratio of history to bounding surface	0.25	0.001	0.001	0.001	0.001	0.25
S^*	size ratio of yield to history surface	0.08	0.2	0.2	0.2	0.2	0.08
ψ	exponent in the hardening modulus	2.5	9.0	9.0	9.0	9.0	2.5
γ_w (kN/m^3)	unit weight of water	9.81	9.81	9.81	9.81	9.81	9.81
γ (kN/m^3)	saturated unit weight of soil	17.44	19.00	N/A	N/A	N/A	N/A
γ_d (kN/m^3)	dry unit weight of soil	N/A	N/A	13.7	13.7	13.7	13.7
γ' (kN/m^3)	$\gamma - \gamma_w$	N/A	9.19	N/A	N/A	N/A	N/A
isotropic linear elastic model							
		silica sand					
E' (kPa)	Young's modulus	46800					
ν'	Poisson's ratio	0.3					
k_v & k_h	vertical and horizontal permeability	drained					
γ_w (kN/m^3)	unit weight of water	9.81					
γ (kN/m^3)	saturated unit weight of soil	19.00					
γ' (kN/m^3)	$\gamma - \gamma_w$	9.19					

Note:

1. For the 3-SKH model the elastic shear modulus was taken as $G'_{max}/p'_r = A(p'/p'_r)^n R_0^m$, where p'_r is a reference pressure equal to 1kPa and R_0 is the overconsolidation ratio in terms of the mean normal effective stress (p'_p/p').
2. For the isotropic linear elastic model the shear modulus is by definition $G' = E'/2(1+\nu')$.

Table 7.3 Summary of material properties for finite element analysis

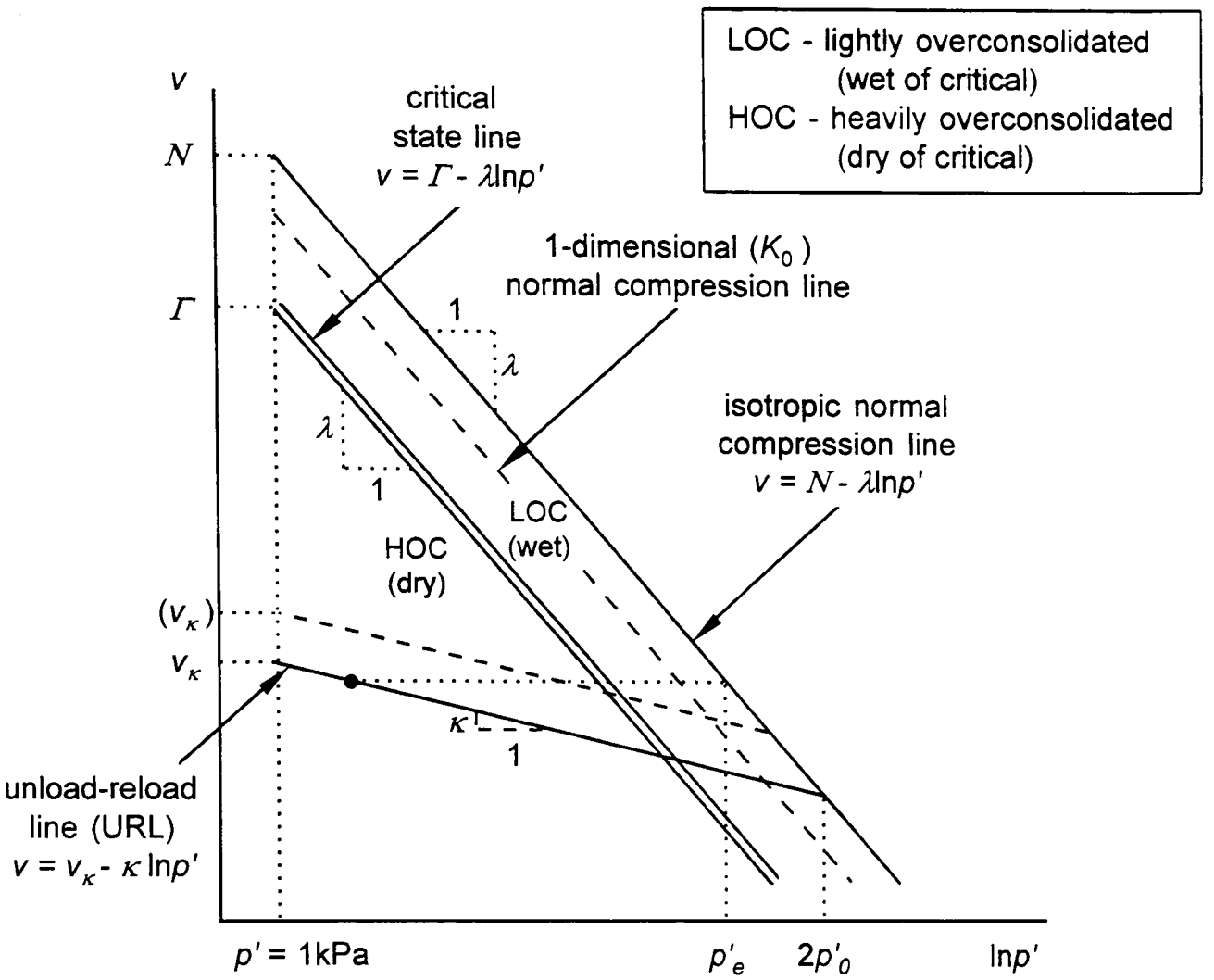

Figure 2.1 (a) Critical state parameters in v:lnp' space

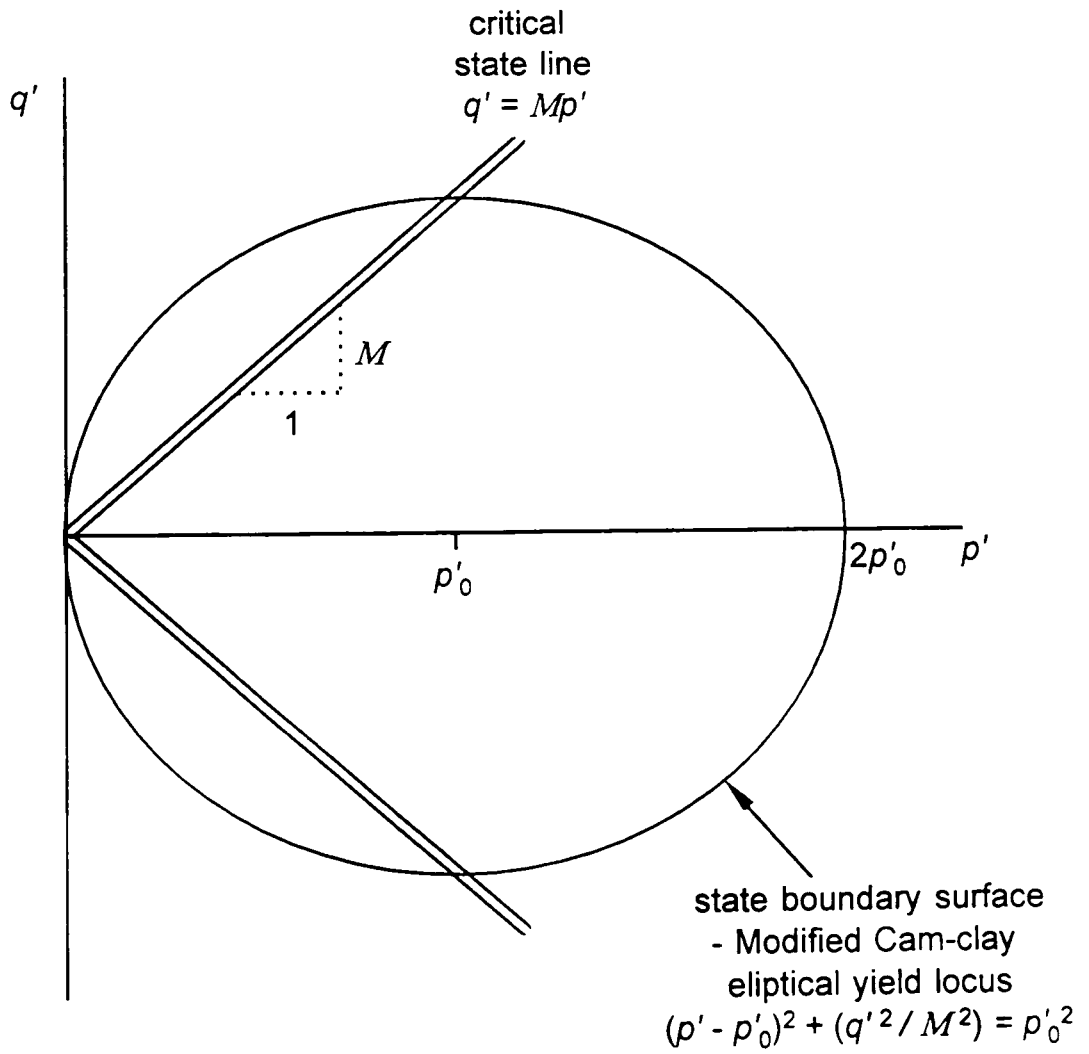

Figure 2.1 (b) Critical state and state boundary surface parameters in q':p' space
(the state boundary surface is projected onto an unload-reload line)

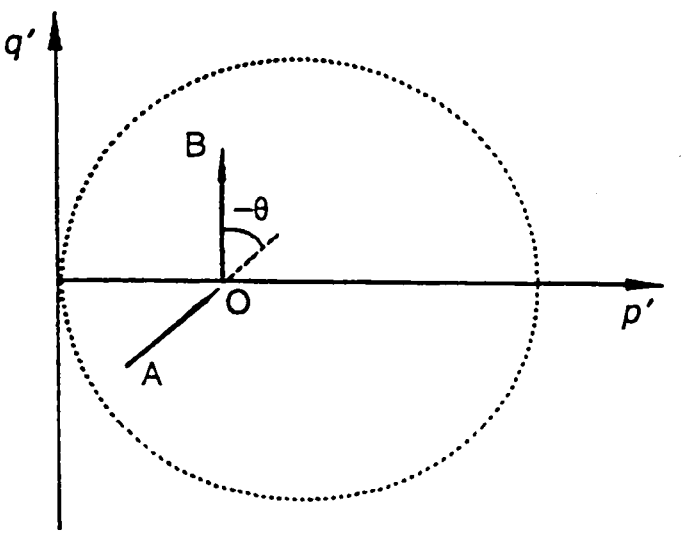

Figure 2.2 (a) Sketched stress probes to illustrate stress path rotation (Stallebrass and Taylor, 1997)

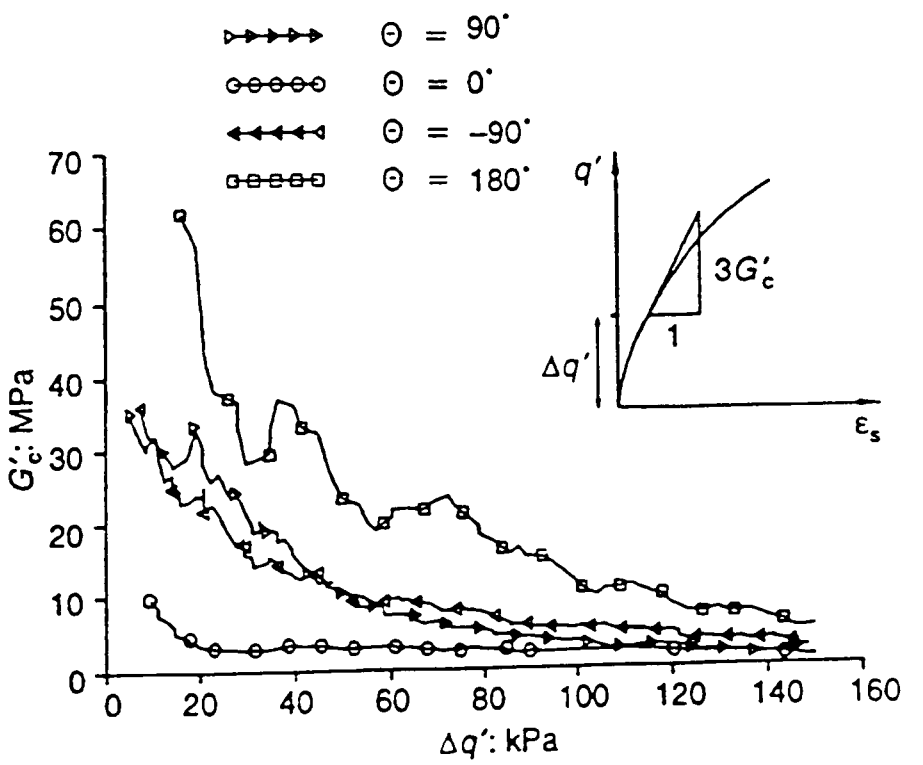

Figure 2.2 (b) Stiffness data for Speswhite kaolin subjected to constant p' shearing following different stress path rotations (Stallebrass and Taylor, 1997)

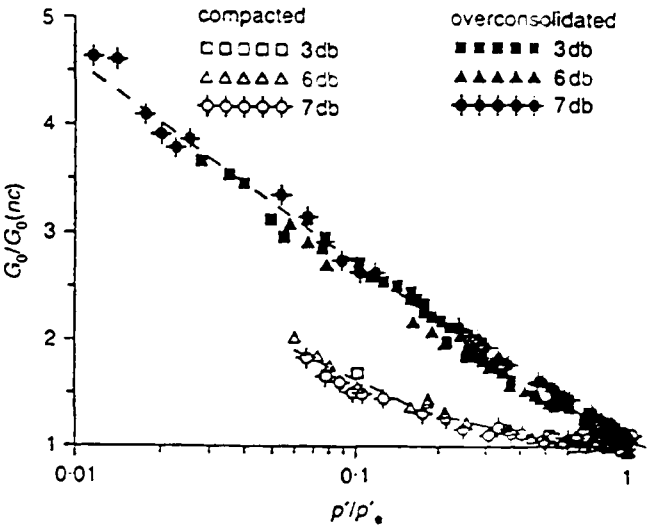

a) Dogs Bay sand (carbonate sand)

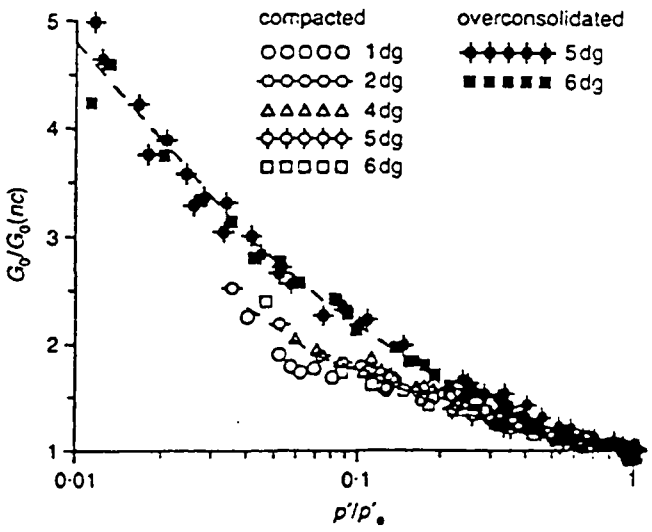

b) Decomposed granite

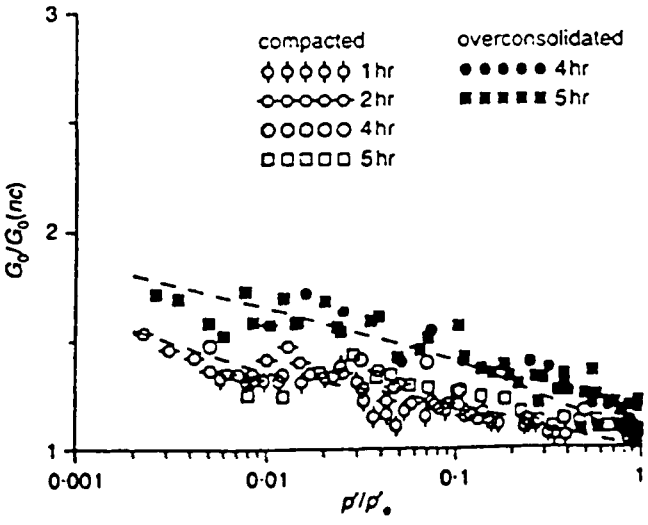

c) Ham River sand (silica sand)

Figure 2.3 Variation of stiffness with normalised volumetric state for three types of sand (Jovicic and Coop, 1997)

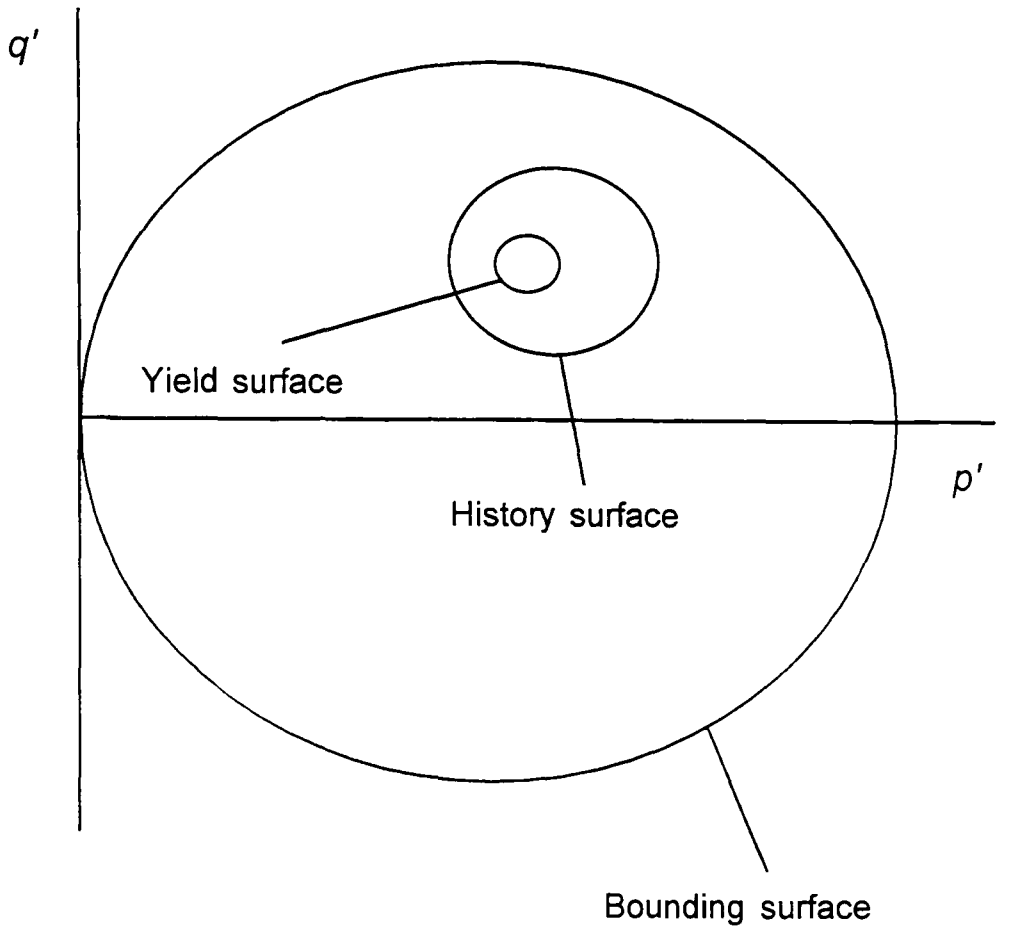

Figure 2.4 Sketch of the basic features of the 3-Surface Kinematic Hardening model

Figure 2.5 Approximate strain limits for reliable measurement of soil stiffness (after Atkinson and Sallfors, 1991) and typical strain ranges for geotechnical structures (after Mair, 1993)

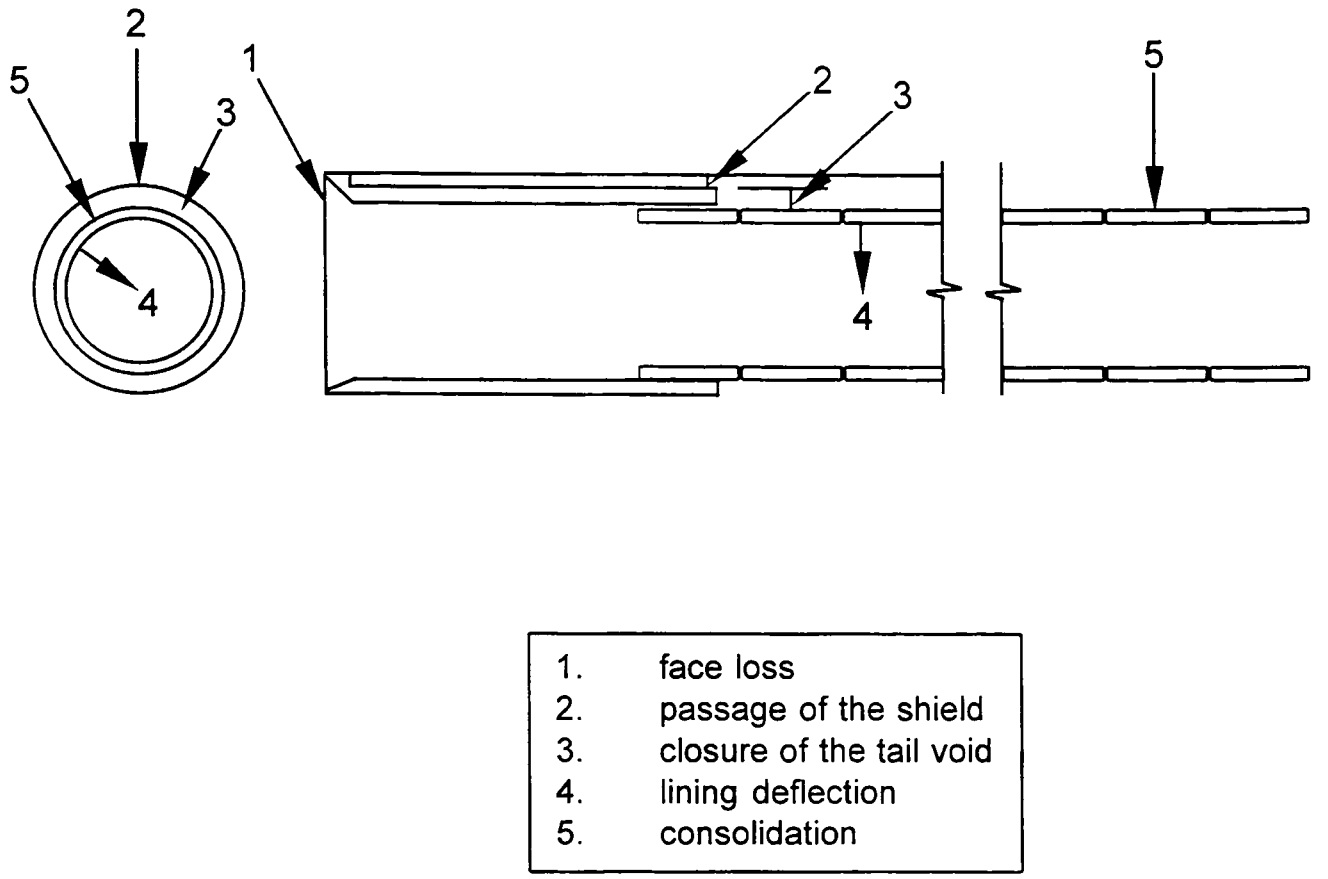

Figure 2.6 Sources of movement at a tunnel heading
(after Mair and Taylor, 1997)

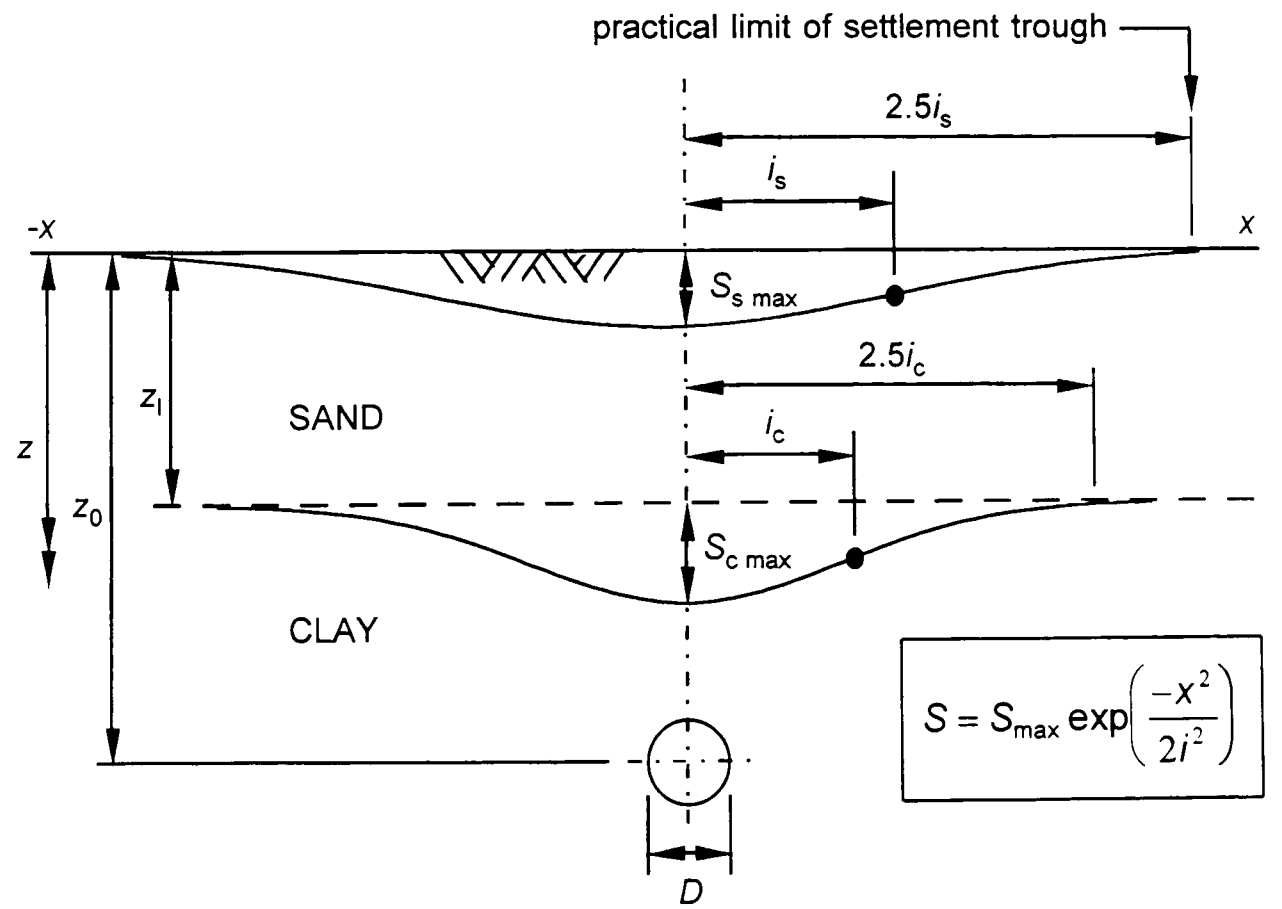

Figure 2.7 Definitions for settlement profiles of Gaussian form

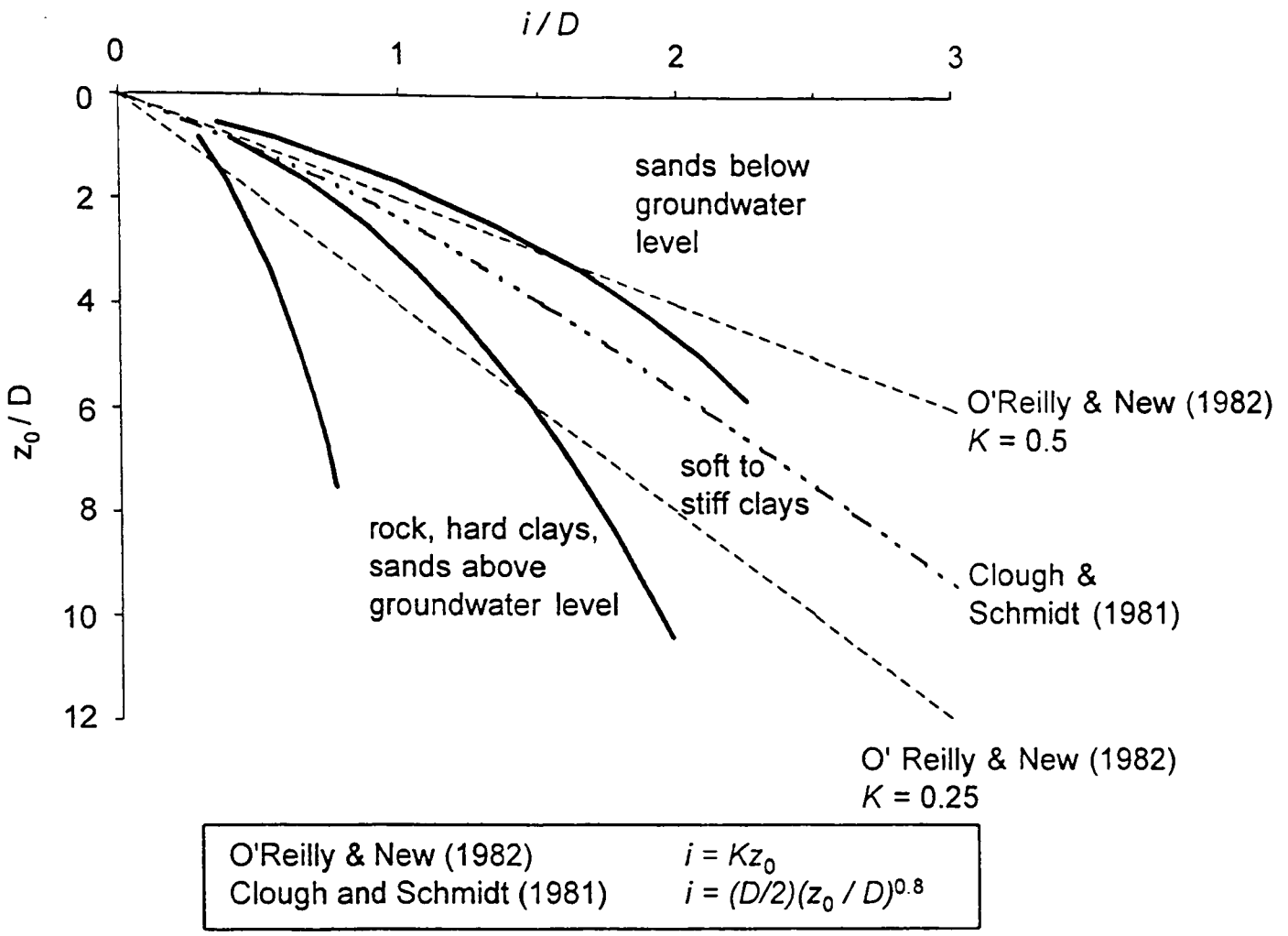

Figure 2.8 Relationships between i at the ground surface and depth of tunnel (originally after Peck, 1969)

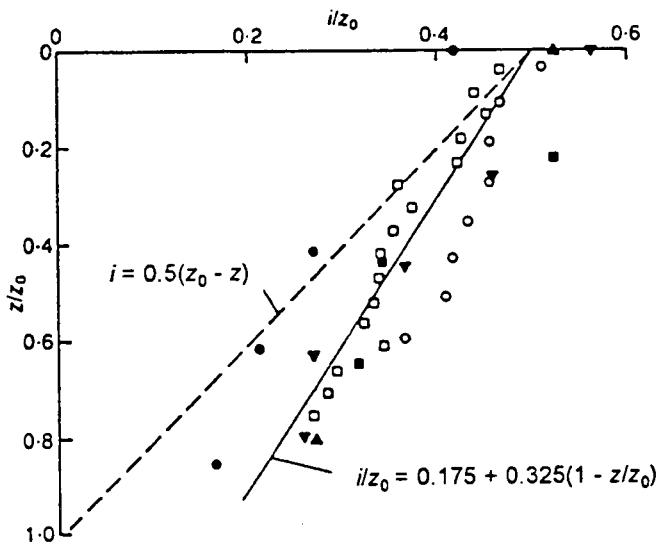

	Location	Soil type	D: m	z_0: m	Reference
•	Green Park	London Clay	4·1	29	Attewell & Farmer (1974)
▲	Regent's Park (northbound)	London Clay	4·1	20	Barratt & Tyler (1976)
▼	Regent's Park (southbound)	London Clay	4·1	34	Barratt & Tylor (1976)
■	Willington Quay	Soft clay	4·3	13.5	Glossop (1978)
○	Centrifuge* model 2DP	Soft clay	0·06	0·13	Mair (1979)
□	Centrifuge* model 2DV	Soft clay	0·06	0·22	Mair (1979)

*Models tested at 75g: equivalent full-scale D = 4·5 m, z_0 = 9·8 m (2DP), 16·5 m (2DV)

Figure 2.9 Variation of i with depth for tunnels in clay only soil profiles (Mair, Taylor and Bracegirdle, 1993)

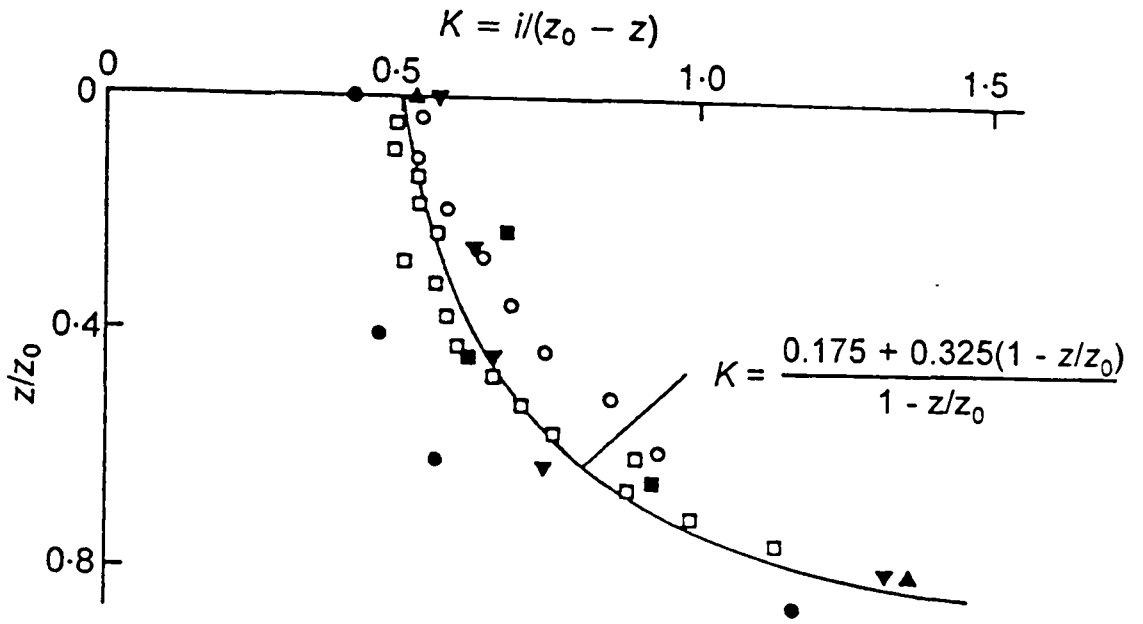

(key to symbols as Figure 2.9)

Figure 2.10 Variation of trough width parameter K with depth for clay only soil profiles (Mair, Taylor and Bracegirdle, 1993)

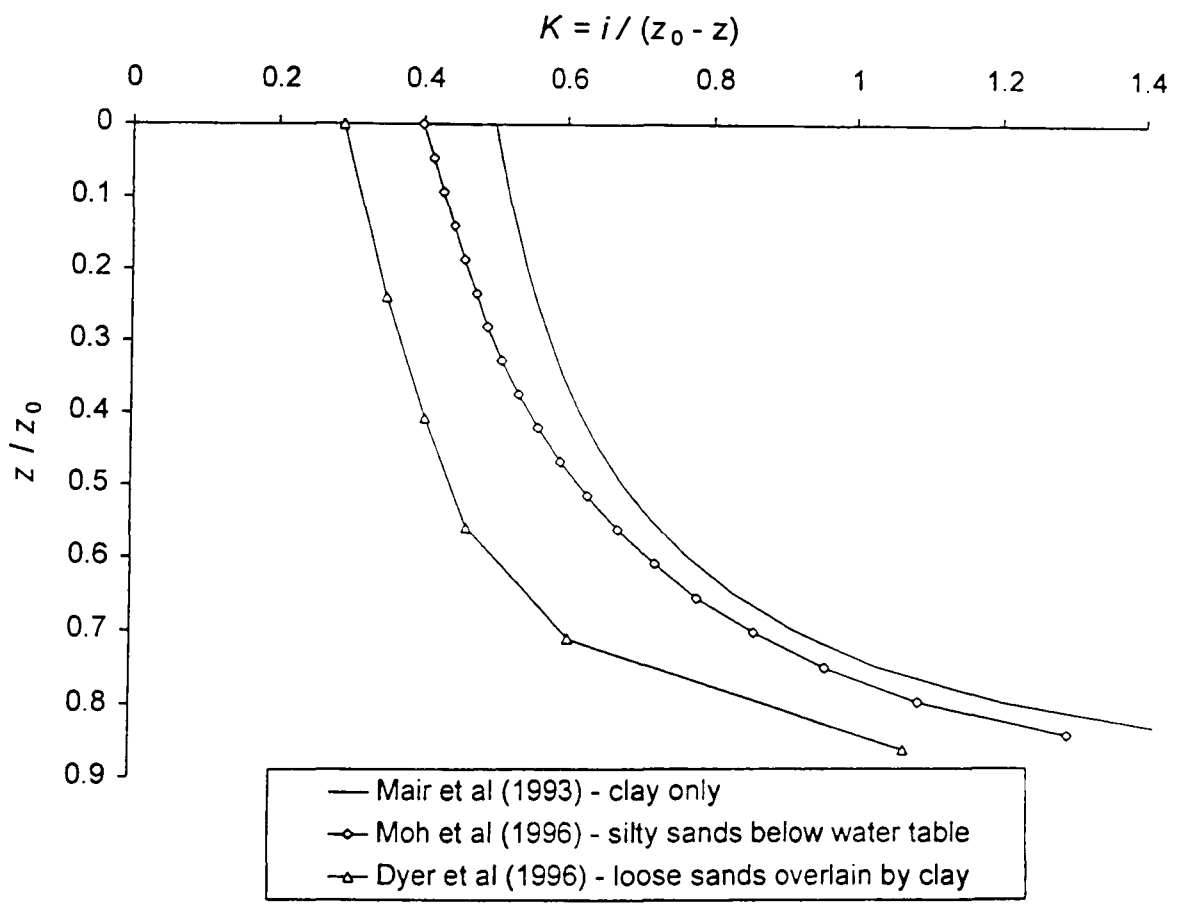

Figure 2.11 Variation of trough width parameter K with depth for different soil types

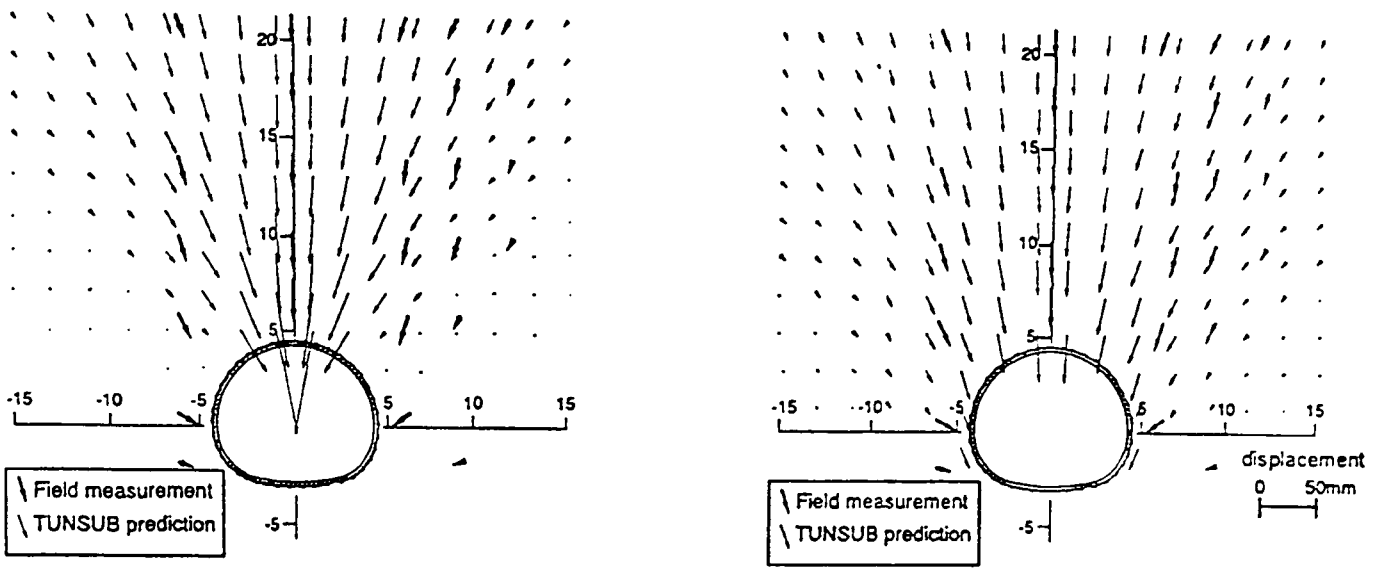

a) Predictions using a point sink at tunnel axis level

b) Predictions using a ribbon sink at tunnel invert level

Figure 2.12 Predicted and measured vectors of movement for the Heathrow Express trial tunnel - type 2 (New and Bowers, 1994)

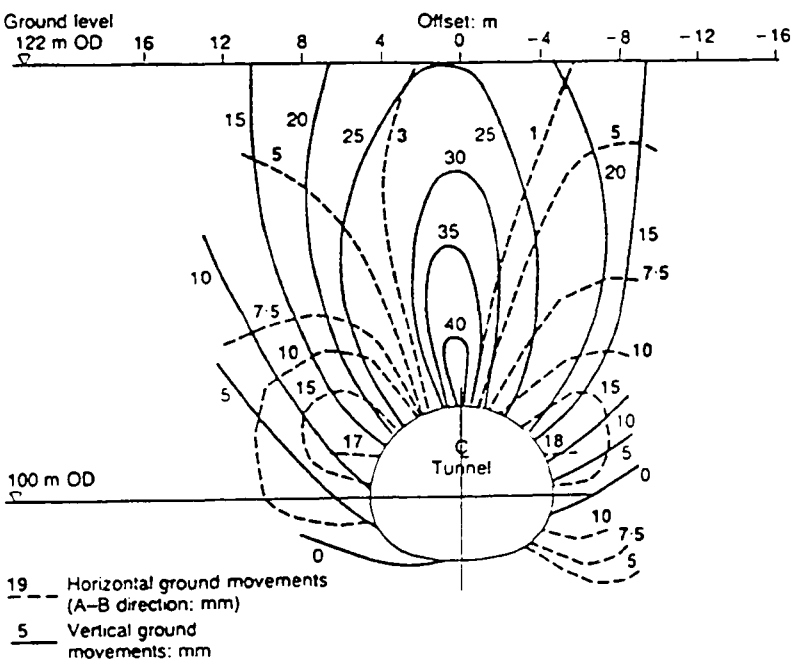

Figure 2.13 Derived contours of vertical and horizontal movement for the Heathrow Express trial tunnel - type 2 (Deane and Bassett, 1995)

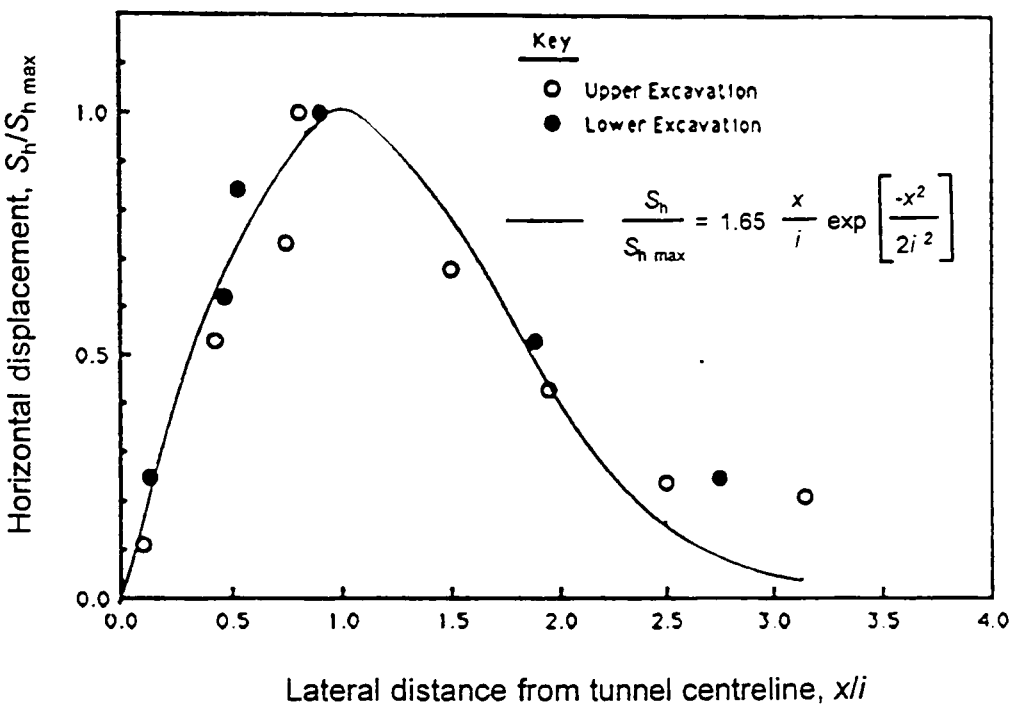

Figure 2.14 Horizontal movements at the ground surface above a tunnel in predominantly sandy strata (Hong and Bae, 1995)

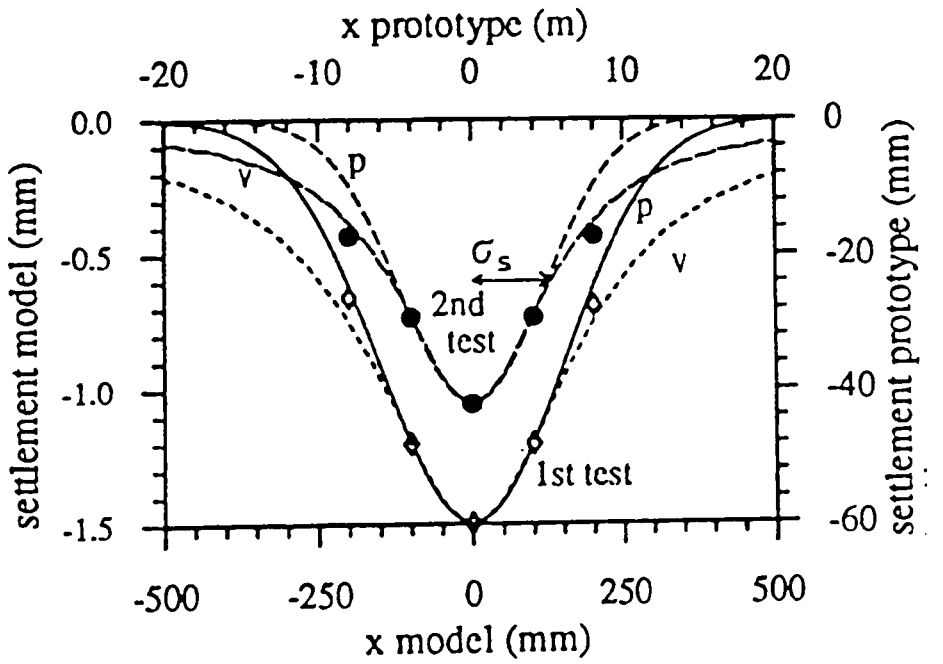

p - Gaussian distribution

v - Analytical solution

Figure 2.15 Surface settlement profiles from centrifuge tests consisting of a tunnel in clay with adjacent piled foundations (Bezuijen and van der Schrier, 1994)

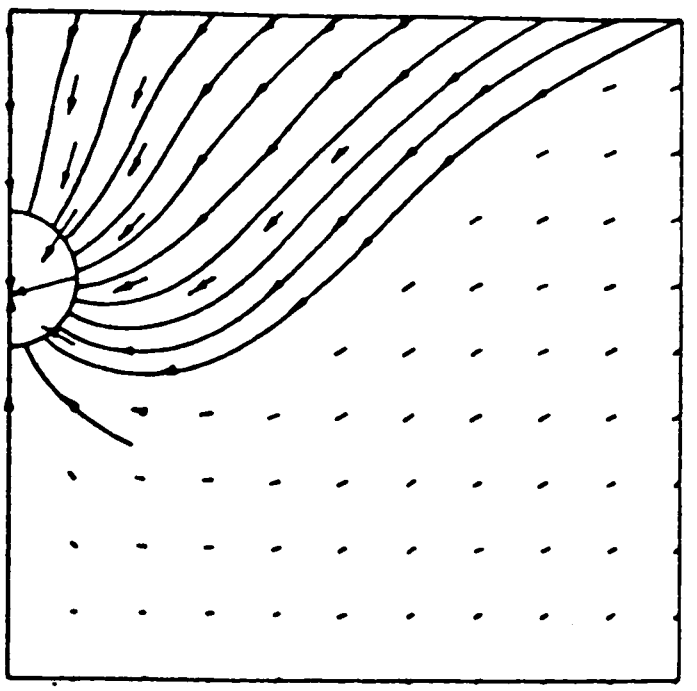

a) Sagaseta - Analytical prediction
(Uriel and Sagaseta, 1989)

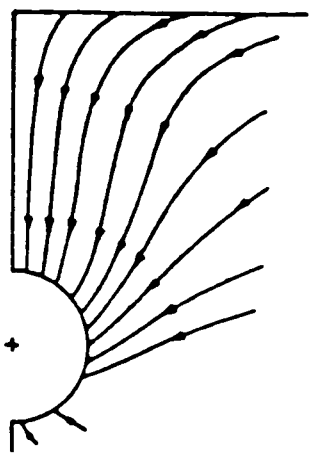

b) Observed patterns
(Cording and Hansmire, 1975)

Figure 2.16 Analytical predictions and observed "stream-lines" of ground movement for the Washington Metro (driven predominantly in sandy gravel with some overlying silty clay)

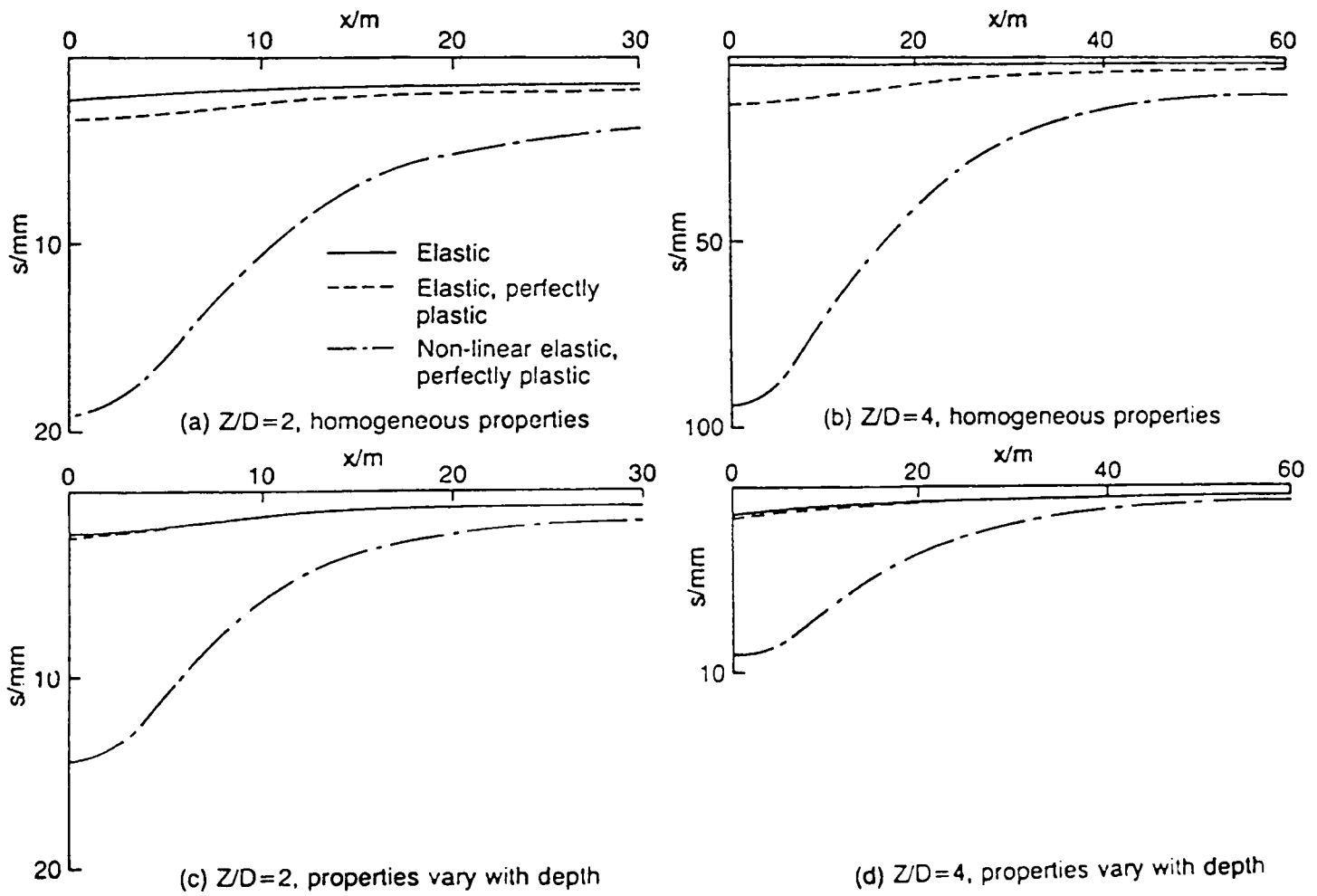

Figure 2.17 Surface settlement profiles from plane strain finite element analyses using different constitutive models (Gunn, 1993)

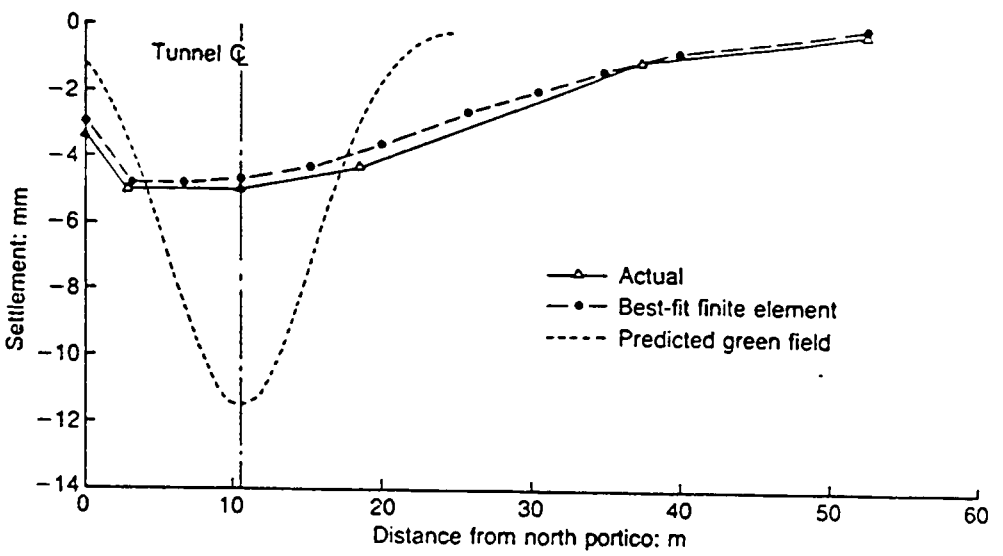

Figure 2.18 Comparison of observed and predicted settlements of the Mansion House, London during construction of the Docklands Light Railway extension (Frischmann et al, 1994)

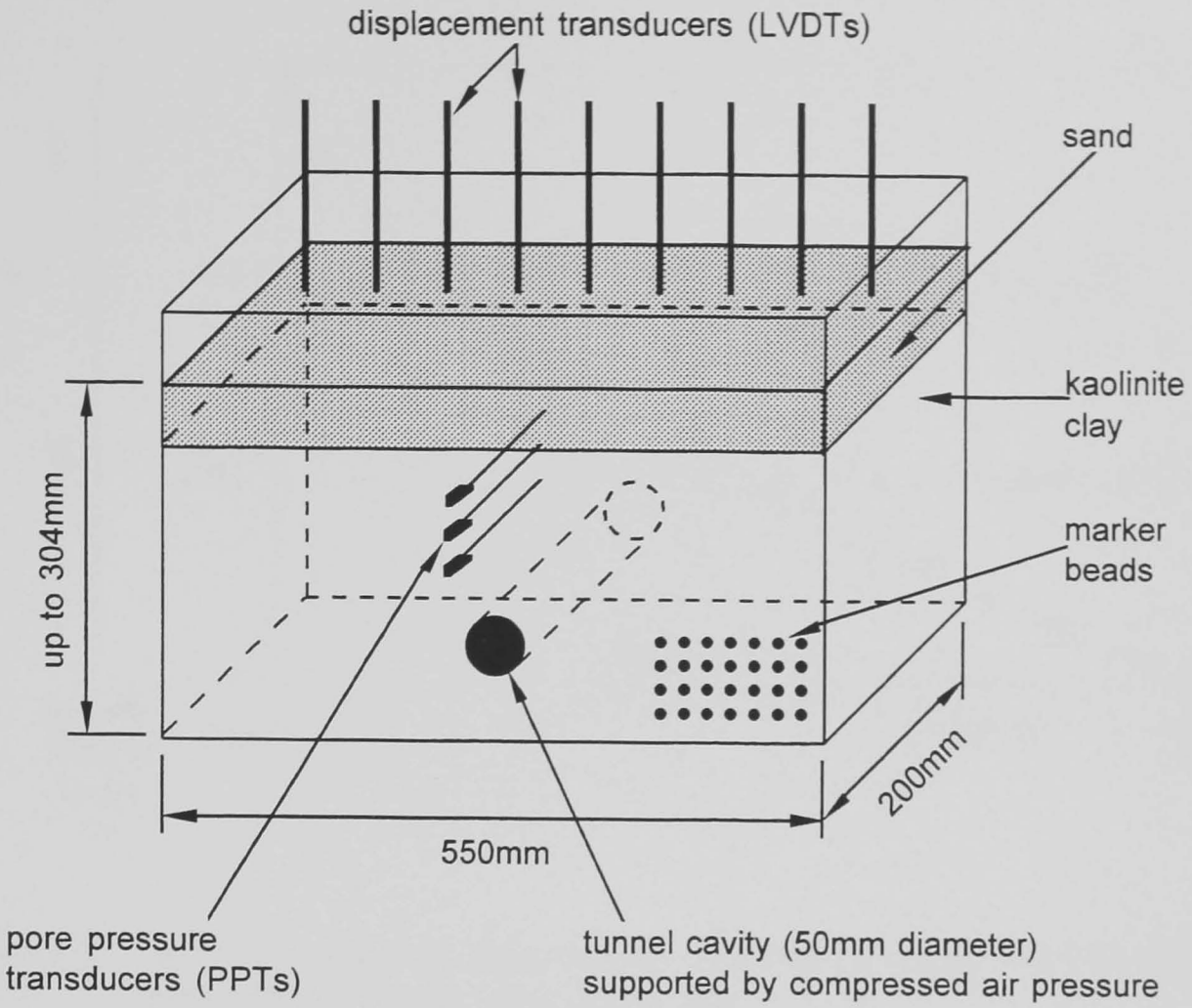

Figure 3.1 Schematic diagram of a typical plane strain centrifuge model (not to scale)

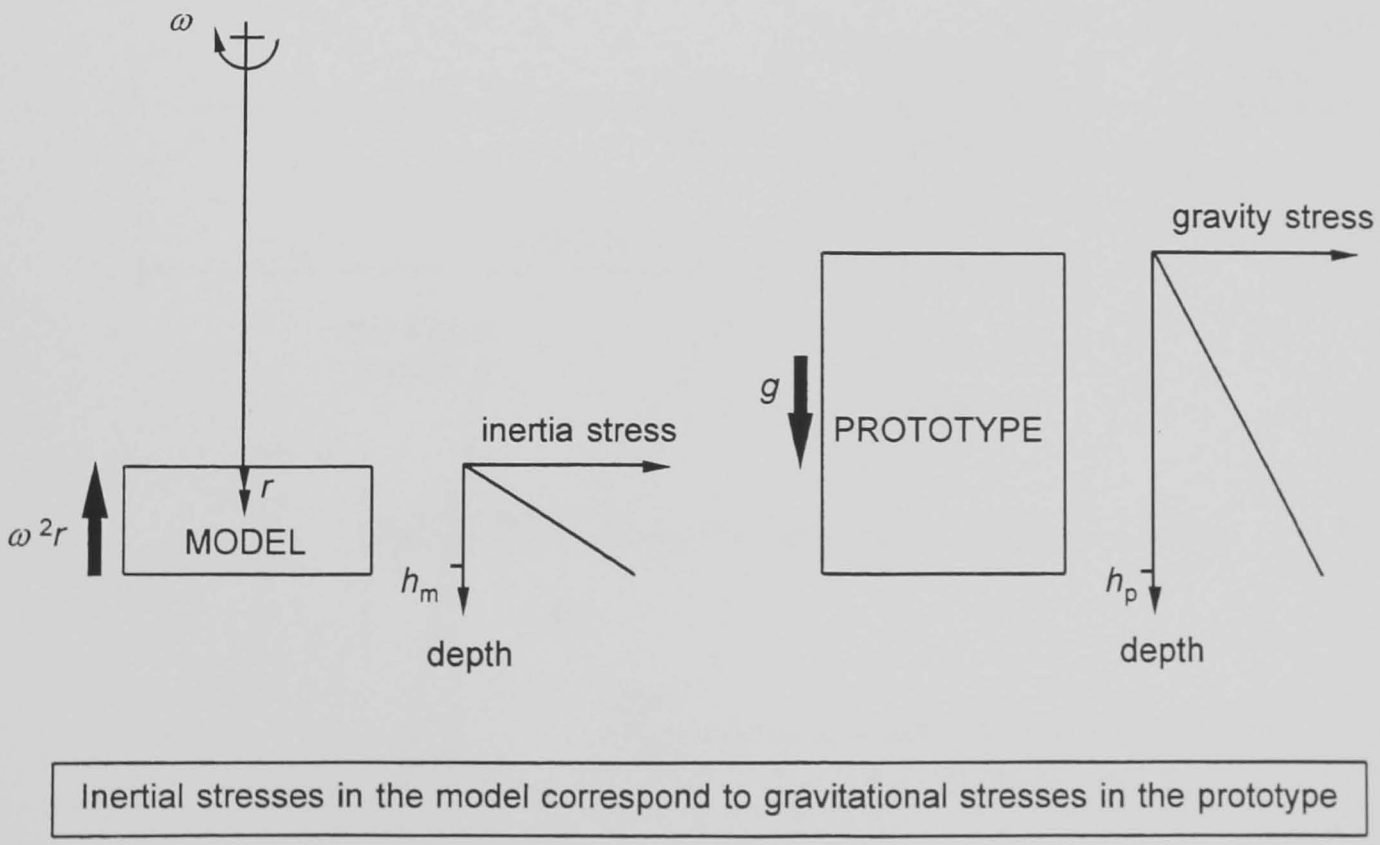

Figure 3.2 Principle of centrifuge modelling

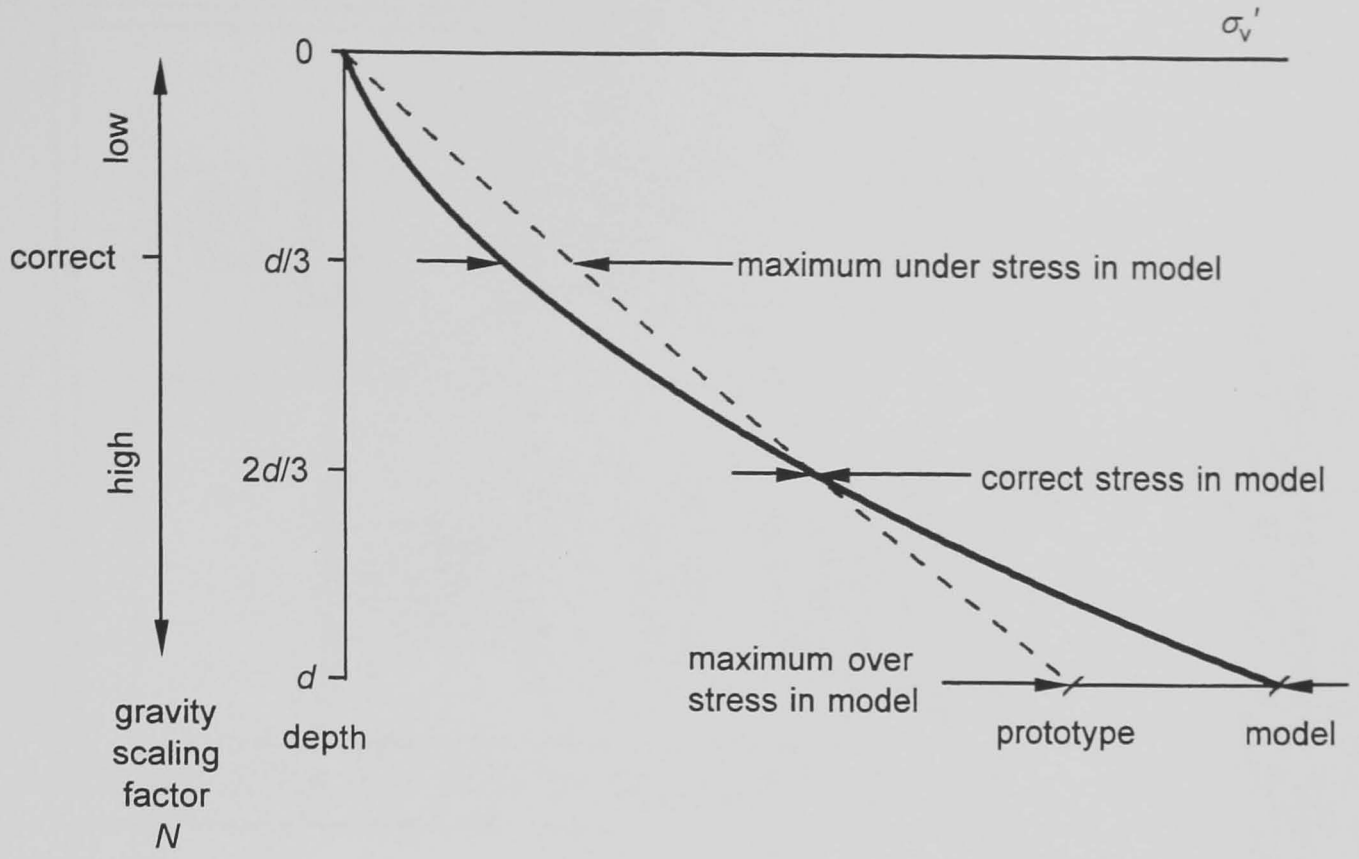

Figure 3.3 Stress variation with depth in a centrifuge model and the corresponding prototype (difference exaggerated x10)

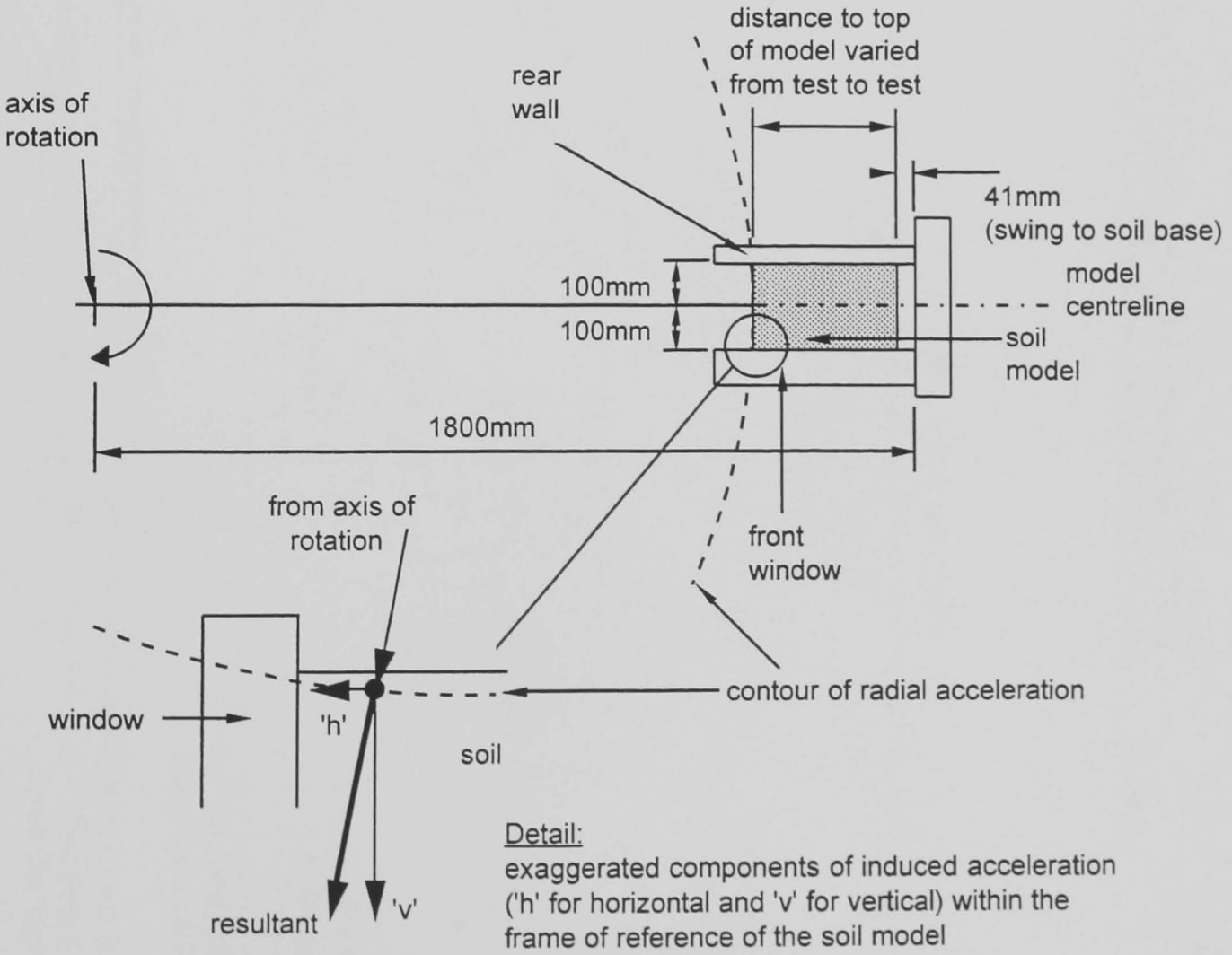

Figure 3.4 Geometry of a typical model on the Acutronic 661 geotechnical centrifuge at City University, London (not to scale), and components of induced acceleration

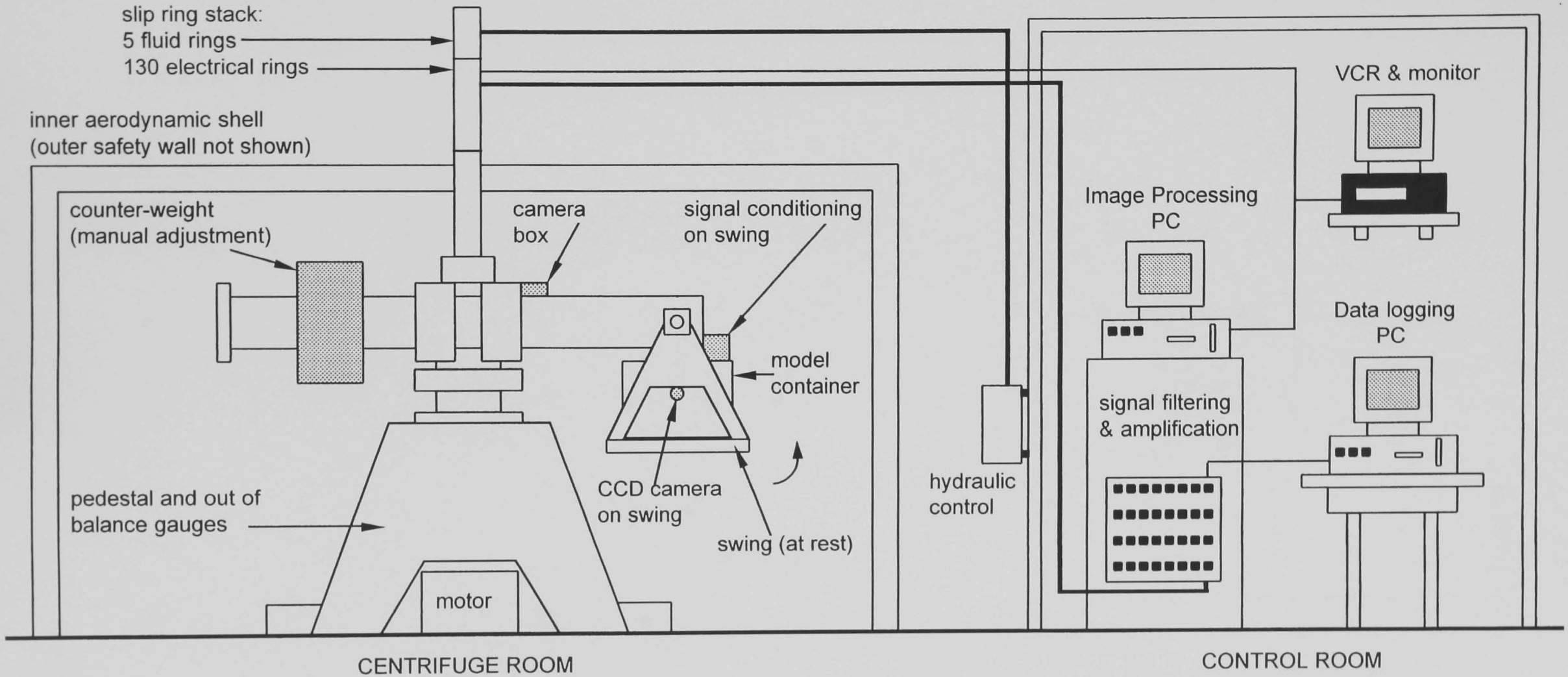

Figure 3.5 Schematic diagram of the Acutronic 661 geotechnical centrifuge testing facility at City University, London (before August 1995, tests RJG1 to RJG16) - capacity 40g.tonnes, radius 1.8m to swing base in flight

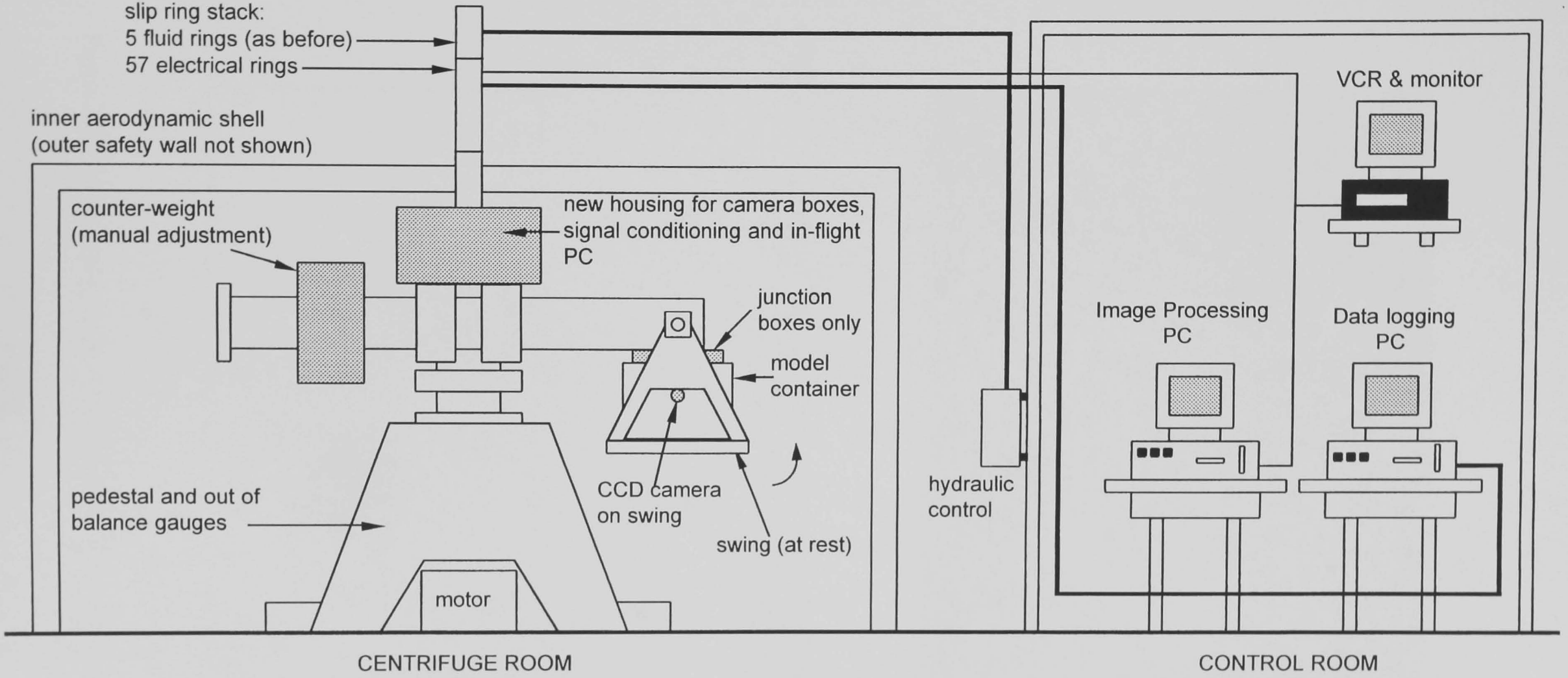

Figure 3.6 Schematic diagram of the Acutronic 661 geotechnical centrifuge testing facility at City University, London (after August 1995, tests RJG17 onwards) - capacity 40*g*.tonnes, radius 1.8m to swing base in flight

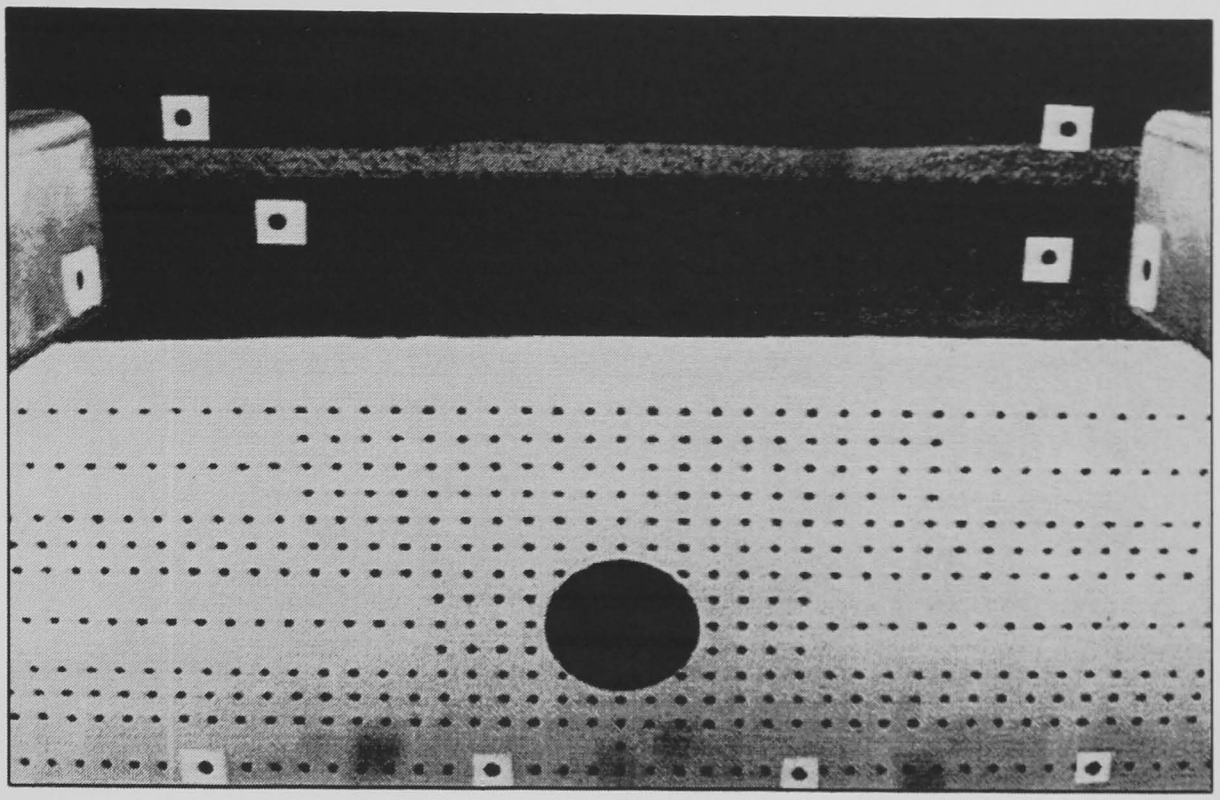

Figure 3.7 Digitised image from the CCD camera in flight (test RJG16 - after reconsolidation and before tunnel pressure reduction)

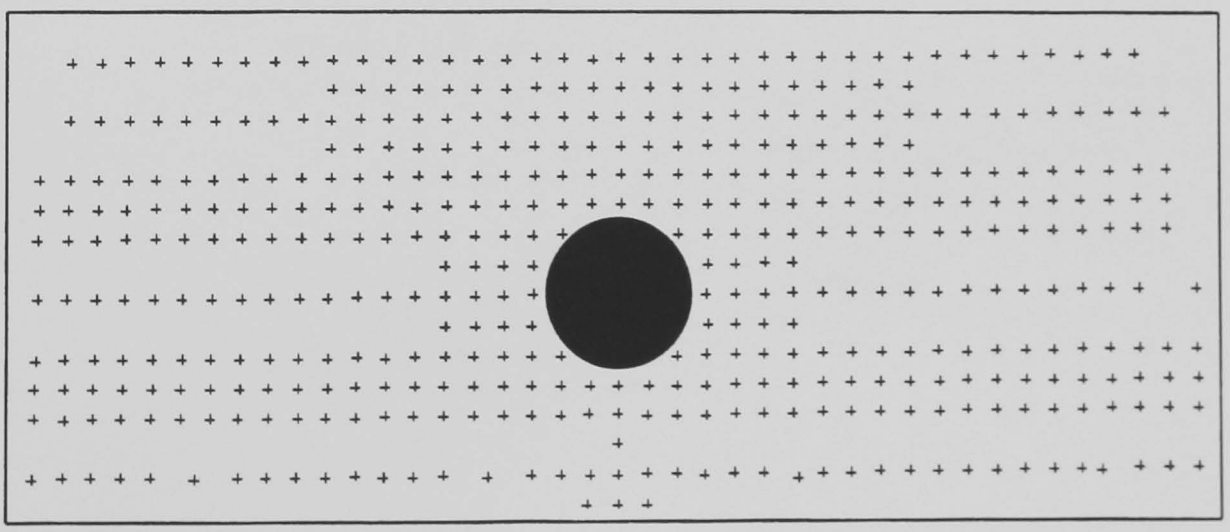

Figure 3.8 Calibrated positions of the targets from Figure 3.7, in the clay layer only

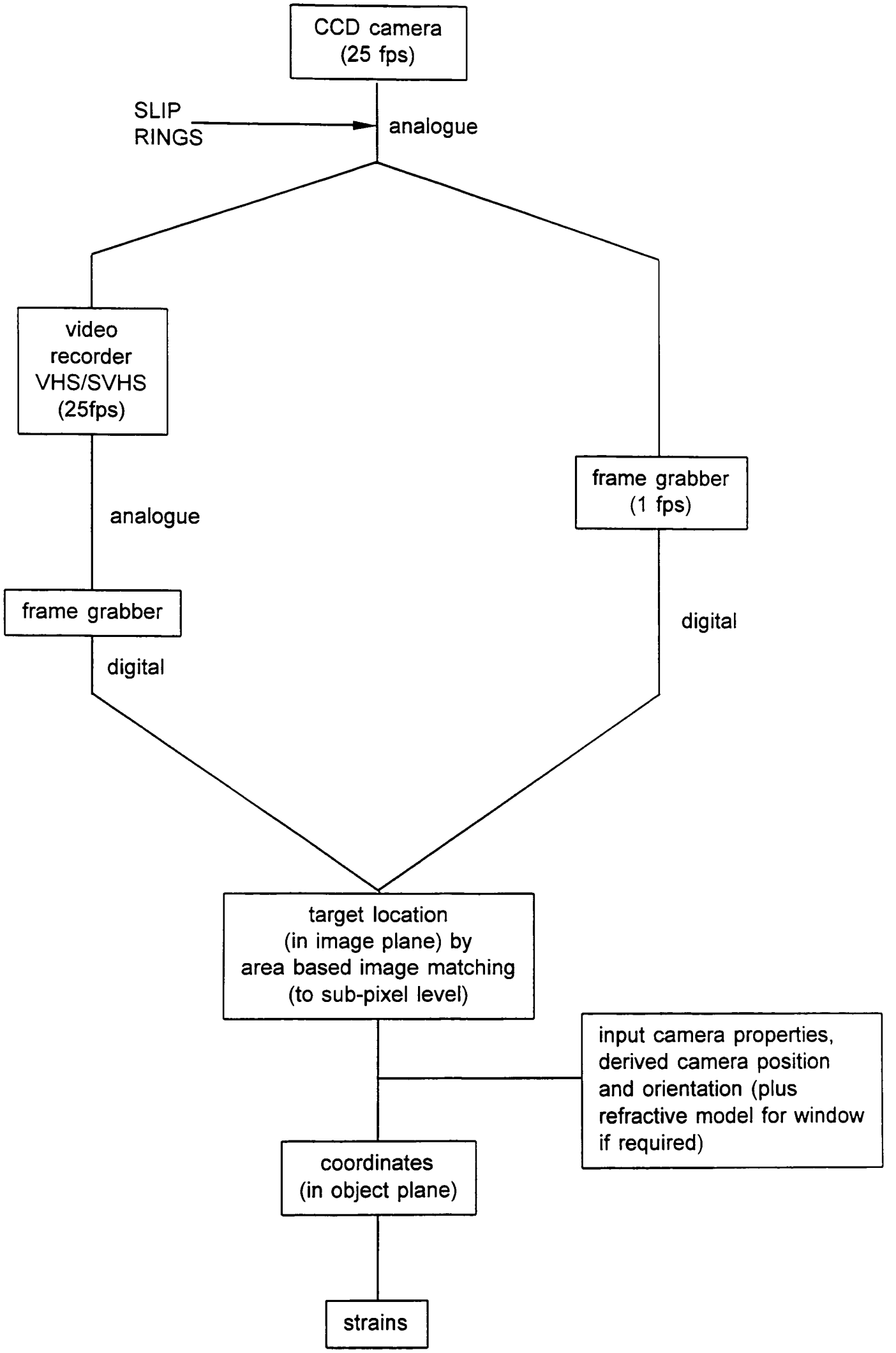

Figure 3.9 Flow chart for image processing system

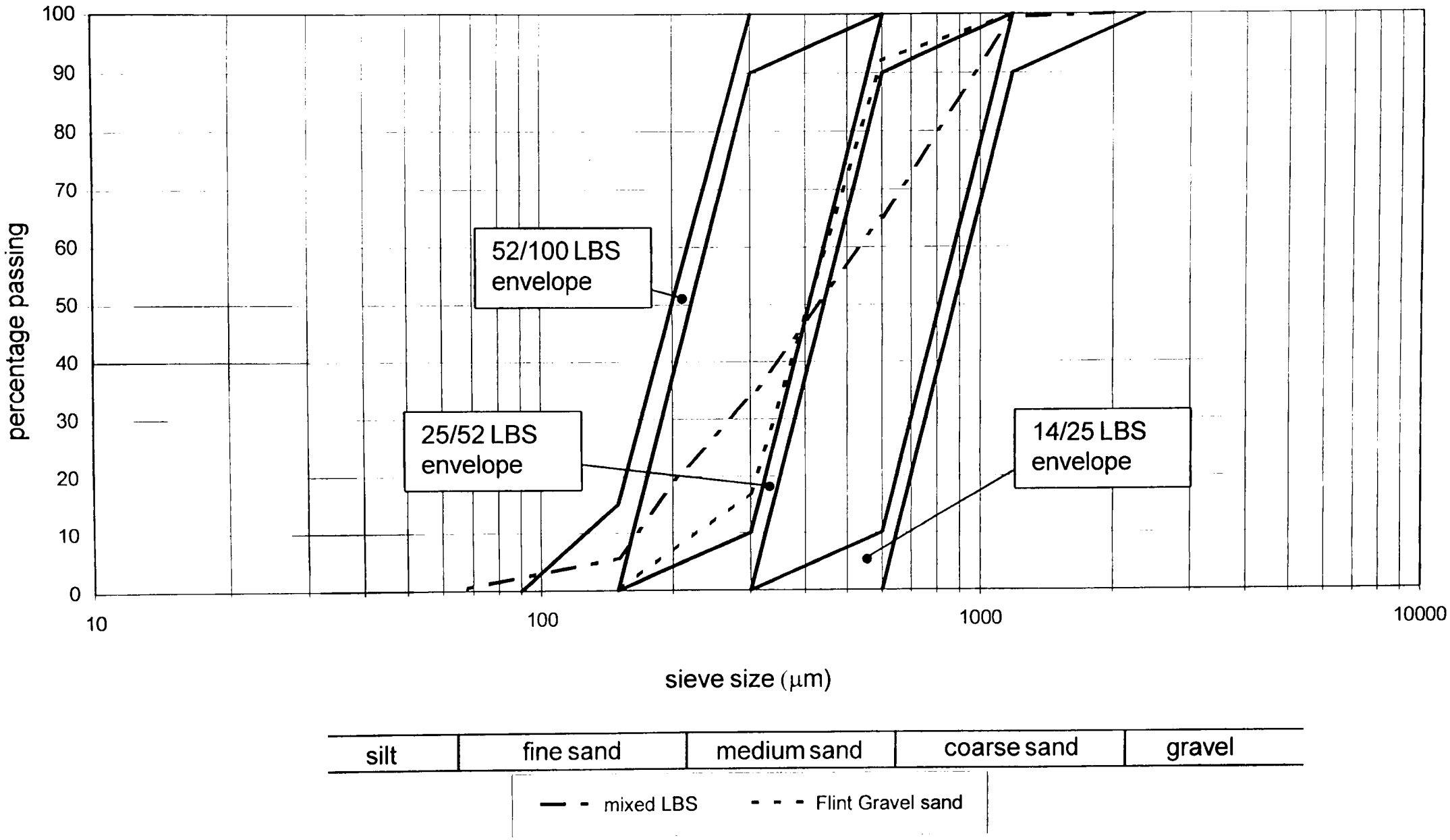

Figure 3.10 Gradings of sands used in tests
(gradings for the Leighton Buzzard Sands from the David Ball Company Ltd., Cambridge)

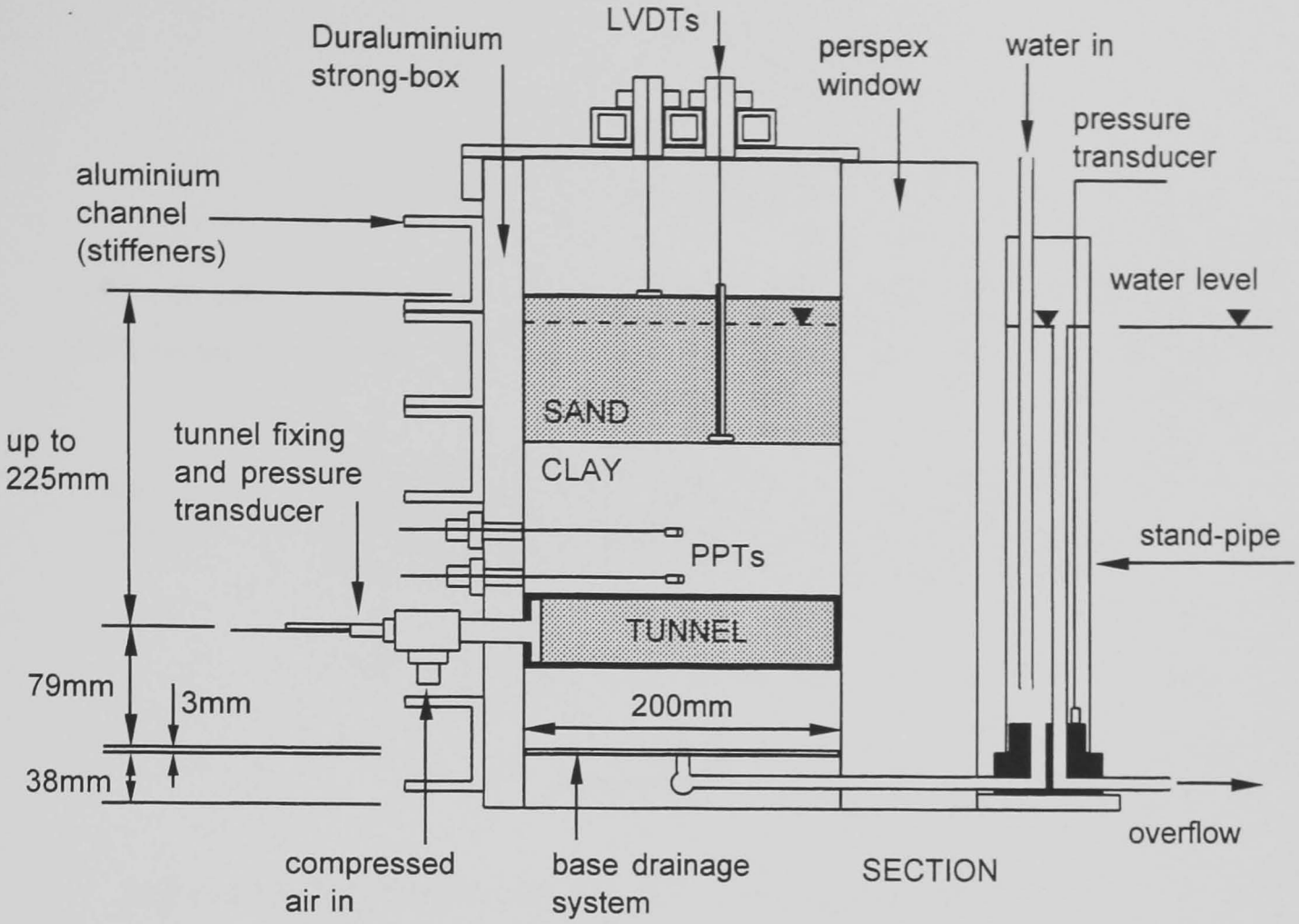

Figure 3.11 Sketched details of typical centrifuge model (not to scale)

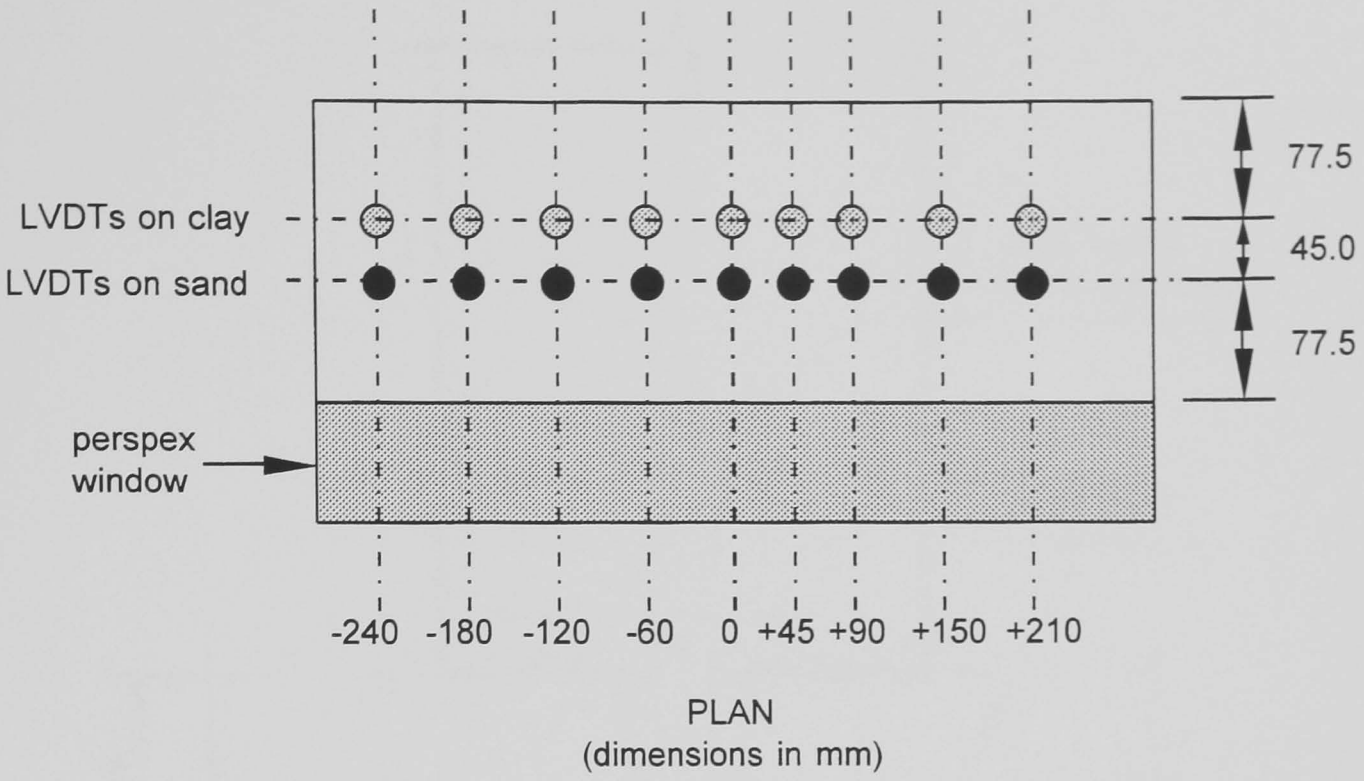

Figure 3.12 Location of displacement transducers (LVDTs)
(not to scale)

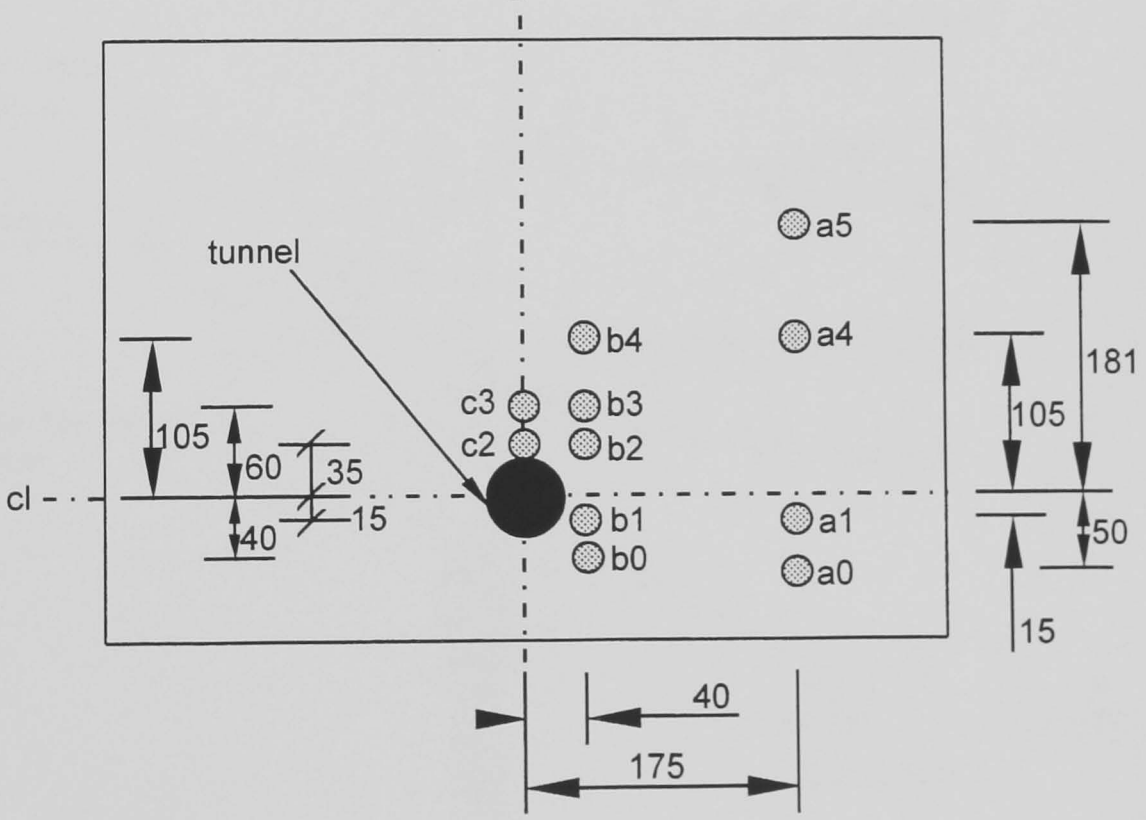

Figure 3.13 Location of ports in rear of strong-box for pore pressure transducers
(not to scale)

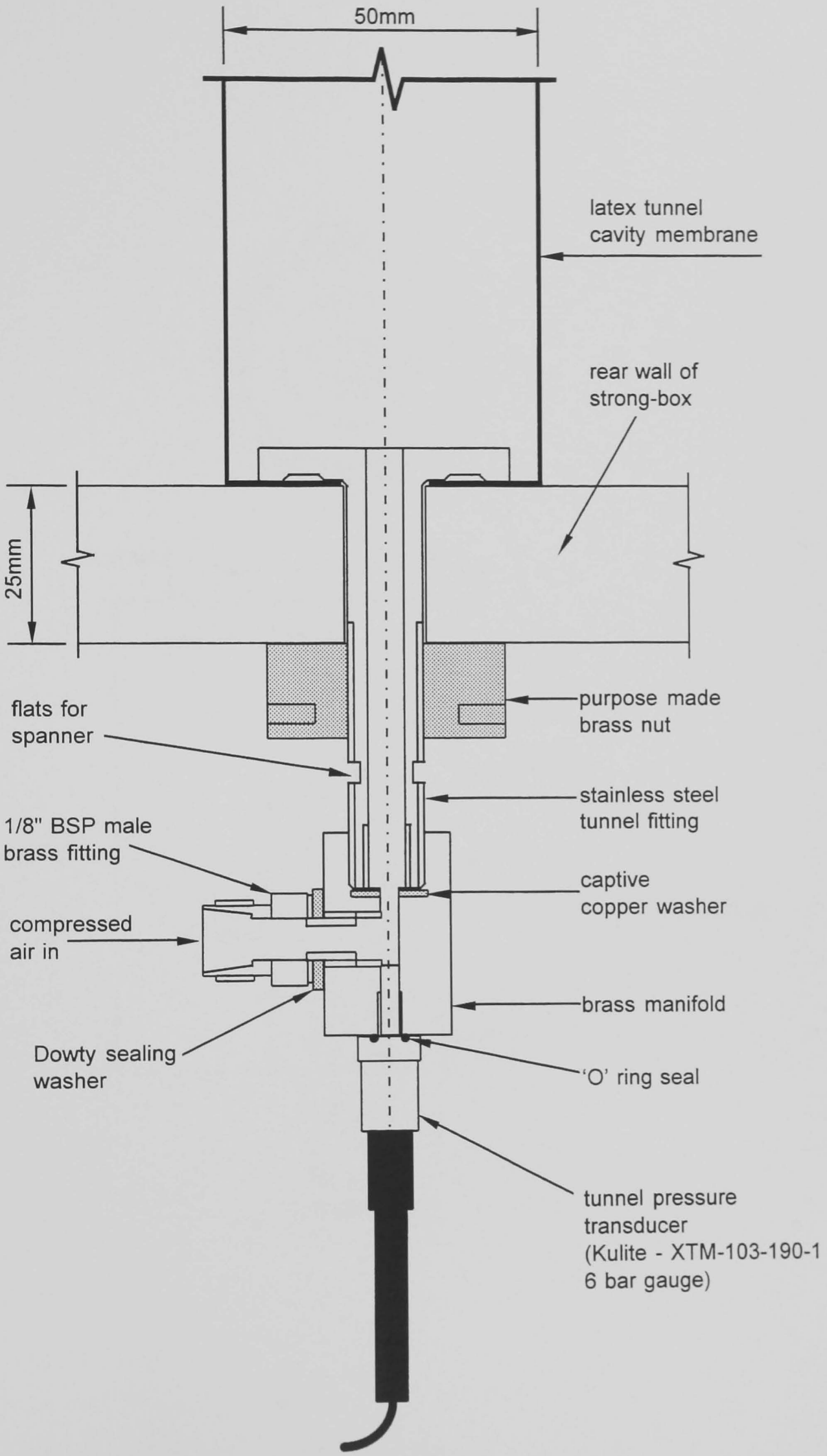

Figure 3.14 Detail of tunnel fixing and tunnel pressure transducer (approximately full scale)

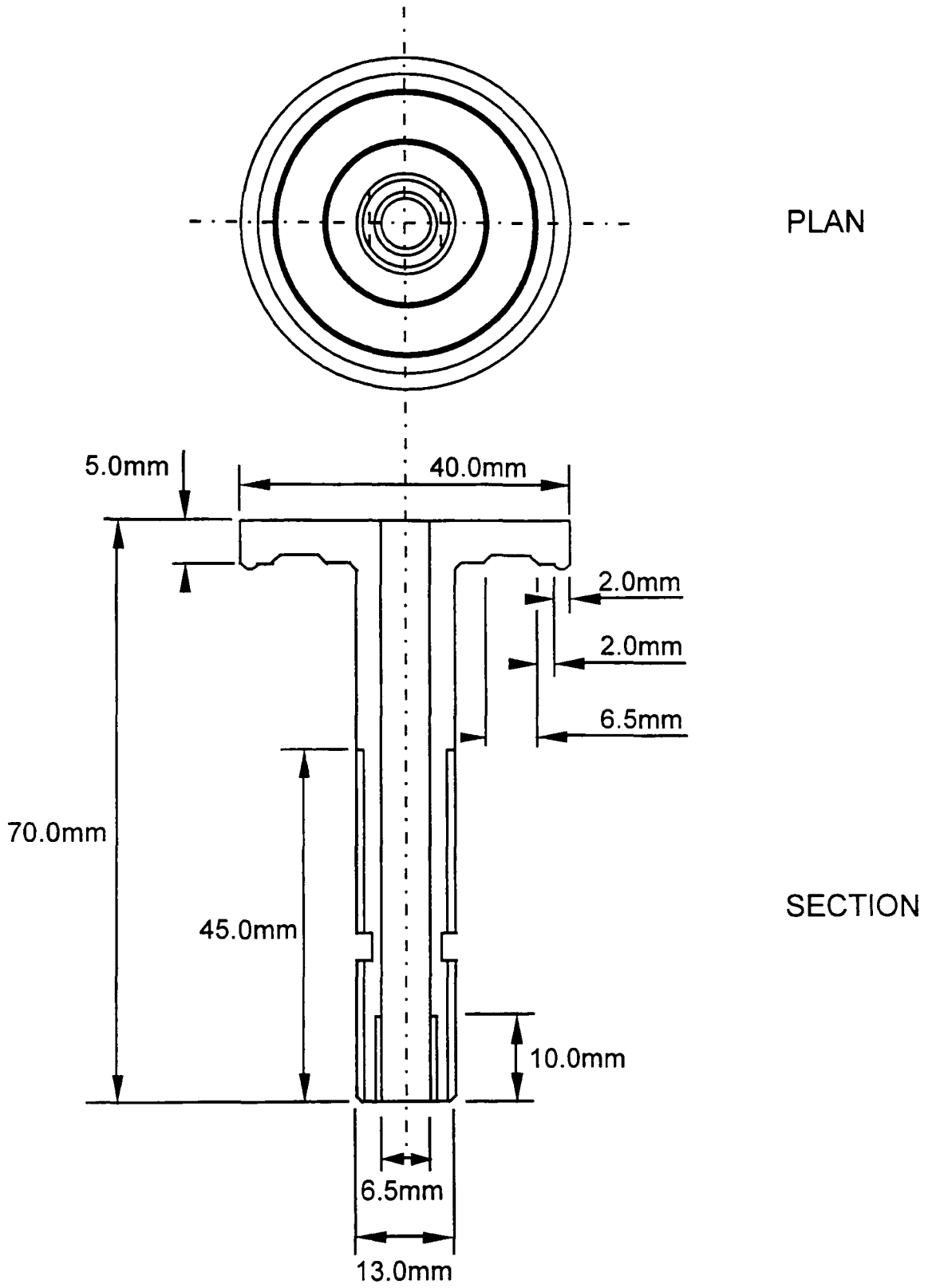

Figure 3.15 Sketch of stainless steel tunnel fitting
(approximately full scale)

Figure 3.16 Preconsolidation of kaolin clay inside centrifuge strong-box and extension with computer controlled consolidation press

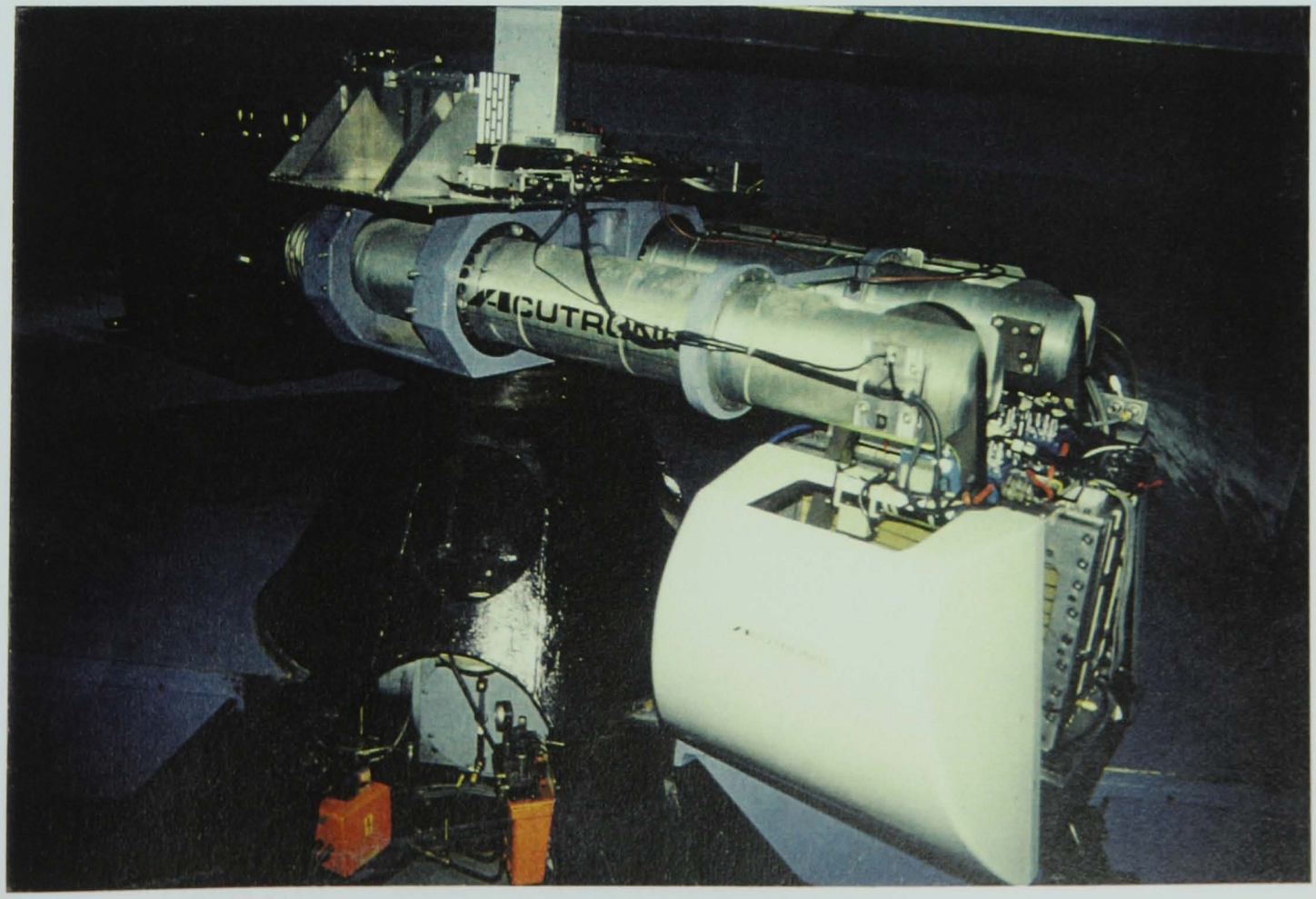

Figure 3.17 Typical centrifuge model assembled on centrifuge swing

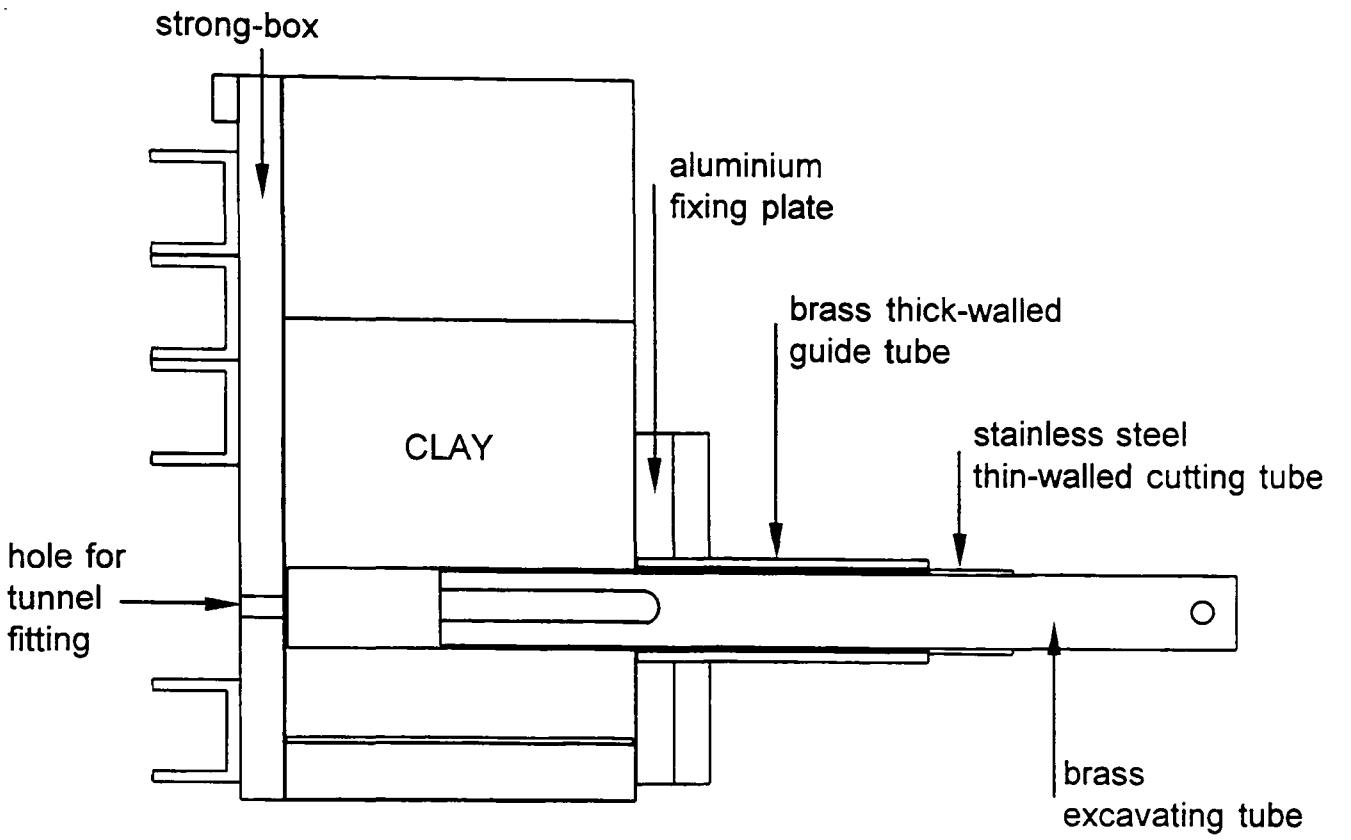

SECTION

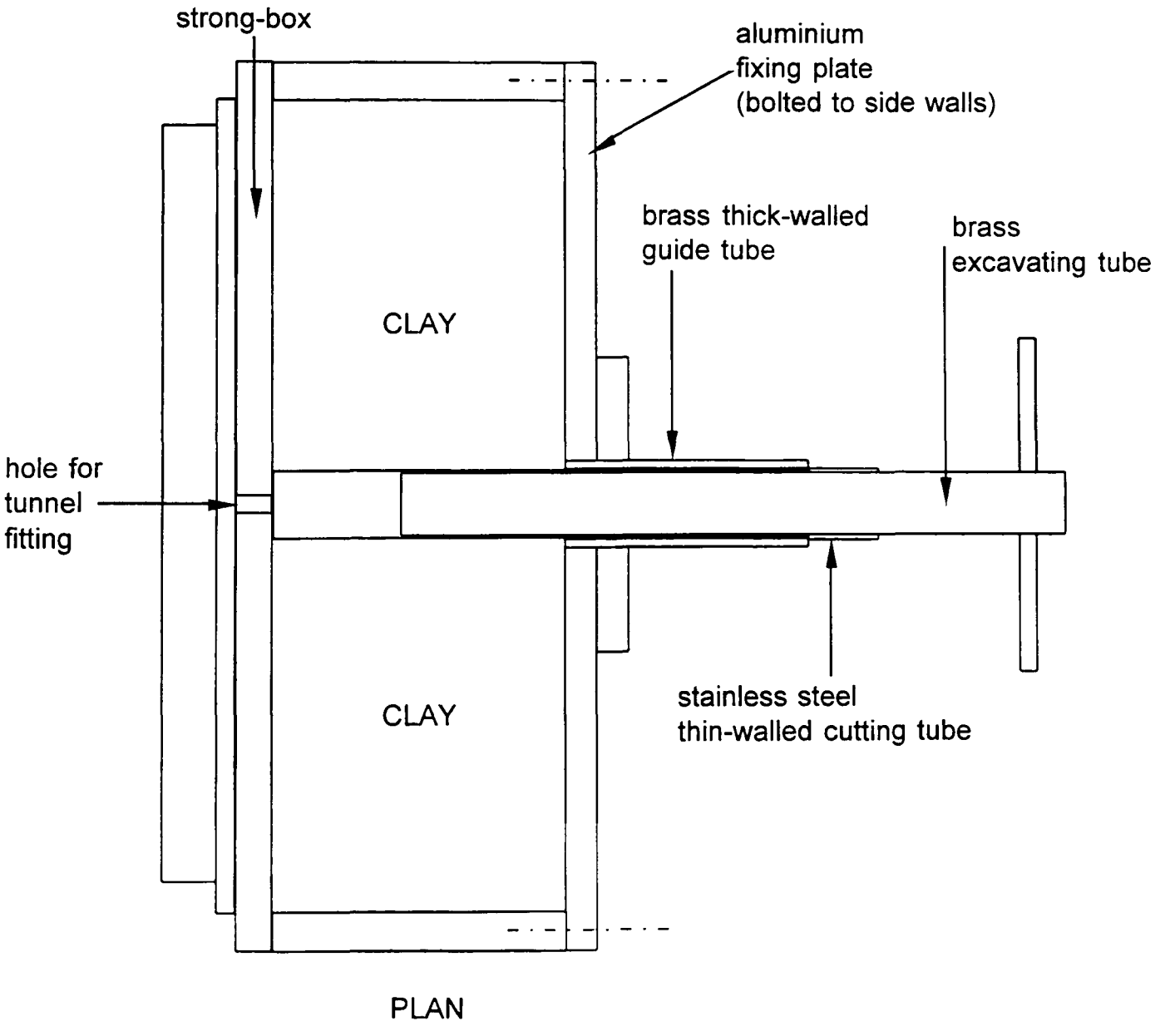

PLAN

Figure 3.18 Details of tunnel cutting equipment
(not to scale)

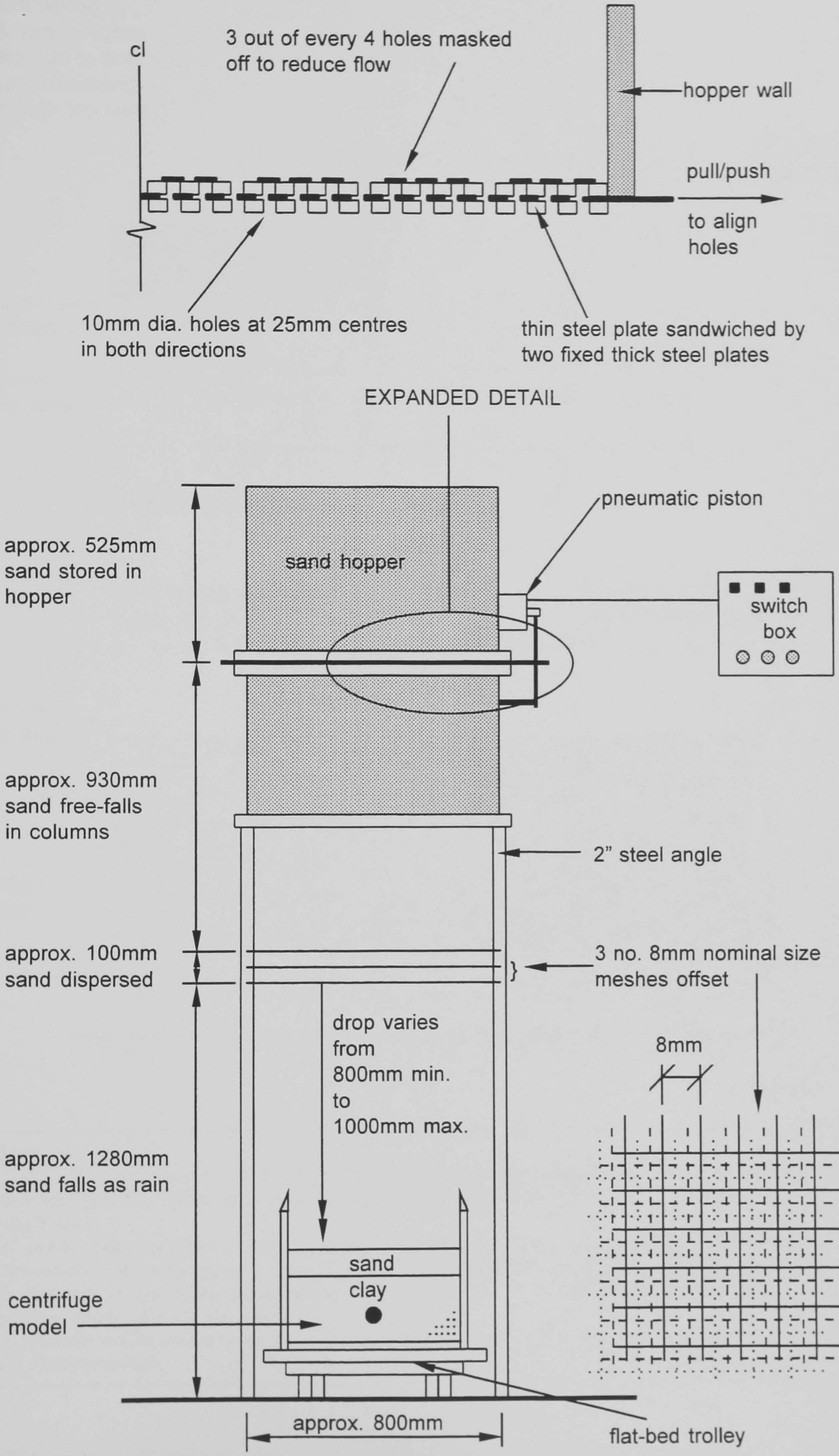

Figure 3.19 Details of sand raining system (not to scale)

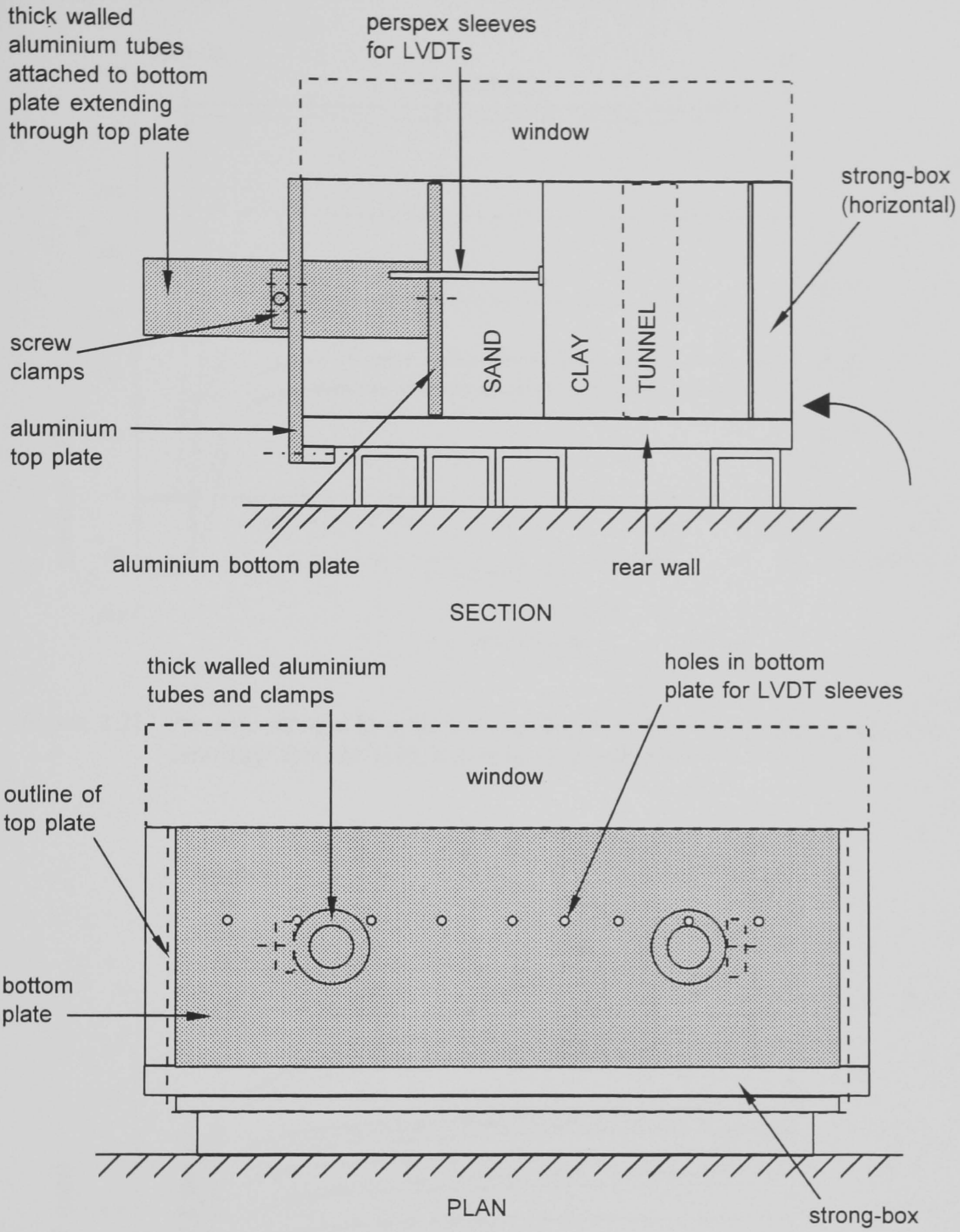

Procedure:

1. After the sand had been placed with the LVDT sleeves in position, the bottom plate was carefully placed over the sleeves by holding the aluminium tubes. At this stage the strong-box was vertical and the window was in place.
2. The top plate was placed over the aluminium tubes and bolted down to the rear wall of the strong-box. The screw clamps were tightened against the aluminium tubes to hold the bottom plate firmly in position.
3. The strong-box was then rocked back onto the rear stiffeners, the bottom plate holding the sand in position, and the window was removed.
4. This allowed the marker beads for image processing to be placed in the sand before carefully reversing the whole procedure.

Figure 3.20 Details of equipment for holding the sand surface during marker placement (not to scale)

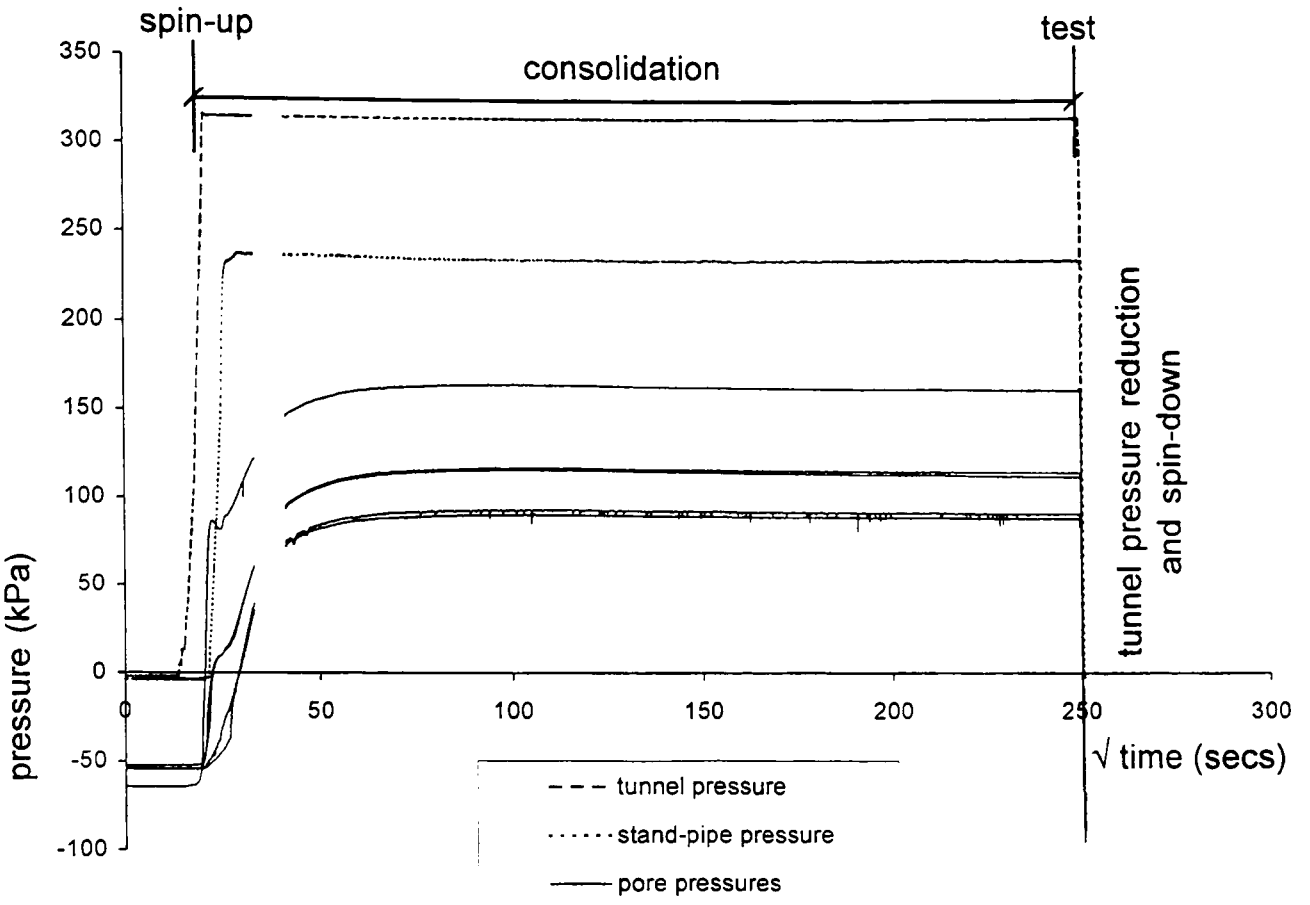

Figure 3.21 Pressure changes in the tunnel, stand-pipe and pore water during a typical centrifuge test (RJG16) from spin-up to spin-down

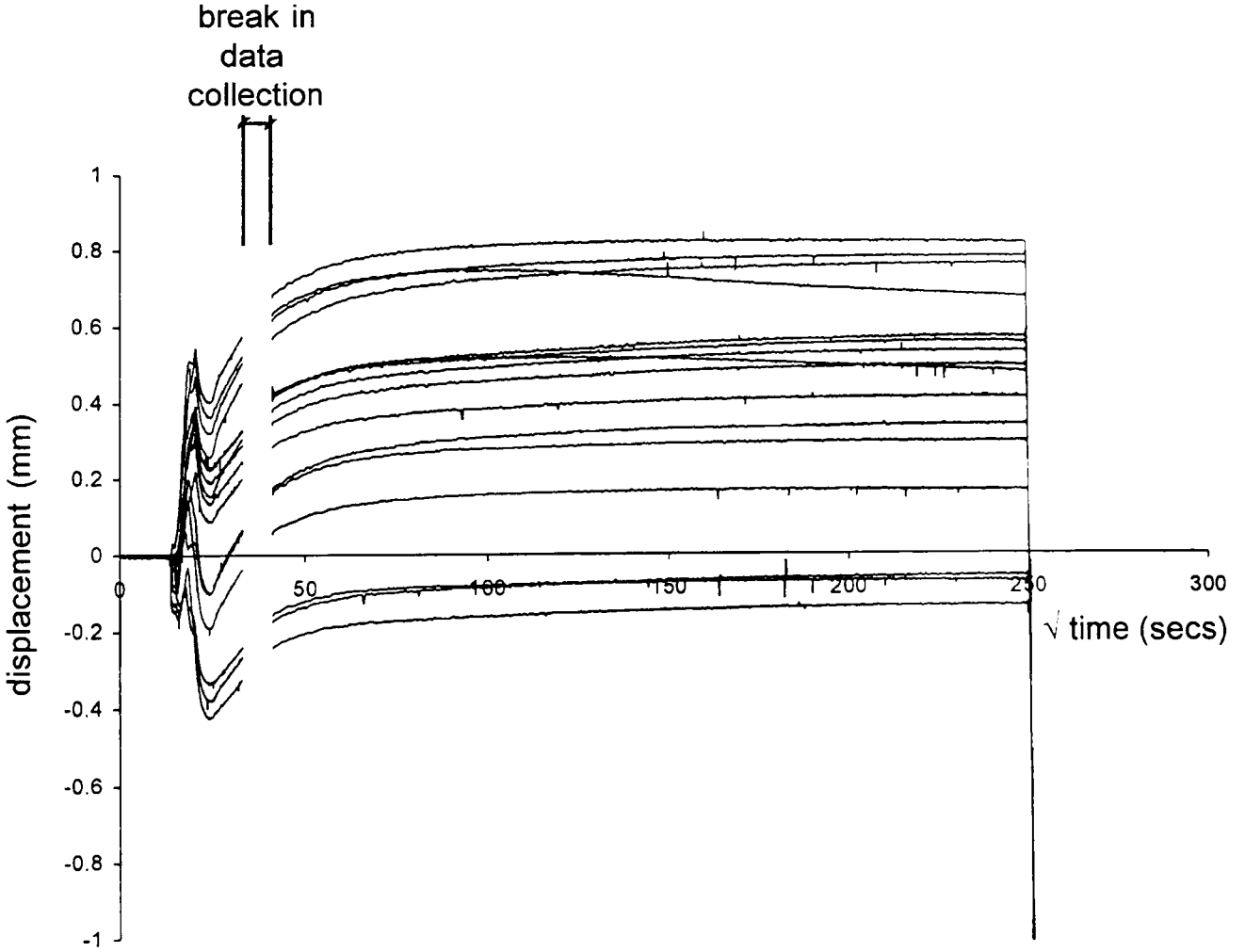

Figure 3.22 LVDT response during a typical centrifuge test (RJG16) from spin-up to spin-down

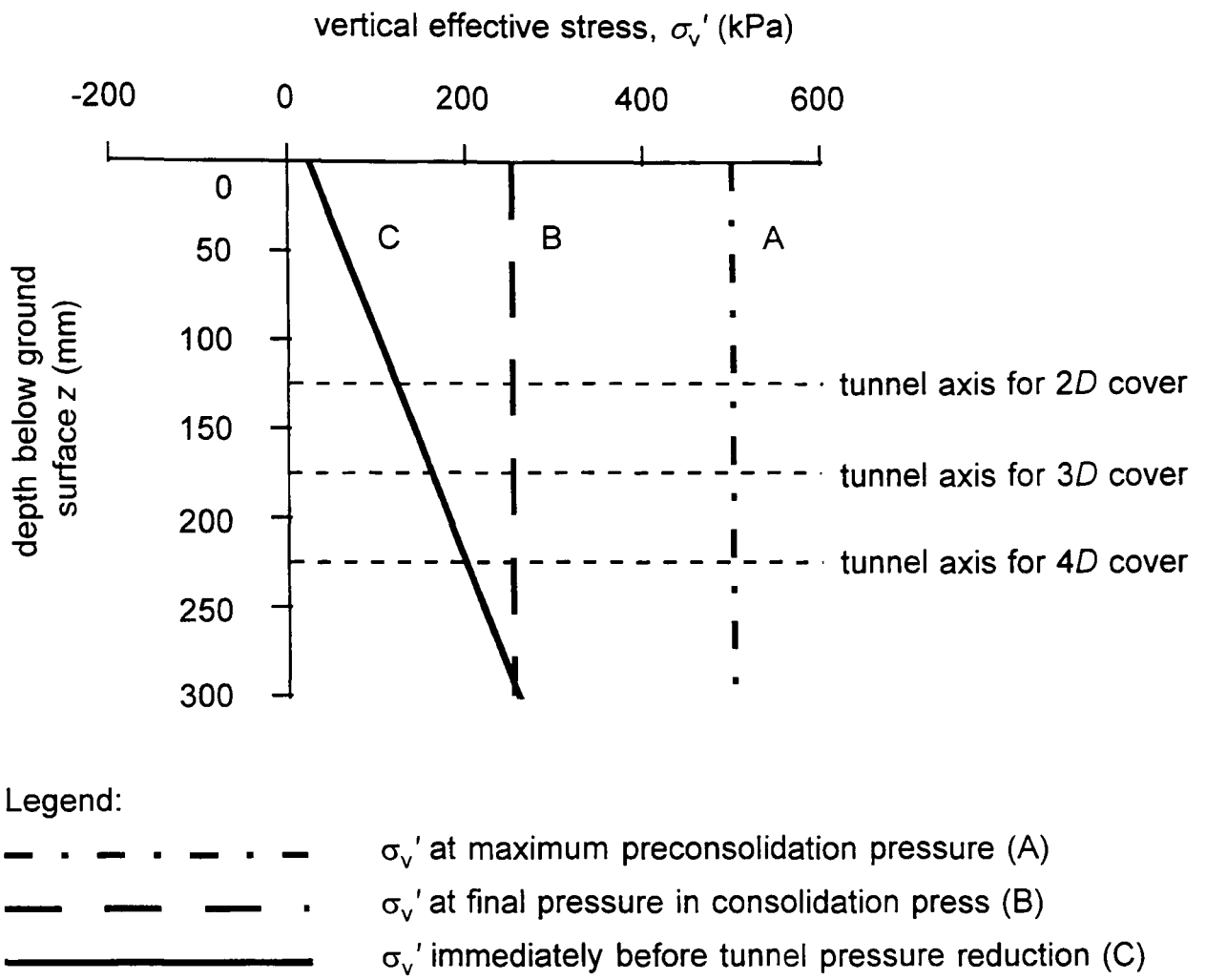

Figure 3.23 Stress history of the clay

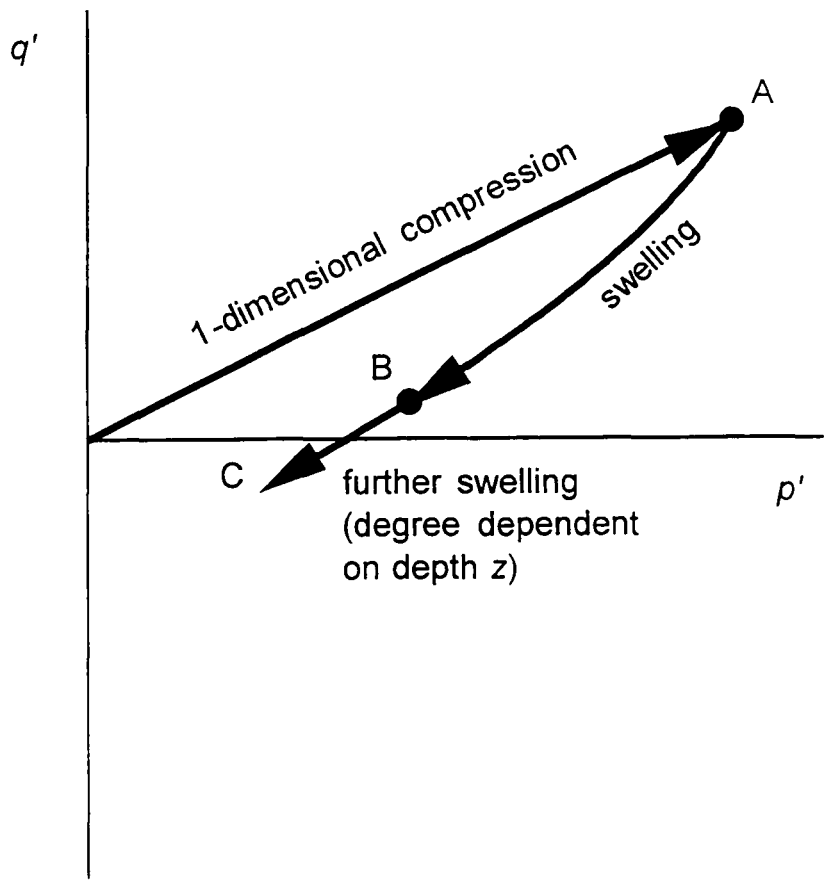

Figure 3.24 Sketched stress paths for elements at tunnel axis level

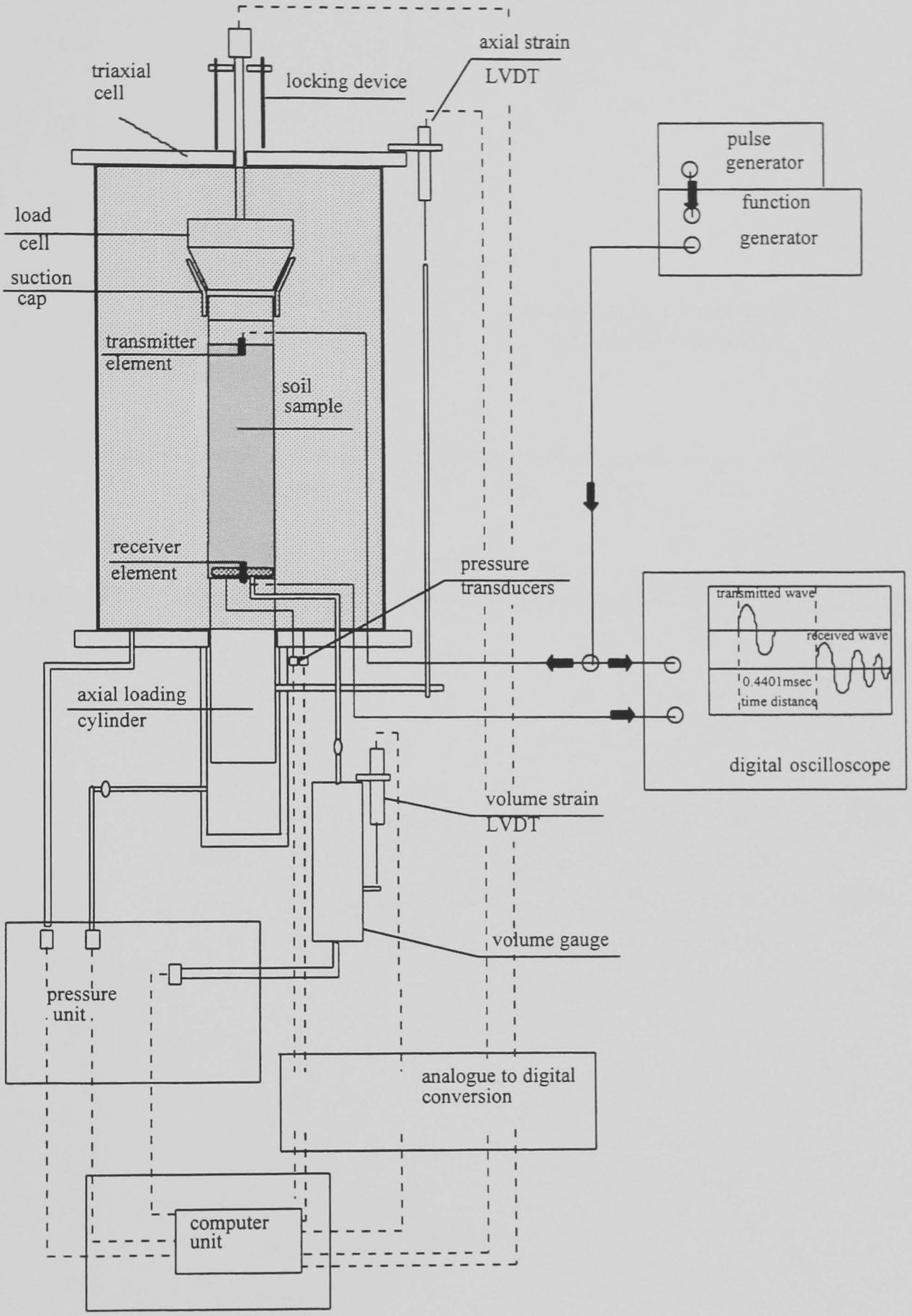

Figure 4.1 Triaxial apparatus showing bender elements (Jovicic, 1997)

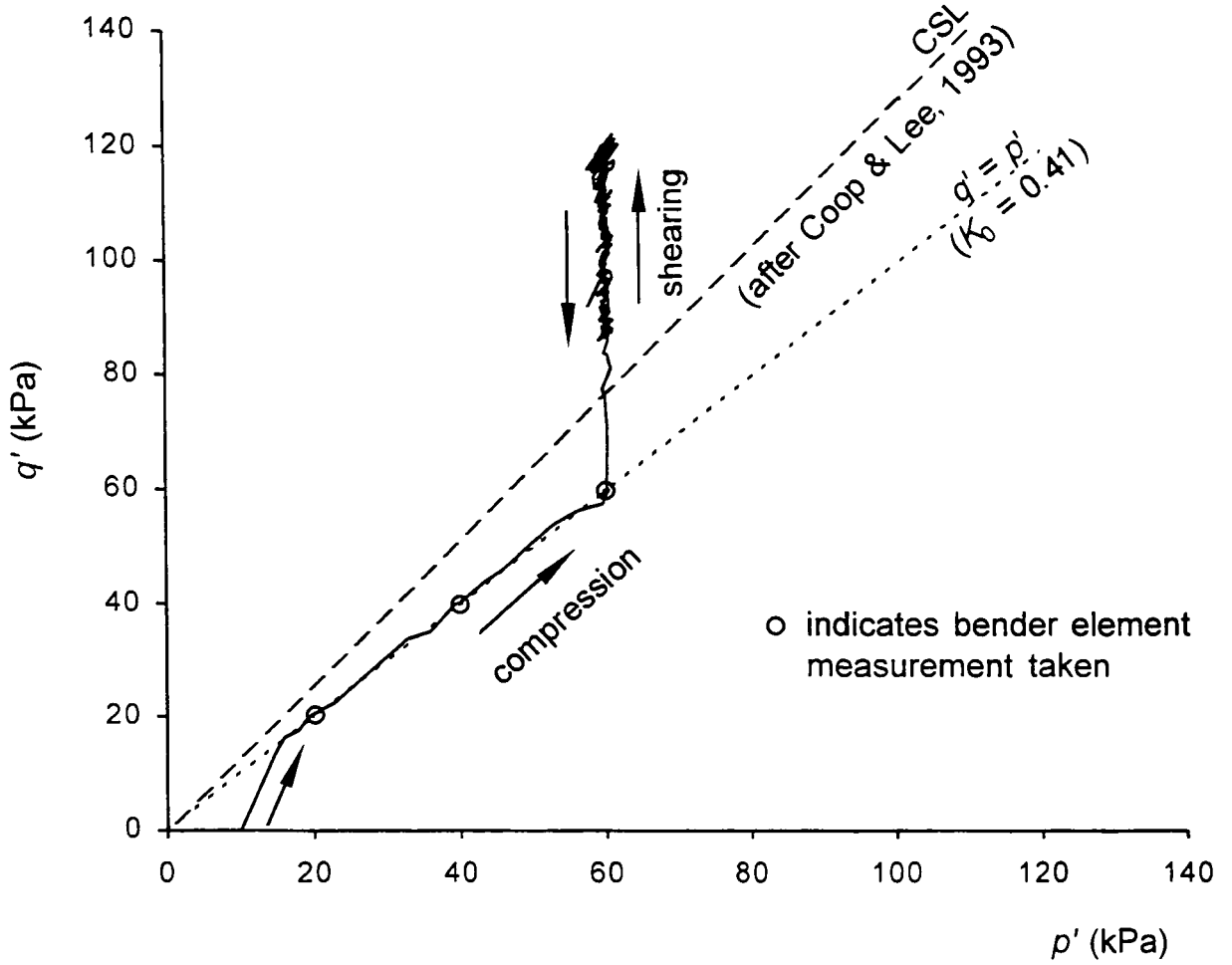

Figure 4.2 Typical stress path for all triaxial tests conducted (from test 7)

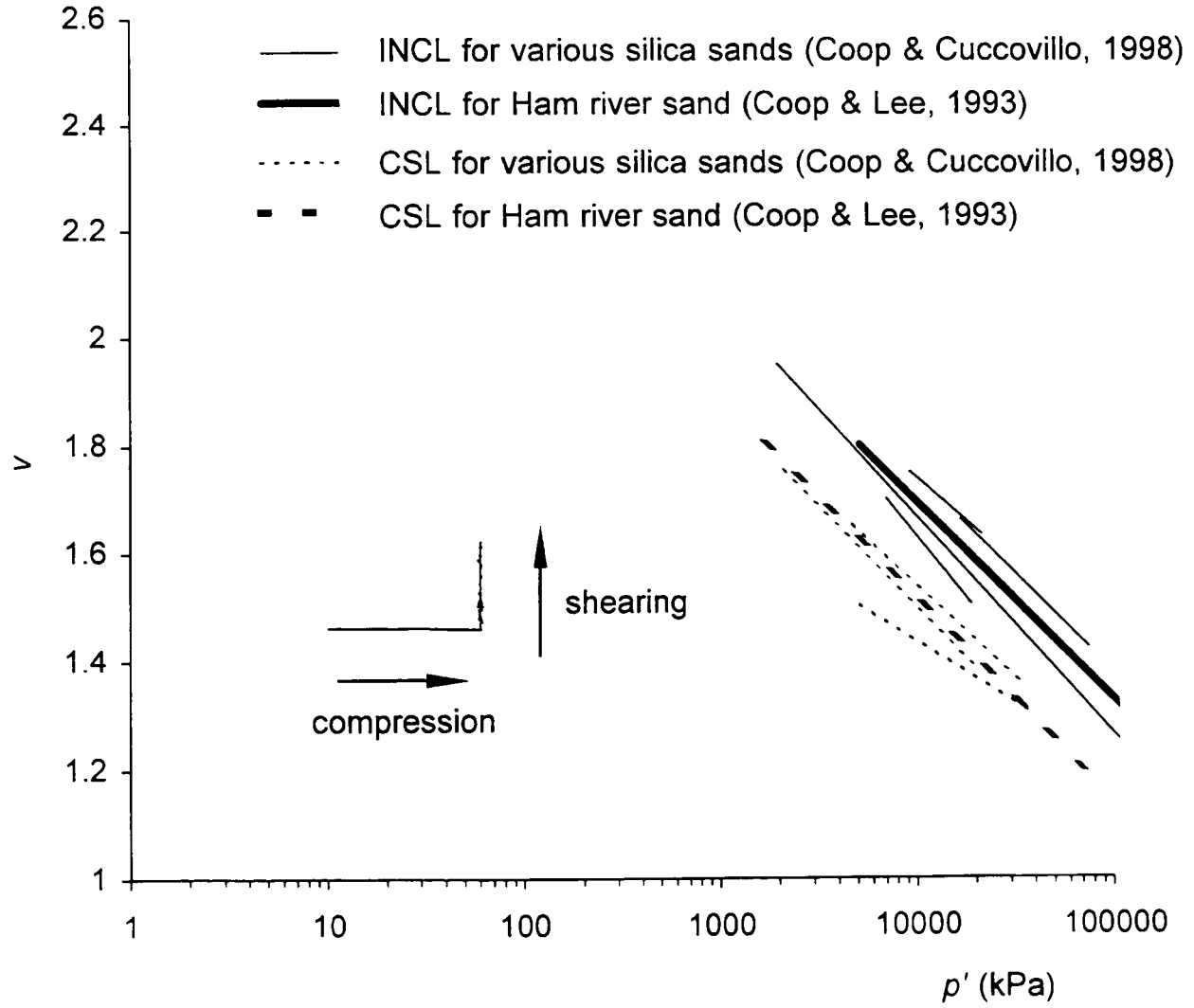

Figure 4.3 Volumetric state from typical triaxial test (from test 7)

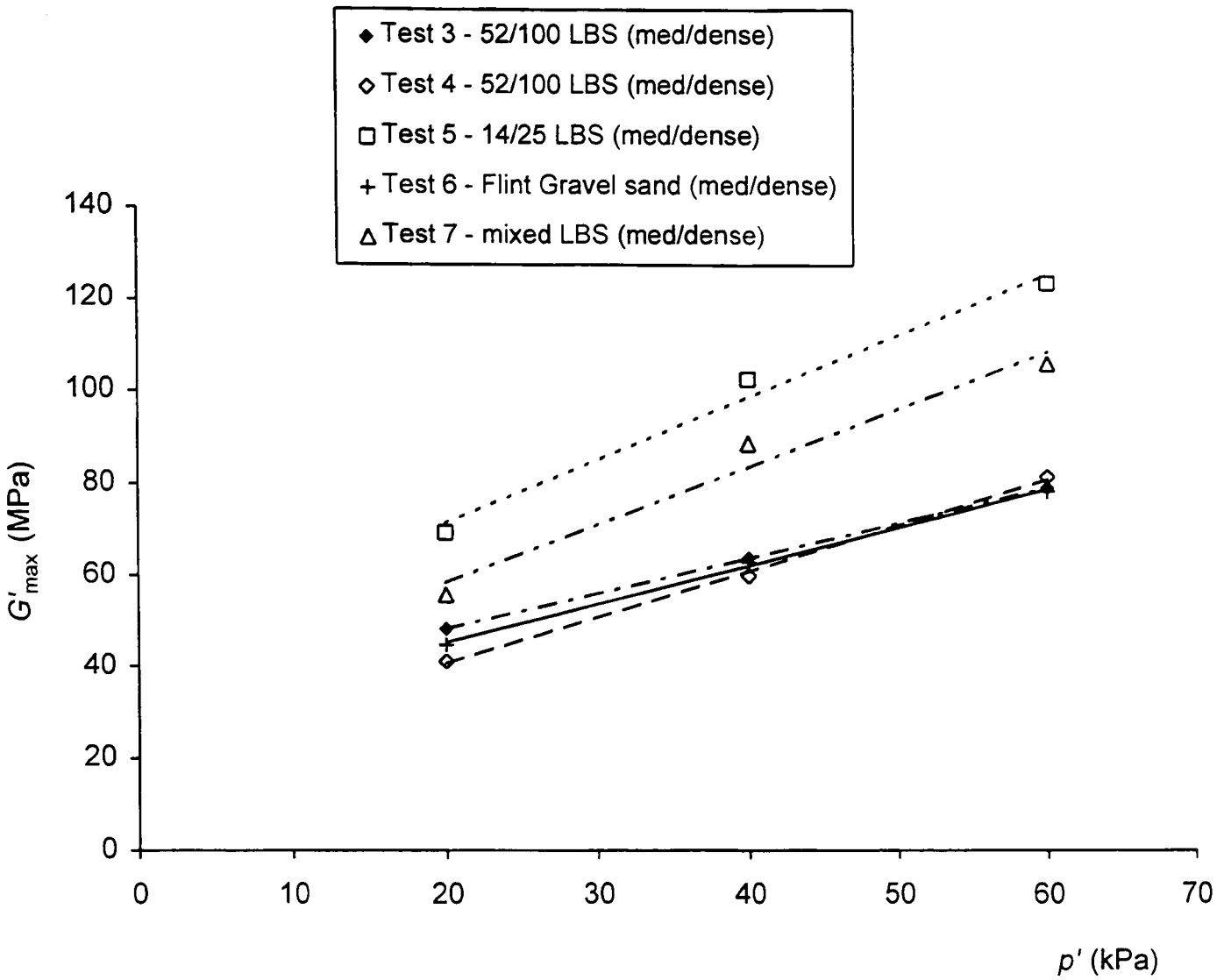

Figure 4.4 G'_{max} of sands from bender element measurements

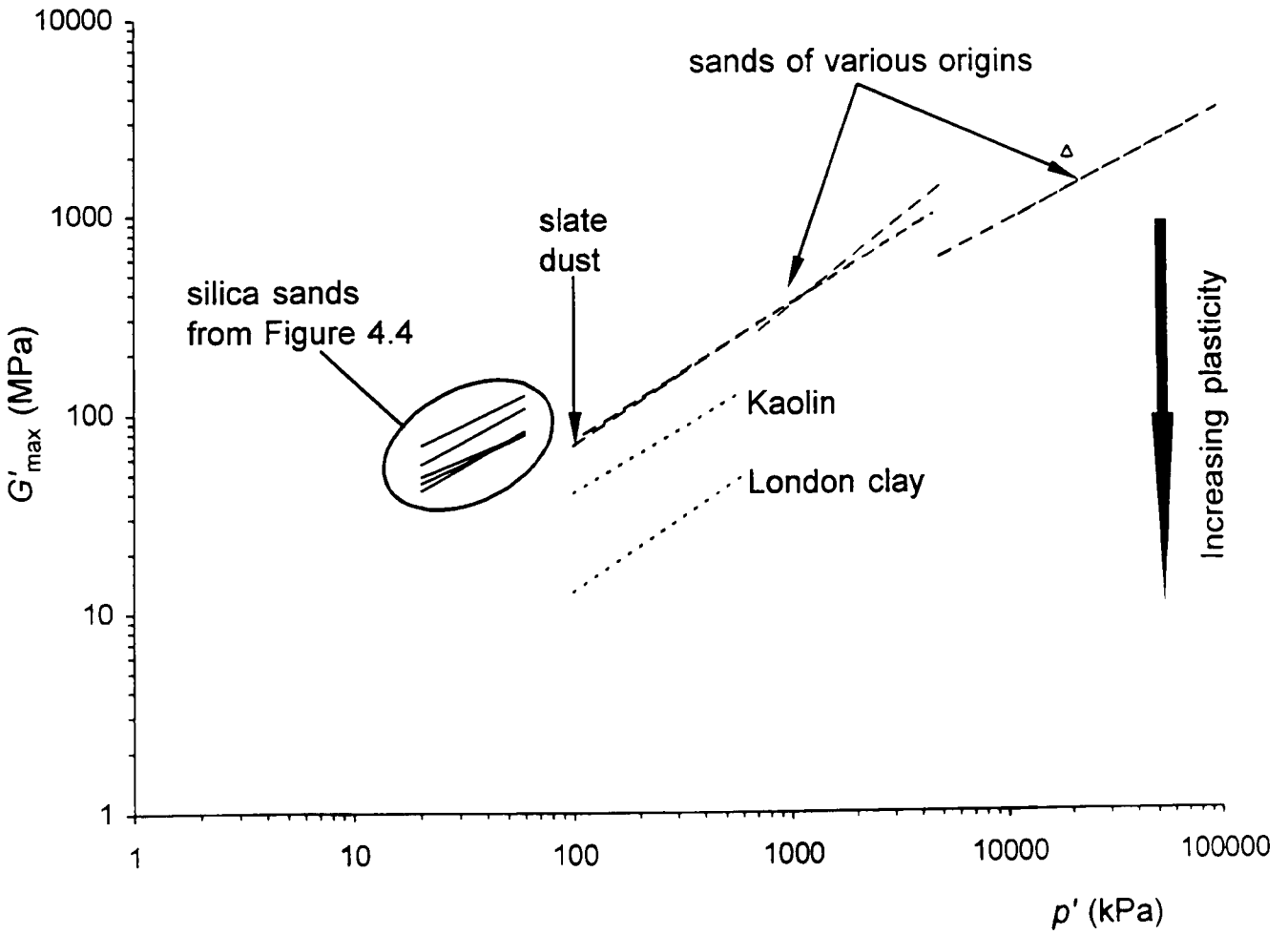

Figure 4.5 $G'_{max\,(oc)}$ of sands from bender element measurements compared to $G'_{max\,(nc)}$ reported for other soils (after Coop, 1998)

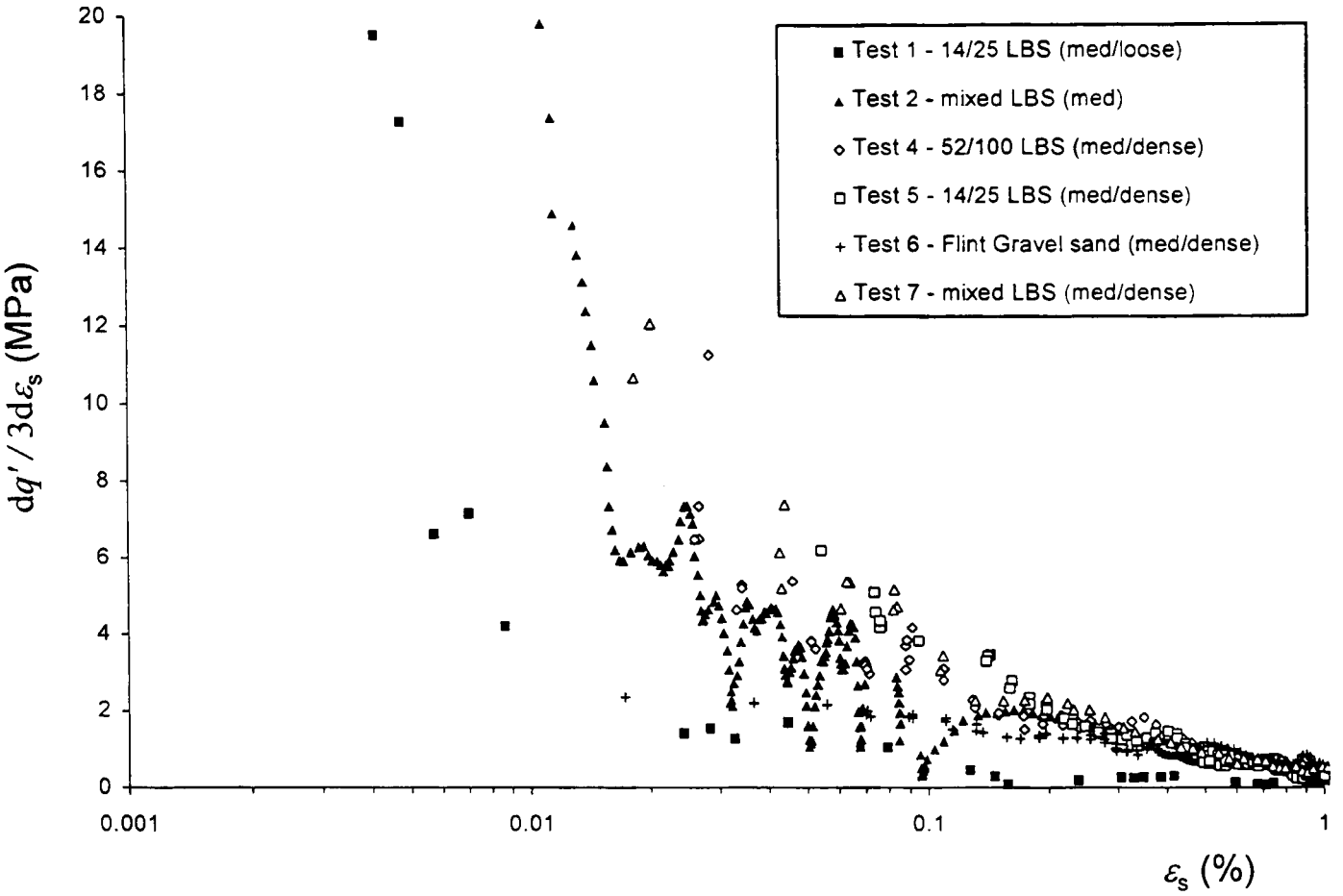

Figure 4.6 Decay of secant shear stiffness with shear strain for sands tested

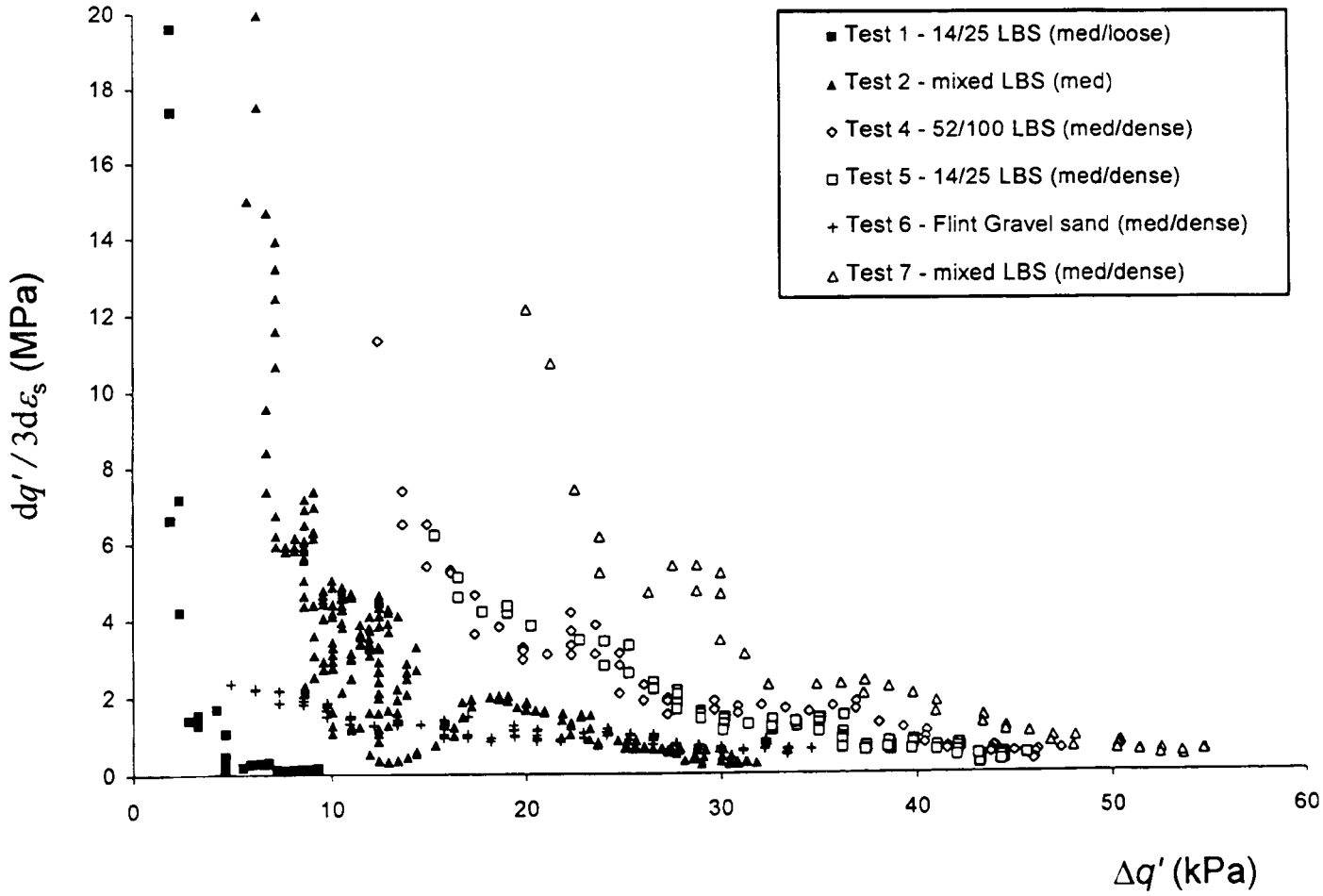

Figure 4.7 Decay of secant shear stiffness with change in deviatoric stress for sands tested

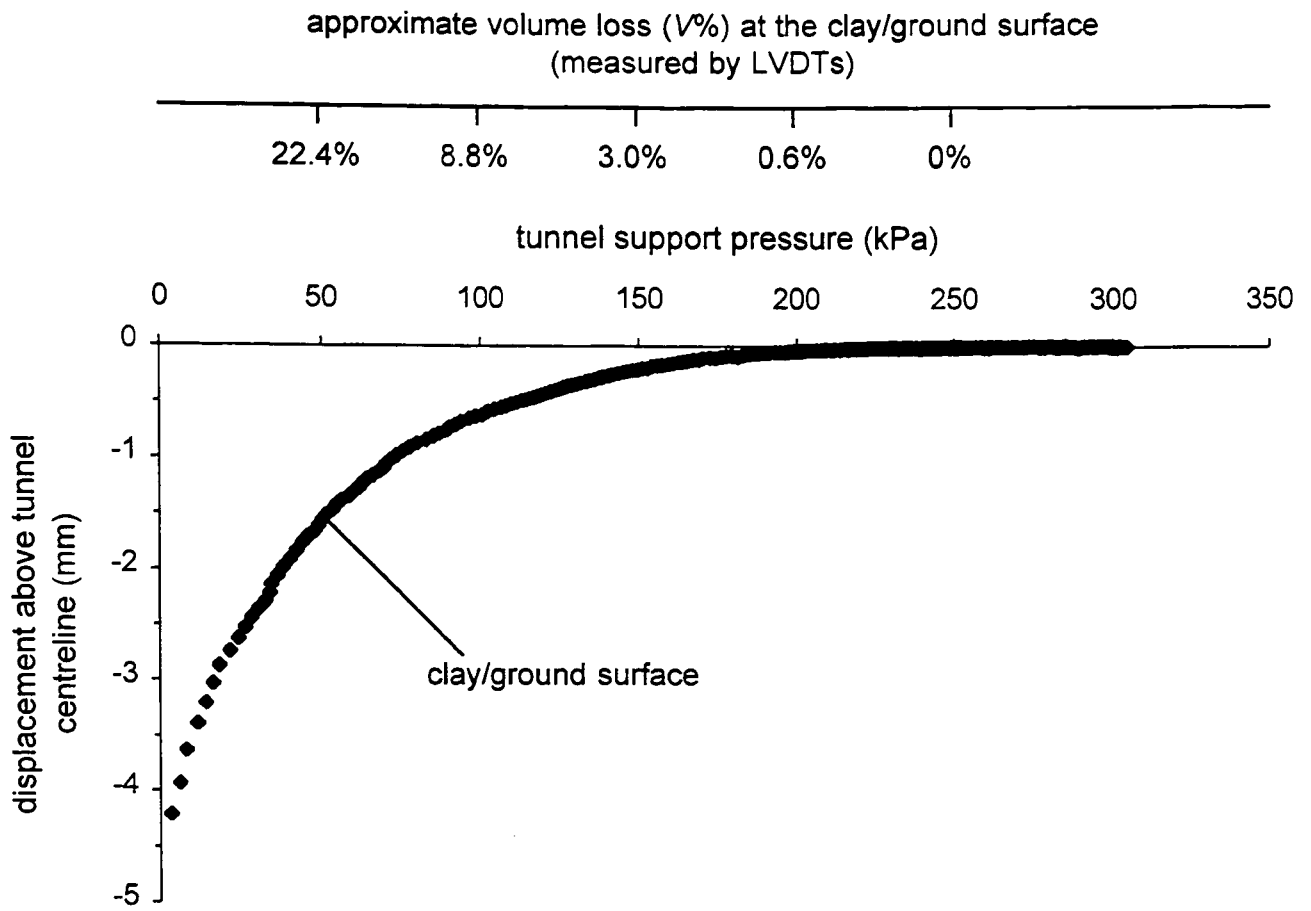

Figure 5.1 Displacement above the tunnel crown at the clay/ground surface during a clay-only centrifuge test, RJG15 (3*D* total cover)

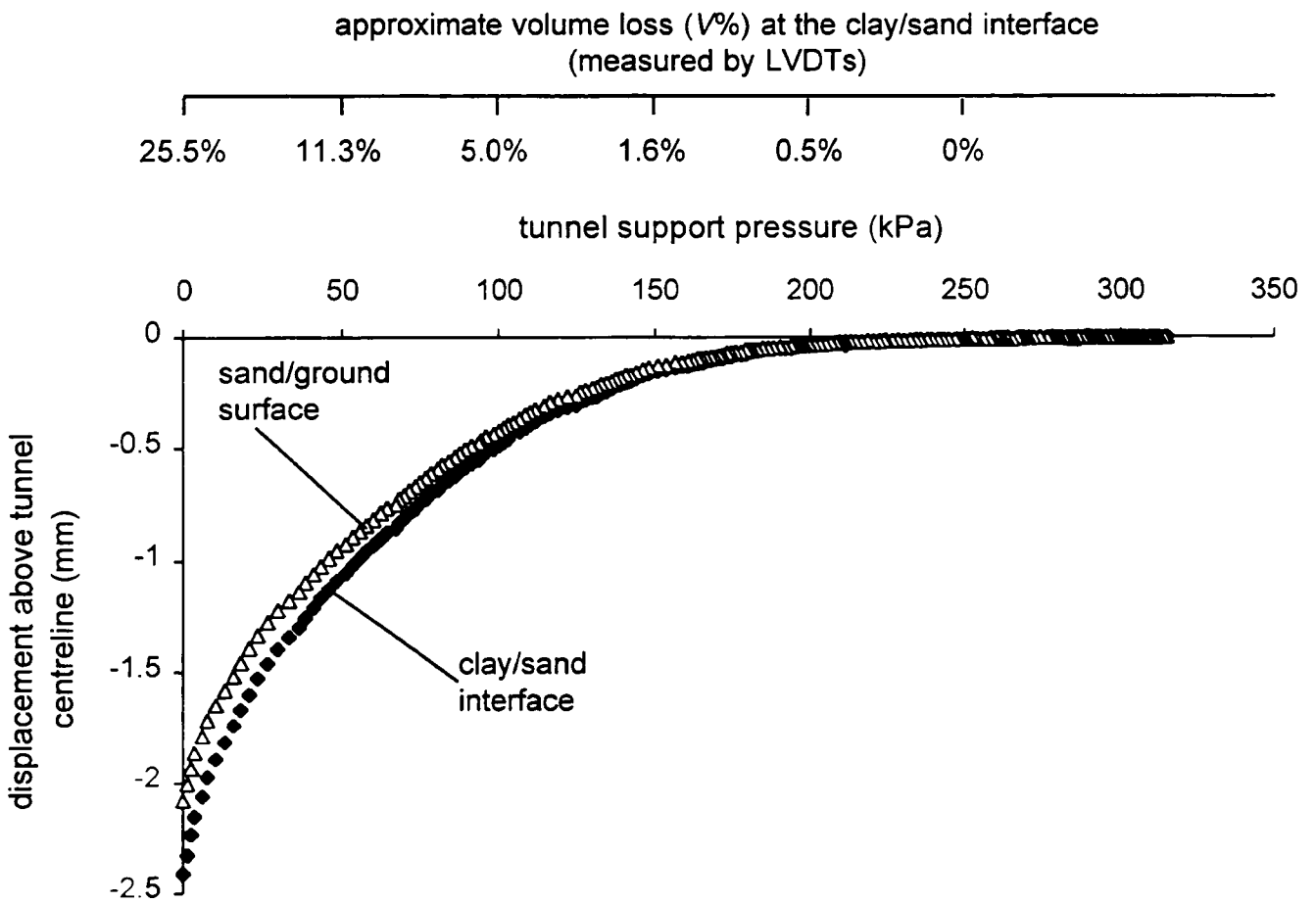

Figure 5.2 Displacement above the tunnel crown at the clay/sand interface and the sand/ground surface during a centrifuge test with overlying sand layer, RJG16 (3*D* total cover)

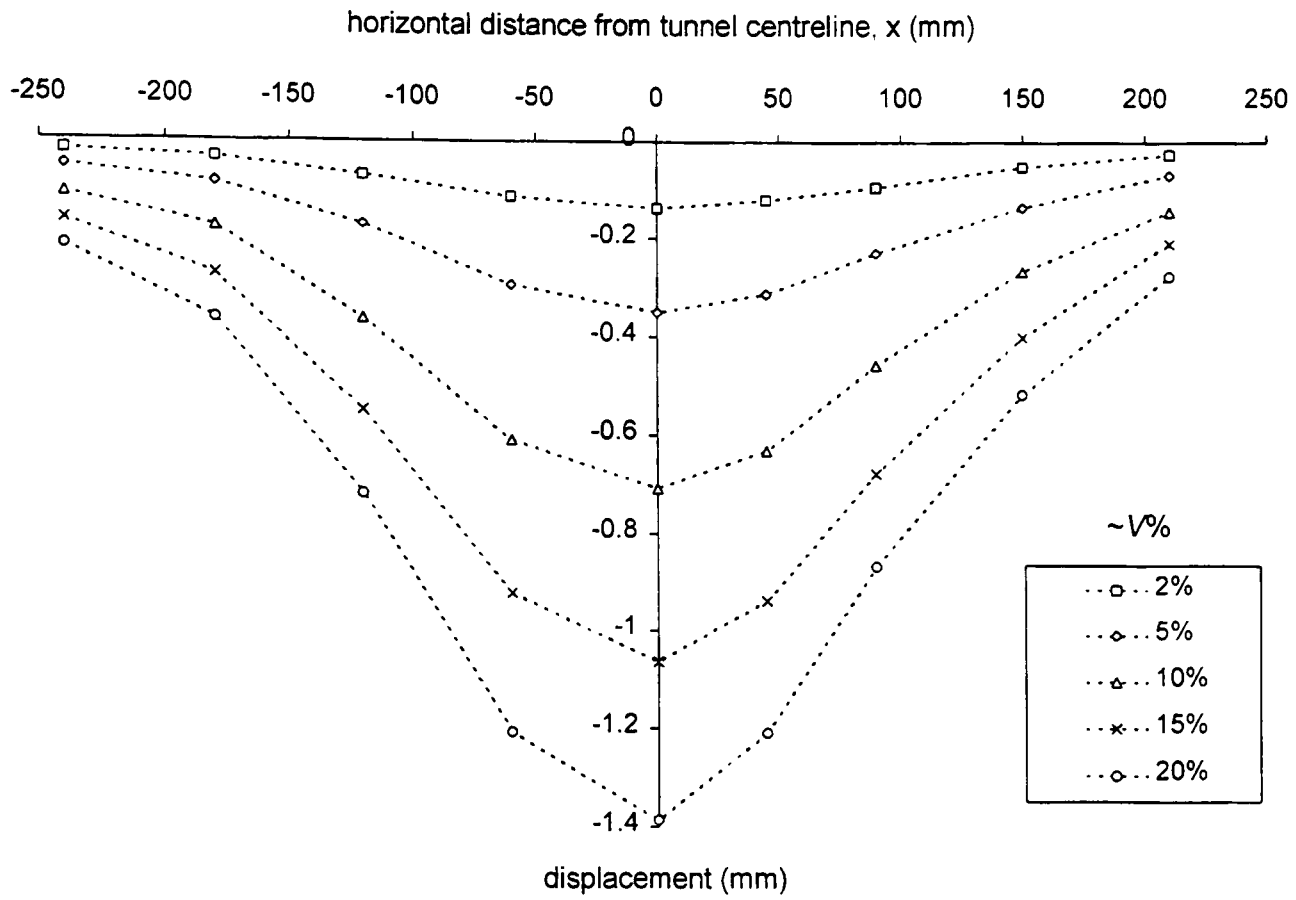

Figure 5.3 Settlement troughs measured by LVDTs at the clay/ground surface during centrifuge test RJG15 (3*D* total cover)

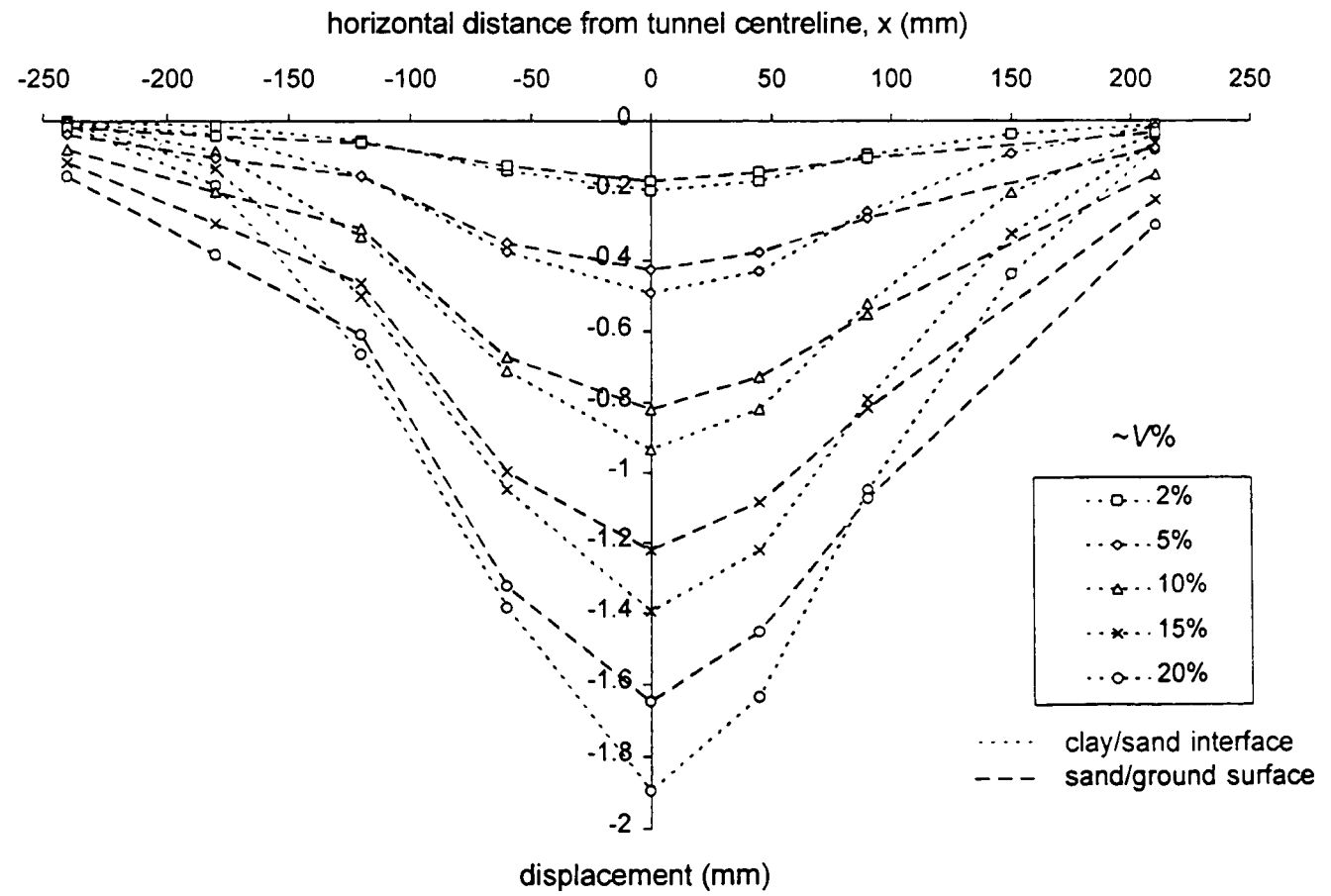

Figure 5.4 Settlement troughs measured by LVDTs at the clay/sand interface and the sand/ground surface during centrifuge test RJG16 (3*D* total cover)

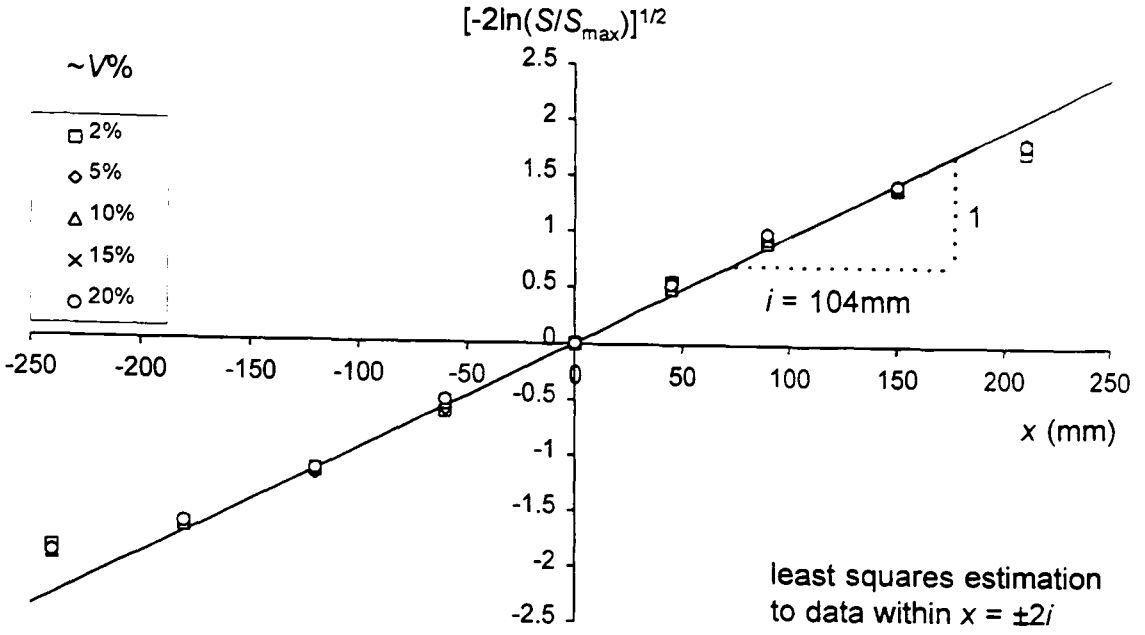

Figure 5.5 Linearised movements at the clay/ground surface during centrifuge test RJG15 (3*D* total cover)

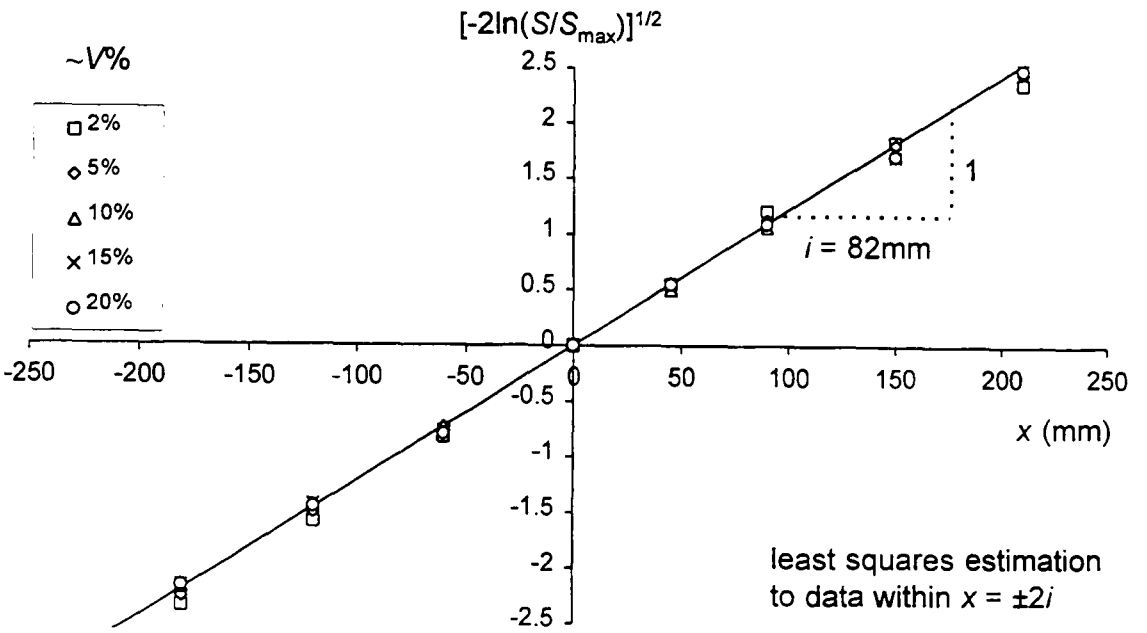

a) clay/sand interface

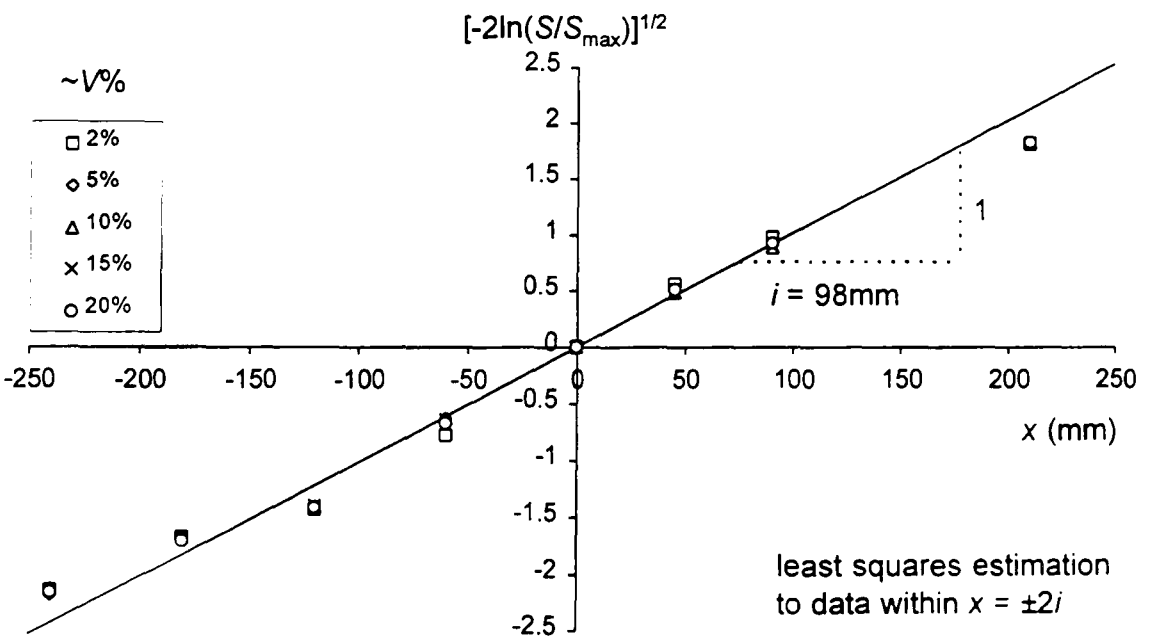

b) sand/ground surface

Figure 5.6 Linearised movements at a) the clay/sand interface and b) the sand/ground surface during centrifuge test RJG16 (3*D* total cover)

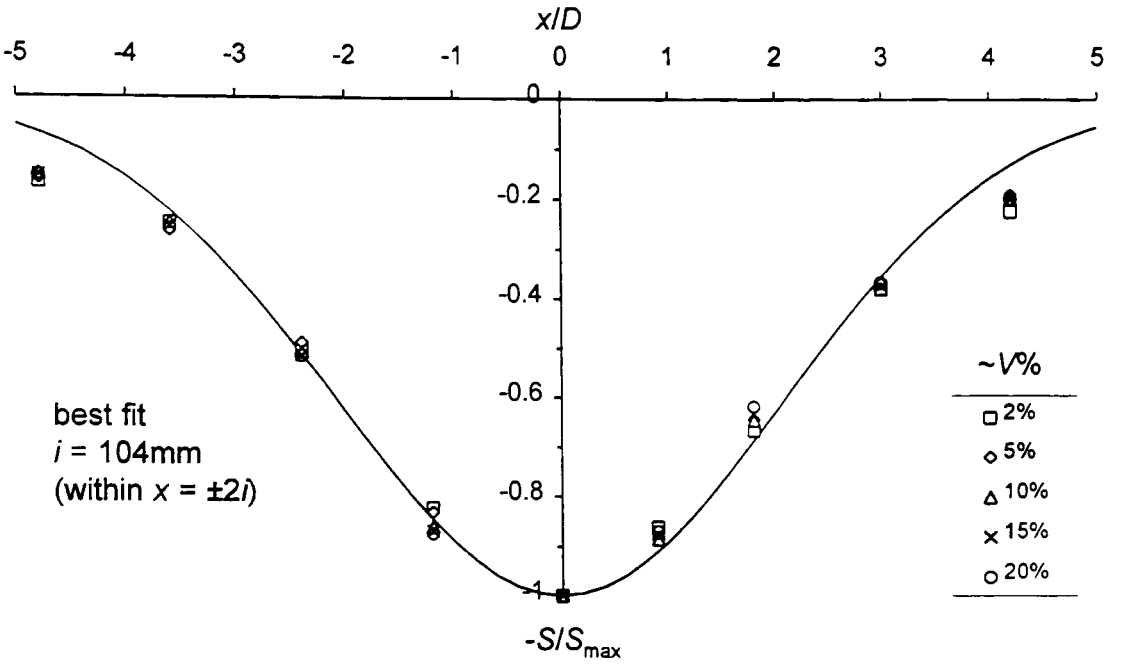

Figure 5.7 Normalised settlement troughs at the clay/ground surface during centrifuge test RJG15 (3*D* total cover)

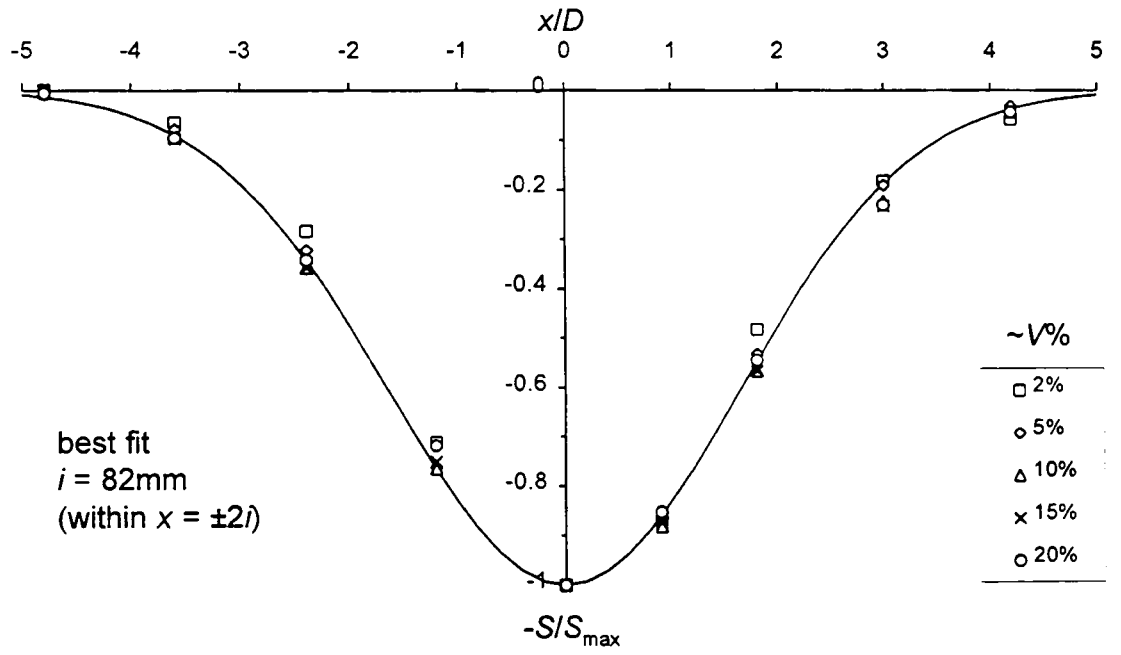

a) clay/sand interface

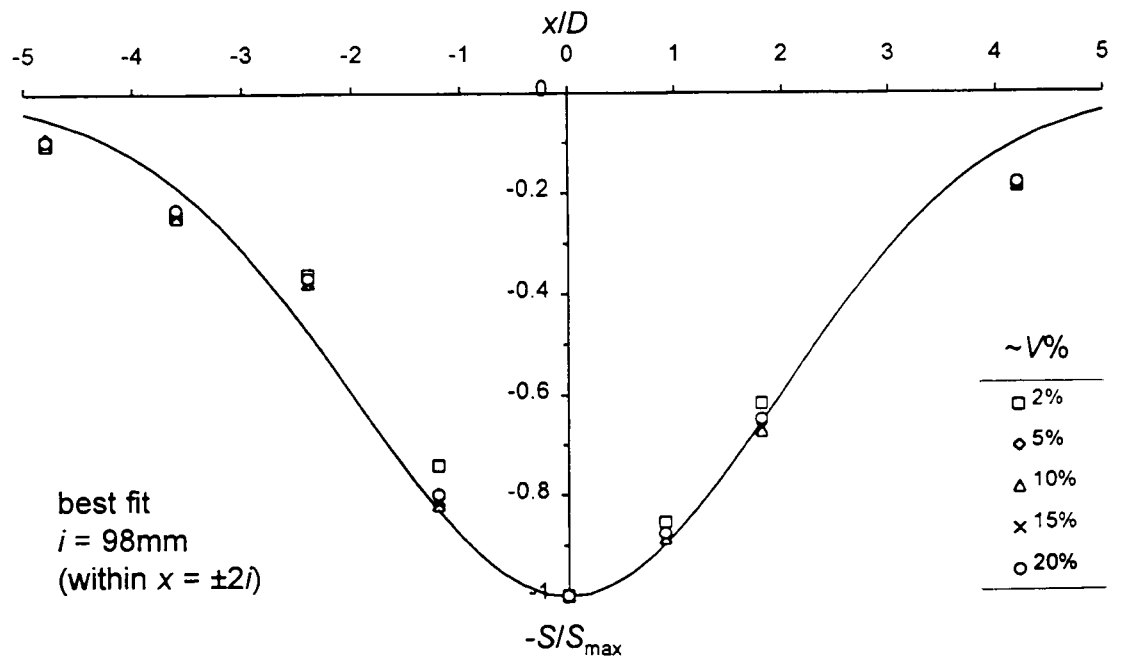

b) sand/ground surface

Figure 5.8 Normalised settlement troughs at a) the clay/sand interface and b) the sand/ground surface during centrifuge test RJG16 (3*D* total cover)

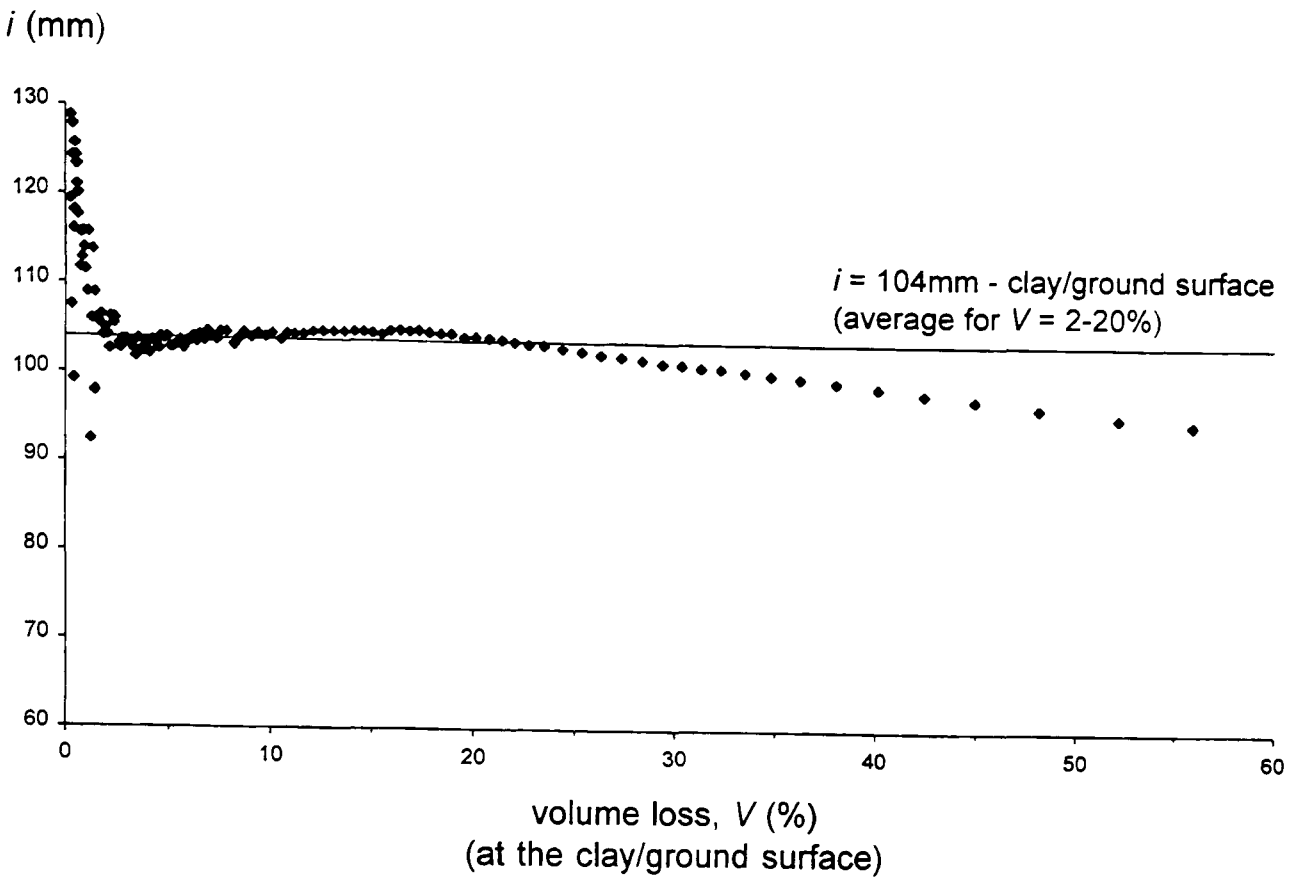

Figure 5.9 Variation of i with volume loss at the clay/ground surface during centrifuge test RJG15 (3D total cover)

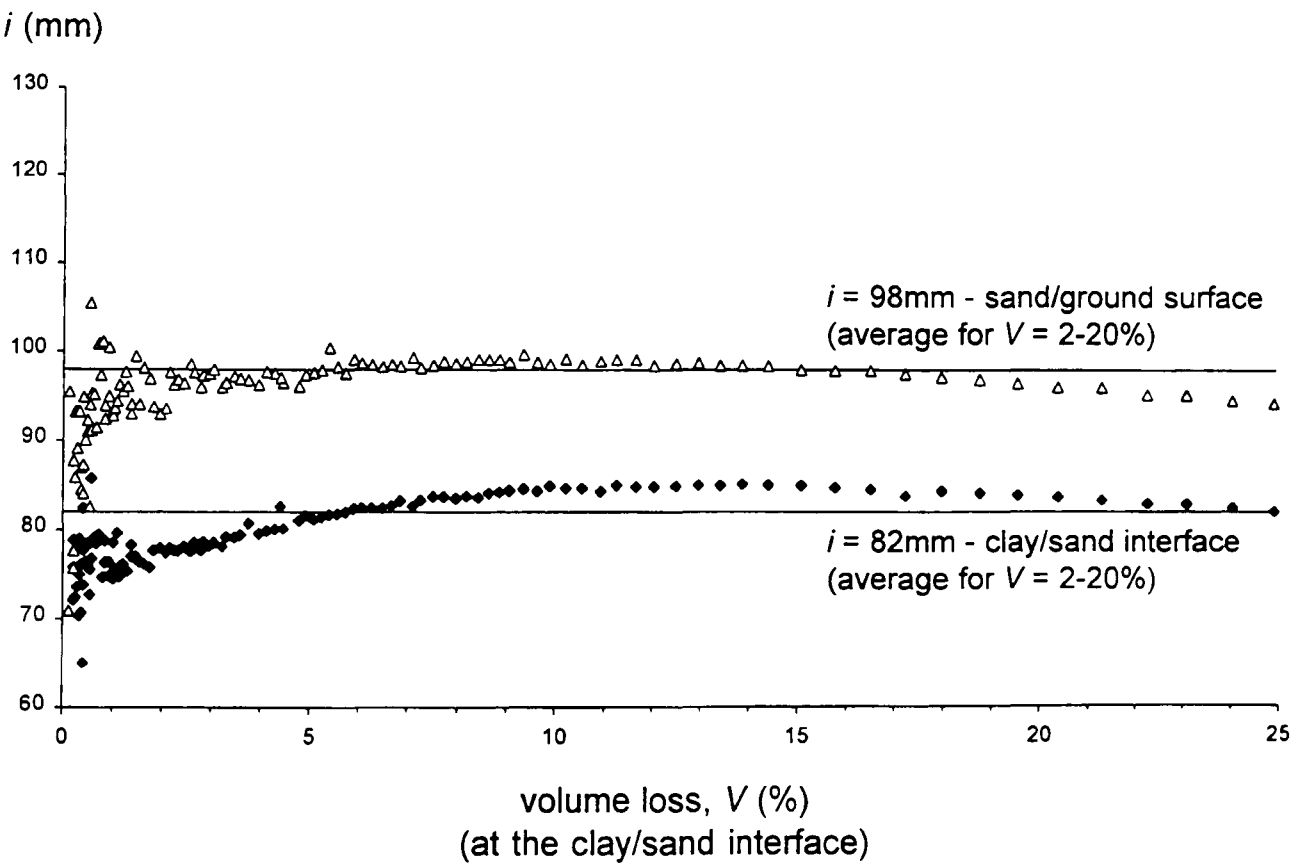

Figure 5.10 Variation of i with volume loss at the clay/sand interface and the sand/ ground surface during centrifuge test RJG16 (3D total cover)

a)

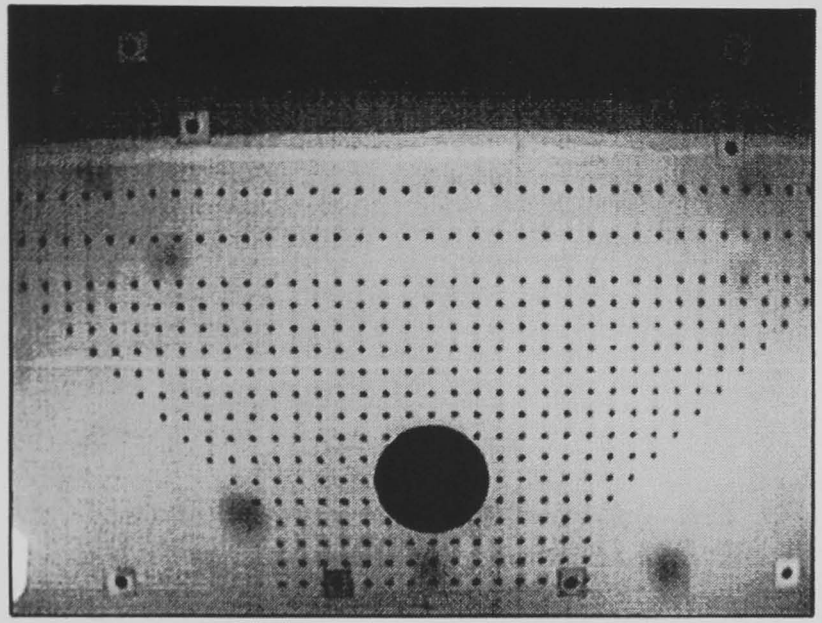

b)

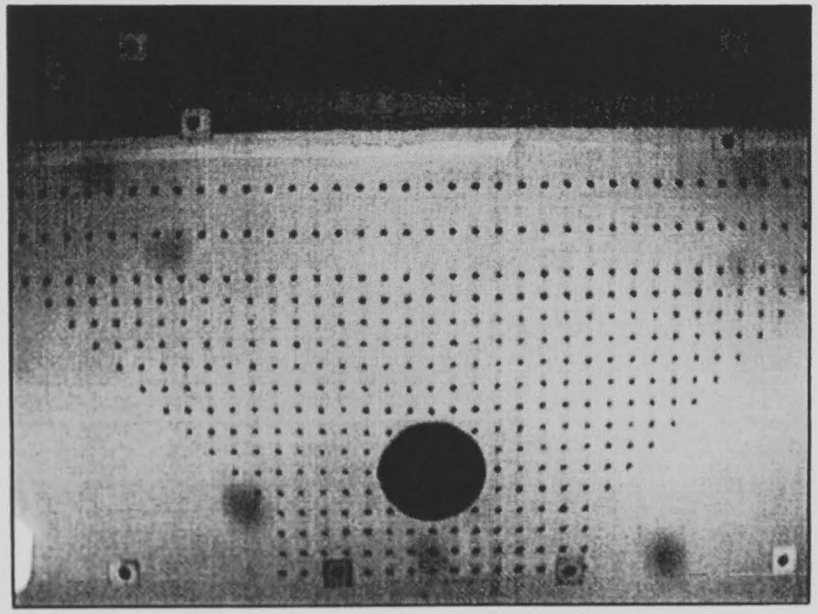

c)

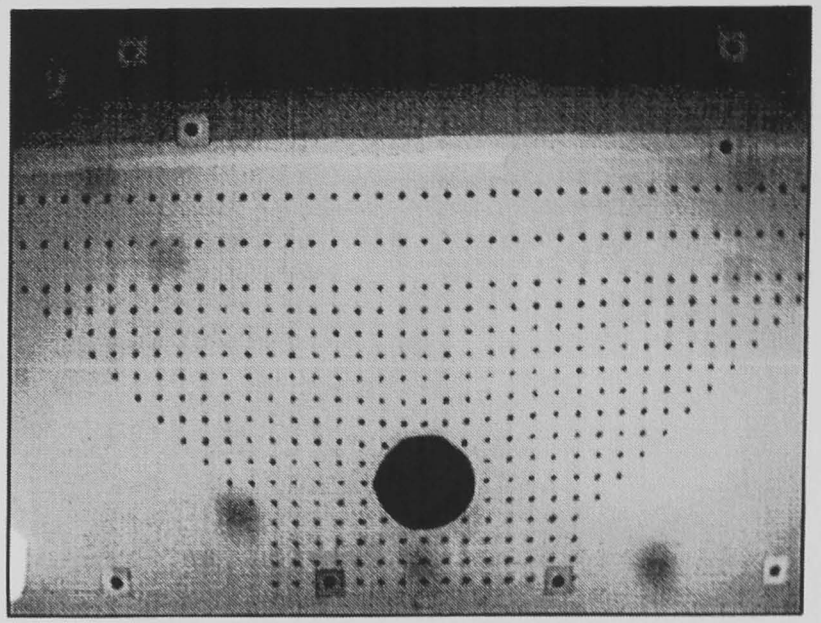

d)

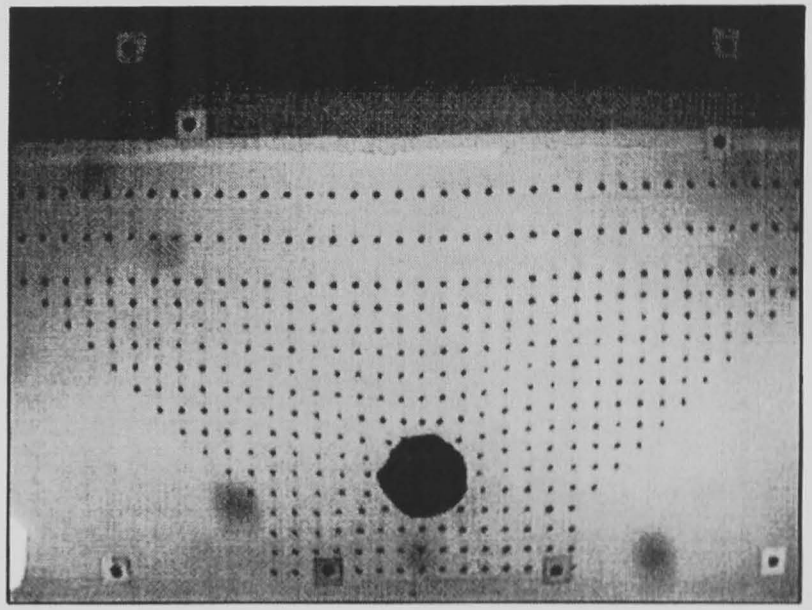

Figure 5.11 Digital images of test RJG20 (1.5*D* sand over 2.5*D* clay above tunnel crown)
a) before reducing the tunnel pressure, b) when $V \sim 10\%$, c) when $V \sim 20\%$ and d) when $V > 40\%$ (effectively well after collapse)

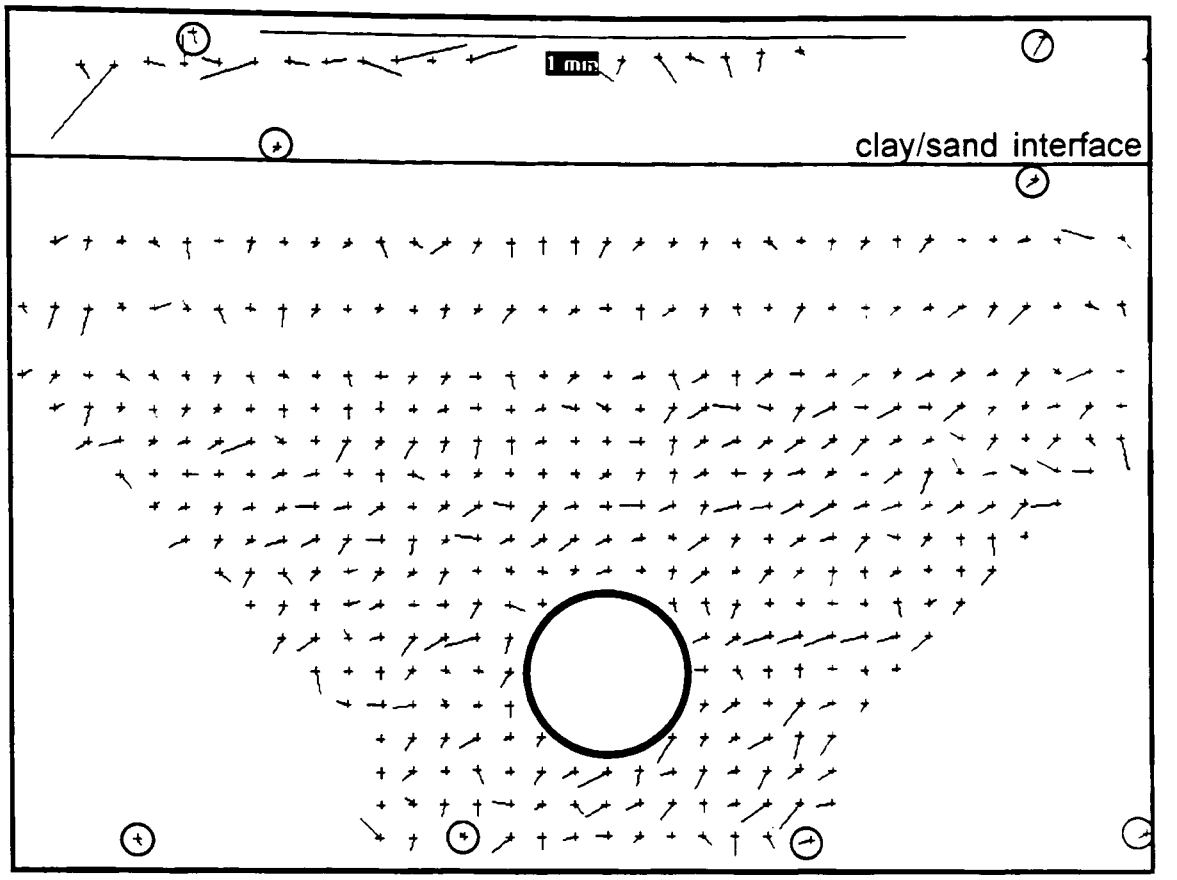

a)
○ indicates control target

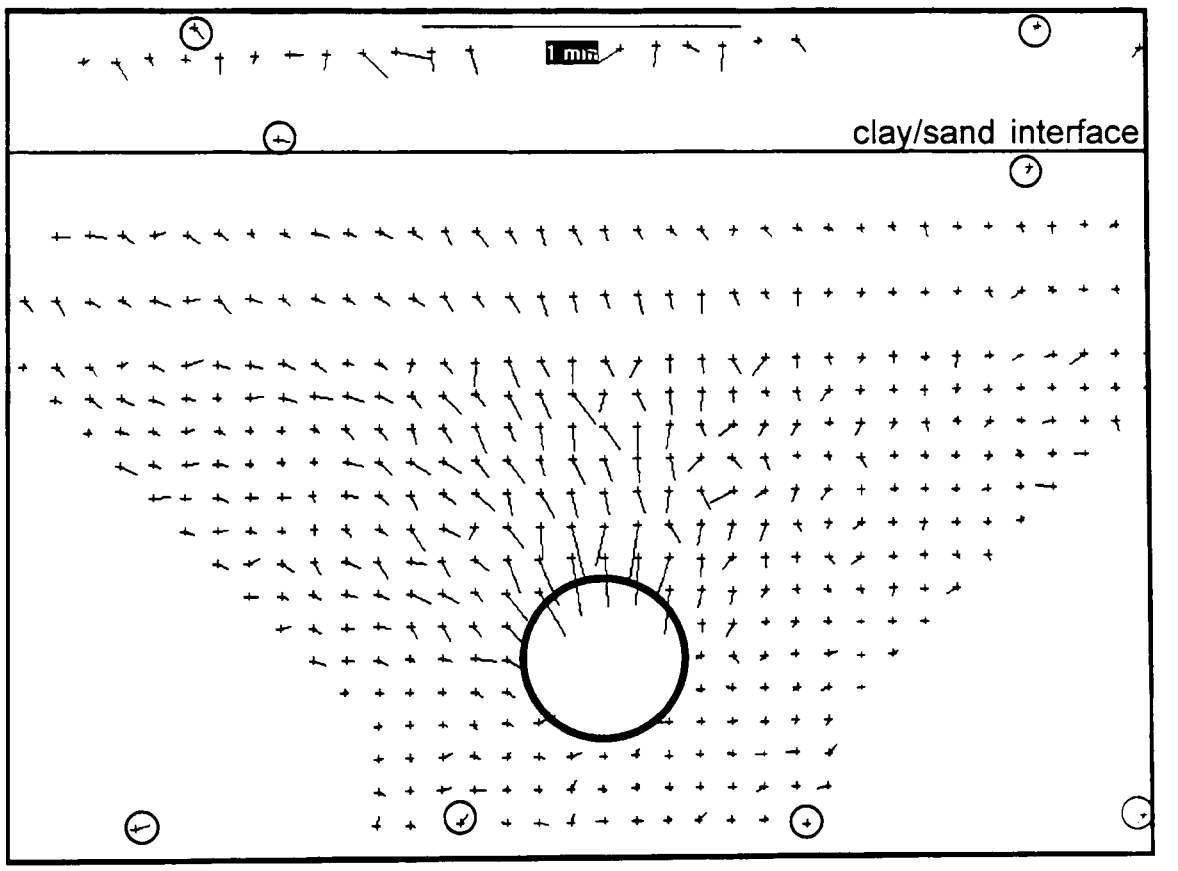

b)
○ indicates control target

Figure 5.12 Calibrated vectors from test RJG20
a) showing level of noise (x200) - from consecutive images before reducing tunnel pressure
b) showing patterns beginning to form (x100) - when movement at the tunnel crown is ~0.15mm (V~1%)

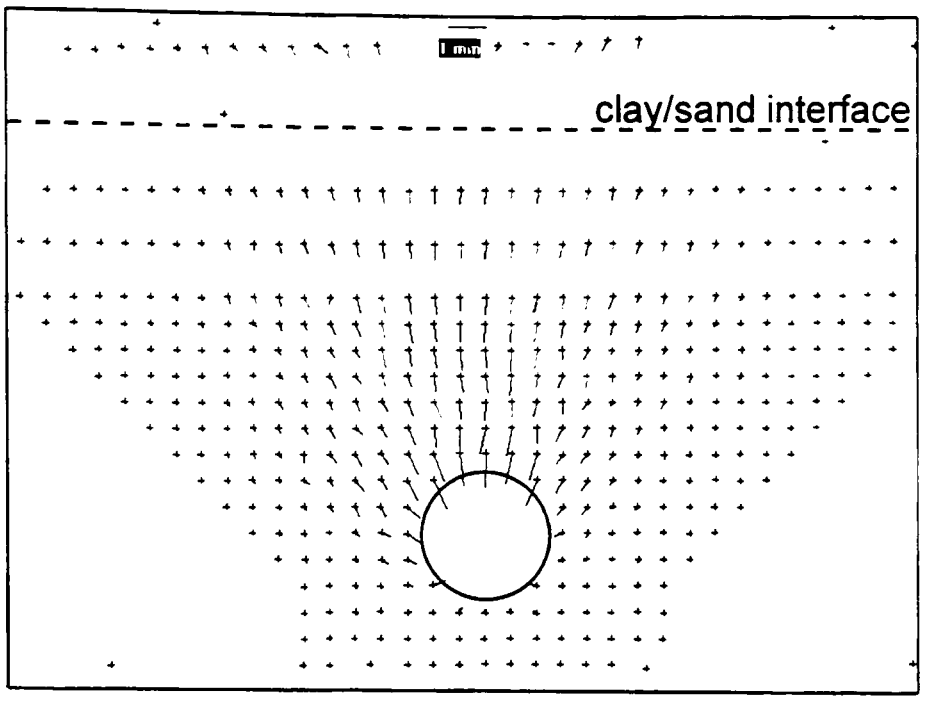

Figure 5.13 Vectors of movement (x15) during centrifuge test RJG20
a) at V~5% (measured by LVDTs)
b) at V~10% (measured by LVDTs)

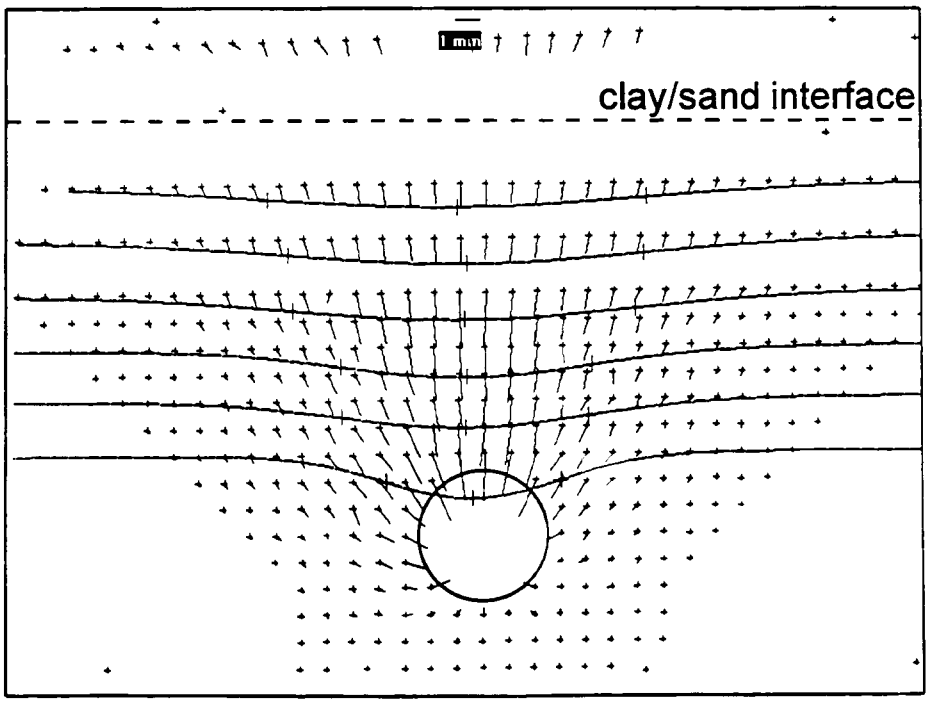

Figure 5.14 Vectors of movement (x10) during centrifuge test RJG20 with best fit Gaussian distributions imposed on subsurface settlement profiles

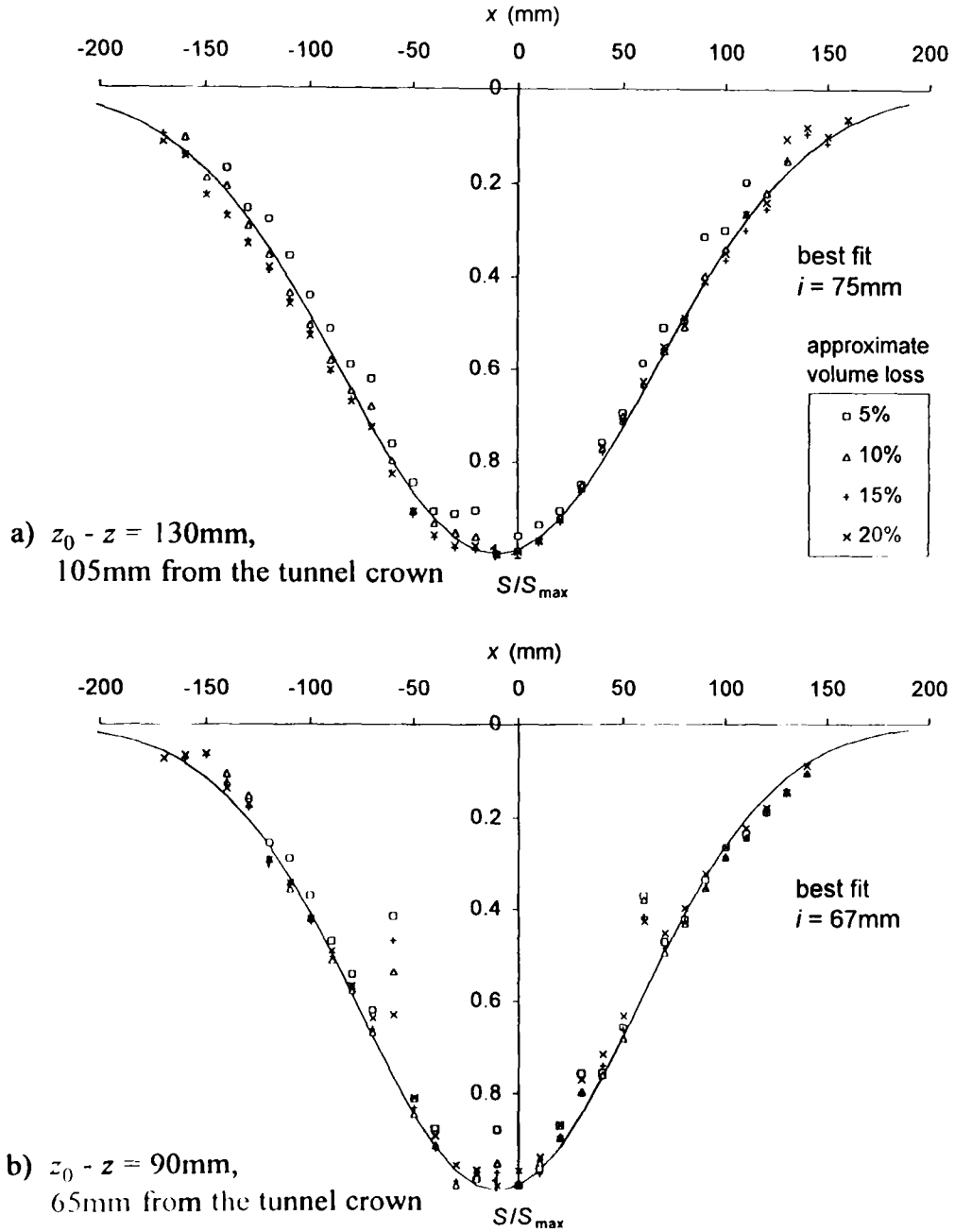

a) $z_0 - z$ = 130mm,
105mm from the tunnel crown

b) $z_0 - z$ = 90mm,
65mm from the tunnel crown

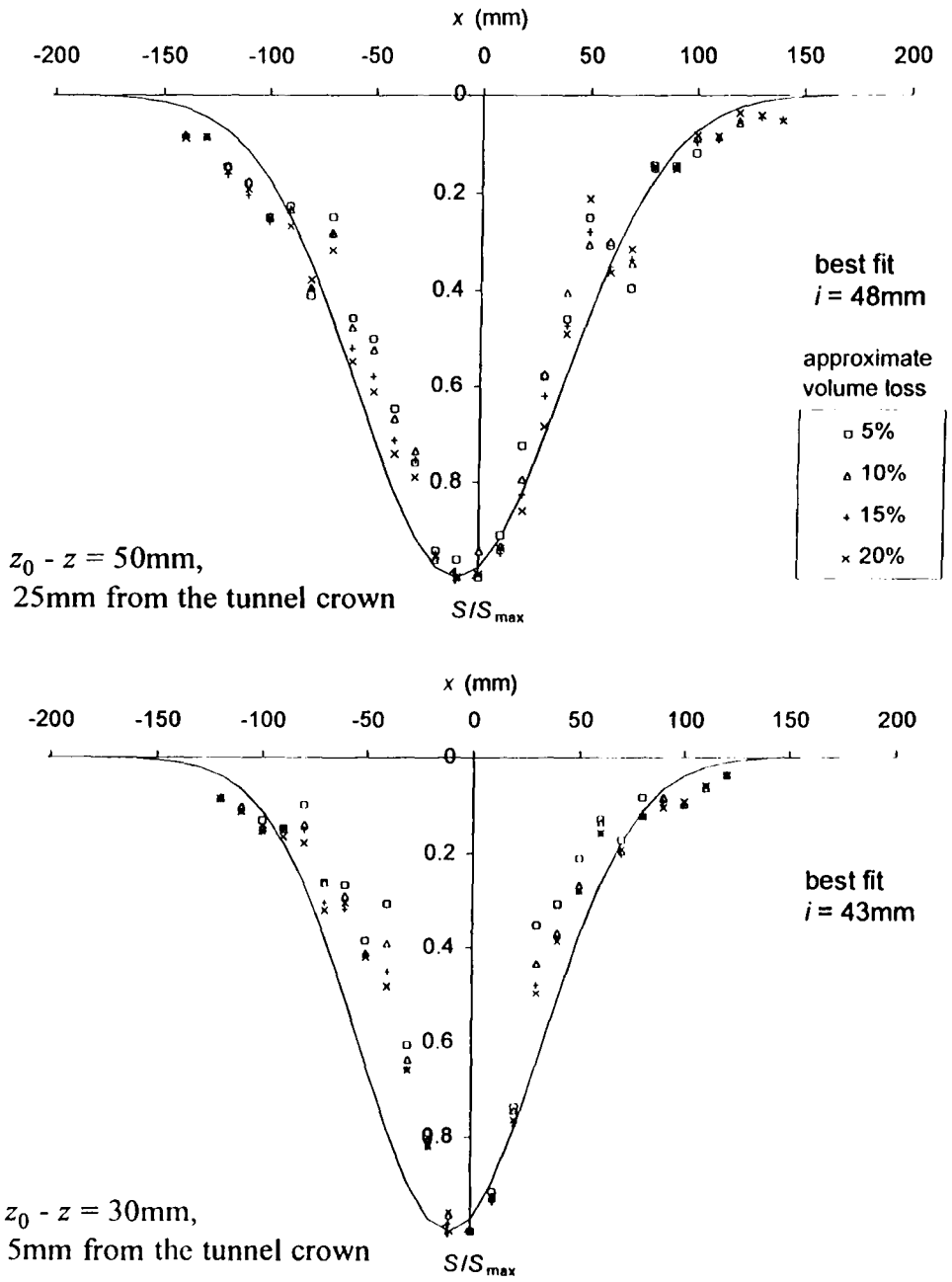

c) $z_0 - z$ = 50mm,
25mm from the tunnel crown

d) $z_0 - z$ = 30mm,
5mm from the tunnel crown

Figure 5.15 Normalised settlement troughs and best fit Gaussian distributions at various subsurface levels in the clay (test RJG20 - 1.5D sand over 2.5D clay above tunnel crown)

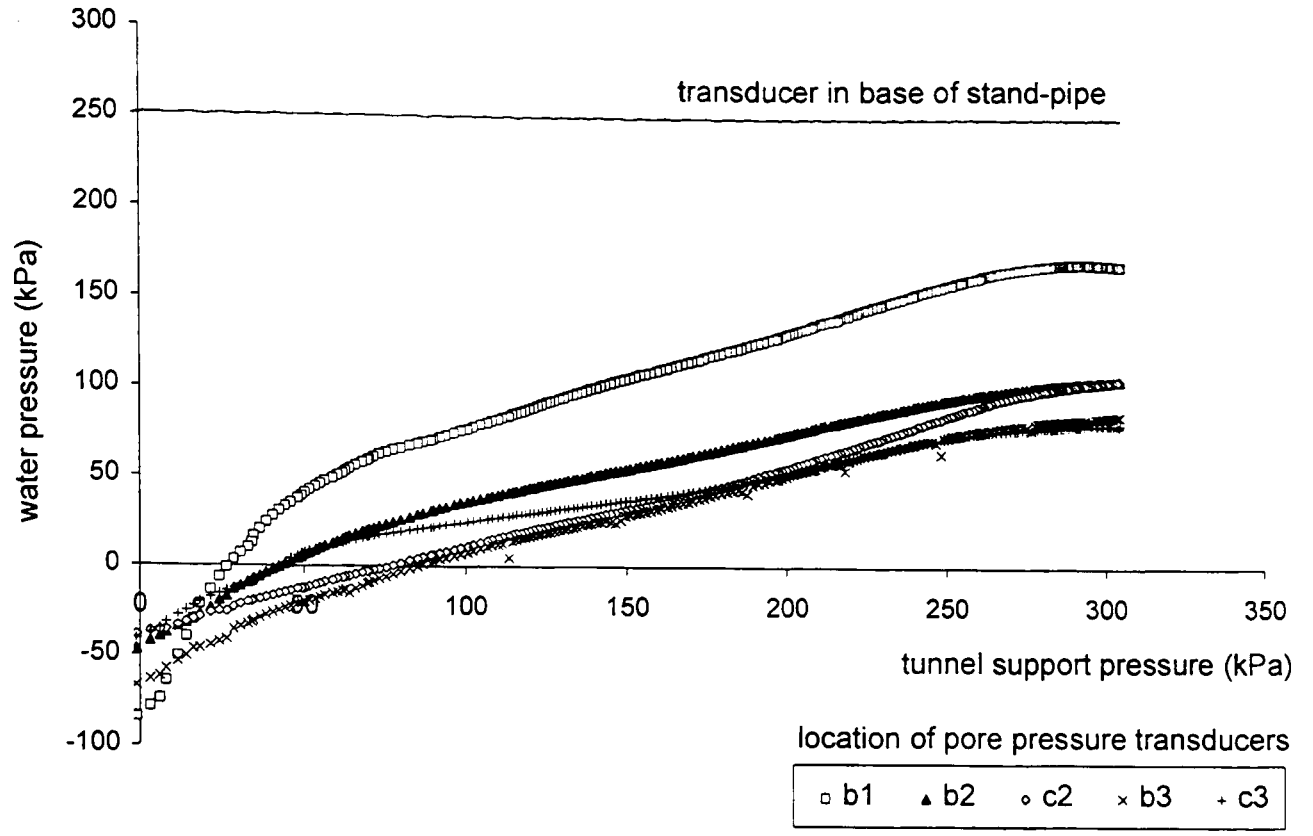

Figure 5.16 Pore pressures during reduction of tunnel support pressure in centrifuge test RJG15 (3*D* clay above tunnel crown)

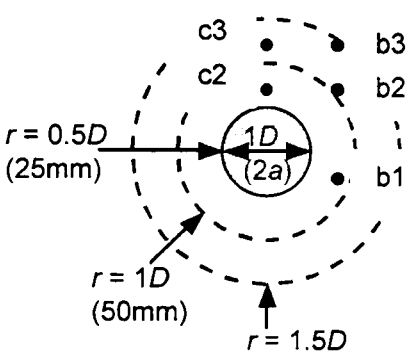

ppt	radius (r)	ppt	radius (r)
b1	42.7mm	c2	35.0mm
b2	53.2mm	c3	60.0mm
b3	72.1mm		

Figure 5.17 Pore pressures during reduction of tunnel support pressure in centrifuge test RJG16 (1.5*D* sand over 1.5*D* clay above tunnel crown)

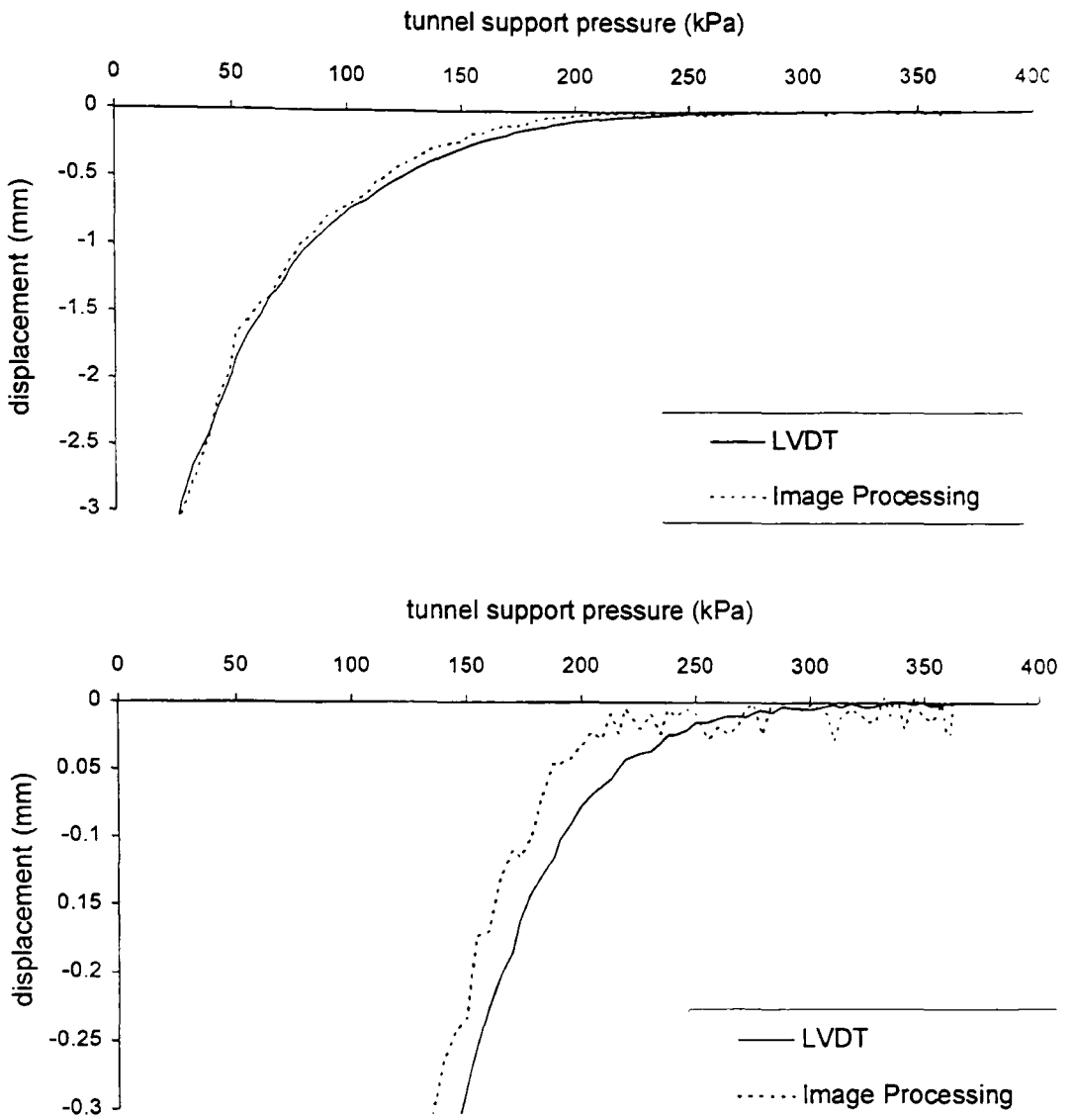

Figure 5.18 Comparison of movement measured above the tunnel centreline at/near the clay surface by a LVDT and by image processing (centrifuge test RJG20)

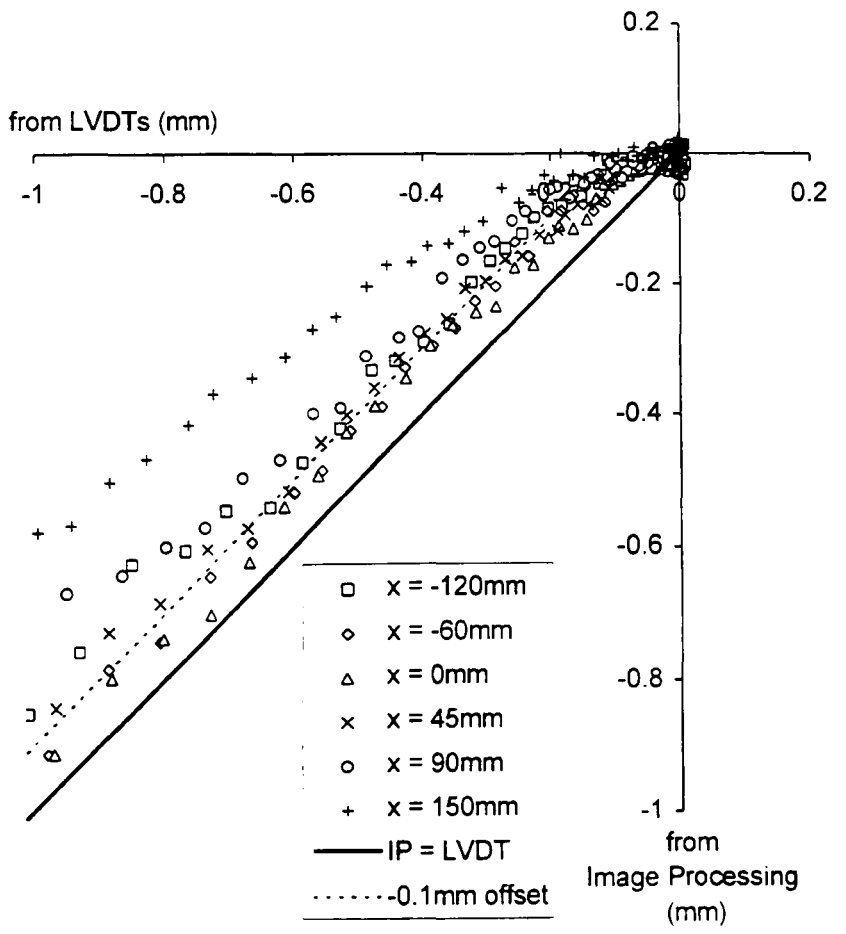

Figure 5.19 Comparison of movements measured at/near the clay surface by LVDTs and by image processing (IP) during centrifuge test RJG20

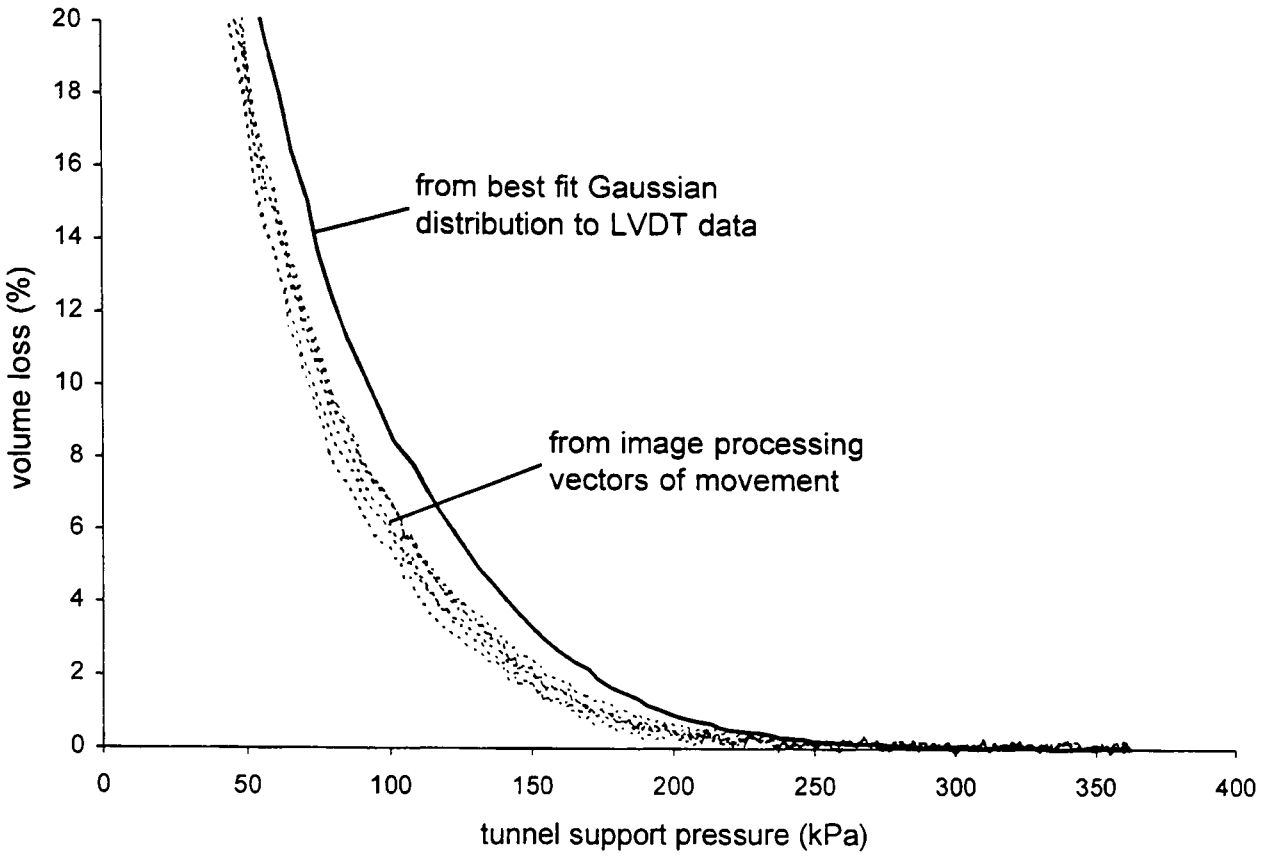

Figure 5.20 Volume losses calculated from LVDT measurements and image processing measurements at various subsurface levels (during centrifuge test RJG20)

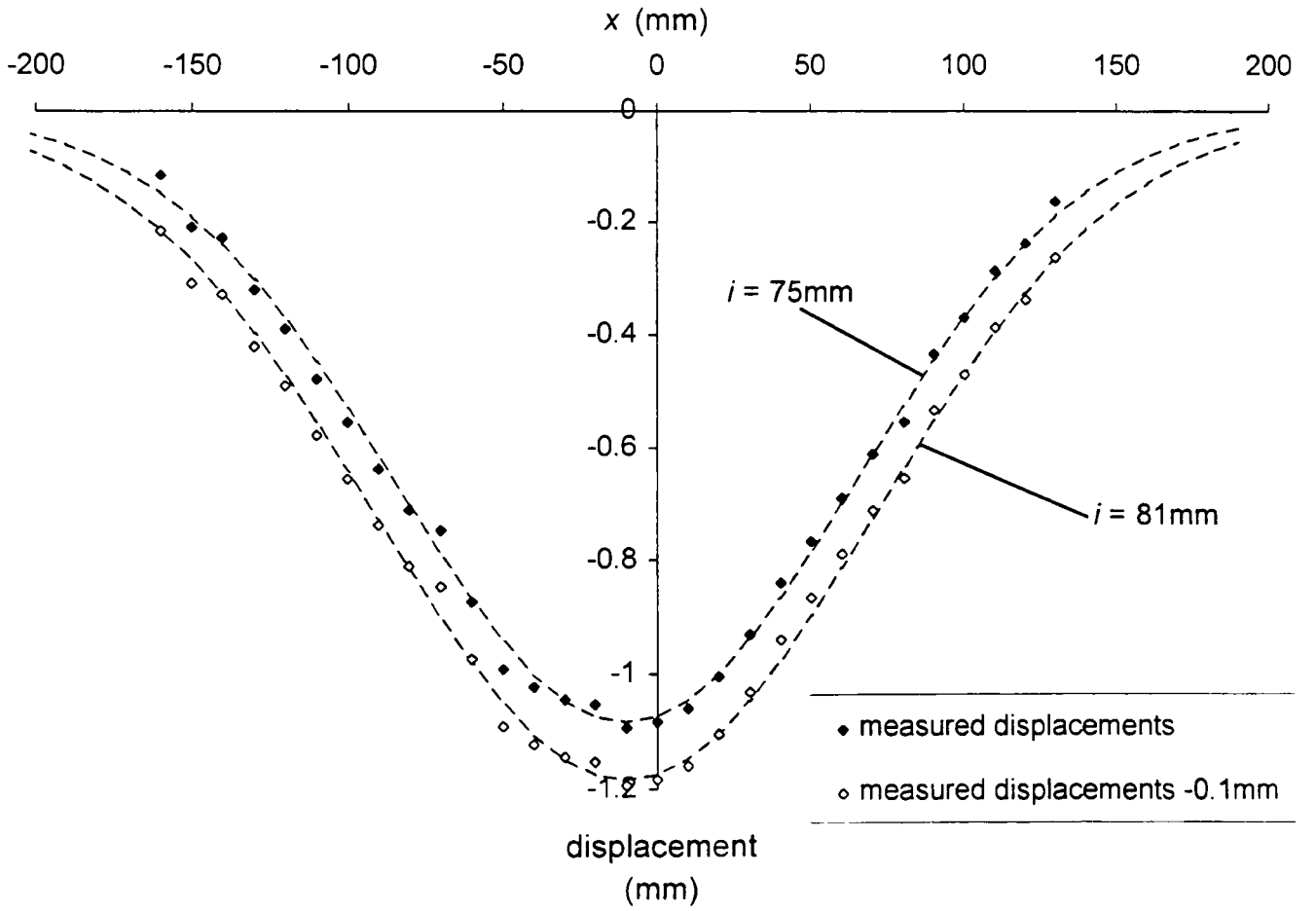

Figure 5.21 Data from image processing near the clay/sand interface with best fit Gaussian distribution compared to the same data -0.1mm displacement (centrifuge test RJG20, for original data V~10%)

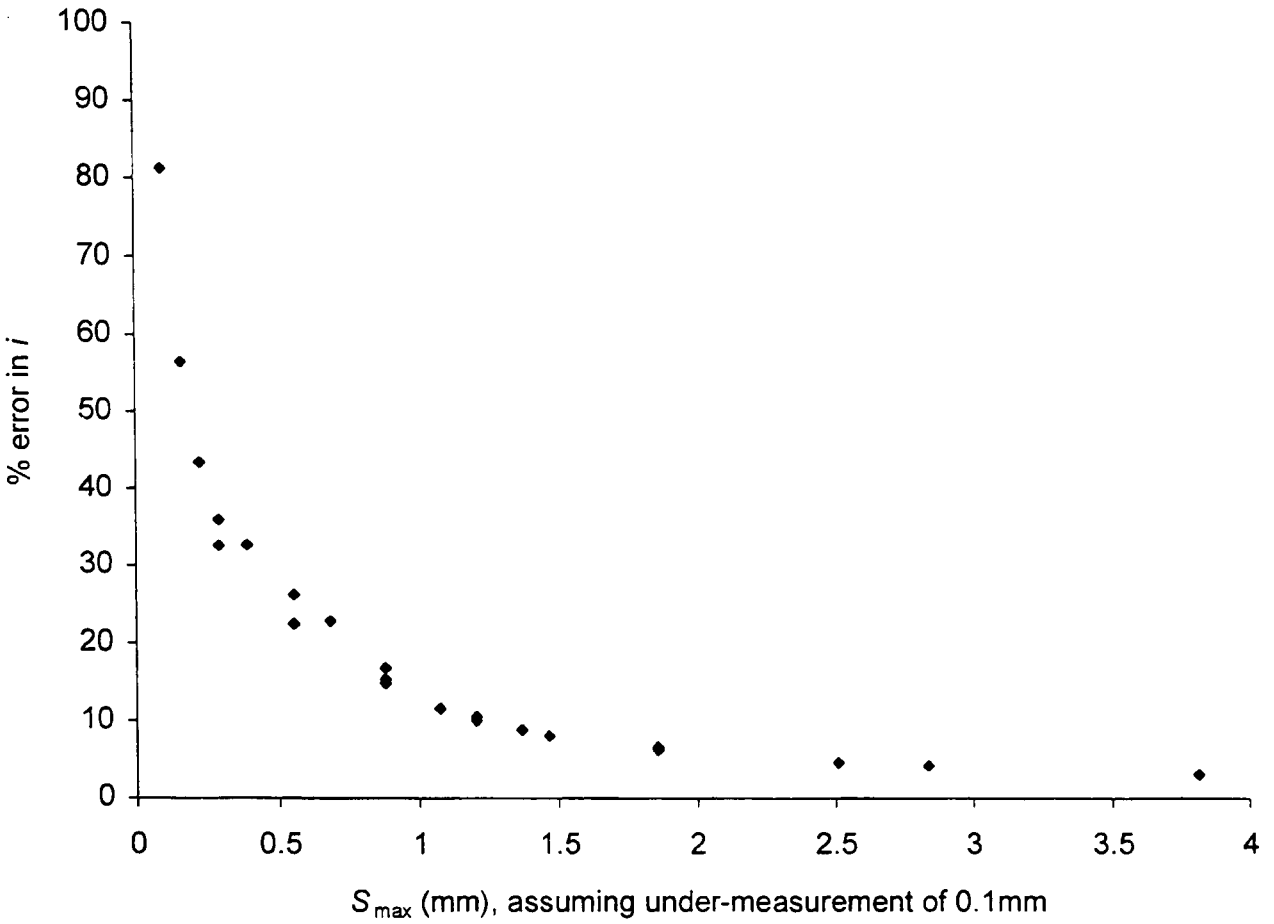

Figure 5.22 Percentage error in i value with increasing S_{max} if settlement under-measured by 0.1mm

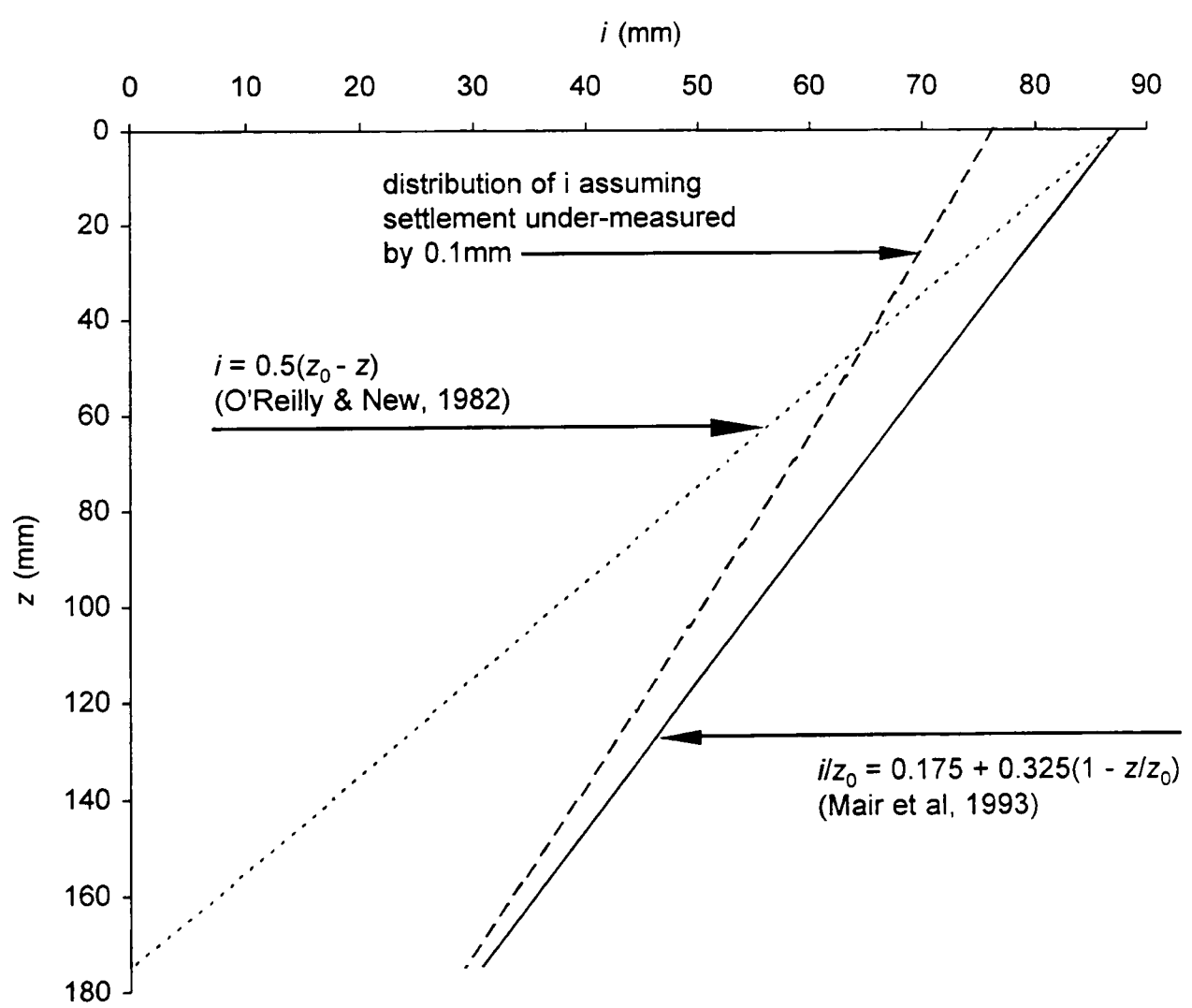

Figure 5.23 Effect on distribution of i with depth if settlement under-measured by 0.1mm, (V_l~10%) for a 3D cover clay test assuming i varies as suggested by Mair et al (1993)

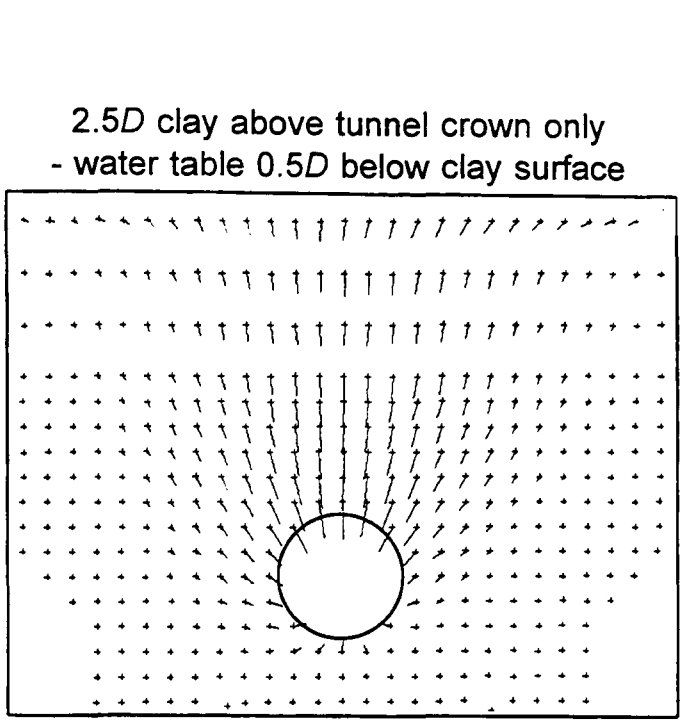

a) RJG17

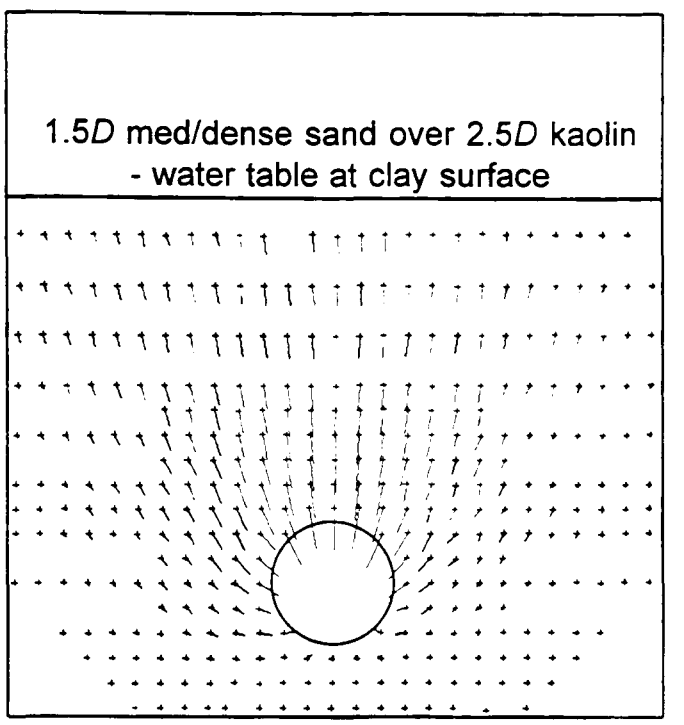

c) RJG19

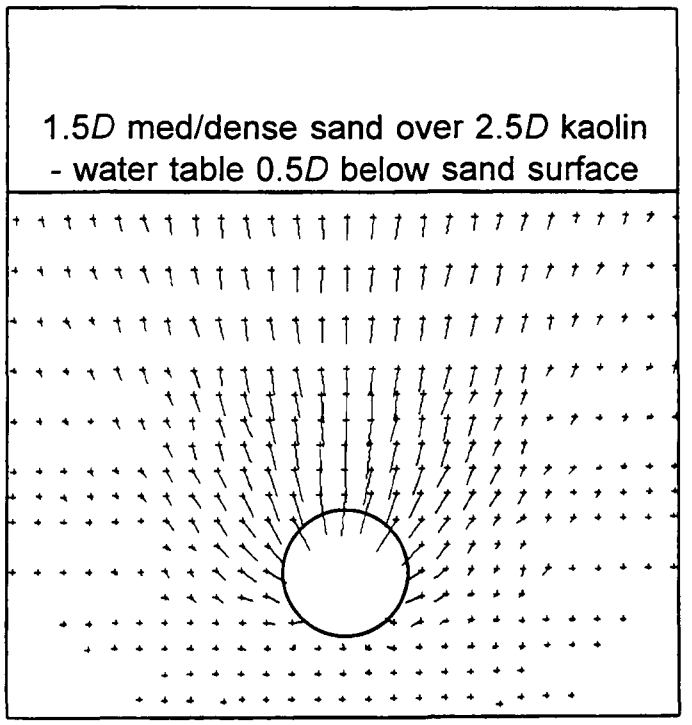

b) RJG18

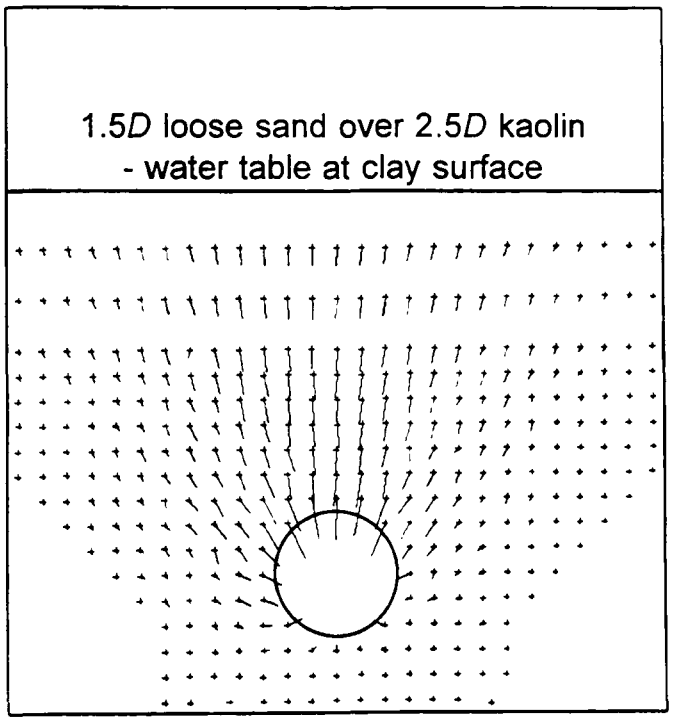

d) RJG20

Figure 5.24 Vectors of movement (x10) in the clay layer for centrifuge tests RJG17 to RJG20 when the movements immediately above the tunnel crown are ~1.7mm (sand 52/100 LBS)

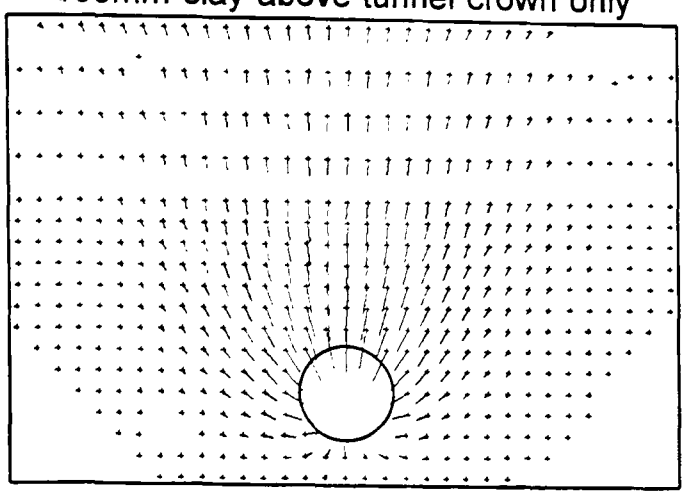

a) TH1

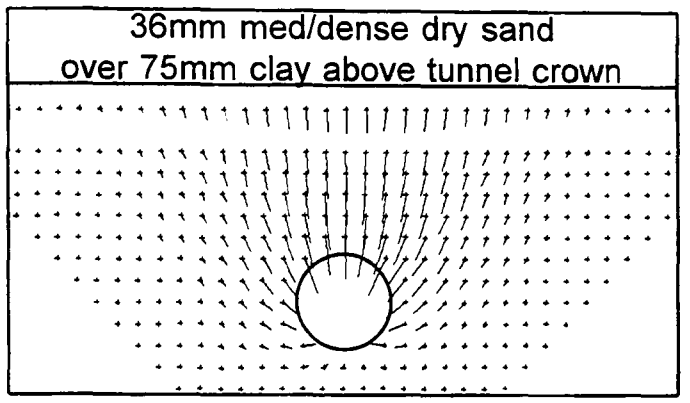

b) TH2

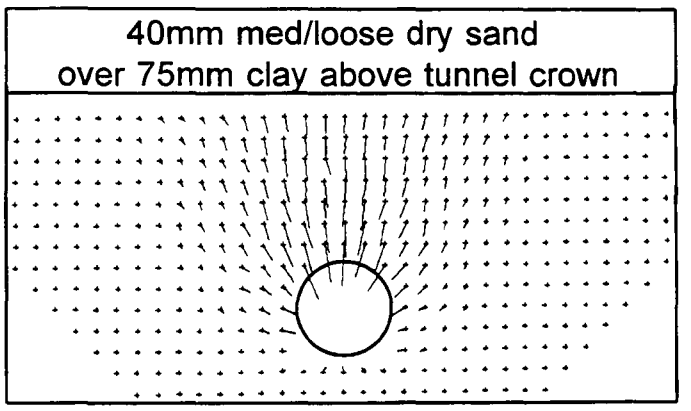

c) TH3

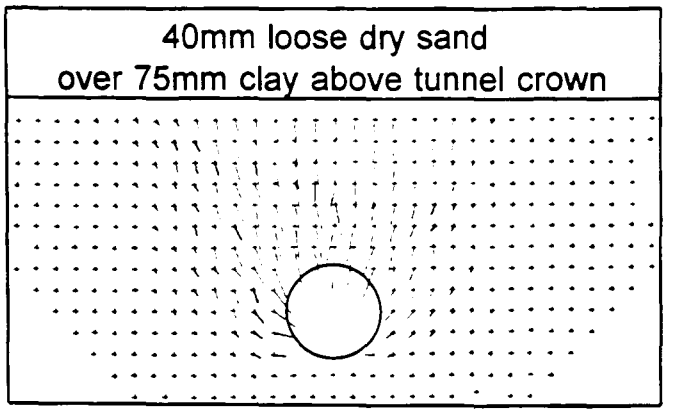

d) TH4

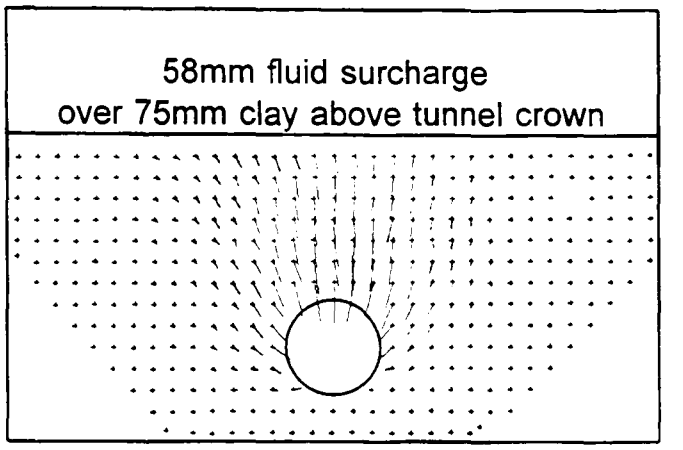

e) TH5

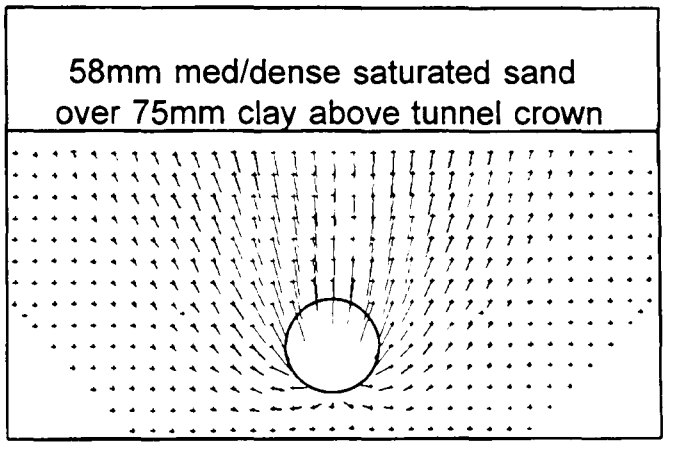

f) MC01

Figure 5.25 Vectors of movement (x10) in the clay layer for tests TH1 to 5 and MC01 when the movements immediately above the tunnel are ~2.0mm (sand 52/100 LBS, σ_v' in the clay layer was the same for each test)

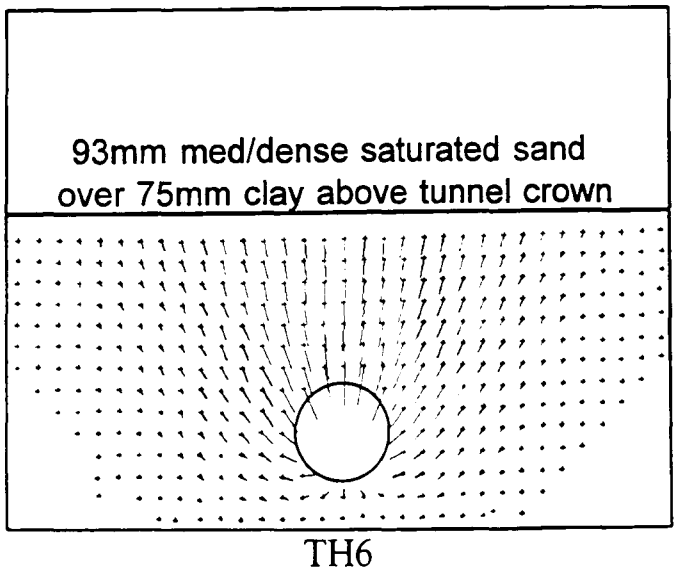

TH6

Figure 5.26 Vectors of movement (x10) in the clay layer for tests TH6 when the vertical movement immediately above the tunnel is ~2.0mm (sand 52/100 LBS)

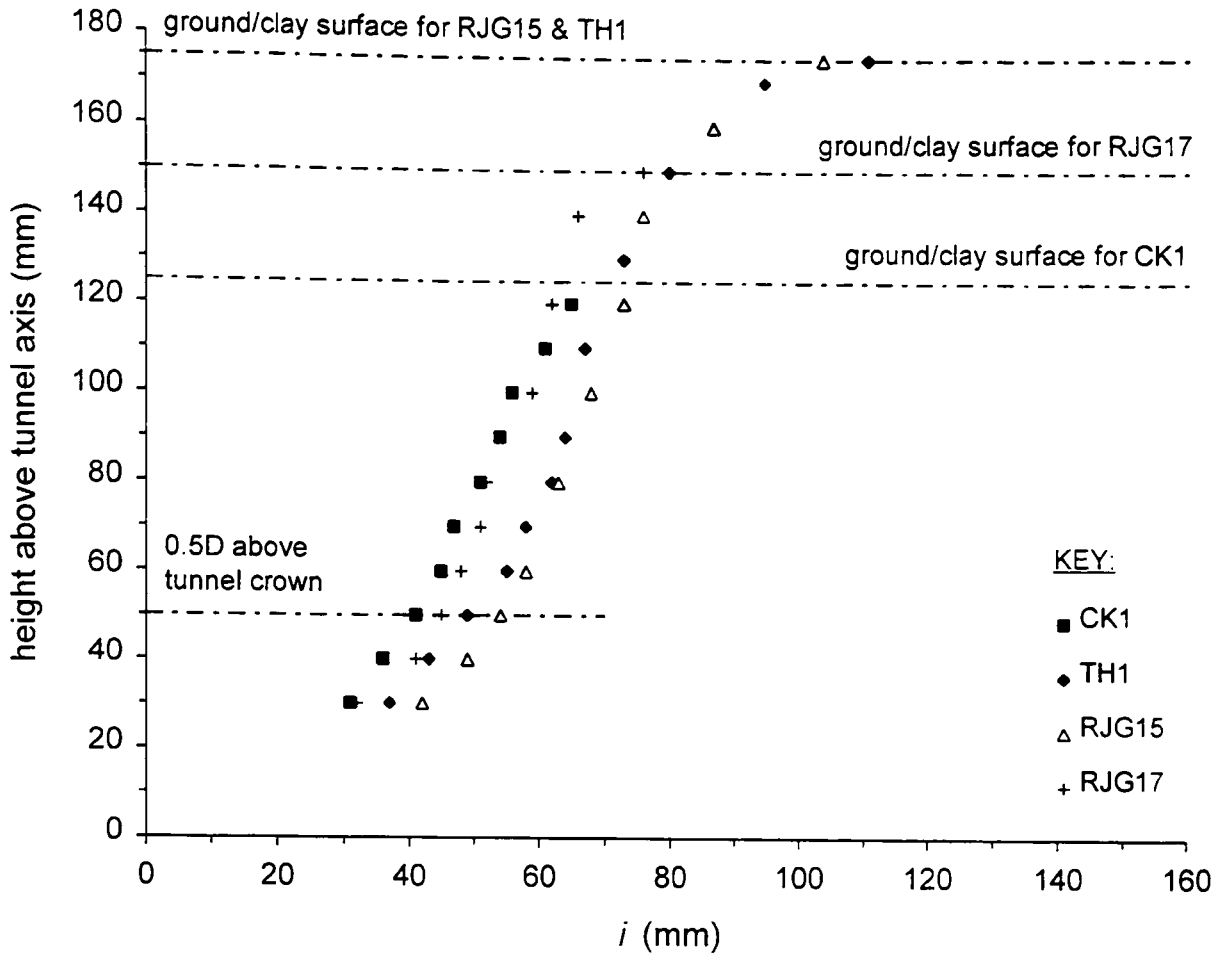

Figure 5.27 Distributions of i with depth for tests with clay only

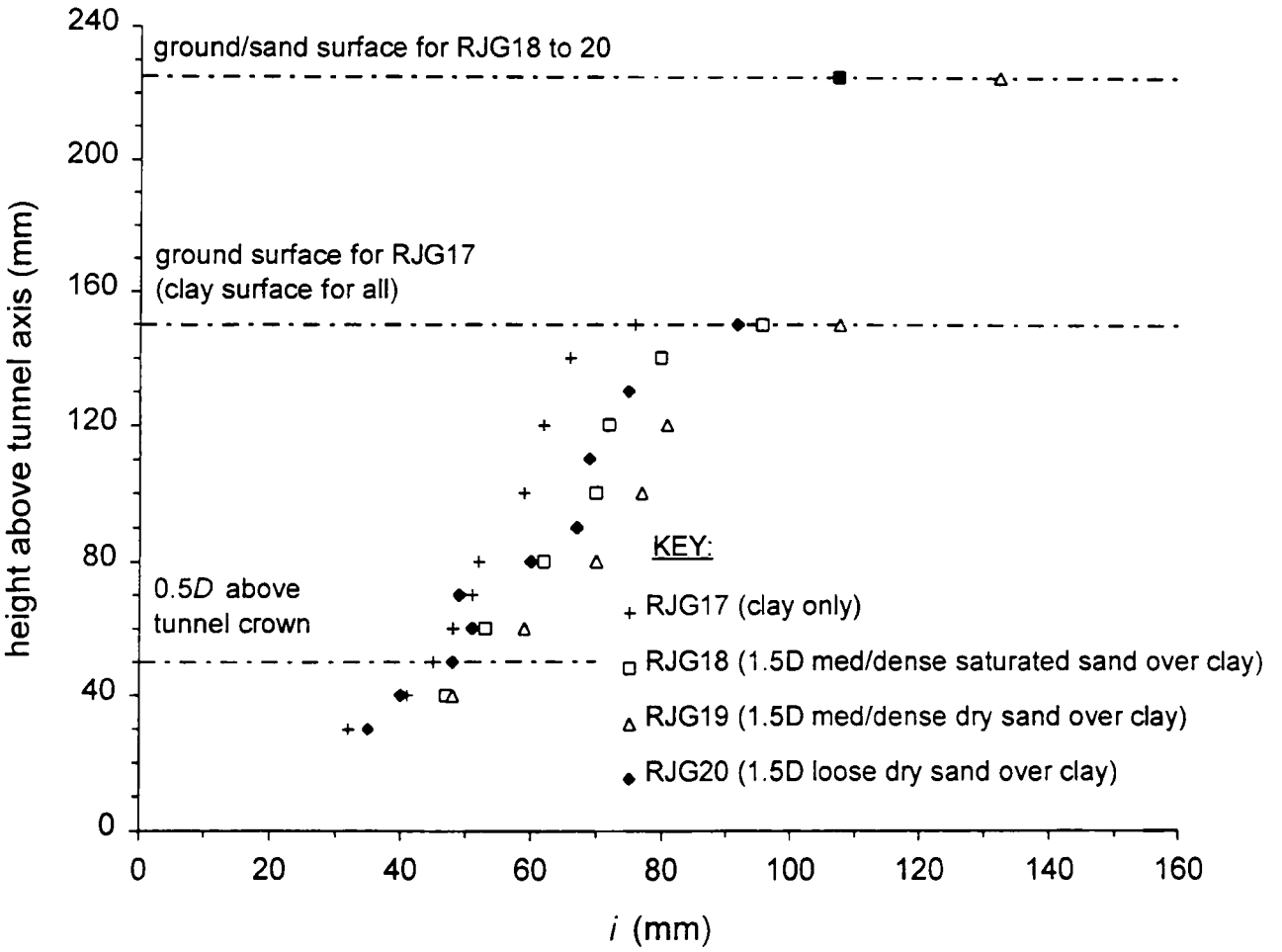

Figure 5.28 Distributions of i with depth for tests RJG17 to 20
(each having 2.5D clay over tunnel crown, sand 52/100 LBS)

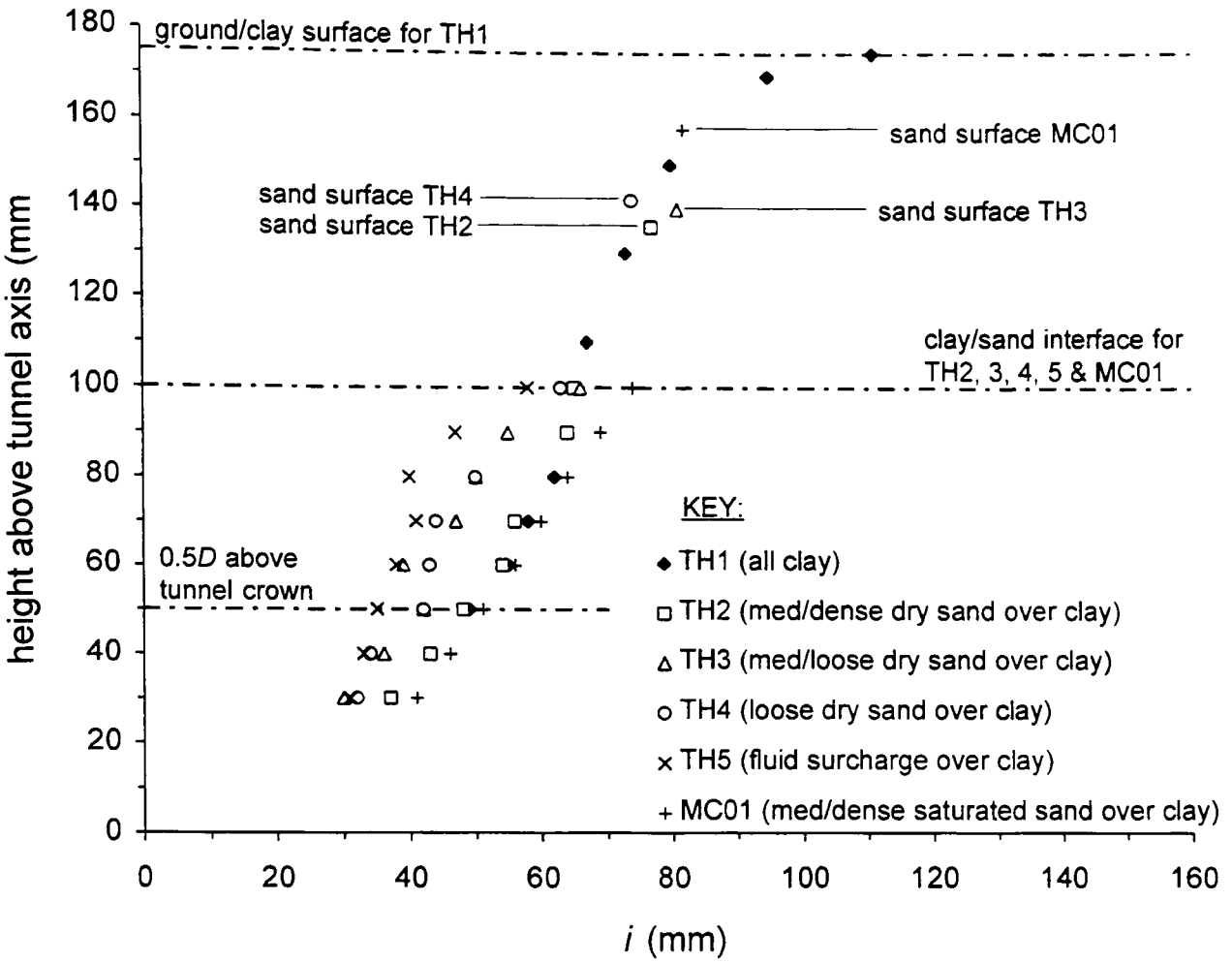

Figure 5.29 Distributions of i with depth for tests TH1 to 5 and MC01 (same σ_v' profile in lower clay layer up to 100mm above tunnel axis, sand 52/100 LBS)

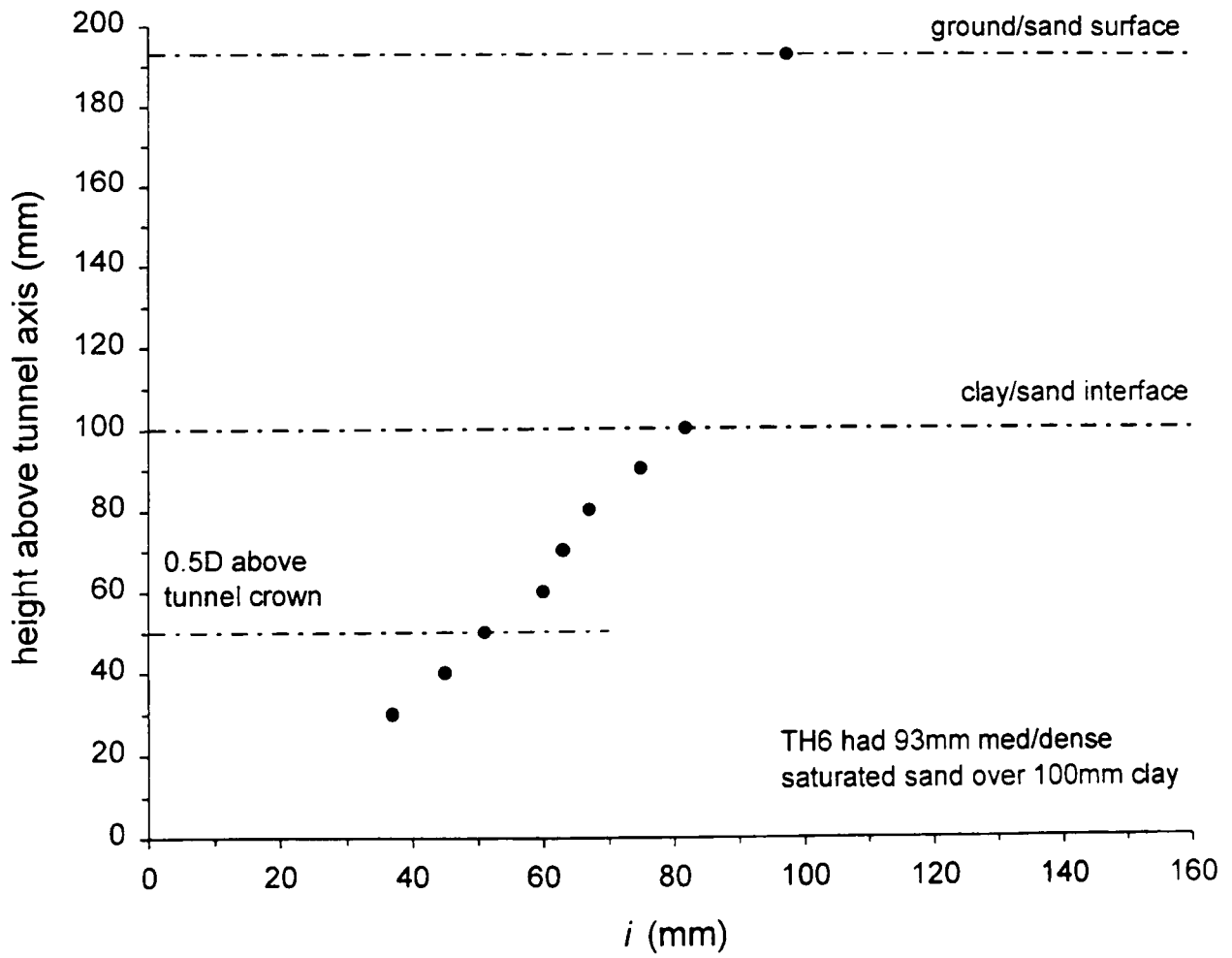

Figure 5.30 Distribution of i with depth for test TH6 (sand 52/100 LBS)

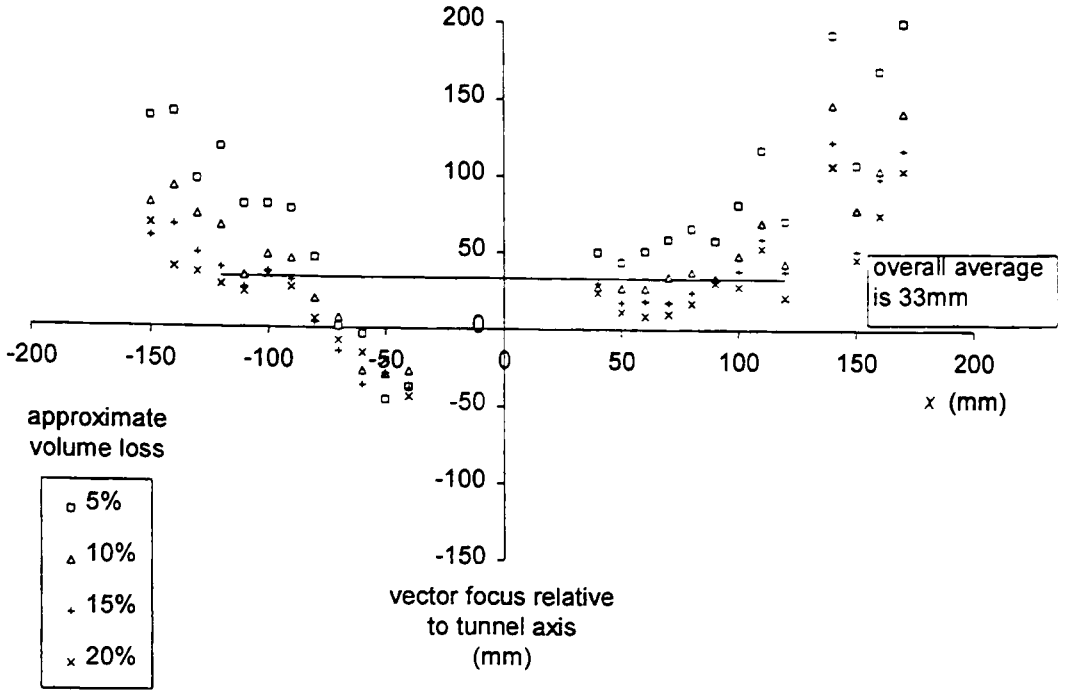

a) 140mm above tunnel axis (10mm from ground surface)

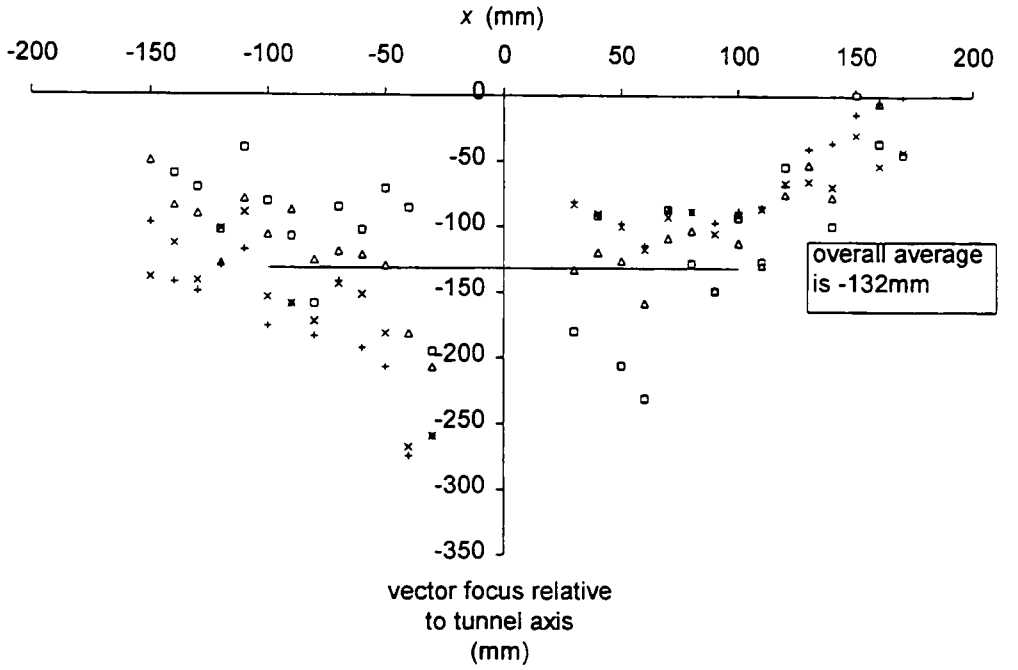

b) 120mm above tunnel axis (30mm from ground surface)

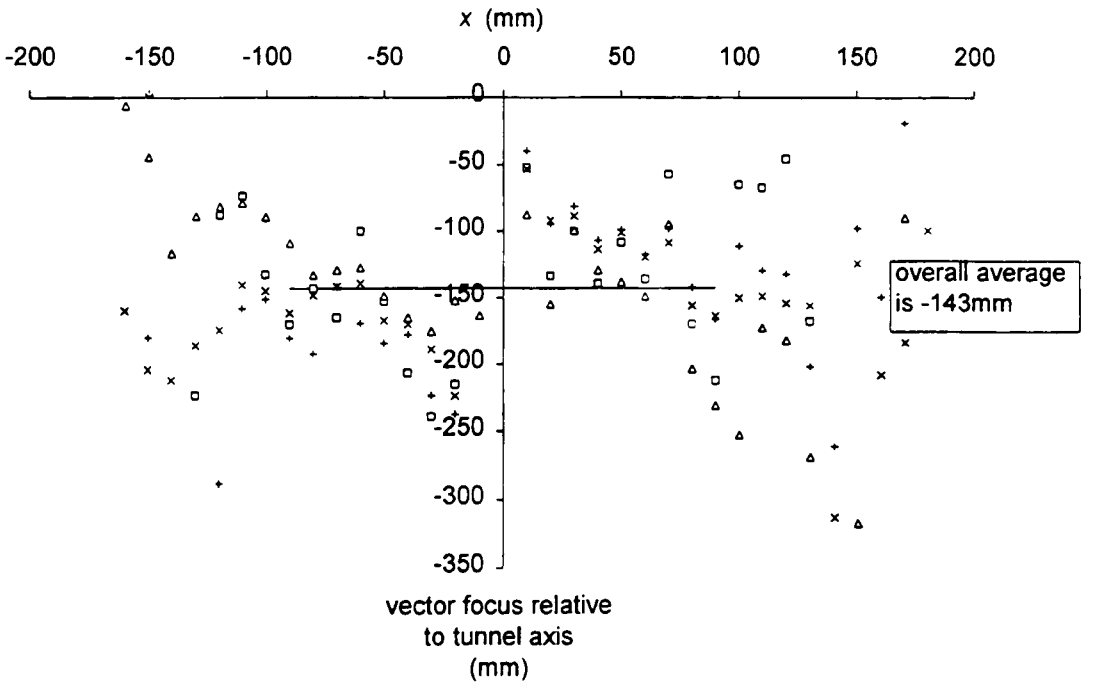

c) 80mm above tunnel axis

Figure 5.31 Focus of vectors of movement at different subsurface levels for centrifuge test RJG17 (2.5*D* kaolin clay only)

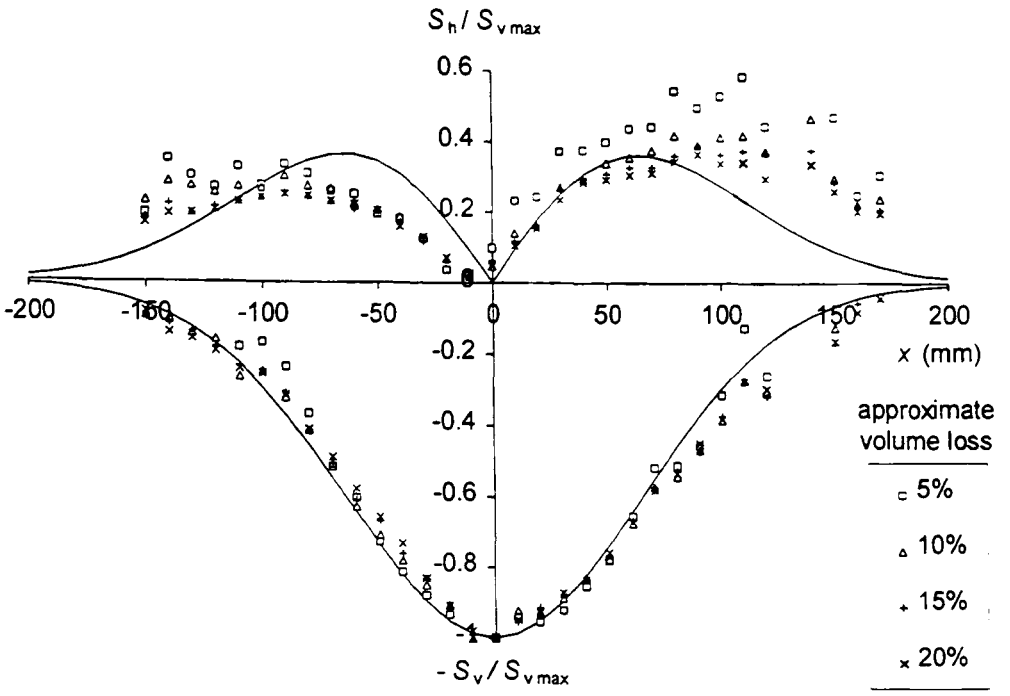

a) 140mm above tunnel axis (10mm from ground surface)

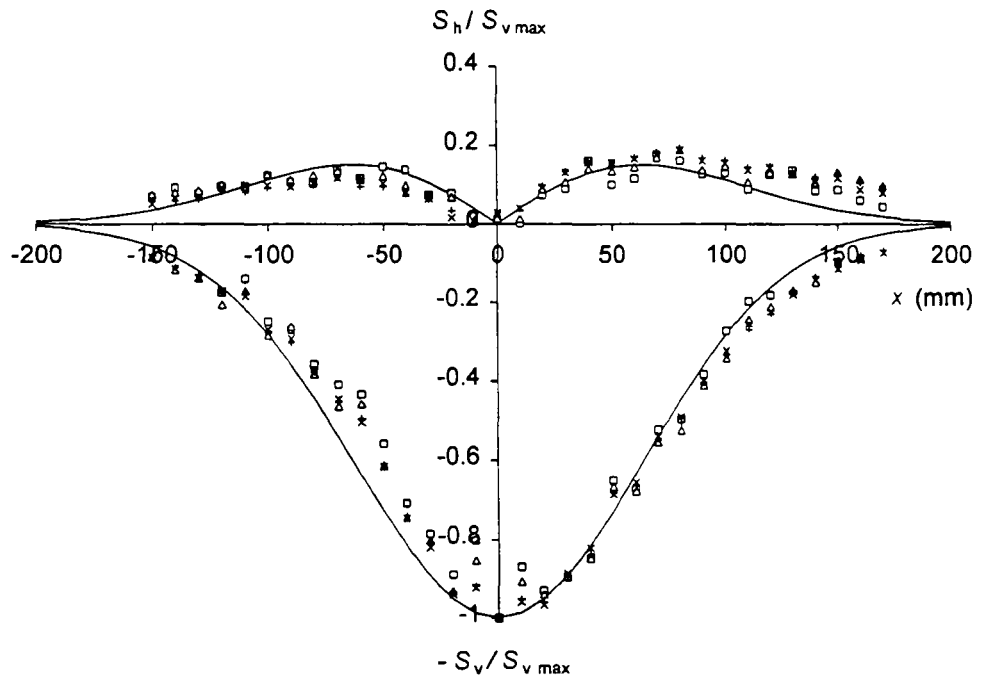

b) 120mm above tunnel axis (30mm from ground surface)

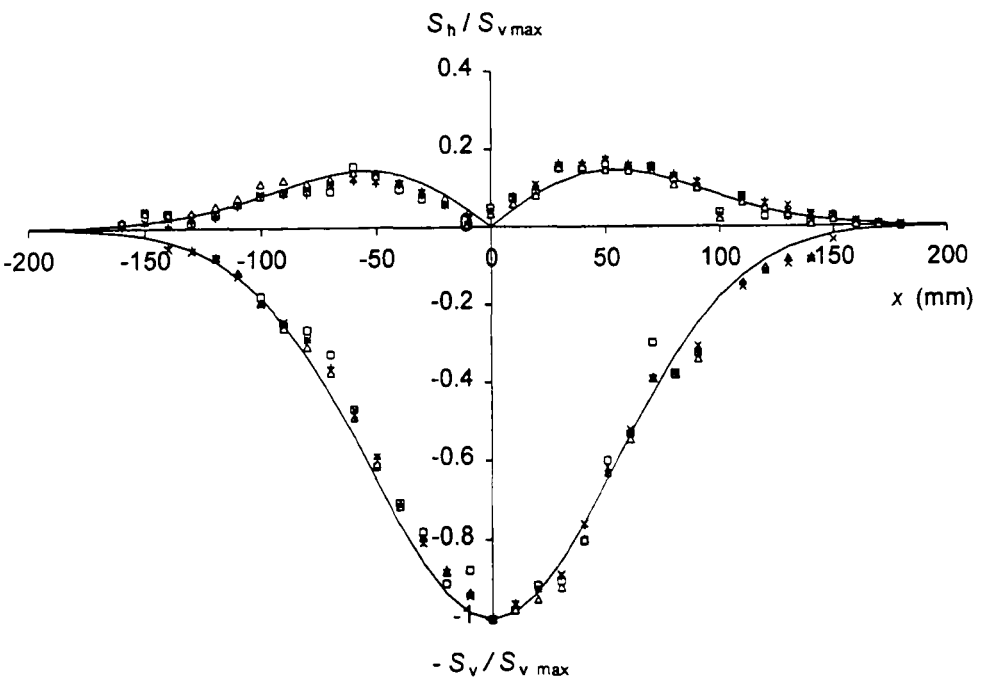

c) 80mm above tunnel axis

Figure 5.32 Vertical and horizontal movement at different subsurface levels for centrifuge test RJG17 (2.5*D* kaolin clay only)

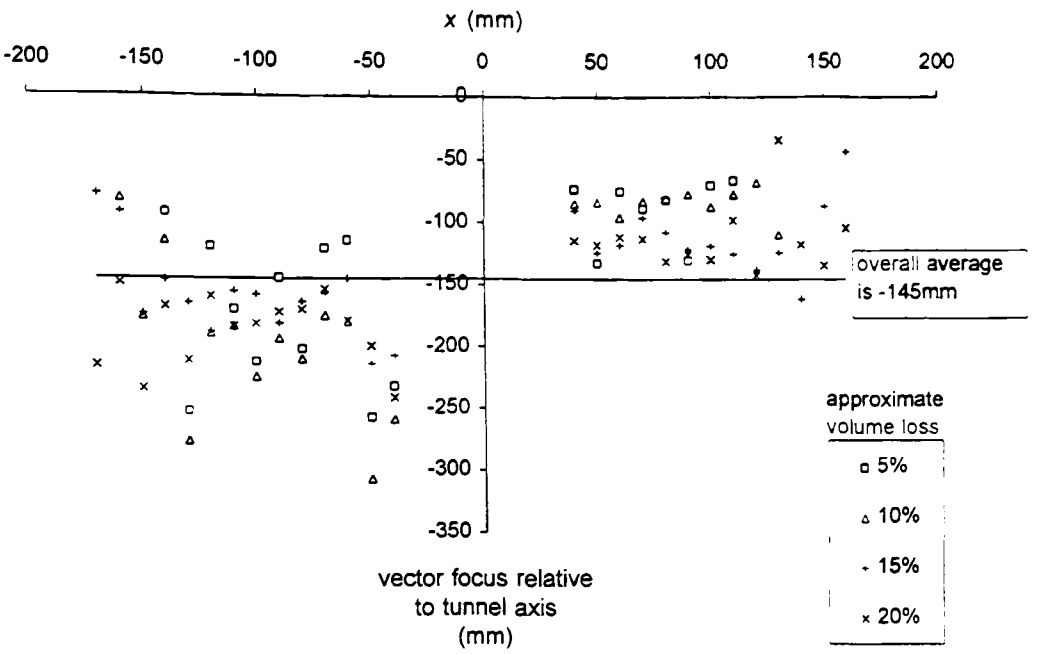

a) 130mm above tunnel axis

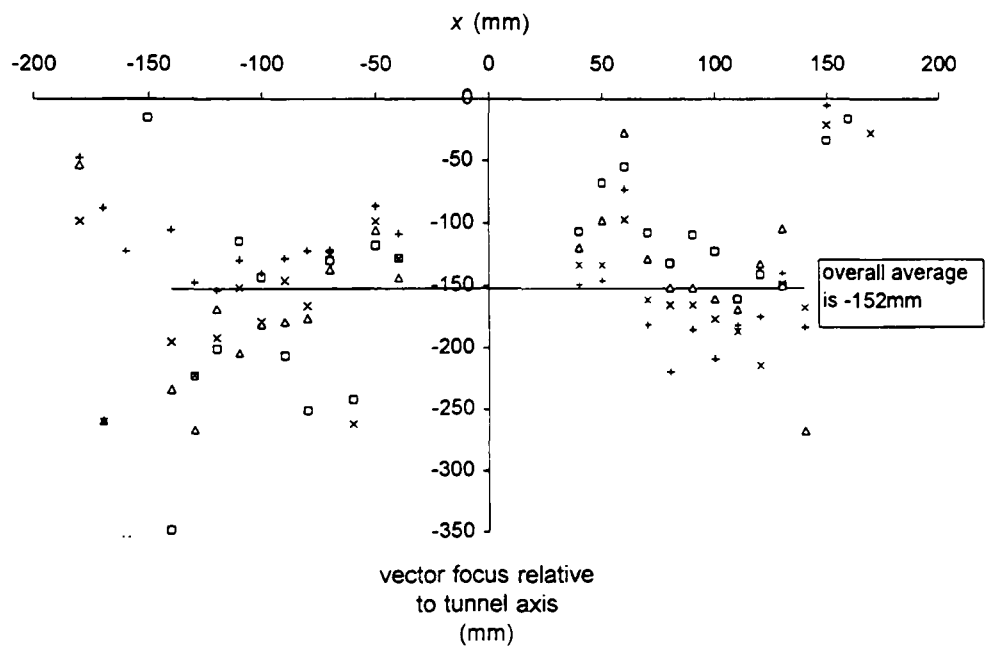

b) 90mm above tunnel axis

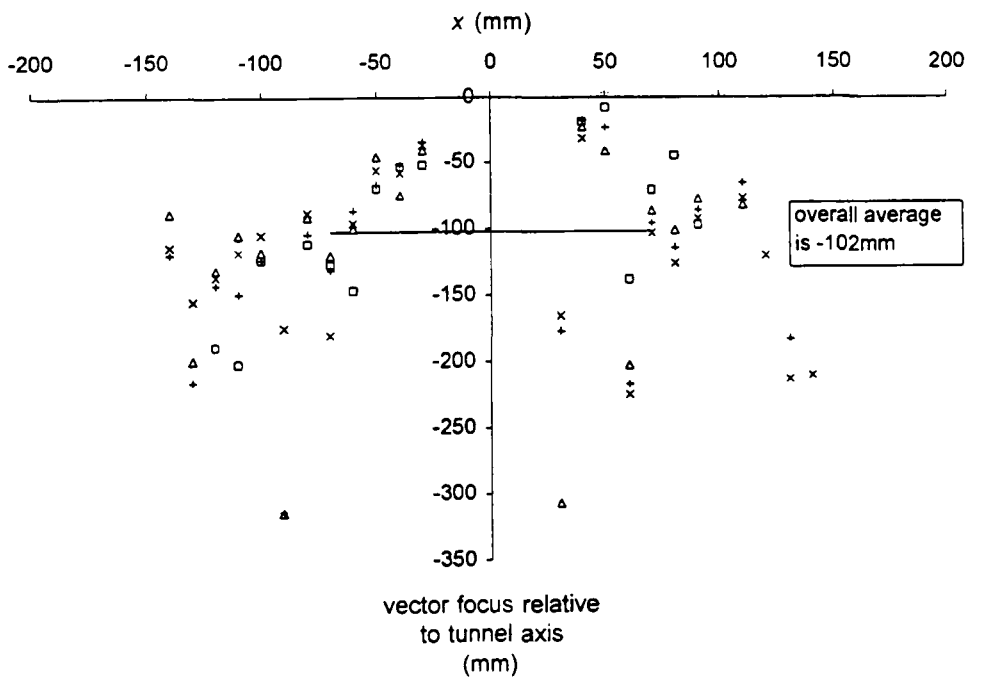

c) 50mm above tunnel axis
(0.5*D* from crown)

Figure 5.33 Focus of vectors of movement at different subsurface levels in the clay for centrifuge test RJG20 (1.5*D* dry loose sand over 2.5*D* kaolin clay)

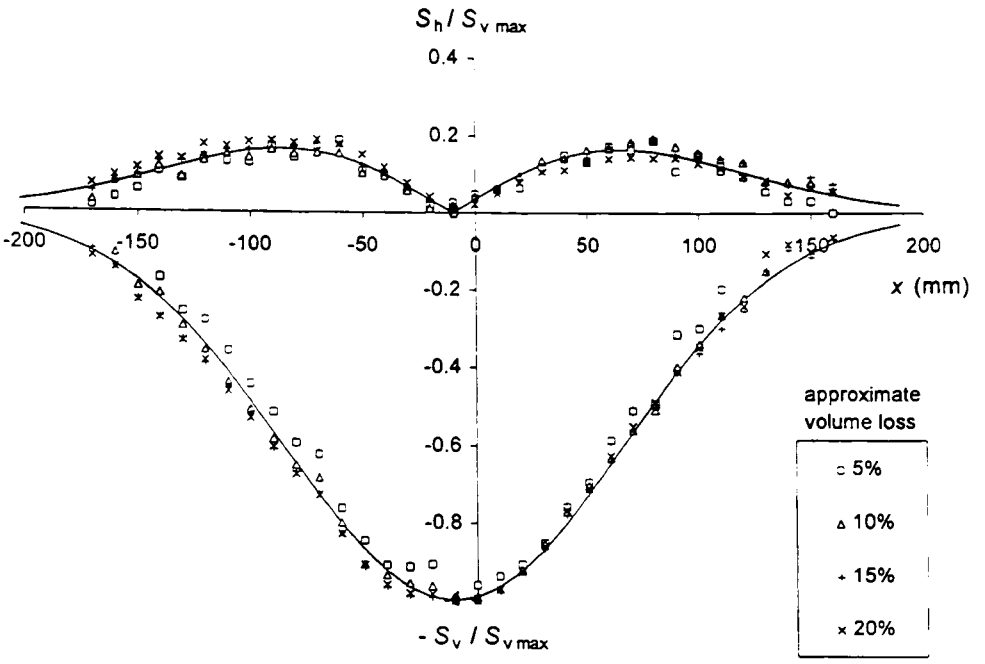

a) 130mm above tunnel axis

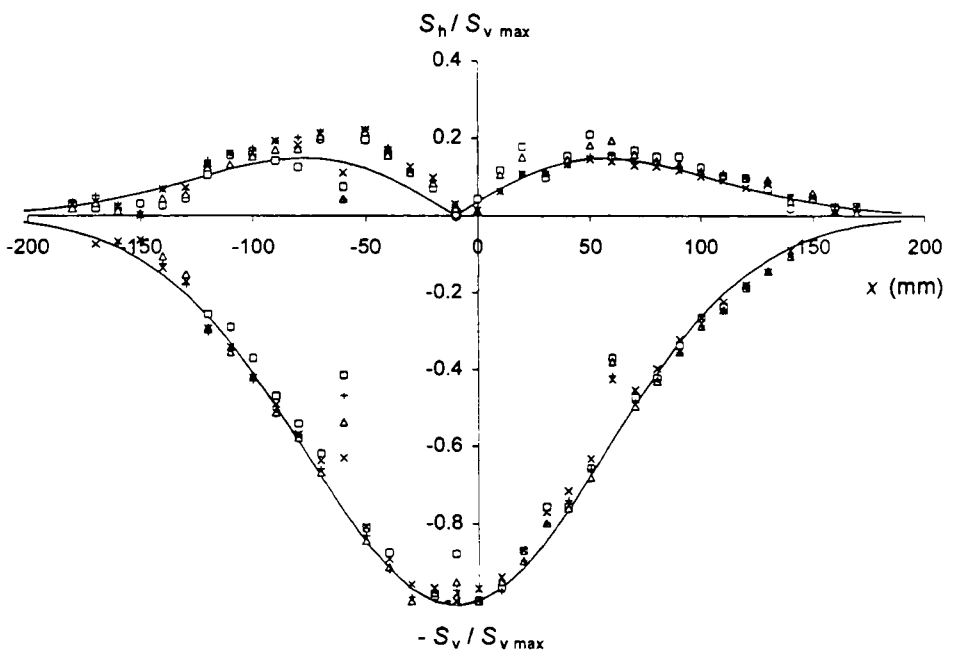

b) 90mm above tunnel axis

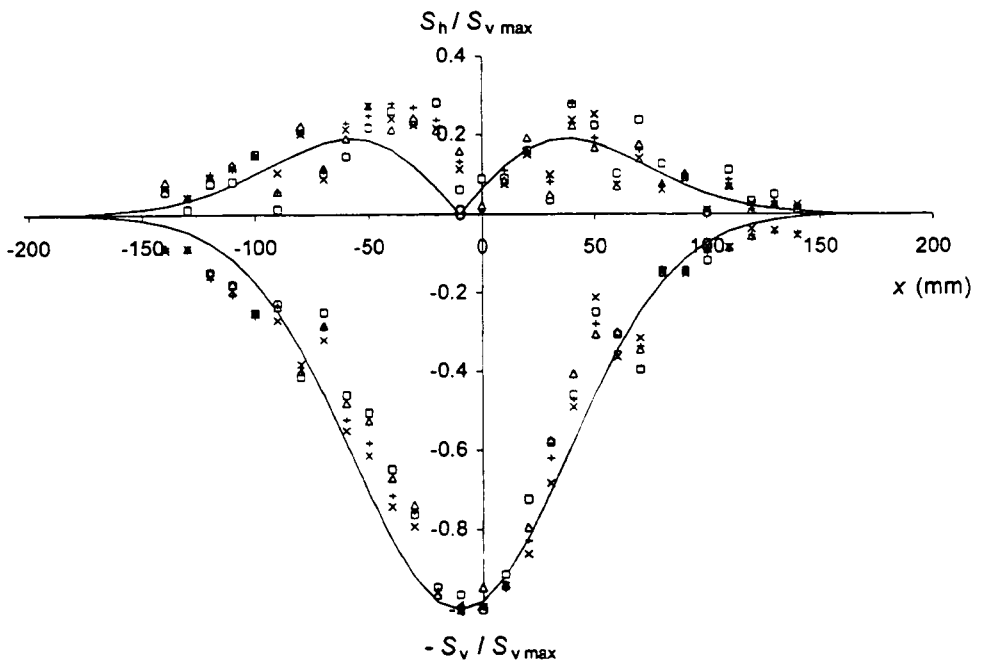

c) 50mm above tunnel axis
(0.5*D* from crown)

Figure 5.34 Vertical and horizontal movement at different subsurface levels in the clay for centrifuge test RJG20 (1.5*D* dry loose sand over 2.5*D* kaolin clay)

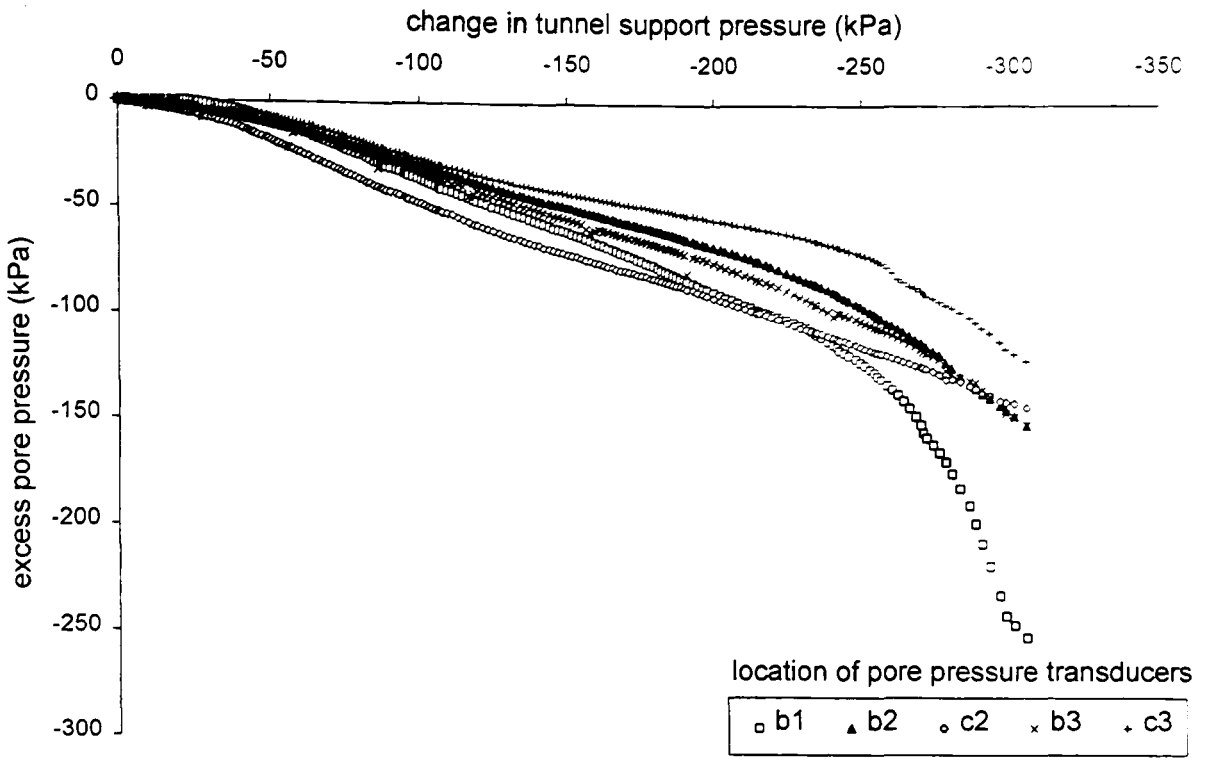

Figure 5.35 Excess pore pressures near the tunnel due to change in tunnel support pressure in centrifuge test RJG15 (only 3*D* clay above the tunnel crown only)

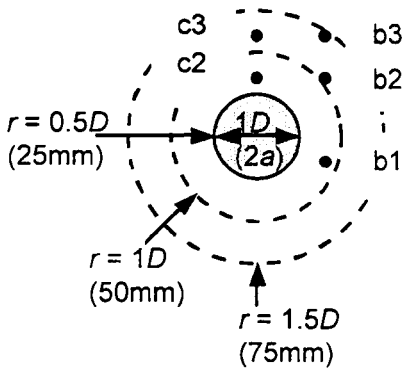

ppt	radius (r)	ppt	radius (r)
b1	42.7mm	c2	35.0mm
b2	53.2mm	c3	60.0mm
b3	72.1mm		

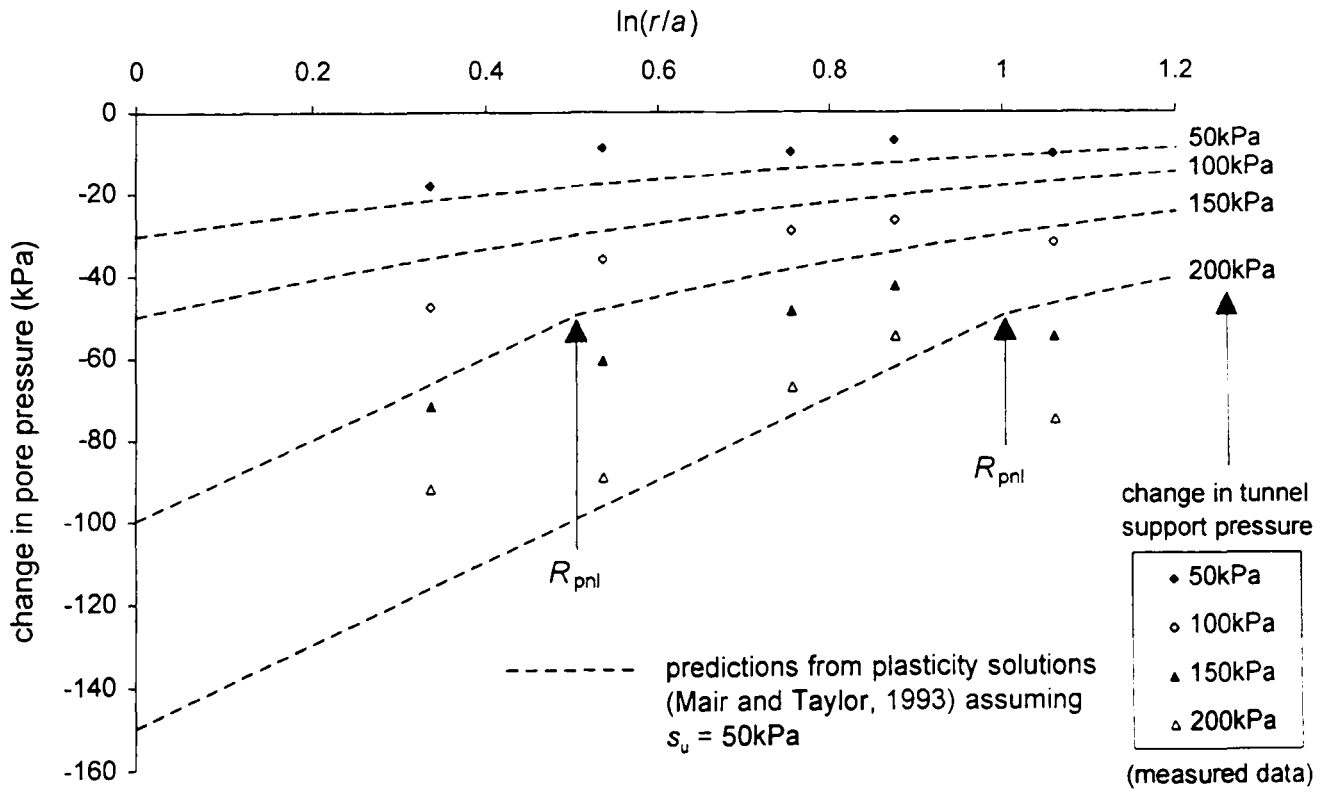

Figure 5.36 Comparison of excess pore pressures around the tunnel in centrifuge test RJG15 with plasticity solutions presented by Mair and Taylor (1993)

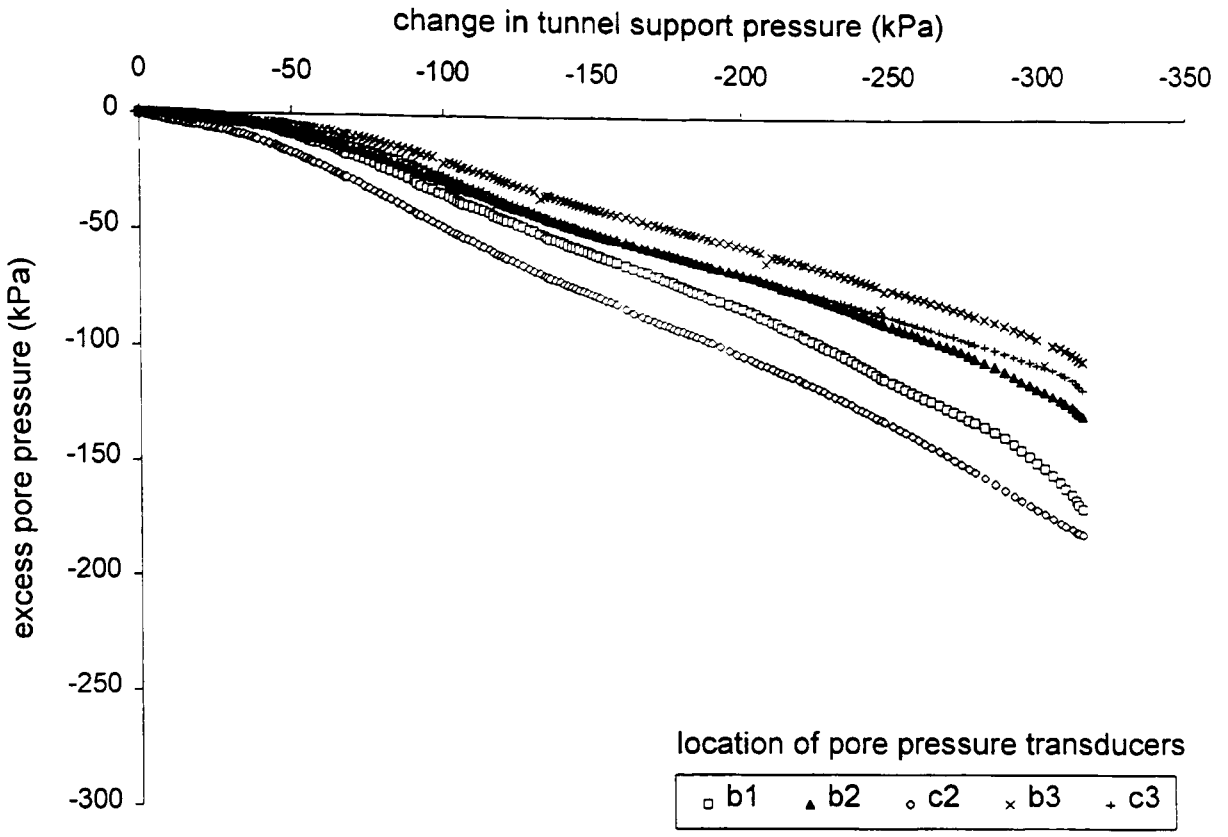

Figure 5.37 Excess pore pressures near the tunnel due to change in tunnel support pressure in centrifuge test RJG16 (1.5*D* sand over 1.5*D* clay above the tunnel crown)

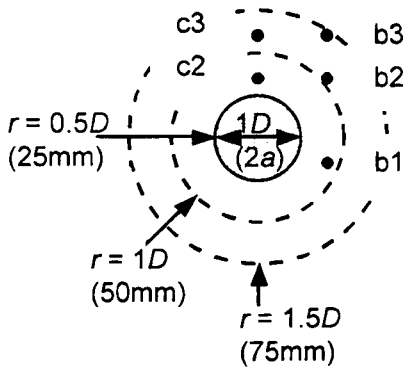

ppt	radius (r)	ppt	radius (r)
b1	42.7mm	c2	35.0mm
b2	53.2mm	c3	60.0mm
b3	72.1mm		

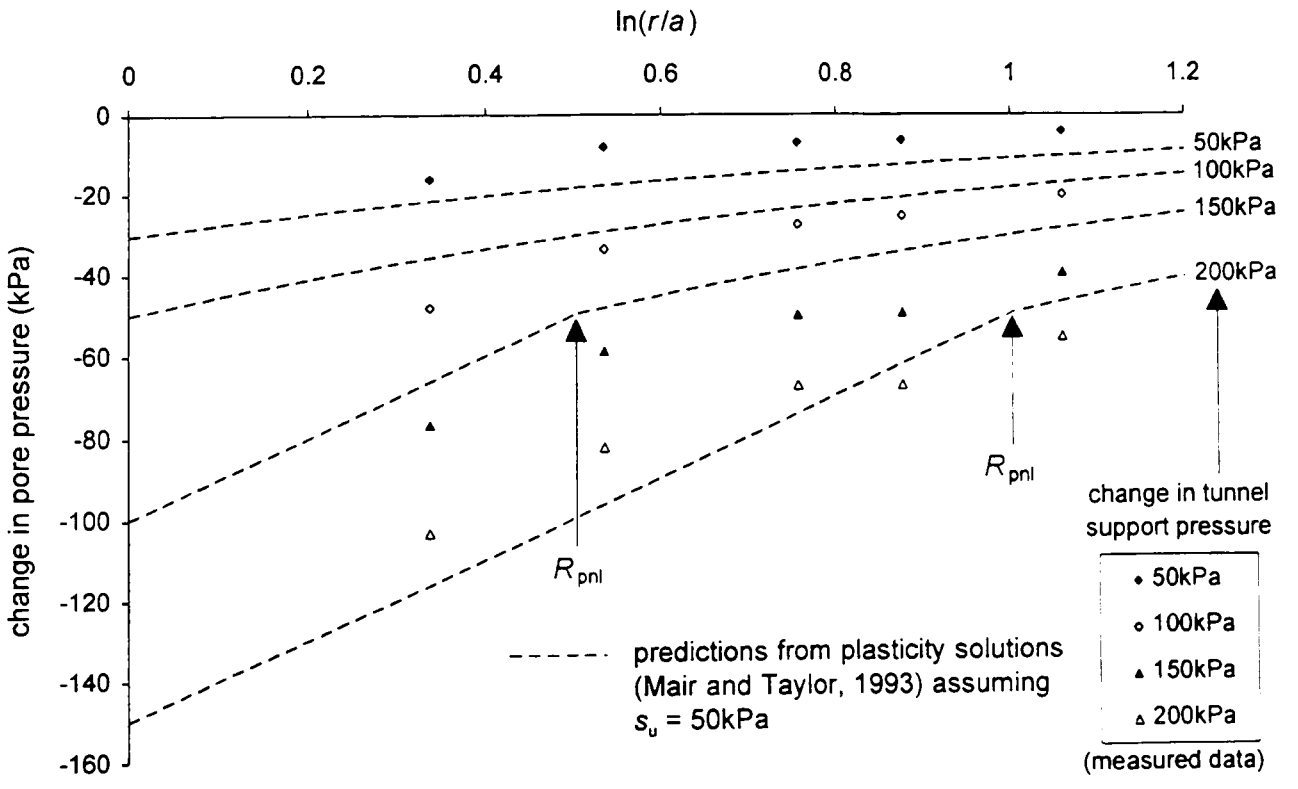

Figure 5.38 Comparison of excess pore pressures around the tunnel in centrifuge test RJG16 with plasticity solutions presented by Mair and Taylor (1993)

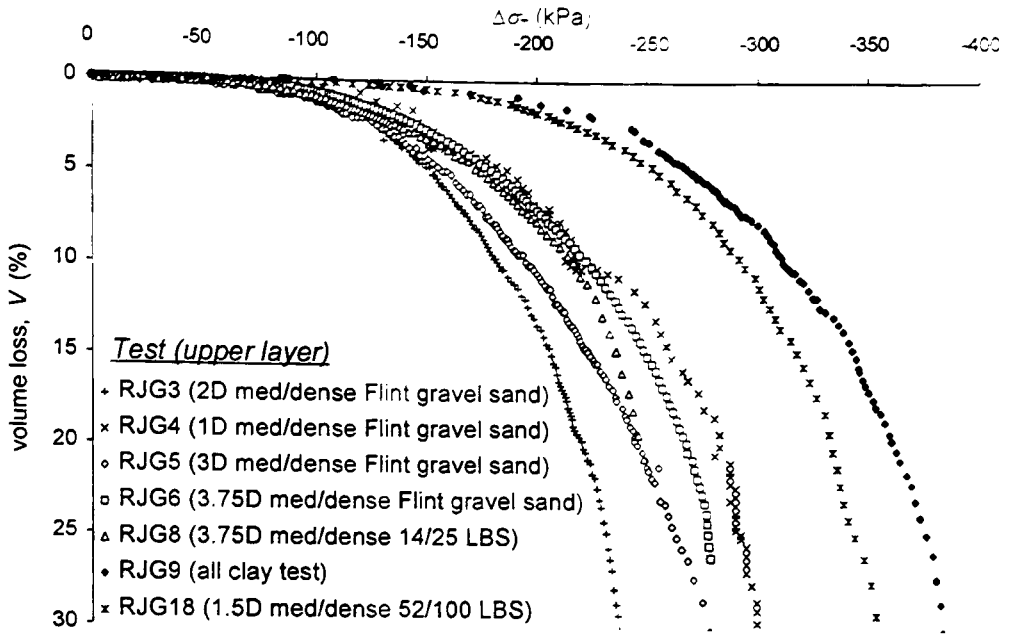

a) RJG3, 4, 5, 6, 8, 9 & 18
(total cover 4*D*, water table near ground surface)

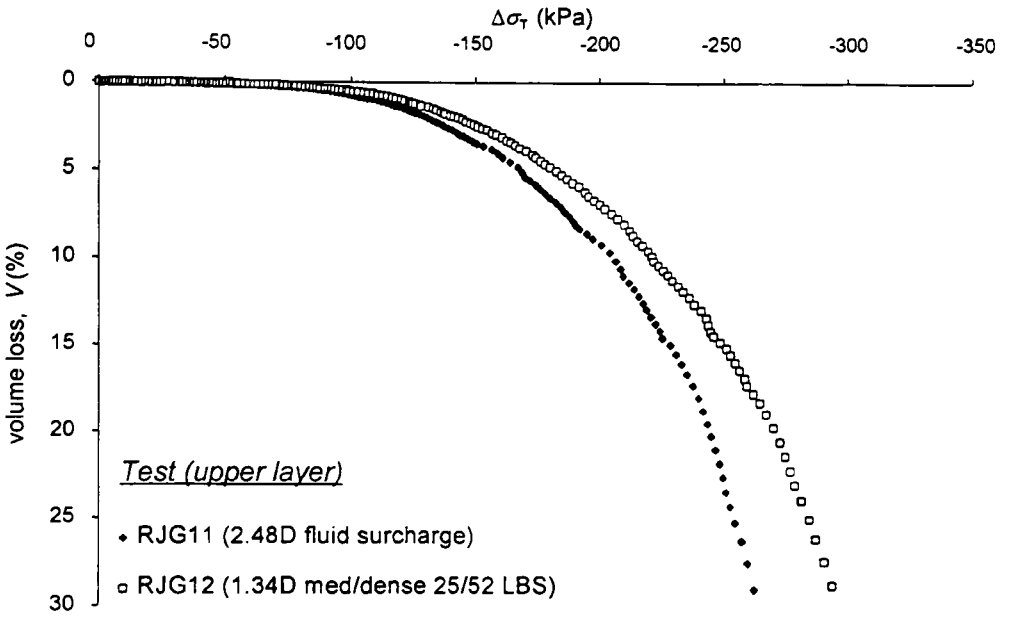

b) RJG11 & 12
(water surcharge equivalent to sand overburden, water table near ground surface)

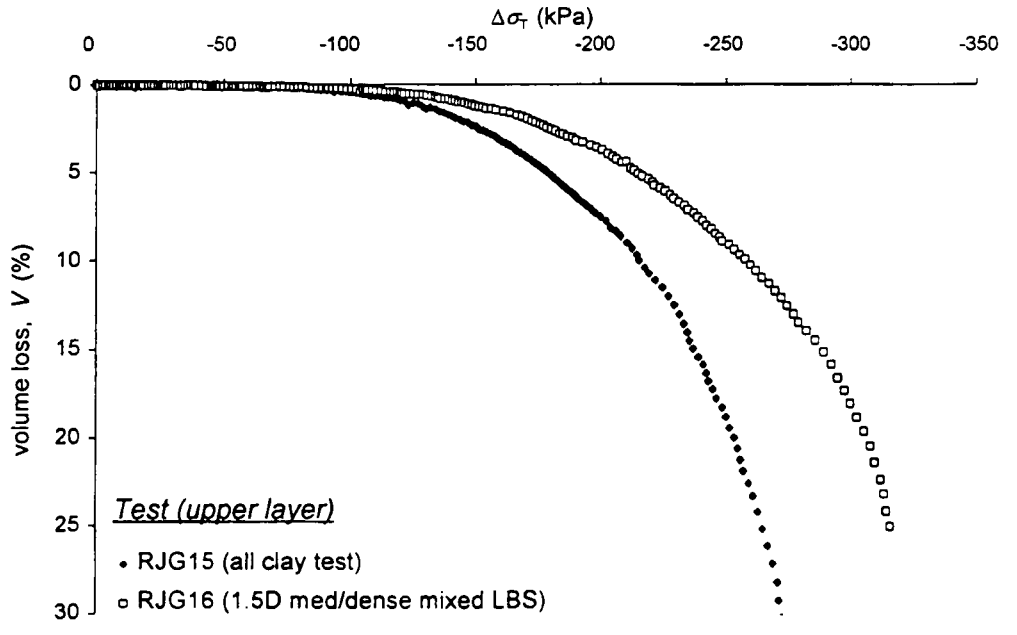

c) RJG15 & 16
(total cover 3*D*, water table near ground surface)

Figure 5.39 Volume loss against change in tunnel support pressure, in groups of tests with similar vertical effective stresses near the tunnel

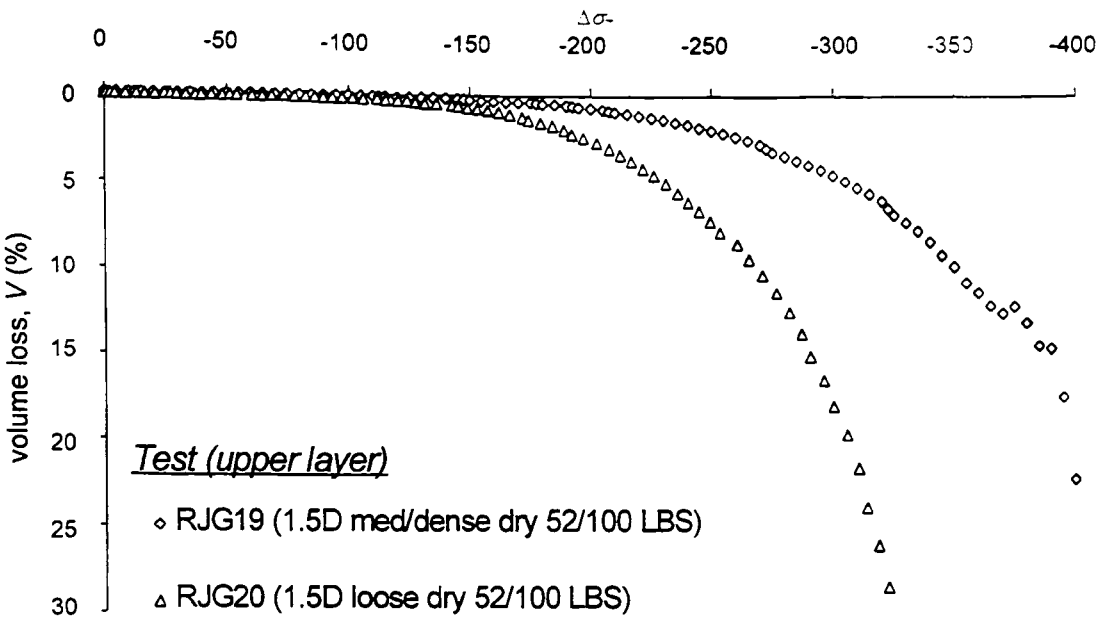

d) RJG19 & 20
(total cover 4*D*, dry sand)

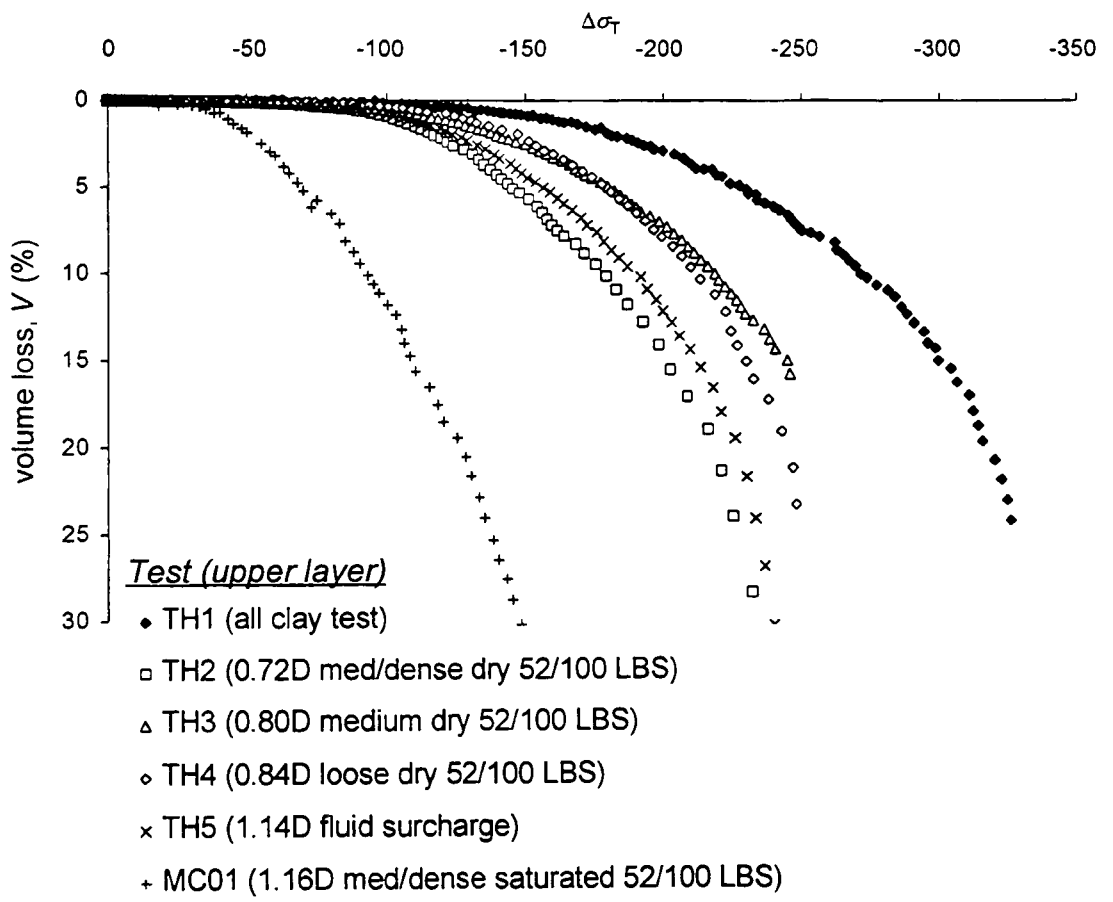

e) TH1 to 5 & MC01
(effective stress in the clay the same by design)

Figure 5.39 (cont'd) Volume loss against change in tunnel support pressure, in groups of tests with similar vertical effective stresses near the tunnel

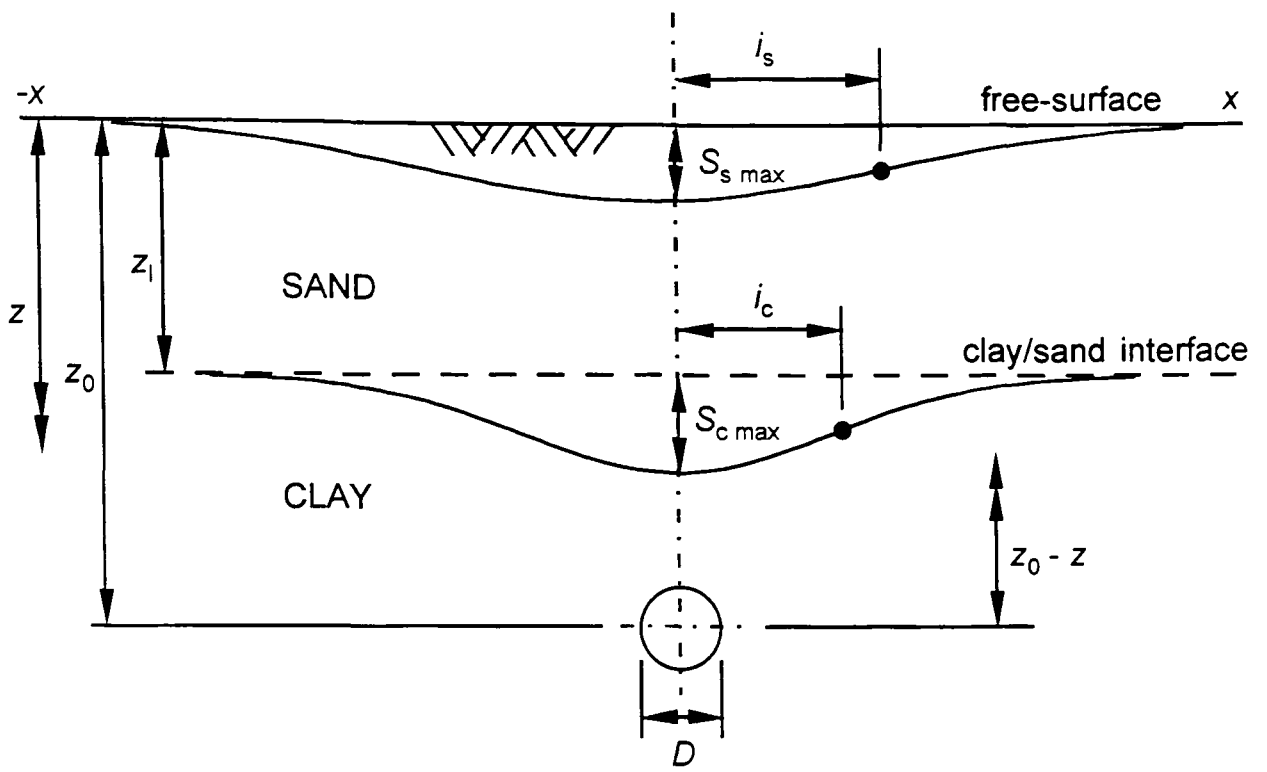

Figure 6.1 Terms defining geometry for ground movements around tunnels in two-layer ground conditions

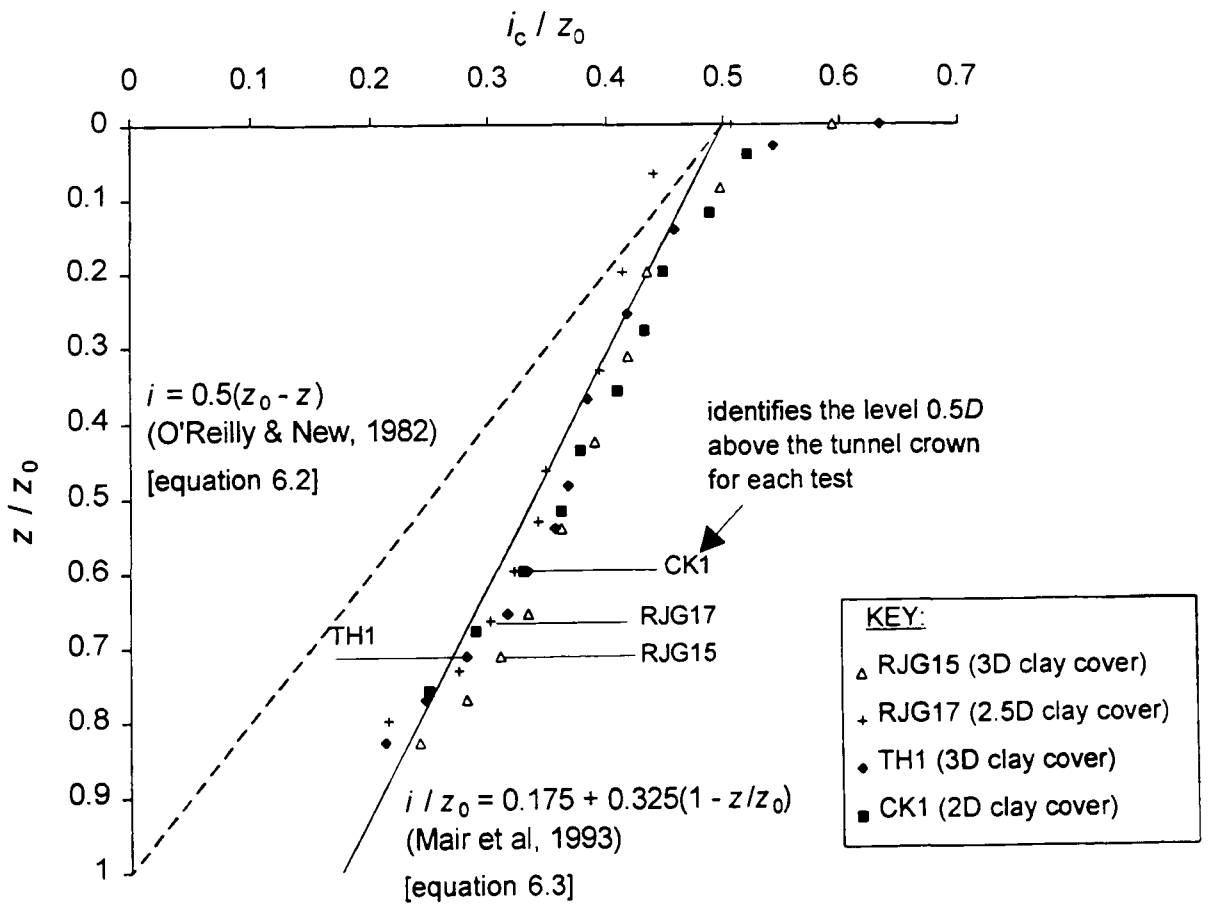

Figure 6.2 i_c / z_0 against z / z_0 for all-clay tests
(determined from LVDT and image processing measurements)

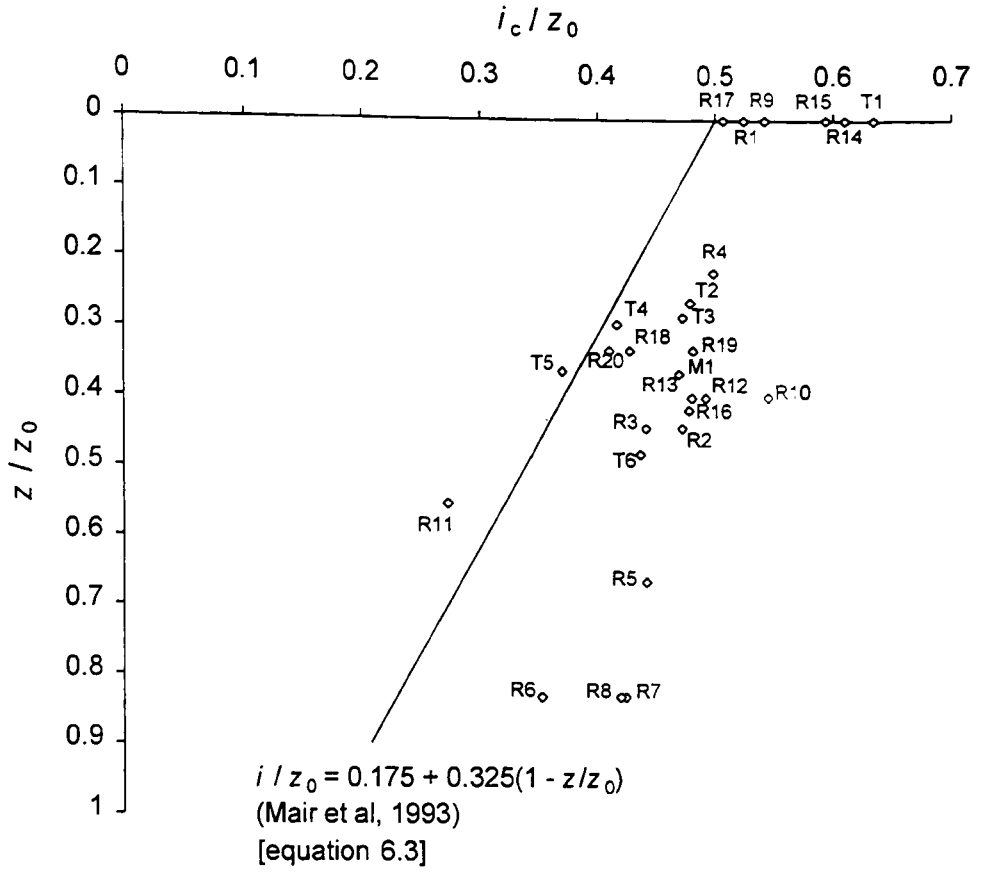

a) labelled by test

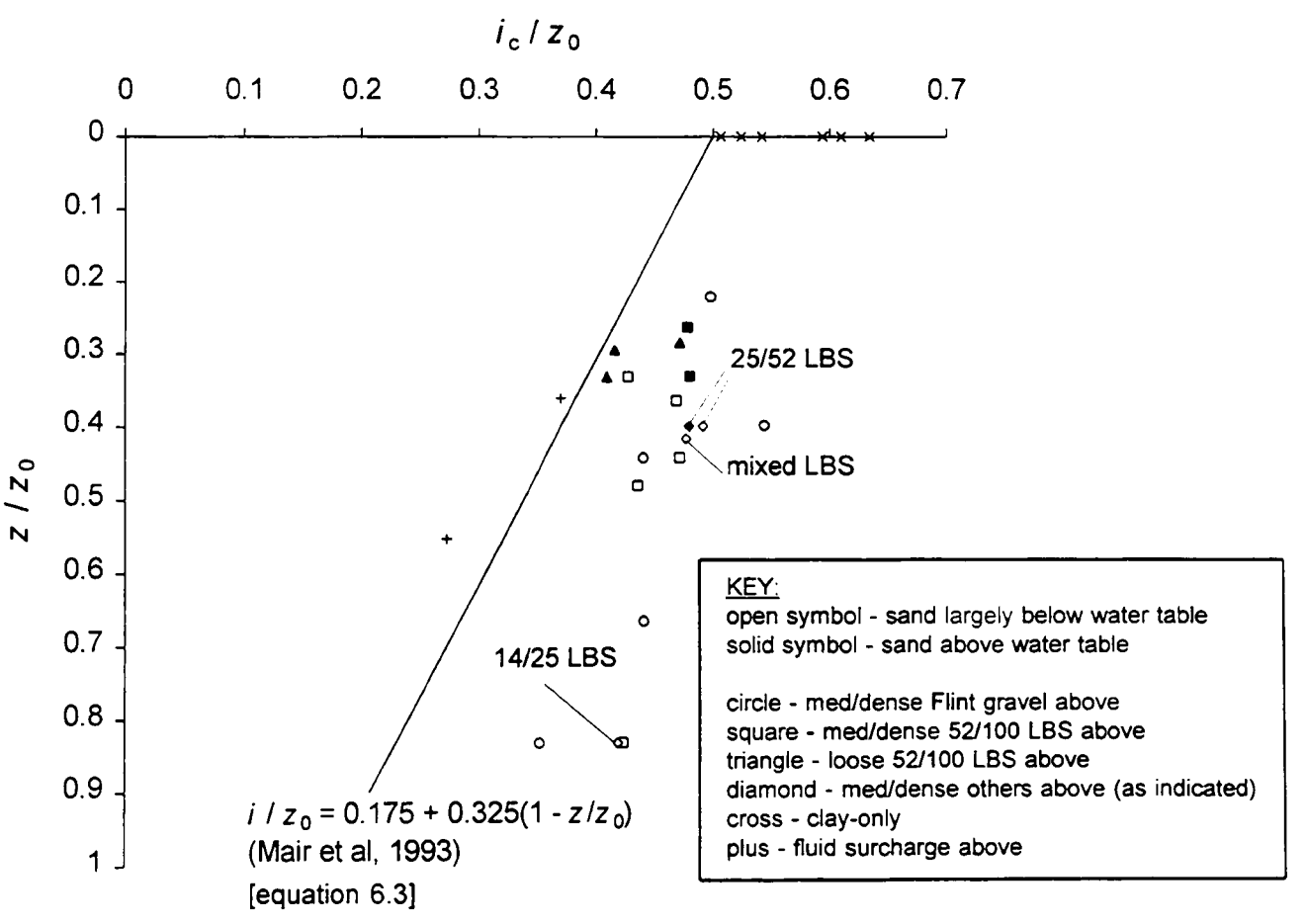

b) identified by type of overlying layer

Figure 6.3 i_c / z_0 against z / z_0 at the clay/sand interface or the clay surface for all centrifuge tests (determined from LVDT measurements)

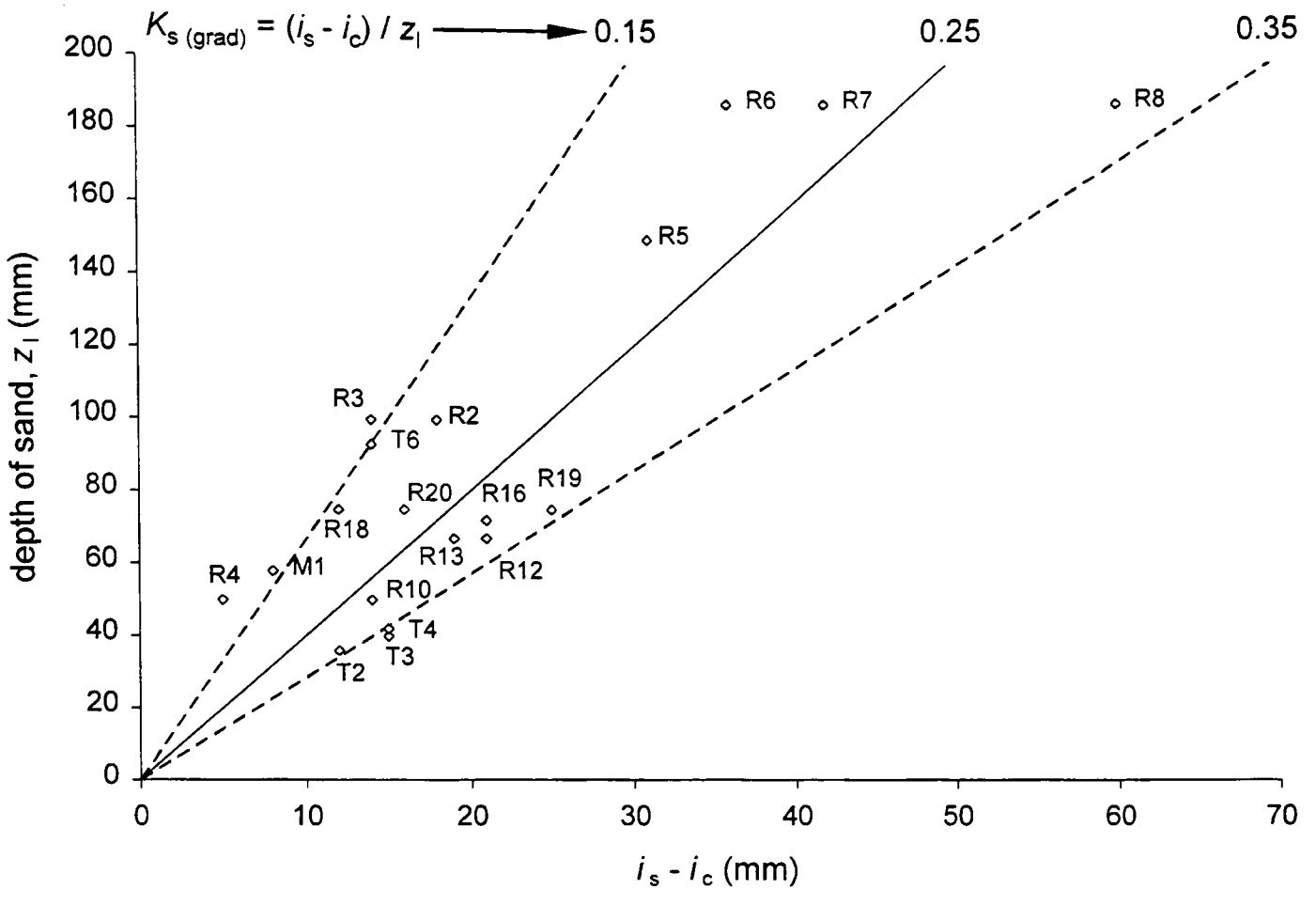

a) labelled by test

b) identified by type and condition of sand

Figure 6.4 Change in value of *i* through the sand layer for all centrifuge tests (determined from LVDT measurements at the sand surface and the clay/sand interface)

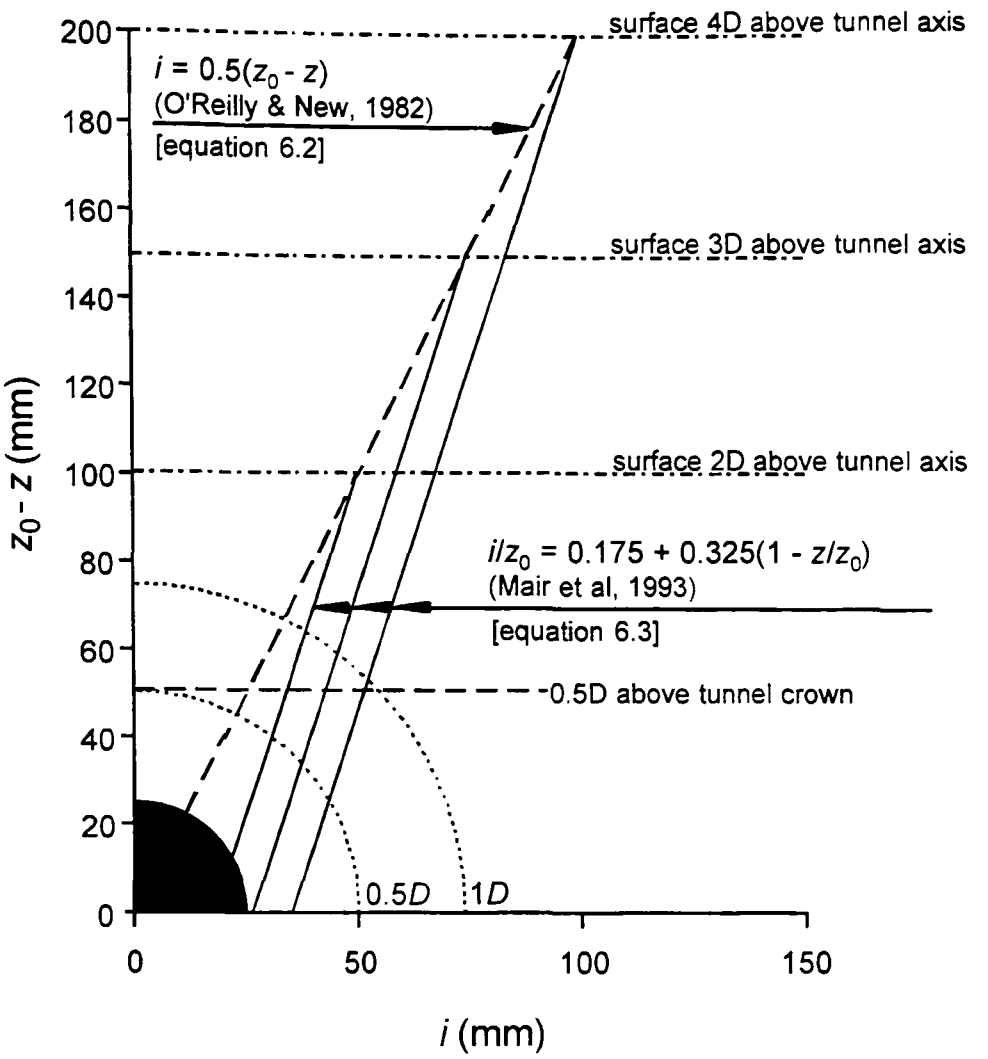

Figure 6.5 Illustration of the commonly applied distributions of i with depth

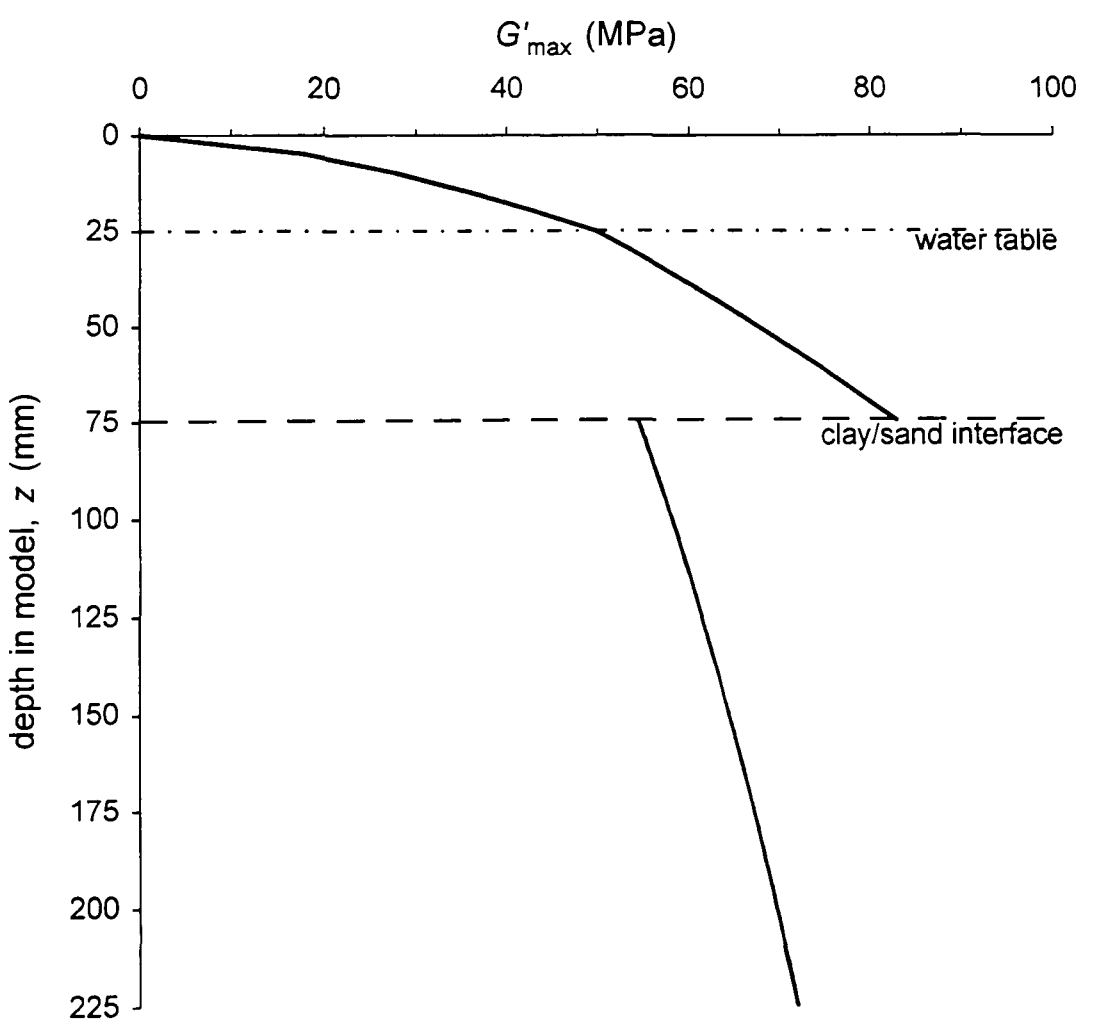

Figure 6.6 Illustration of the assumed distribution of G'_{max} with depth for a typical centrifuge test (RJG18 - 1.5D sand over 2.5D clay above crown)

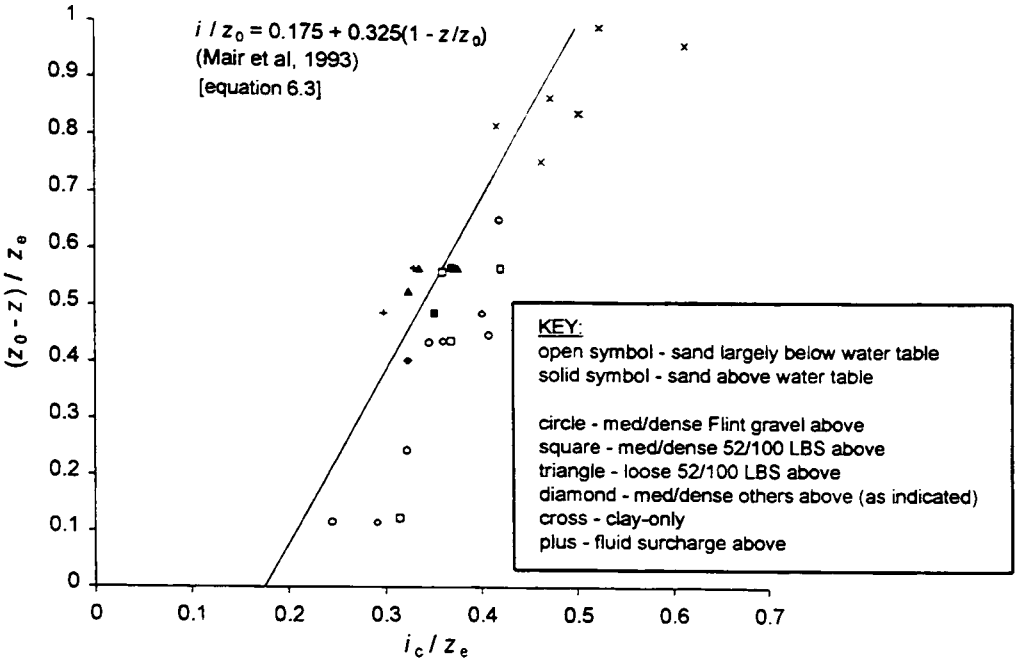

a) LVDTs at the clay/sand interface or clay/ground surface

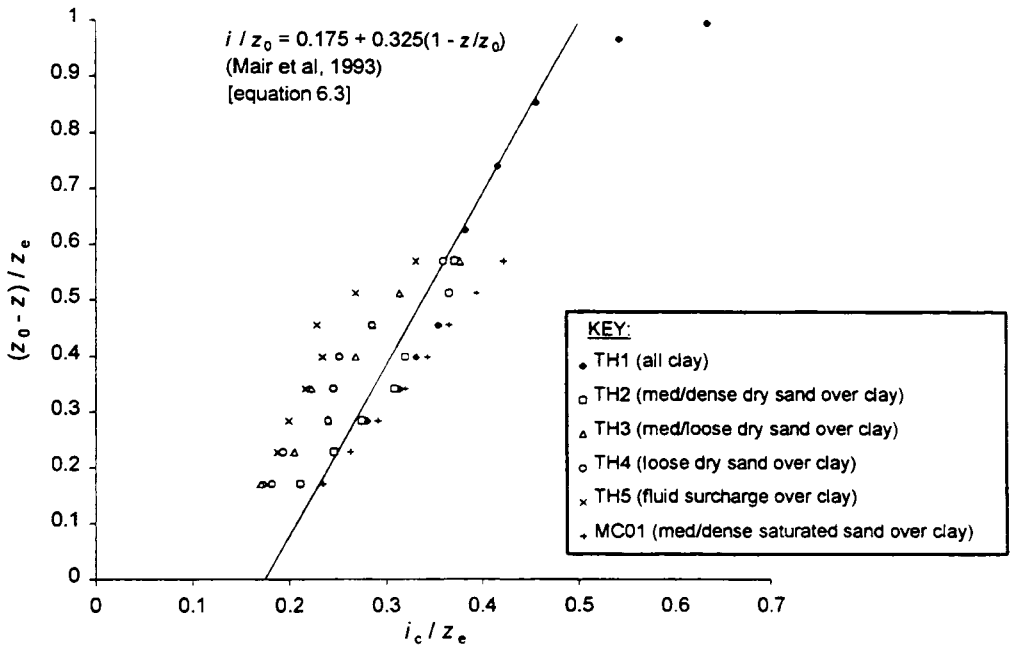

b) test series TH1 to 5 and MC01

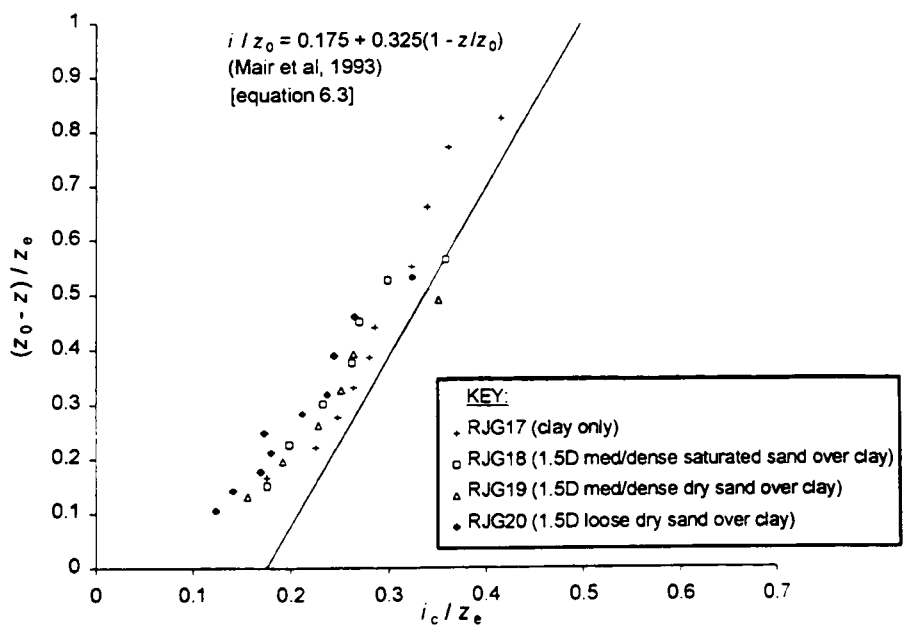

c) test series RJG17 to 20

Figure 6.7 i_c / z_e against $(z_0 - z) / z_e$ in the clay layer (where z_e is calculated to account for σ_v' in the clay)

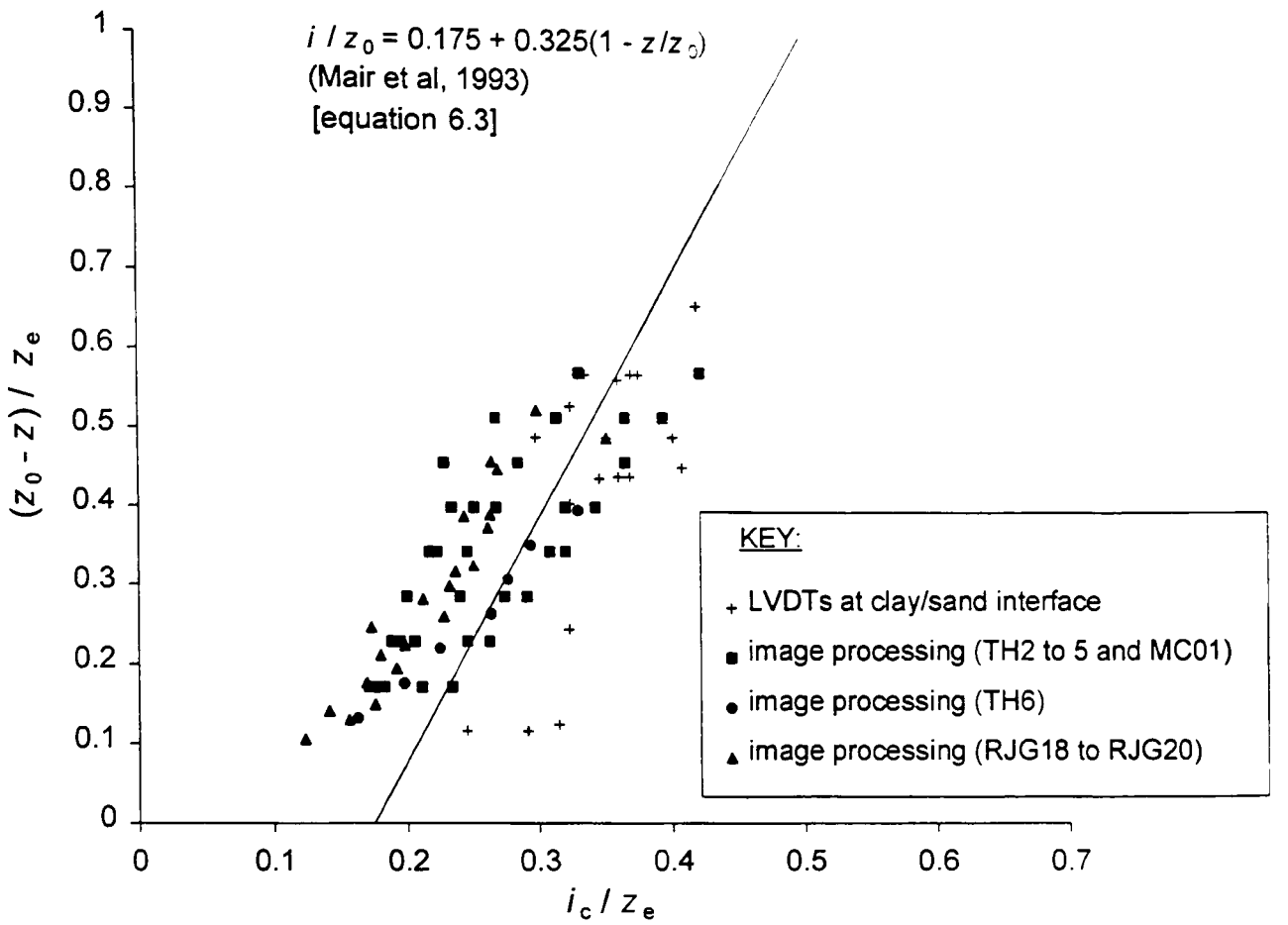

a) compared to Mair et al (1993) for all-clay soil profiles

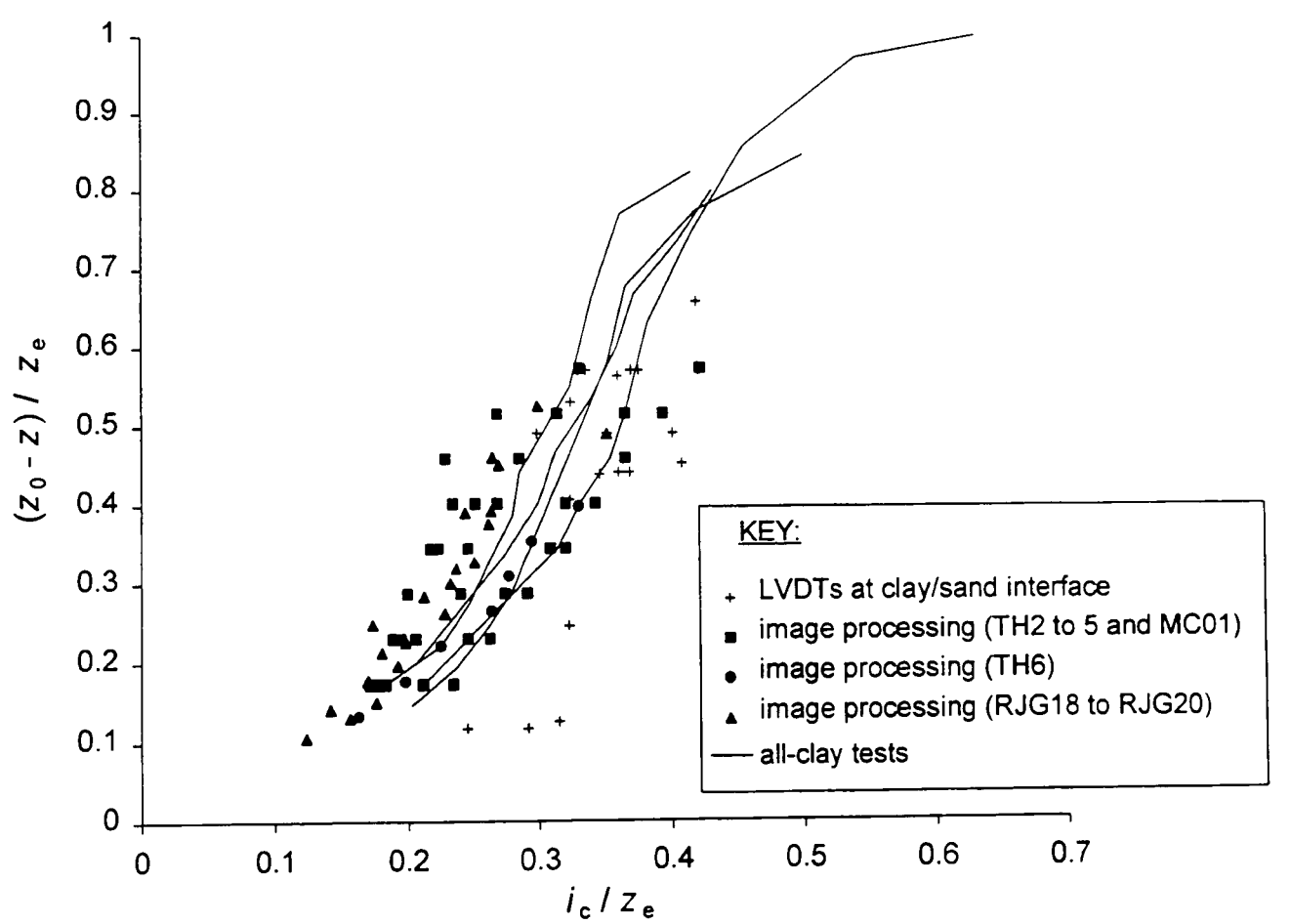

b) compared to the all-clay centrifuge tests

Figure 6.8 i_c / z_e against $(z_0 - z) / z_e$ for all centrifuge test data (where z_e is calculated to account for σ_v' in the clay layer)

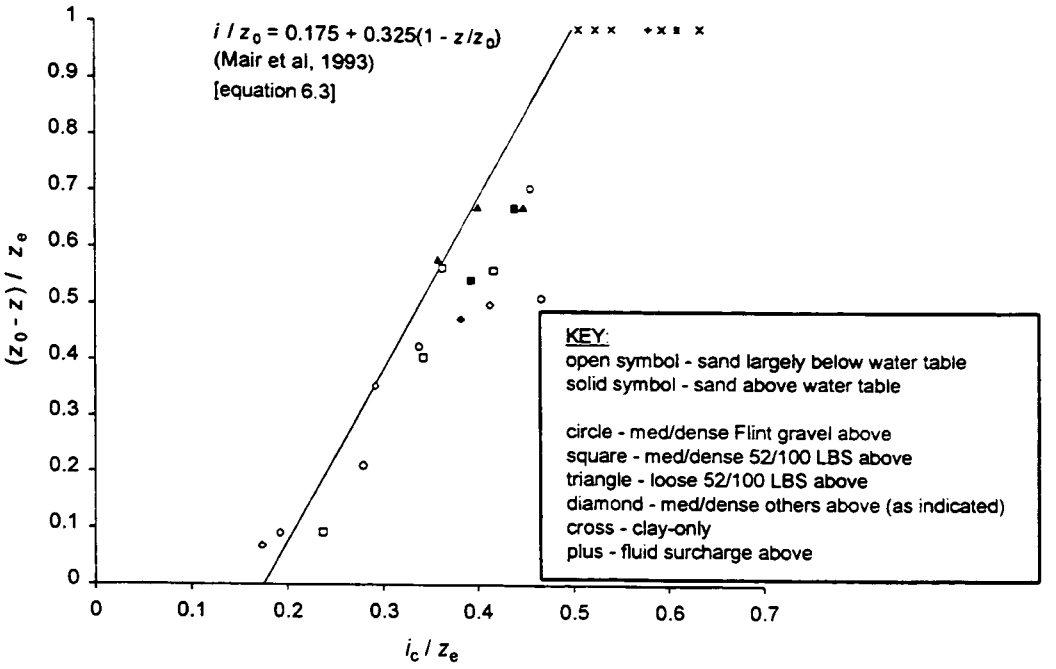

a) LVDTs at the clay/sand interface or clay/ground surface

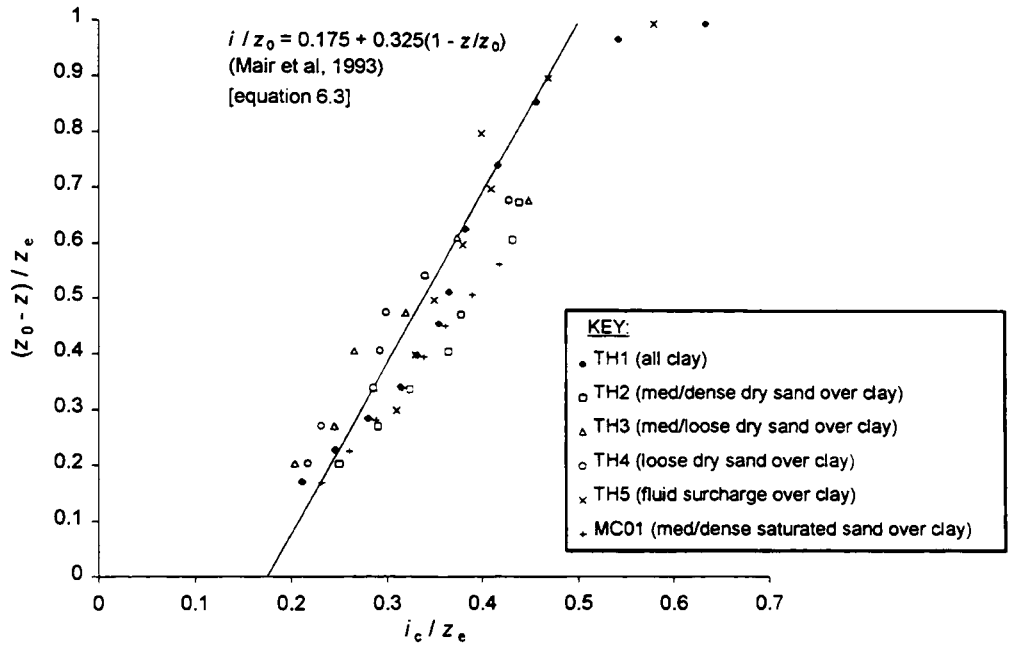

b) test series TH1 to 5 and MC01

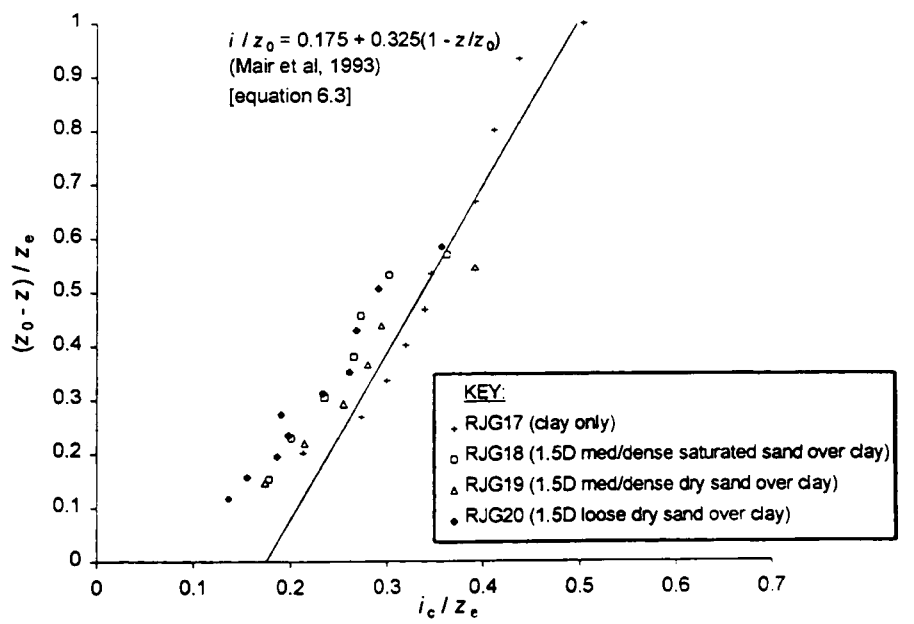

c) test series RJG17 to 20

Figure 6.9 i_c / z_e against $(z_0 - z) / z_e$ in the clay layer (where z_e is factored for the ratio of shear stiffnesses at the clay/sand interface)

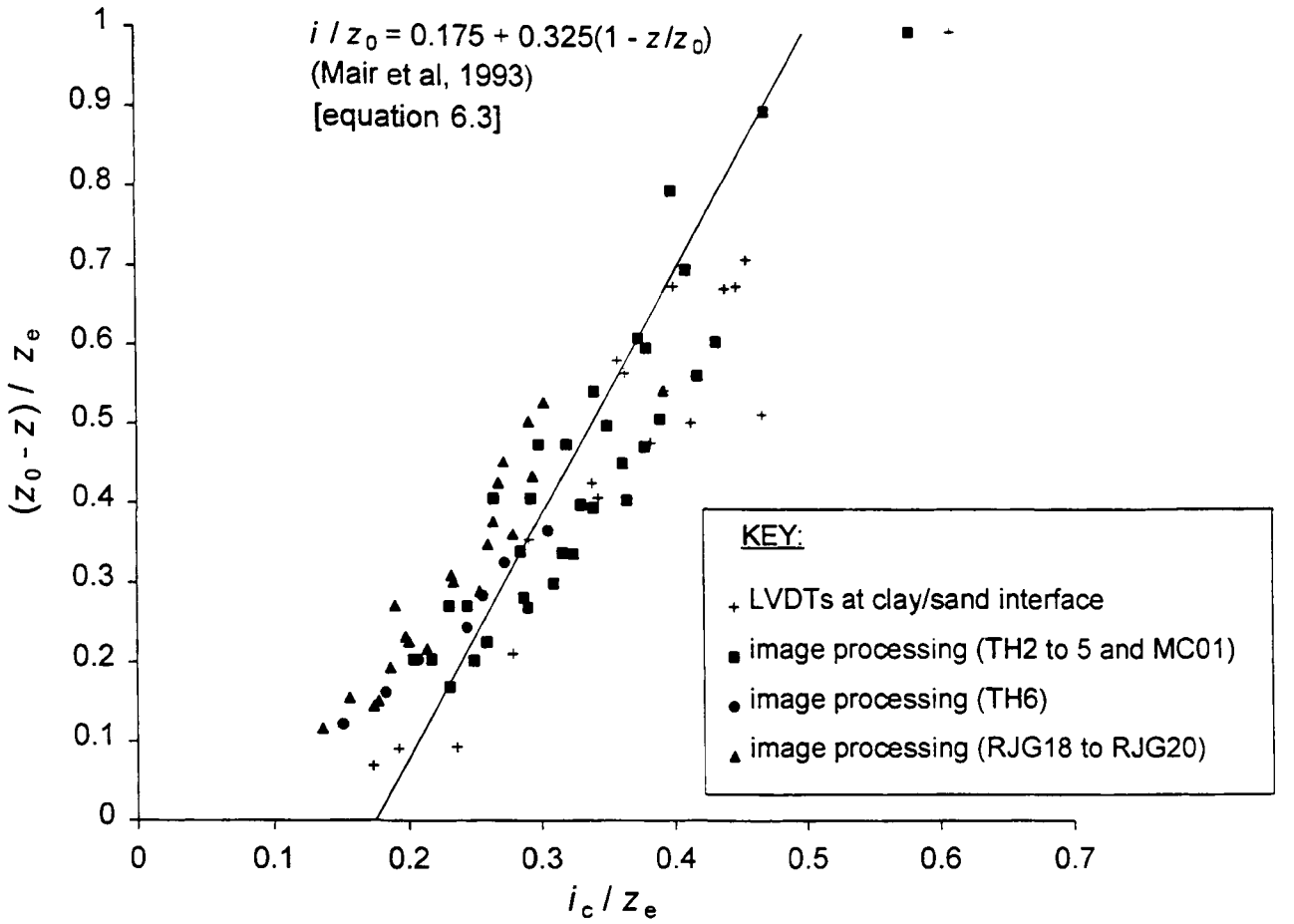

a) compared to Mair et al (1993) for all-clay soil profiles

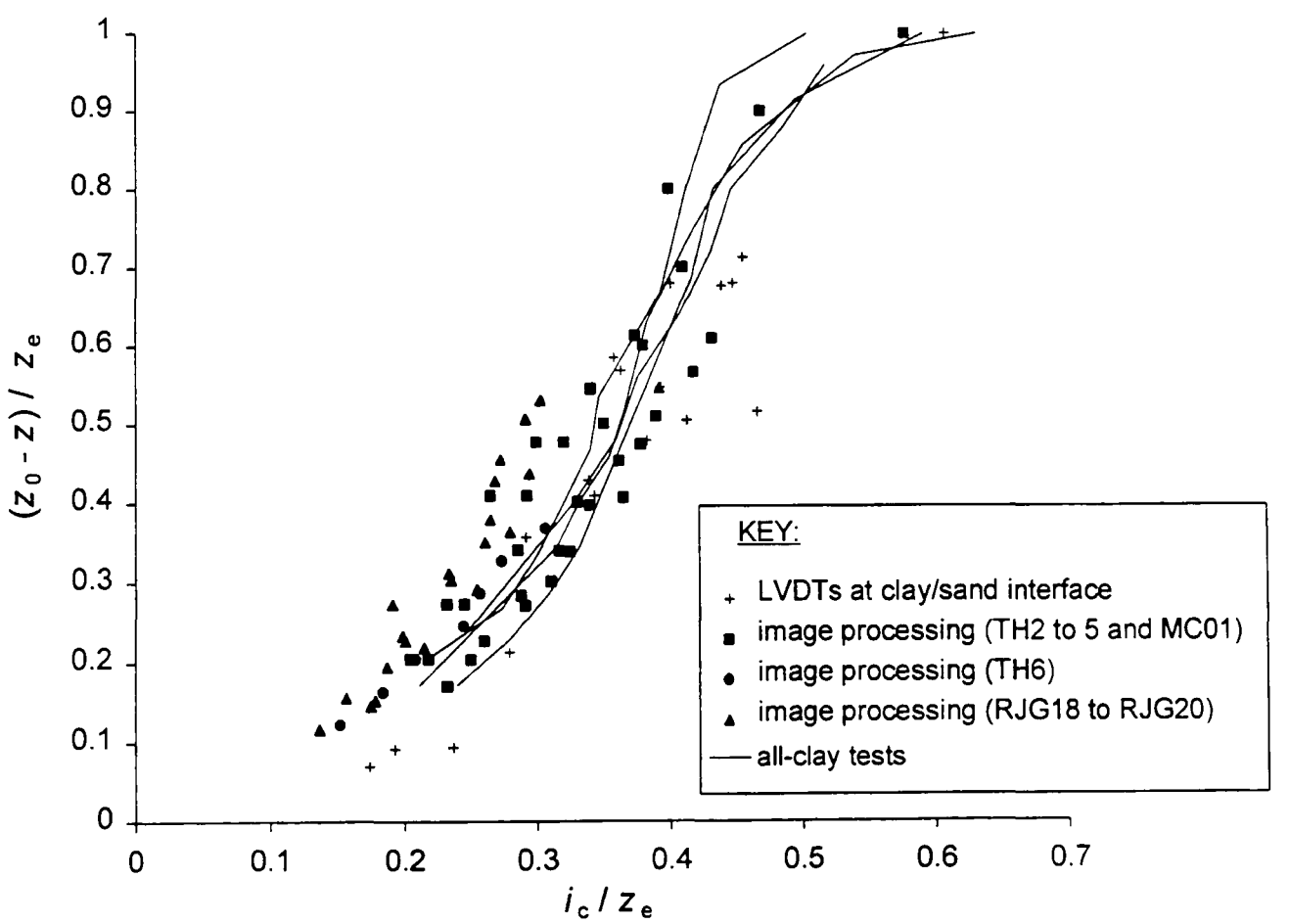

b) compared to the all-clay centrifuge tests

Figure 6.10 i_c / z_e against $(z_0 - z) / z_e$ for all centrifuge test data (where z_e is factored for the ratio of shear stiffnesses at the clay/sand interface)

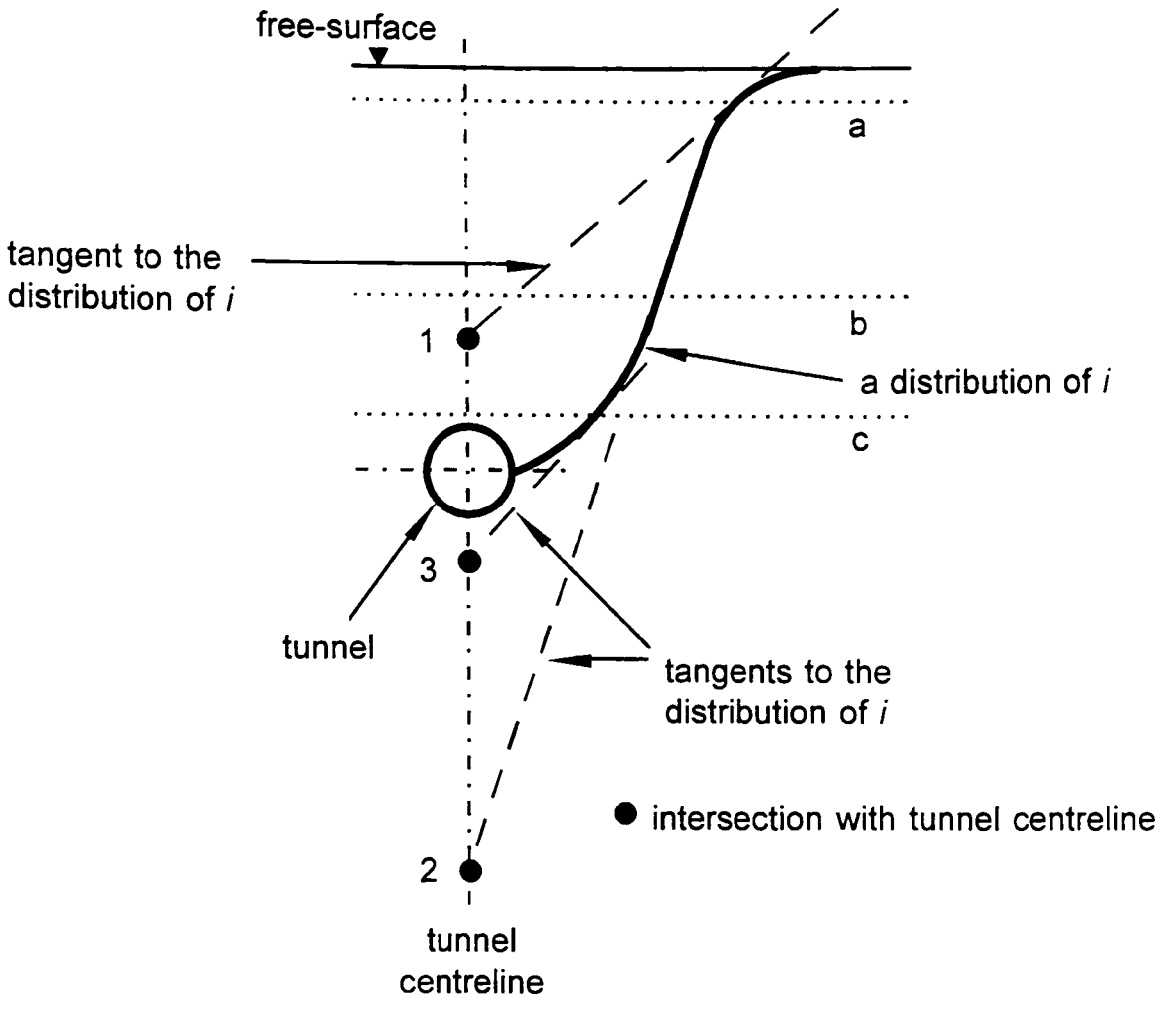

a) intersections of tangents to the distribution of *i* with the tunnel centreline

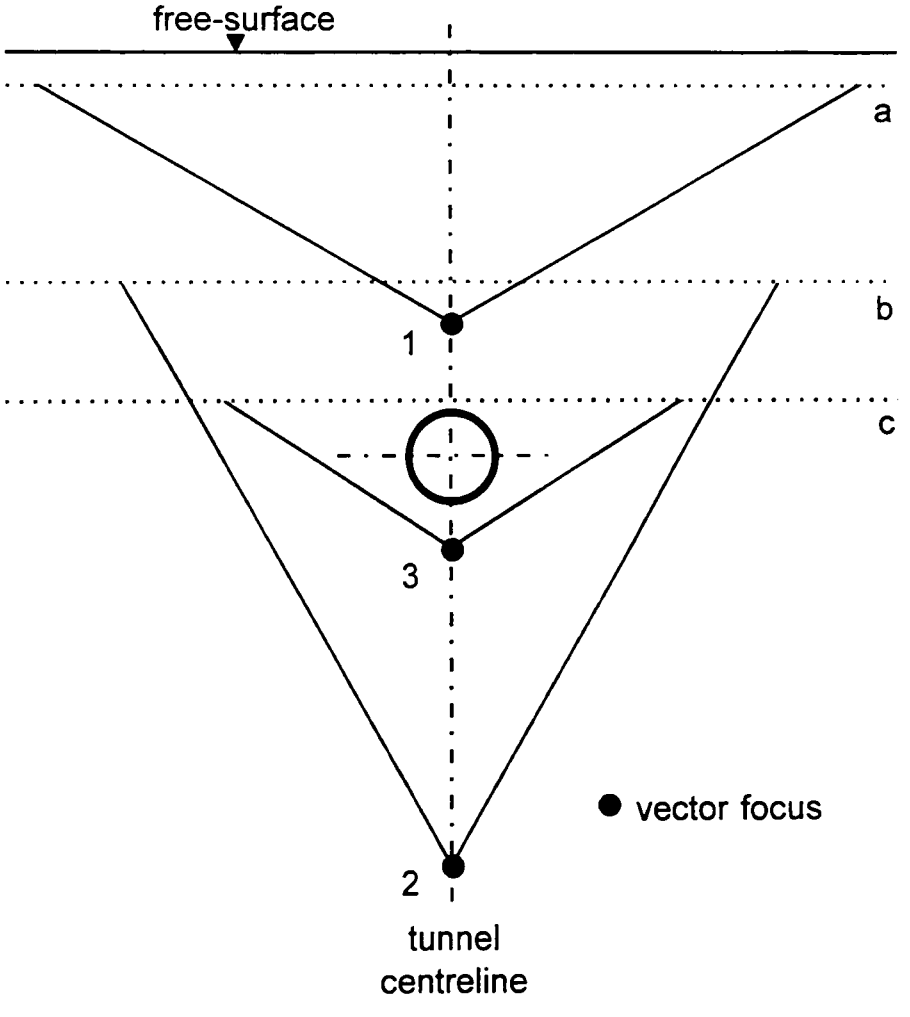

b) vectors focus on the intersections of the tangents to the distribution of *i* with the tunnel centreline

Figure 6.11 Implications of a distribution of *i* with depth assuming constant volume conditions

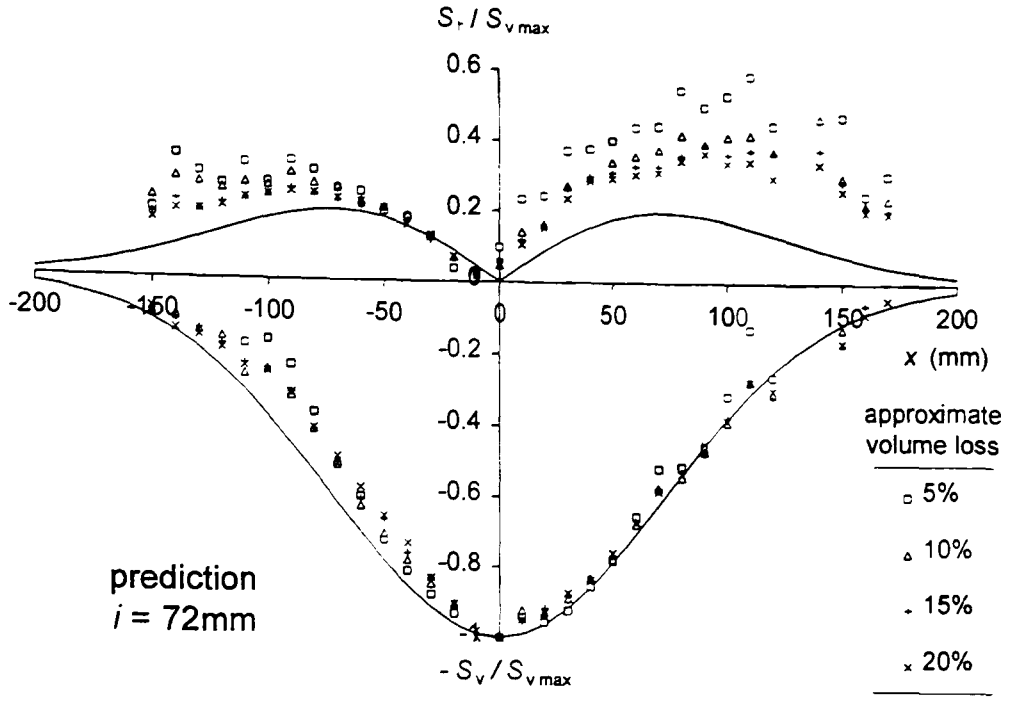

a) 140mm above tunnel axis (10mm from ground surface)

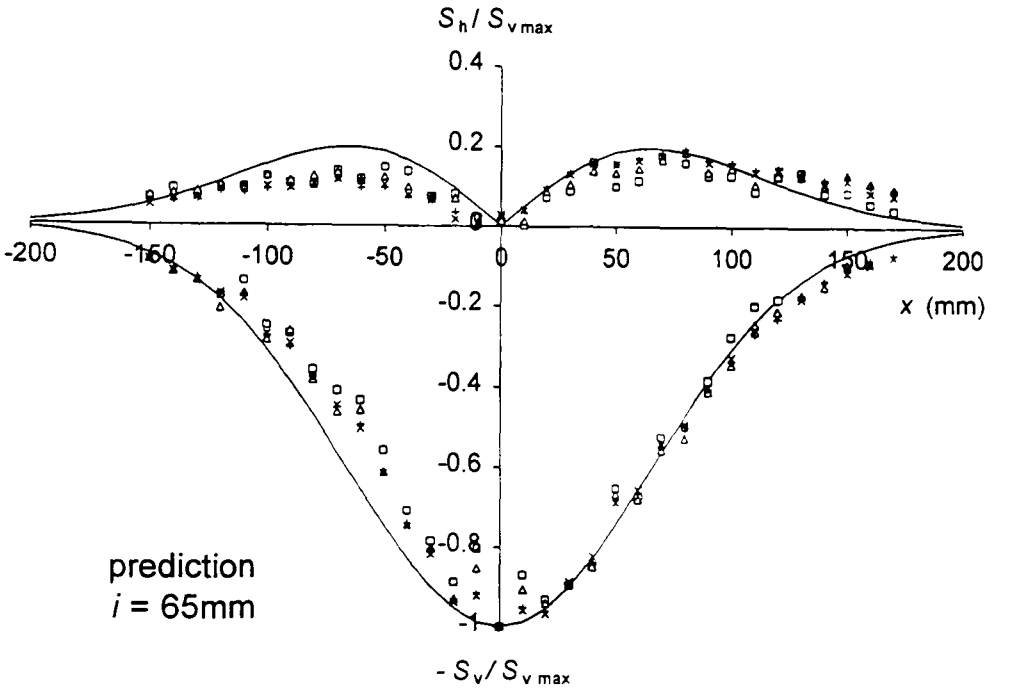

b) 120mm above tunnel axis (30mm from ground surface)

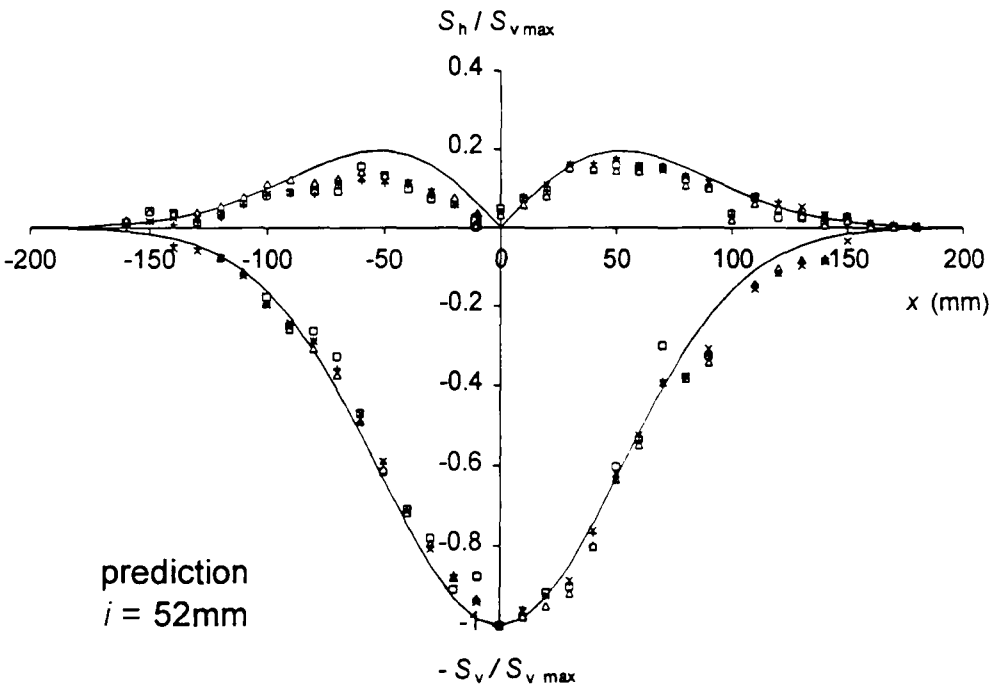

c) 80mm above tunnel axis

Figure 6.12 Comparison of predicted vertical and horizontal movement at different subsurface levels with measurements for centrifuge test RJG17 (2.5*D* clay only above crown)

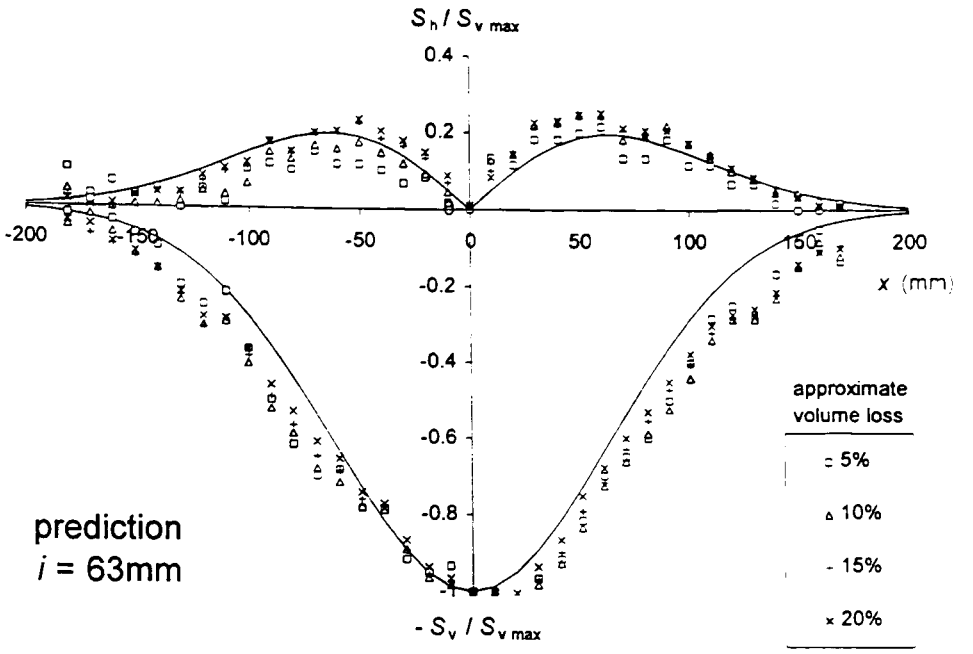

a) Movements 90mm above tunnel axis - equation 6.15 (after Mair et al, 1993)

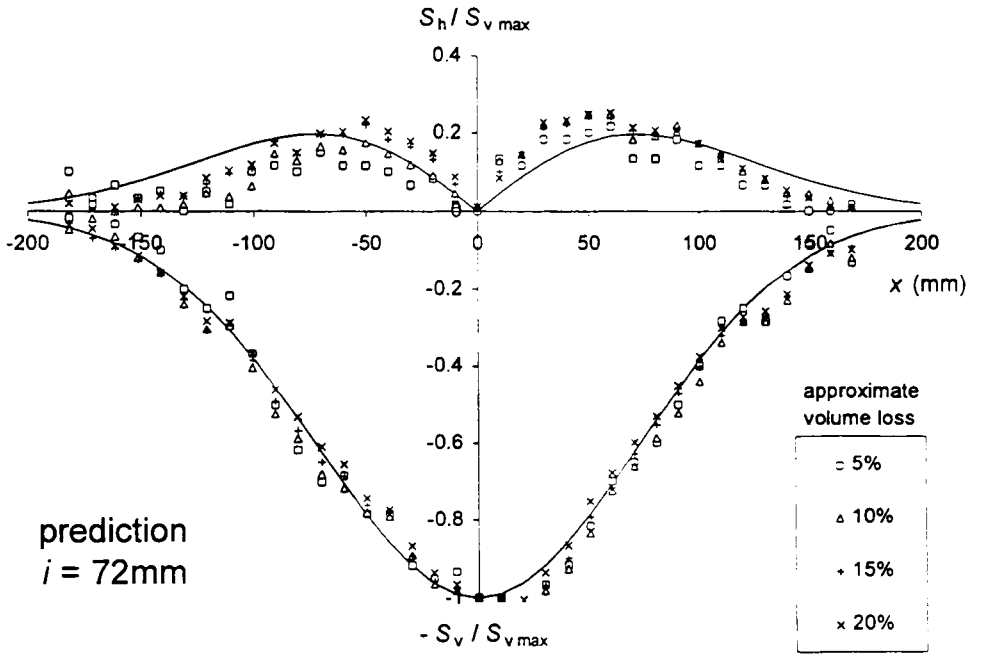

b) Movements 90mm above tunnel axis - equation 6.16 (accounting for stiffness)

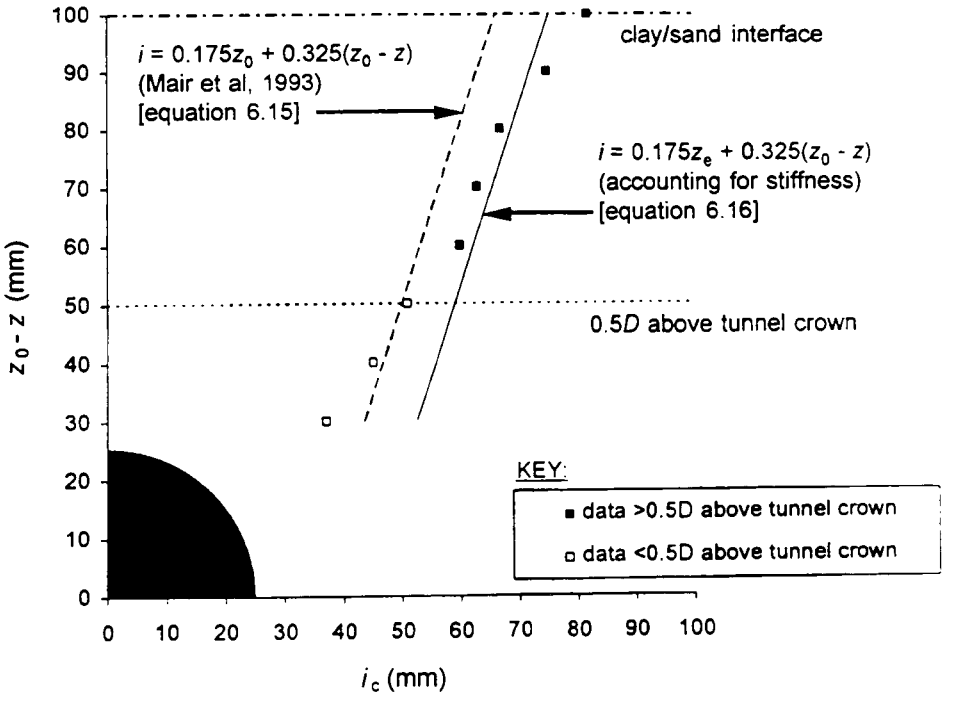

c) Distribution of i_c with depth

Figure 6.13 Comparison of predictions with measured data in the clay layer for centrifuge test TH6 (93mm saturated sand over 75mm clay above crown)

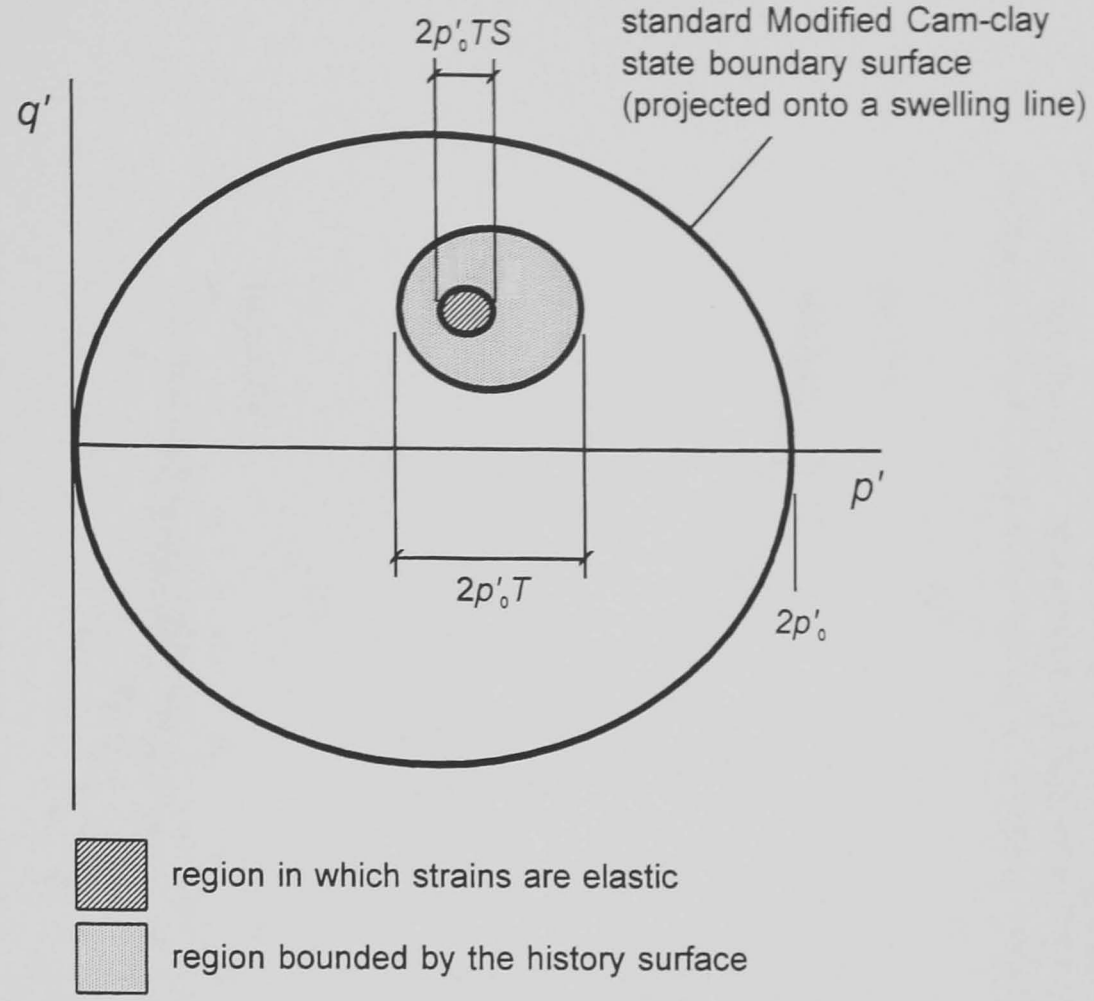

Figure 7.1 Definition of the parameters T and S for the 3-Surface Kinematic Hardening model

A - current stress state
B & C - conjugate points with same outward normal as A

$\underline{\gamma}$ - vector of movement of yield surface, parallel to and of magnitude AB
$\underline{\beta}$ - vector of movement of history surface, parallel to and of magnitude BC

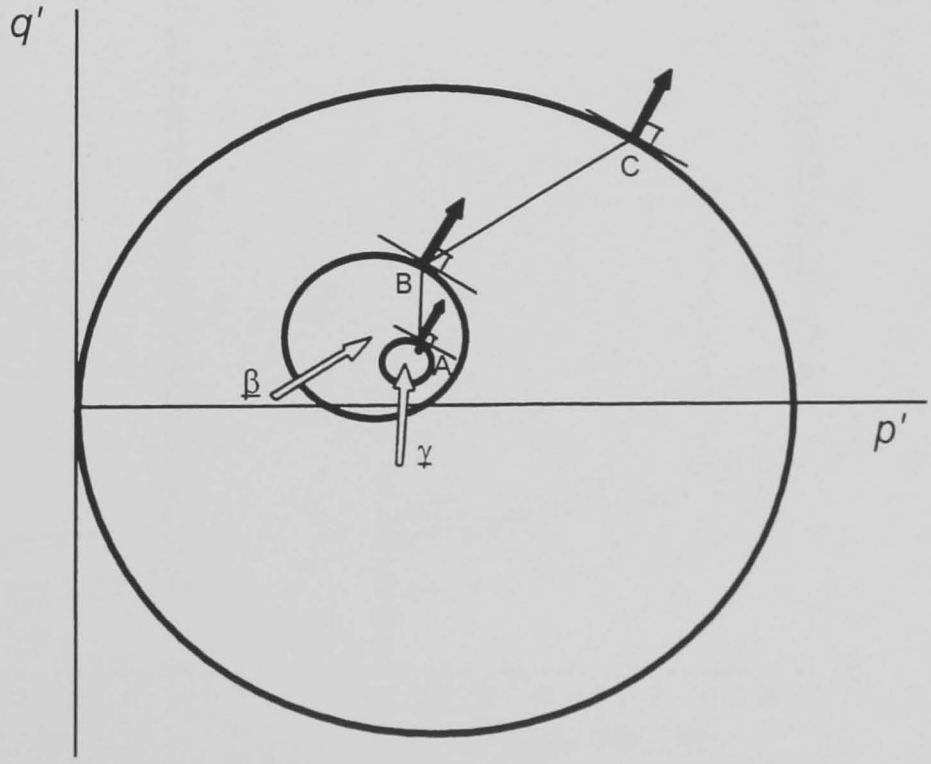

Figure 7.2 Sketch illustrating the rule for the translation of the kinematic surfaces

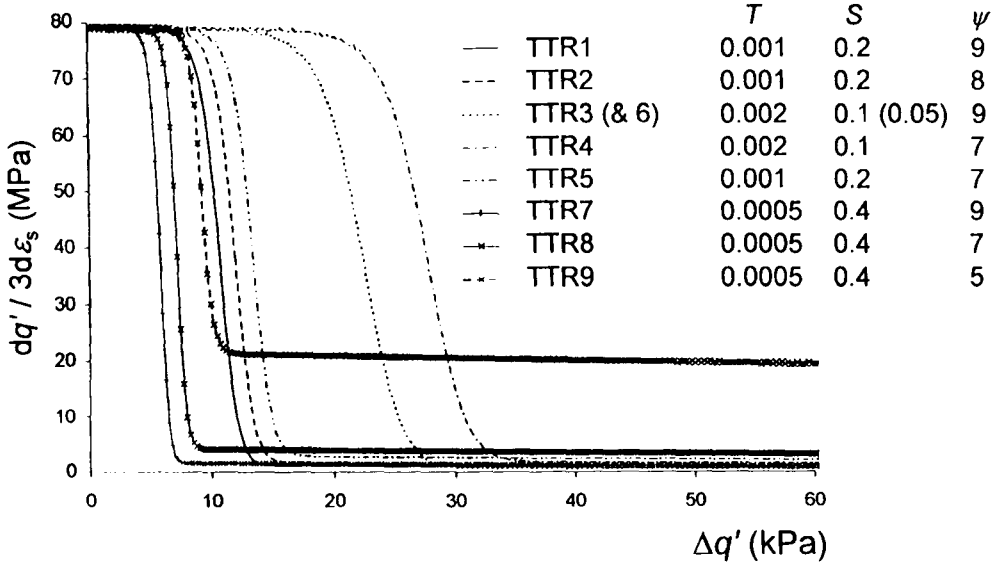

(a)

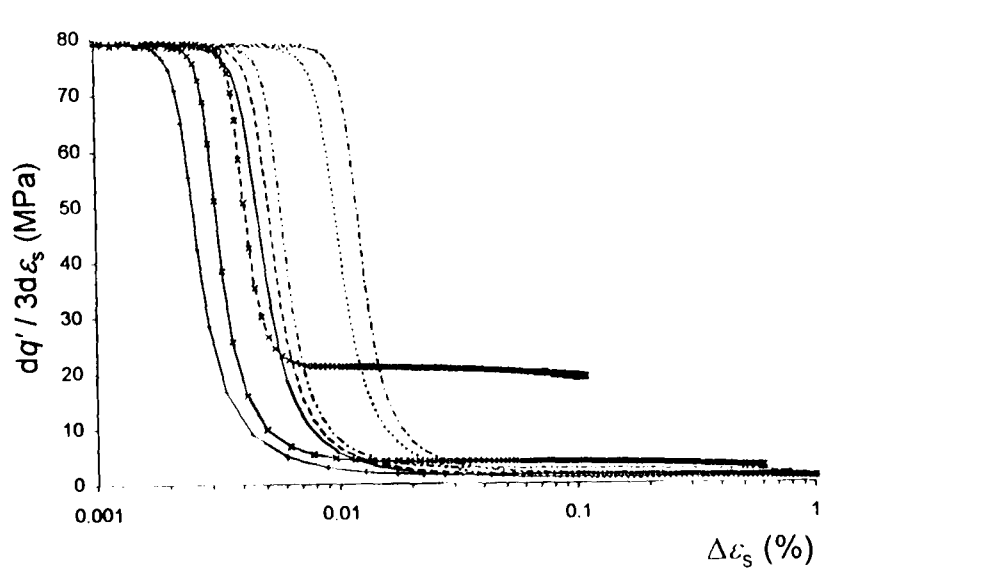

(b)

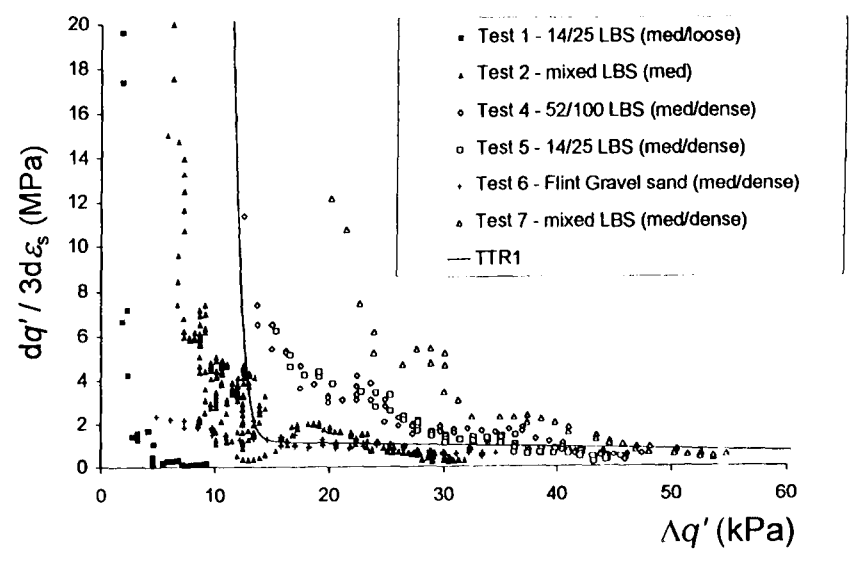

(c)

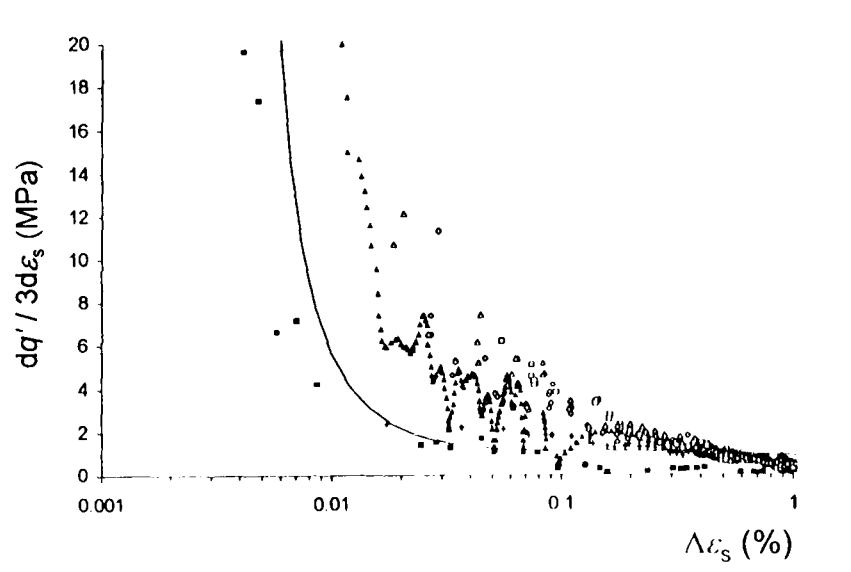

(d)

Figure 7.3 Determination of the 3-SKH model parameters T, S and ψ for sands (by modelling the triaxial tests with a 2 element axi-symmetric FEA) a) Effect on stiffness with $\Delta q'$ of varying the parameters, b) Effect on stiffness with $\Delta\varepsilon_s$ of varying the parameters, c) Comparison of results from FEA with triaxial test data with $\Delta q'$, d) Comparison of results from FEA with triaxial test data with $\Delta\varepsilon_s$

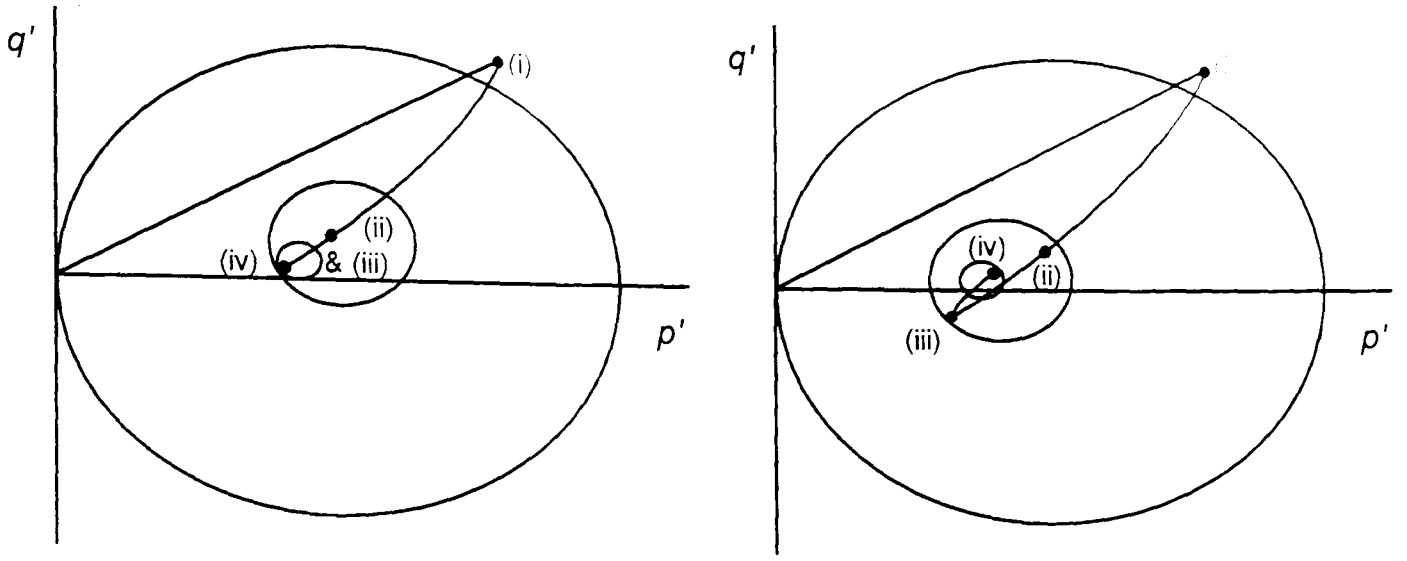

a) 1-dimensional compression (i)
swelling in the consolidation press (ii)
no extra swelling during model preparation (iii)
swelling due to centrifuge acceleration (iv)
(RC3A)

b) 1-dimensional compression (i)
swelling in the consolidation press (ii)
swelling during model preparation (iii)
compression due to centrifuge acceleration (iv)
(RC3AM)

Figure 7.4 Sketched stress paths and orientations of the kinematic surfaces for different stress histories ending at the same σ'_v (applicable to soil in the lower regions of the model)

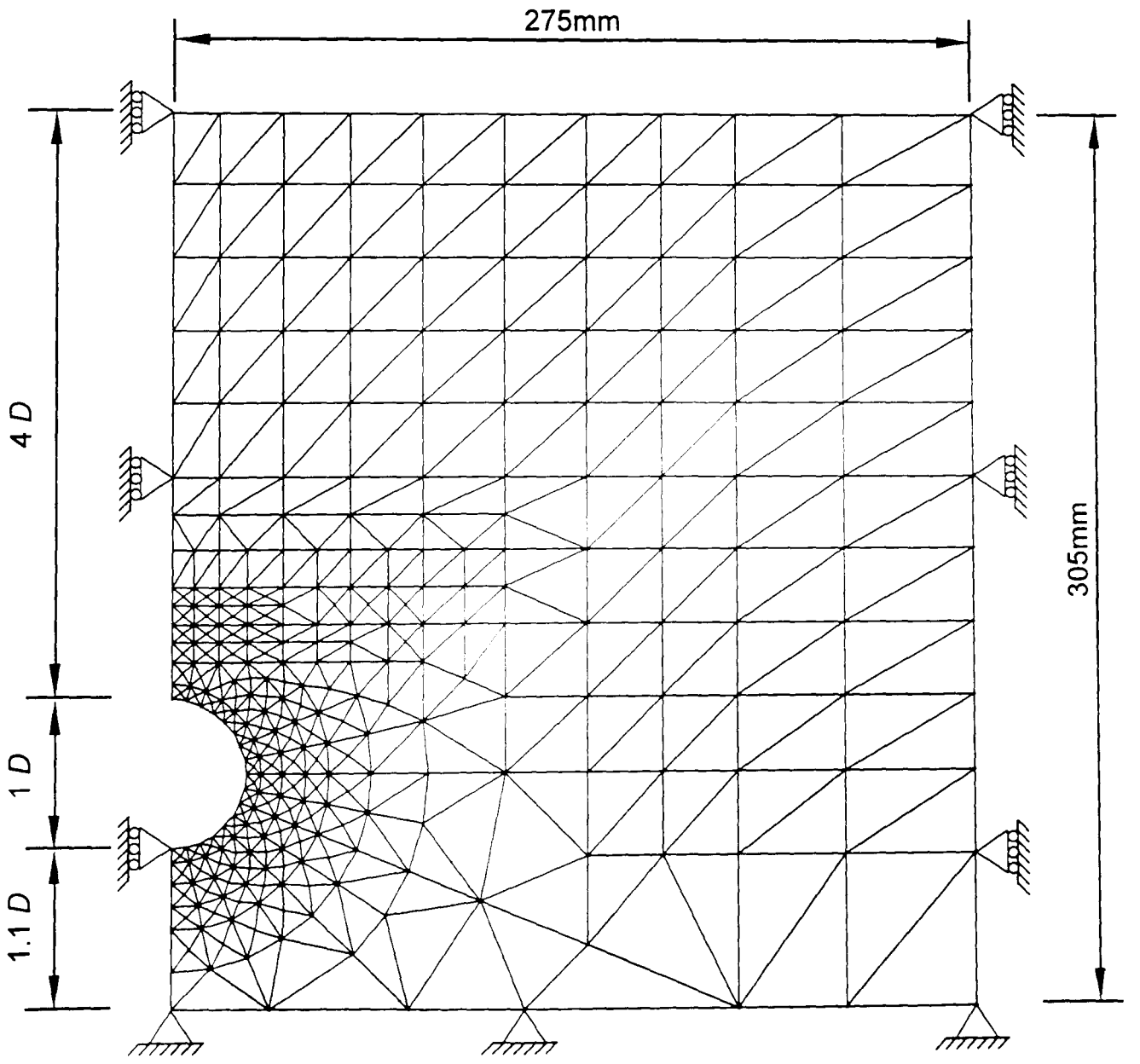

Figure 7.5 Standard finite element mesh (for analyses with 4*D* total soil cover)

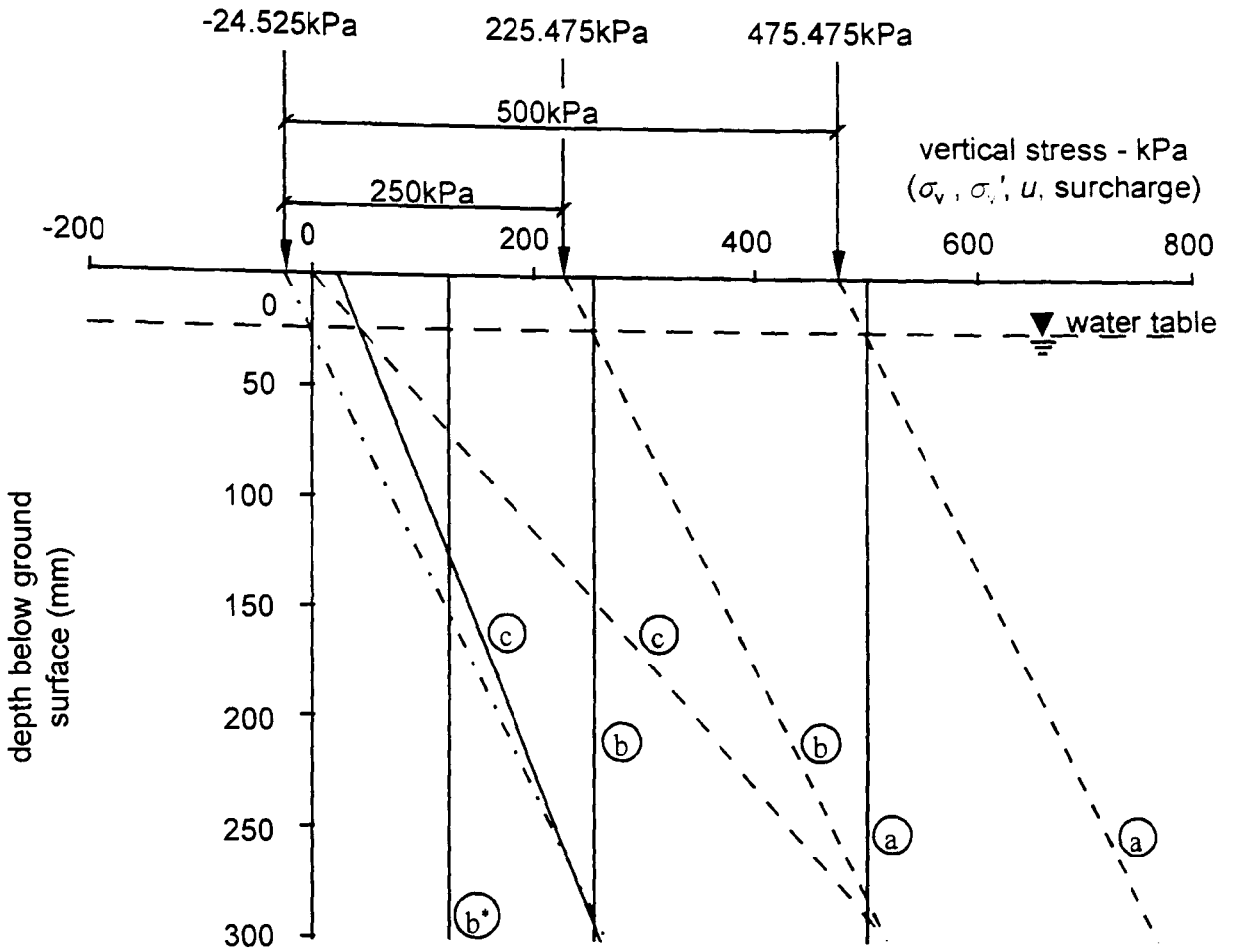

Legend:

vertical effective stress (σ_v') profile

vertical total stress (σ_v) profile

pore water pressure (u) profile - hydrostatic for 100g

Notes:
All distributions are for equilibrium conditions.

In situ conditions (a)
Water table usually 25mm below surface with equilibrium u profile specified as hydrostatic for 100g (CRISP does not apply accelerations to pore water).
All analyses began with 56.25g applied to the clay which produced a σ_v profile parallel to the u profile. It was offset from the u profile by 500kPa by applying a surcharge to the clay surface, so producing a σ_v' profile which was a constant 500kPa with depth.

1st loading stage (b)
250kPa surcharge removed from clay surface so σ_v and σ_v' profiles offset by -250kPa.
(b^* is σ_v' profile if clay allowed to swell further, eg. during model preparation, as in RC3AM.)

2nd loading stage (c)
Further surcharge removed from clay surface and acceleration increased to 100g. σ_v and σ_v' profiles offset and gradients altered.
(if sand layer was to be added sufficient surcharge was left to balance the weight of the sand.)

The next stage in the analyses was to replace the elements in the tunnel with a supporting pressure equal to σ_v at tunnel axis level. No significant change in equilibrium vertical stress distributions should occur. When sand was present in the analyses, this stage was followed by the building of the sand layers during which further surcharge was removed to balance the load on the clay from the sand above. No significant change in vertical stress distributions should occur.
(c) therefore represents the equilibrium stress distributions before the tunnel pressure reduction.

Figure 7.6 Illustration of typical history for finite element analysis

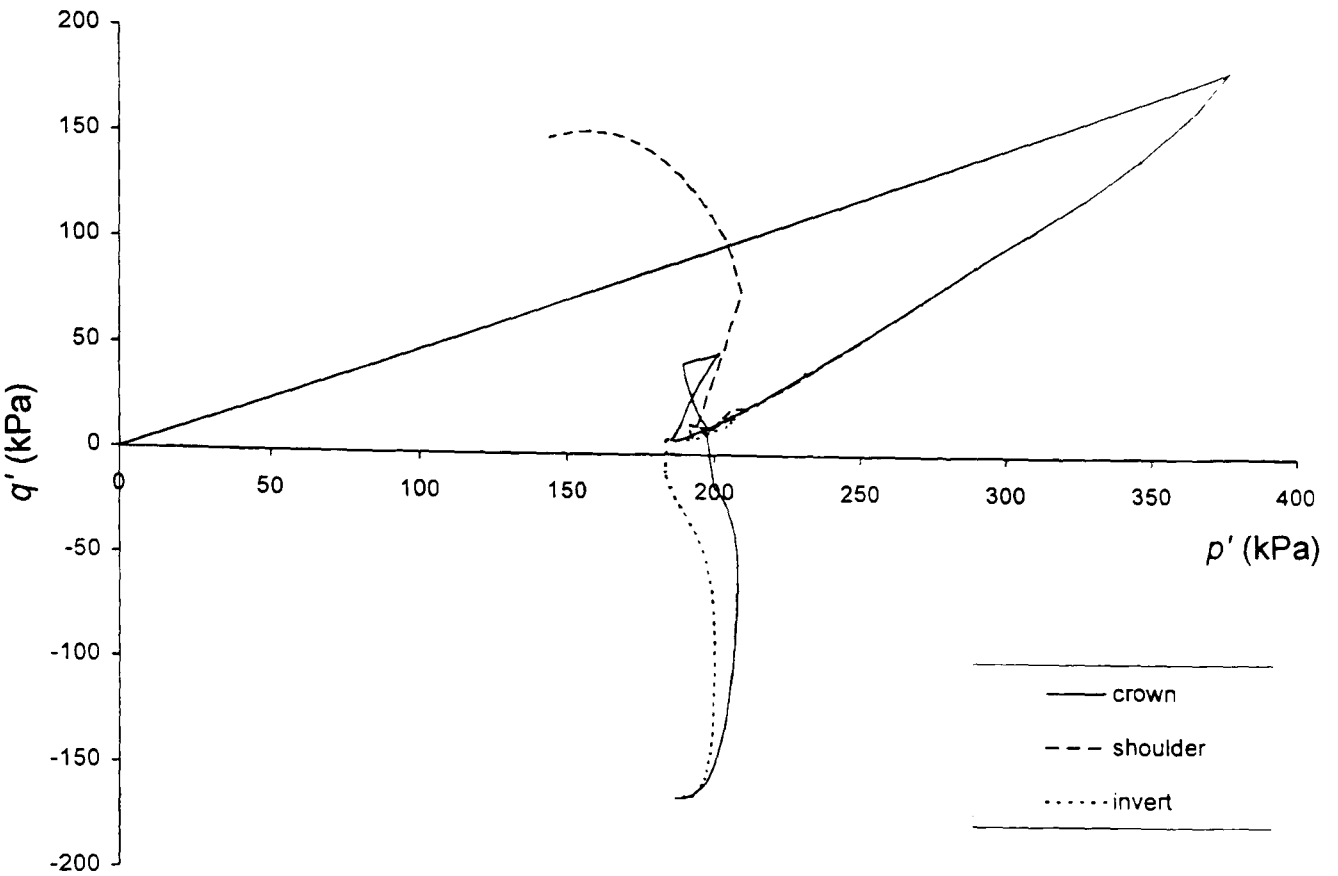

Figure 7.7 Effective stress paths for elements near the tunnel during finite element analysis RC4 (K_0 compression followed by swelling and then σ_T reduction)

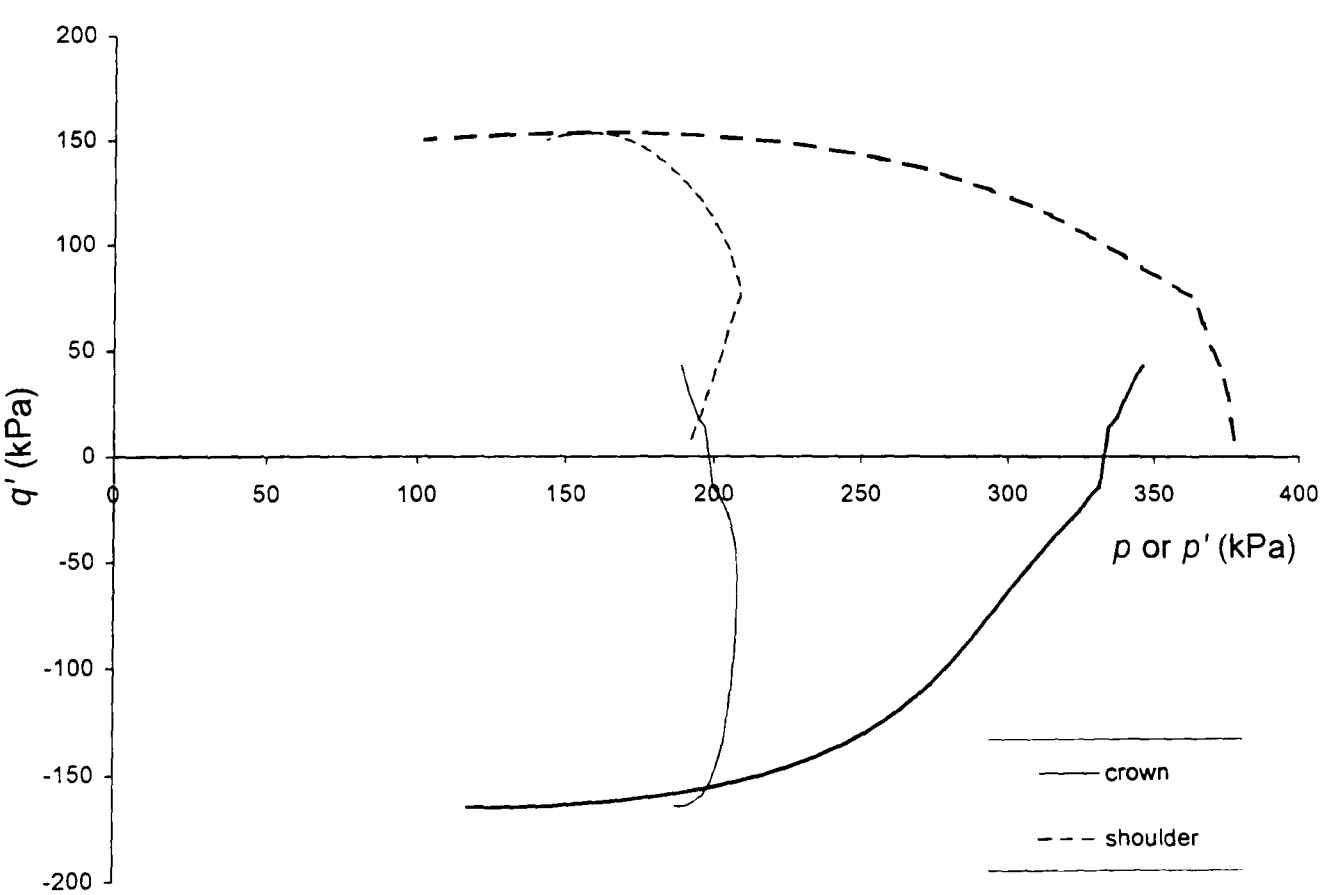

Note:
The thicker lines are total stress paths and the thinner lines are effective stress paths

Figure 7.8 Total and effective stress paths near the tunnel crown and shoulder during finite element analysis RC4 for σ_T reduction phase

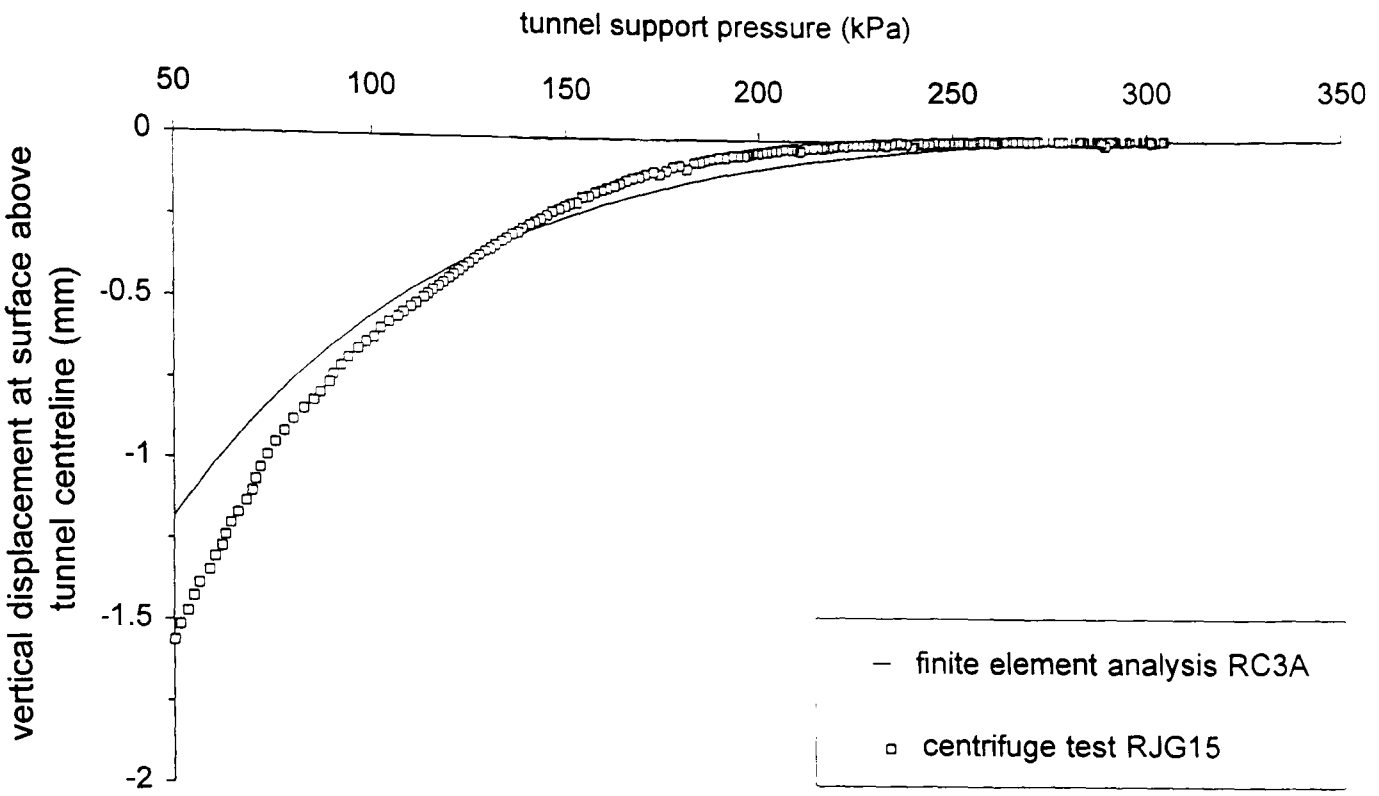

Figure 7.9 Surface settlement above tunnel centreline for 3*D* clay cover only: comparison of finite element analysis (RC3A) prediction with LVDT data from centrifuge test RJG15

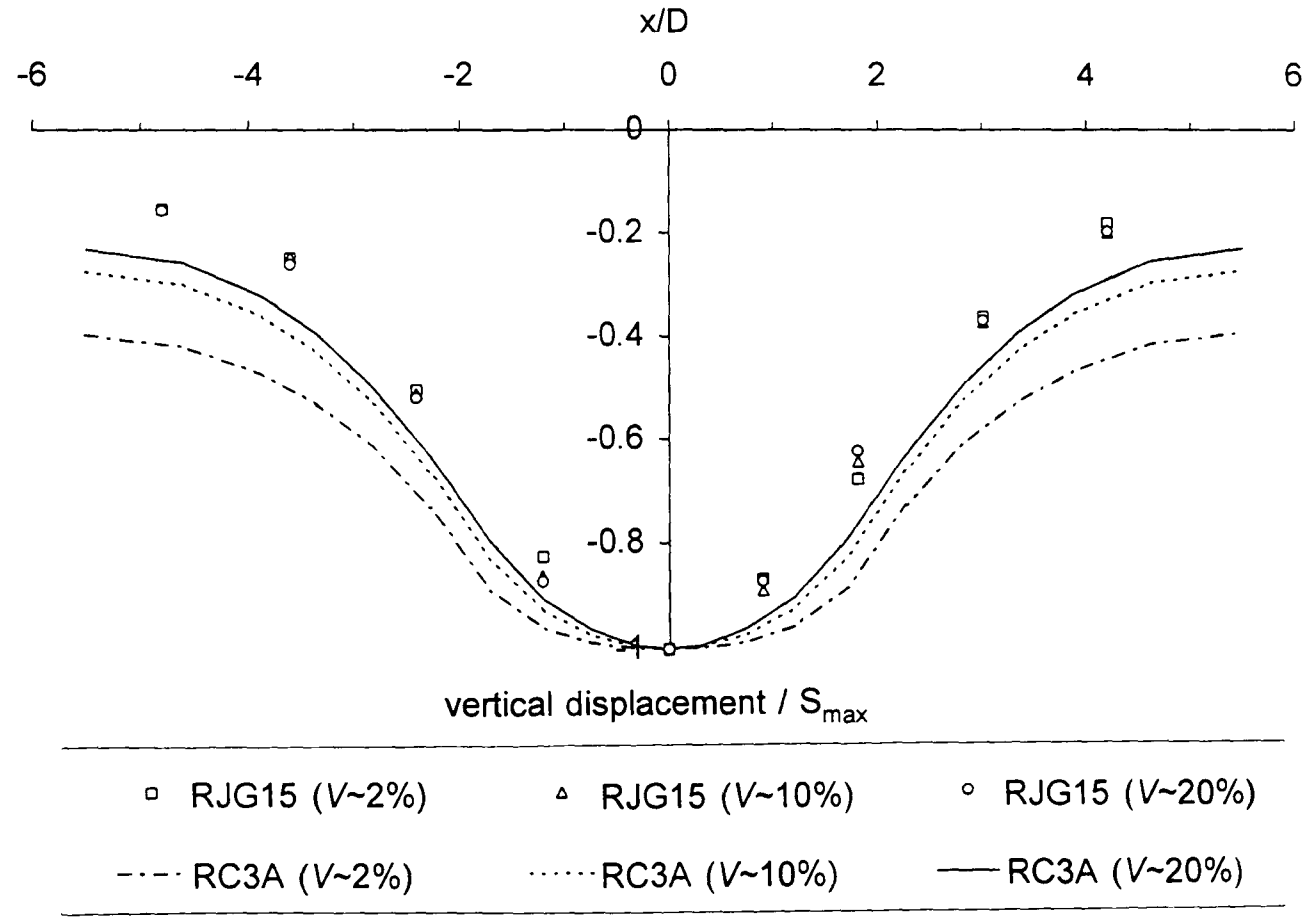

Figure 7.10 Normalised surface settlement troughs above tunnel for 3*D* clay cover only: comparison of finite element analysis (RC3A) prediction with LVDT data from centrifuge test RJG15

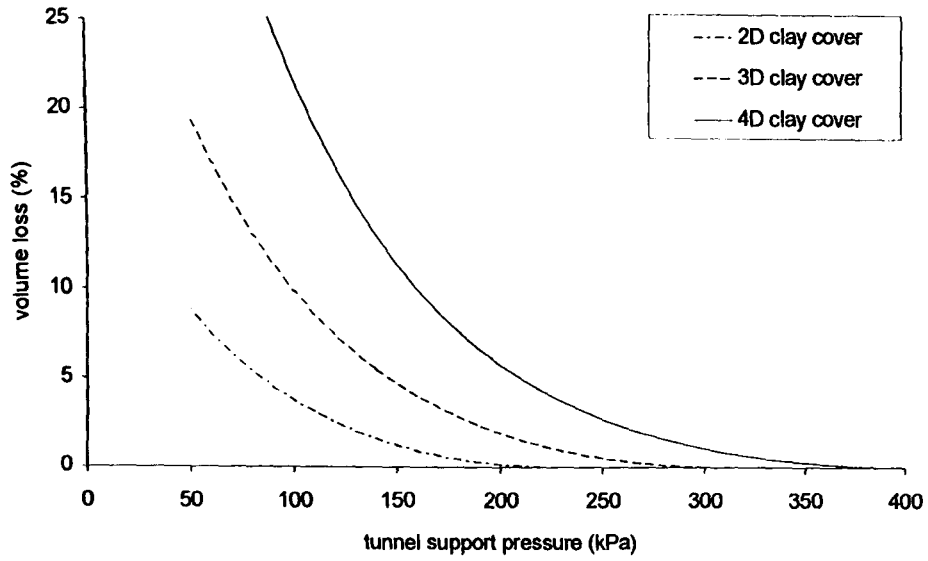

(a)

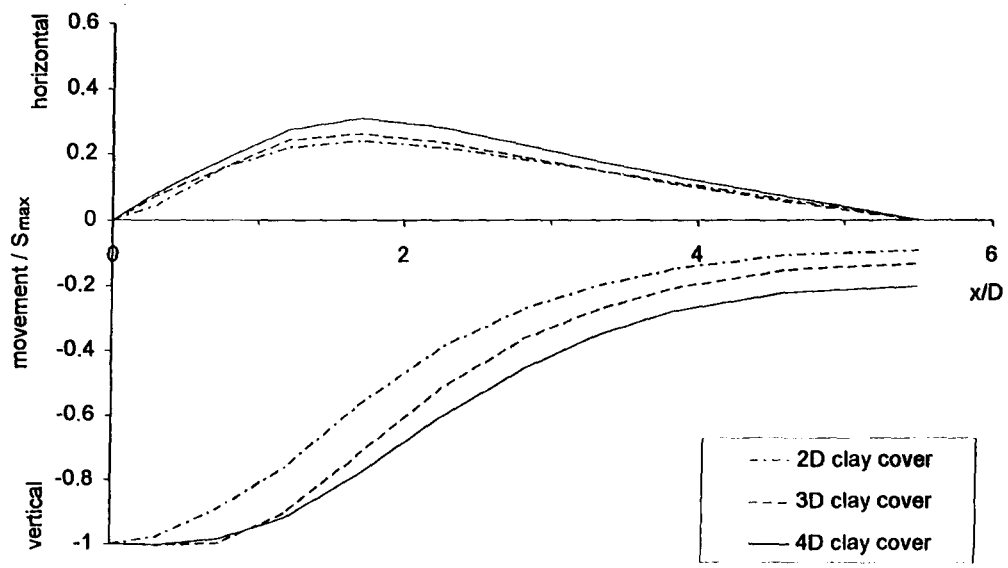

(c)

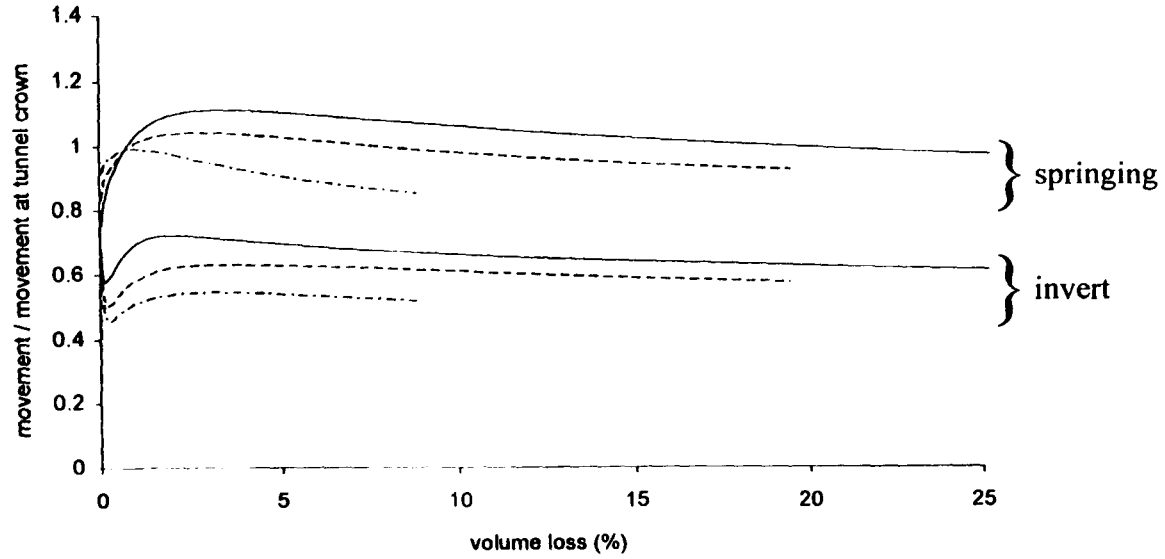

(b)

(d)

Figure 7.11 Effect of depth of clay cover above tunnel crown
(2*D* cover - RC2, 3*D* cover - RC3A, 4*D* cover - RC4).
a) volume loss against tunnel support pressure, b) movements around tunnel, c) normalised movements 1*D* above tunnel crown,
d) normalised movements at surface, (all at $V \sim 5\%$ where applicable)

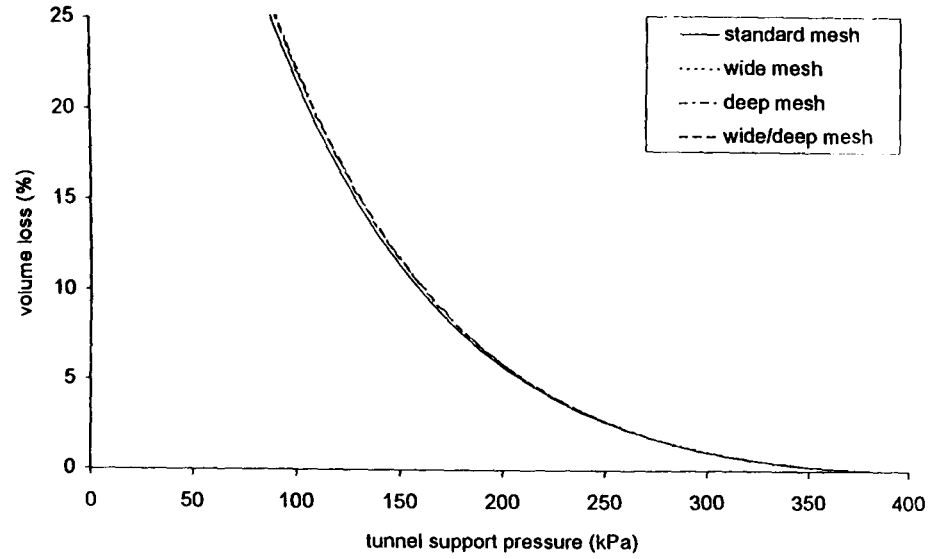

(a)

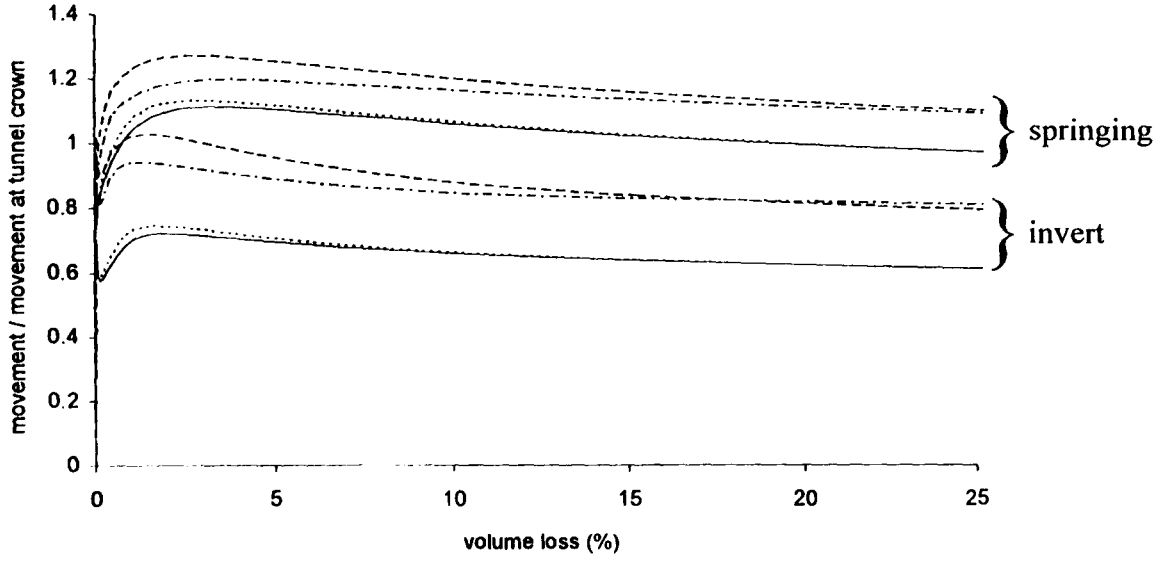

(b)

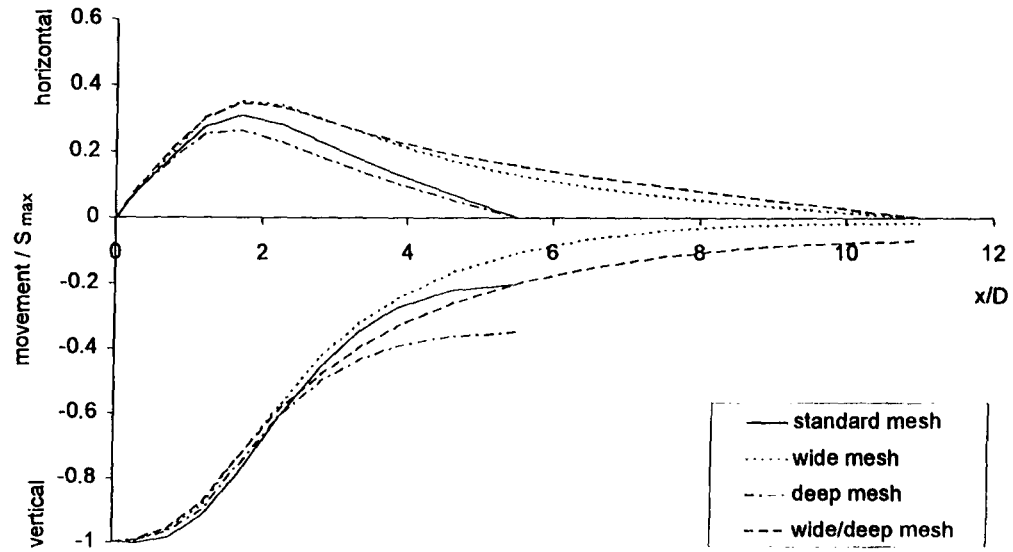

(c)

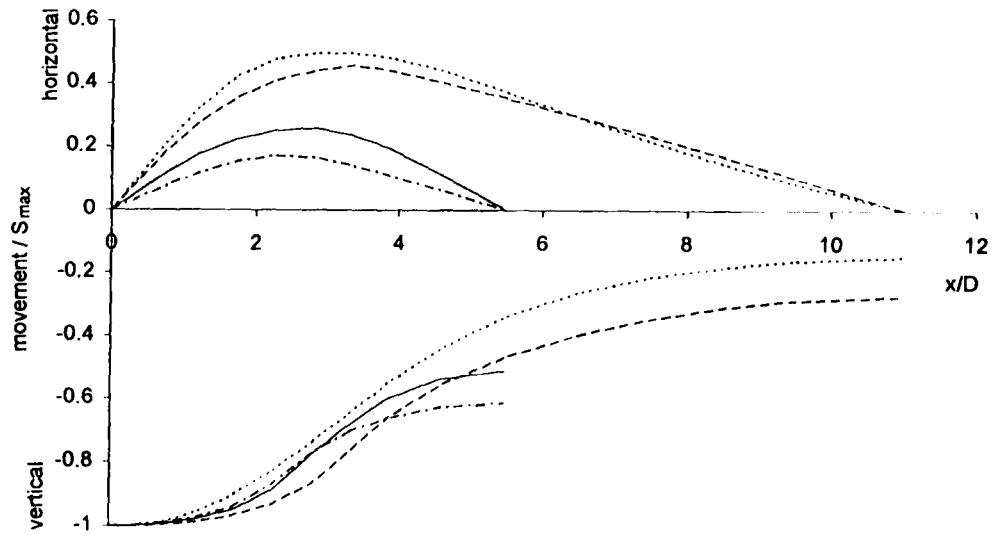

(d)

Figure 7.12 Effect of boundary proximity for 4*D* clay cover analyses
(standard mesh - RC4, wide mesh - RC4W, deep mesh - RC4D, wide/deep mesh - RC4WD).
a) volume loss against tunnel support pressure, b) movements around tunnel, c) normalised movements 1*D* above tunnel crown,
d) normalised movements at surface (4*D* above tunnel crown), (all at $V \sim 5\%$ where applicable)

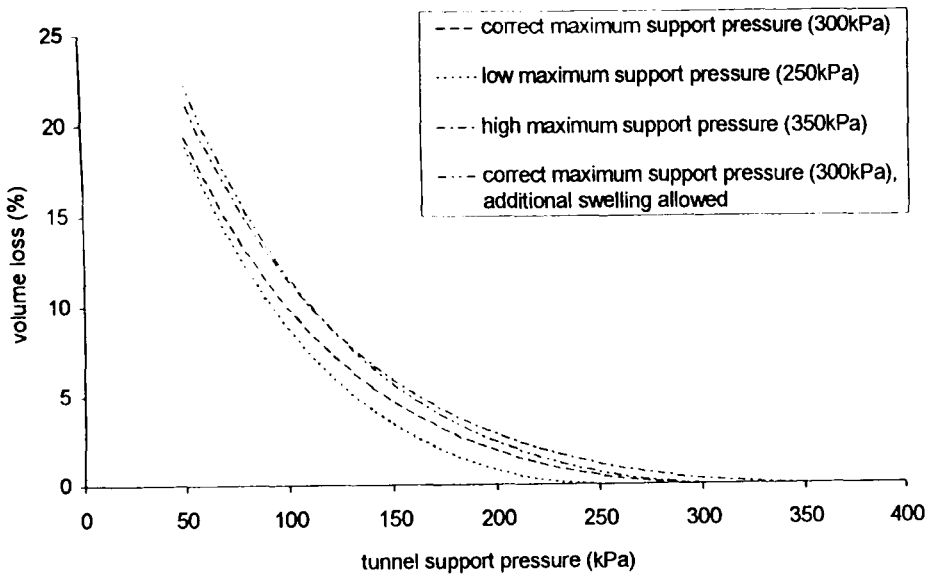

(a)

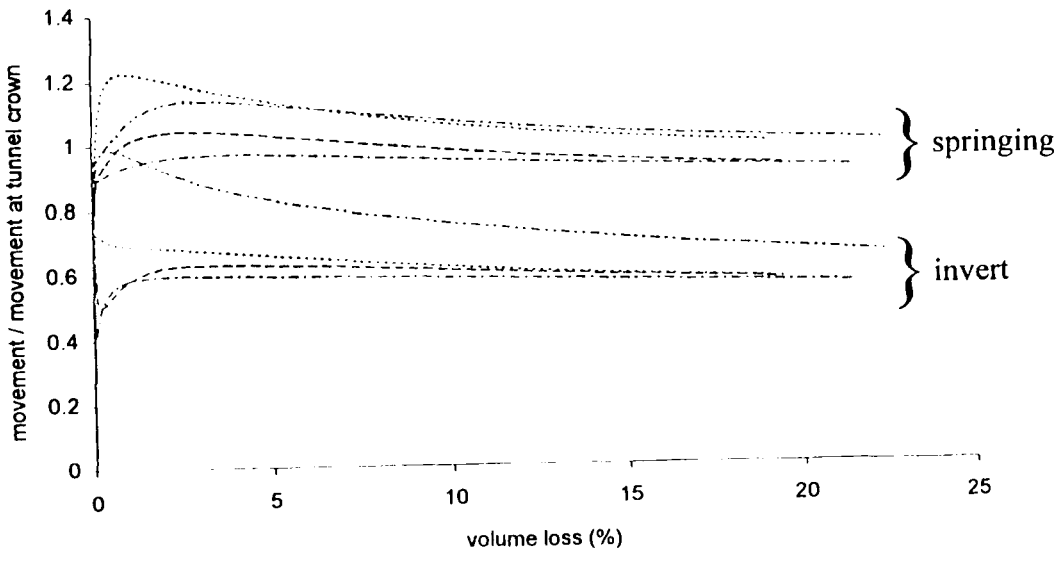

(b)

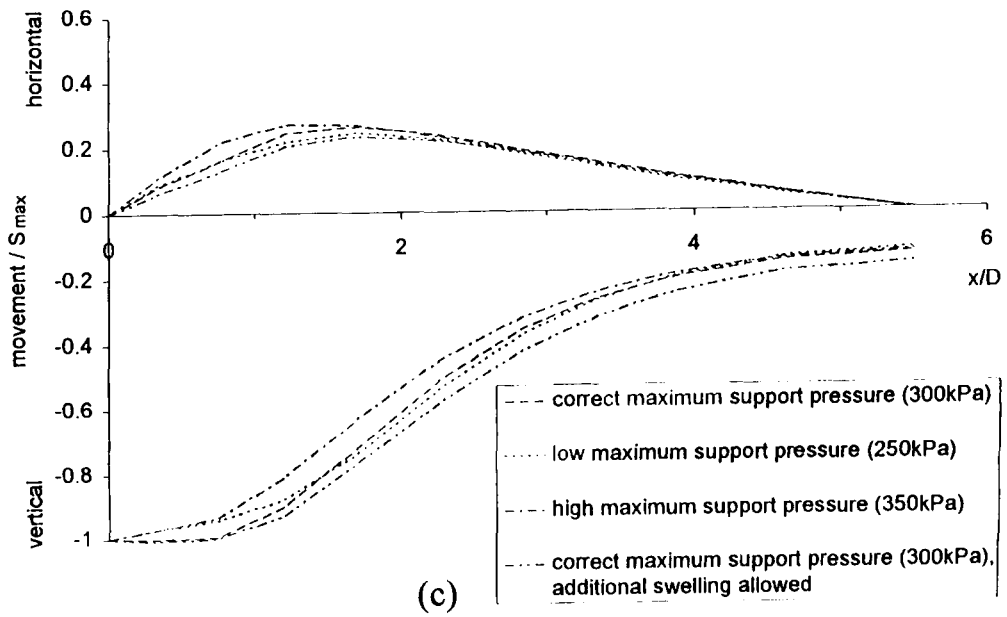

(c)

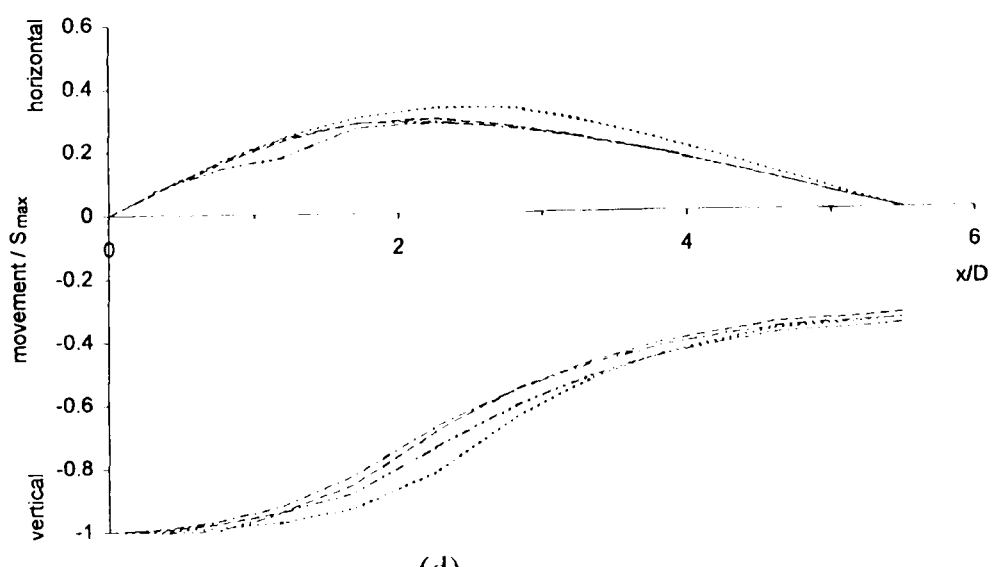

(d)

Figure 7.13 Effect of stress history for 3*D* clay cover analyses
($\sigma_{T\,max}$ = 300kPa - RC3A, $\sigma_{T\,max}$ = 250kPa - RC3B, $\sigma_{T\,max}$ = 350kPa - RC3C, $\sigma_{T\,max}$ = 300kPa with additional swelling allowed - RC3AM).
a) volume loss against tunnel support pressure, b) movements around tunnel, c) normalised movements 1*D* above tunnel crown,
d) normalised movements at surface (3*D* above tunnel crown), (all at $V \sim 5\%$ where applicable)

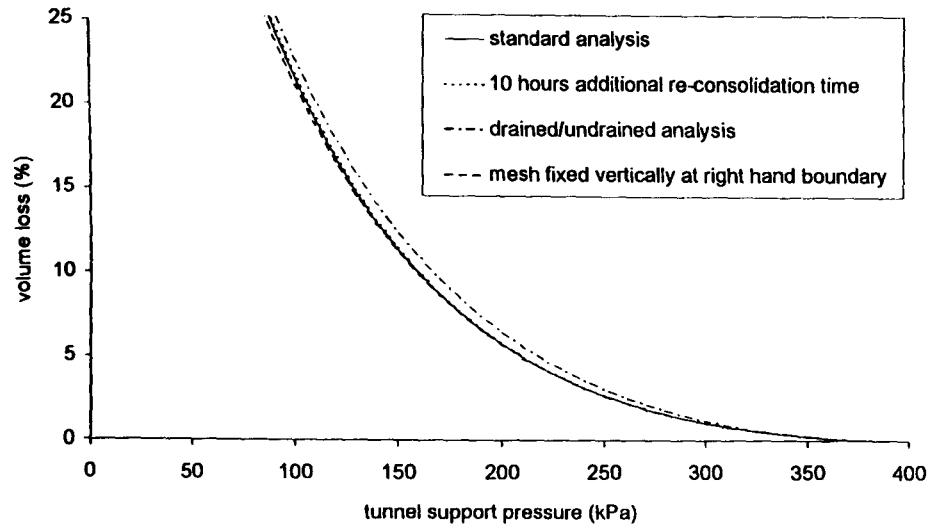

(a)

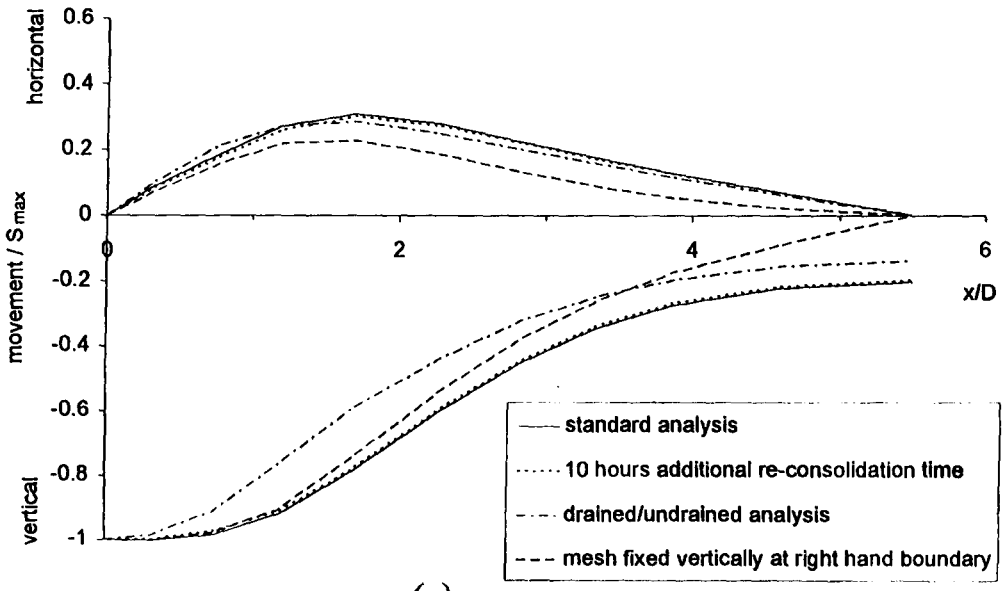

(c)

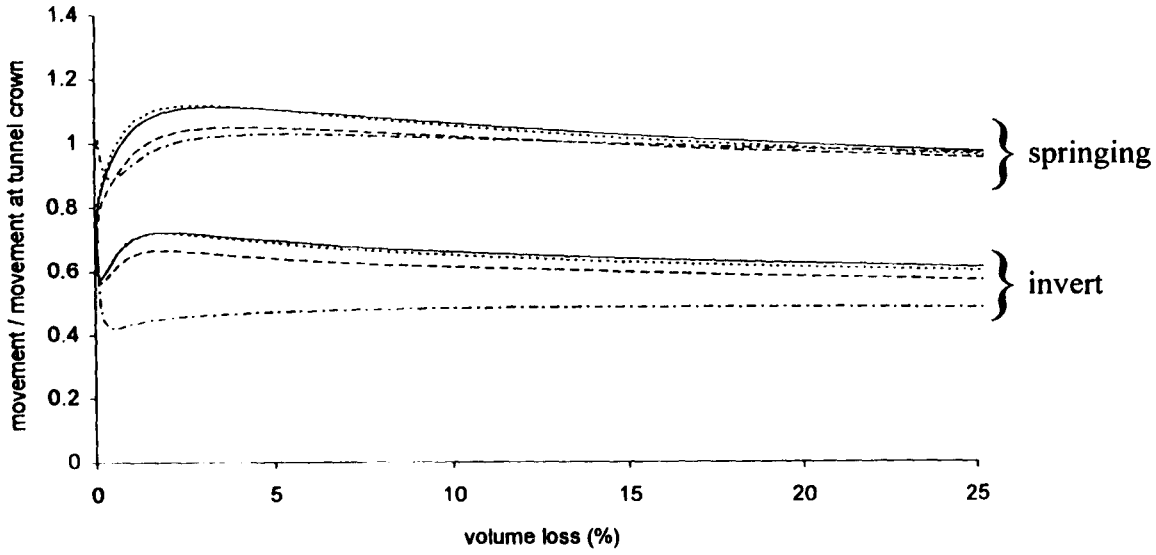

(b)

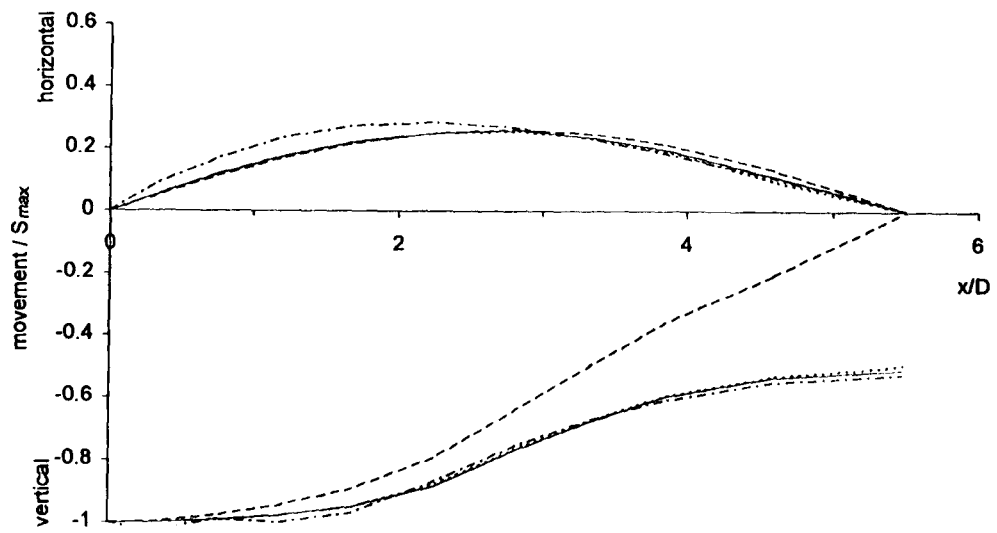

(d)

Figure 7.14 Effect of re-consolidation time, drained/undrained conditions and vertically fixing the right hand boundary for 4*D* clay cover analyses (standard analysis - RC4, additional re-consolidation - RC4X, drained/undrained analysis - RC4U, fixed right hand boundary - RC4P). a) volume loss against tunnel support pressure, b) movements around tunnel, c) normalised movements 1*D* above tunnel crown, d) normalised movements at surface (4*D* above tunnel crown), (all at $V \sim 5\%$ where applicable)

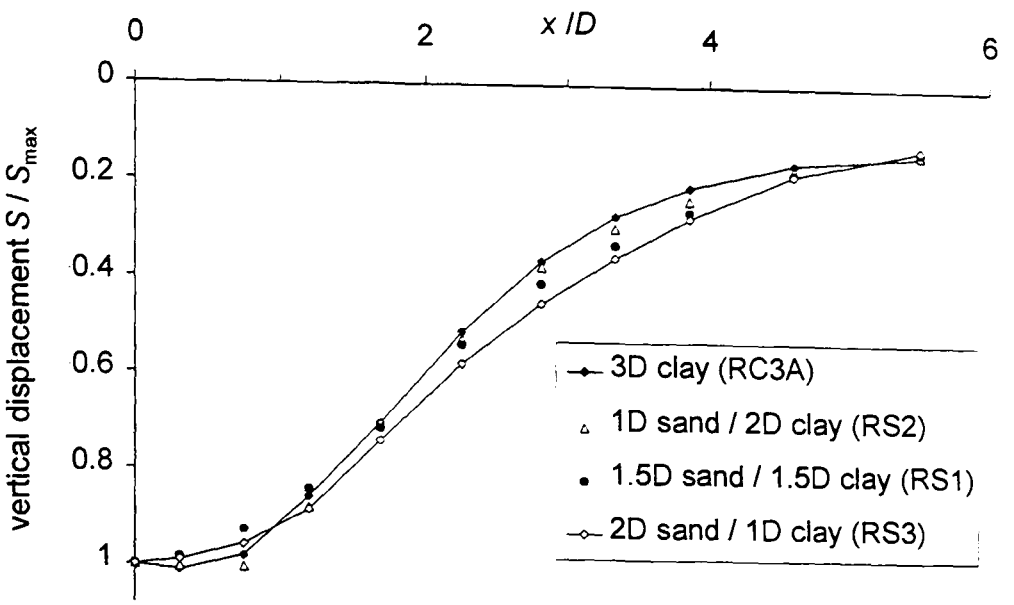

a) Vertical displacement of clay 1*D* above tunnel crown - LE model for sand

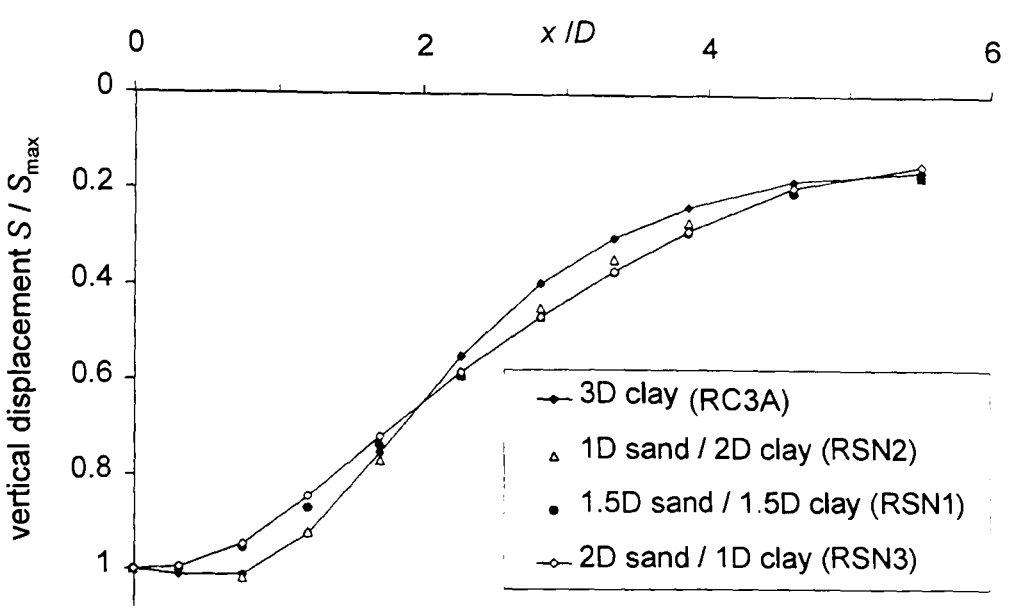

b) Vertical displacement of clay 1*D* above tunnel crown - 3-SKH model for sand

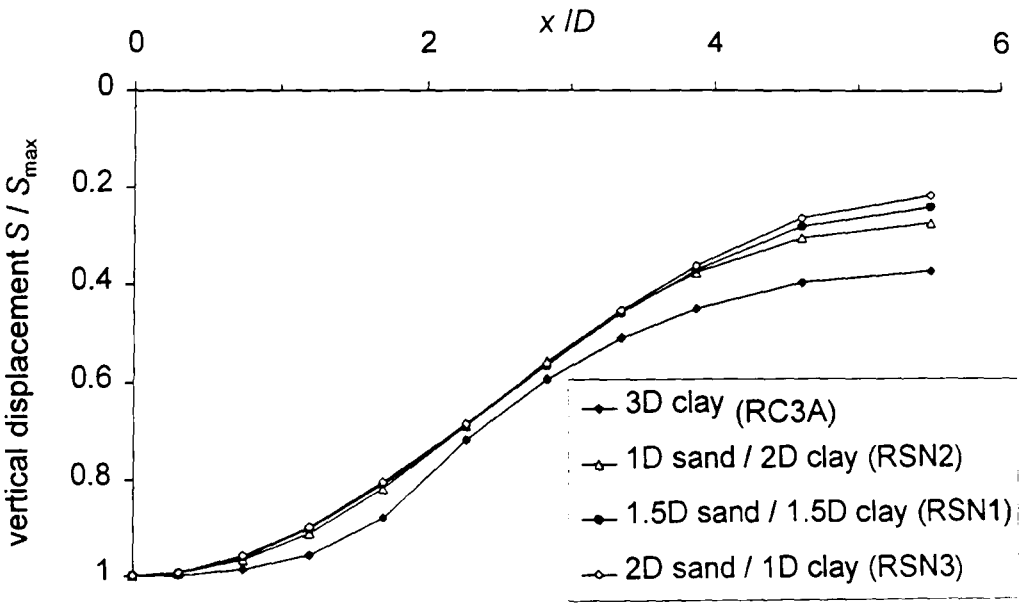

c) Vertical displacement at the surface 3*D* above tunnel crown - 3-SKH model for sand

Figure 7.15 Normalised settlement half-troughs for 3*D* total cover, varying proportions of sand over clay (σ_T = 180kPa, $V \sim 3\%$): comparison of finite element analyses using a LE model and the 3-SKH model for the upper sand layer

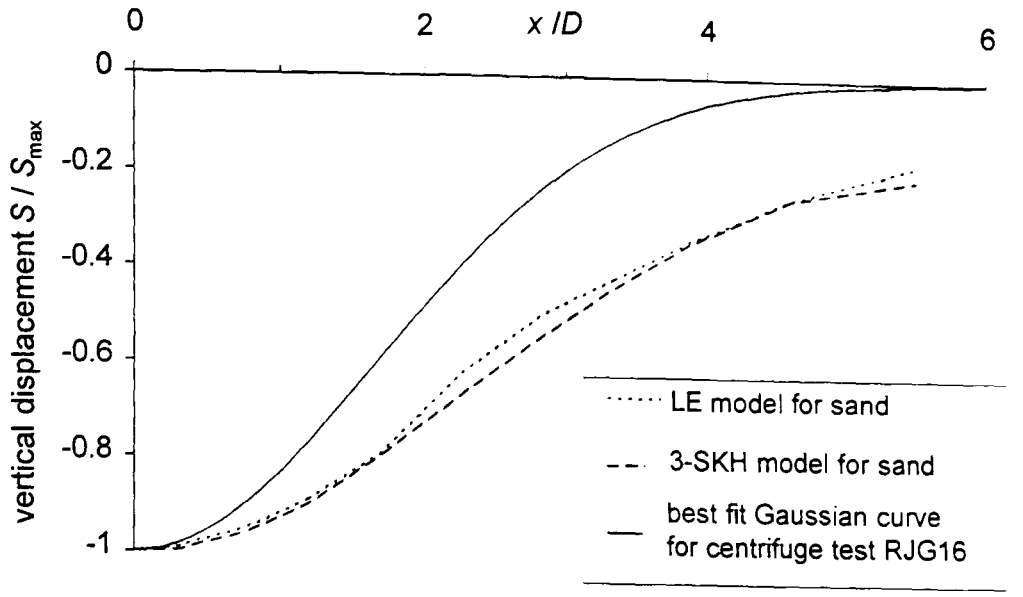

a) 1.5*D* sand / 1.5*D* clay (analyses RS1 & RSN1)

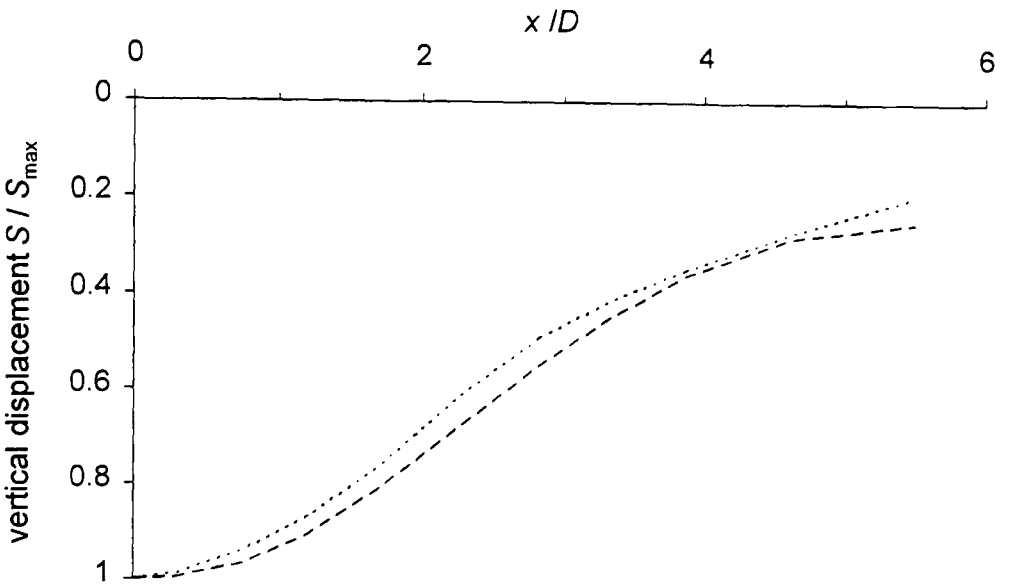

b) 1*D* sand / 2*D* clay (analyses RS2 & RSN2)

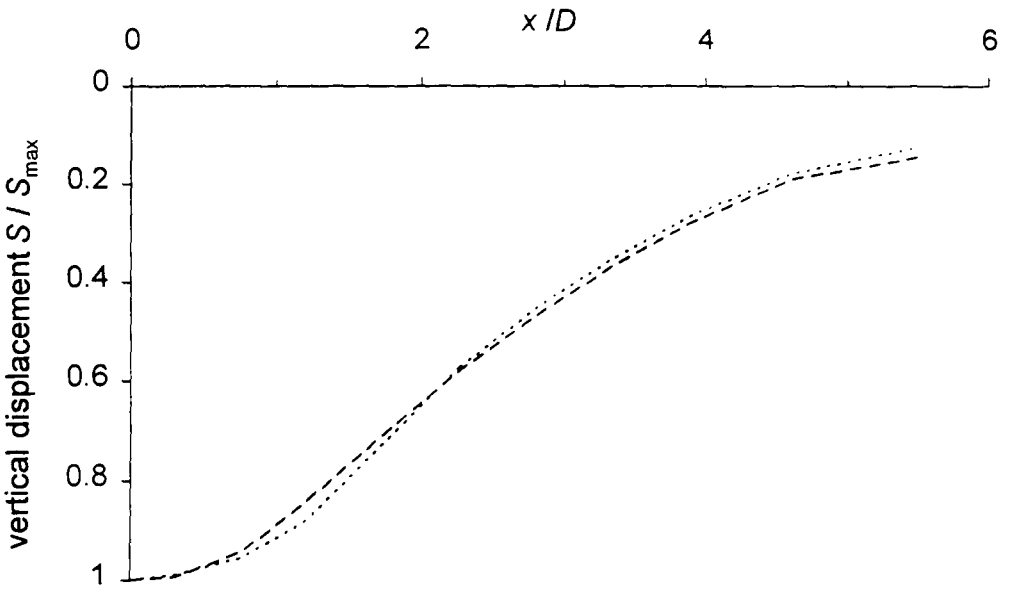

c) 2*D* sand / 1*D* clay (analyses RS3 & RSN3)

Figure 7.16 Normalised settlement half-troughs at the clay/sand interface for 3*D* total cover, varying proportions of sand over clay (σ_T = 180kPa, V ~ 3%): comparison of finite element analyses using a LE model and the 3-SKH model for the upper sand layer

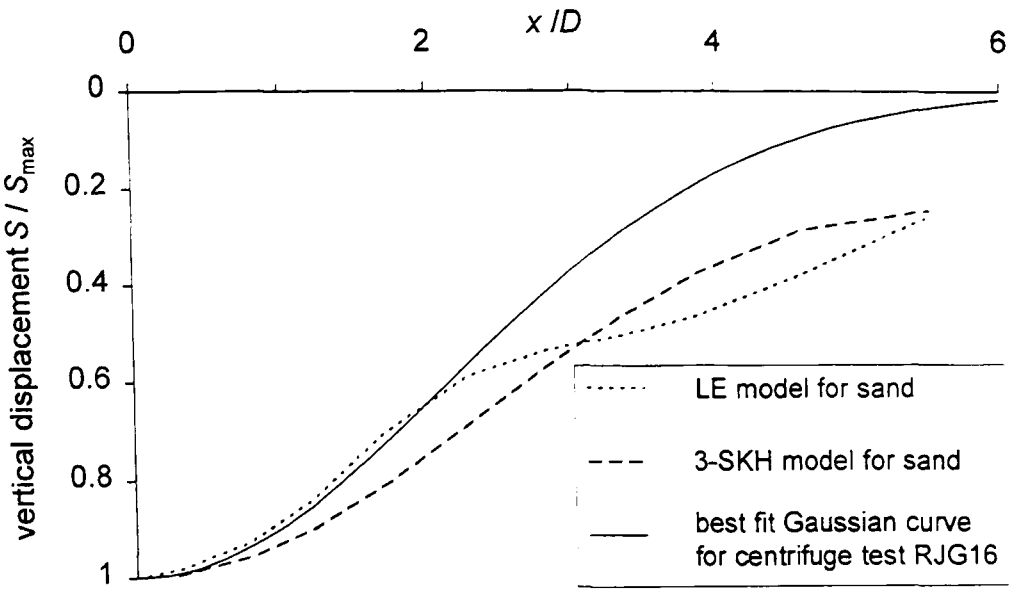

a) 1.5*D* sand / 1.5*D* clay (analyses RS1 & RSN1)

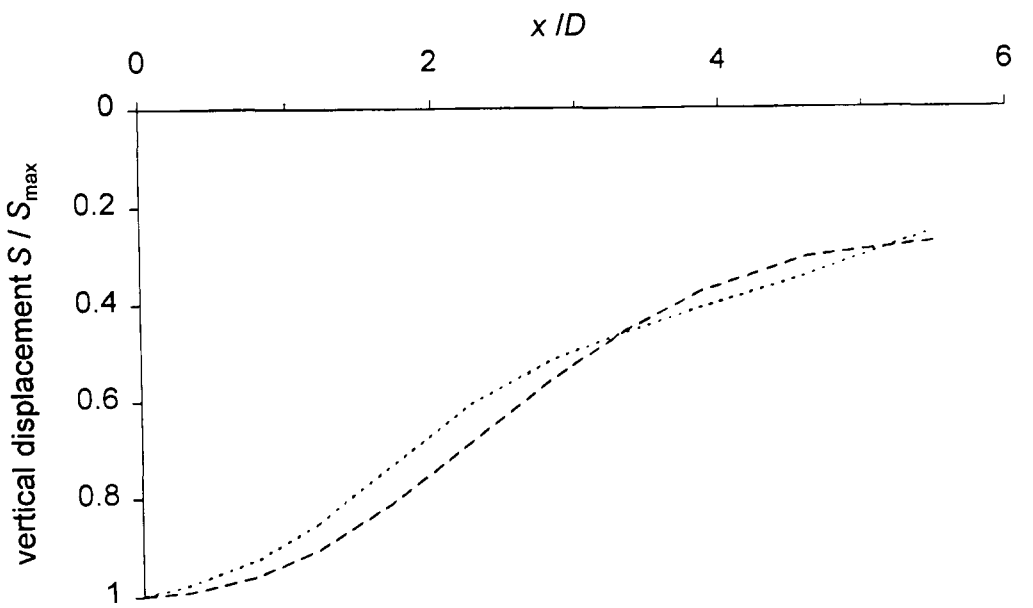

b) 1*D* sand / 2*D* clay (analyses RS2 & RSN2)

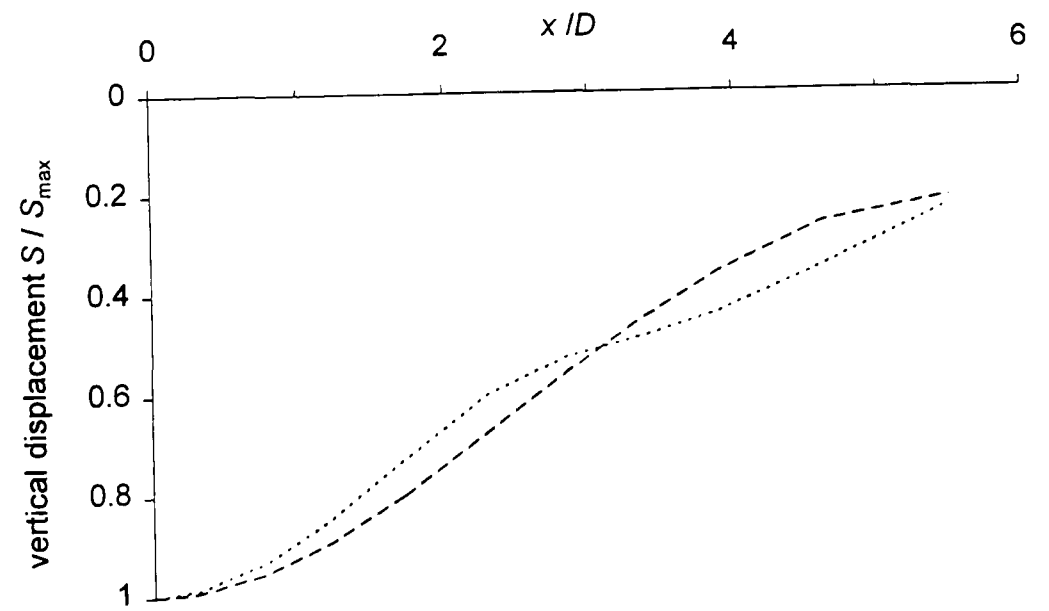

c) 2*D* sand / 1*D* clay (analyses RS3 & RSN3)

Figure 7.17 Normalised settlement half-troughs at the upper sand surface for 3*D* total cover, varying proportions of sand over clay (σ_T = 180kPa, $V \sim 3\%$): comparison of finite element analyses using a LE model and the 3-SKH model for the upper sand layer

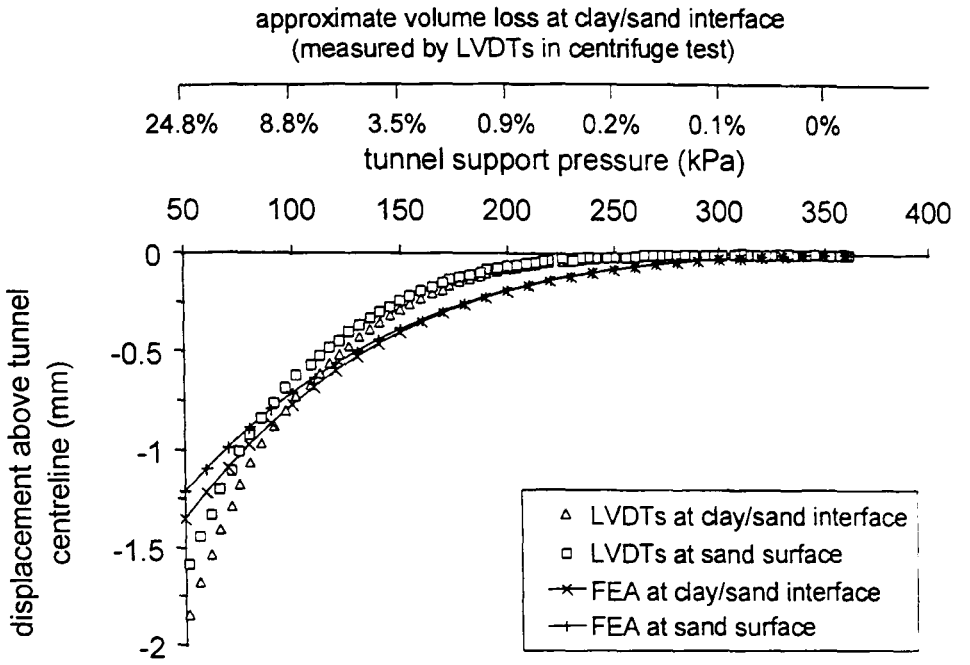

Figure 7.18 Comparison of displacements above the tunnel crown from centrifuge test RJG20 and corresponding finite element analysis RSG1

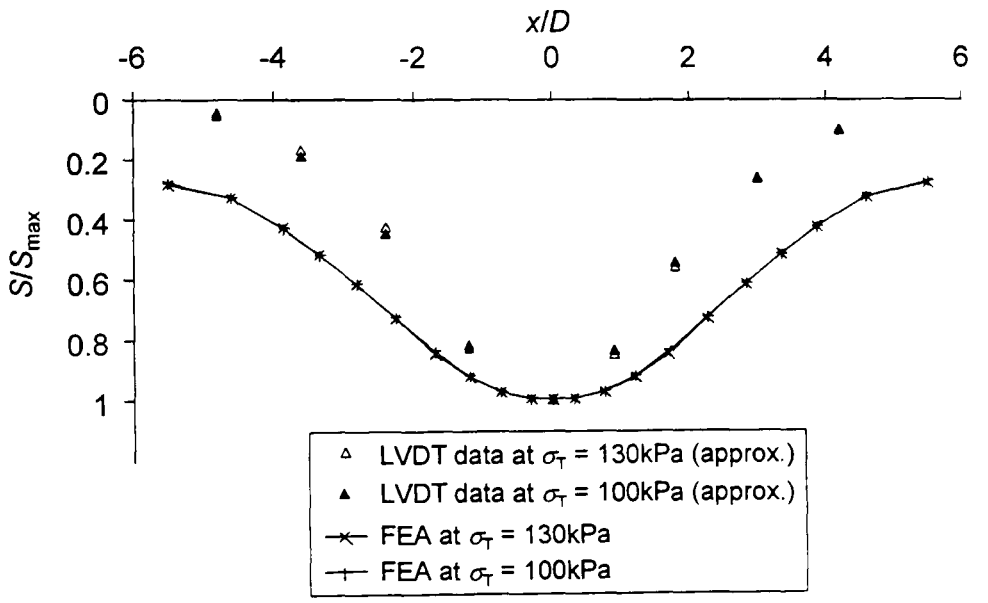

a) clay/sand interface

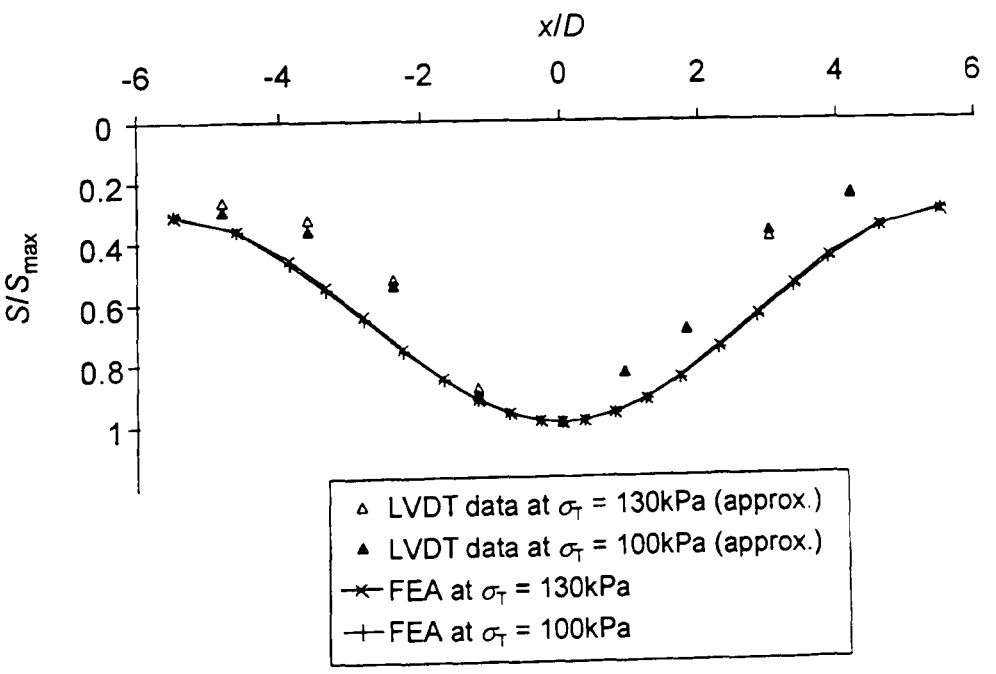

b) upper sand surface

Figure 7.19 Comparison of normalised settlement troughs from centrifuge test RJG20 and corresponding finite element analysis RSG1

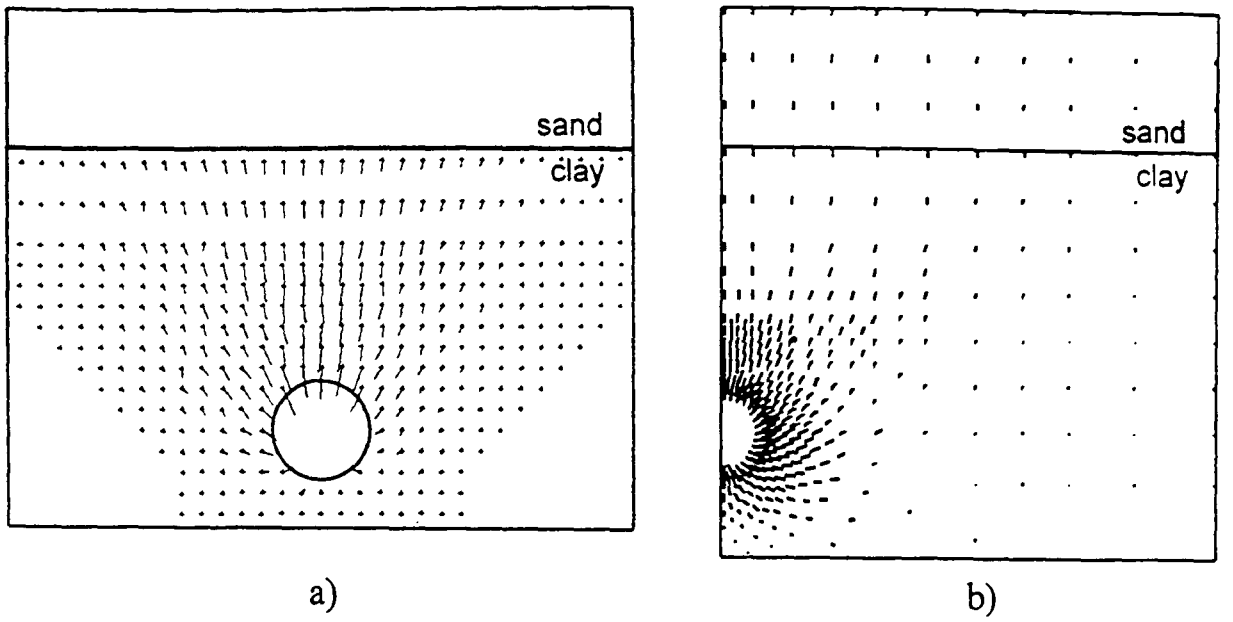

Figure 7.20 Vectors of movement from a) centrifuge test RJG20 and b) the corresponding finite element analysis RSG1 at similar σ_T

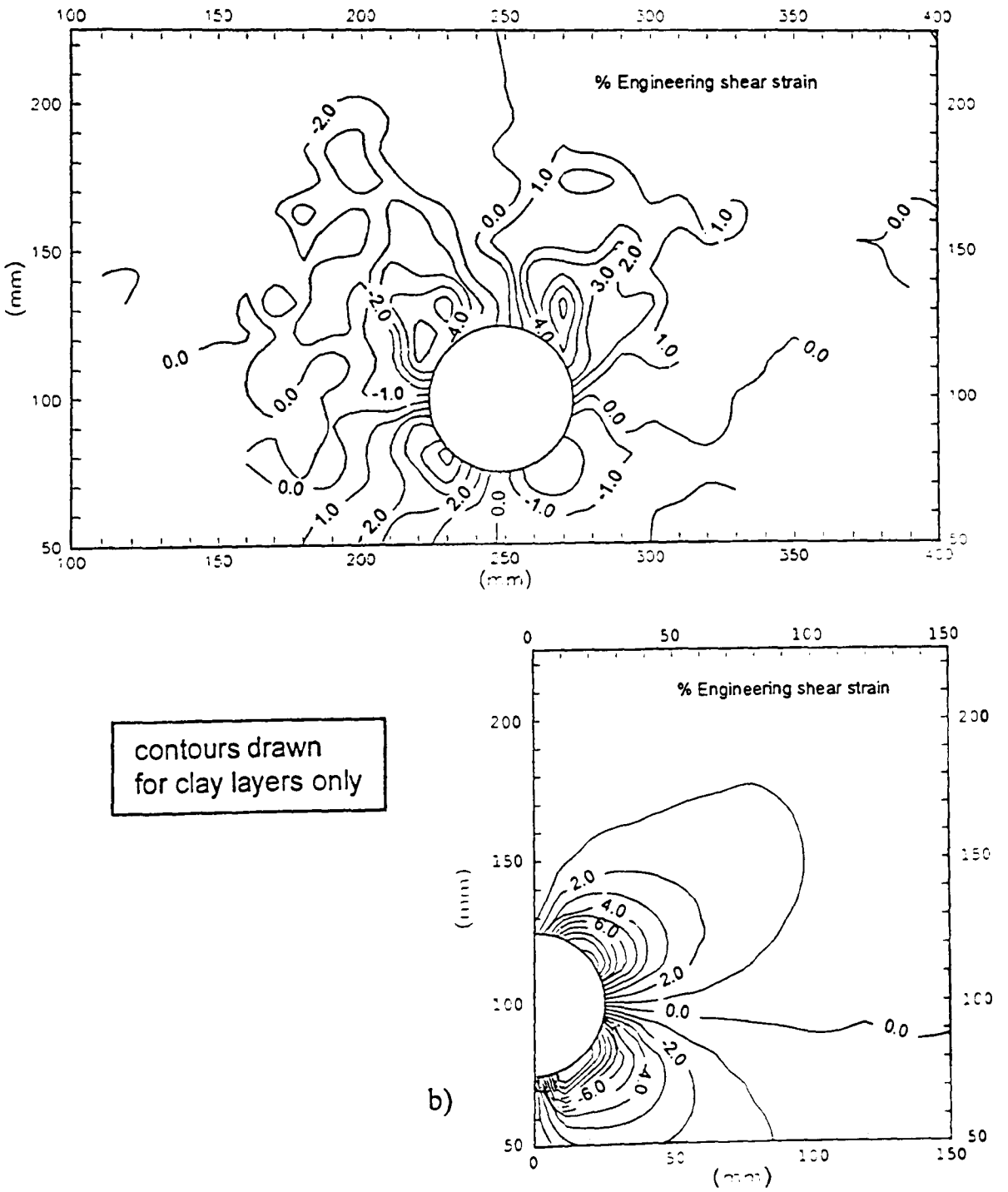

Figure 7.21 Contours of engineering shear strain from a) centrifuge test RJG20 and b) the corresponding finite element analysis RSG1 at similar σ_T

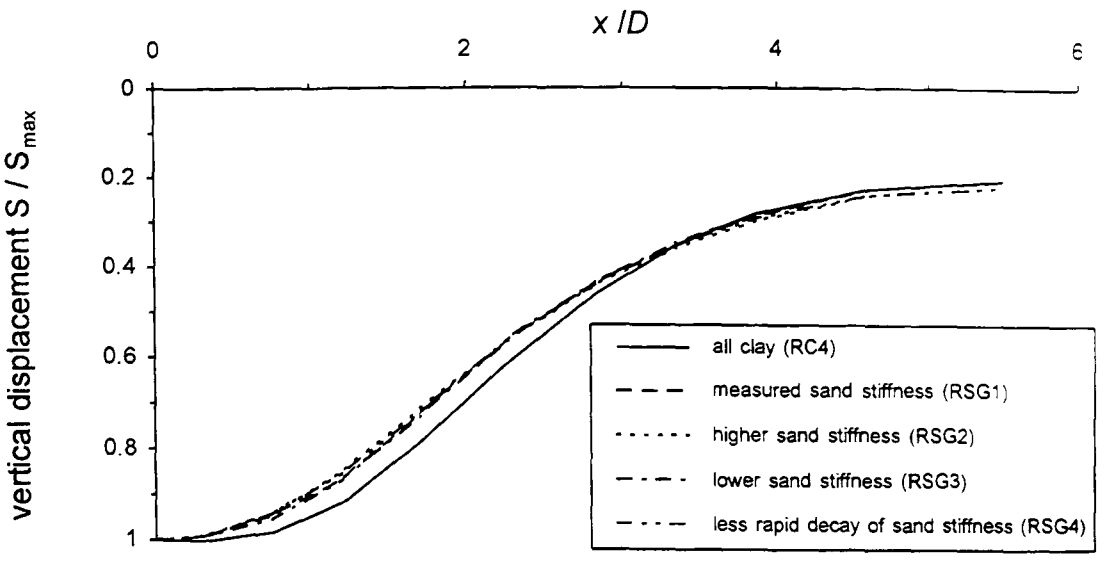

a) Vertical displacement 1*D* above tunnel crown

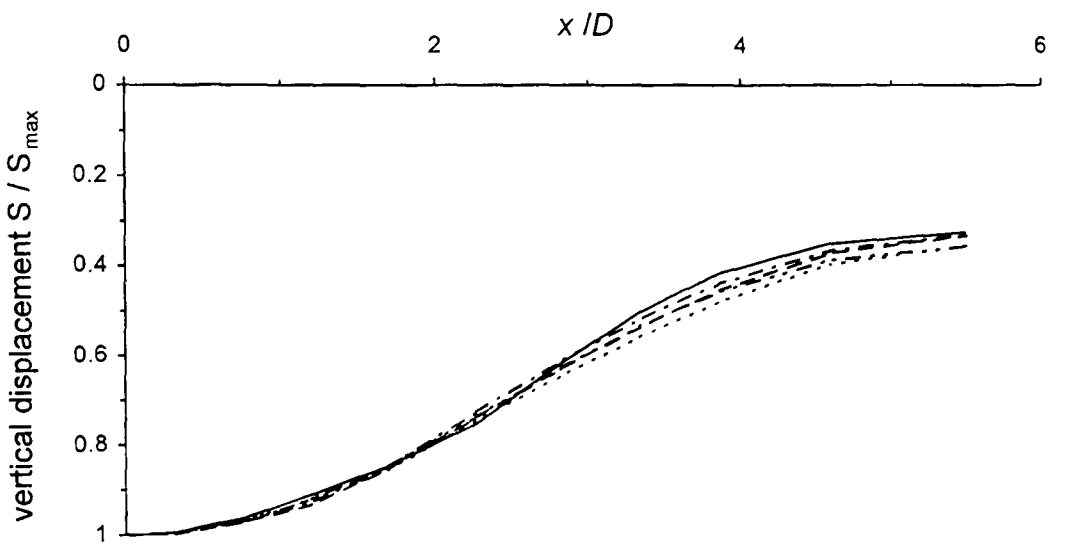

b) Vertical displacement 2.5*D* above tunnel crown (clay/sand interface if present)

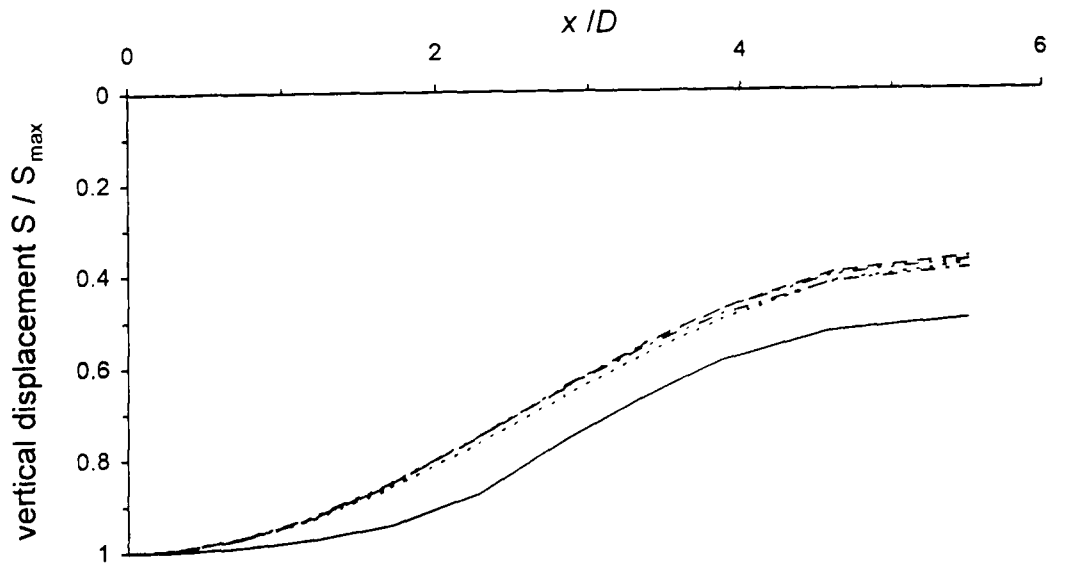

c) Vertical displacement 4*D* above tunnel crown (ground surface)

Figure 7.22 Normalised settlement half troughs with varying stiffness characteristics of the surface layer (4*D* total cover with top 1.5*D* sand except for all-clay analysis, $V_s \sim 5\%$) - RC4, RSG1, RSG2, RSG3, RSG4

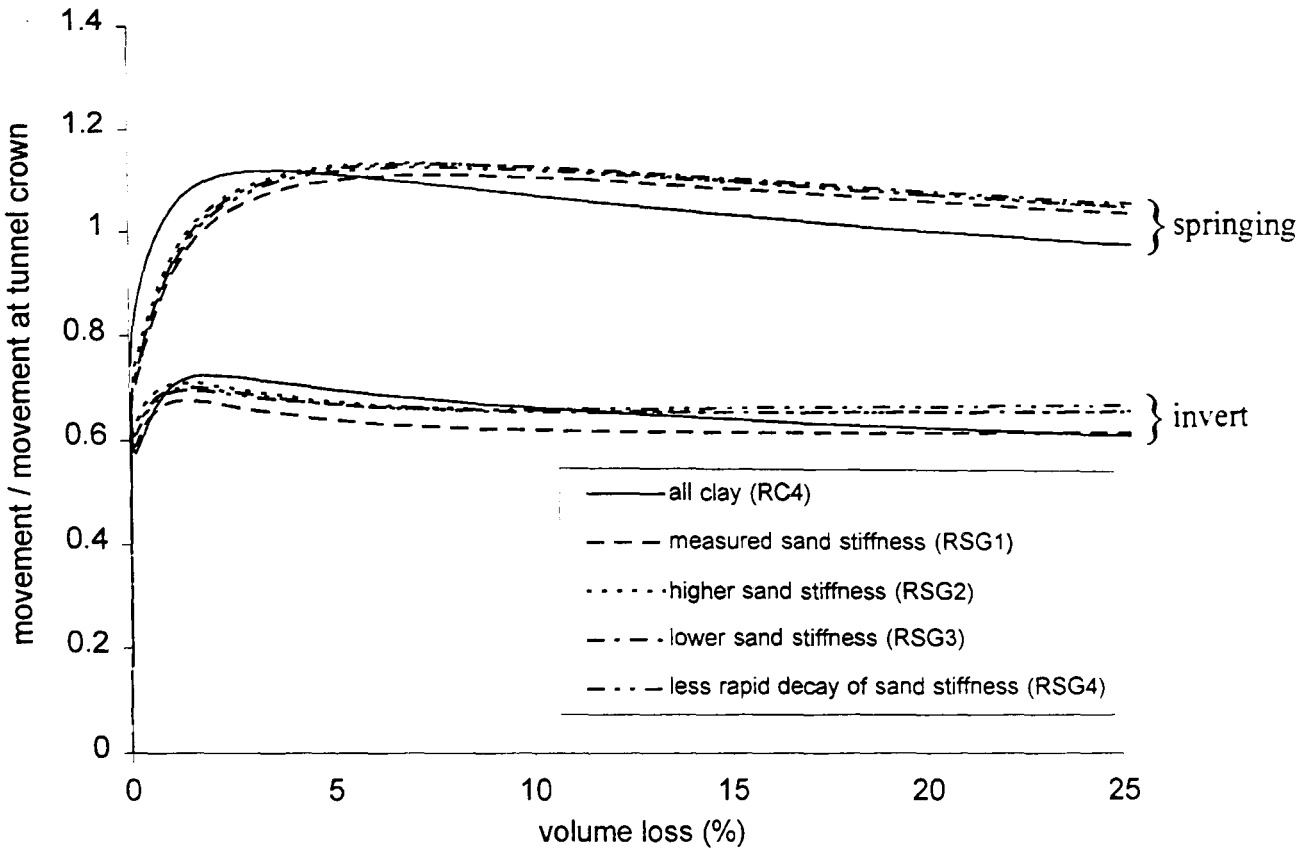

Figure 7.23 Effect of stiffness characteristics of the surface layer on movements around the tunnel (4*D* total cover with top 1.5*D* sand except for all-clay analysis) (RC4, RSG1, RSG2, RSG3, RSG4)

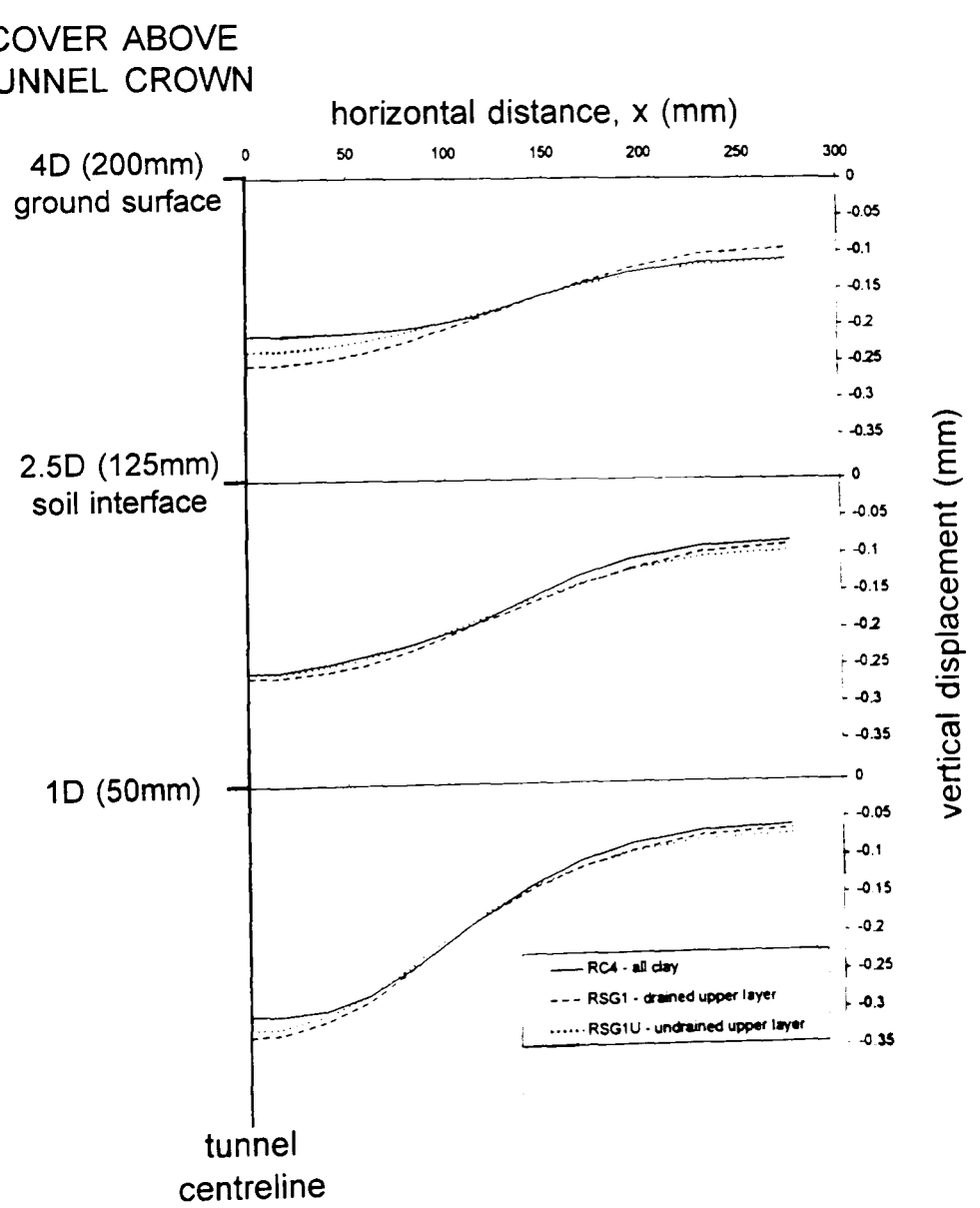

Figure 7.24 Settlement troughs at various depths with 4*D* total cover showing effect of drainage conditions in upper soil layer (RC4, RSG1, RSG1U)

APPENDIX A FOCUS OF VECTORS OF GROUND MOVEMENT DUE TO TUNNELLING ASSUMING GAUSSIAN SETTLEMENT PROFILES AND CONSTANT VOLUME CONDITIONS

Note:- For the purposes of this theoretical examination of vector focus it is convenient to re-define the distance from the tunnel axis to the horizon of interest as z_*, and so in the notation used in the main body of the dissertation $z_* = (z_0 - z)$.

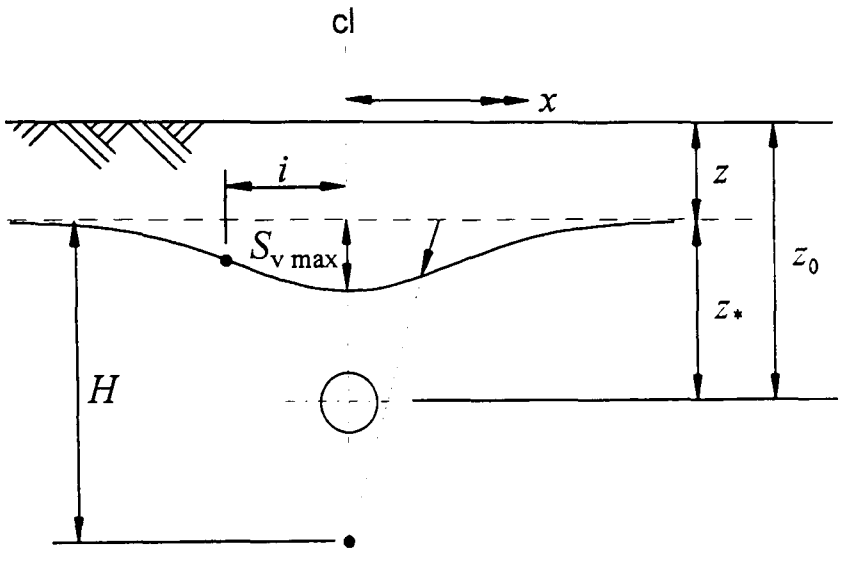

At any horizon above the tunnel, assume that the vertical ground settlement profile takes the form of a Gaussian distribution as

$$S_v = \frac{V}{\sqrt{2\pi}.i} \exp\left(\frac{-x^2}{2i^2}\right) . \qquad \text{A.1}$$

If $i = Kz_*$,

$$S_v = \frac{V}{\sqrt{2\pi}} \frac{1}{Kz_*} \exp\left(\frac{-x^2}{2K^2 z_*^2}\right) . \qquad \text{A.2}$$

Assume that any vector of ground movement above the tunnel is directed towards any point on the vertical axis of the tunnel, which is a distance H below the horizon of interest. The horizontal movement is then described by;

$$S_h = \frac{x}{H} S_v , \qquad \text{A.3}$$

so that,

$$S_h = \frac{V}{\sqrt{2\pi}} \frac{1}{Kz_*} \frac{x}{H} \exp\left(\frac{-x^2}{2K^2 z_*^2}\right) . \qquad \text{A.4}$$

For constant volume conditions there must be zero volumetric strain in any element of soil, so

$$\varepsilon_v + \varepsilon_h = 0 . \qquad \text{A.5}$$

The vertical strain in the ground is given by;

$$\varepsilon_v = \frac{dS_v}{dz_*} \quad , \tag{A.6}$$

and noting that K=f(z_*), from equation A.2;

$$\frac{dS_v}{dz_*} =$$

$$\frac{V}{\sqrt{2\pi}}\left[\exp\left(\frac{-x^2}{2K^2z_*^2}\right)\left(-\frac{1}{Kz_*^2}-\frac{1}{K^2z_*}\frac{dK}{dz_*}\right)+\frac{1}{Kz_*}\exp\left(\frac{-x^2}{2K^2z_*^2}\right)\left(\frac{2x^2}{2K^2z_*^3}+\frac{2x^2}{2z_*^2K^3}\frac{dK}{dz_*}\right)\right] \tag{A.7}$$

so,

$$\varepsilon_v = \frac{V}{\sqrt{2\pi}}\exp\left(\frac{-x^2}{2K^2z_*^2}\right)\frac{1}{Kz_*^2}\left(\frac{x^2}{K^2z_*^2}+\frac{x^2}{K^3z_*}\frac{dK}{dz_*}-1-\frac{z_*}{K}\frac{dK}{dz_*}\right) . \tag{A.8}$$

The horizontal strain in the ground is given by;

$$\varepsilon_h = \frac{dS_h}{dx} \quad , \tag{A.9}$$

and noting that by definition H = f(z_*), but H = f(x) also, from equation A.4;

$$\frac{dS_h}{dx} = \frac{V}{\sqrt{2\pi}}\frac{1}{Kz_*}\left[\frac{1}{H}\exp\left(\frac{-x^2}{2K^2z_*^2}\right)+\frac{x}{H}\exp\left(\frac{-x^2}{2K^2z_*^2}\right)\frac{-2x}{2K^2z_*^2}-\frac{x}{H^2}\frac{dH}{dx}\exp\left(\frac{-x^2}{2K^2z_*^2}\right)\right] \tag{A.10}$$

so,

$$\varepsilon_h = \frac{V}{\sqrt{2\pi}}\exp\left(\frac{-x^2}{2K^2z_*^2}\right)\frac{1}{Kz_*^2}\left(\frac{z_*}{H}-\frac{z_*}{H}\frac{x^2}{K^2z_*^2}-\frac{z_*x}{H^2}\frac{dH}{dx}\right) . \tag{A.11}$$

For zero volumetric strain, from equations A.5, A.8 and A.11;

$$\frac{x^2}{K^2z_*^2}+\frac{x^2}{K^3z_*}\frac{dK}{dz_*}-1-\frac{z_*}{K}\frac{dK}{dz_*}+\frac{z_*}{H}-\frac{z_*}{H}\frac{x^2}{K^2z_*^2}-\frac{z_*x}{H^2}\frac{dH}{dx}=0 \tag{A.12}$$

so,

$$\frac{x^2}{K^2z_*^2}\left(1-\frac{z_*}{H}+\frac{z_*}{K}\frac{dK}{dz_*}\right)-\left(1-\frac{z_*}{H}+\frac{z_*}{K}\frac{dK}{dz_*}\right)-\frac{z_*x}{H^2}\frac{dH}{dx}=0 . \tag{A.13}$$

If it is assumed that at any particular horizon the vectors of movement focus on a single point which lies on the vertical centreline of the tunnel, ie. $dH/dx = 0$ at any z_*, equation A.13 is satisfied if

$$1-\frac{z_*}{H}+\frac{z_*}{K}\frac{dK}{dz_*}=0 \tag{A.14}$$

which gives;

$$\frac{z_*}{H}=1+\frac{z_*}{K}\frac{dK}{dz_*} . \tag{A.15}$$

i varies with depth and the distribution may be considered to be linear except in the vicinity of the tunnel or a free-surface. The tangent to the distribution of i with depth intersects the vertical axis of the tunnel at H_*, as shown below.

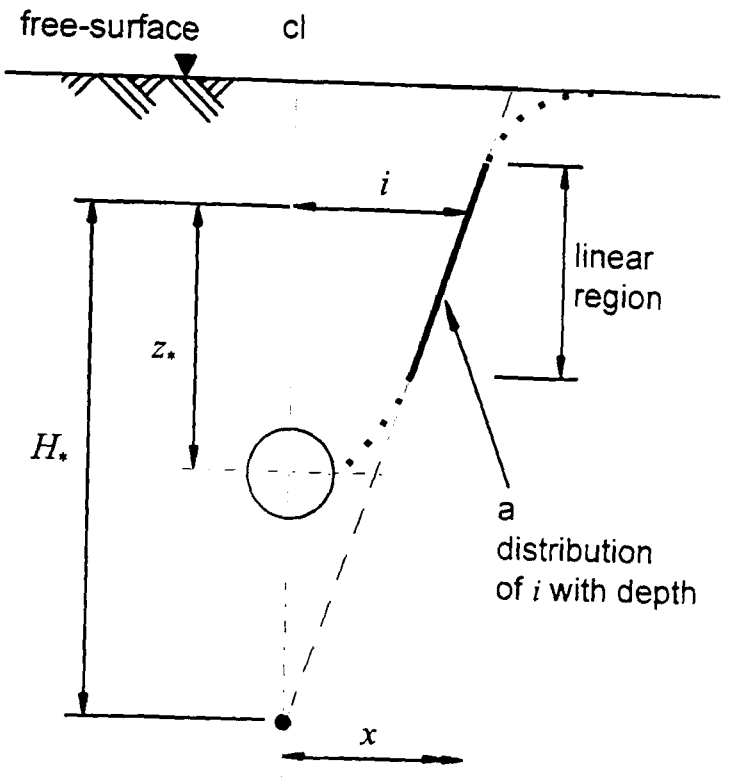

As $i = Kz_*$ and $K = f(z_*)$;

$$\frac{di}{dz_*} = K + z_* \frac{dK}{dz_*}, \qquad \text{A.16}$$

and

$$\frac{1}{K}\frac{di}{dz_*} = 1 + \frac{z_*}{K}\frac{dK}{dz_*}. \qquad \text{A.17}$$

Therefore, substituting equation A.15 above;

$$\frac{z_*}{H} = \frac{1}{K}\frac{di}{dz_*} \qquad \text{A.18}$$

or

$$\frac{di}{dz_*} = \frac{Kz_*}{H} = \frac{i}{H}, \qquad \text{A.19}$$

so at any particular z_*, $H=H_*$.

Assuming vertical ground settlement profiles of Gaussian form, constant volume conditions and that the vectors of ground movement at a given horizon above the tunnel focus on a single point on the vertical axis of the tunnel, the point of focus lies at the intersection of the tangent to the distribution of i with the vertical centreline of the tunnel.